EPRI

Development of Energy Production Systems from Heat Produced in Deuterated Metals

Volume 1

Technical Report

Energy Production Processes in Deuterated Metals

Volume 1

TR-107843-V1

Final Report, June 1998

EPRI Project Manager
T.O. Passell

DISCLAIMER OF WARRANTIES AND LIMITATION OF LIABILITIES

ORGANIZATION(S) THAT PREPARED THIS REPORT

Sri International
Lockheed Martin Company

ORDERING INFORMATION

CITATIONS

This report was prepared by

SRI International
333 Ravenswood Ave.
Menlo Park, CA 94025-3493.

Lockheed Martin Company
3251 Hanover St.
Palo Alto, CA 94304-1191

Principal Investigators

M.C.H. McKubre
S. Crouch-Baker
A. Hauser
N. Jevtic
S. I. Smedley
F. L. Tanzella
M. Williams
S. Wing

Non-SRI Contributors

B. Bush
F. McMohon
M. Srinivasan
A. Wark
D. Warren

The report is a corporate document that should be cited in the literature in the following manner:

Energy Production Processes in Deuterated Metals: Volume 1, EPRI, Palo Alto, CA,: 1998. Report TR-107843-V1.

REPORT SUMMARY

EPRI sponsored an experimental program to investigate the idea that heat, and possibly nuclear products, could be created electrolytically in palladium lattices. Observations using high precision mass flow calorimetry revealed that excess heat could be produced in electrochemical cells with palladium cathodes and a heavy water electrolyte in a more or less reproducible manner, when a number of criteria were satisfied. This excess heat generated is far too large to be a chemical or metallurgical transformation. By inference, a nuclear reaction of some as yet undetermined nature is the hypothesized heat source. This report details the observation of excess powers documented in calorimetry experiments.

Background
Palladium (Pd) cathodes electrochemically charged with deuterium (D) to unusually high D/Pd ratios have exhibited episodes of heat in excess of measured electrical inputs. While investigators have not yet definitively observed nuclear reaction products commensurate with the excess heat, they have detected suggestive evidence of nuclear reactions in the form of helium-4 (^{4}He), in the cell vapor space in a few cases.

Objective
To measure, optimize, and control the excess heat produced in highly deuterated Pd cathodes; to measure any signatures of possible nuclear reactions associated with the production of the excess heat.

Approach
The project team designed electrochemical cells within totally closed, precision flow calorimeters equipped with catalytic recombiners of the electrochemically produced D and oxygen gases. These systems were sensitive to excess heat episodes in the range above 50 mW, during inputs ranging from 1-45 W. Approximately 38 separate cells/calorimeters operated for periods of several days to several weeks each, with one cell operating nearly 3 mo. Separately, the team operated 107 open cells to test various procedures for attaining the high cathode D/Pd atomic ratios, believed to be a key condition for obtaining excess heat. They measured loading every few minutes by monitoring the electrical resistance of the cathode relative to its value in the pure metal, which has a known functional dependence with respect to D/Pd ratios. They accomplished loading with a combination of initial low cathode current densities of ~20-50 mA/cm^2, followed by current ramps up to ~1.0 A/cm^2. Current reversals to

deload or "strip" the cathodes of D and clean the surface by temporarily making it an anode resulted in high loadings. Lithium deuteroxide was almost always the electrolyte at a concentration of 1.0 mol/l, with occasional additions of 100-200 ppm of aluminum, boron, silicon, or copper.

Results

Four conditions were characteristic of all cells yielding episodes of excess heat: a D/Pd ratio >0.9, initial heat appearance times of 8-23 days, cathodic current densities above 0.1 A/cm^2, and high D fluxes across the cathode surface. Excess powers in the range of 5-30% were observed and measured to an accuracy of ~0.4%. These excess powers integrated to a total of about 0.1 to 1.1 MJ for a ~1.0-2.5 g (1/100 to 1/40 mol) Pd cathode. Thus, the excess heats ranged from 4-67 MJ per mol Pd, well above the largest known heats of chemical or metallurgical transformations. ^{4}He, measured in helium-tight cells designed to exclude atmospheric helium, indicated that this may be the ash of a nuclear reaction heat source. The absence of tritium, neutrons, and ^{3}He shows this hypothetical nuclear reaction to be something other than the D+D reaction observed in "hot fusion" research (unless the rare reaction pathway producing ^{4}He has somehow become completely dominant over the two pathways producing tritium and neutrons).

EPRI Perspective

Though the heat-producing phenomena were obtained in only about one-fifth of the cells, this work confirms the claims of Fleischmann, Pons, and Hawkins concerning the production of excess heat in D-loaded Pd cathodes at levels too large to be chemical transformations. Further work on this subject remains to demonstrate which nuclear reactions, if any, are generating the ^{4}He and excess heat. The only way to achieve this is to observe in generally quantitative fashion the nuclear reaction products, or "ashes." At this time, investigators believe that the most likely ashes to be found will be ^{4}He observable in the vapor phase of closed cells. This study provides information that will be valuable for long-term utility planning concerning potential heat sources that might become available several decades into the future. However, the specific reaction(s) producing the heat and ^{4}He must be determined to maximize this phenomena for practical uses in the power industry. Related EPRI reports address the *Development of Advanced Concepts for Nuclear Processes in Deuterated Metals* (TR-104195) and Cavitation-Induced Excess Heat in Deuterated Metals (TR-108474). Also available are Proceedings: Fourth International Conference on Cold Fusion (TR-104188, Vols. 1-4).

TR-107483

Interest Categories

Advanced nuclear technology

Keywords

Electrochemical power generation	Deuterium
Palladium	Cold fusion
Heavy water	Heat source independent

ABSTRACT

Since first announced in 1989 by Fleischmann, Pons, and Hawkins, "cold fusion" has been the subject of widespread interest and intense controversy. Observations using high precision mass flow calorimetry revealed that excess heat could be produced in electrochemical cells with palladium cathodes and a heavy water electrolyte in a more or less reproducible manner, when a number of criteria were satisfied. This excess heat generated is far too large to be a chemical or metallurgical transformation. By inference, a nuclear reaction of some as yet undetermined nature is the hypothesized heat source. While nuclear reaction products commensurate with the excess heat have not yet been definitively observed, suggestive evidence of nuclear reactions has been detected in the form of helium-4 in the vapor space in a few cases. This report describes the characteristics of cells yielding episodes of excess power as well as separate cells devoted to studies of deuterium loading in palladium. Inserted at the back cover of the report is a CD-ROM containing original data of all the cells reported, the subdirectory/folder names corresponding to the experiment designations used in the text. The format (ISO 9660 standard) is one readable by either PC or Macintosh computers. This enormous data base is provided as tables of parameters measured for each cell such as time of measurement, cell voltage, cell current, temperatures at various places within the calorimeter, gas overpressure, and many others. The data are "tab delimited" and can easily be imported into a spreadsheet type program such as Microsoft Excel. To look at a file, start Excel, then using the open command, locate the file on the CD-ROM and open the file. If a subdirectory has no files in it, then there are no data files associated with that cell/experiment.

CONTENTS

LIST OF FIGURES

LIST OF TABLES

1

INTRODUCTION

An experimental program sponsored by the Electric Power Research Institute (EPRI) was undertaken at SRI International to investigate the idea that heat, and possibly nuclear products, could be created in palladium lattices under electrolytic conditions. Several types of experiments were performed to determine the factors that control the extent of deuterium (D) loading in the Pd lattice and to search for unusual calorimetric and nuclear effects.

Following the results reported in 1989 by Fleischmann et al.[1] considerable effort has been expended to test the hypothesis that the electrochemical loading of deuterium into palladium leads to the production of more energy than is predicted to arise from known chemical or electrochemical phenomena. In the period 1989-1992, work was performed at SRI, again under the sponsorship of EPRI, in order to confirm the reality of excess heat production. The results of this study are described in the EPRI final report TR-104195. In a nutshell, using high precision mass flow calorimetry, excess heat production was observed in electrochemical cells containing palladium cathodes in a more-or-less reproducible manner when a number of criteria were satisfied. These included attainment of a high loading of deuterium in the cathode (in excess of approximately 0.9), the use of electrochemical currents above a threshold value, and the satisfaction of a cathode "incubation" time of several hundred hours.

In addition to these calorimetric studies, a comprehensive series of experiments was undertaken earlier in order to study the loading behavior of hydrogen and deuterium into palladium. With appropriate control of the interfacial conditions, it was shown that it is possible to load both H and D into Pd to molar ratios of approximately unity. Electrode preconditioning apparently plays a significant role in the ability to attain and maintain high loading under electrochemical conditions. It was found that helium implantation provided a suitable means of surface activation to facilitate loading; the presence of such implanted helium, however, was not obviously implicated in the generation of excess power. The overall conclusions of the loading studies were that, by careful control of the electrode pretreatment, the electrolyte composition, and the current density, Pd can be loaded to an atomic ratio $D/Pd \approx 1$ and this loading sustained for periods of weeks.

We were unable to account for the observed excess heat by any artifact known to us and were forced to conclude that the source of the excess power is a property of the

D/Pd system. Further, we could not account for the measured excess power and energy by any chemical or mechanical process with which we were familiar.

Encouraged by the calorimetric results obtained during 1989-1992, as well as by the progress made in understanding some of the critical loading-related issues, it was decided to continue the investigation, although with a somewhat different emphasis-including that of addressing directly the potentially nuclear aspects of the heat producing process. It is the execution of the calorimetric and loading-related aspects of this continuation which forms the substance of the present report. *The results of the nuclear portion of this program are described in a separate, companion report (vol. 2).* In the present study, three broad tasks were undertaken:

1. To continue the study of excess heat production in electrochemical cells utilizing palladium cathodes, and further investigate those materials science issues which affect deuterium loading.

In addition to mass flow calorimetry, a variety of calorimetric systems were employed in order to provide more flexibility in the choice of operational protocols as well as for use with simultaneous nuclear detection systems. Similarly, a variety of cell designs, cathode materials, electrode pretreatments and experiment operation protocols were used. As in our previous study, axial cathode resistance measurements were employed in order to measure in-situ the cathode loading. Such measurements were carried out in calorimetric experiments as well as in the degree-of-loading farm, a collection of cells designed to study loading-related issues.

2. To identify the nuclear product(s) associated with excess heat production. Three potential products were given priority in this respect: γ-rays, He and tritium.

3. To investigate *in-situ* the temporal and quantitative correlations between excess heat production and nuclear product formation.

As part of tasks (2) and (3), mass flow and heat flow calorimetries were carried out in systems designed to retain any He produced for subsequent batch analysis; further, calorimetric systems were assembled for operation with simultaneous high-sensitivity γ-ray detection. In addition, cell components were retrospectively analyzed for both γ-ray and tritium production.

The experiments described briefly above, and in more detail in the following chapters, were carried out in a purpose-built laboratory. This facility was constructed in order to enable experiments which involve the potentially hazardous production of deuterium and oxygen mixtures to be carried out safely and efficiently.

1. M. Fleischmann, S. Pons and M. Hawkins, "Electrochemically Induced Nuclear Fusion of Deuterium", J. Electroanal. Chem., *261* (1989), p. 301 and errata, *203* (1989), p. 87.

2

DEGREE-OF-LOADING STUDIES

Introduction and Overview

As part of an EPRI-sponsored program in the Energy Research Center (ERC) at SRI, we have investigated the uptake of hydrogen and its isotopes into palladium. Up to ten electrolytic cells have been used at a time in what is referred to as the Degree-of-Loading (DoL) farm. Four point *in-situ* resistance measurements have been employed to infer the degree of loading using calibration data from the literature. Relatively high degrees of deuterium loading have been achieved in the majority of the electrolysis experiments by careful manipulation of the electrochemical and cathode metallurgical conditions. Specifically, 81% of the palladium cathodes were charged with deuterium to an atomic D/Pd ratio > 0.85, and 61% of the electrodes reached loadings of greater than 0.90. Although these statistics are based on the value of peak loading achieved and invariably maintained for only a small part of the total electrolysis time, the metric is nonetheless rather significant considering that most deuterium charging of palladium by electrochemical means reaches a D/Pd ratio of only 0.70.

Attainment of very high degrees of loading is of particular interest because the ERC previously established that an atomic ratio of 0.90 is the minimum loading threshold required for the observation of anomalous excess heat generation in deuterated palladium cathodes. It was shown that this difficult-to-achieve loading criteria is a necessary, but not sufficient, condition for the heat effects. Additionally, it is widely recognized that a lack of reproducibility associated with this system is a cause for concern among researchers in the field. Thus, the overall objective of the DoL work therefore has been to determine the factors that control the extent of deuterium uptake in palladium so that one can reproducibly achieve high degrees of electrolytic loading on demand.

It might be possible to obtain this goal by using the DoL farm to screen a large number of variables in order to learn which parameters are most important. However, an underlying premise of our works is that a fundamental understanding of the H(D)/Pd system is very much needed and will serve to guide future electrochemical loading and calorimetric experiments.

We have characterized the H(D)/Pd system by building on the past success of the ERC's pioneering work involving electrolytic loading. In particular, the electrochemical

cell design and materials of construction employed in the early DoL studies - a helical platinum anode coiled around the palladium cathode and enclosed in a quartz body - proved to be an excellent starting point for this investigation. Significant improvements to the DoL supporting apparatus included the following: The commercially available constant-temperature (35°C) water bath was replaced with a box constructed in-house out of transparent Lexan (polycarbonate). The see-through bath allowed the electrolyte level in the DoL cells to be readily observed and easily maintained by making water additions by visual inspection during electrolysis (as opposed to estimating the water loss using Faraday's law). The water was replaced with circulating ambient air to prevent the possibility of bath water (normal light water) contaminating the electrolytic cells containing high purity heavy water based electrolyte.

All cell modifications, however, were not positive. For example, small changes in the anode-to-cathode aspect ratios appear to yield poor loading performance. This somewhat unexpected result supports the claim that the group's original electrolytic cell design was better. Even more importantly, these subtle geometrical changes in electrode configuration and their subsequent detrimental effects clearly demonstrate that the attainment of a highly uniform current distribution at the cathode is of paramount importance with respect to achieving extremely high degrees of loading.

Other key variables were identified to play a major role in the loading process. Of particular importance, an electrode pre-conditioning annealing step in an oxygen-gettered environment was determined to be a necessary requirement for the attainment of highly loaded deuterated palladium. Better results have been obtained using a vacuum (as opposed to a D_2) anneal at 850°C for three (instead of 48 hours). Additionally, silica and aluminum, when added to the 1M LiOD/D_2O electrolyte, serve as surface modifying agents that enhance loading and promote the longevity of loading, respectively. The role of current density is recognized to be of great importance in the loading process, so various current protocols have been investigated. Low to moderate cathodic current densities (below 200 mA/cm²) and small constant current steps (40 mA/cm²) enabled high degrees of loading to be obtained without the onset of significant spontaneous deloading. Anodic current is required to strip the absorbed deuterium out of the palladium lattice. Stripping in the form of low anodic current-density steps (20 mA/cm²), pulses and/or open-circuit deloads appeared to provide a suitable means of reactivating the electrode surface to facilitate re-loading. Overall loading also was shown to be improved with each repeated cycle of the cathodic-load/anodic-strip current protocol.

The remaining variable of significance to be discussed here is the source of the cathode material and its effect on electrolytic loading. Despite reports in the literature of observed binary heat effects (and presumed loading behavior) in deuterated palladium from different suppliers, we were able to obtain reasonably good loadings (atomic ratios above 0.85, but not always above the 0.90 threshold value) seemingly independent of the metal source, provided that the design criteria and electrolysis

conditions presented above were met. Although overall good loadings have been obtained, variability in the DoL data appears to be prominent when the response profiles versus time are examined more closely. For example, may unexplained and seemingly unaccountable responses have been observed in the resulting DoL profiles. We also have seen batch-to-batch variations among some (six) separate shipments of Engelhard palladium.

In addition to delineating the effect that these key variables have on electrolytic loading, the DoL work has proven to be most beneficial for supplementing the other critical areas of the ERC's exploratory research program. Specifically, it is important for the future support of the group to meet the EPRI milestone of correlating the observed excess heat with a nuclear signature. A strategy for this purpose involved selecting a DoL cell, based on high cathode loading as the criteria, and transferring the entire cell to an air-cooled Seebeck heat flow calorimeter designed to operate in the environment of a Ge detector for gamma rays. Additionally, all post-mortem DoL electrodes were installed inside an NaI annulus and on top of the Ge detector for counting purposes. Thus, the DoL farm serves as a useful pre-loading station for the group's calorimetric and nuclear detection investigation.

In conclusion, the ERC's degree-of-loading research program has been very successful, based on the experimental results summarized above. Ironically, our loading success rate may have resulted from having been too conservative with the experimental design and not having tried enough provocative new ideas. Despite this success, assessment of our understanding the H(D)/Pd system is decidedly mixed. On one hand, we have gained an empirical understanding of the electrochemical and metallurgical conditions that give rise to high degrees of loading. This pragmatic approach has enabled us to establish useful loading criteria from which future DoL characterization experiments can be based, as well as being most beneficial to the group's on-going calorimetric work. On the other hand, we have not obtained the fundamental and mechanistic understanding of the system that we would like, and need to have, in order to correlate the attainment of loading with changes in the molecular structure of the palladium due to metallurgical processing conditions.

Consequently, future degree-of-loading research is required, including both experimental and theoretical work. Various electrochemical methods and spectroscopic surface analysis techniques should be applied to assess the electrocatalytic activity of the palladium metal and/or alloy, as well as the microscopic profiles of surface composition. Existing mathematical models should be developed further to describe the overall rate of the deuterium-palladium electrode reaction in terms of the experimentally controllable variables. This should be useful for elucidating electrochemical mechanisms and for ascertaining fundamental system properties, including intrinsic kinetic parameters and diffusion coefficients. Finally, such an approach is necessary to obtain a comprehensive quantitative understanding of the

electrochemical loading process such that the deuterium electrode reproducibility and stability may be improved and then optimized.

Experimental Approach

The focus of this work has been to use measurements of the Pd solid phase resistivity to monitor on-line the degree of loading as a function of the key experimental variables. Two different approaches have been taken. In each, the functionality between the resistance $R/R°$ ratio and atomic D/Pd ratio was calibrated primarily by reference to the works of Baranowski and Smith.

The first experimental set up consists of a series of up to ten electrolytic cells, which is referred to as the degree-of-loading "farm". This approach is used to study simultaneously a number of different variables that affect loading, as well as the reproducibility of loading. It is used to investigate the effect of electrode preconditioning steps, including etching and annealing. Results from the DoL farm are reported here.

Space for
Recombiner
Catalyst

Silica
Support
Rod

Pt
Reference
Electrode

Pd Cathode

Silica Cell

Pt Anode

Electrochemical cell for Pd
resistance measurements
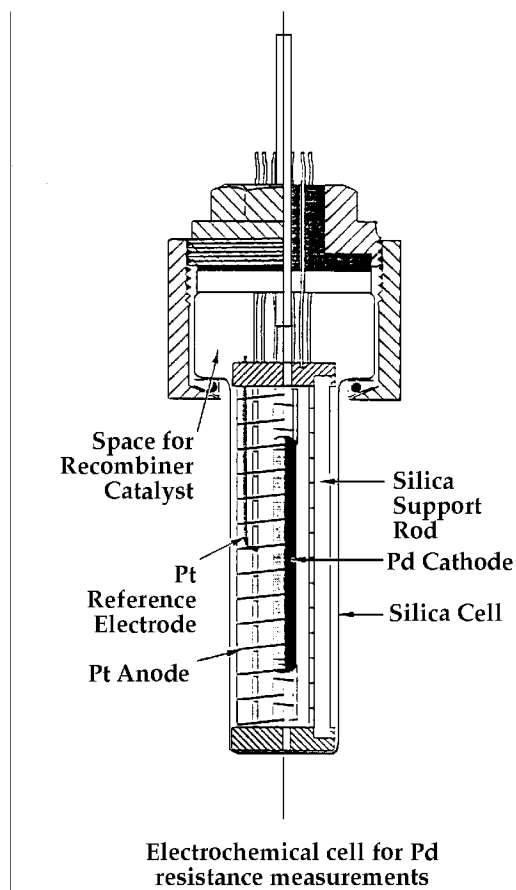
Figure 2-1
Degree of Loading Cell

Experiment Description and Results

Our efforts for the past 1-1/2 years to characterize the H(D)-Pd system using the degree-of-loading farm are summarized in the following tables for farms A through Q. We have attempted to provide a comprehensive description of each electrolytic loading experiment. This includes information identifying the particular cathode, and a summary of experimental conditions and the resulting loading behavior. Each electrolysis experiment is assigned a DoL catalogue designation, which includes a letter A through Q (excluding O) for the farm name followed by a number corresponding to the farm's data-collection position. The cathode is also assigned a P#, where the numbering is a continuation from the original DoL studies. A description of each of the palladium cathodes is given, including its source, dimensions, preparation and axial resistivity, R_o, prior to loading. The electrolyte and additives to the electrolyte, if any, are specified. Loading is quantified in terms of the D/Pd atomic ratio. Tabulated values of the cathode's best loading corresponds to a single value of the resistance ratio, $(R/R_p)_{,om}$, at the point during the electrolysis, where the cathode has achieved the highest degree of loading. The time and current density at maximum loading are specified. Also included in this section are the loading response profiles versus time, for farms E through L.

Summary of Results and Discussion

As was stated in the Introduction, the ERC first demonstrated that high loaded deuterated palladium is a necessary, but not sufficient, condition for the generation of anomalous heat by electrolytic means. Specifically, it was found that an atomic ratio of 0.9 is the minimum loading threshold required for the heat effects. Due to the importance of loading, we have characterized the H(D)-Pd system by building on the past success of the group's pioneering DoL work. This has included continuing to screen variables that are thought to play an important role in the loading process. Additionally, we have attempted to address the reproducibility issues that researchers in this field have had to be concerned with since the cold fusion announcement by Fleischmann and Pons in 1989.

Table 2-1 provides a summary of our DoL investigation, including the experimental conditions and loading results. We have been able to obtain relatively high degrees of loading in the majority of the electrolysis experiments. Of the 83 palladium cathodes that were employed in fully functional DoL electrolytic cells (20 cells have been excluded due to experimental difficulties), 81% of the cathodes were charged with deuterium to an atomic D/Pd ratio of greater than 0.85. Also, 61% of the total reached loadings of above 0.9. Next, we want to examine these results to answer questions such as: what are the critical variables that contribute to the loading success? which do not? and how can the reproducibility of the system be improved? How can maintenance of high loading over a long enough time be achieved?

Table 2-1
Degree of Loading Summary

Expt	Cathode	Source	Dimens.	Electrolyte	Additive	Cathode Preparation
A1	P86	E#2	3 * 0.3	1 M LiOH	Al	dub notch,spot weld,anneal,etch
A2	P87	E#2	3 * 0.3	1 M LiOD	Al	dub notch,spot weld,anneal,etch
A3	P88	E#2	3 * 0.3	1 M LiOD	Al	dub notch,spot weld,anneal,etch
A4	P89	E#2	3 * 0.3	1 M LiOH	Al	dub notch,spot weld,anneal,etch
B1	P90	E	5.3 * 0.1	1 M LiOD	Al	spot weld, no anneal, etch
B2	P91	E	5.3 * 0.1	1 M LiOD	Al	spot weld, no anneal, etch
B3	P92	Aithaca	5.3 * 0.1	1 M LiOD	Al	spot weld, no anneal, etch
B4	P93	Aithaca	5.3 * 0.1	1 M LiOD	Al	spot weld, no anneal, etch
C1	P94	E#3	4 * 0.3	1 M LiOD	Al	dub notch,spot weld,anneal,etch
C2	P95	E#3	4 * 0.3	1 M LiOD	Al	dub notch,spot weld,anneal,etch
C3	P96	E#3	4 * 0.3	1 M LiOD	Al	SonoBond, anneal, etch
C4	P97	E#3	4 * 0.3	1 M LiOD	Al	SonoBond, anneal, etch
D1	P98	E#3	3 * 0.3	1 M LiOD		SonoBond, D2 anneal, etch
D2	P99	E#3	3 * 0.3	1 M LiOD		SonoBond, D2 anneal, etch
D3	P100	E#3	3 * 0.3	1 M LiOD		SonoBond, no anneal, etch
D4	P101	E#3	3 * 0.3	1 M LiOD		SonoBond, no anneal, etch
D5	P102	E#3	3 * 0.3	1 M LiOD		SonoBond, vacuum anneal, etch
D6	P103	E#3	3 * 0.3	1 M LiOD		SonoBond, vacuum anneal, etch
D7	P104	NRL(30um)	3 * 0.4	1 M LiOD		dub notch, spot weld, etch
D8	P105	NRL(30um)	3 * 0.4	1 M LiOD		dub notch, spot weld, etch
D9	P106	NRL(600um)	3 * 0.4	1 M LiOD		dub notch, spot weld, etch
D10	P107	NRL(600um)	3 * 0.4	1 M LiOD		dub notch, spot weld, etch
E1/K1/A1	P108	E#3	3 * 0.3	1 M LiOD	Al	E control (weld,vac anneal,etch)
E2	P109	E#3	3 * 0.3	1 M LiOD	Al	E control (weld,vac anneal,etch)
E3	P110	E#3	3 * 0.3	1 M LiOD	Al	SonoBond, vac anneal, etch
E4	P111	E#3	3 * 0.3	1 M LiOD	Al	SonoBond, vac anneal, etch
E5/J1	P112	E#2	3 * 0.3	1 M LiOD	Al	E control (weld, vac anneal,etch)
E6	P113	E#3	3 * 0.3	1 M LiOD	Al	annealed & reused P102
E7	P114	E#3	3 * 0.3	1 M LiOD	Al	E control w/ Ni Anode
E8	P115	E#3	3 * 0.3	1 M LiOD	Al	E control w/ Ni Anode
E9	P116	E#3	3 * 0.3	1 M LiOD	Al	E control w/Ni Anode, PTFE Cell
E10	P117	E#3	3 * 0.3	1 M LiOD	Al	E control w/Ni Anode, PTFE Cell
F3	P118	E#3	3 * 0.3	1 M LiOD	Al	spot weld, 48 h anneal, etch
F4	P119	E#3	3 * 0.3	1 M LiOD	Al	spot weld, 48 h anneal, etch
F6	P120	E#3	3 * 0.3	1 M LiOD	Al	E control
F7	P121	E#3	3 * 0.3	1 M LiOD	Al	stab weld, anneal, etch
F9	P122	E#3	3 * 0.3	1 M LiOD		E control w/ boron
F10	P123	E#3	3 * 0.3	1 M LiOD	Al	stab weld,anneal,etch w/Pd anode
GG2/G10	P124	E	3 * 0.1	1 M LiOD	Al	Weld, vac anneal, Ar cool, etch
GG4/G8	P125	E#3 sand cast	2.5 * 0.3	1 M LiOD	Al	Same as HH cells
GG7/G7	P126	NRL(600um)	3 * 0.4	1 M LiOD	Al	spot weld, no anneal, etch
GG8	P127	NRL(600um)	3 * 0.4	1 M LiOD	Al	annealed & reused P100

Table 2-1 (cont.)
Degree of Loading Summary

Expt	Cathode	Source	Dimens.	Electrolyte	Additive	Cathode Preparation
GG9/G9	P128	E#3	3 * 0.3	1 M LiOD	Al	spot weld, no anneal, etch
H1	P129	JM	3 * 0.2	1 M LiOD	Al	spot weld, no anneal, no etch
H2	P130	JM	3 * 0.2	1 M LiOD	Al	spot weld, no anneal, no etch
H3	P131	JM	3 * 0.2	1 M LiOD	Al	spot weld, no anneal, etch
H4	P132	JM	3 * 0.2	1 M LiOD	Al	spot weld, no anneal, etch
H5	P133	JM	3 * 0.2	1 M LiOD	Al	spot weld, anneal, etch
H6	P134	JM	3 * 0.2	1 M LiOD	Al	spot weld, anneal, etch
I 1	P135	reused E#1 (P55)	3 * 0.3	1 M LiOD		etch, anneal,spot weld,etch
I 2/II9	P136	reused E#1 (P44)	3 * 0.3	1 M LiOD		polish, anneal,spot weld,etch
I 3/A1.3	P137	reused E#1 (P53)	3 * 0.28	1 M LiOD		machine,anneal,spot weld,etch
I 4	P138	reused E#1 (P38)	3 * 0.28	1 M LiOD		machine,anneal,spot weld
I 5/A2.1	P139	E#2	3 * 0.28	1 M LiOD	Al	machine,anneal,spot weld,etch
I 6	P140	E#2	3 * 0.28	1 M LiOD		machine,anneal,spot weld,etch
I 7	P141	E#3	3 * 0.28	1 M LiOD	Al	machine,anneal,spot weld,etch
I 8	P142	E#3	3 * 0.28	1 M LiOD		machine,anneal,spot weld,etch
I 9	P143	JM	3 * 0.38	1 M LiOD	Al	machine,anneal,spot weld,etch
I 10	P144	JM	3 * 0.38	1 M LiOD		machine,anneal,spot weld,etch
J1	P145	JM	3.8 * 0.2	1 M LiOD	Al	spot weld
J2	P146	JM	3.8 * 0.2	1 M LiOD		spot weld
J3	P147	IB	3.8 * 0.3	1 M LiOD	Al	spot weld
J4	P148	IB	3.8 * 0.3	1 M LiOD		spot weld
J5	P149	IB square	3 * 0.28	1 M LiOD	Al	spot weld
J6	P150	IB square	3 * 0.28	1 M LiOD		spot weld
K1	P151	E#4	3 * 0.3	1 M LiOD		machine,cut,dgrease,anneal,sptwld
K2	P152	E#4	3 * 0.3	1 M LiOD		machine,cut,dgrease,anneal,sptwld
K3	P153	E#4	3 * 0.3	1 M LiOD	Al	machine,cut,dgrease,anneal,sptwld
K4	P154	E#4	3 * 0.3	1 M LiOD	Al	machine,cut,dgrease,anneal,sptwld
K5	P155	reused E#1 (P45)	3 * 0.28	1 M LiOD		machine,cut,dgrease,anneal,sptwld
K6	P156	reused E#1 (P46)	3 * 0.28	1 M LiOD		machine,cut,dgrease,anneal,sptwld
K7	P157	JM	3 * 0.2	1 M LiOD		cut,degrease,anneal,spot weld
K8	P158	JM	3 * 0.2	1 M LiOD	Al	cut,degrease,anneal,spot weld
K9	P159	JM	3 * 0.1	1 M LiOD		cut,degrease,anneal,spot weld
K10	P160	JM	3 * 0.1	1 M LiOD	Al	cut,degrease,anneal,spot weld
L1	P161	used E#1 (p61)	3 * 0.3	1 M LiOD	B	mchn,ct,dgrs,anel,spwld,ech,rns
L2	P162	used E#1 (p73)	3 * 0.3	1 M LiOD	(+) B	mchn,ct,dgrs,anel,spwld,ech,rns
L4(LL11)	P163	used E#1 (p85)	3 * 0.3	1 M LiOD	Be	mchn,ct,dgrs,anel,spwld,ech,rns
L7	P164	JM	3 * 0.1	1 M LiOD	Cu	cut,dgrs,anneal,sptwld,etch,rinse
L8(LL10)	P165	JM	3 * 0.1	1 M LiOD	(+)Cu	cut,dgrs,anneal,sptwld,etch,rinse
L9(LL9)	P166	JM	3 * 0.1	1 M LiOD	(+)Cu	cut,dgrs,anneal,sptwld,etch,rinse
L11	P167	JM	3 * 0.1	1 M LiOD	Tl	cut,dgrs,anneal,sptwld,etch,rinse
L12	P168	JM	3 * 0.1	1 M LiOD	(+)Tl	cut,dgrs,anneal,sptwld,etch,rinse
M1	P169	JM	3 * 0.4	1 M LiOD		cut,dgrs,anneal,sptwld,etch,rinse
M2	P170	JM	3 * 0.4	1 M LiOD	Cu	cut,dgrs,anneal,sptwld,etch,rinse

Table 2-1 (cont.)
Degree of Loading Summary

Expt	Cathode	Source	Dimens.	Electrolyte	Additive	Cathode Preparation
M3	P171	JM	3 * 0.1	1 M LiOD		cut,dgrs,anneal,sptwld,etch,rinse
M4	P172	JM	3 * 0.1	1 M LiOD	Cu	cut,dgrs,anneal,sptwld,etch,rinse
M5	P173	JM	3 * 0.1	1 M LiOD		cut,dgrs,anneal,sptwld,etch,rinse
M6	P174	JM	3 * 0.1	1 M LiOD	Al	cut,dgrs,anneal,sptwld,etch,rinse
M7	P175	JM	3 * 0.1	1 M LiOD		cut,dgrs,anneal,sptwld,etch,rinse
M8	P176	JM	3 * 0.1	1 M LiOD	Si	cut,dgrs,anneal,sptwld,etch,rinse
N9	P177	E#5	3 * 0.3	1 M LiOD	(+) Cu	cut,dgrs,anneal,sptwld,etch,rinse
N10	P178	E#5	3 * 0.3	1 M LiOD		cut,dgrs,aneal,sptwld,rinse
N11	P179	E#5	3 * 0.3	1 M LiOD	(+) Cu	cut,dgrs,anneal,sptwld,etch,rinse
N12	P180	E#5	3 * 0.3	1 M LiOD		cut,dgrs,aneal,sptwld,rinse
P1	P181	E#2	3 * 0.28	1 M LiOD		cut,dgrs,anneal,sptwld,etch,rinse
P2(PP7)	P182	E#2	3 * 0.28	npe 1 M LiOD	+ Al	cut,dgrs,anneal,sptwld,etch,rinse
P3(PP6)	P183	E#3	3 * 0.28	1 M LiOD	+ Al	cut,dgrs,anneal,sptwld,etch,rinse
P4	P184	E#3	3 * 0.28	1 M LiOD		cut,dgrs,anneal,sptwld,etch,rinse
P5(PP5)	P185	E#4	3 * 0.28	npe 1 M LiOD		cut,dgrs,anneal,sptwld,etch,rinse
P6	P186	E#4	3 * 0.28	1 M LiOD		cut,dgrs,anneal,sptwld,etch,rinse
P7	P187	E#5	3 * 0.28	1 M LiOD		cut,dgrs,anneal,sptwld,etch,rinse
P8(PP8)	P188	E#5	3 * 0.28	npe 1 M LiOD	+ Al	cut,dgrs,anneal,sptwld,etch,rinse
Q1	P189	E#3	3 * 0.28	1 M LiOD		cut,dgrs,anneal,sptwld,etch,rinse
Q2	P190	E#3	3 * 0.28	pe 1 M LiOD	+ Al	cut,dgrs,anneal,sptwld,etch,rinse
Q3	P191	E#5	3 * 0.28	1 M LiOD	+ Al	cut,dgrs,anneal,sptwld,etch,rinse
Q4	P192	E#5	3 * 0.28	pe 1 M LiOD	+ Al	cut,dgrs,anneal,sptwld,etch,rinse

Table 2-1 (cont.)
Degree of Loading Summary

Expt	Ro	Best	Best	Load # or	Start date	Finish	Duration	Comments
	/mOhm	(R/Ro)	(D/Pd)	Time/h : i		date	\h	
		Min	Max	i / mAcm^{-2}				
A1	0.46	1.55	0.964	#0 : 140	5/28/93	6/29/93	640	
A2	0.45	1.71	0.914	#2 : 140	5/28/93	6/29/93	640	
A3	0.44	1.64	0.935	#5 : 180	5/28/93	6/29/93	640	
A4	0.46	1.38	1.018	#4,5 : 180	5/28/93	6/29/93	640	
B1	3.83	1.87	0.854	#4 : 80	6/29/93	7/21/93	576	
B2	4.17	1.76	0.899	#4 : 640	6/29/93	7/21/93	576	
B3	4.81	1.94	0.805	#1 : 40	6/29/93	7/9/93	235	
B4	4.84	1.91	0.829	#3 : 20	"	"	"	
C1	0.61	1.75	0.902	#3 : 80	7/9/93	7/27/93	216	
C2	0.63	1.74	0.905	#2 : 40	7/9/93	7/27/93	216	
C3	0.73	1.76	0.899	#1 : 80	7/9/93	7/27/93	216	
C4	0.72	1.7	0.917	#2,3 : 320	7/9/93	7/27/93	216	
D1	0.49	2	0.739		7/30/93	9/14/93	1104	pre-electrolysis
D2	0.51	2	0.739		7/30/93	9/14/93	1104	anodic strip
D3	0.54	2	0.739		7/30/93	9/14/93	1104	& MOM problems
D4	0.52	2	0.739		7/30/93	9/14/93	1104	"
D5	0.51	2	0.739		7/30/93	9/14/93	1104	"
D6	0.51	2	0.739		7/30/93	9/14/93	1104	"
D7	0.24	2	0.739		7/30/93	9/14/93	1104	"
D8	0.23	2	0.739		7/30/93	9/14/93	1104	"
D9	0.23	2	0.739		7/30/93	9/14/93	1104	"
D10	0.22	2	0.739		7/30/93	9/14/93	1104	"
E1/K1/A1	0.48	1.6	0.948	2650 : 80	9/16/93	2/25/94	3900	>BB>Air Seebeck
E2	0.47	1.6	0.948	1275 : 80	9/16/93	2/10/94	3600	
E3	0.49	1.72	0.911	475 : 80	9/16/93	11/16/93	1440	
E4	0.48	1.88	0.848	25 : 20	9/16/93	11/16/93	1440	
E5/J1	0.56	1.45	0.997	1275 : 80	9/16/93	2/25/94	3900	> NaI detector
E6	0.51	1.78	0.892	250 : 160	9/16/93	11/16/93	1440	
E7	0.47	1.73	0.908	975 : 80	9/16/93	11/16/93	1440	
E8	0.45	1.75	0.902	2650 : 80	9/16/93	1/23/94	1440	
E9	0.47	1.84	0.868	975 : 80	9/16/93	11/16/93	3500	
E10	0.47	1.85	0.864	475 : 80	9/16/93	11/16/93	1440	
F3	0.54	1.66	0.929	1000 : 80	11/24/93	2/25/94	2230	
F4	0.55	1.6	0.948	1000 : 80	11/24/93	2/10/94	1900	
F6	0.52	1.5	0.980	425 : 80	11/24/93	2/25/94	2230	
F7	0.38	1.68	0.923	425 : 80	11/24/93	2/10/94	1900	
F9	0.53	1.65	0.932	560 : 120	11/24/93	2/10/94	1900	
F10	0.39	1.85	0.864	450 : 80	11/24/93	2/10/94	1900	
GG2/G10	4.49	1.7	0.917	830 : 40	2/10/94	4/6/94	1300	
GG4/G8	0.40	1.71	0.914	290 : 80	2/10/94	4/7/94	1350	
GG7/G7	0.24	1.93	0.814	300 : 80	2/10/94	4/6/94	1300	
GG8	0.30	/	/	/	2/10/94	2/24/94	350	
GG9/G9	0.55	1.77	0.895	930 : 80	2/10/94	4/6/94	1300	
H1	0.95	1.78	0.892	925 : 120	2/24/94	4/6/24	960	

Table 2-1 (cont.)
Degree of Loading Summary

Expt	Ro	Best	Best	Load # or	Start	Finish	Duration	Comments
	/mOhm	(R/Ro)	(D/Pd)	Time/h : i	date	date	\h	
		Min	Max	i / mAcm^{-2}				
H2	1.00	1.75	0.902	800 : 80	2/24/94	4/6/24	960	
H3	0.99	1.8	0.885	625 : 80	2/24/94	4/6/24	960	
H4	0.98	1.8	0.885	620 : 80	2/24/94	4/6/24	960	
H5	0.95	1.78	0.892	930 : 80	2/24/94	4/6/24	960	
H6	1.00	1.78	0.892	750 : 40	2/24/94	4/6/24	960	
I 1	0.46	1.66	0.929	670 : 80	4/13/94	5/20/94	890	
I 2	0.42	1.53	0.970	120 : 80	"	6/3/94	1210	II 9 +ext rcmbnr >L 13
I 3/A1.3	0.50	1.63	0.938	175 : 80	"	4/28/94	360	> A1.3 > A1.3G
I 4	0.49	1.58	0.954	810 : 80	"	5/20/94	890	
I 5	0.55	1.44	1.000	685 : 80	"	5/17/94	810	> A2.1 > L14
I 6	0.54	1.73	0.908	680 : 80	"	5/20/94	890	
I 7	0.56	1.57	0.957	685 : 80	"	6/8/94	1200+	slow strip
I 8	0.57	1.6	0.948	680 : 80	"	6/8/94	1200+	slow strip
I 9	0.29	1.76	0.899	680 : 80	"	5/25/94	1000	
I 10	0.28	1.71	0.914	190 : 120	"	present	1000+	+ int. Recombiner
J1	1.24	1.94	0.805	155 : 120	5/25/94	6/8/94	330	
J2	1.25	1.85	0.864	330 : 80	5/25/94	6/8/94	330	
J3	0.55	1.92	0.821	320 : 80	5/25/94	6/8/94	330	
J4	0.54	2	0.739	330 : 80	5/25/94	6/8/94	330	
J5	0.41	1.89	0.854	320 : 80	5/25/94	6/8/94	330	
J6	0.40	1.87	0.854	310 : 80	5/25/94	6/8/94	330	
K1	0.47	1.59	\	75 : 40	6/10/94	6/29/94	450	
K2	0.48	1.34	\	110 : 80	6/10/94	6/29/94	450	
K3	0.45	1.53	\	210 : 80	6/10/94	8/4/94	1270	
K4	0.46	1.45	\	100 : 80	6/10/94	6/29/94	450	
K5	0.56	1.39	\	660 : 40	6/10/94	7/8/94	665	> open L15
K6	0.56	1.38	\	660 : 40	6/10/94	8/4/94	1270	
K7	0.99	1.64	\	330 : 40	6/10/94	6/29/94	450	
K8	0.96	1.77	\	250 : 80	6/10/94	6/29/94	450	
K9	3.56	1.65	\	350 : 40	6/10/94	6/29/94	450	
K10	3.63	1.49	\	1070 : 20	6/10/94	8/4/94	1270	
L1	0.55	1.7	0.917	650 : 80	7/1/94	8/2/94	700	
L2	0.58	1.5	0.980	250 : 40	7/1/94	7/22/94	500	
L4	0.58	1.68	0.923	720 : 80	7/1/94	8/17/94	1050	
L7	3.45	1.69	0.920	350 : 40	7/1/94	8/4/94	750	
L8	3.47	1.4	1.010	1050 : 80	7/1/94	8/19/94	1100	
L9	3.81	1.34	< 1	1050 : 80	7/1/94	8/19/94	1100	
L11	3.47	1.76	\	410 : 120	7/1/94	8/4/94	750	
L12	3.21	\	\	\	7/1/94	8/4/94	800	
M1	0.23	1.8	0.880	365 : 120	8/10/94	9/7/94	650	
M2	0.23	1.9	0.836	360 : 120	8/10/94	9/7/94	650	
M3	3.35	\	\	\	8/10/94	9/9/94	340	Removed 8/16 - 9/1/94
M4	3.24	1.85	0.864	450 : 160	8/10/94	9/9/94	700	
M5	3.40	1.66	0.930	320 : 40	8/10/94	9/7/94	650	

Table 2-1 (cont.)
Degree of Loading Summary

Expt	Ro	Best	Best	Load # or	Start date	Finish	Duration	Comments
	/mOhm	(R/Ro)	(D/Pd)	Time/h : i		date	\h	
		Min	Max	i / mAcm^{-2}				
M6	3.30	1.9	0.836	450 : 160	8/10/94	9/7/94	650	
M7	3.29	1.9	0.836	175 : 80	8/10/94	9/9/94	700	
M8	3.35	1.93	0.814	370 : 120	8/10/94	9/9/94	700	
N9	0.43	1.99	0.752	25:20	8/19/94	9/1/94	350	
N10	0.42	1.98	0.764	100:40	8/19/94	9/1/94	350	
N11	0.52	\	\	\	8/19/94	9/1/94	350	Bad relay system
N12	0.40	\	\	\	8/19/94	9/1/94	350	Bad relay system
P1	0.49	1.685	0.922	635 : 80	9/9/94	10/21/94	2500	
P2	0.50	1.58	0.954	1355:120	9/9/94	12/23/94	2500	
P3	0.52	1.6	0.948	1355:120	9/9/94	12/23/94	2500	
P4	0.52	1.63	0.938	780:80	9/9/94	10/21/94	2500	> G Cell
P5	0.50	1.66	0.929	1355:120	9/9/94	11/ /1994	2500	> L Cell
P6	0.52	1.65	0.932	780:80	9/9/94	10/21/94	2500	
P7	0.50	1.575	0.955	780:80	9/9/94	10/21/94	2500	
P8	0.52	1.58	0.954	780:80	9/9/94	12/23/94	2500	
Q1	0.50	1.6	0.948	415:160	10/21/94	11/ /1994	1500	> L Cell
Q2	0.49	1.77	0.895	480:40	10/21/94	12/23/94	1500	
Q3	0.52	1.67	0.926	1075:120	10/21/94	12/23/94	1500	
Q4	0.52	1.69	0.920	315:80	10/21/94	12/23/94	1500	

The key variables that we have found using the DoL farm to affect electrolytic loading of palladium with hydrogen and its isotopes are summarized in Table 2-2. The analysis is made by making a qualitative assessment of the loading data, without making reference to specific loading response profiles.

The role of the electrochemical cell is recognized to be important to the electrolytic loading process. In particular, the electrode design and materials of construction have been identified as being critical factors for attaining high loadings. At the center of our DoL electrolytic cell configuration is the anode-cathode assembly. It consists of a helical platinum anode (instead of nickel or palladium) symmetrically coiled around the palladium cathode. Both are positioned inside a quartz cell body (as opposed to Teflon). Although changes in the anode-to-cathode geometrical ratios were not explored using the DoL farm, modifications to the existing DoL electrode configuration were made when the new calorimeters were designed and built. The changes in the aspect ratios of the anode-cathode assembly have been identified as being the most likely source for the poor loading performance in the new calorimeters. Attainment of a highly uniform current distribution to the cathode therefore has been determined to be of paramount importance to the success of the loading experiment. It is suggested here that if modifications in the calorimeter's cell design were made such that current losses at the ends of the cathode are minimized, then higher degrees of loading would be achieved in the calorimeter comparable to that in the DoL farm. Only then will the observation of excess heat be possible.

Table 2-2
Summary of DoL Farm Results

- Electrolyte loading cell & supporting apparatus design
  - proper anode-to-cathode geometrical aspect ratios yield highly uniform current distribution required for loading
  - large head space over body of cell is beneficial
  - regulation of cell temperature using convective ambient air (instead of water bath) reduces probability of electrolyte's isotopic purity becoming compromised during electrolysis
  - transparent Lexan box (instead of opaque water bath) enables electrolyte level to be readily observed and maintained

- Electrochemical cell materials
  - Pd cathode: see table 2-3 for effects of metal source on loading
  - Pt anode better than Pd and Ni
  - quartz body superior to Teflon (PTFE)
  - 1 M LiOD electrolyte
  - + pre-electrolysis (cleaning) of electrolyte yields better initial loading rates

- Surface modifying agents
  - silicates enhance loading
  - aluminum increases longevity of loading
  - copper increases overpotential of undesired D_2 evolution reaction
  - boron changes loading characteristics of machined cathodes
  - thallium & beryllium do not appear to promote loading

- Electrode Preparation
  - annealing in O_2-gettered environment is critical
  - + 3 hours at 850°C better than 48 hours
  - + vacuum better than D_2 anneal

  - surface treatments are beneficial secondary effects
    - + machining
    - + polishing
    - + etching

  - electrical contacts for in-situ 4 wire resistance
    - + end posts and single small notches better than double notches at ends of cathode
    - + spot welded and posts better than sonobonding

- Current Protocols
  - low to moderate cathodic currents (below 200 mA/cm^2) and small current steps (40 mA cm^2) yield loading without initiating spontaneous deloading
  - low anodic current steps (20 mA/cm^2) and pulses reactivates surface and promotes re-loading
  - repeated cathodic-load/anodic-strip cycles enhances loading with each cycle

Improvements to the DoL supporting apparatus include the following. Water additions to the electrolytic cells are a necessary requirement for the continuous operation of the DoL farm. Although Faraday's law provides a good indication of the amount of water that is consumed due to electrolysis, it is only, at best, an approximation of the amount of water that needs to be added during the course of an experiment. Thus, visual inspection of the water level in the electrolytic cells is the best means for ensuring that the proper amount of water is added. For this reason (as well as for safety concerns), the commercially available constant temperature bath was replaced with a box constructed in-house out of transparent Lexan (polycarbonate).

The isotopic purity of the electrolyte is very critical for accurately determining loading in our electrolysis experiments. Therefore, when we learned of the possibility that the electrolyte was becoming contaminated with water from the constant-temperature bath, temperature regulation of the electrolytic cells was changed from the use of 35°C bath water to that of convective ambient air. Thus, the probability of water contamination of the cells was greatly decreased.

Other key variables identified in this study to play a major role in the loading process involve electrode preparation, surface modifying agents, and current protocols. Each will be briefly discussed next.

The condition of the cathode surface has been shown to significantly affect loading performance. Of particular importance, an electrode preconditioning annealing step in an oxygen-gettered (oxygen free) environment was determined to be a necessary requirement for the attainment of highly loaded deuterated palladium. Better results have been obtained using a vacuum (as opposed to a D_2 anneal at 850°C for three (instead of 48) hours. Additionally, silicate and aluminum, when added to the 1M $LiOD/D_2O$ electrolyte, serve as surface modifying agents that enhance loading and promote the longevity of loading, respectively.

The role of current density is recognized to be of great importance in the loading process, so various current protocols have been investigated. Low to moderate cathodic current densities (below 200 mA/cm²) and small constant current steps (40 mA/cm²) enabled high degrees of loading to be obtained without the onset of significant spontaneous deloading. Anodic current is required to strip the absorbed deuterium out of the palladium lattice. Stripping in the form of low anodic current-density steps (20 mA/cm²), pulses and/or open-circuit deloads appeared to provide a suitable means of reactivating the electrode surface to facilitate re-loading. Overall loading also was shown to be improved with each repeated cycle of the cathodic-load/anodic-strip current protocol.

The remaining variable of significance to be discussed here is the source of the cathode material and its effect on electrolytic loading. Table 2-3 lists the source of palladium that has been used in the DoL farm and provides an indication of the loading performance

of each. 90% of the Pd that was employed in functional electrolytic cells in the DoL farm was supplied by either Engelhard (63%) or Johnson Matthey (28%). Engelhard 1 mm diameter Pd and five different lots of 3 mm diameter Pd were used, with a third of the total being Engelhard lot 3 (designated E3). JM Pd was employed in 1, 2 and 4 mm diameters.

The results summarized in Table 2-3 indicate that high degrees of loading were generally obtained using the DoL farm.

We were able to obtain intermediate level loadings (atomic ratios above 0.85, but not always above 0.9) in Pd metal samples obtained from different suppliers and in different lots from the same suppliers, provided that the design criteria and electrolysis conditions presented above, were met. Although overall good loadings have been obtained, variability in the DoL data appears to be prominent when the loading response profiles are examined more closely. The statistics reported in Table 2-3 were computed for cathodes which at any time exceeded the stipulated loading thresholds. Many unexplained and seemingly unaccountable responses were observed in the temporal response of loading at constant current and with varying current. Specifically, our ability to obtain and maintain atomic ratios of $D/Pd \geq 0.9$ for long periods of time at current densities greater than 100 mA cm^{-2}, was very much less with any metal source other than Engelhard lot #1 (designated as E1). The statistical weight of this observation is greatly enhanced when data from our previous phase of work[2] are included.

In addition to providing fundamental information on the key variables which affect electrolytic loading, the DoL experiments were used to support two other important aspects of the experimental program. Using high loading as the criterion, DoL cells were selected and transferred to an air-cooled Seebeck heat-flow calorimeter designed to operate in the environment of a Ge detector for gamma rays.

Table 2-3
Effect of Palladium Source on Deuterium Uptake of Metal Lattice

Source of Pd	# of (Cathodes)	% of Cathodes Loading to D/Pd Ratios of:		
		^{3} 0.85	^{3} 0.90	^{3} 0.95
E1	(7)	100	100	43
E2	(7)	100	100	43
E3	(27)	100	81	30
E4	(2)	100	100	0
E5	(6)	67	67	33
1 mmE	(3)	100	67	0
JM	(23)	65	30	9
Misc	*(8)*	*(25)*	*(0)*	*(0)*
Total	**(83)**	**81**	**61**	**22**

Reproducibility of Engelhard Pd Lot 3

Pd Cathode (3.0 x 3 cm); Pt Anode; 1 M LiOD/D2O; Quartz Cell
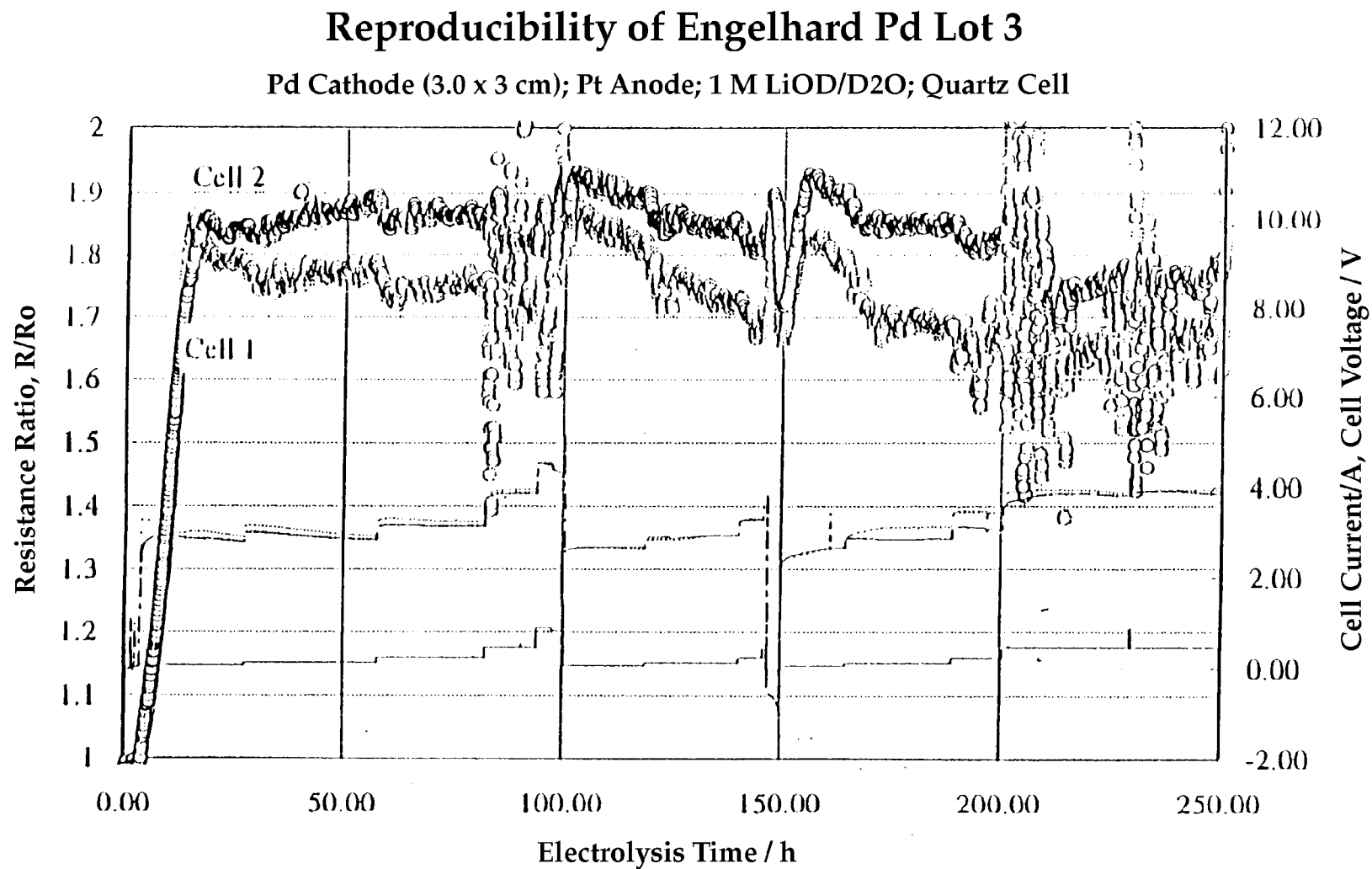
Figure 2-2
DoL farm E Cells # 1, 2

Reproducibility of Engelhard Pd

Pd Cathode (0.3 x 3 cm); Pt Anode; 1 M LiOD/D2O; Quartz Cell
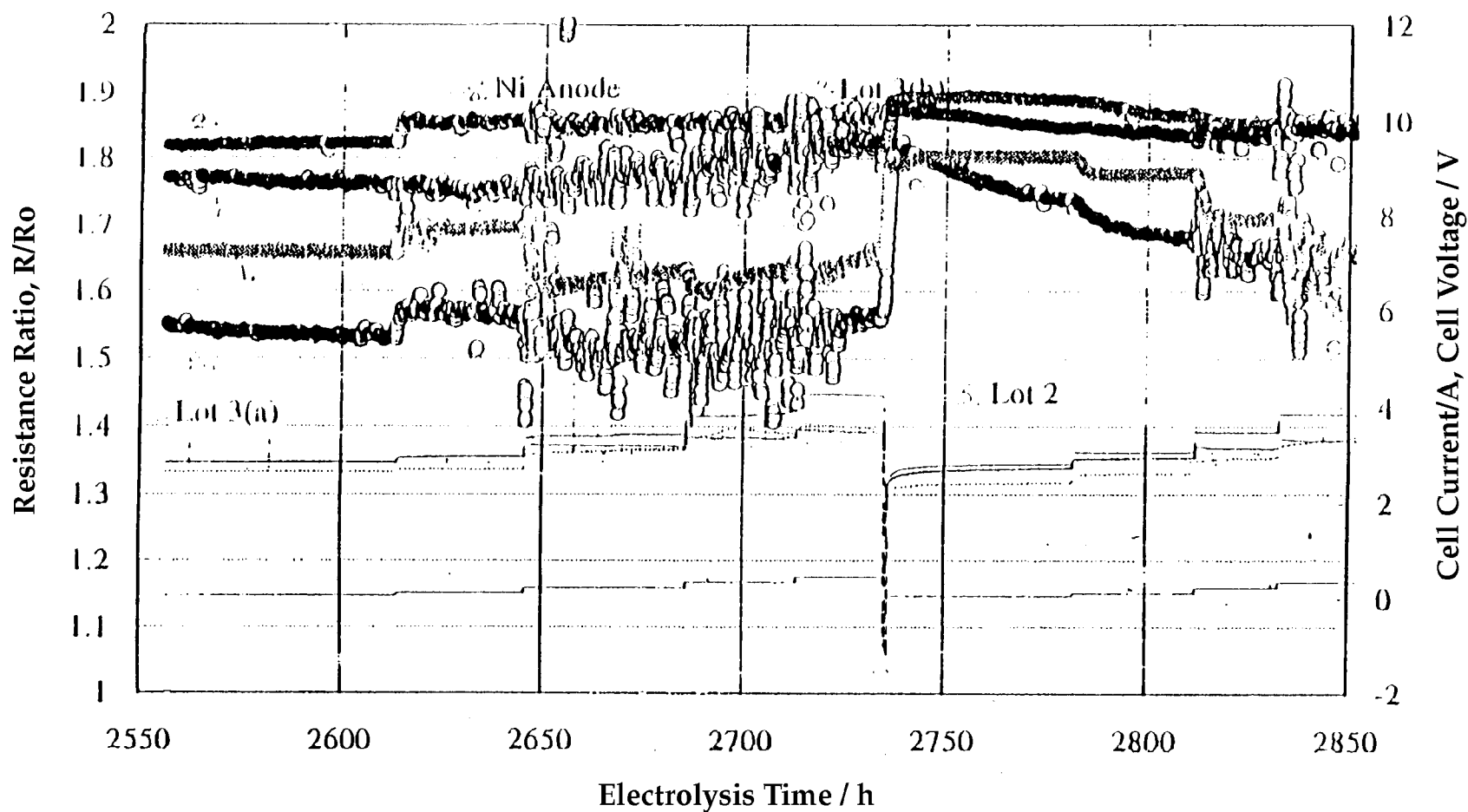
Figure 2-3
DoL Farm E Cells # 1, 2, 5, 8

Reproducibility of Engelhard Pd

Pd Cathode (0.3 x 3 cm); Pt Anode; 1 M LiOD/D2O; Quartz Cell

Figure 2-4
DoL Farm E Cells # 1, 2, 5, 8

Reproducibility of Engelhard Pd

Pd Cathode (0.3 x 3 cm); Pt Anode; 1 M LiOD/D2O; Quartz Cell
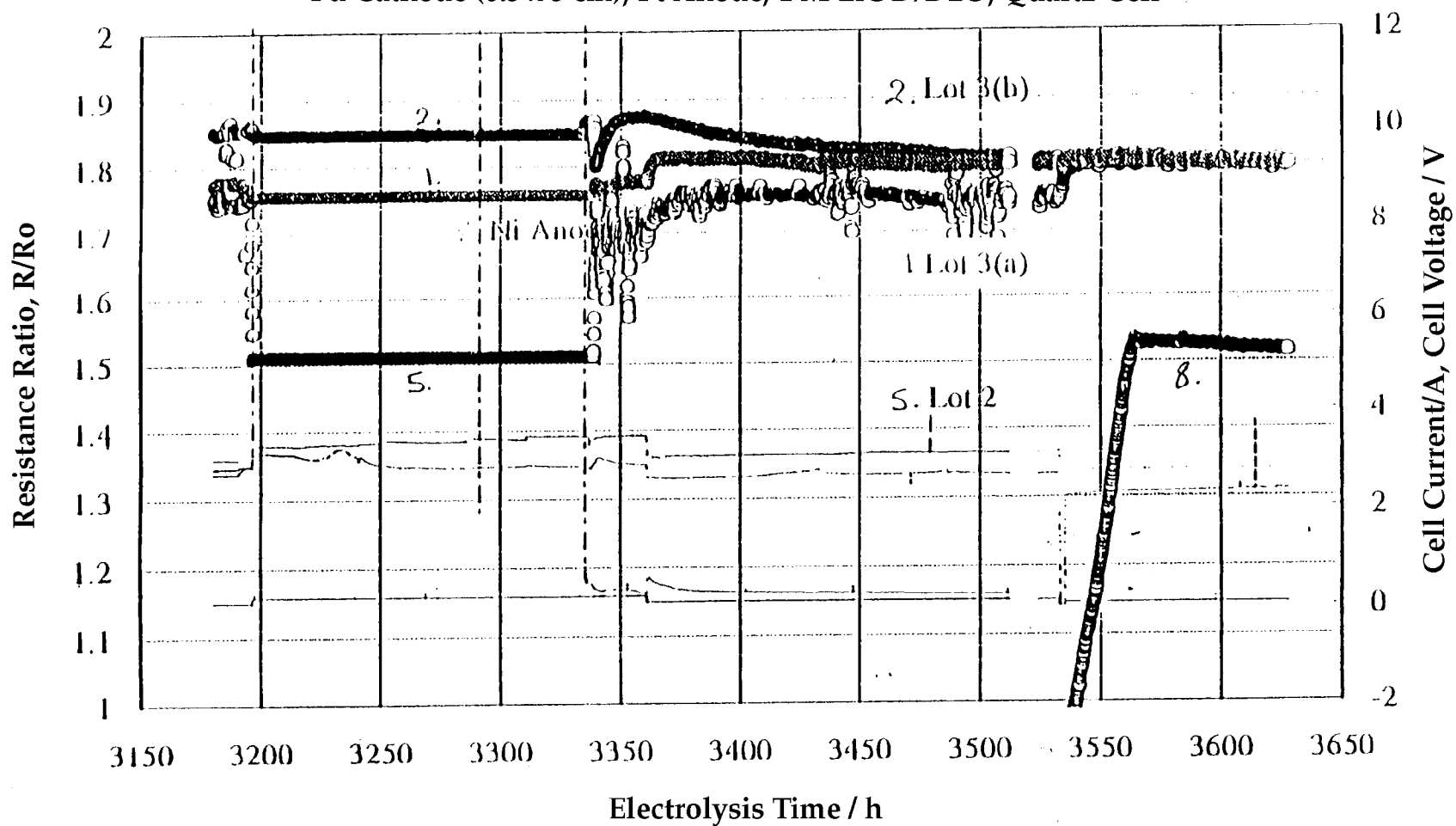
Figure 2-5
DoL Farm E Cells # 1, 2, 5, 8

Reproducibility of Engelhard Pd

Pd Cathode (0.3 x 3 cm); Pt Anode; 1 M LiOD/D2O; Quartz Cell
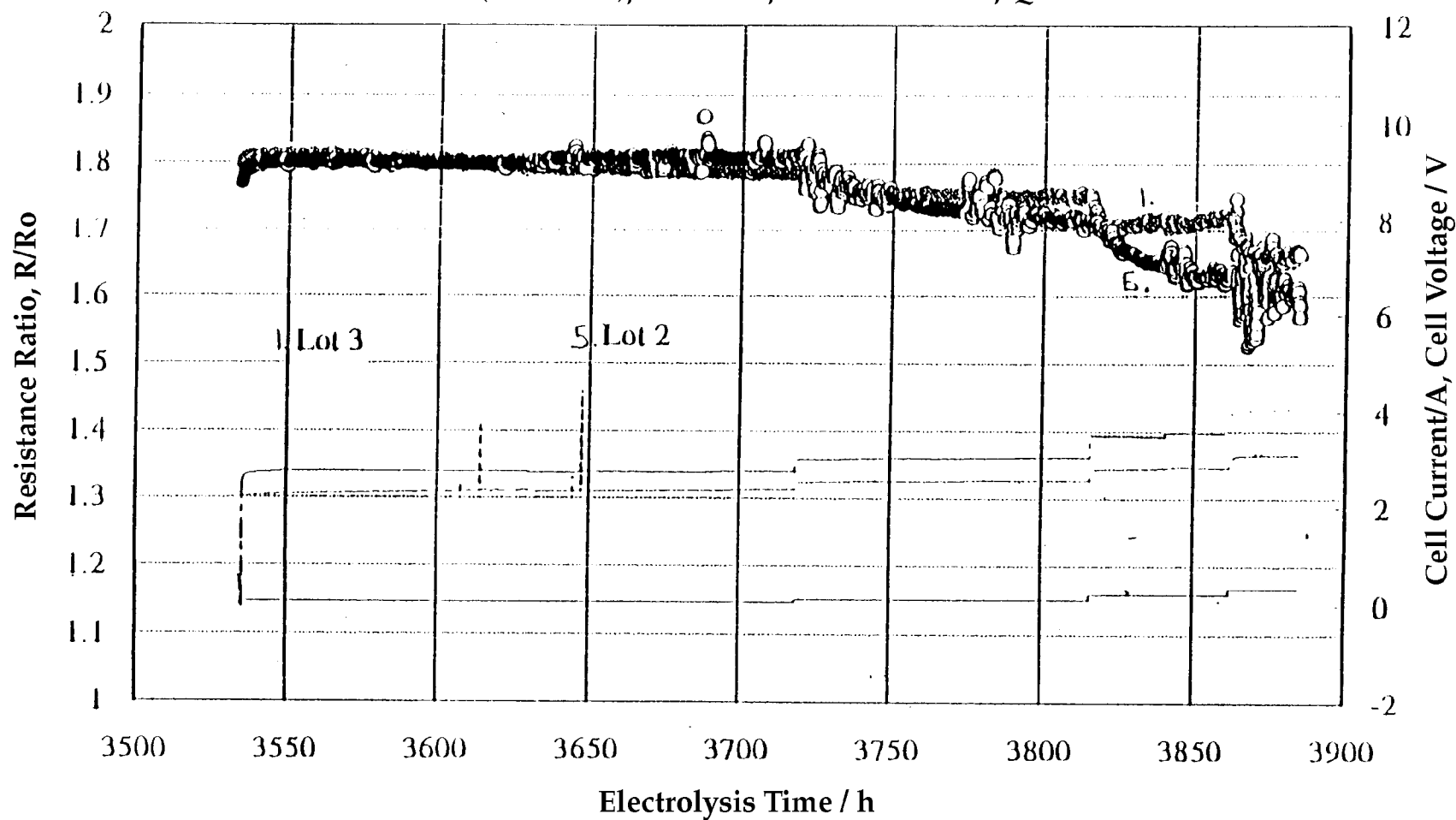
Figure 2-6
DoL Farm E Cells # 1, 5

Effect of Time of Annealing at 850 C on Loading

Engelhard Lot 3 Pd Cathode (0.3 x 3 cm); Pt Anode; 1 M LiOD/D2O; Quartz Cell
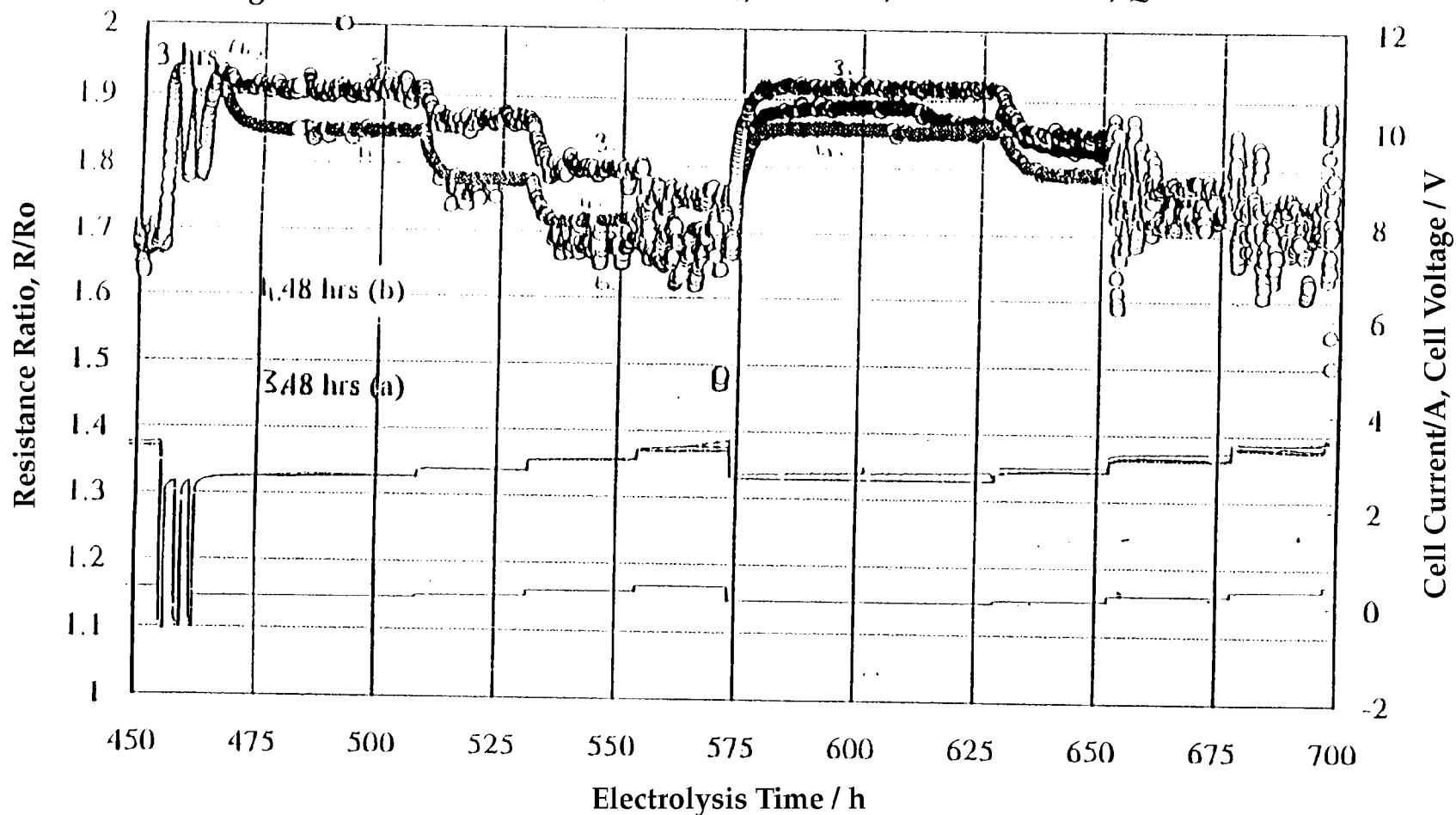
Figure 2-7
DoL Farm F Cells # 3, 4, 6

Effect of Time of Annealing at 850 C on Loading

Engelhard Lot 3 Pd Cathode (0.3 x 3 cm); Pt Anode; 1 M LiOD/D2O; Quartz Cell
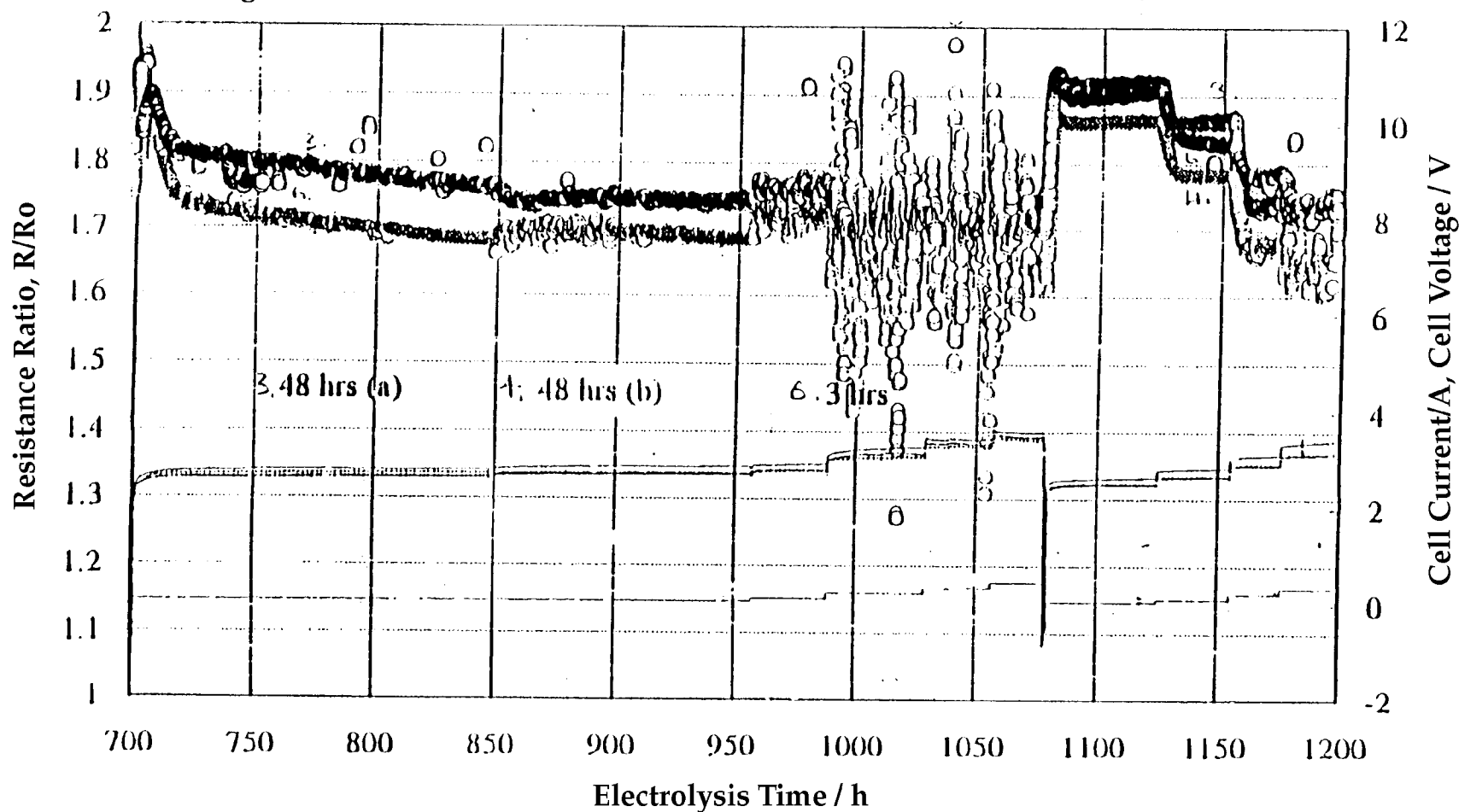
Figure 2-8
DoL Farm F Cells # 3, 4, 6

Effect of Time of Annealing at 850 C on Loading

Engelhard Lot 3 Pd Cathode (0.3 x 3 cm); Pt Anode; 1 M LiOD/D2O; Quartz Cell
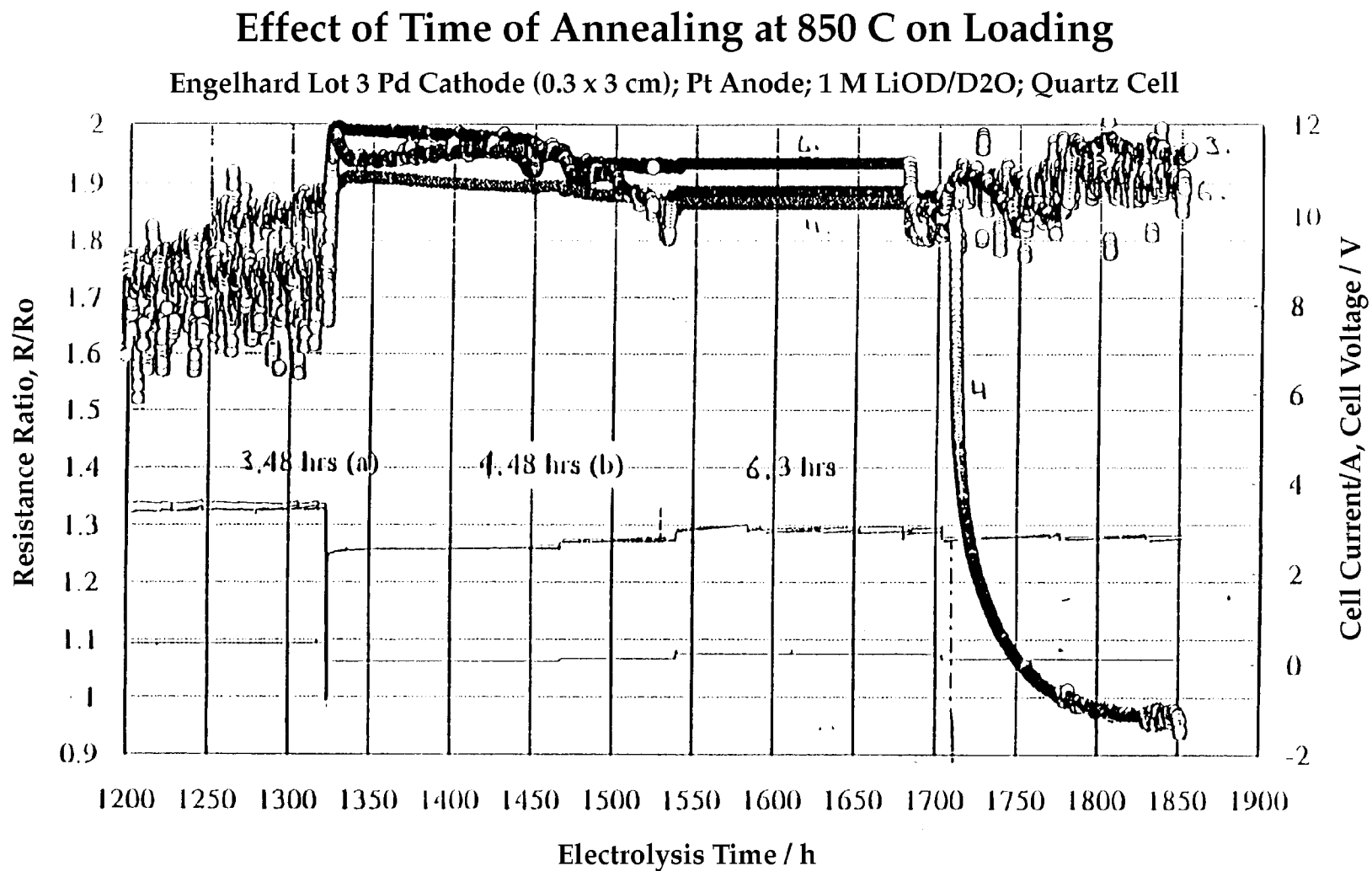
Figure 2-9
DoL Farm F Cells # 3, 4, 6

Effect of Stab Weld on Loading

Engelhard Lot 3 Pd Cathode (0.3 x 3 cm); Pt Anode; 1 M LiOD/D2O; Quartz Cell
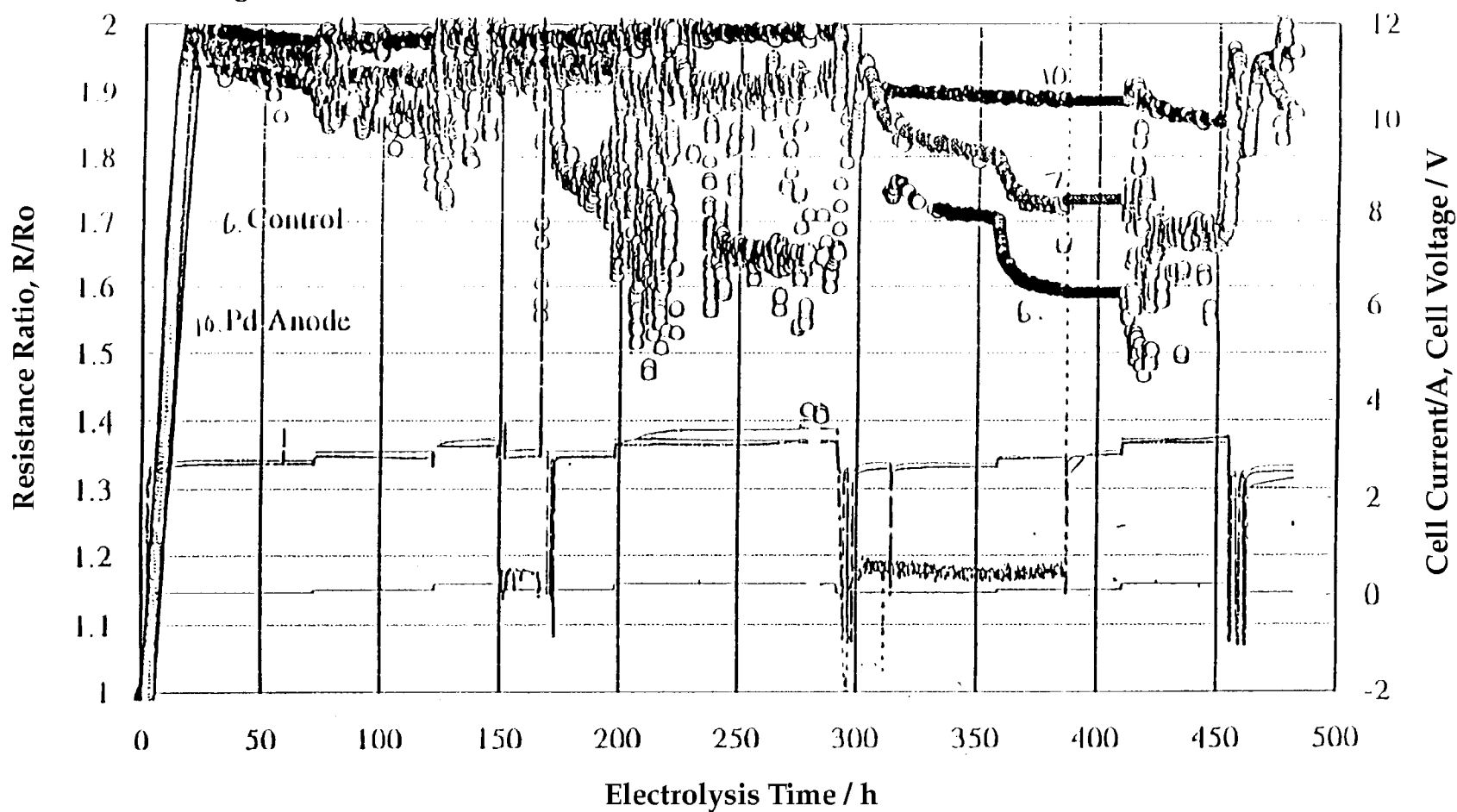
Figure 2-10
DoL Farm F Cells # 6, 7, 10

Effect of Stab Weld on Loading

Engelhard Lot 3 Pd Cathode (0.3 x 3 cm); Pt Anode; 1 M LiOD/D2O; Quartz Cell
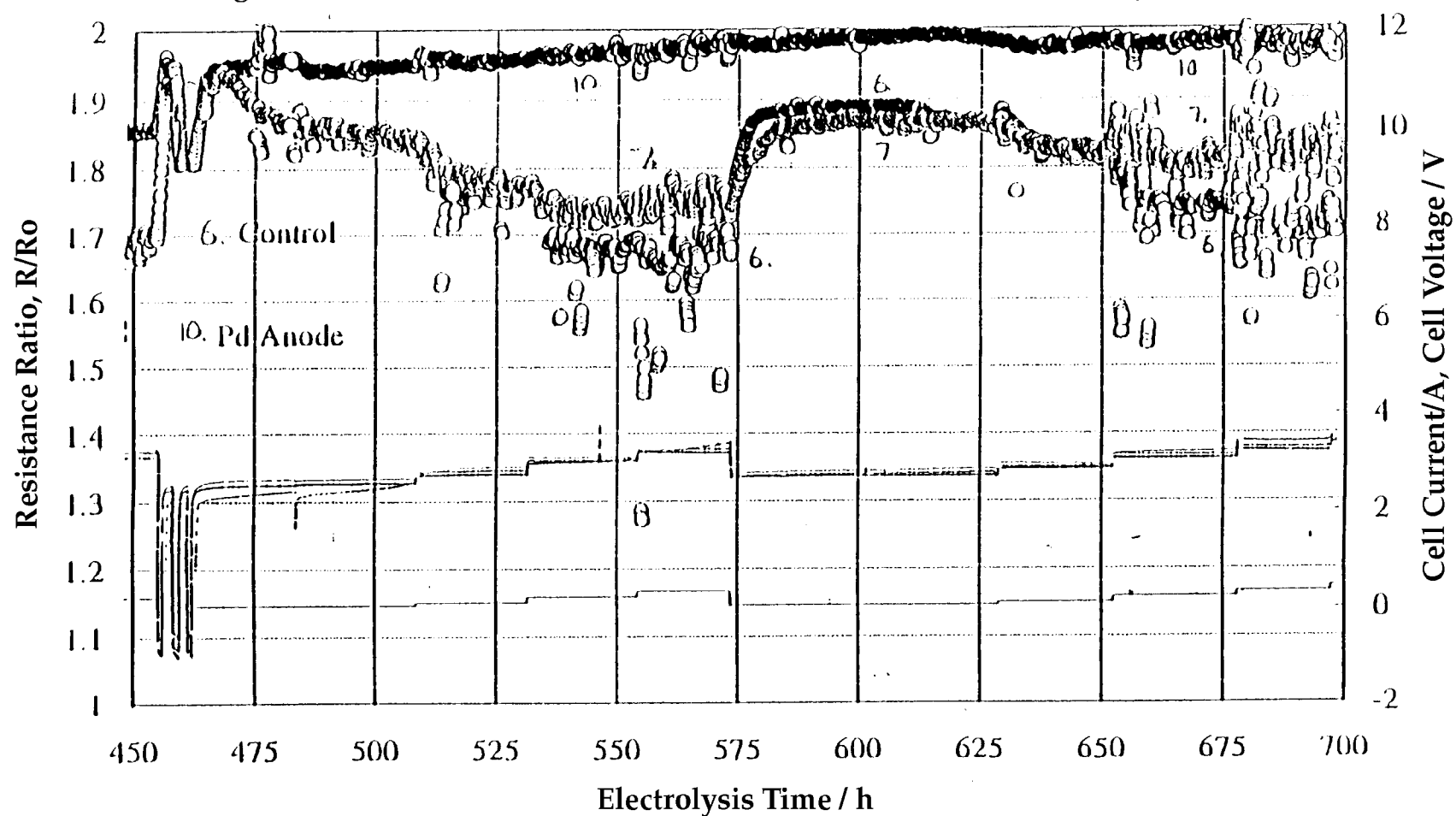
Figure 2-11
DoL Farm F Cells # 6, 7, 10

Effect of Stab Weld on Loading

Engelhard Lot 3 Pd Cathode (0.3 x 3 cm); Pt Anode; 1 M LiOD/D2O; Quartz Cell
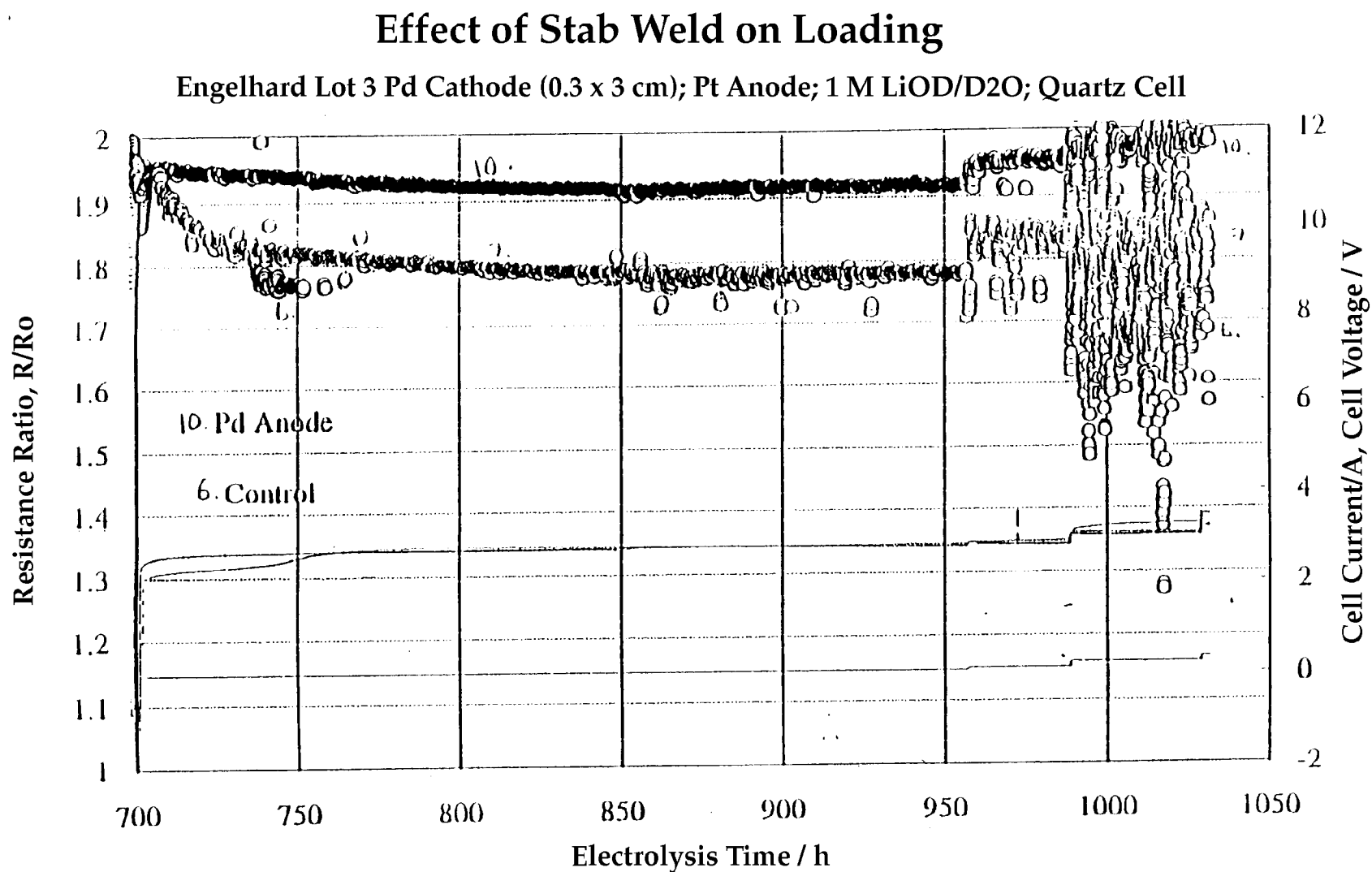
Figure 2-12
DoL Farm F Cells # 6, 7, 10

Effect of Stab Weld on Loading

Engelhard Lot 3 Pd Cathode (0.3 x 3 cm); Pt Anode; 1 M LiOD/D2O; Quartz Cell
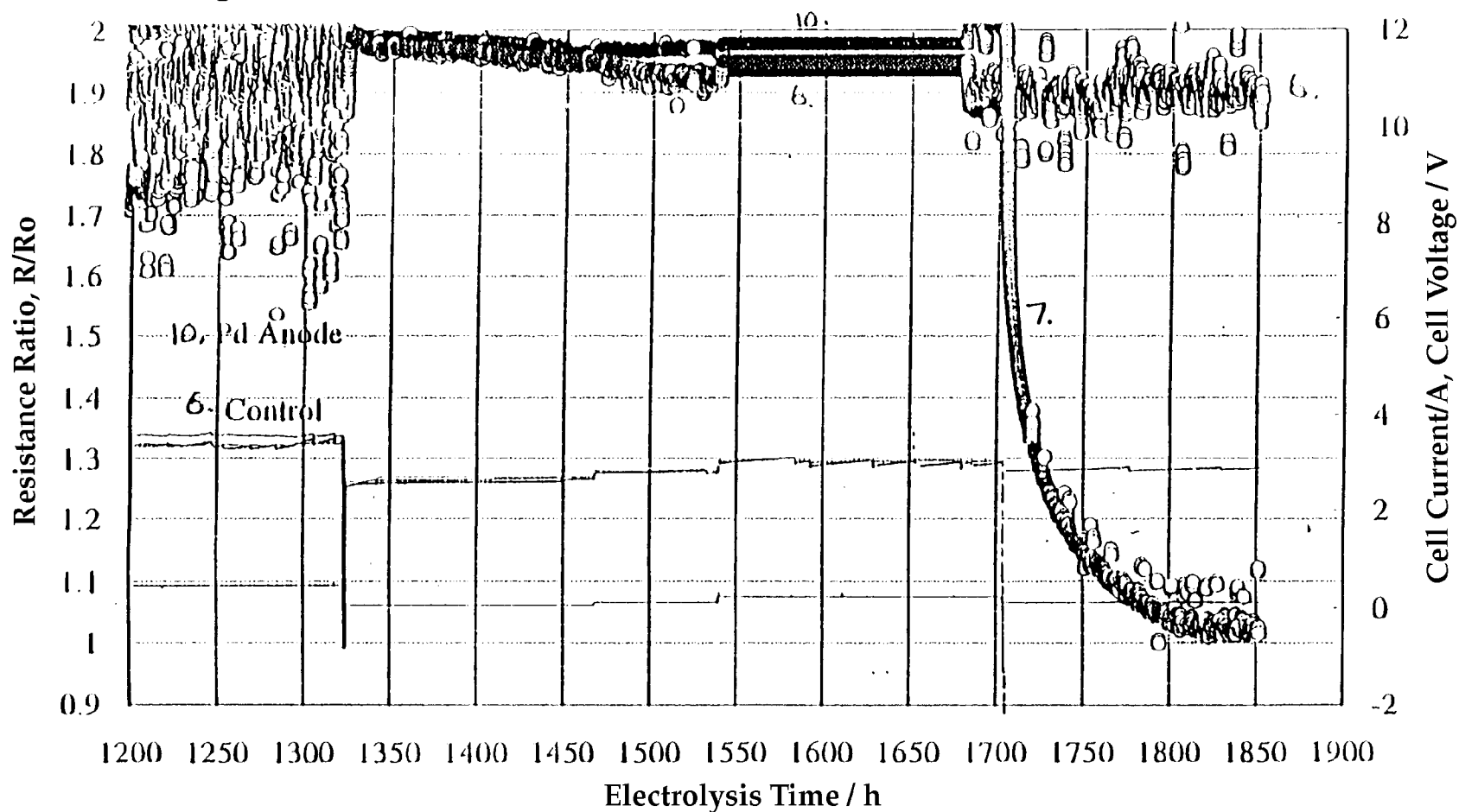
Figure 2-13
DoL Farm F Cells # 6, 7, 10

Effect of Boron on Loading

Engelhard Lot 3 Pd Cathode (0.3 x 3 cm); Pt Anode; 1 M LiOD/D2O; Quartz Cell
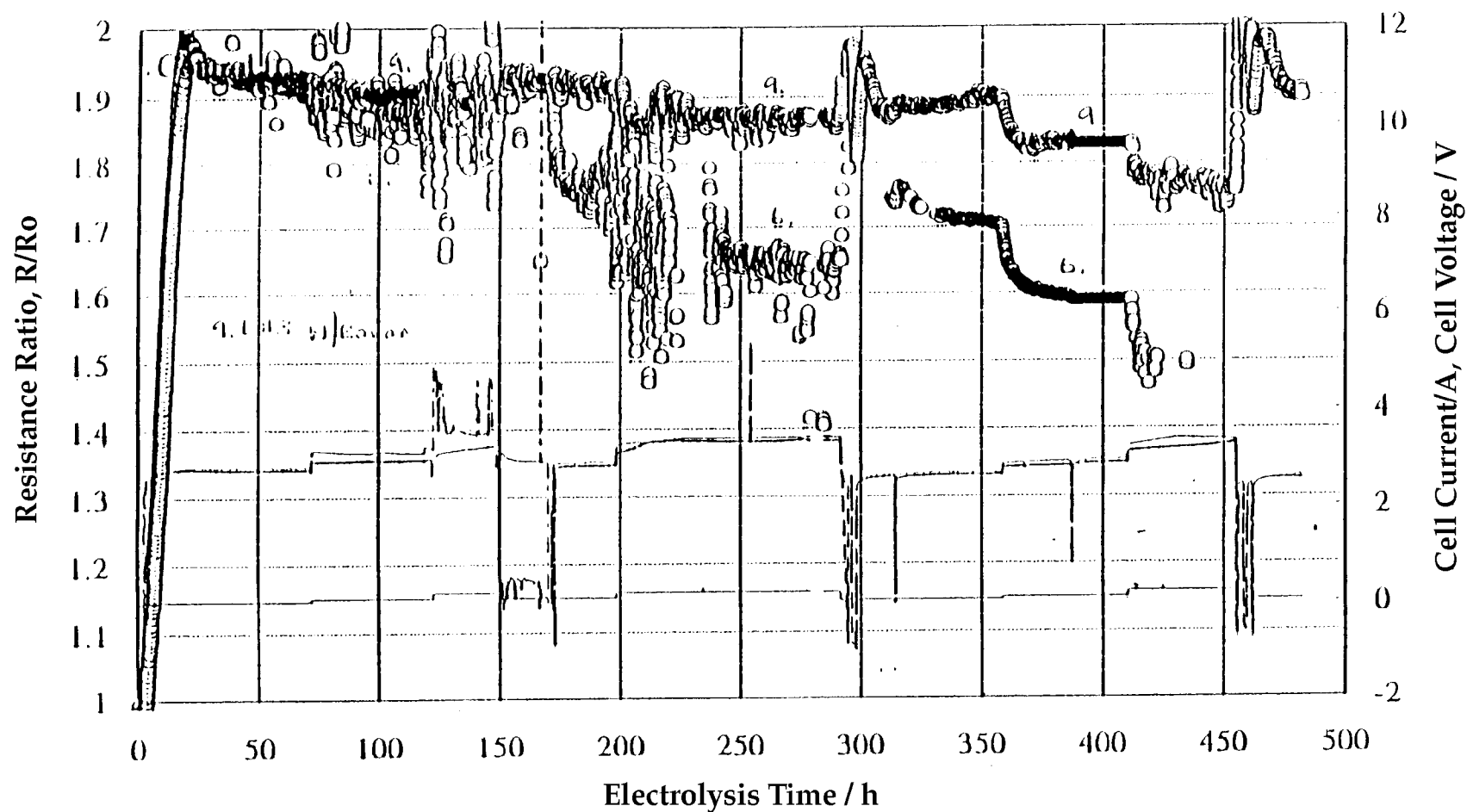
Figure 2-14
DoL Farm F Cells # 6, 9

Effect of Boron on Loading

Engelhard Lot 3 Pd Cathode (0.3 x 3 cm); Pt Anode; 1 M LiOD/D2O; Quartz Cell
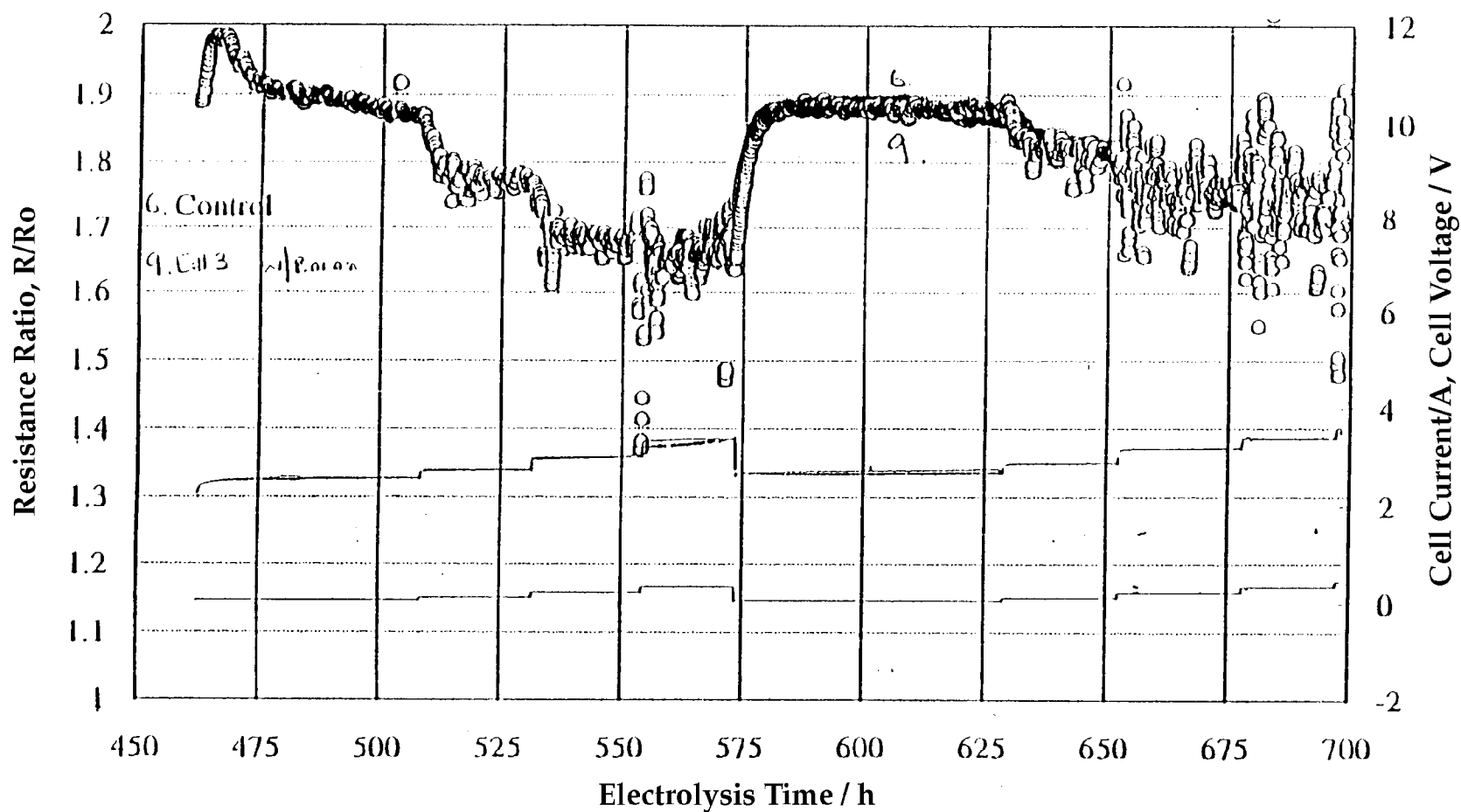
Figure 2-15
DoL Farm F Cells # 6, 9

Effect of Boron on Loading

Engelhard Lot 3 Pd Cathode (0.3 x 3 cm); Pt Anode; 1 M LiOD/D2O; Quartz Cell
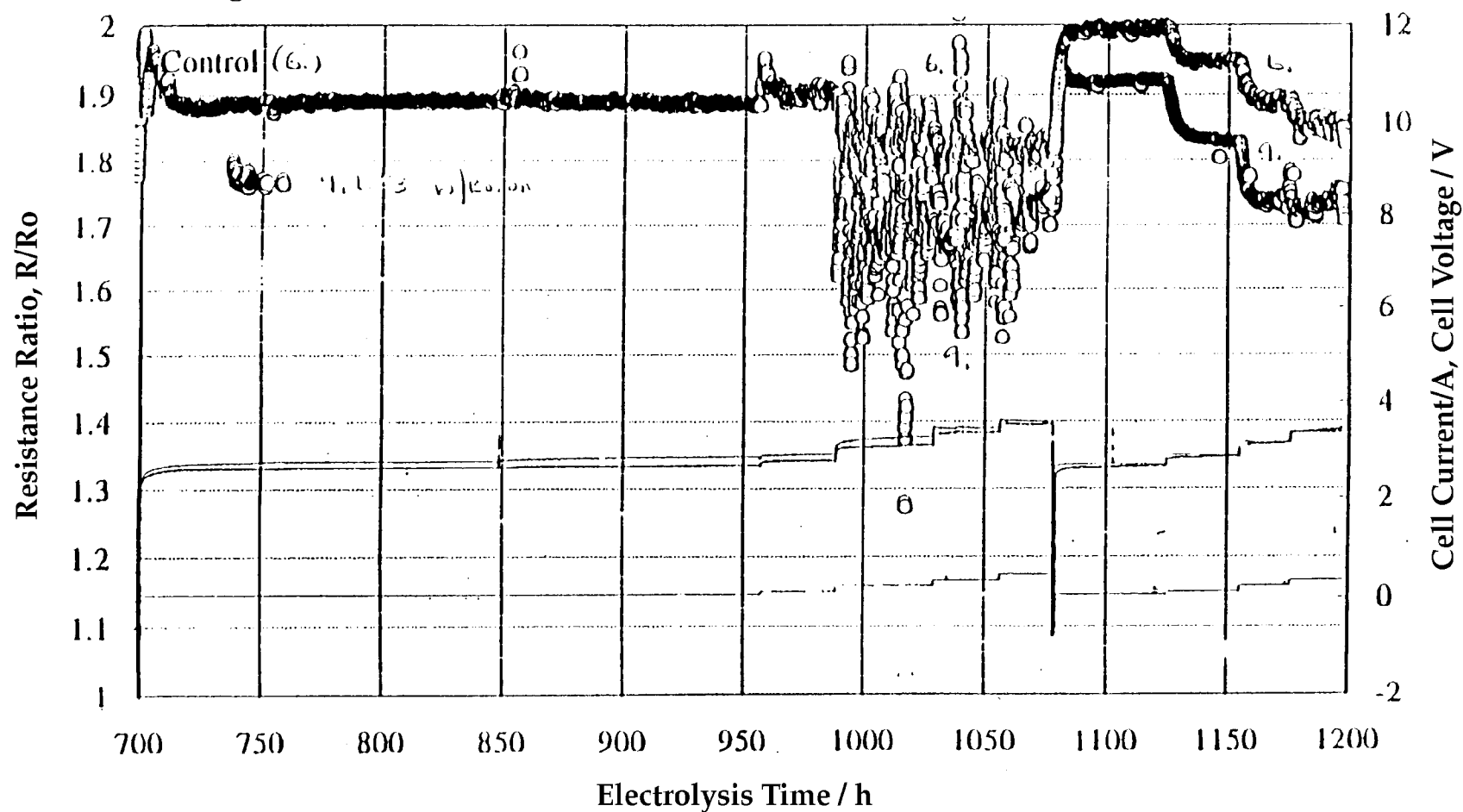
Figure 2-16
DoL Farm F Cells # 6, 9

Effect of Boron on Loading

Engelhard Lot 3 Pd Cathode (0.3 x 3 cm); Pt Anode; 1 M LiOD/D2O; Quartz Cell
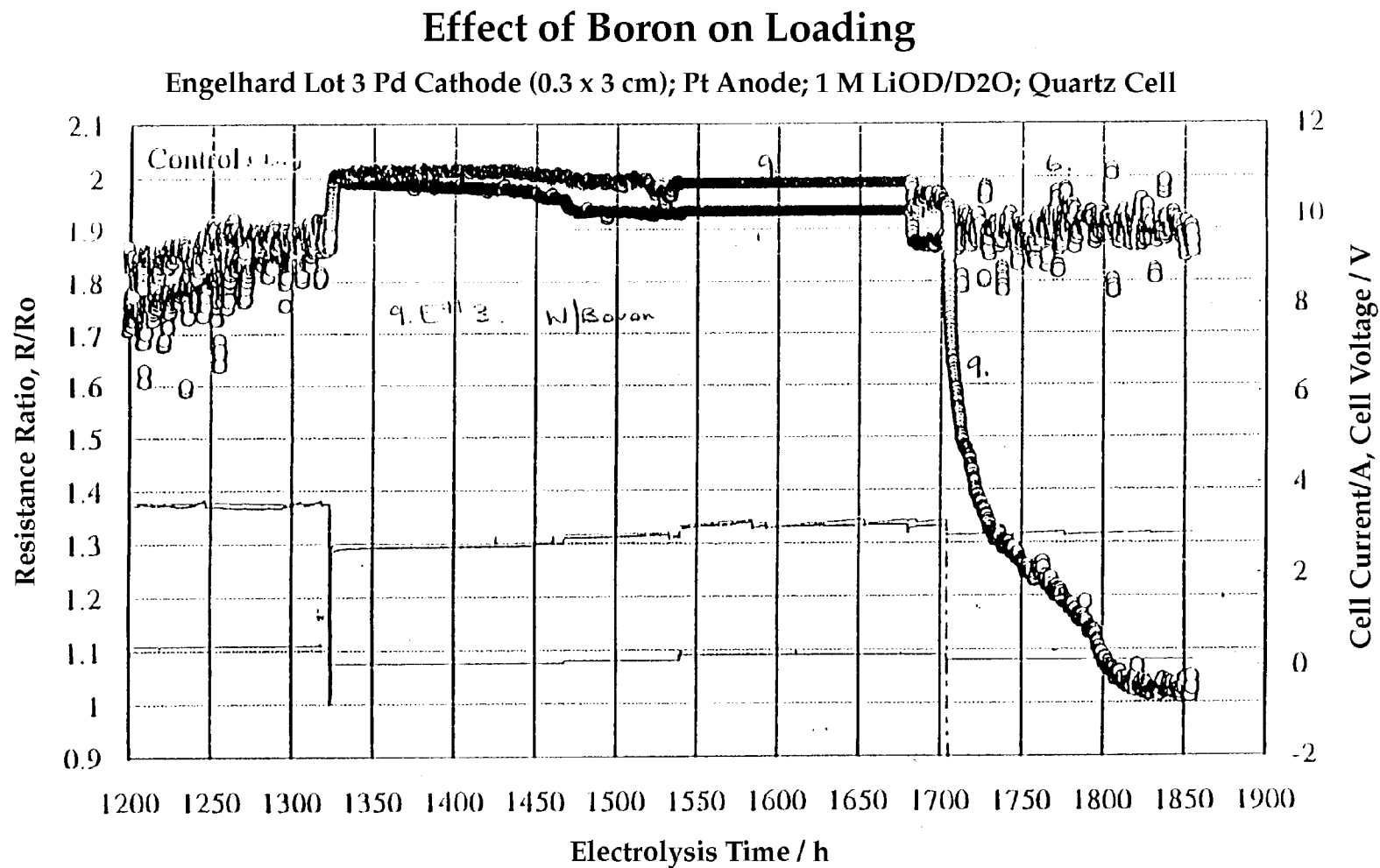
Figure 2-17
DoL Farm F Cells # 6, 9

Effect of Pd Source on Loading

Pd Cathode; Pt Anode; 1 M LiOD/D2O; Quartz Cell
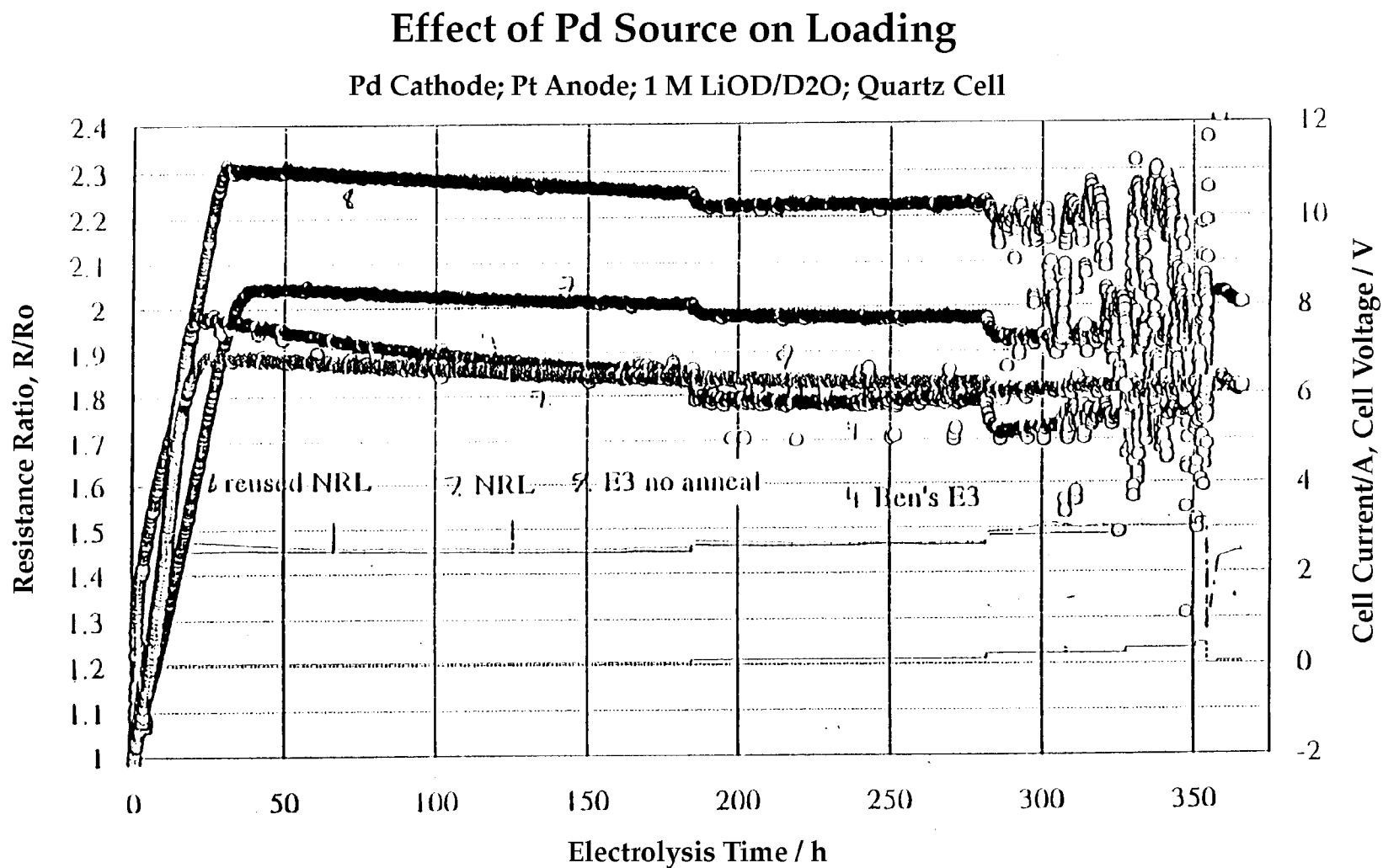
Figure 2-18
DoL Farm GG Cells # 4, 7, 8, 9

Effect of Pd Source on Loading

Pd Cathode; Pt Anode; 1 M LiOD/D2O; Quartz Cell
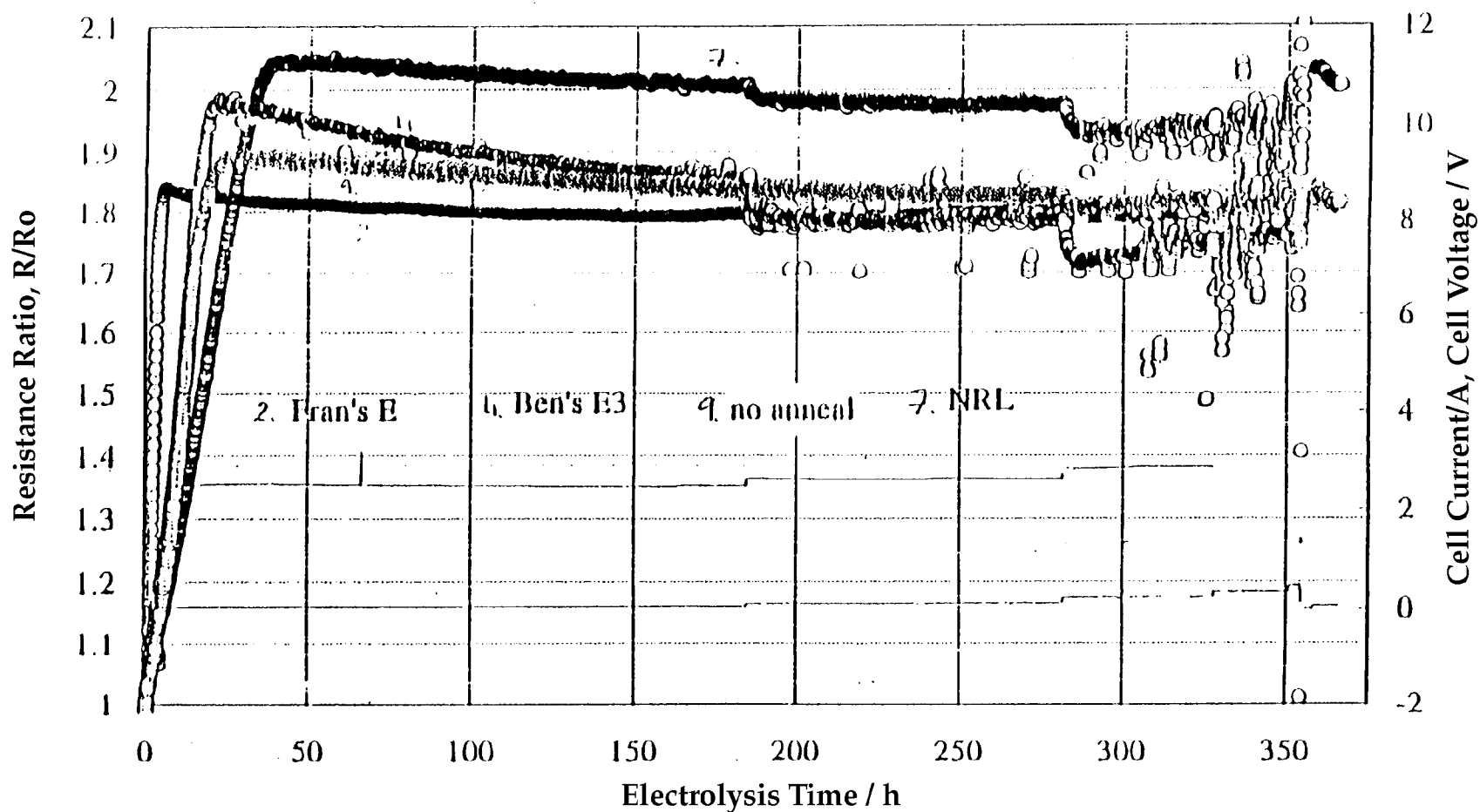
Figure 2-19
DoL Farm GG Cells # 2, 4, 7, 9

Reproducibility of Engelhard Pd

Pd Cathode (0.3 x 3 cm); Pt Anode; 1 M LiOD/D2O; Quartz Cell

Figure 2-20
DoL Farm GG Cells # 2, 4, 7, 9

Reproducibility of Engelhard Pd

Pd Cathode (0.3 x 3 cm); Pt Anode; 1 M LiOD/D2O; Quartz Cell
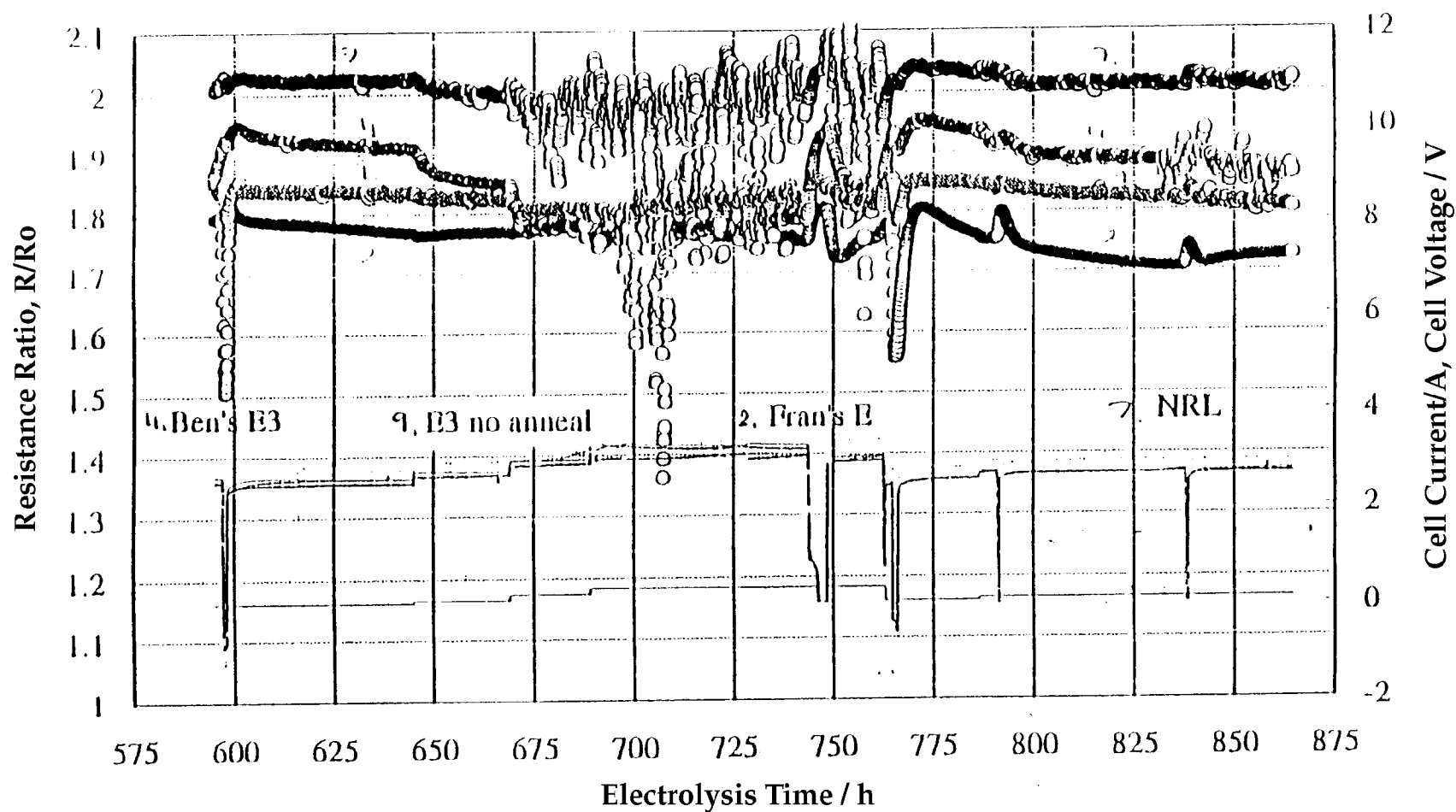
Figure 2-21
DoL Farm GG Cells # 2, 4, 7, 9

Reproducibility of Engelhard Pd

Pd Cathode (0.3 x 3 cm); Pt Anode; 1 M LiOD/D2O; Quartz Cell
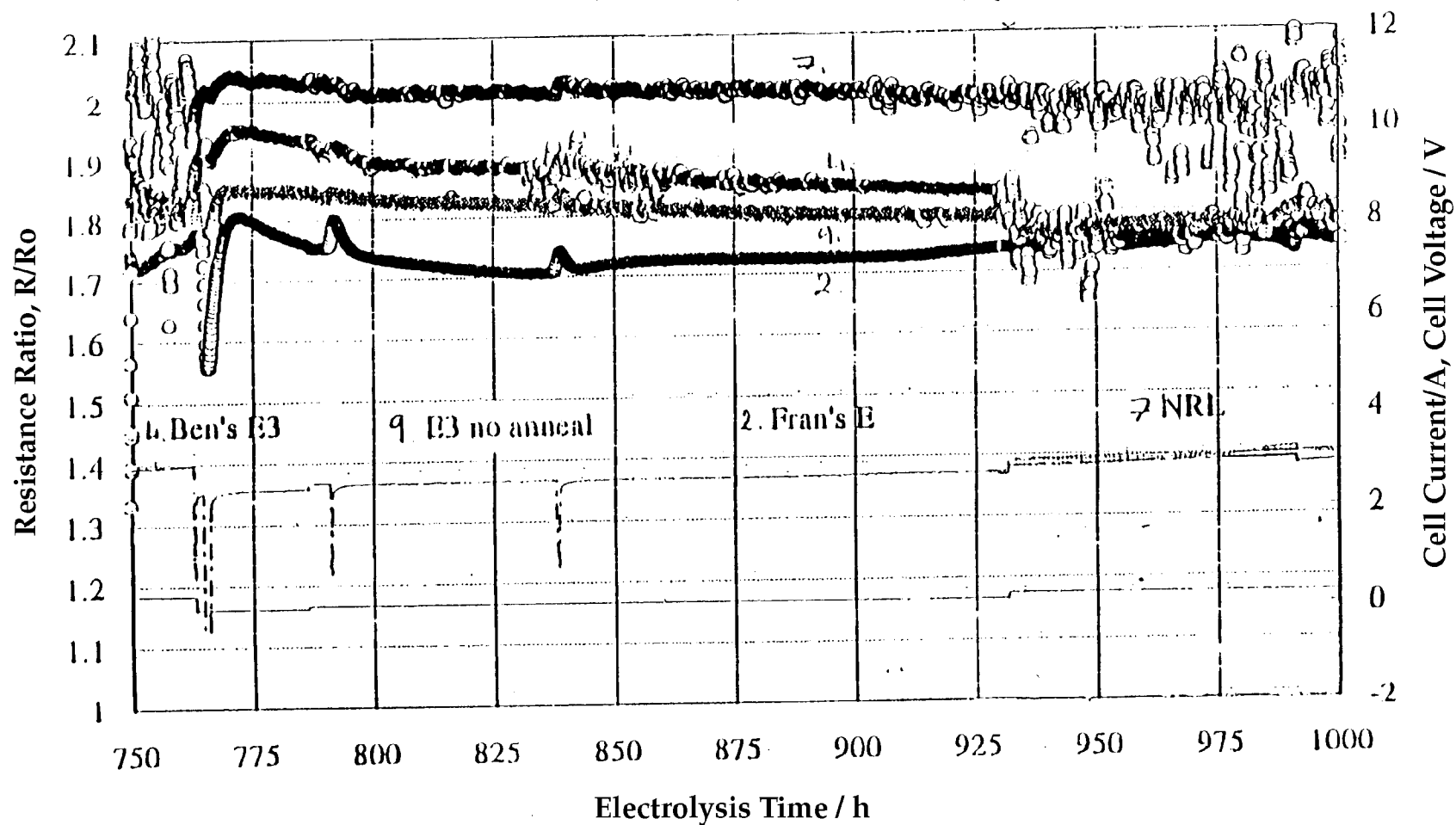
Figure 2-22
DoL Farm GG Cells # 2, 4, 7, 9

Reproducibility of Engelhard Pd

Pd Cathode (0.3 x 3 cm); Pt Anode; 1 M LiOD/D2O; Quartz Cell

Figure 2-23
DoL Farm GG Cells # 2, 4, 7, 9

Reproducibility of Engelhard Pd

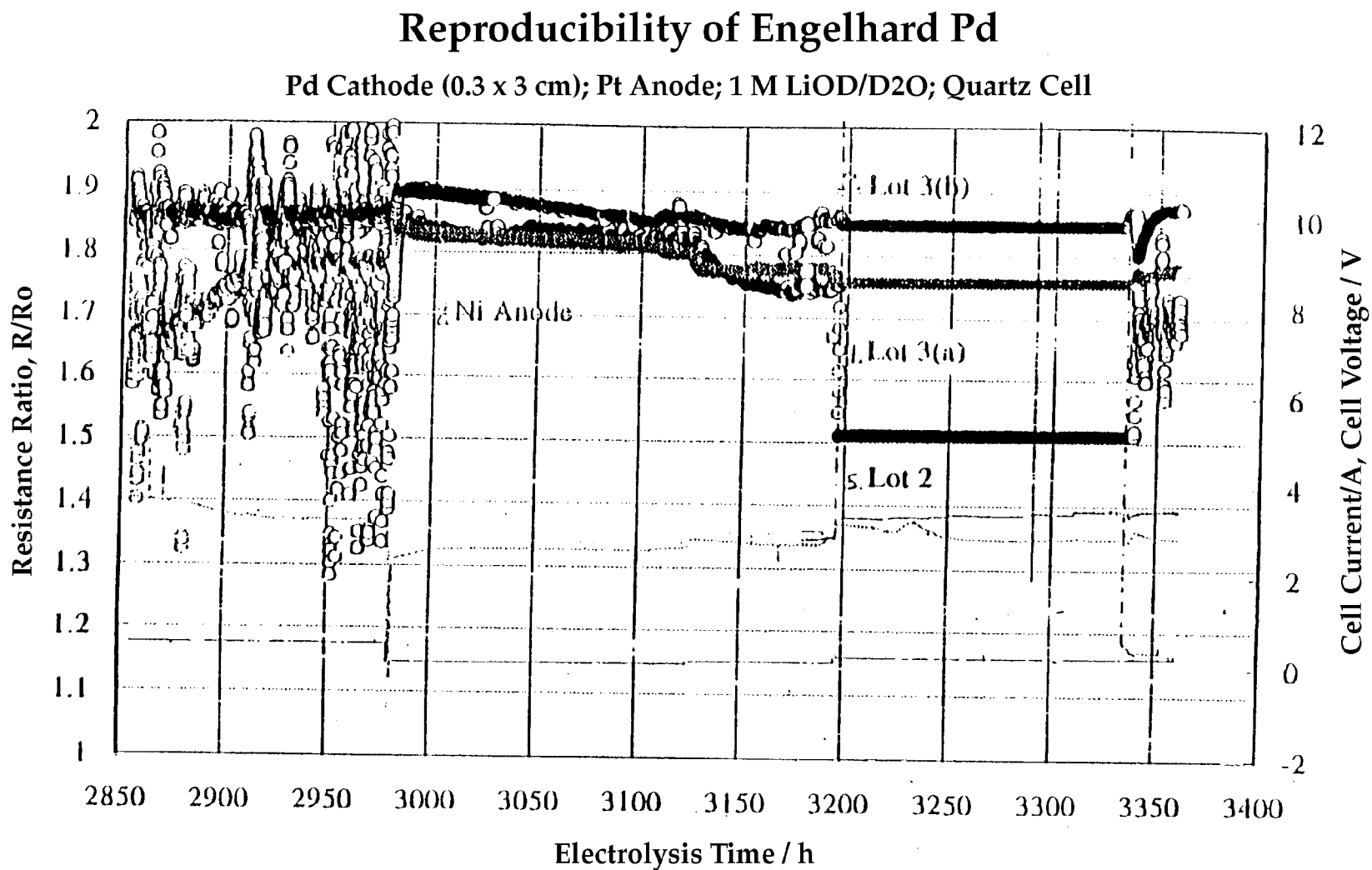## Pd Cathode (0.3 x 3 cm); Pt Anode; 1 M LiOD/D2O; Quartz Cell
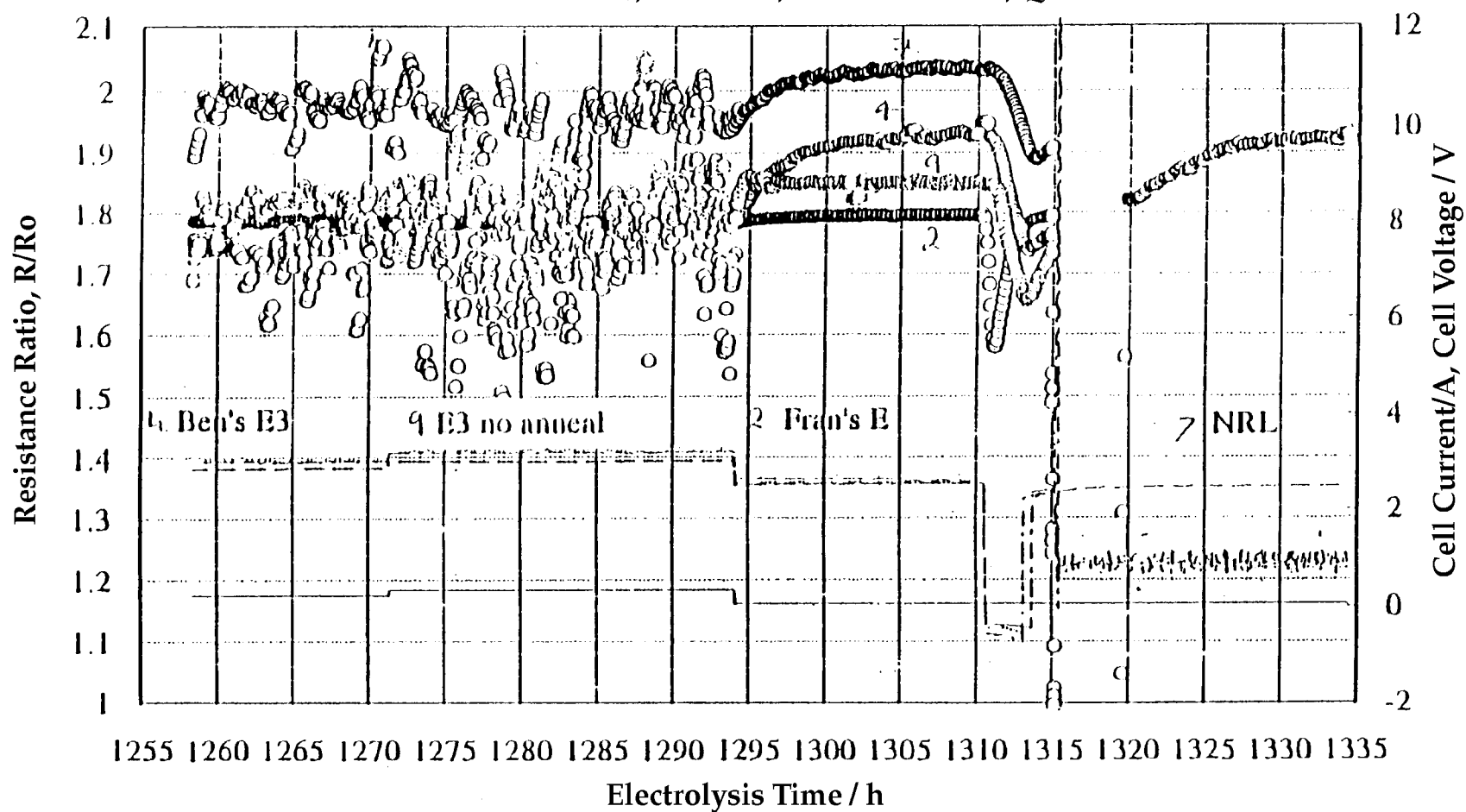
Figure 2-24
DoL Farm GG Cells # 2, 4, 7, 9

Effect of Electrode Pretreatment on Loading

JM Pd Cathode (0.2 x 3 cm); Pt Anode; 1 M LiOD/D2O; Quartz Cell
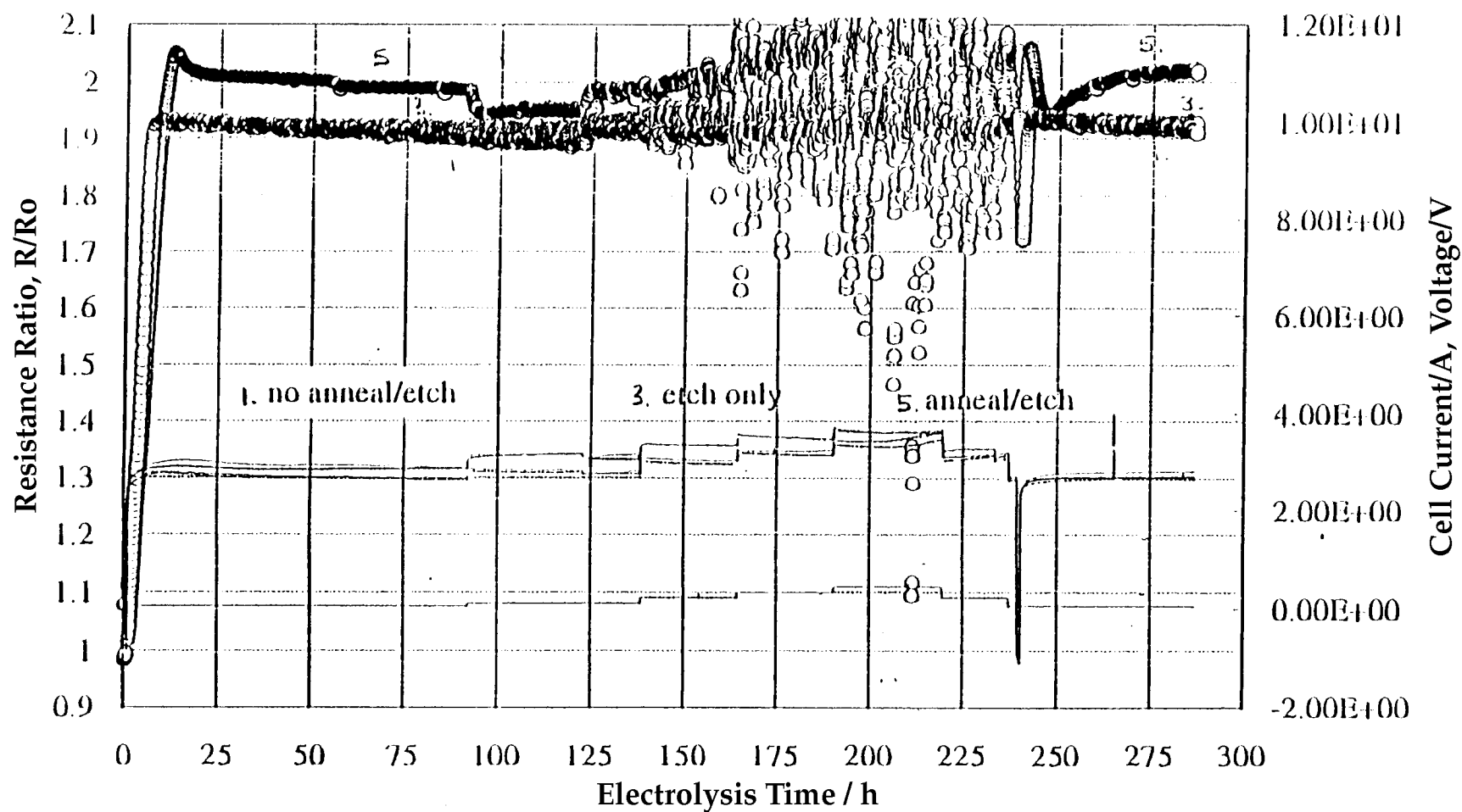
Figure 2-25
DoL Farm H Cells # 1, 3, 5

Effect of Electrode Pretreatment on Loading

JM Pd Cathode (0.2 x 3 cm); Pt Anode; 1 M LiOD/D2O; Quartz Cell
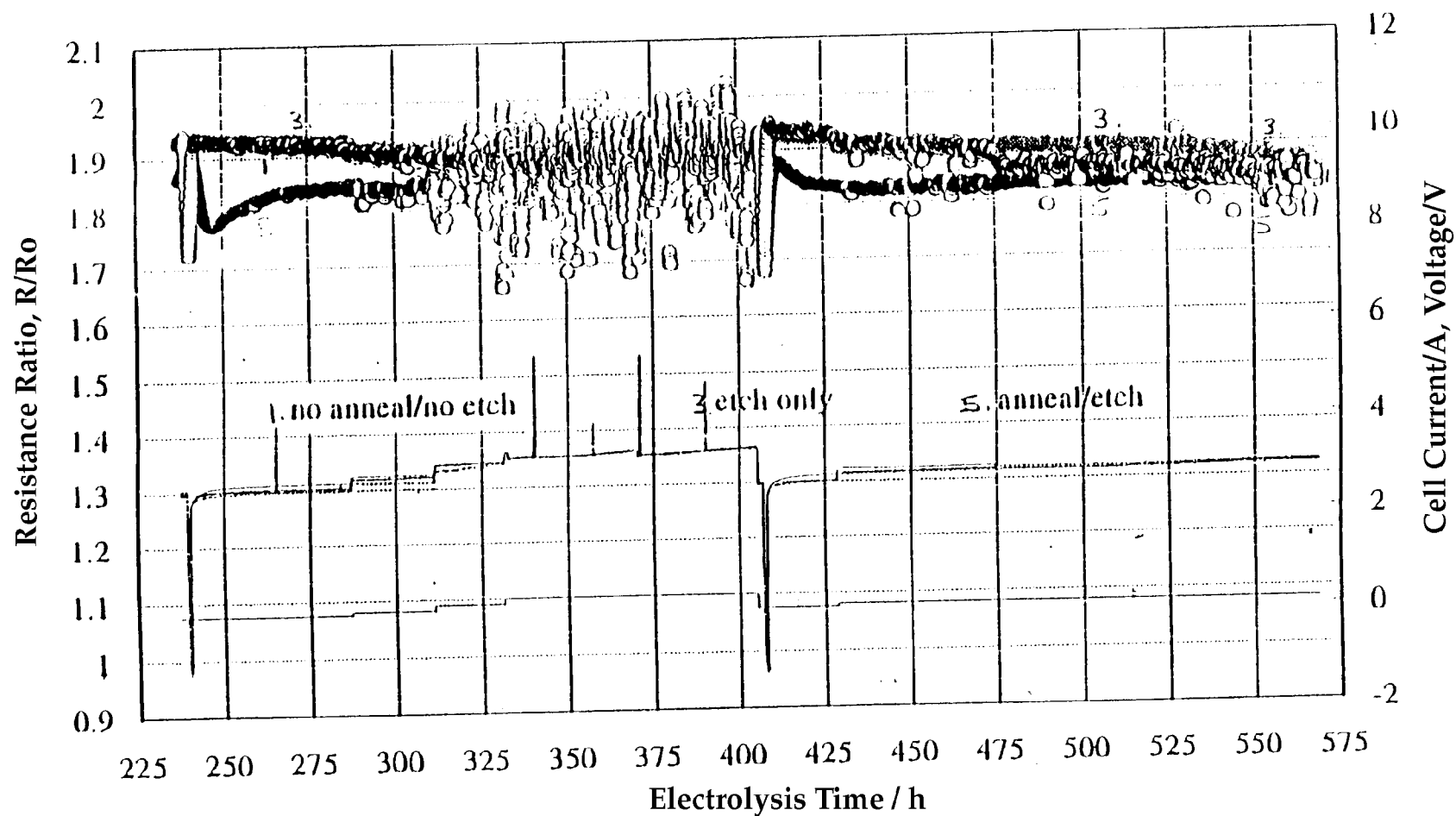
Figure 2-26
DoL Farm H Cells # 1, 3, 5

Effect of Electrode Pretreatment on Loading

JM Pd Cathode (0.2 x 3 cm); Pt Anode; 1 M LiOD/D2O; Quartz Cell
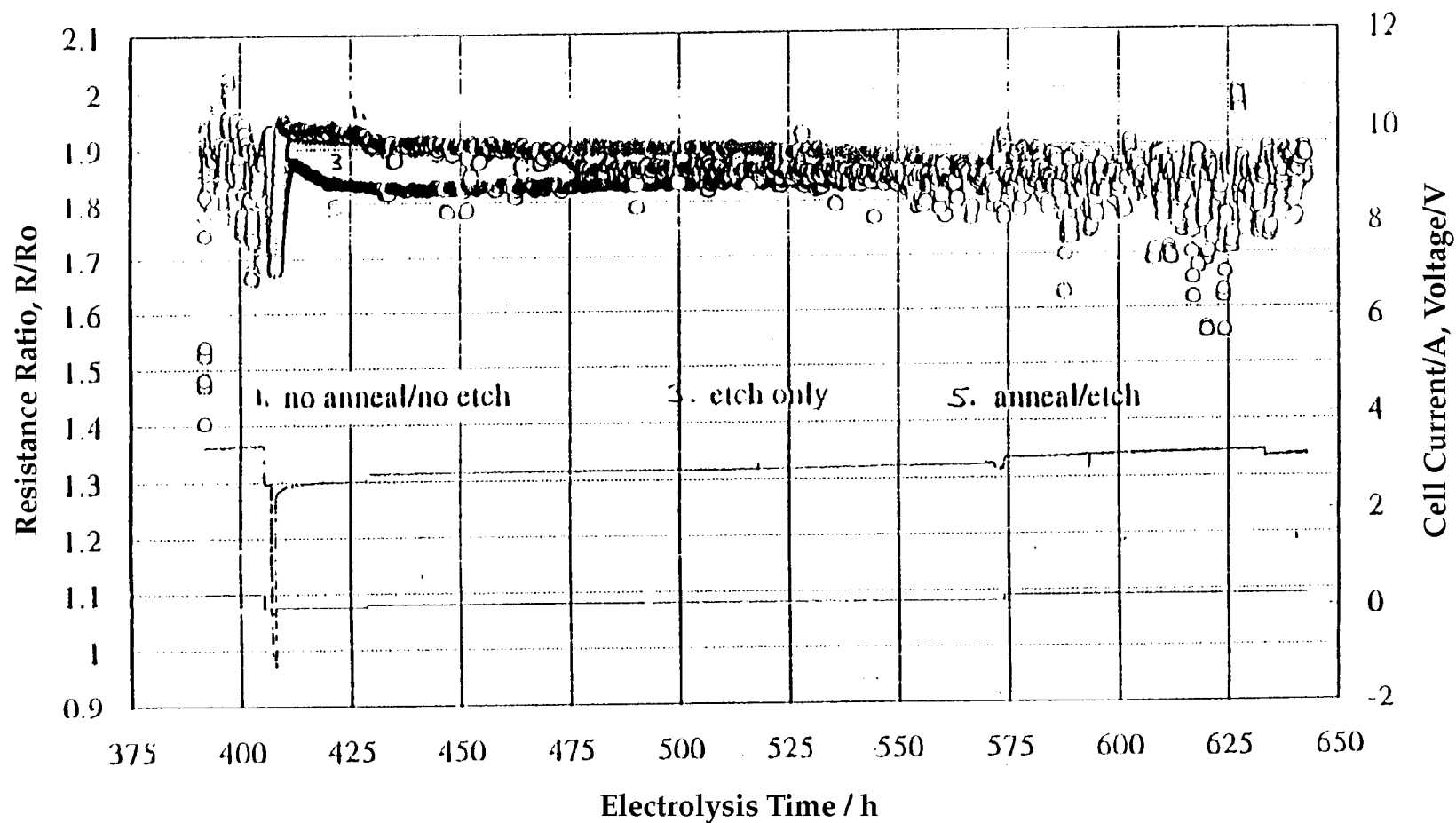
Figure 2-27
DoL Farm H Cells # 1, 3, 5

2-40

Effect of Electrode Pretreatment on Loading

JM Pd Cathode (0.2 x 3 cm); Pt Anode; 1 M LiOD/D2O; Quartz Cell
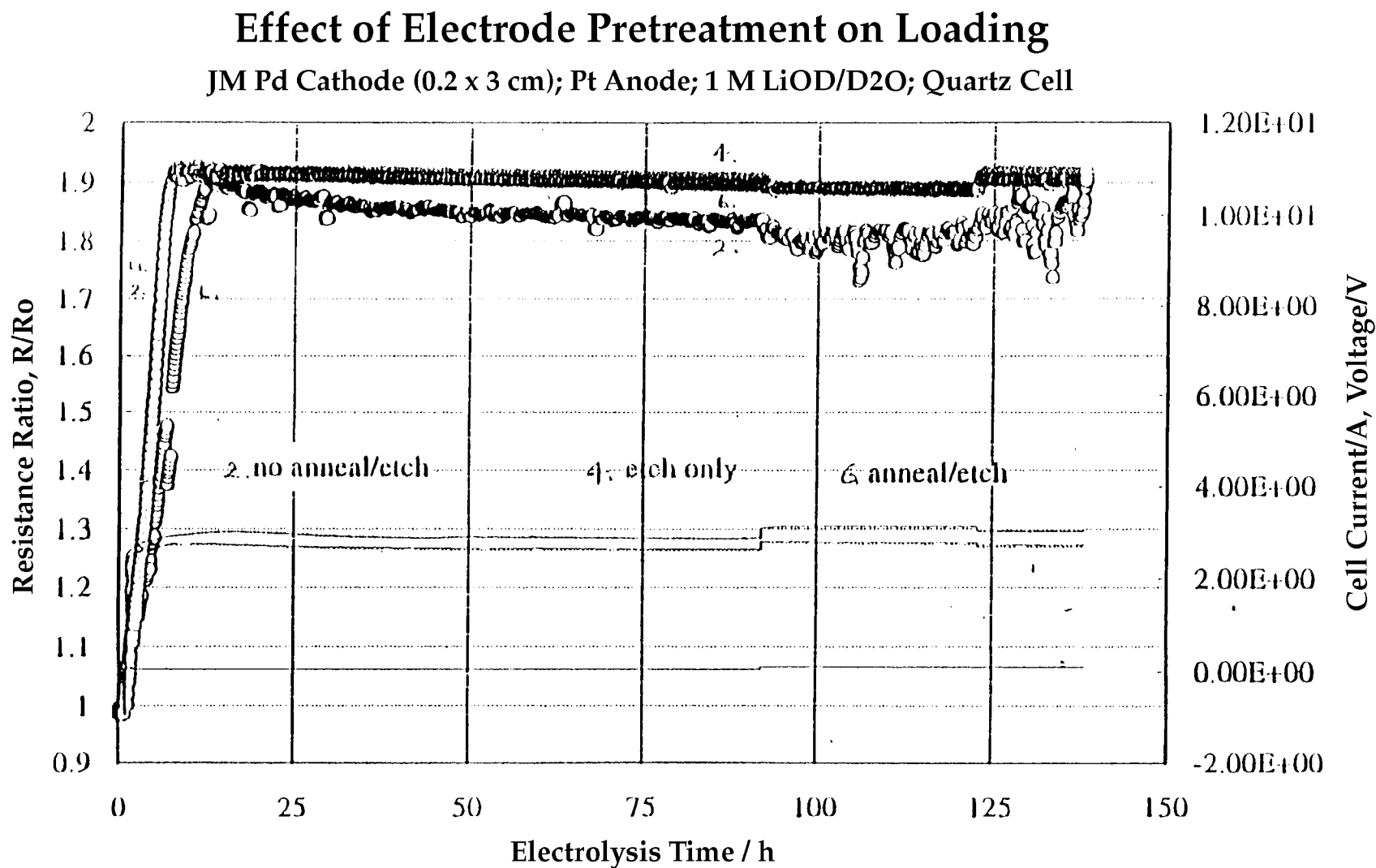
Figure 2-28
DoL Farm H Cells # 2, 4, 6

Effect of Electrode Pretreatment on Loading

JM Pd Cathode (0.2 x 3 cm); Pt Anode; 1 M LiOD/D2O; Quartz Cell
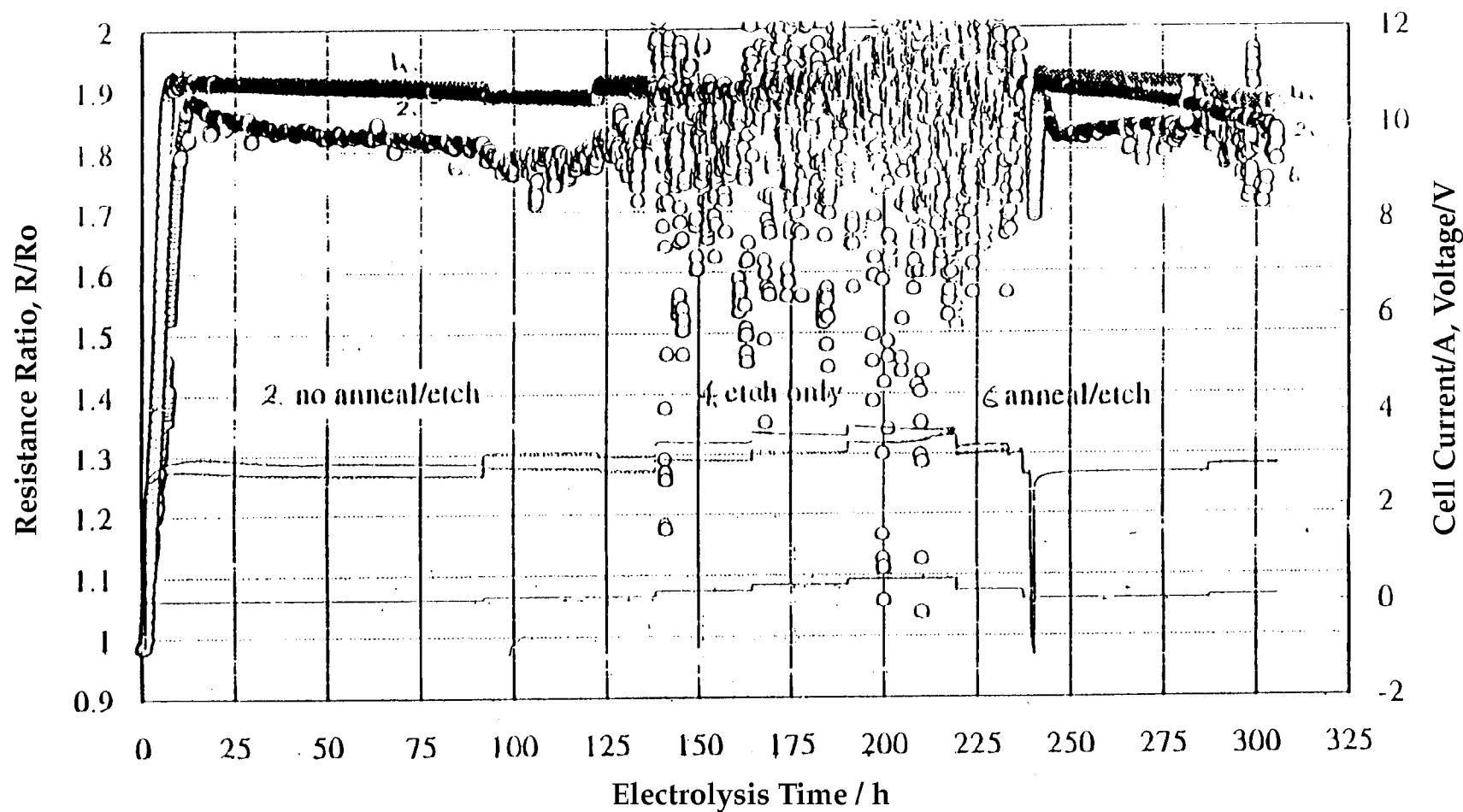
Figure 2-29
DoL Farm H Cells # 2, 4, 6

Effect of Electrode Pretreatment on Loading

JM Pd Cathode (0.2 x 3 cm); Pt Anode; 1 M LiOD/D2O; Quartz Cell
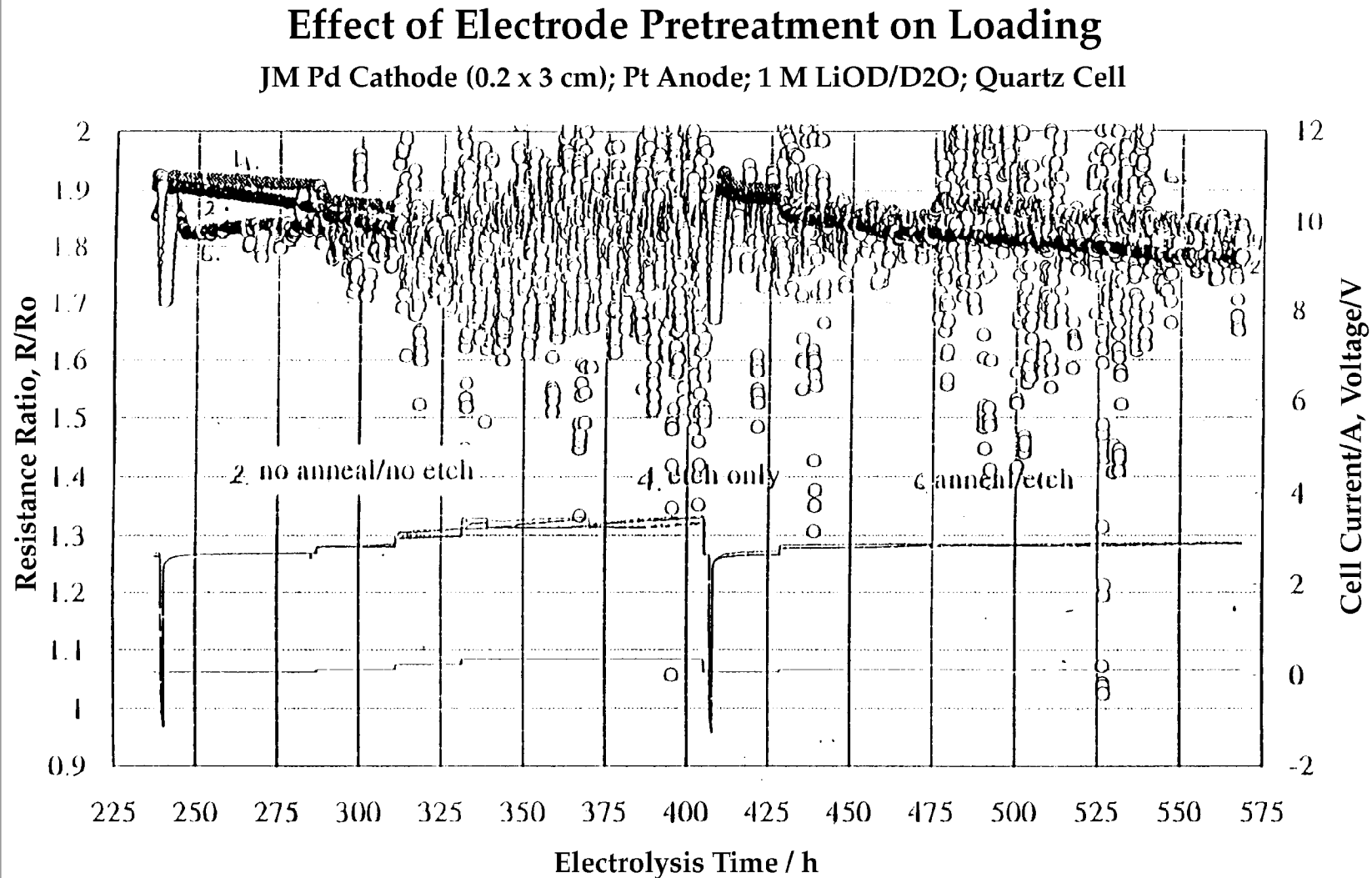
Figure 2-30
DoL Farm H Cells # 2, 4, 6

Effect of Electrode Pretreatment on Loading

JM Pd Cathode (0.2 x 3 cm); Pt Anode; 1 M LiOD/D2O; Quartz Cell
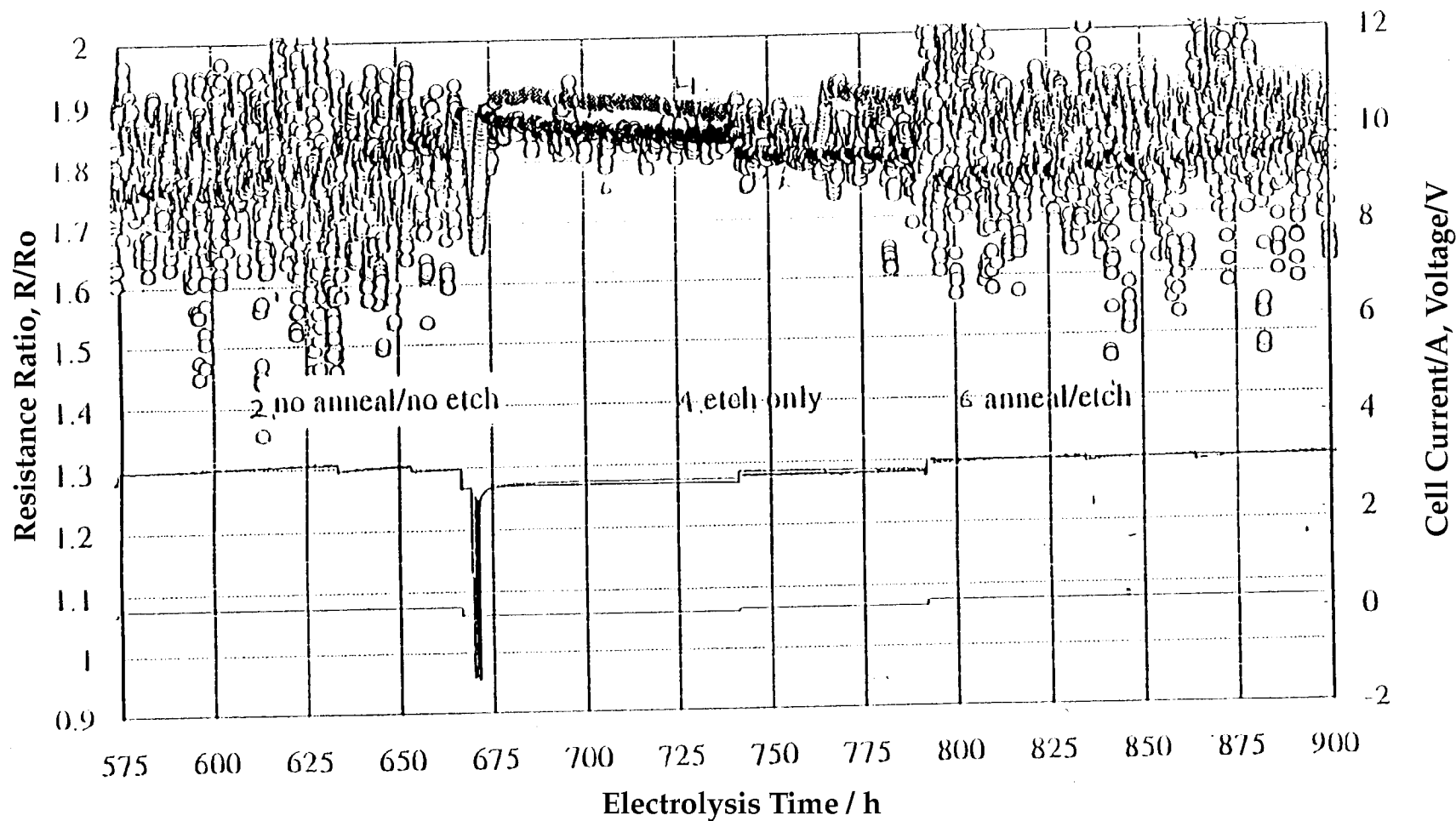
Figure 2-31
DoL Farm H Cells # 2, 4, 6

Effect of Electrode Pretreatment on Loading

JM Pd Cathode (0.2 x 3 cm); Pt Anode; 1 M LiOD/D2O; Quartz Cell
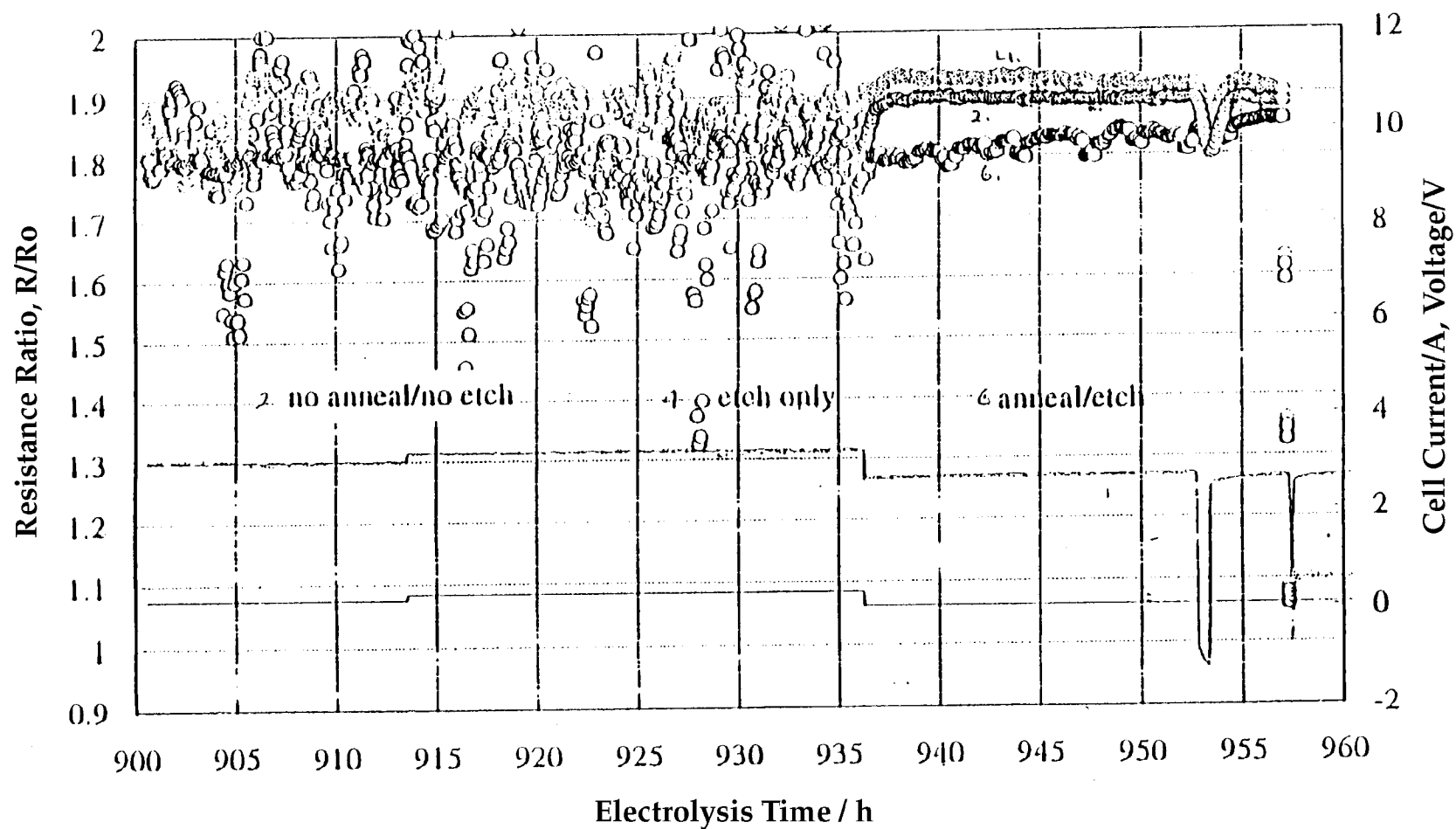
Figure 2-32
DoL Farm H Cells # 2, 4, 6

Effects of Electrode Surface Preparation

Reused E1 Pd Cathode (0.3 x 3 cm); Pt Anode; 1 M LiOD/D2O; Quartz Cell

Machine, Degrease, Anneal, Spot Weld, Etch

1 - etch (no machining)

2 - polish (no machining)

3 - control

4 - no final etch

Resistance Ratio, R/Ro (y-axis, left)

Cell Current/A, Voltage/V (y-axis, right)

Electrolysis Time / h (x-axis)
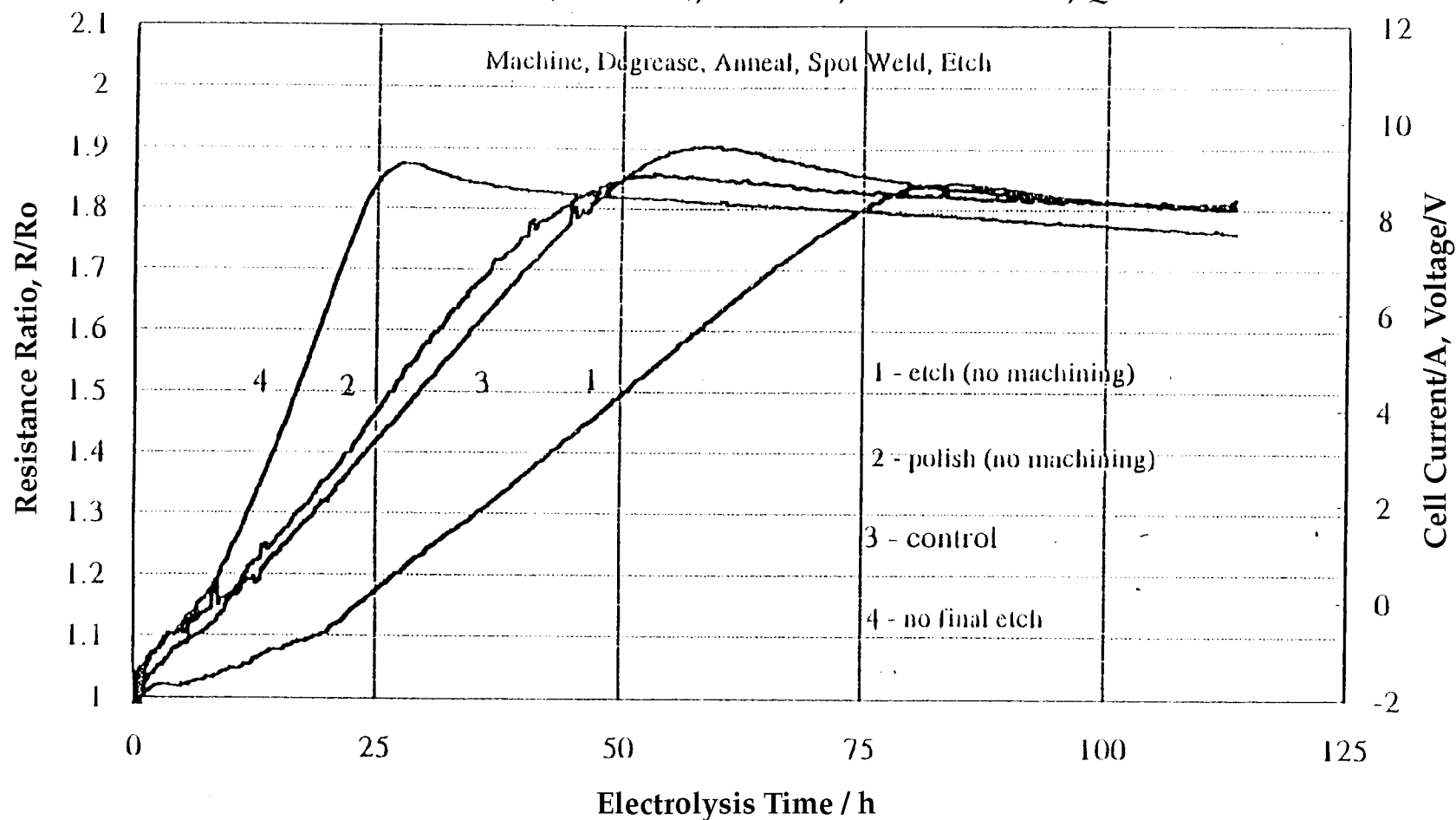
Figure 2-33
DoL Farm I Cells # 1, 2, 3, 4

Effects of Electrode Surface Preparation

Reused E1 Pd Cathode (0.3 x 3 cm); Pt Anode; 1 M LiOD/D2O; Quartz Cell
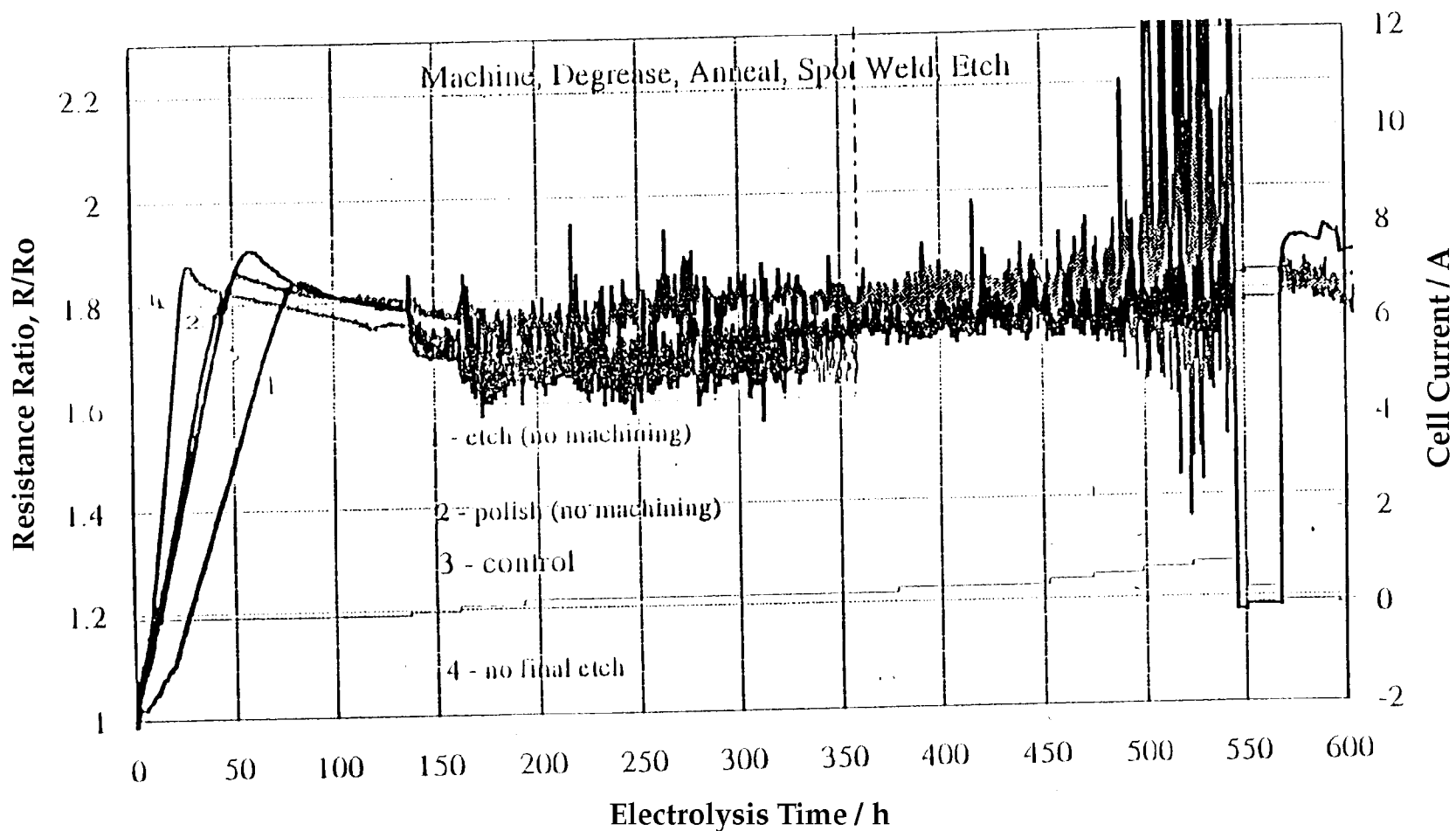
Figure 2-34
DoL Farm I Cells # 1, 2, 3, 4

Effects of Electrode Surface Preparation

Reused E1 Pd Cathode (0.3 x 3 cm); Pt Anode; 1 M LiOD/D2O; Quartz Cell
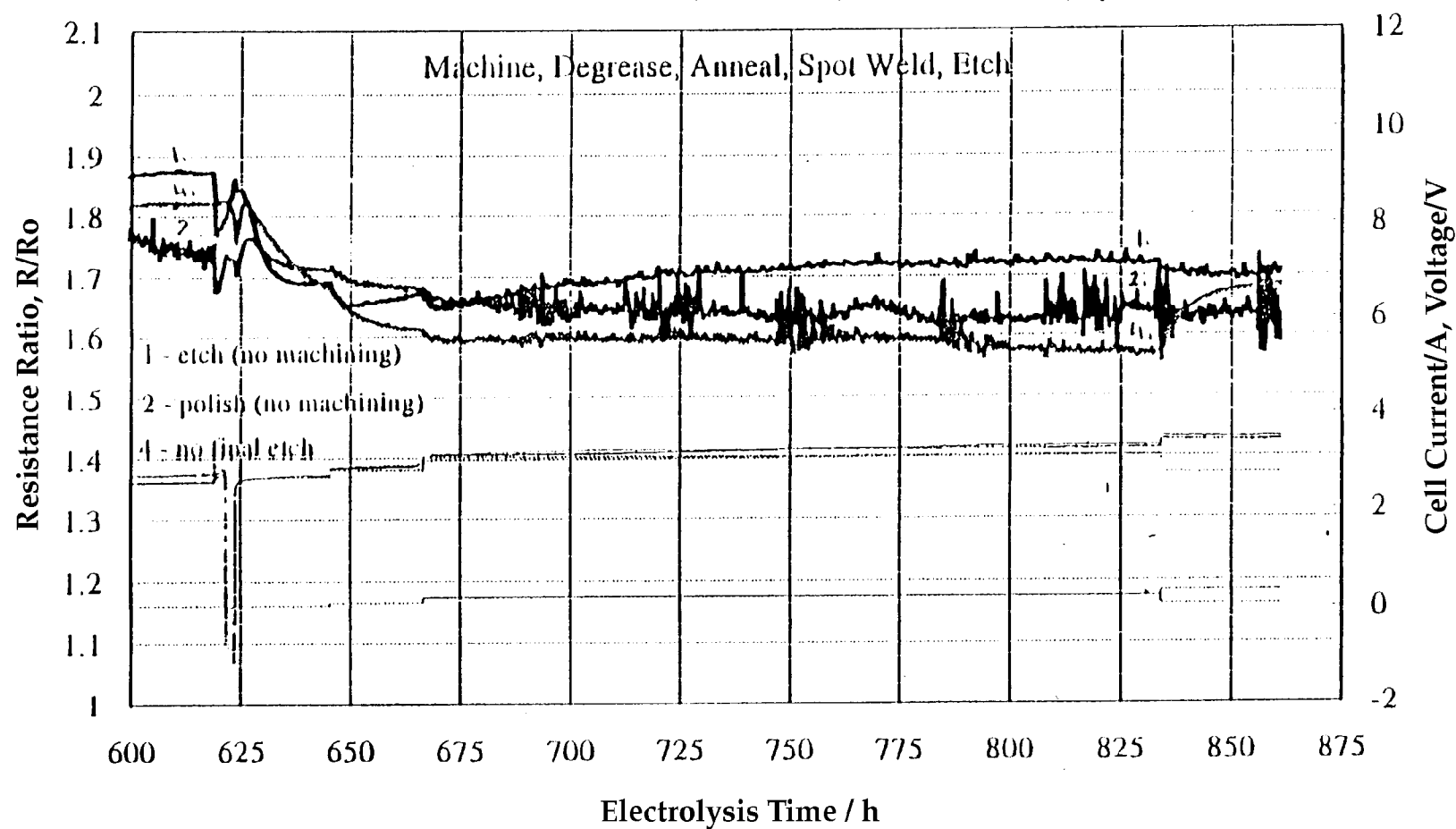
Figure 2-35
DoL Farm I Cells # 1, 2, 4

Reproducibility of Pd

Pd Cathode (0.3 x 3 cm); Pt Anode; 1 M LiOD/D2O; Quartz Cell
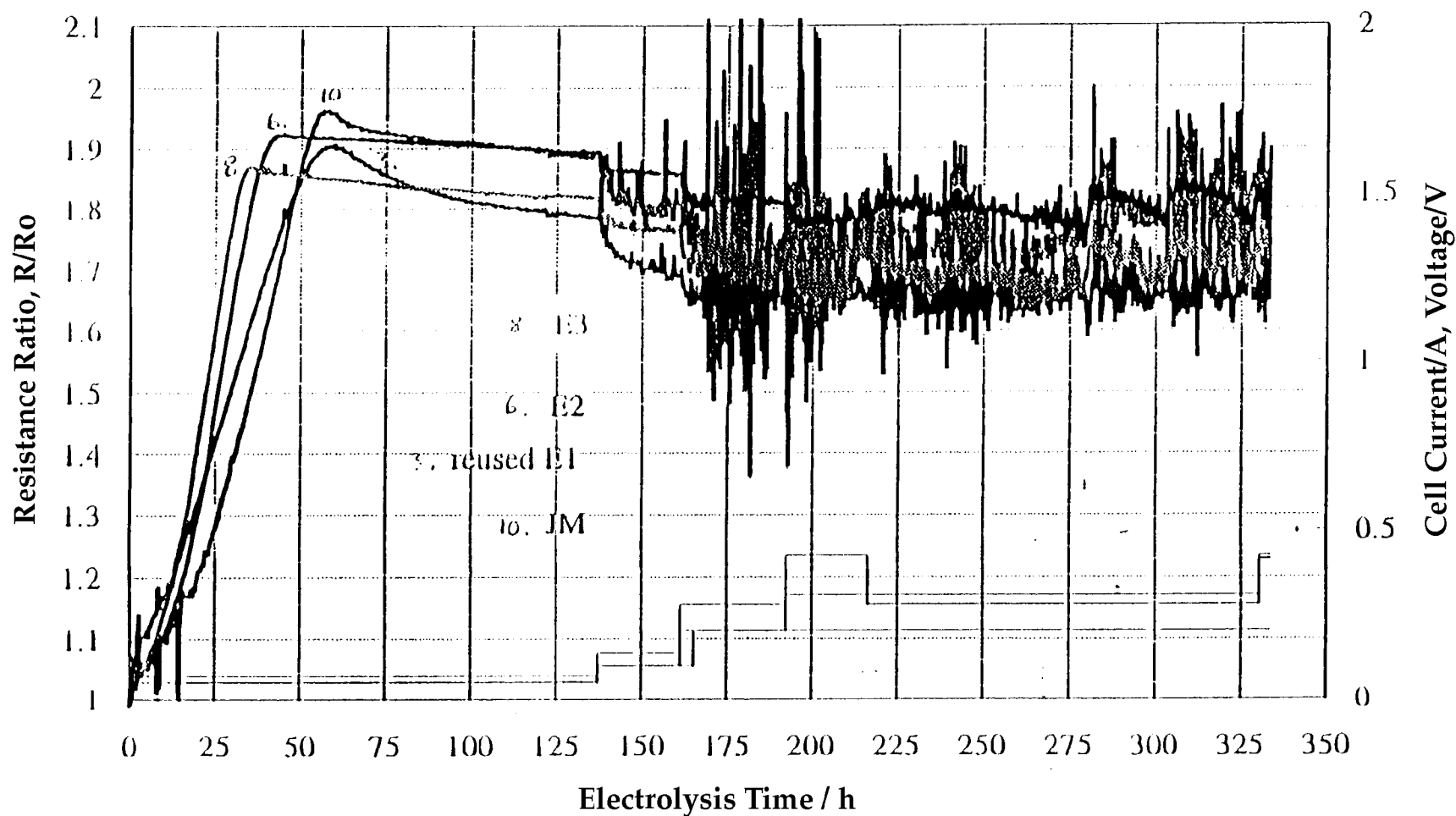
Figure 2-36
DoL Farm I Cells # 3, 6, 8, 10

Reproducibility of Pd

Pd Cathode (0.3 x 3 cm); Pt Anode; 1 M LiOD/D2O; Quartz Cell
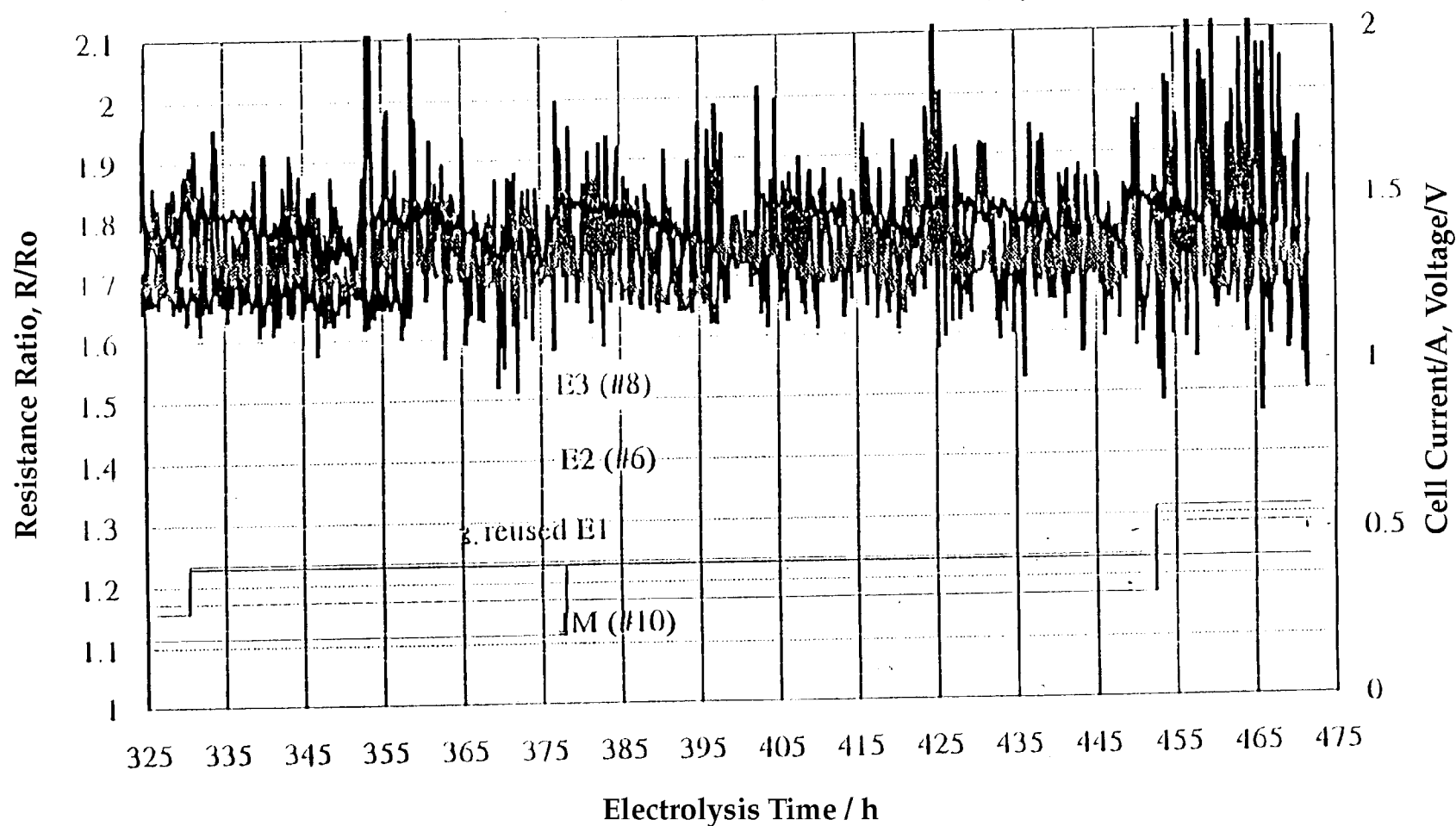
Figure 2-37
DoL Farm I Cells # 3, 6, 8, 10

Reproducibility of Pd

Pd Cathode (0.3 x 3 cm); Pt Anode; 1 M LiOD/D2O; Quartz Cell
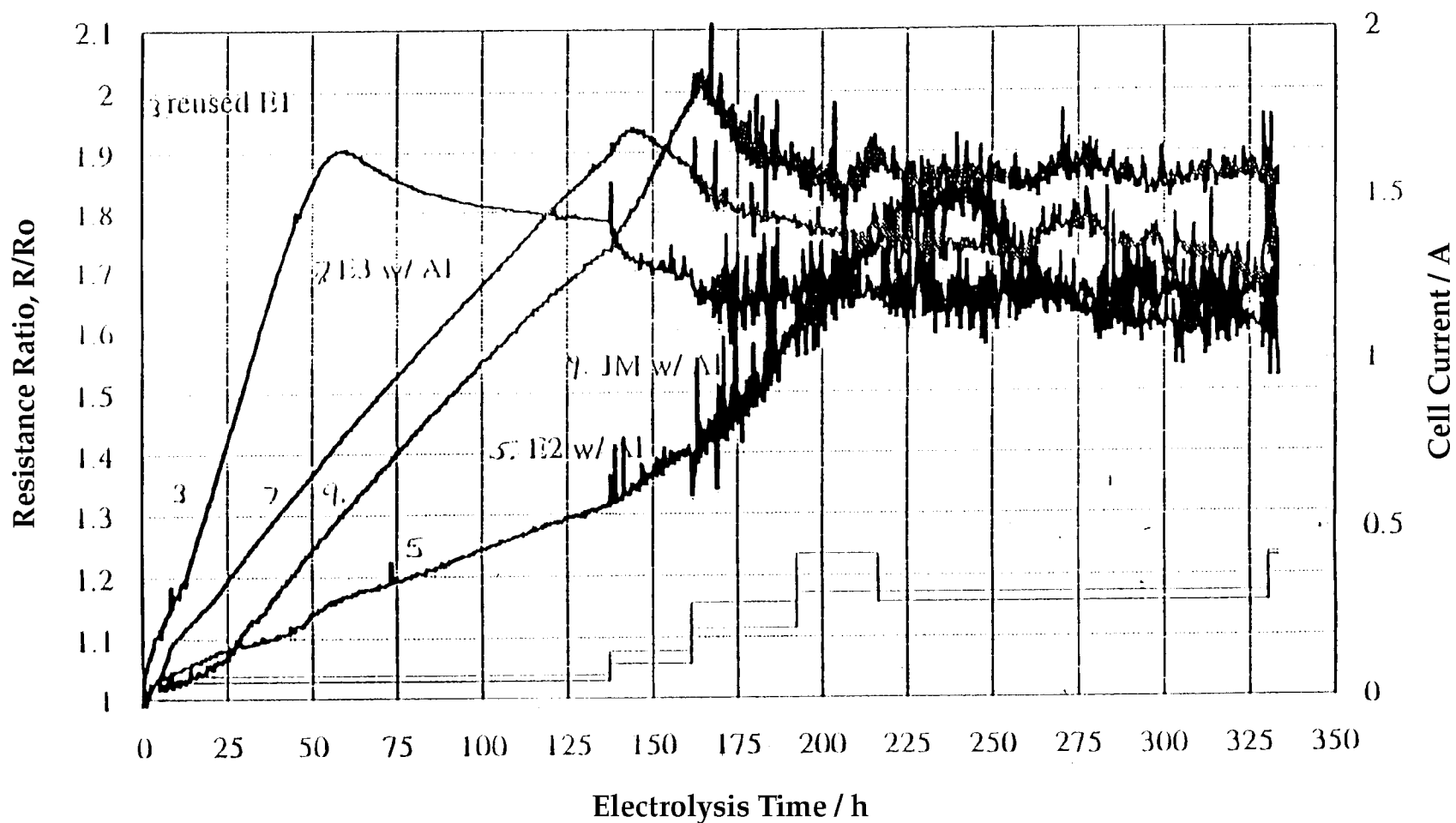
Figure 2-38
DoL Farm I Cells # 3, 5, 7, 9

Reproducibility of Pd

Pd Cathode (0.3 x 3 cm); Pt Anode; 1 M LiOD/D2O; Quartz Cell
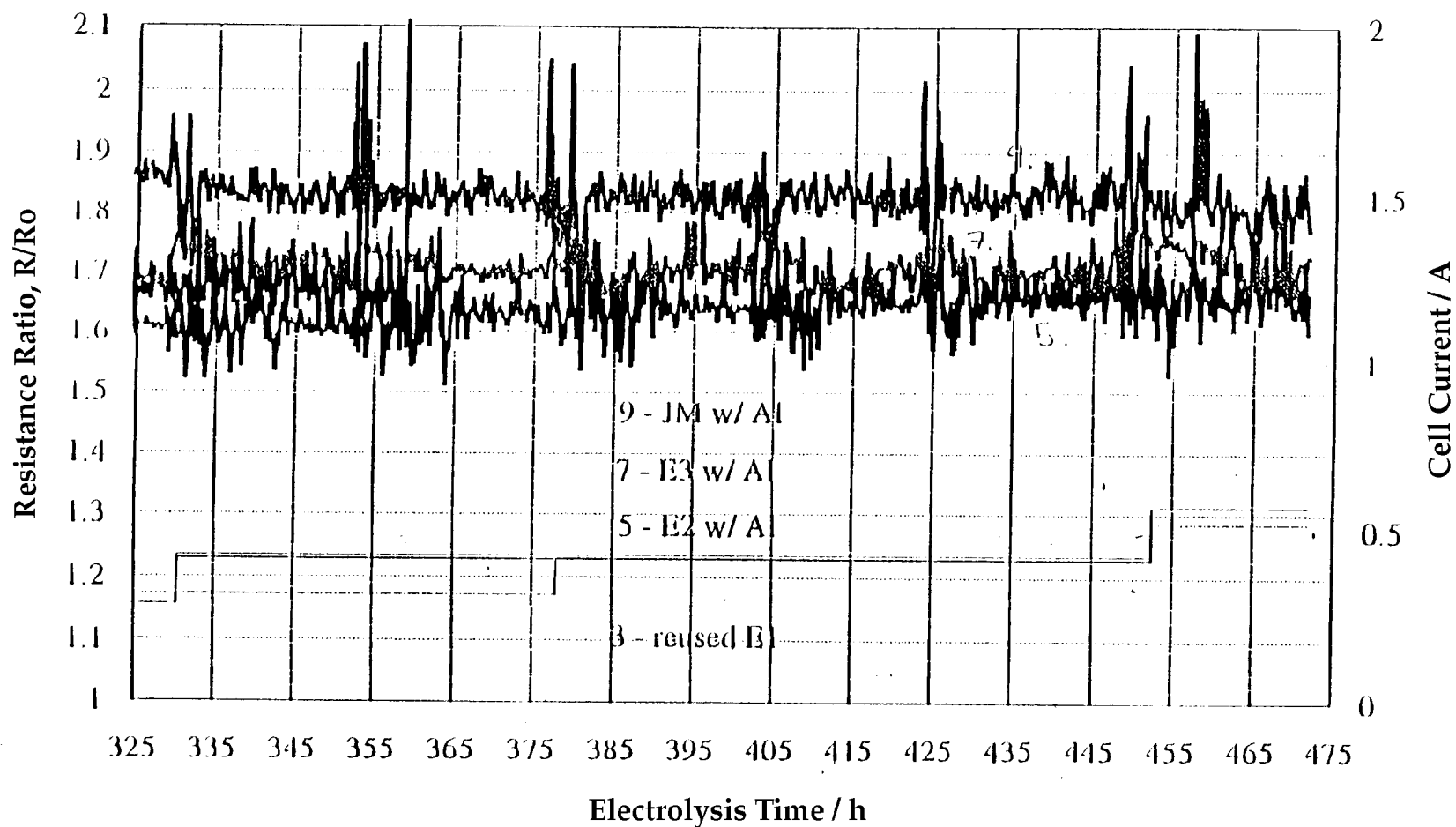
Figure 2-39
DoL Farm I Cells # 3, 5, 7, 9

Reproducibility of Pd

Pd Cathode (0.3 x 3 cm); Pt Anode; 1 M LiOD/D2O; Quartz Cell
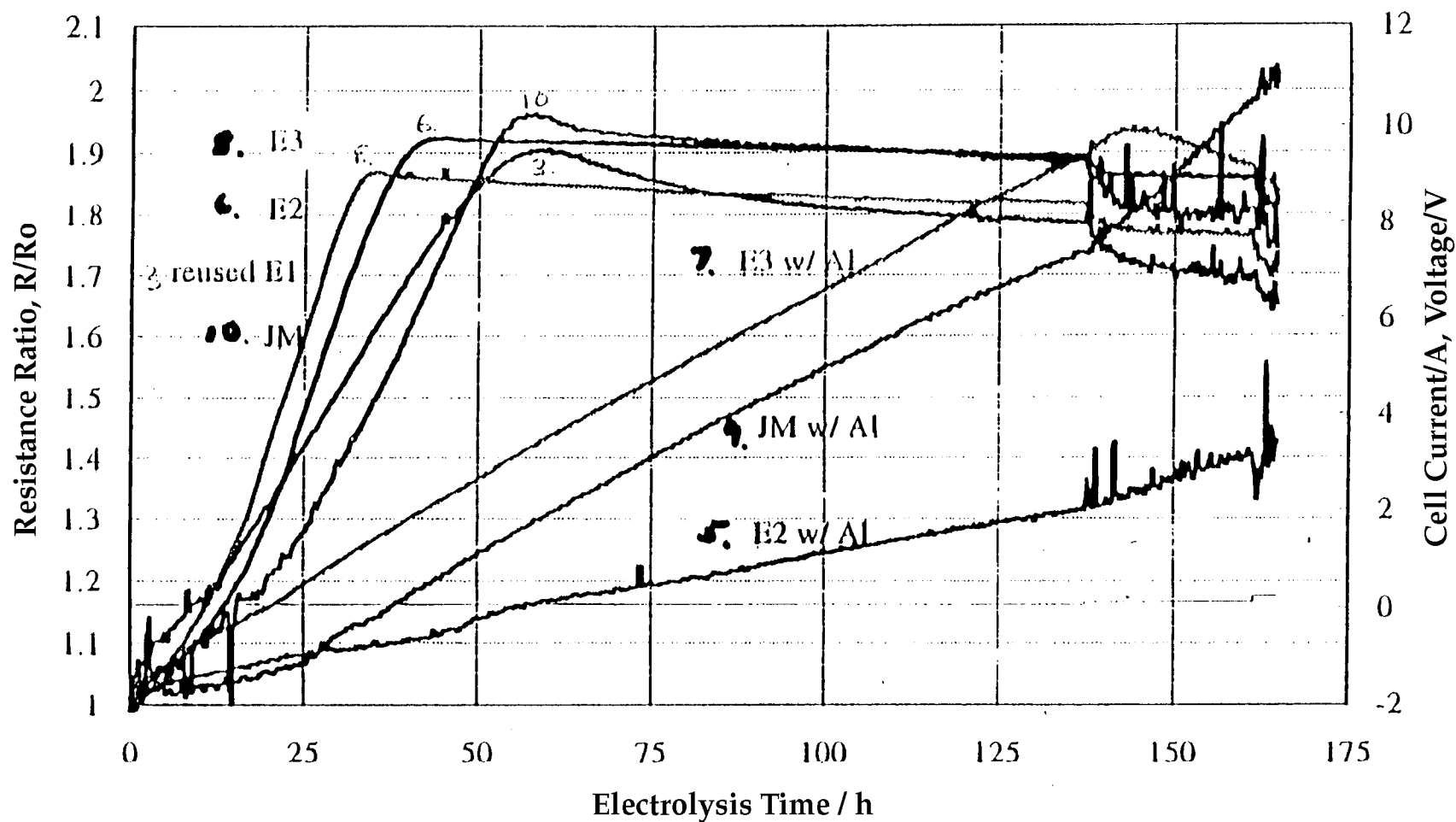
Figure 2-40
DoL Farm I Cells # 3, 5-10

Reproducibility of Pd

Pd Cathode (0.3 x 3 cm); Pt Anode; 1 M LiOD/D2O; Quartz Cell
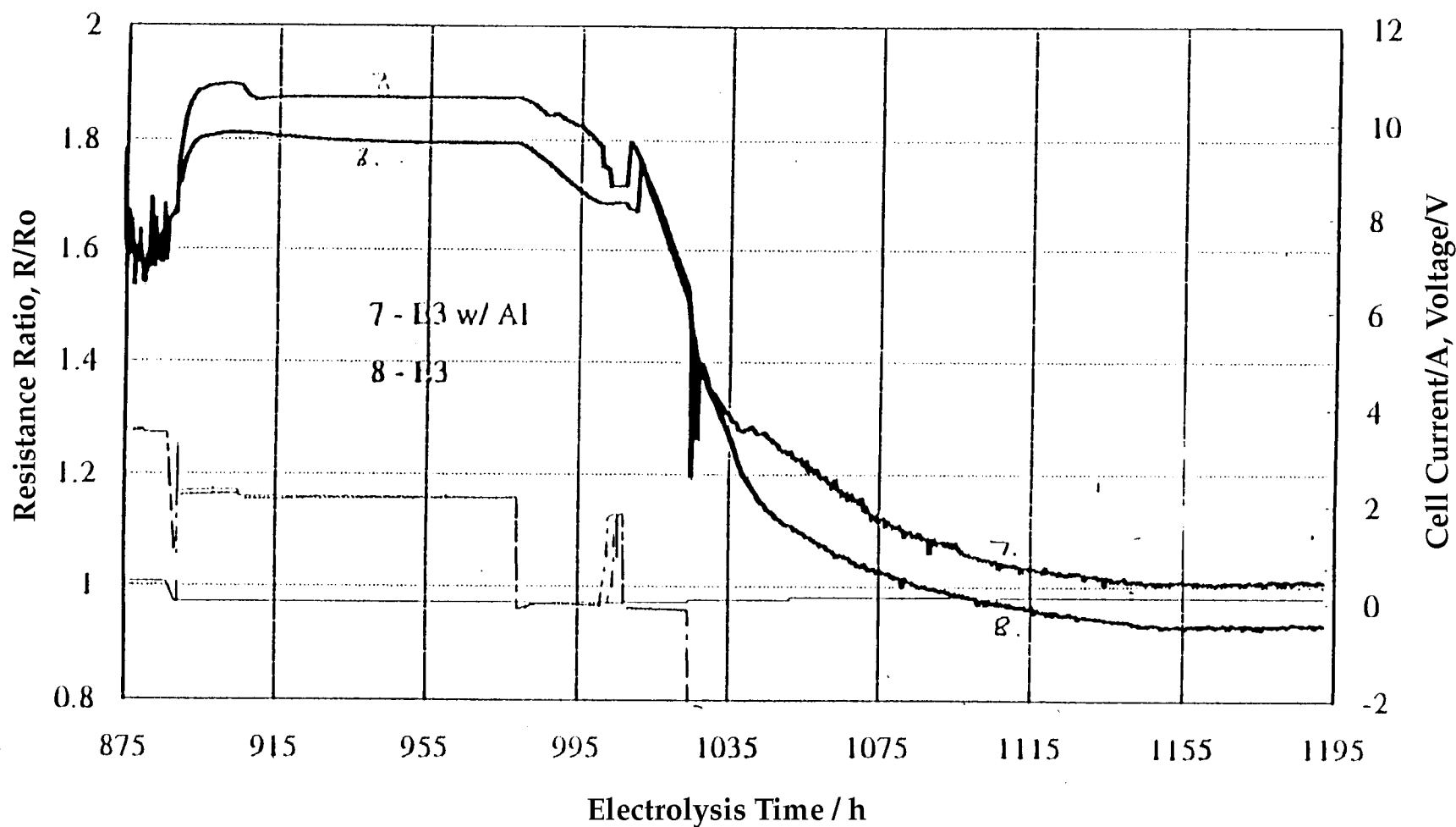
Figure 2-41
DoL Farm I Cells # 7, 8

Effects of Electrode Surface Preparation

Reused E1 Pd Cathode (0.3 x 3 cm); Pt Anode; 1 M LiOD/D2O; Quartz Cell
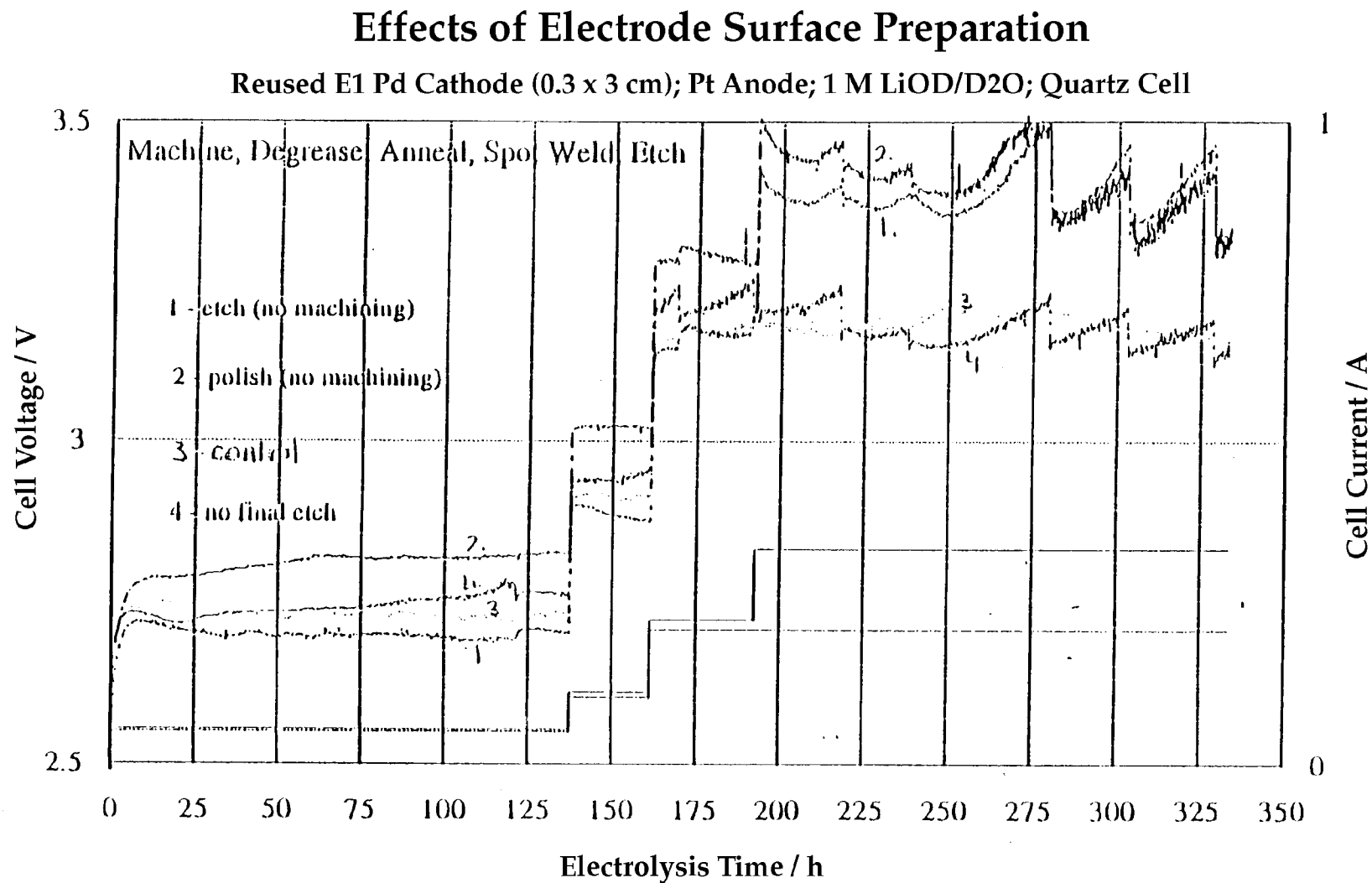
Figure 2-42
DoL Farm I Cells # 1, 2, 3, 4

Effects of Electrode Surface Preparation

Reused E1 Pd Cathode (0.3 x 3 cm); Pt Anode; 1 M LiOD/D2O; Quartz Cell
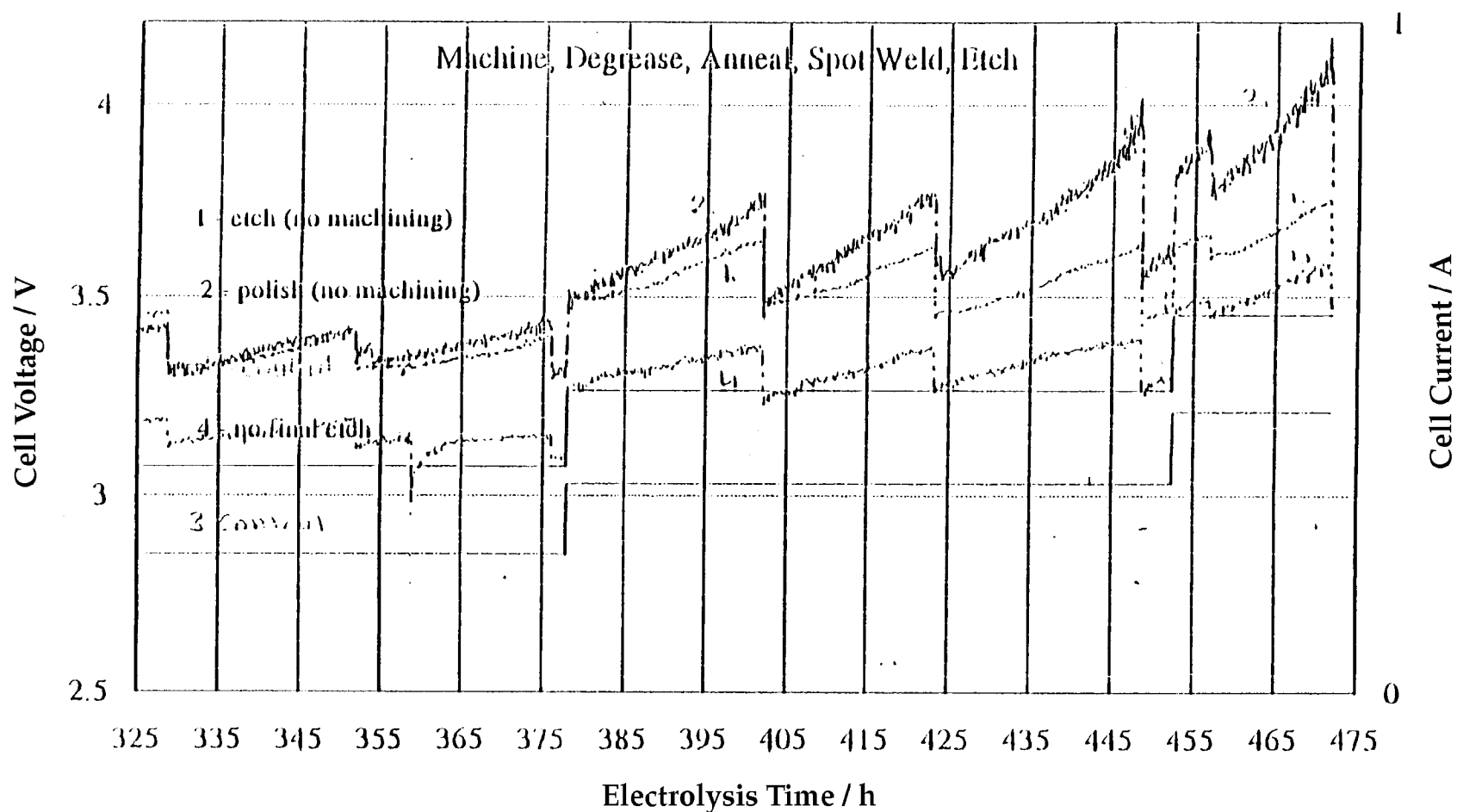
Figure 2-43
DoL Farm I Cells # 1, 2, 3, 4

Effects of Electrode Surface Preparation

Reused E1 Pd Cathode (0.3 x 3 cm); Pt Anode; 1 M LiOD/D2O; Quartz Cell

Machine, Degrease, Anneal, Spot Weld, Etch

1 - etch (no machining)

2 - polish (no machining)

4 - no final etch

Cell Voltage / V

Cell Current / A

Electrolysis Time / h
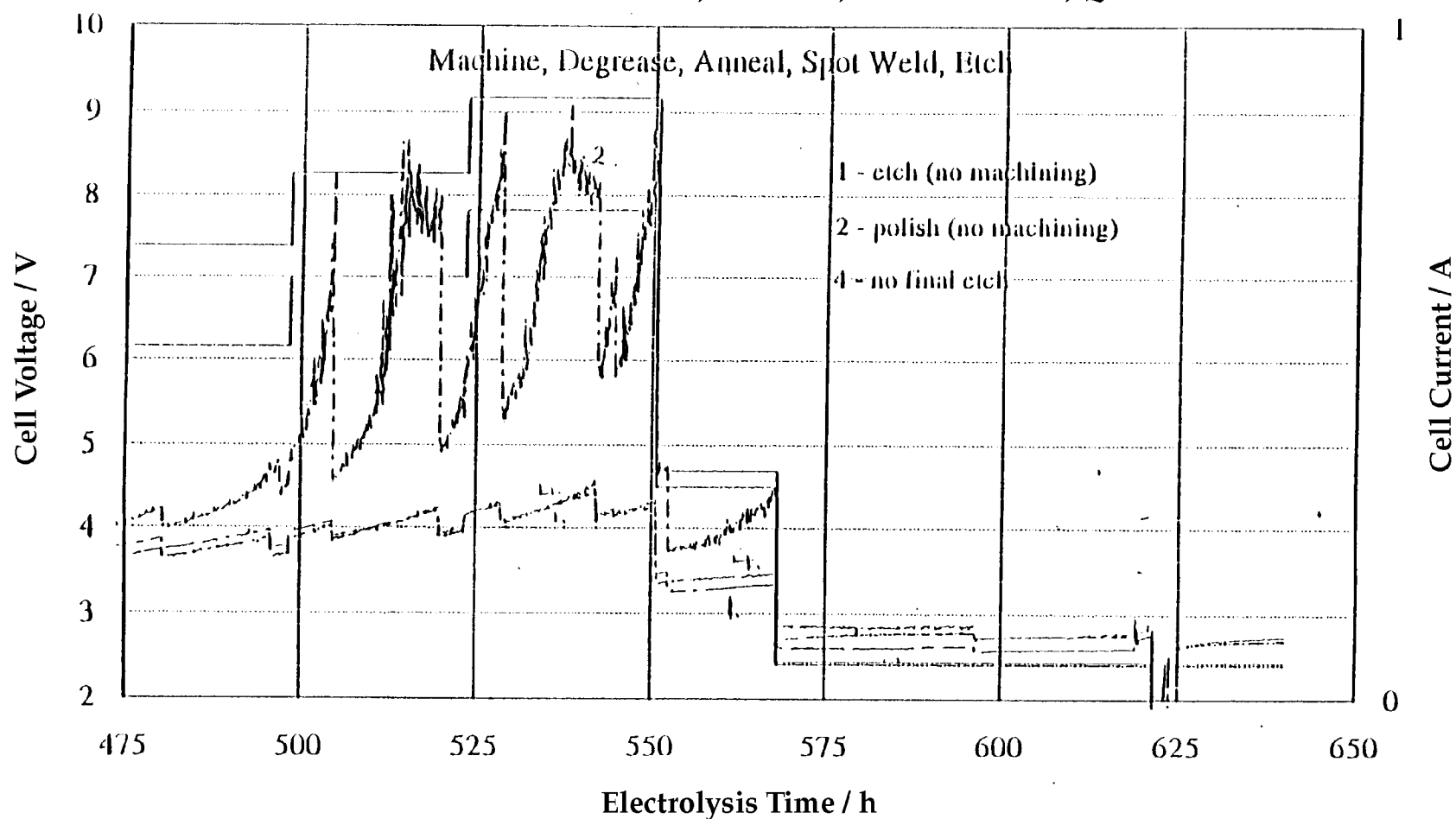
Figure 2-44
DoL Farm I Cells # 1, 2, 4

Effects of Electrode Surface Preparation

Reused E1 Pd Cathode (0.3 x 3 cm); Pt Anode; 1 M LiOD/D2O; Quartz Cell

Machine, Degrease, Anneal, Spot Weld, Etch

1 - etch (no machining)

2 - polish (no machining)

4 - no final etch

Cell Voltage / V

Cell Current / A

Electrolysis Time / h
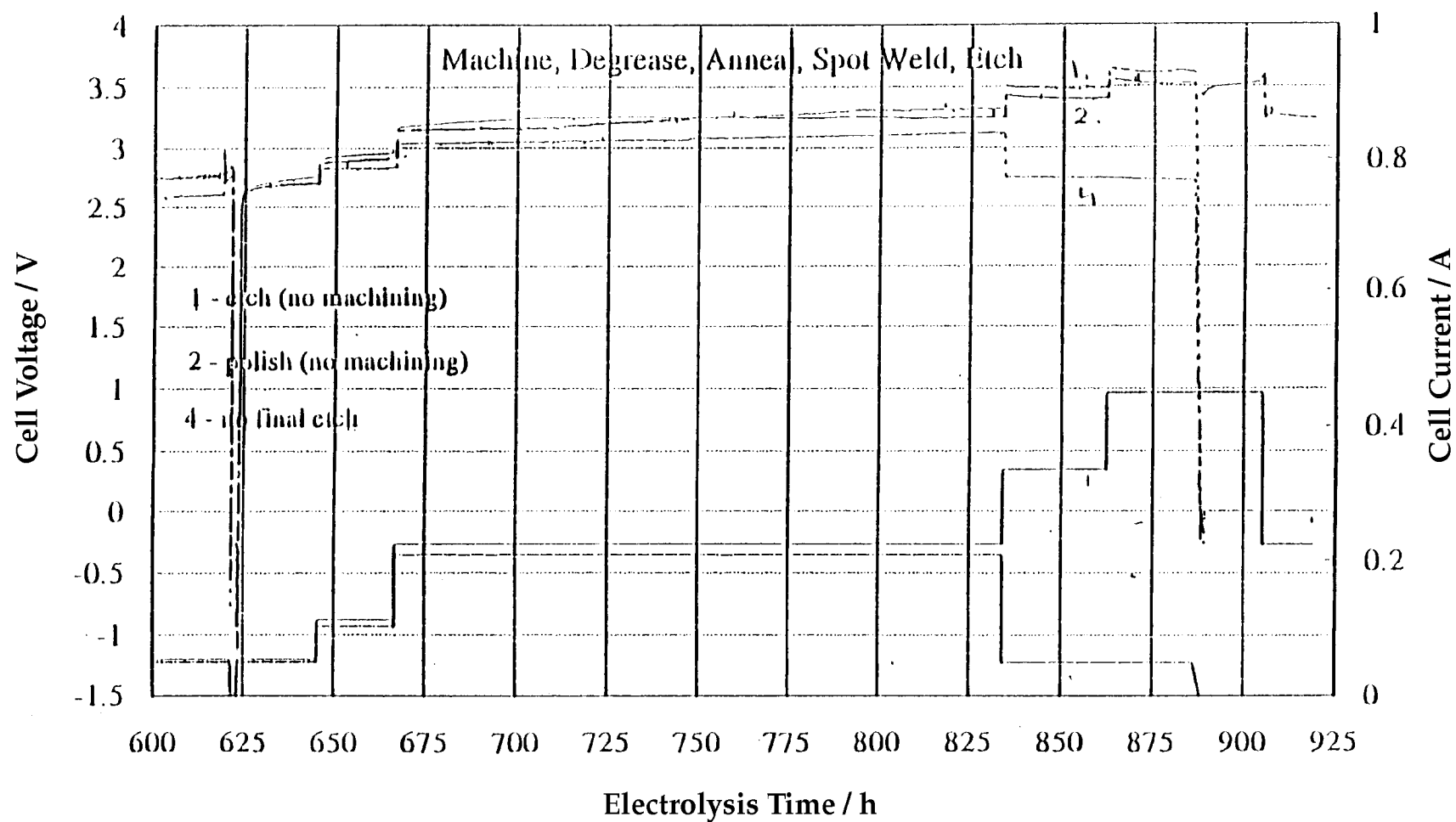
Figure 2-45
DoL Farm I Cells # 1, 2, 4

Reproducibility of Pd

Pd Cathode (0.3 x 3 cm); Pt Anode; 1 M LiOD/D2O; Quartz Cell
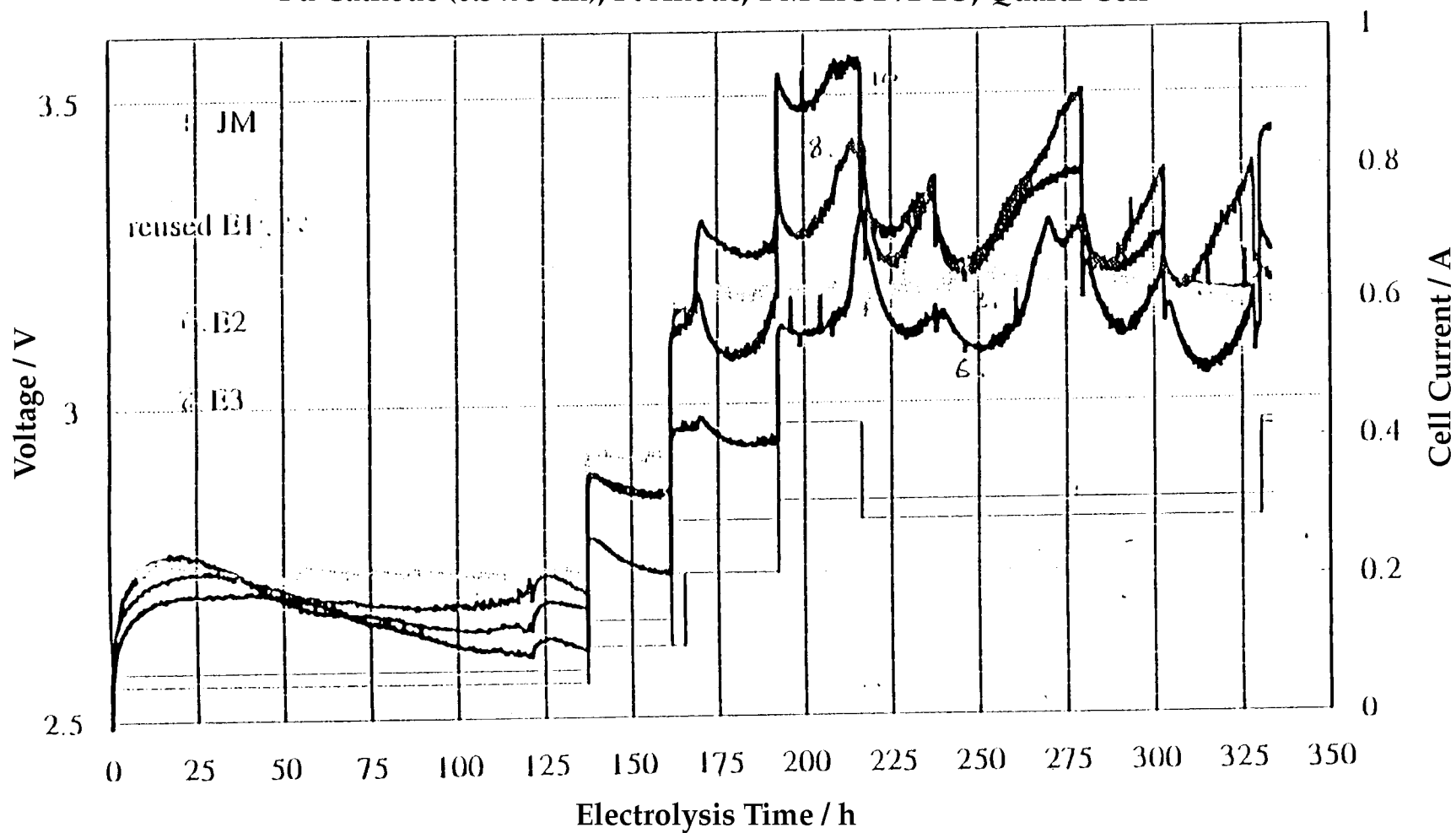
Figure 2-46
DoL Farm I Cells # 3, 6, 8, 10

Reproducibility of Pd

Pd Cathode (0.3 x 3 cm); Pt Anode; 1 M LiOD/D2O; Quartz Cell
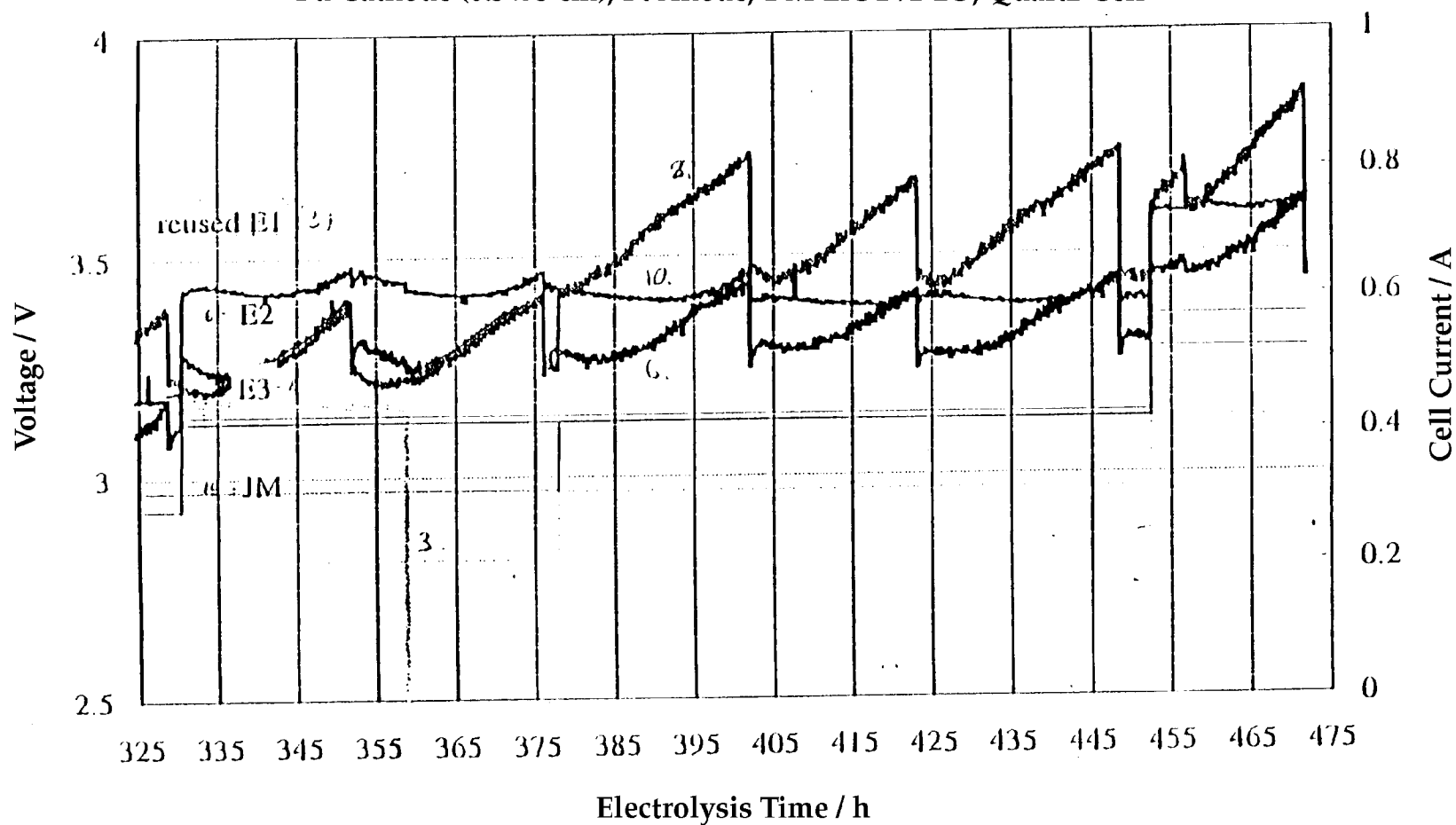
Figure 2-47
DoL Farm I Cells # 3, 6, 8, 10

Reproducibility of Pd

Pd Cathode (0.3 x 3 cm); Pt Anode; 1 M LiOD/D2O; Quartz Cell

6. E2
8. E3
10. JM
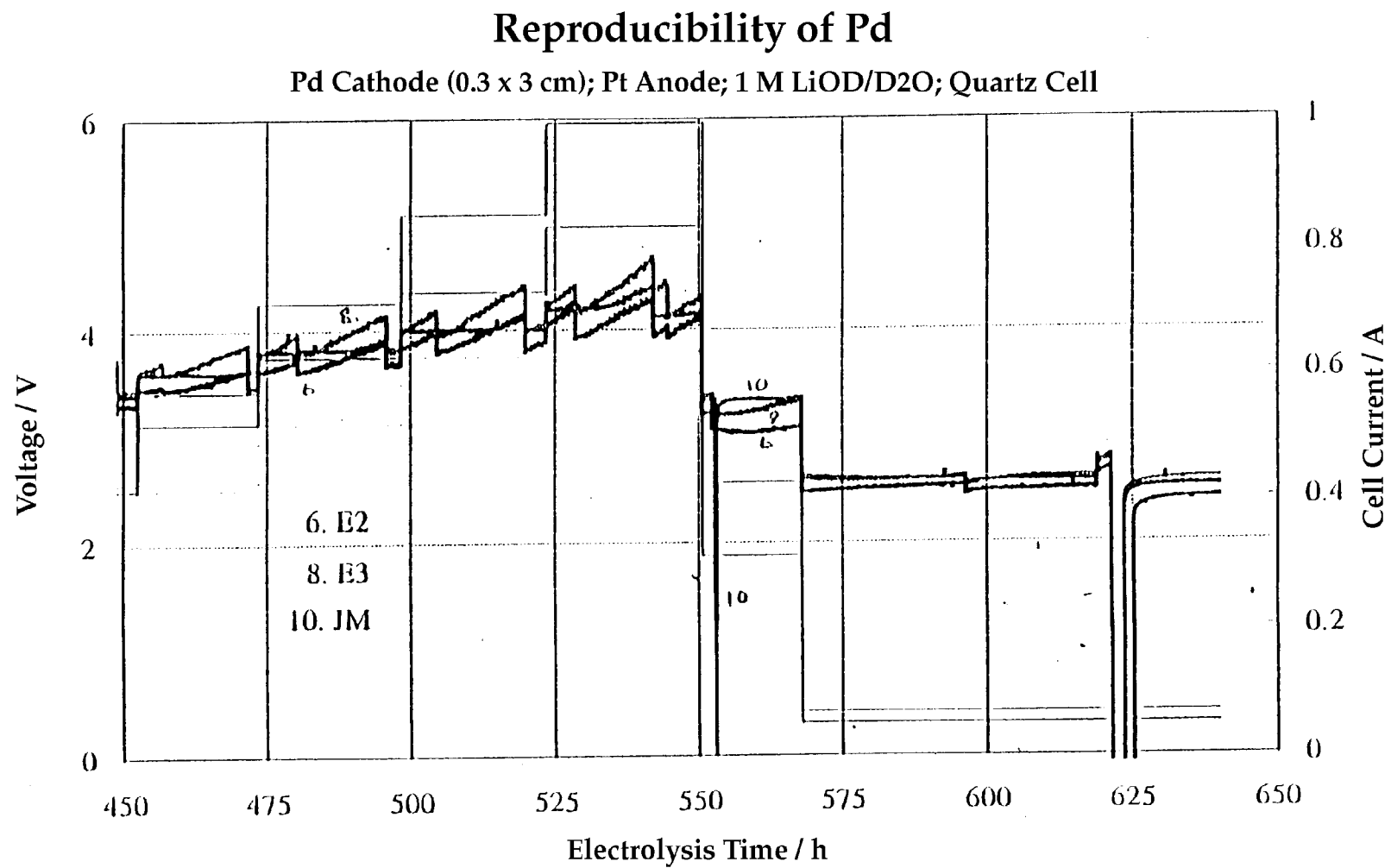
Figure 2-48
DoL Farm I Cells # 6, 8, 10

Reproducibility of Pd

Pd Cathode (0.3 x 3 cm); Pt Anode; 1 M LiOD/D2O; Quartz Cell


6 - E2 w/ Al

8 - E3 w/ Al

10 - JM w/ Al
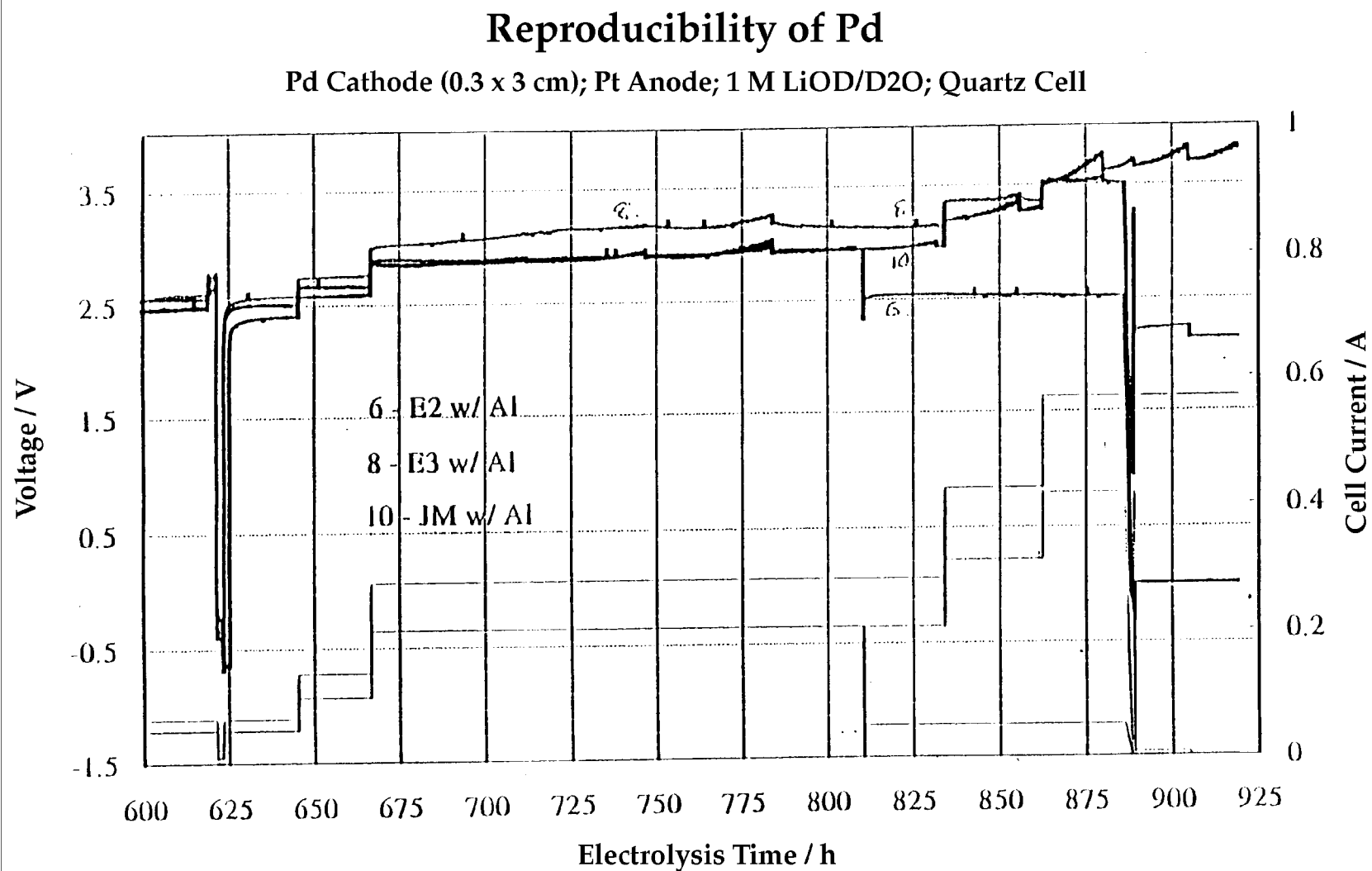
Figure 2-49
DoL Farm I Cells # 6, 8, 10

Reproducibility of Pd

Pd Cathode (0.3 x 3 cm); Pt Anode; 1 M LiOD/D2O; Quartz Cell
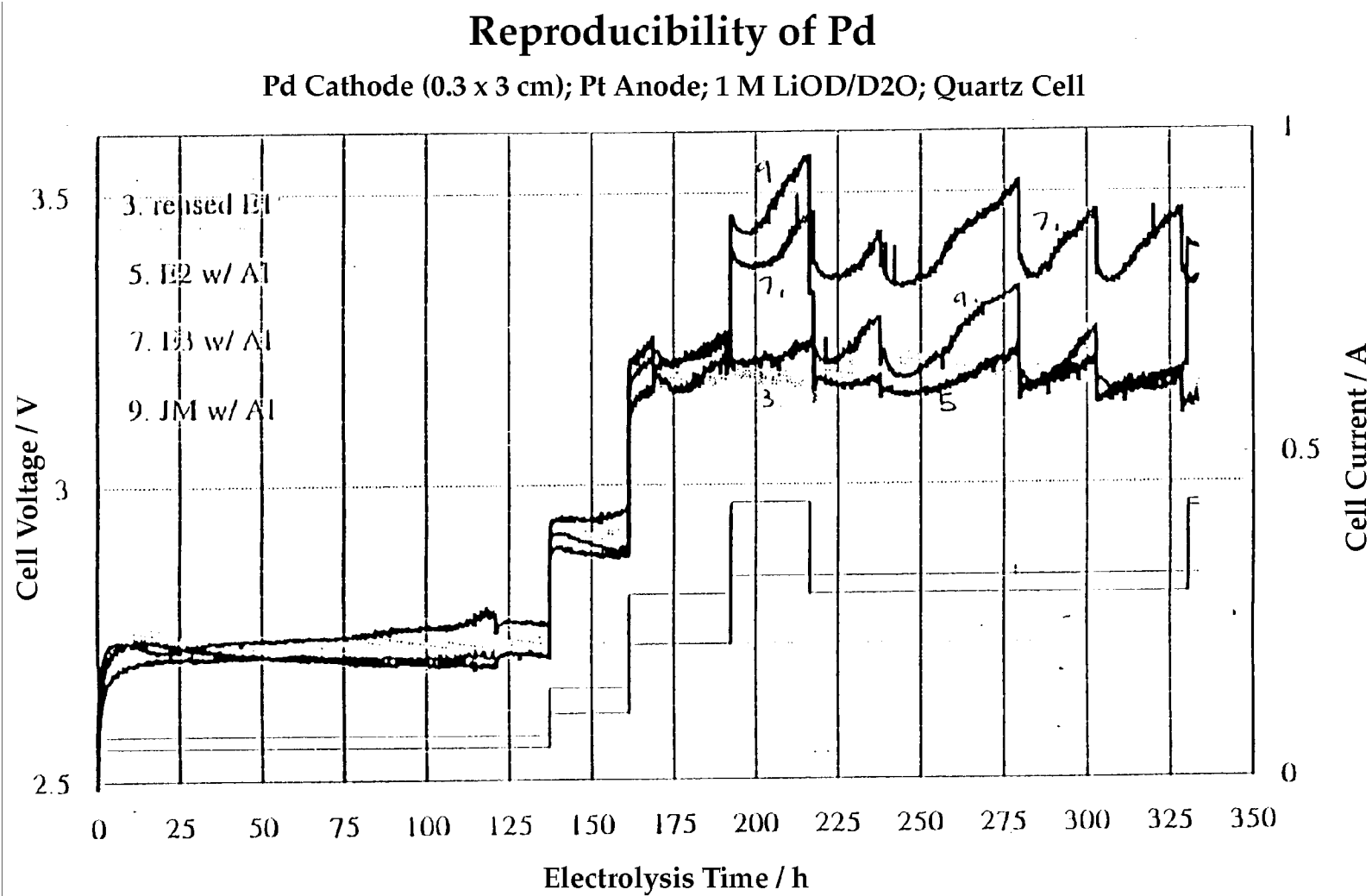
Figure 2-50
DoL Farm I Cells # 3, 5, 7, 9

Reproducibility of Pd

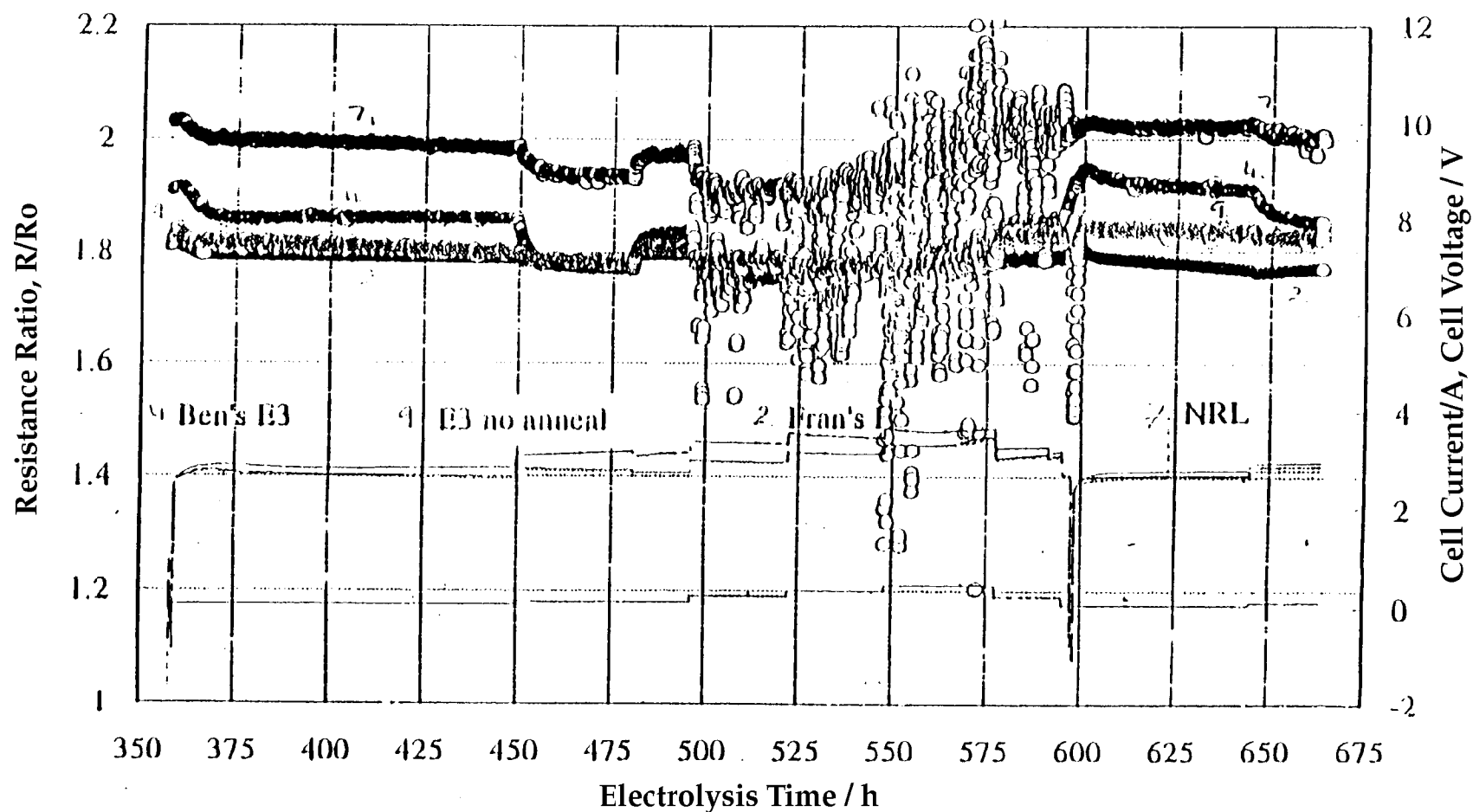## Pd Cathode (0.3 x 3 cm); Pt Anode; 1 M LiOD/D2O; Quartz Cell

5 - E2 w/ Al

7 - E3 w/ Al

9 - JM w/ Al

Electrolysis Time / h
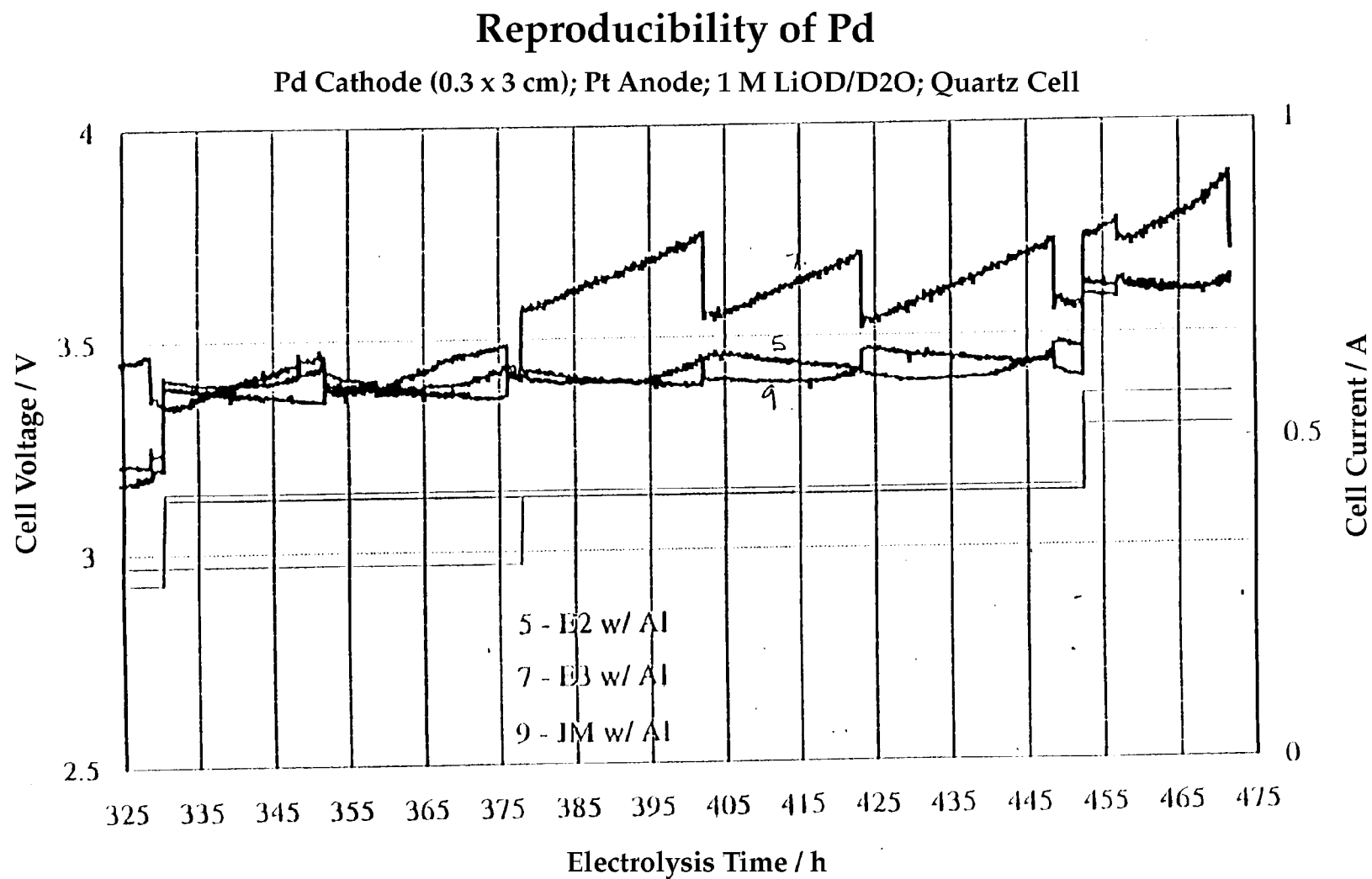
Figure 2-51
DoL Farm I Cells # 5, 7, 9

Reproducibility of Pd

Pd Cathode (0.3 x 3 cm); Pt Anode; 1 M LiOD/D2O; Quartz Cell

5 — E2 w/ Al
7 — E3 w/ Al
9 — JM w/ Al
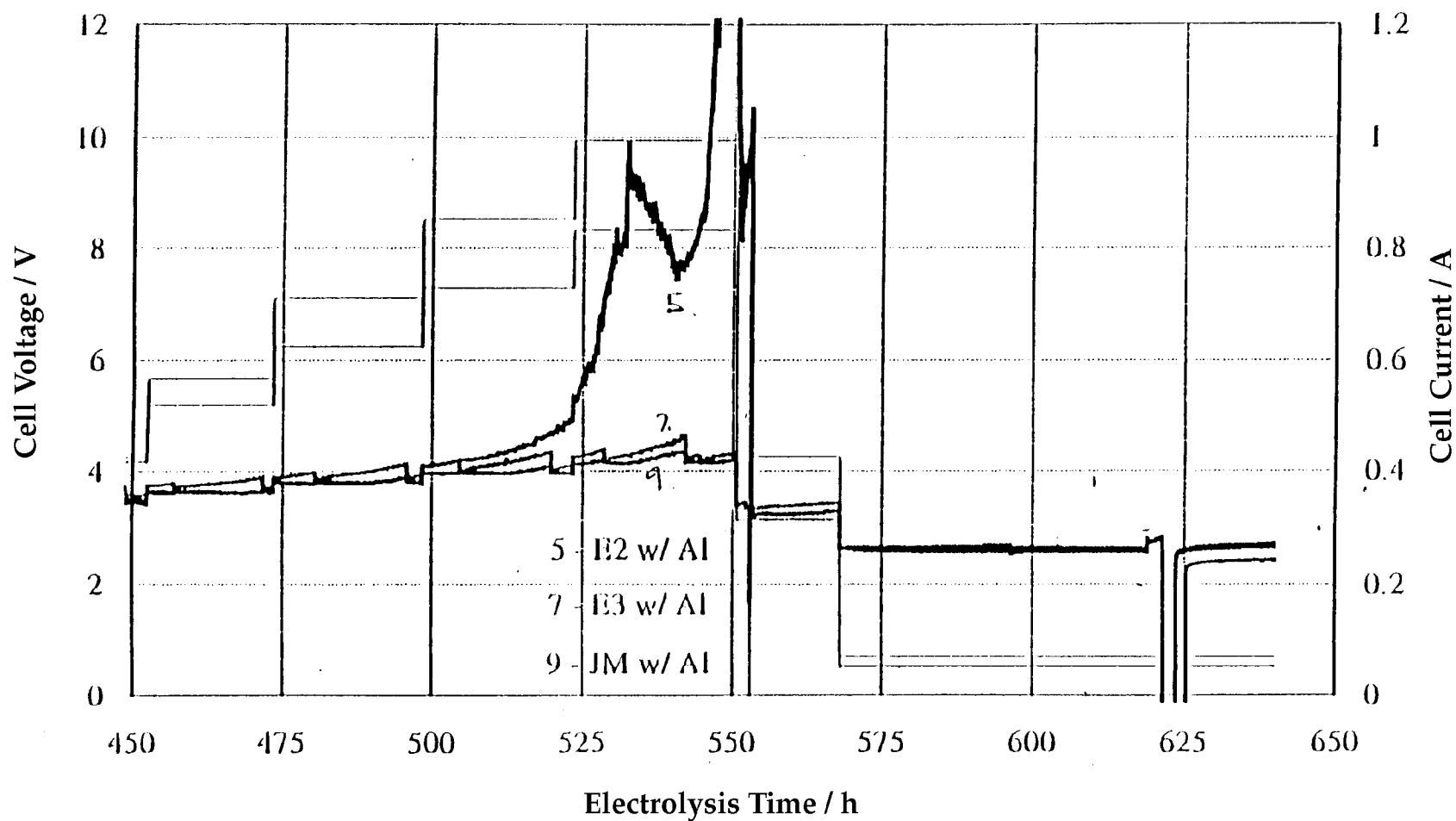
Figure 2-52
DoL Farm I Cells # 5, 7, 9
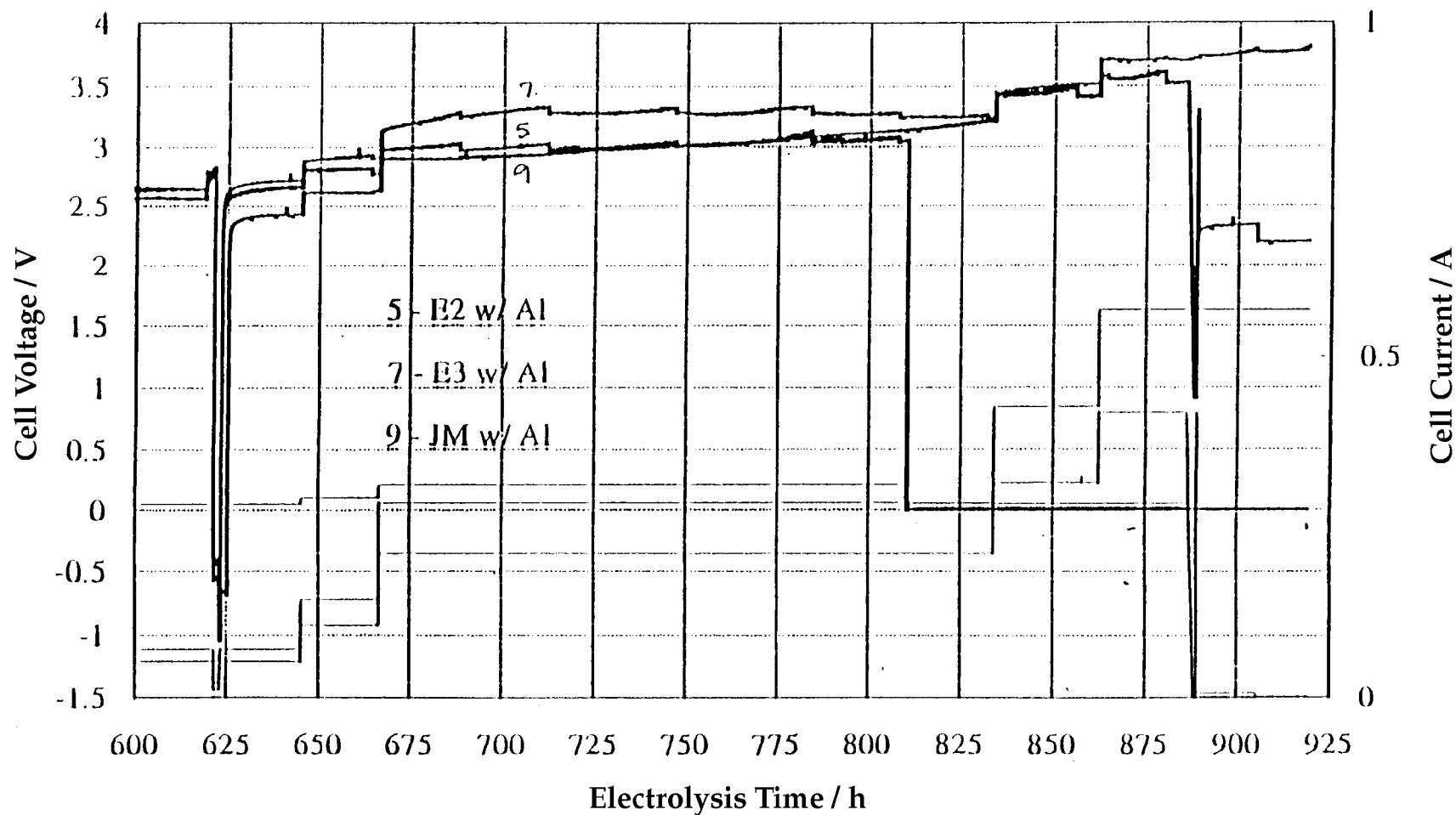
Figure 2-53
DoL Farm I Cells # 5, 7, 9

Reproducibility of Pd

Pd Cathode (0.3 x 3 cm); Pt Anode; 1 M LiOD/D2O; Quartz Cell
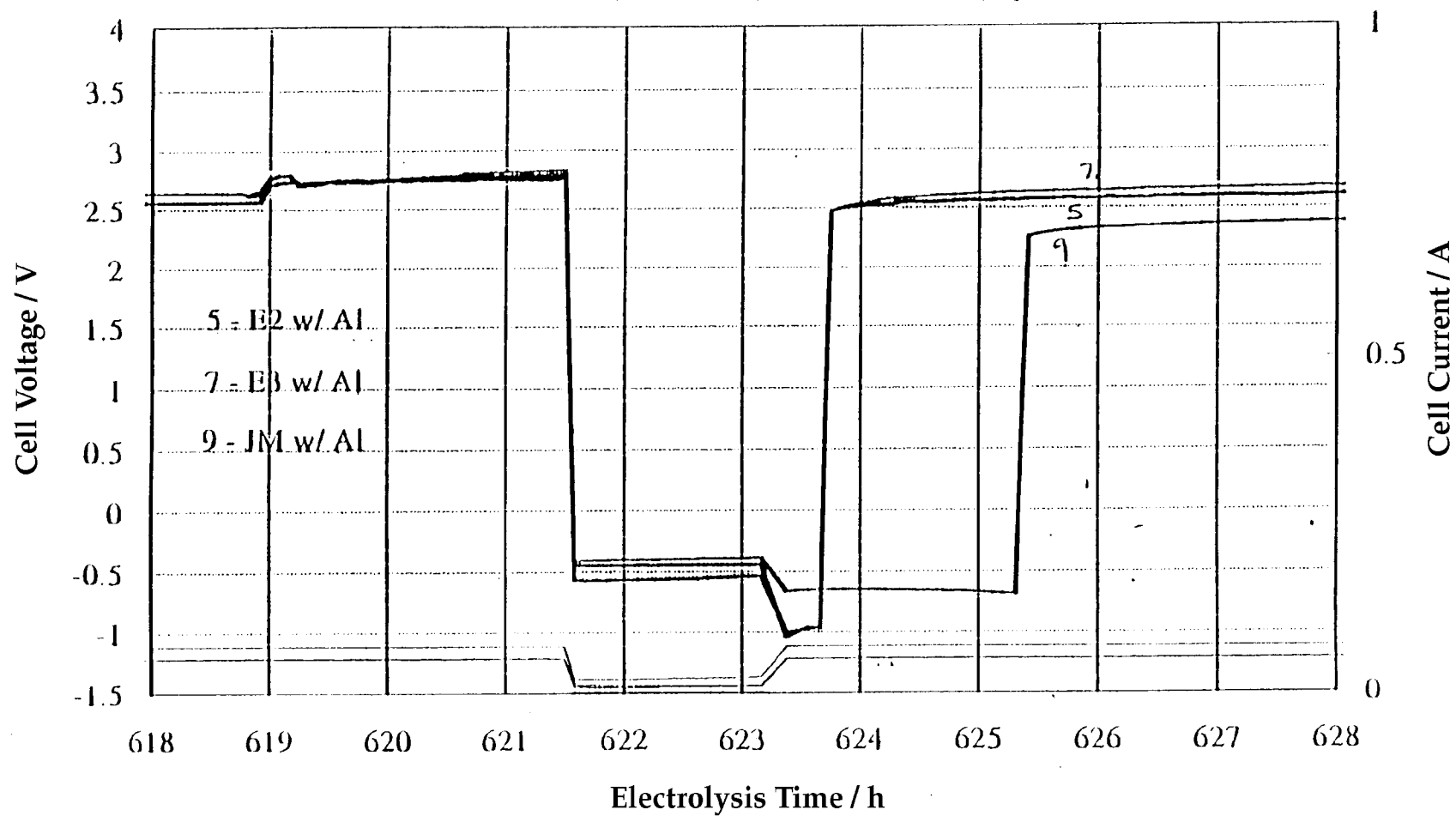
Figure 2-54
DoL Farm I Cells # 5, 7, 9

Reproducibility of Pd

JM Cathode (0.2 x 3.8 cm); IB Pd Cathode (0.3 x 3.8cm); Pt Anode; 1 M LiOD/D2O; Quartz Cell
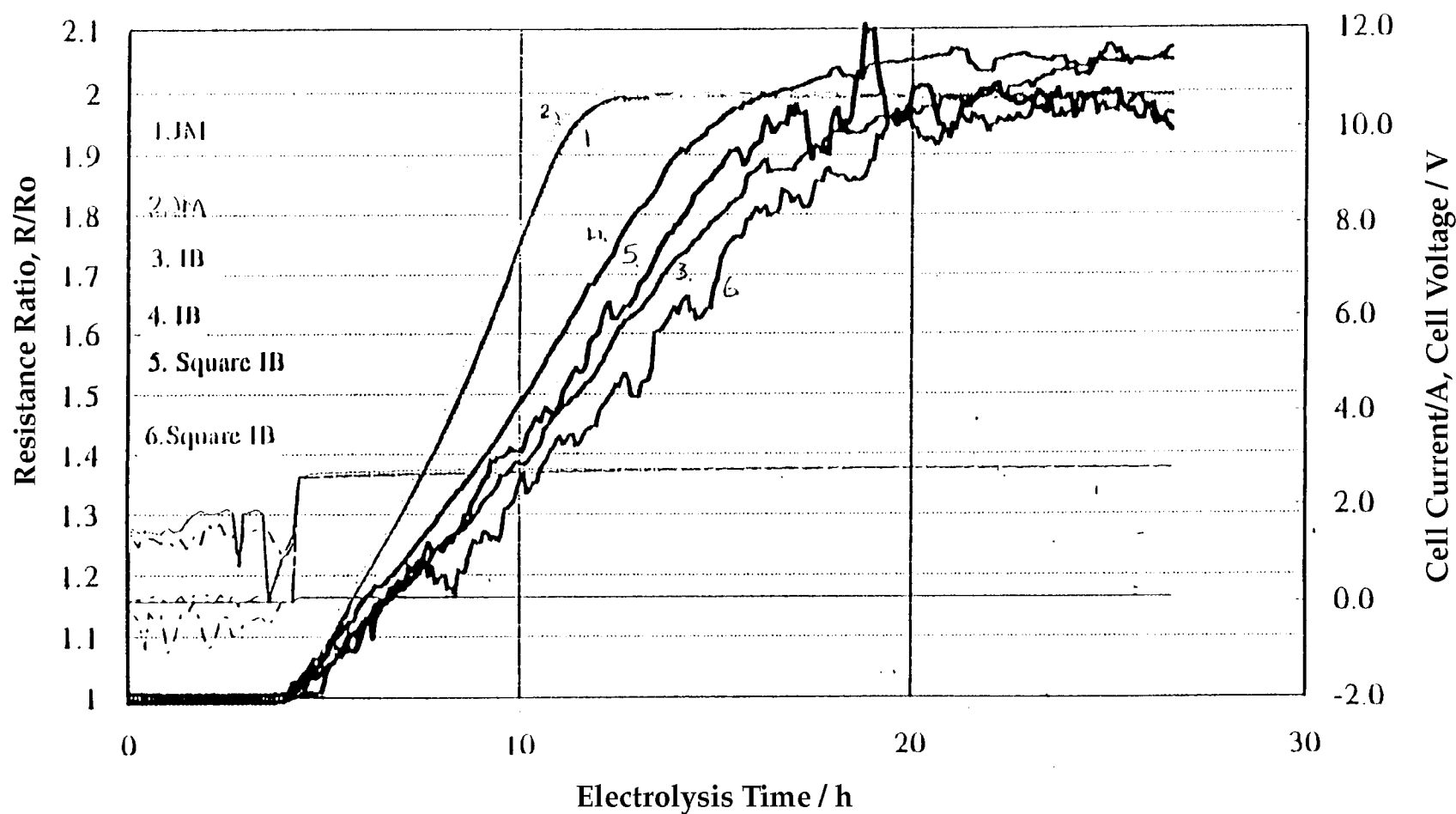
Figure 2-55
DoL Farm J Cells # 1-6

Reproducibility of Pd

JM Cathode (0.2 x 3.8 cm); IB Pd Cathode (0.3 x 3.8cm); Pt Anode; 1 M LiOD/D2O; Quartz Cell
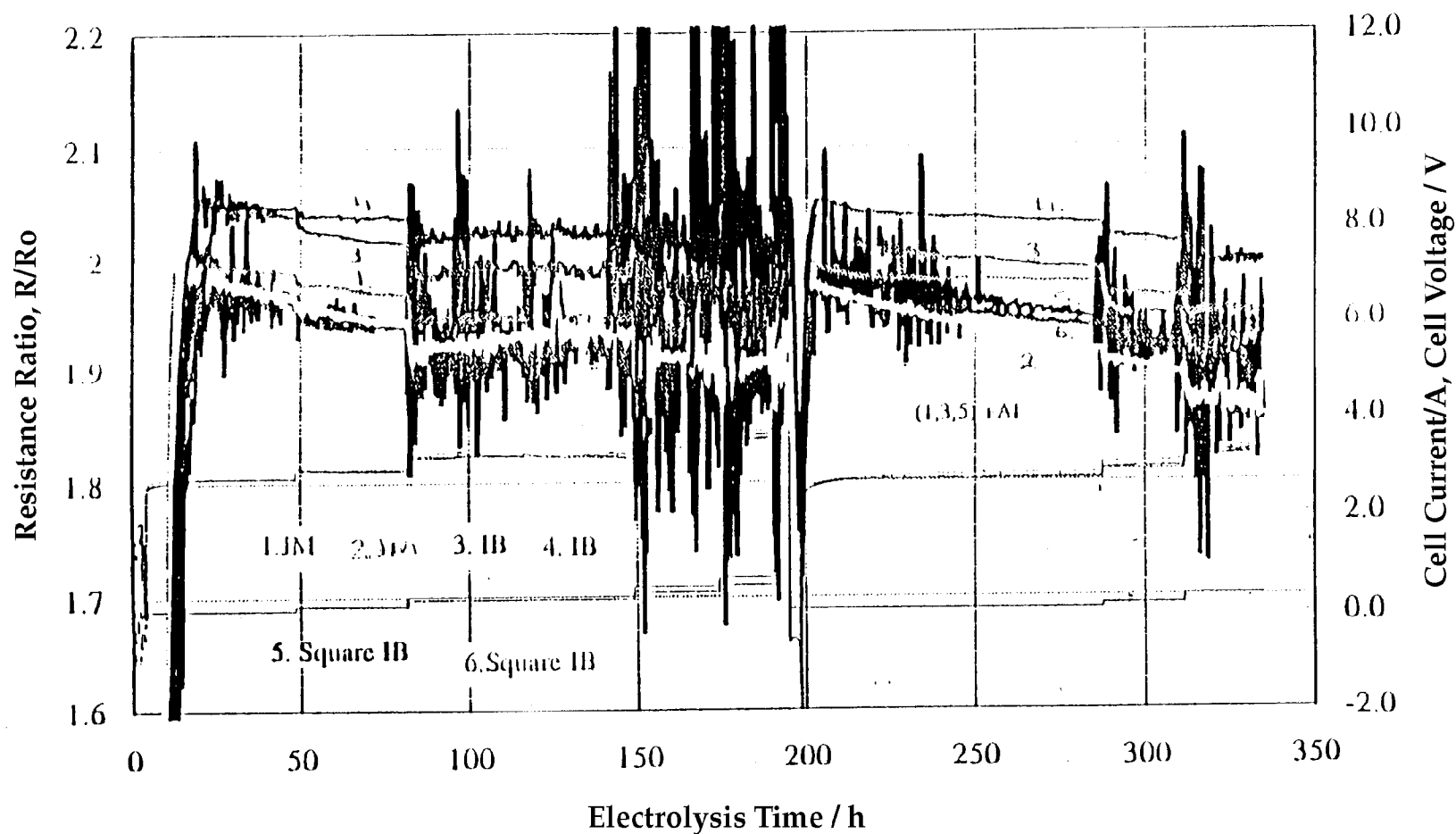
Figure 2-56
DoL Farm J Cells # 1-6

Reproducibility of Pd

Englehard #4 Cathode (0.3 x 3 cm); Pt Anode; 1 M LiOD/D2O; Quartz Cell
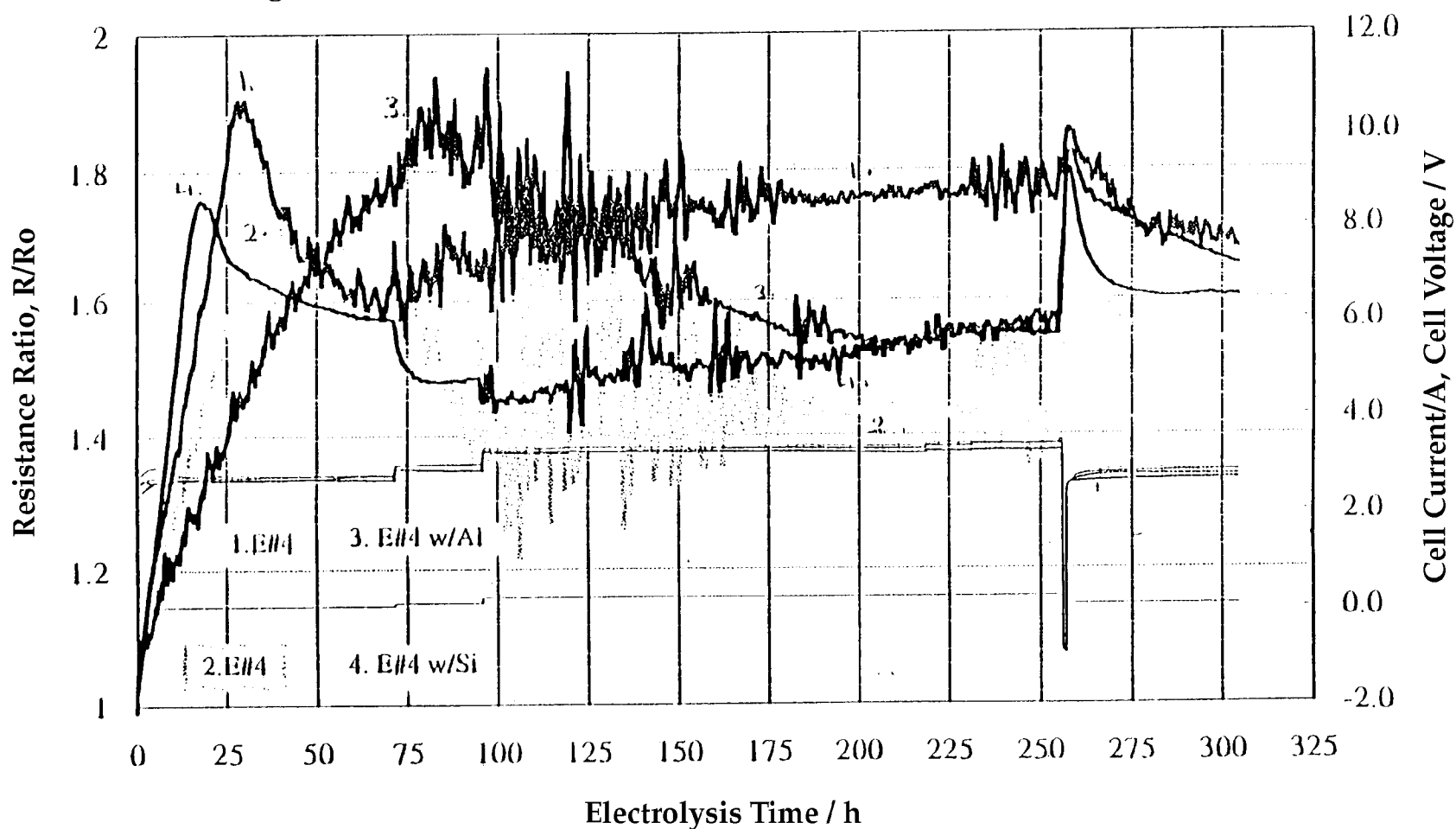
Figure 2-57
DoL Farm K Cells # 1-4

Reproducibility of Pd

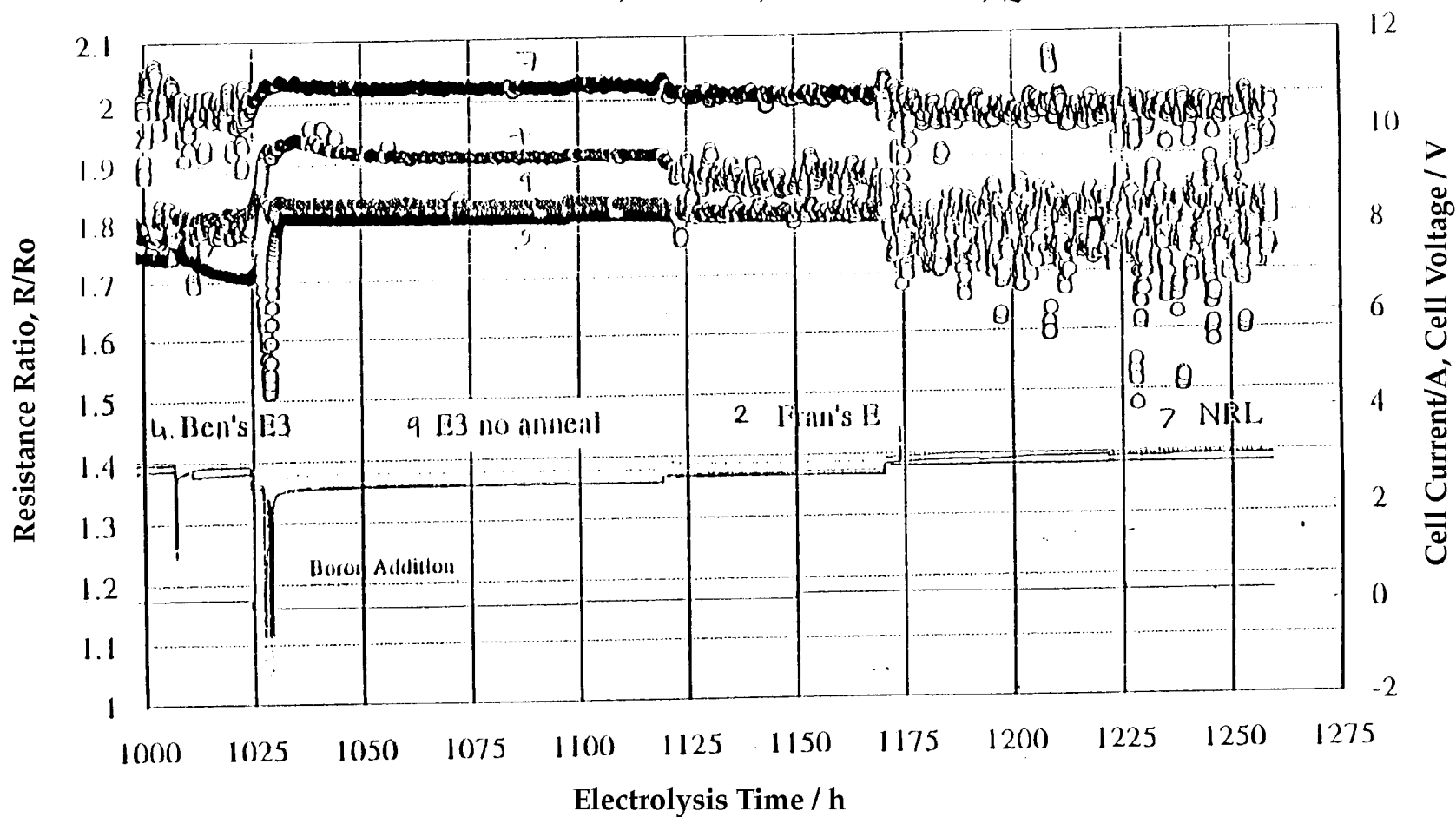## Englehard #4 Cathode (0.3 x 3 cm); Pt Anode; 1 M LiOD/D2O; Quartz Cell

Electrolysis Time / h
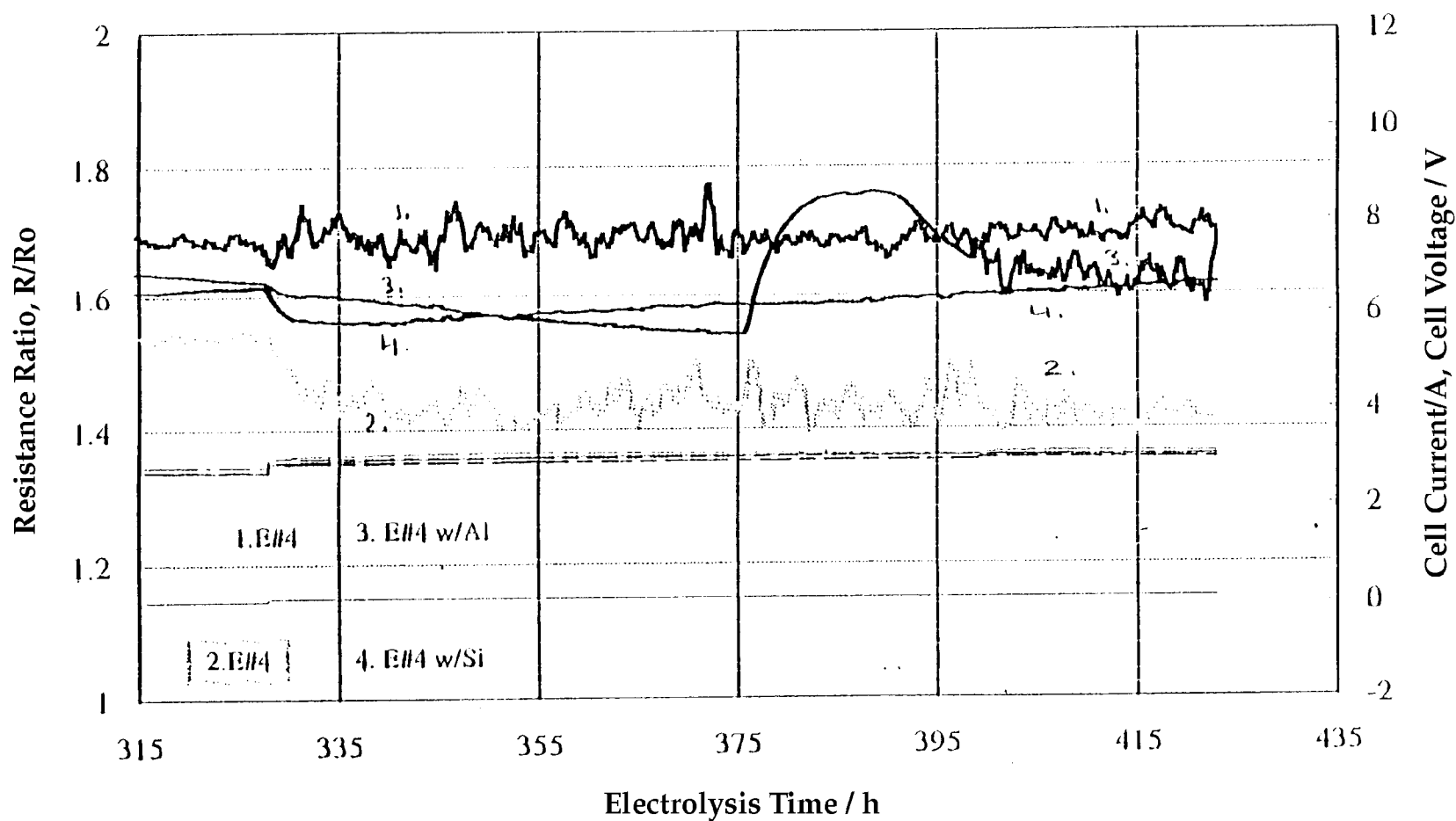
Figure 2-58
DoL Farm K Cells # 1-4

Reproducibility of Pd

Used E1 Pd Cathode (0.28 x 3 cm); Pt Anode; 1 M LiOD/D2O; Quartz Cell
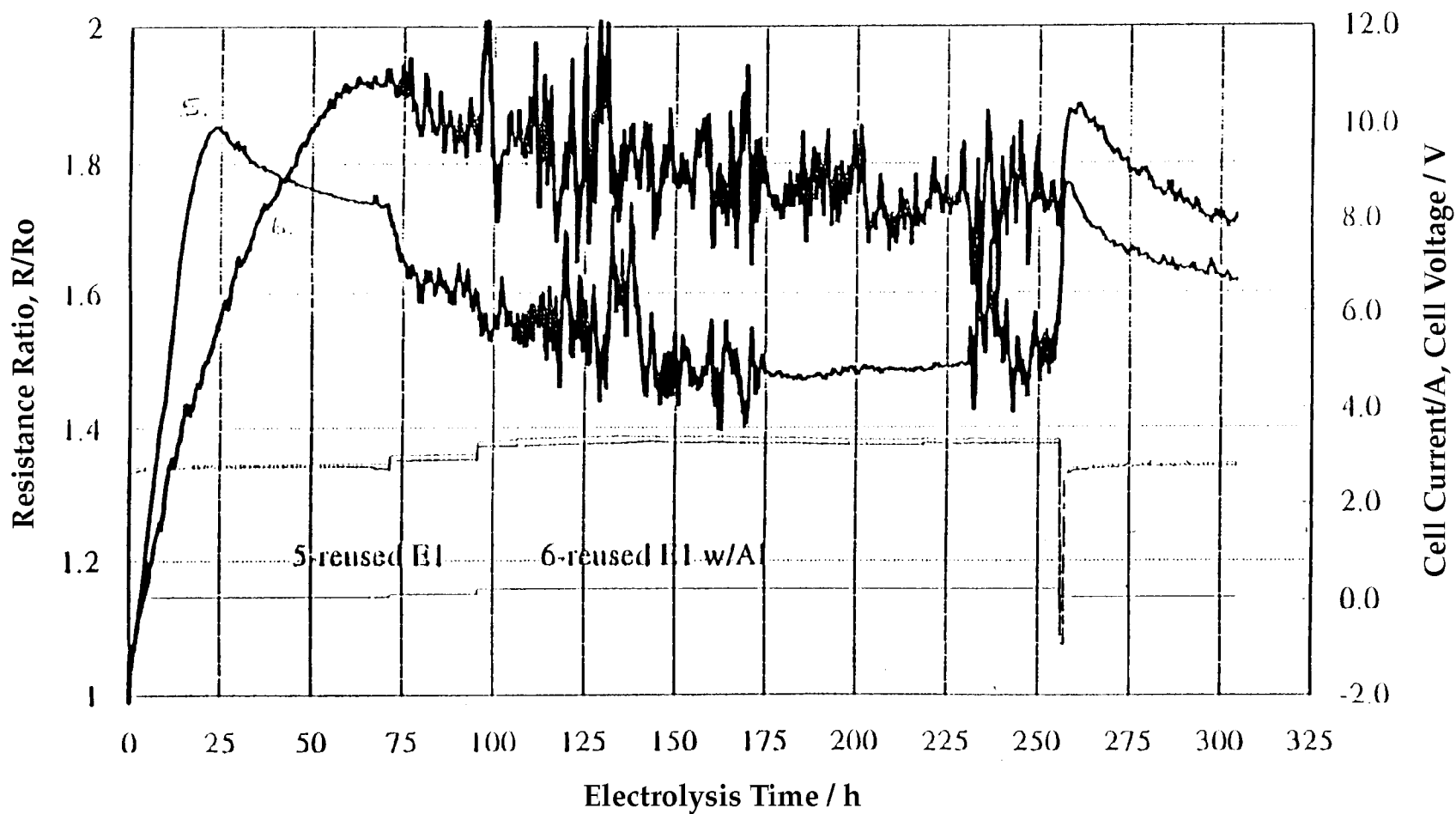
Figure 2-59
DoL Farm K Cells # 5, 6

Reproducibility of Pd

Used E1 Pd Cathode (0.28 x 3 cm); Pt Anode; 1 M LiOD/D2O; Quartz Cell
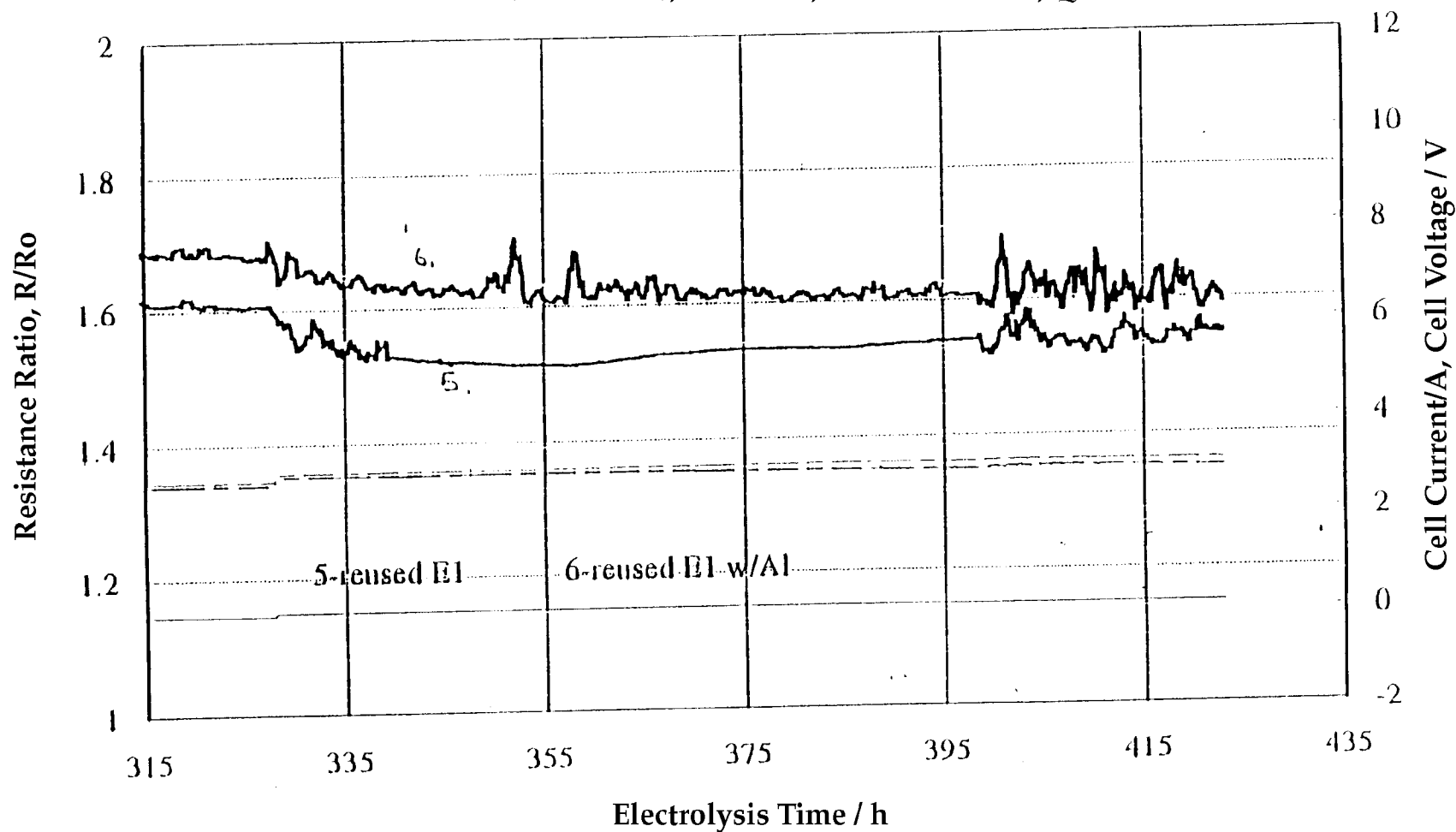
Figure 2-60
DoL Farm K Cells # 5, 6

Reproducibility of Pd

Used E1 Pd Cathode (0.28 x 3 cm); Pt Anode; 1 M LiOD/D2O; Quartz Cell
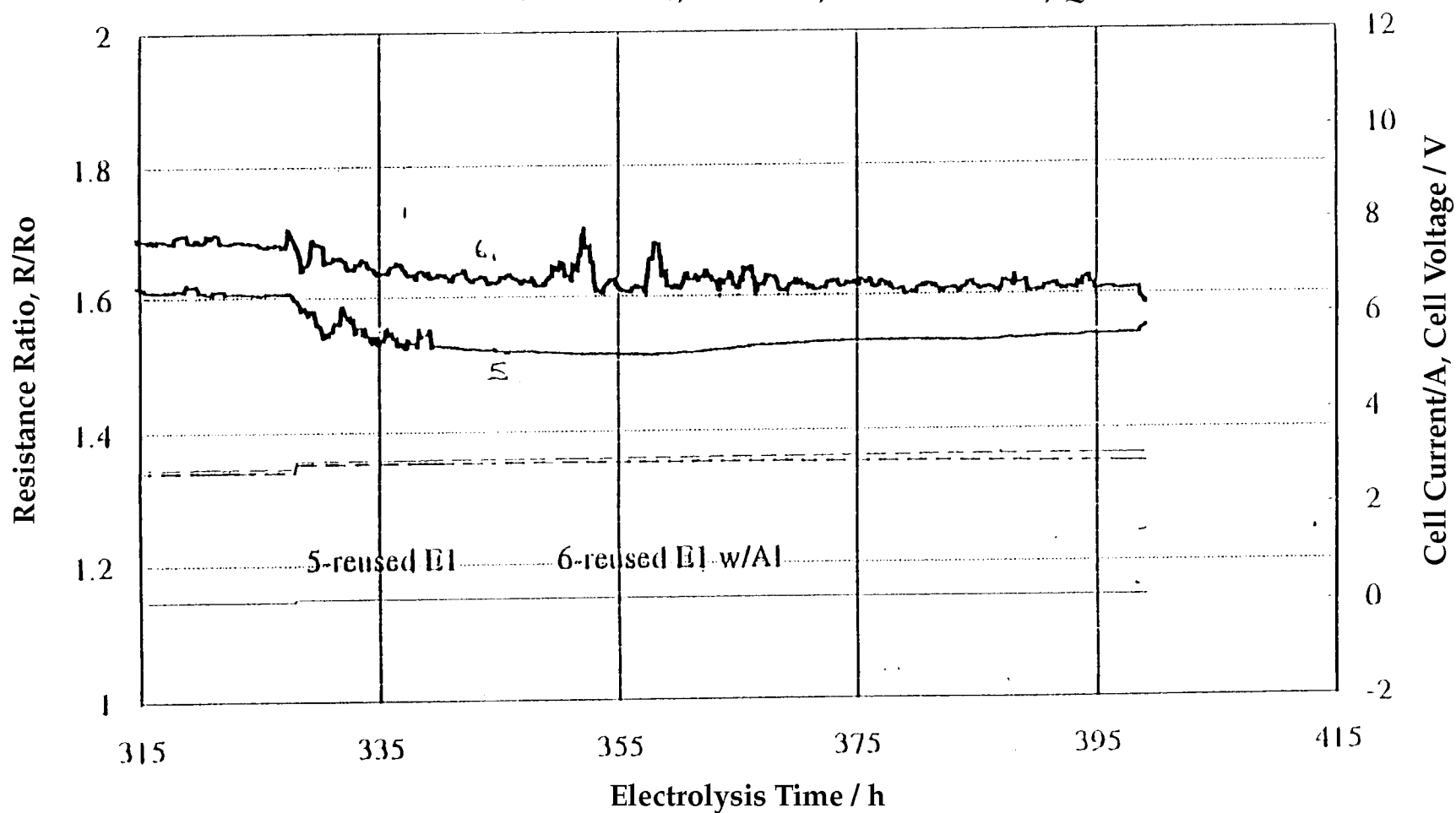
Figure 2-61
DoL Farm K Cells # 5, 6

Reproducibility of Pd

JM Pd Cathode (0.2 x 3 cm) or (0.1 x 3 cm); Pt Anode; 1 M LiOD/D2O; Quartz Cell
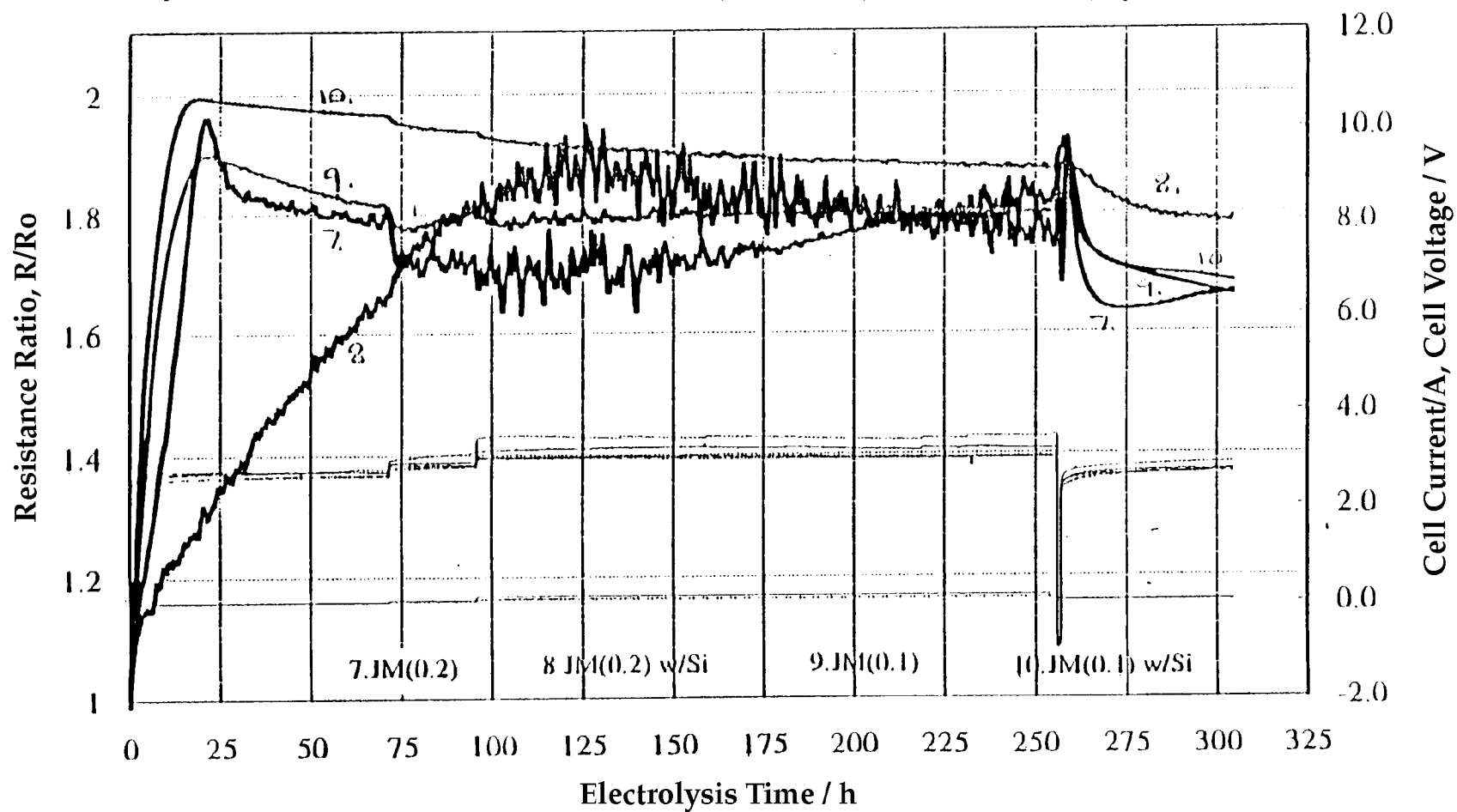
Figure 2-62
DoL Farm K Cells # 7-10

Reproducibility of Pd

JM Pd Cathode (0.2 x 3 cm) or (0.1 x 3 cm); Pt Anode; 1 M LiOD/D2O; Quartz Cell
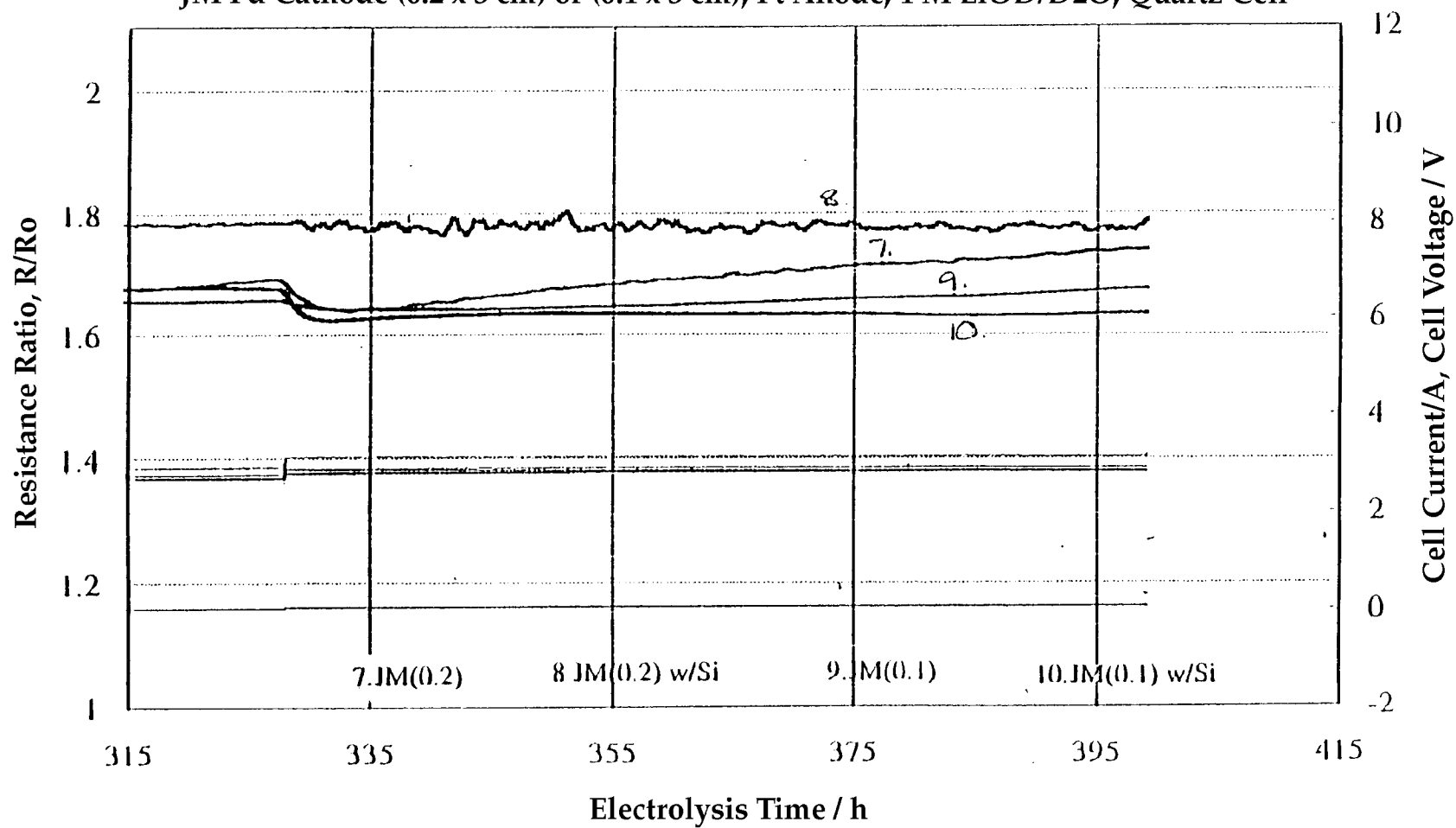
Figure 2-63
DoL Farm K Cells # 7-10

Reproducibility of Pd

Engelhard #1 Cathode (0.3 x 3 cm); Pt Anode; 1 M LiOD/D2O; Quartz Cell
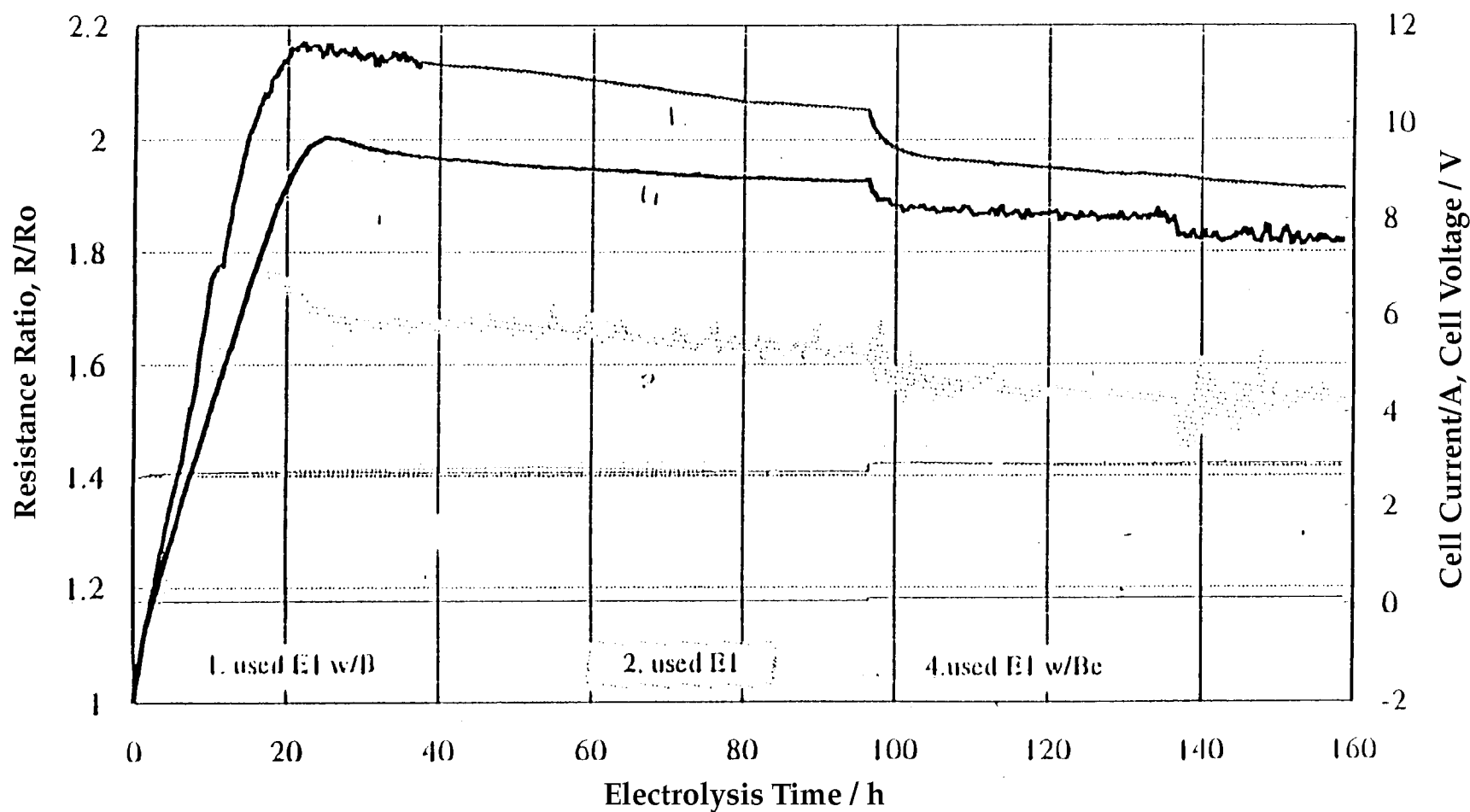
Figure 2-64
DoL Farm L Cells # 1, 2, 4

Reproducibility of Pd

Engelhard #1 Cathode (0.3 x 3 cm); Pt Anode; 1 M LiOD/D2O; Quartz Cell
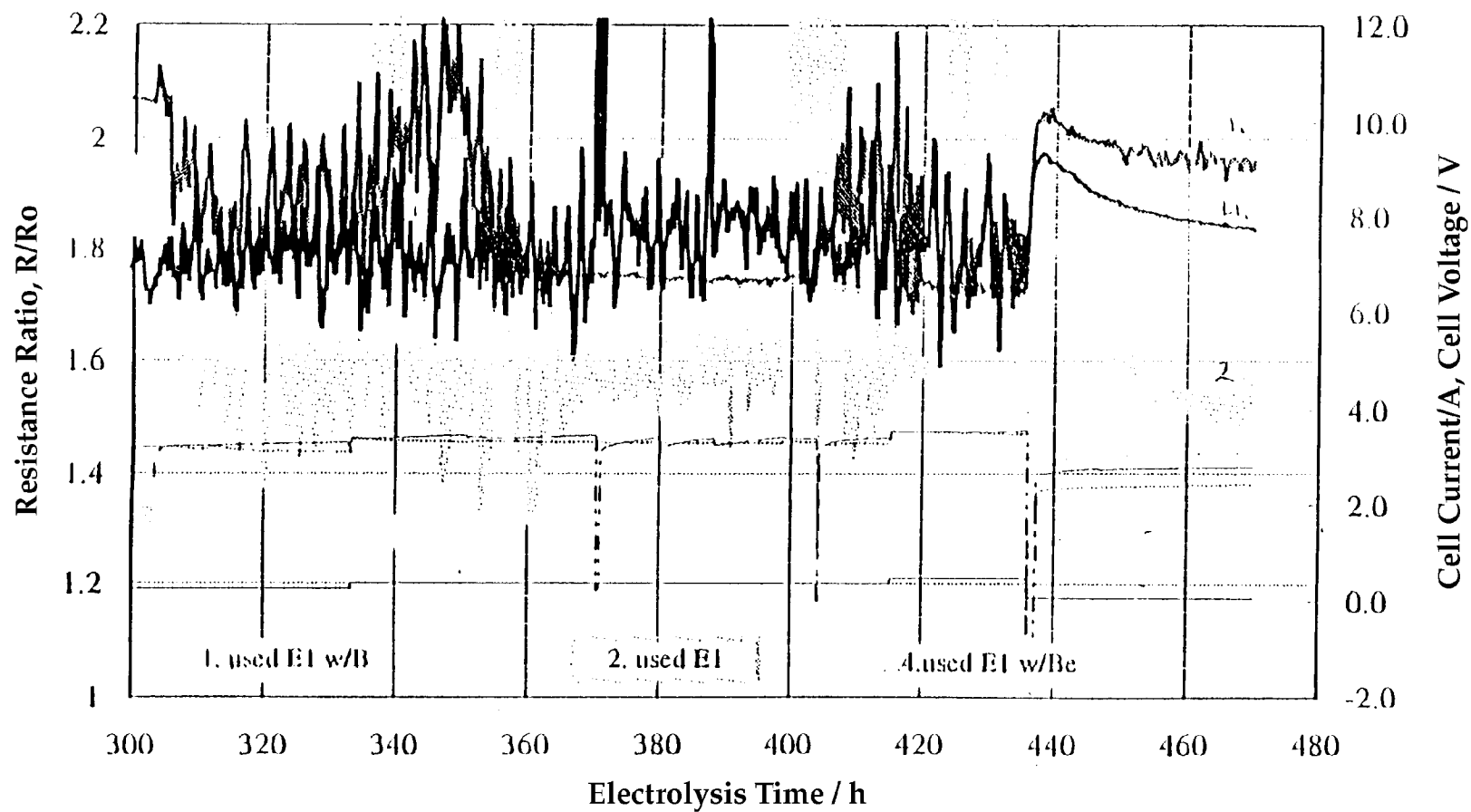
Figure 2-65
DoL Farm L Cells # 1, 2, 4

Reproducibility of Pd

Engelhard #1 Cathode (0.3 x 3 cm); Pt Anode; 1 M LiOD/D2O; Quartz Cell
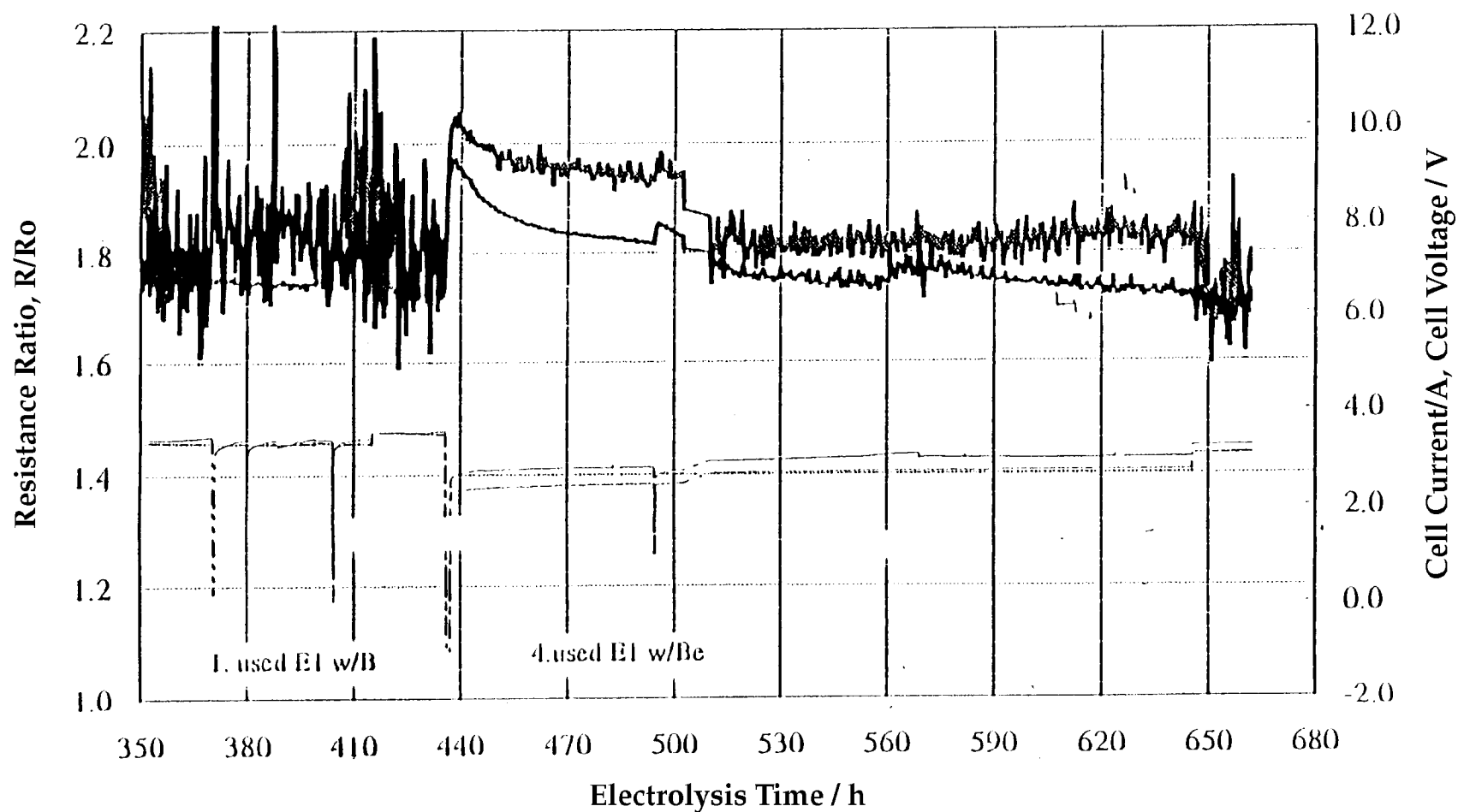
Figure 2-66
DoL Farm L Cells # 1, 4

Reproducibility of Pd

JM Pd Cathode (0.1 x 3 cm); Pt Anode; 1 M LiOD/D2O; Quartz Cell
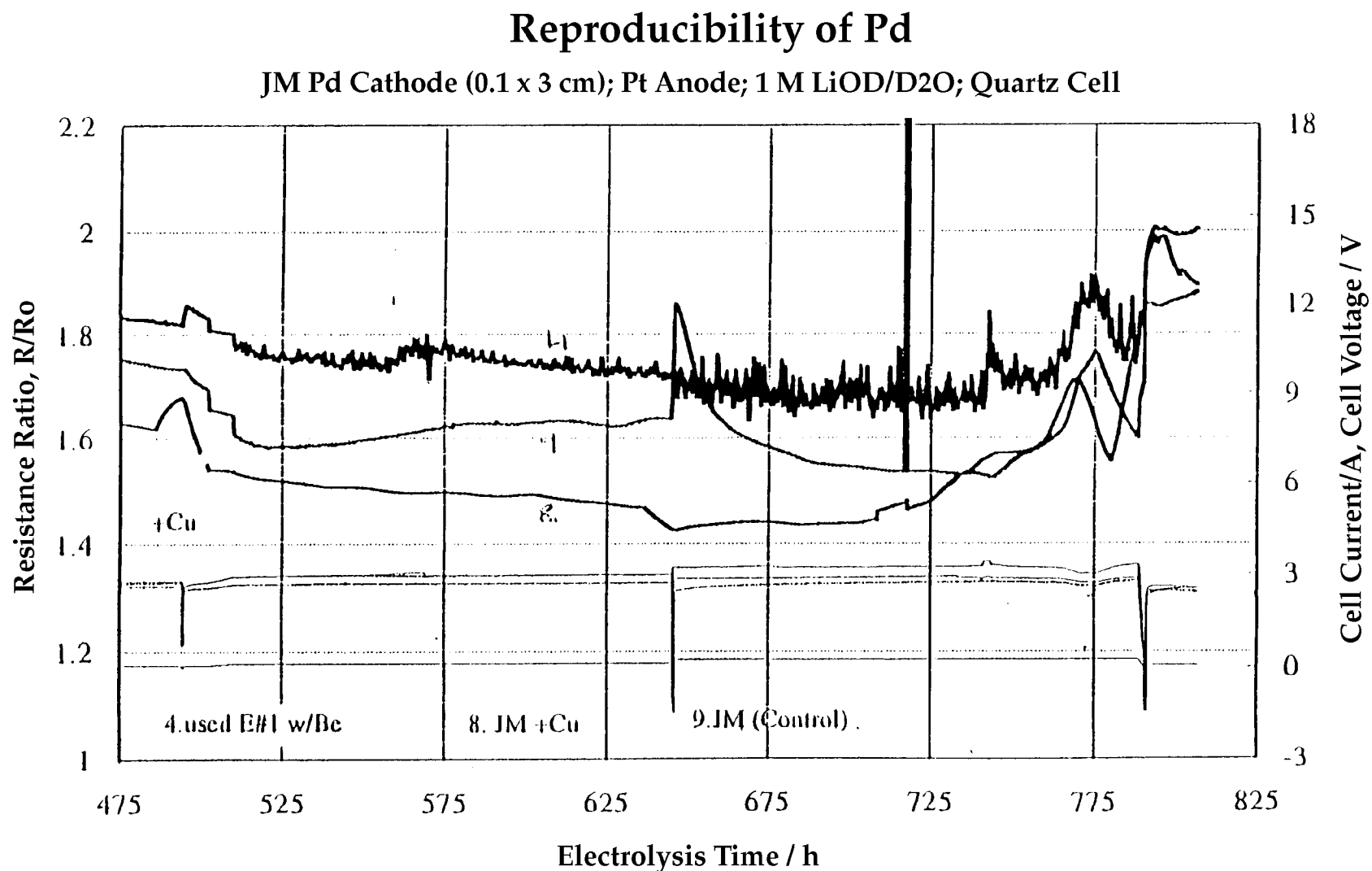
Figure 2-67
DoL Farm L Cells # 4, 8, 9

Reproducibility of Pd

JM Pd Cathode (0.1 x 3 cm); Pt Anode; 1 M LiOD/D2O; Quartz Cell
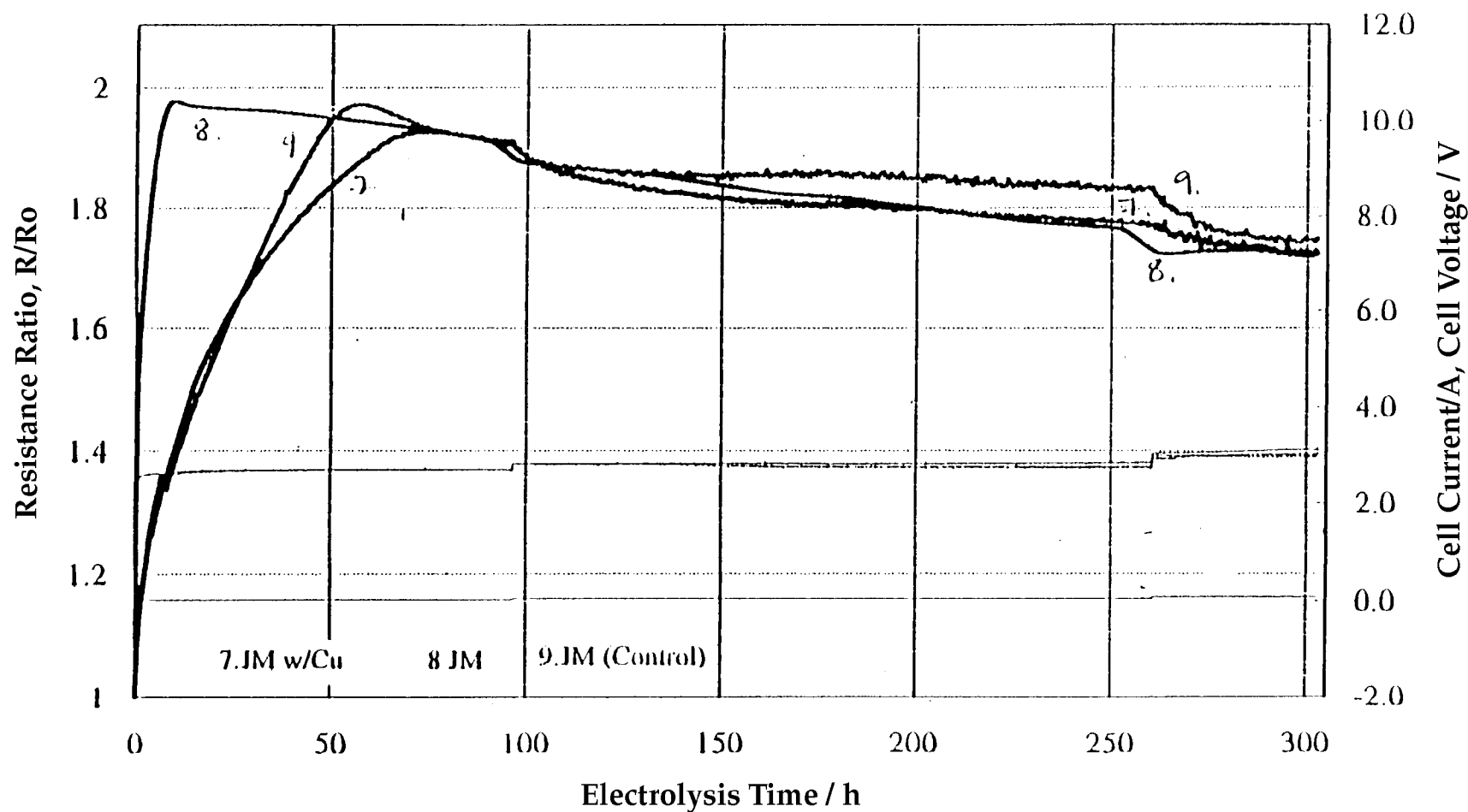
Figure 2-68
DoL Farm L Cells # 7, 8, 9

Reproducibility of Pd

JM Pd Cathode (0.1 x 3 cm); Pt Anode; 1 M LiOD/D2O; Quartz Cell
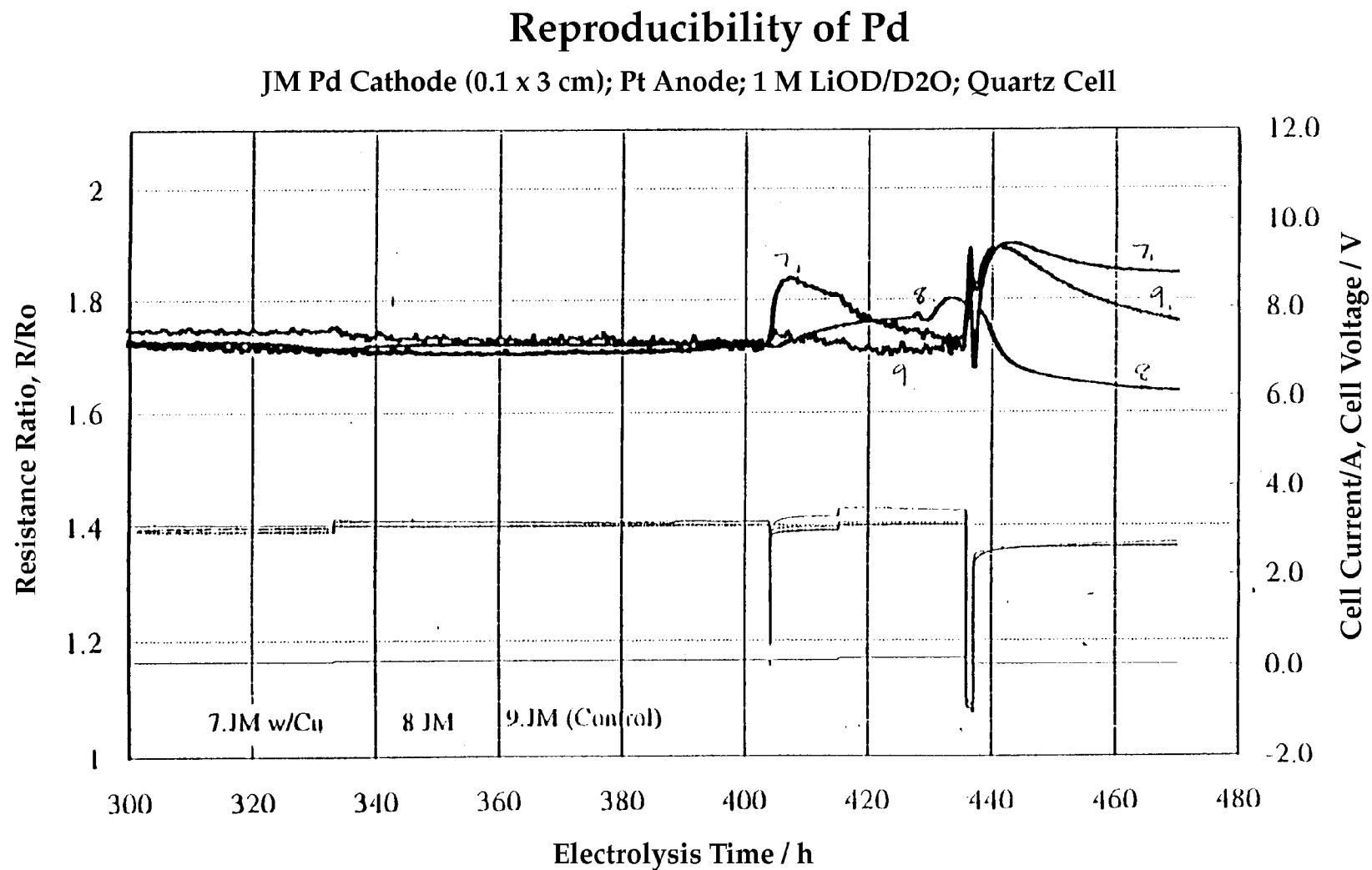
Figure 2-69
DoL Farm L Cells # 7, 8, 9

Reproducibility of Pd

JM Pd Cathode (0.1 x 3 cm); Pt Anode; 1 M LiOD/D2O; Quartz Cell
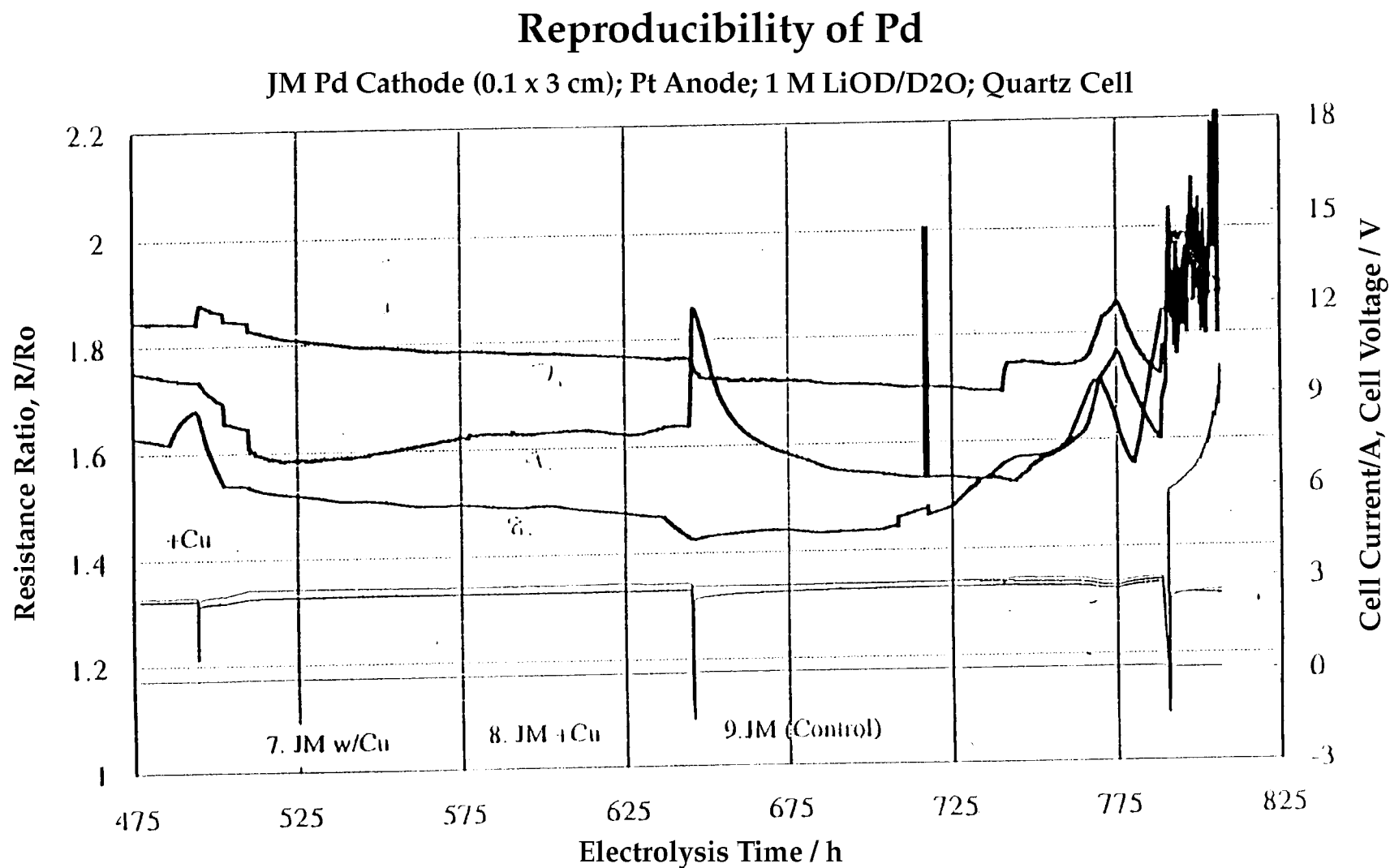
Figure 2-70
DoL Farm L Cells # 7, 8, 9

Reproducibility of Pd

Pd Cathode [( ) x 3.0 cm]; Pt Anode; 1 M LiOD/D2O; Quartz Cell
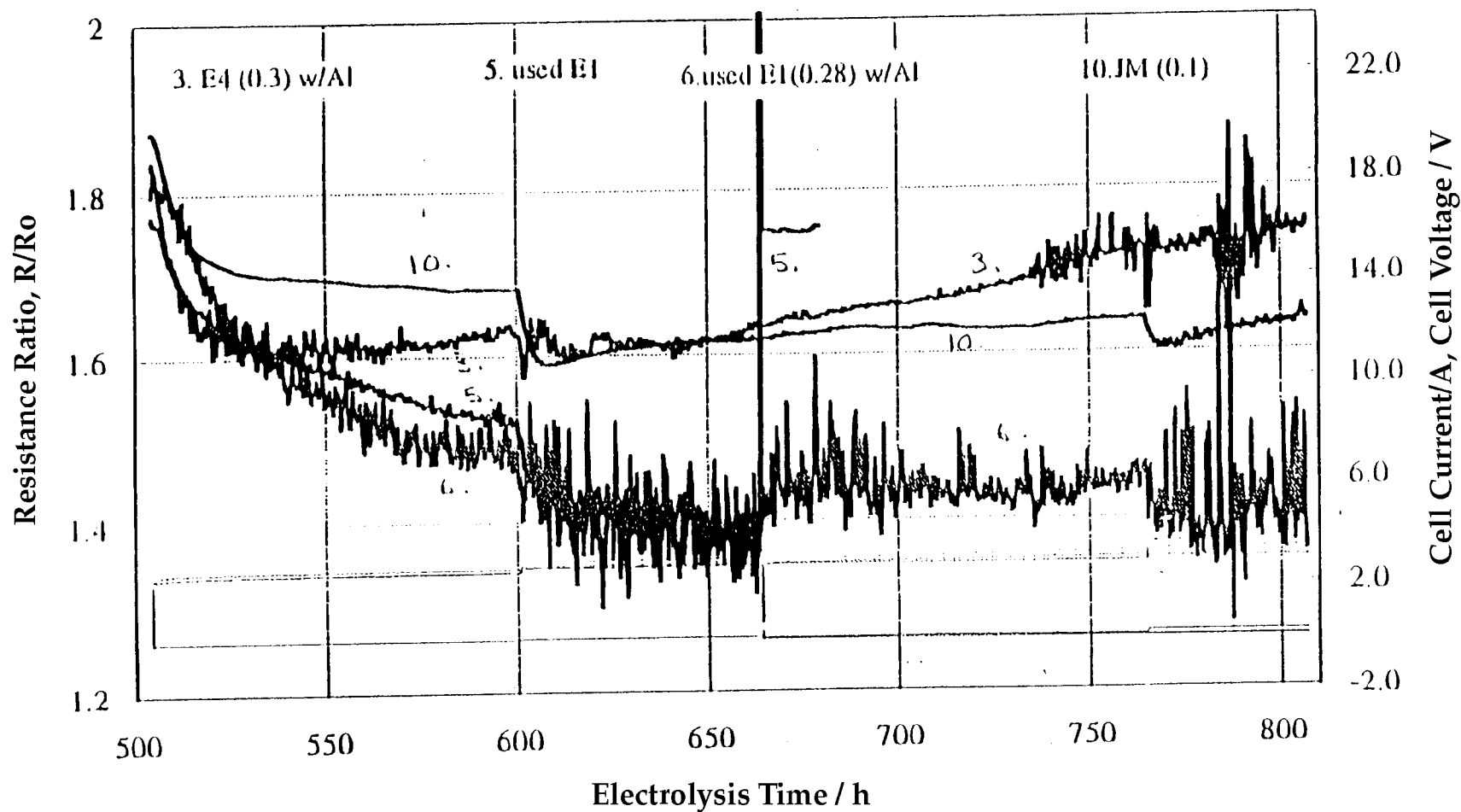
Figure 2-71
DoL Farm L Cells # 3, 5, 6, 10

Reproducibility of Pd

Pd Cathode [( ) x 3.0 cm]; Pt Anode; 1 M LiOD/D2O; Quartz Cell
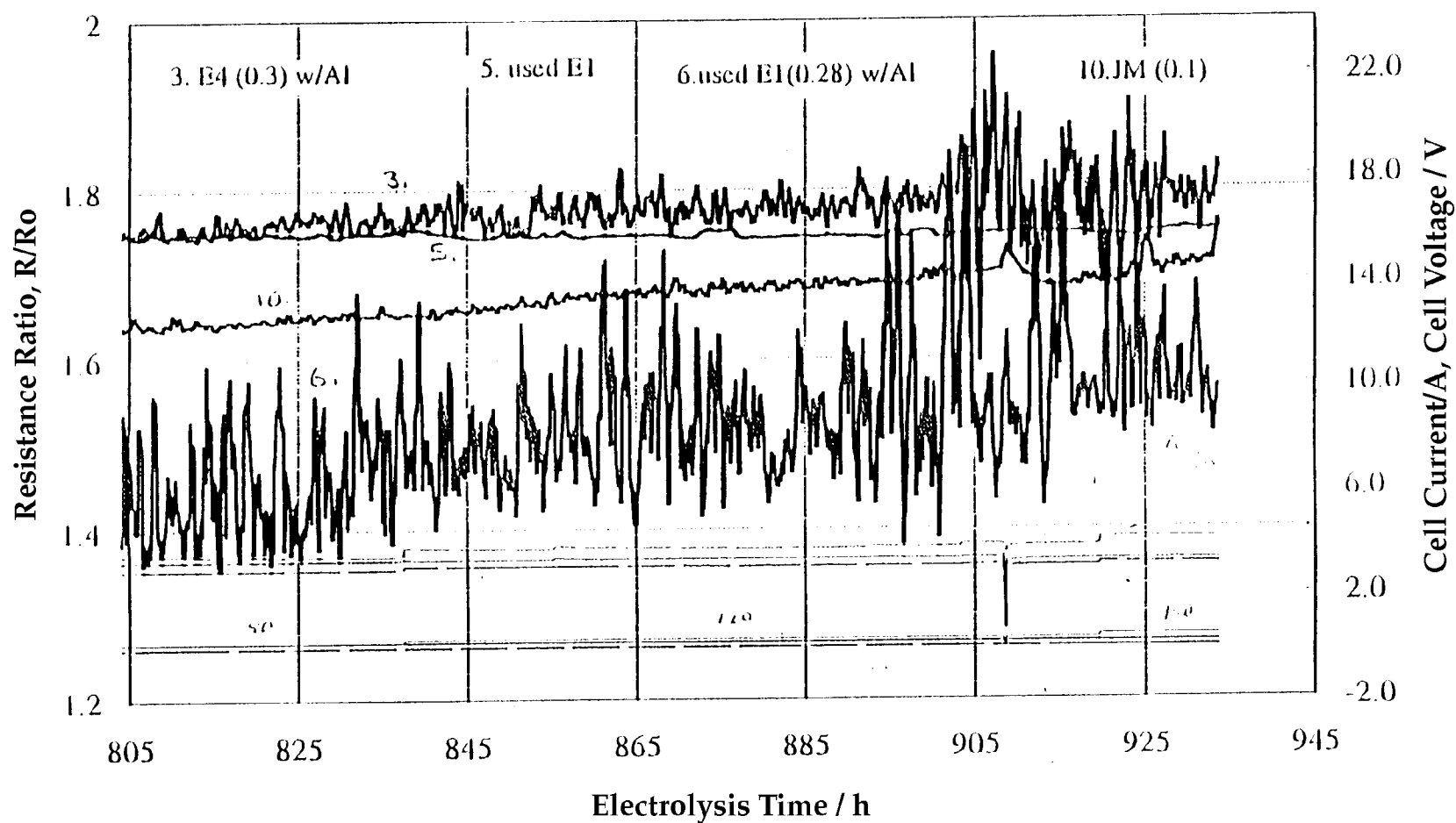
Figure 2-72
DoL Farm L Cells # 3, 5, 6, 10

Reproducibility of Pd

Pd Cathode [( ) x 3.0 cm]; Pt Anode; 1 M LiOD/D2O; Quartz Cell
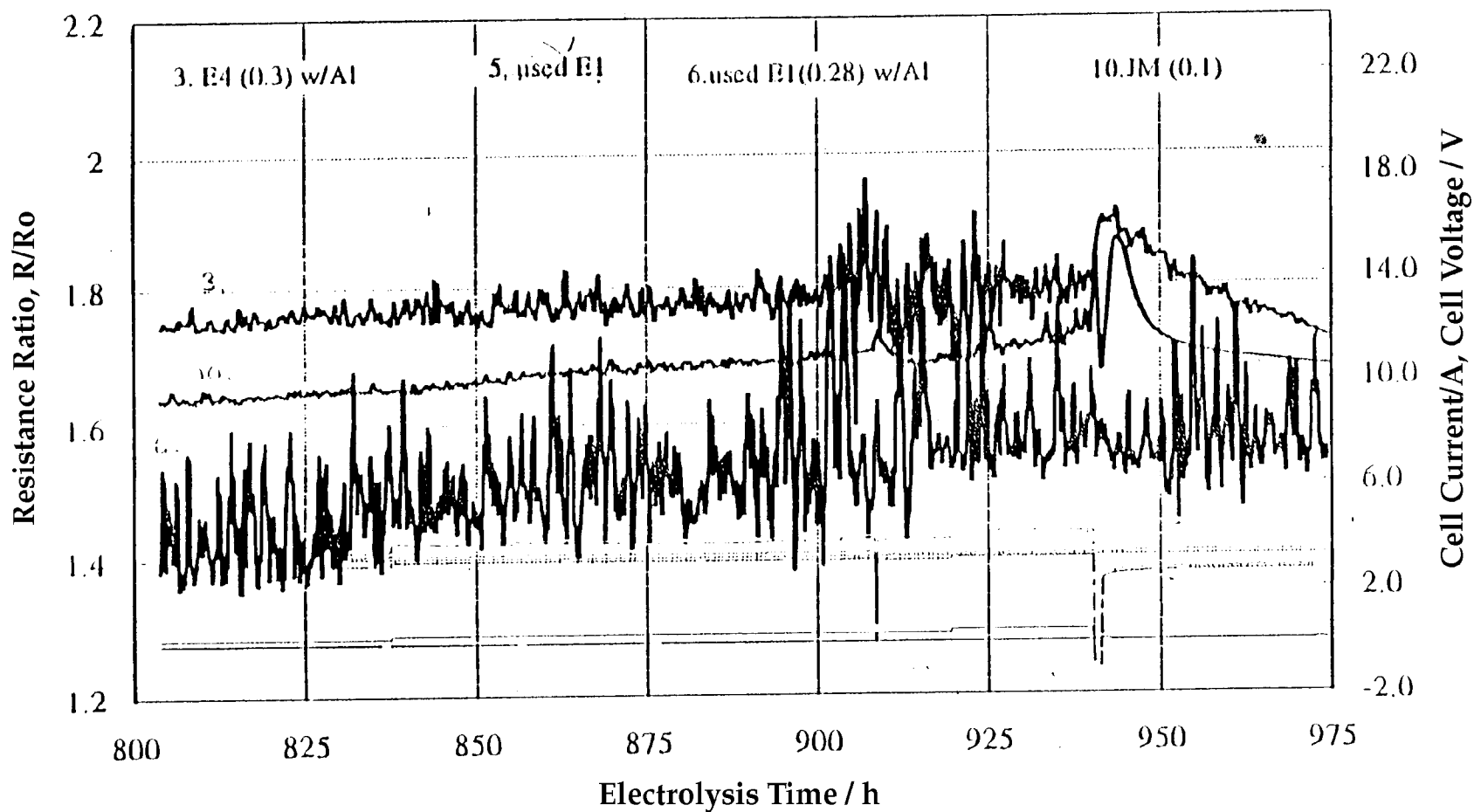
Figure 2-73
DoL Farm L Cells # 3, 6, 10

Reproducibility of Pd

Pd Cathode [( ) x 3.0 cm]; Pt Anode; 1 M LiOD/D2O; Quartz Cell
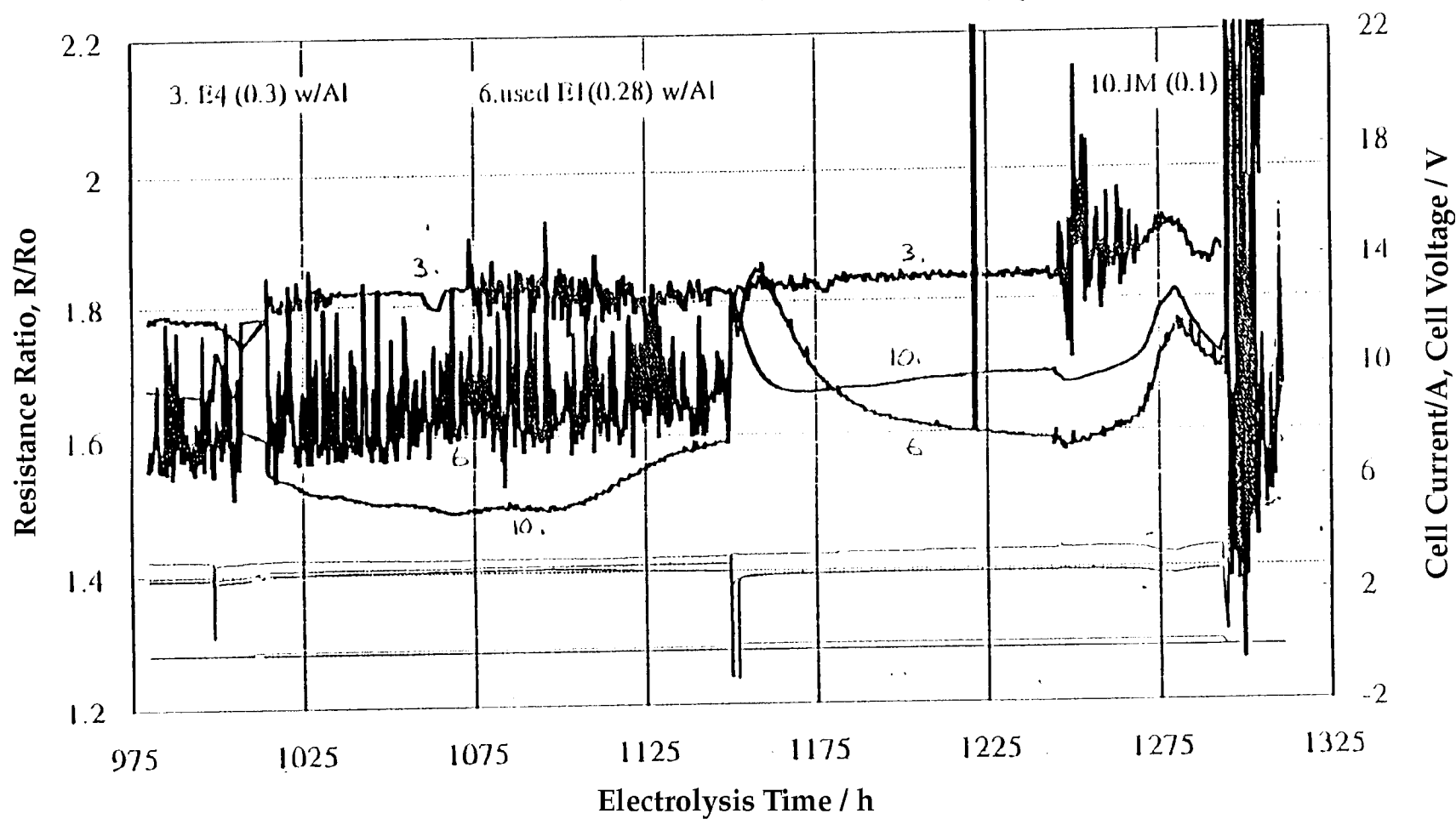
Figure 2-74
DoL Farm L Cells # 3, 6, 10

Table 2-4
Summary of DoL Farm A Results

Expt.	Cell (p 86-89)	†R° mΩ	(R/R°)$_{min}$	(D[H]/Pd)$_{max}$	Time/h: i/mA cm^{-2}
A1	E#2 (3*0.3) cm	0.461	1.55	0.93	30 : 400
A2	"	0.448	1.71	0.914	213 : 400
A3	"	0.435	1.64	0.935	377.5 : 500
A4	"	0.461	1.38	>1	329 : 500

Cells:

Container - Quartz
Anode - 16 cm^3 [0.05 x 100 cm] Pt coil
Cathodes: Engelhard, Lot 2 palladium
            Dub notch, spot weld, anneal, etch

Electrolyte
A1, A4; 20 ml of 1M LiOH/H$_2$O (Aldrich) + Al
A2, A3; 20 ml of 1 M LiOD/D$_2$O (Aldrich) + Al

Protocol for A cells
Seven Loading cycles of current steps up to 1A.
Intermediate anodic strips.

†Determined with no electrolyte.

Table 2-5
Summary of DoL Farm B Results

Expt.	Cell (P 90-93)	†R° mΩ	$(R/R°)_{min}$	$(D[H]/Pd)_{max}$	Time/h: i/mA cm^{-2}
B1	E#2	3.830	1.87	0.854	385.6 : 80
B2	"	4.165	1.76	0.899	178.6 : 640
B3	Aithica	4.813	1.96	0.786	215.4 : 320
B4	"	4.840	1.91	0.829	117.7 : 20

Cells:

Container - Quartz
Anode - 16 cm³ [0.05 x 100 cm] Pt coil
Cathodes: B1, B2; Engelhard Lot 2 palladium (unannealed)
B3, B4; Aithica Chemical Corp. palladium (unannealed)
1.665 cm² active area of Pd [5.3 cm length x 1 mm diam]
0.942 cm² monitored area of Pd [3 cm length x 1 mm diam]

Electrolyte

20 ml of 1M LiOD/D₂O (Ontario Hydro) + Al

Protocol for B cells

Three Loading cycles of current steps (6 hrs) of 20, 40, 80, 160, 320, 640 mA cm² 960 & 1280 mA cm^{-2} used in third load
Intermediate anodic strips
Aluminum added after first strip

B1, B2; Additional loading cycle of current steps of 20, 40, 80, 160, 320, 530 mA cm²

†Determined with no electrolyte.

Table 2-6
Summary of DoL Farm C Results

Expt.	Cell (P 94-979)	$^\dagger R°$ mΩ	(R/R°)$_{min}$	(D[H]/Pd)$_{max}$	Time/h: i/mA cm^{-2}
C1	E#2 (0.3 * 4) cm	0.607	1.75	0.902	287.5 : 300
C2	"	0.626	1.74	0.905	118.9 : 150
C3	"	0.729	1.76	0.899	25.3 : 300
C4	"	0.720	1.70	0.917	332 : 1200

Cells:

Container - Quartz
Anode - 16 cm^3 [0.05 x 100 cm] Pt coil
Cathodes: C1, C2 - Dub notch, spot weld, anneal, anneal, etch
          C3, C4 - Sonobond end weld, anneal, anneal, etch

Electrolyte

D52 & D53 - 1M LiOD/D$_2$O (Ohtario Hydro & topped w/Aldrich D$_2$O)

Protocol for C cells

Three loading cycles of current steps (12, 24, 24 hrs) of:
20, 40, 80, 160, 320, 530 mA/cm^2;
200 and 530 mA cm^2 used twice in 3rd load

Intermediate anodic strips with Al addition at end of 2nd strip

†Determined with no electrolyte.

Table 2-7
Summary of DoL Farm D Results

Expt.	Cell (P 98-107)	†R° mΩ	(R/R°)$_{min}$	(D[H]/Pd)$_{max}$	Time/h: i/mA cm^{-2}
D1	NRL (0.4 * 3) cm	0.235	2.00	0.74	40
D2	"	0.228	2.00	0.74	40
D3	"	0.234	2.00	0.74	40
D4	"	0.221	2.00	0.74	40
D5	E#3 (0.3 * 3) cm	0.509	2.00	0.74	40
D6	"	0.511	2.00	0.74	40
D7	"	0.490	2.00	0.74	40
D8	"	0.505	2.00	0.74	40

Cells:

Container - Quartz
Anode - 16 cm³ [0.05 x 100 cm] Pt coil
Cathodes: D1-D4; NRL palladium
                D1, D2; small grain size; D3, D4; large grain size
D5-D8; Engelhard Lot #3 palladium; D5, D6; vacuum annealed
                                D7, D8; deuterium annealed

Electrolyte
20 ml of 1M LiOD/D$_2$O (Aldrich) + Al

Protocol for D cells
One loading cycle of current steps (24 hrs) of 20, 40, 80, 160, 320 mA cm⁻³

†Determined with no electrolyte.

Table 2-8
Summary of DoL Farm E Results

Expt.	Cell (P 108-117)	$^{\dagger}R°$ mΩ	$(R/R°)_{min}$	$(D[H]/Pd)_{max}$	Time/h: i/mA cm^{-2}
E1	E#3 (3 * 0.3) cm	0.483	1.6	0.948	2650 : 80
E2	"	0.4.69	1.6	0.948	1275 : 80
E3	"	0.492	1.72	0.911	475 : 80
E4	"	0.478	1.88	0.848	25 : 20
E5	E#3 (0.3 * 3) cm	0.557	1.45	0.997	1275 : 80
E6	"	0.511	1.78	0.892	250 : 160
E7	"	0.471	1.73	0.908	975 : 80
E8	"	0.451	1.75	0.902	2650 : 80
E9	"	0.471	1.84	0.868	975 : 80
E10	"	0.472	1.85	0.864	475 : 80

Cells:

Container - E1 - E8 Quartz, E9, E10; PTFE
Anode - E1-E6; 16 cm² [0.05 x 100 cm] Pt coil: E7-E10; Ni
Cathodes: E1, E2, E5, E7-E10; E control (weld, vac anneal, etch)
            E3, E4; SonoBond, vac anneal, etch
            E6; annealed & reused P102

Electrolyte
20 ml of 1M LiOD/D$_2$O (Aldrich) + Al

Protocol for E cells
Eleven loading cycles, with current strepping in the range of 20 mA cm² 240 mA cm^{-2}

Intermediate anodic strips

†Determined with no electrolyte.

Table 2-9
Summary of DoL Farm F Results

Expt.	Cell (P 118-123)	$^\dagger R^\circ$ mΩ	$(R/R^\circ)_{min}$	$(D[H]/Pd)_{max}$	Time/h: i/mA cm^{-2}
F3	E#3 (3 * 0.3) cm	0.54	1.66	0.929	1000 : 80
F4	"	0.55	1.6	0.948	1000 : 80
F6	"	0.52	1.5	0.980	425 : 80
F7	"	0.38	1.68	0.923	425 : 80
F9	"	0.53	1.65	0.932	560 : 120
F10	"	0.39	1.85	0.864	450 : 80

Cells:

Container - Quartz
Anode - 16 cm^3 [0.05 x 100 cm] Pt coil
        [F10; Pd anode]
Cathodes: F6, F9; E control; weld, vacuum anneal, etch
        F3, F4; spot weld, 48 hour anneal, etch
        F7, F10; stab weld, anneal, etch

Electrolyte
20 ml of 1M LiOD/D$_2$O (Aldrich) + Al
F9; Boron addition instead of aluminum

Protocol for G cells
1st loading cycle of current steps of 20, 40, 80, 120 mA/cm^2
2nd loading cycle of current steps of 20, 40, 80, 20, 40, 20, 40, 20, 40, 80, 120, 160 mA/cm^2
3rd loading cycle of current steps of 20, 40, 80, 120, 160, 200, 240, 280, 320 mA/cm^2
4th loading cycle of current steps of 20, 40, 80, 120 mA/cm^2
5th loading cycle of current steps of 20, 40, 80, 40 mA/cm^2

†Determined with no electrolyte.

Table 2-10
Summary of DoL Farm G Results

Expt.	Cell (P 124-128)	†R°mΩ	(R/R°)$_{min}$	(D[H]/Pd)$_{max}$	Time/h: i/mA cm^{-2}
GG2	E#1 (3 * 0.1) cm	4.49	1.7	0.917	830 : 40
GG4	E#3 (2.5*0.3) cm	0.398	1.71	0.914	290 : 80
GG7	NRL (3*0.4) cm	0.242	1.93	0.814	300 : 80
GG9	"	0.545	1.77	0.895	930 : 80

Cells:

Container - Quartz
Anode - 16 cm^2 [0.05 x 100 cm] Pt coil

Cathodes: GG7, GG9; Spot weld, no anneal, etch
          F3, F4; spot weld, 48 hour anneal, etch

Electrolyte
20 ml of 1M LiOD/D$_2$O (Aldrich) + Al

Protocol for F cells
1st loading cycle of current steps of 20, 40, 80, 120, 160 mA/cm^2
2nd loading cycle of current steps of 20, 40, 80, 120, 160, 80 mA/cm^2
3rd loading cycle of current steps of 20, 40, 80, 120 mA/cm^2
4th loading cycle of current steps of 20, 40, 80, 120 mA/cm^2

†Determined with no electrolyte.

2-94

Table 2-11
Summary of DoL Farm H Results

Expt.	Cell (P 124-134)	$^\dagger R^\circ m\Omega$	$(R/R^\circ)_{min}$	$(D[H]/Pd)_{max}$	Time/h: i/mA cm^{-2}
H1	JM (3 * 0.2)	0.95	1.78	0.892	925 : 120
H2	"	1.0	1.75	0.902	800 : 80
H3	"	0.985	1.80	0.885	625 : 80
H4	"	0.975	1.80	0.885	620 : 80
H5	"	0.95	1.78	0.892	930 : 80
H6	"	1.0	1.78	0.892	750 : 40

Cells:

Container - Quartz
Anode - 16 cm² [0.05 x 100 cm] Pt coil

Cathodes: H1, H2; Spot weld, no anneal, etch
           H3, H4; Spot weld, no anneal, etch

Electrolyte
20 ml of 1M LiOD/D₂O (Aldrich) + Al

Protocol for H cells
1st loading cycle of current steps of 20, 40, 80, 120, 160, 80 mA/cm²
2nd loading cycle of current steps of 20, 40, 80, 120 mA/cm²
3rd loading cycle of current steps of 20, 40 mA/cm²
4th loading cycle of current steps of 20, 40, 80, 120 mA/cm²

†Determined with no electrolyte.

Table 2-12
Summary of DoL Farm I Results

Expt.	Cell (P 135-144)	†R°mΩ	(R/R°)$_{min}$	(D[H]/Pd)$_{max}$	Time/h: i/mA cm^{-2}
I1	used E#1 (3 * 0.3) cm	0.455	1.66	0.929	650 : 40 670 : 80
I2	"	0.422	1.62	0.942	800 : 80
I3	used E#1 (3*0.28) cm	0.5	1.63	0.938	175 : 80
I4	"	0.491	1.58	0.954	810 : 80
I5	E#2 (3 * 0.28) cm	0.55	1.44	1.0	810 : 80
I6	"	0.54	1.73	0.908	680 : 80
I7	E#3 (3*0.28) cm	0.56	1.57	0.957	685 : 80
I8	"	0.565	1.6	0.948	680 : 80
I9	JM (3*0.38) cm	0.29	1.76	0.899	680 : 80
I10	"	0.28	1.73	0.908	800 : 80

Cells:

Container - Quartz
Anode - 16 cm² [0.05 x 100 cm] Pt coil

Cathodes: I1; etch, anneal, spot weld, etch
    I2; polish, anneal, spot weld, etch
    I4; machine, anneal, spot weld
   I3, I5-I6; machine, anneal, spot weld, etch

Electrolyte
20 ml of 1M LiOD/D₂O (Aldrich)

Protocol for I cells
1st loading cycle of current steps of 20, 40, 80, 120, 160, 80 mA/cm²
2nd loading cycle of current steps of 20, 40, 80, 120 mA/cm²
3rd loading cycle of current steps of 20, 40 mA/cm²
4th loading cycle of current steps of 20, 40, 80, 120 mA/cm²

†Determined with no electrolyte.

Table 2-13
Summary of DoL Farm J Results

Expt.	Cell (P 145-150)	$^{\dagger}R^{\circ}\,m\Omega$	$(R/R^{\circ})_{min}$	$(D[H]/Pd)_{max}$	Time/h: i/mA cm^{-2}
J1	JM (3.8 * 0.2) cm	1.24	1.94	0.805	155 : 120
J2	"	1.25	1.85	0.864	330 : 80
J3	IB (3.8*0.3) cm	0.55	1.92	0.821	320 : 80
J4	"	0.54	2.0	0.739	320 : 80
J5	square IB (3*0.28) cm	0.41	1.89	0.854	320 : 80
J6	"	0.40	1.87	0.854	310 : 80

Cells:

Container - Quartz
Anode - 16 cm^2 [0.05 x 100 cm] Pt coil

Cathodes: J1-J6; spot weld

Electrolyte
20 ml of 1M LiOD/D$_2$O (Aldrich)

Protocol for J cells
1st loading cycle of current steps of 20, 40, 80, 120, 160, mA/cm^2
2nd loading cycle of current steps of 20, 40, 80 mA/cm^2

†Determined with no electrolyte.

Table 2-14
Summary of DoL Farm K Results

Expt.	Cell	†R° mΩ	$(R/R°)_{min}$	$(D/Pd)_{max}$	Time/h: i/mA cm^{-2}
K1	E#4 (0.3)	0.47	1.6	0.948	70 : 20
K2	"	0.48	1.4	1.012	100 : 80
K3	"	0.45	1.53	see DoL KL	—
K4	"	0.46	1.46	0.993	100 : 80
K5	used E#1 (0.28)	0.56	1.48	see DoL KL	—
K6	"	0.56	1.6	see DoL KL	—
K7	JM (0.2)	0.99	1.64	0.935	330 : 40
K8	"	0.99	1.77	0.895	245 : 80
K9	JM (0.1)	3.56	1.65	0.932	340 : 40
K10	"	3.63	1.63	see DoL KL	—

Cells:

Container - Quartz
Anode - 16 cm² [0.05 x 100 cm] Pt coil

Cathodes: E Pd; machine, cut, degrease, anneal, spot weld, D_2O rinse.
　　　　　JM Pd; cut, degrease, anneal spot weld, D_2O rinse

Electrolyte
20 ml of 1M LiOD/D_2O (Aldrich)
Cells #3,4,8,10; + Al

Protocol for E1-10 cells
1st loading cycle of current steps of 20, 40, 80, 120 mA/cm²
2nd loading cycle of current steps of 20, 40 mA/cm²

†Determined with no electrolyte.

Table 2-15
Summary of Farm K; Effect of Additives on Initial Loading Rates

Cell	Cathode Material	Cathode Dimensions (cm)	Initial Electrolyte Additive	$(R/R^\circ)_{max}$: Time (hours)
K1	E#4	(0.3 * 3)	None	1.9 : 30
K2	E#4	(0.3 * 3)	None	1.7 : 40
K3	E#4	(0.3 * 3)	Al	1.88 : 80
K4	E#4	(0.3 * 3)	Si	1.75 : 18
K5	used E#1	(0.28 * 3)	None	1.85 : 23
K6	used E#1	(0.28 * 3)	Al	1.93 : 70
K7	JM	(0.2 * 3)	None	1.96 : 20
K8	JM	(0.2 * 3)	Si	1.87 : 125
K9	JM	(0.1 * 3)	None	1.9 : 20
K10	JM	(0.1 * 3)	Si	1.99 : 18

Cells:

Container - Quartz
Anode - 16 cm² [0.05 x 100 cm] Pt coil

Cathodes: K1-K6; Machine, cut, degrease, anneal, spot weld
        K7-K10; Cut, degrease, anneal, spot weld

Protocol for K cells

Initial loading at 20 mA cm⁻²

Table 2-16
Summary of DoL Farm L Results

Expt.	Cell (p 161-168)	$^\dagger R°$ mΩ	$(R/R°)_{mix}$	$(D[H]/Pd)_{max}$	Time/h: i/mA cm^{-2}
L1	used E#1 (3 * 0.3) cm	0.55	1.7	0.917	650 : 80
L2	"	0.58	1.5	0.98	250 : 40
L4	used E#1 (3*0.3) cm	0.58	1.68	0.923	720 : 80
L7	JM (3*0.1) cm	3.45	1.69	0.92	350 :40
L8	"	3.47	1.4	1.01	1050 : 80
L9	"	3.81	1.34	>1	1050 : 80

Cells:

Container - Quartz
Anode - 16 cm^2 [0.05 x 100 cm] Pt coil

Cathodes: L,L2,L4; Used Engelhard Lot 1, p61, p73, p85 respectively
Machine, cut, degrease, anneal, spot weld etch
L7, L8, L9; Johnson Matthey; No machine

Electrolyte
20 ml of 1M LiOD/D$_2$O (Aldrich)

Initial Additions
Cell #1; +B   Cell #4; + Be   Cell #7 + Cu
Cell #3,6; + Al

Protocol for L cells
1st loading cycle of current steps of 20, 40, 80, 120, 160, mA/cm^2
2nd loading cycle of current steps of 20, 40, 80, 120 mA/cm^2
Intermediate anodic strip
L8, L9, L4 additional loading cycle of 20, 40, 80, 20, 40, 80 mA/cm^2

†Determined with no electrolyte.

Table 2-17
Summary of DoL Farm M Results

Expt.	Cell (p 169-176)	†R° mΩ	(R/R°)$_{mix}$	(D[H]/Pd)$_{max}$	Time/h: i/mA cm^{-2}
M1	JM (3 * 0.4) cm	0.23	1.8	0.88	365 : 120
M2	"	0.23	1.9	0.836	360 : 120
M3	JM (3*0.1) cm	3.35	—	—	—
M4	"	3.24	1.85	0.864	450 : 160
M5	"	3.4	1.66	0.93	320 : 40
M6	"	3.3	1.9	0.836	450 : 160
M7	"	3.29	1.9	0.836	175 : 80
M8	"	3.35	1.93	0.814	370 : 120

Cells:

Container - Quartz
Anode - 16 cm² [0.05 x 100 cm] Pt coil

Cathodes: Johnson Matthey palladium
M1-M8; Cut, degrease, anneal, spot weld, etch rinse

Electrolyte
20 ml of 1M LiOD/D₂O (Aldrich)

Initial Additions
Cell #1; Cu   Cell #4; Cu   Cell #7 + Cu
Cell #6; Al   Cell #8; Si

Protocol for M cells
1st loading cycle of current steps of 20, 40, 80, 120 mA/cm²
2nd loading cycle of current steps of 20, 40, 80, 120, 160 mA/cm²
3rd loading cycle of current steps of 20, 40 mA/cm²

Initial Additions
Cell #1; Cu   Cell #4; Cu
Cell #6; Al   Cell #8; Si

Intermediate anodic strip

†Determined with no electrolyte.

Table 2-18
Summary of DoL Farm N Results

Expt.	Cell (P 175-180)	$^{\dagger}R^{\circ}$ mΩ	$(R/R^{\circ})_{mix}$	$(D[H]/Pd)_{max}$	Time/h: i/mA cm^{-2}
N9	E#5 (3 * 0.3) cm	0.43	1.99	0.752	25 : 20
N10	"	0.42	1.98	0.764	100 : 40

Cells:

Container - Quartz
Anode - 16 cm² [0.05 x 100 cm] Pt coil

Cathodes: N9; Cut, anneal, degrease, spot weld, etch rinse
　　　　　　N10; Cut, anneal, degrease, spot weld, rinse

Electrolyte
20 ml of 1M LiOD/D2O (Aldrich)

Protocol for N cells
Both loading cycles of current steps of 20, 40, 80, 120 mA cm²

†Determined with no electrolyte.

2-102

Table 2-19
Summary of DoL Farm P Results

Expt.	Cell	†R° mΩ	(R/R°)$_{mix}$	Time/hours
P1	E#2 (3 * 0.28) cm	0.492	2.01	55
P2	"	0.502	2.01	30
P3	E#3 (3*0.28) cm	0.517	1.98	90
P4	"	0.518	2.0	37
P5	E#4 (3*0.28) cm	0.501	2.04	75
P6	"	0.515	2.0	43
P7	E#5 (3*0.28) cm	0.496	2.0	55
P8	"	0.517	2.0	38

Cells:

Container - Quartz
Anode - 16 cm² [0.05 x 100 cm] Pt coil

Electrolyte
20 ml of 1M LiOD/D$_2$O (Aldrich)

Protocol for P cells
Initial loading at 20 mA cm⁻²

†Determined with no electrolyte.

Table 2-20
DoL Farm PPQ Experimental Design

Cell	Cathode Source 0.3 x 3 cm	Comments	Electrolyte	R°
Q1	E lot 3	long anode cage	Control	.50
Q2	"	"	clean	.49
Q3	E lot 5	control	control	.52
Q4	"	"	clean	.52
PP5	E lot 4 (P5)		new clean	.51
PP6	E lot 3 (P3)		—	.52
PP7	E lot 2 (P2)		new clean	.51
PP8	E lot 5 (P8)		new clean	.52

1 M LiOD/D$_2$O, Pt [0.05 x 100 cm] Anode, Quartz Cell

Cathode Preparation

E Pd - cut, degrease, anneal, spot weld, etch, D$_2$O rinse

3

CALORIMETRY

Calorimetry Types

In the calorimetric study of electrochemical systems, the essential measurement is that of the difference between the power dissipated by the electrochemical cell and the power input to the cell. Assuming that the mode of operation of the cell itself determines the rate of energy storage within the cell and its surroundings, and that this process is understood, the presence of anomalous heat producing or consuming reactions within the cell may be inferred from the absence of the simple, expected, power balance. In most cases, the determination of the input power is straightforward in the event that only electrical systems are involved; similarly, the nature of the possible energy storage within a cell, for the experiments performed here, is simply related to the "open" or "closed" nature of the experiment. Most difficulties are encountered in the accuracy and reliability of the calorimetric determination of the power dissipation from the cell.

In this study, two different calorimetric principles "heat flow" and "mass flow" have been employed for output power determination. This redundancy of method allowed us to operate essentially identical electrochemical experiments in different calorimeters, which permitted us to separate the excess power effects from any possible systematic error due to a particular calorimetric design. Any systematic errors introduced by one calorimeter would presumably not be manifest in a different calorimeter design. In fact, among the heat flow calorimeters we used three different calorimeter types to further extend the redundancy of method.

In the first, "heat flow" type, the power dissipated from the cell is assumed to be proportional to the temperature difference across the cell boundary. In order to increase the reliability of the method with respect to problems introduced by the inevitable temperature distribution within the cell boundary it (the boundary) is normally chosen to have the largest thermal resistance in the system. Furthermore, the best results are to be expected when the system is isoperibolic, such that problems introduced by environmental fluctuations are minimized (for example, immersion in a constant temperature water bath is to be preferred to forced air-cooling). The temperature difference across the cell boundary may be measured directly, by temperature measurements inside and outside the cell, or indirectly using thermoelectric elements

attached to the cell (in this case, the temperature difference across the element is recorded and the system should therefore be designed so that the thermoelectric elements intercept most of the output power). The major problem with these modes of operation is the extent to which the measured temperature (or thermoelectric voltage) is "representative" *i.e.* a true measure of the thermal state of the system. For this reason, open cells are to be preferred over closed cells (in order to minimize the spatial temperature variation within the system) and, for thermoelectric measurement, it is preferable to cover as much of the cell surface as possible with thermoelectric elements. Unavoidable problems, however, remain; for example, the effects of inadequate stirring at low electrochemical currents with respect to local temperature measurements (thereby necessitating auxiliary stirring), the need to calibrate thermoelectric elements for performance variations with mean device temperature, and the unpredictable occurrence of recombination in an open system. Heat flow systems, however, do possess some advantages over more sophisticated approaches; for example, relative ease of system design and operation (there are usually no moving parts in a heat flow calorimeter), relative ease of data analysis and, as a result of these factors, the capacity to operate a large number of identical systems at minimal cost. Ultimately, however, the "trustworthiness" of any form of heat flow calorimetry is always an issue.

"Mass flow" calorimetry represents a more sophisticated approach which overcomes many, if not all, of the disadvantages of heat flow calorimetry. In this approach, *all* of the power output from the cell is intercepted by a moving fluid (in our case, water); the temperature change of this fluid, together with its flow rate and heat capacity, determine the rate of power dissipation. The moving fluid is preferably surrounded by an adiabatic jacket in order that all of the absorbed energy is detected by the outlet temperature sensors. Notice that, in this respect, a key problem in the design of heat flow calorimeters is present in the mass flow case, *i.e.* the measurement of a representative fluid temperature. Care must be taken with respect to fluid mixing and temperature sensor placement in order to ensure that representative mass flow fluid temperature measurements are made. This being the case, mass flow calorimeters are intrinsically more trustworthy but generally less sensitive than heat flow calorimeters.

Heat Flow. The principles used to design the heat flow calorimeter were guided by the needs that these calorimeters (1) be easy to use, (2) be inexpensive, (3) allow for radiation detection (4) allow for other intrusive detectors, (5) operate at temperatures significantly above ambient and (6) be able to "farm" cells that have performed well in the degree of loading (DoL) experiments. These experiments could be operated thermodynamically open or closed (with a recombiner catalyst). The power input to the cells was directly measured from the cells' and/or heaters' voltage and current. The output power was measured indirectly by either using a calibrated temperature difference measurement or a calibrated heat flow measurement. All temperatures were measured using 100% Pt Resistive Temperature Detectors (RTD's). When using an open cell, which was most common in the heat flow calorimeters, the thermoneutral potential

of the D₂O electrolysis reaction (1.54 V) was subtracted from the cell voltage before multiplying by the cell's current. This accounts for the thermodynamic potential energy being carried away by the D_2 and O_2 relative to their energy as D_2O. Any D_2O vapor carried with these gases would be accounted for in the calibration of the heat flow measurement's efficiency.

Six different cells were used as isoperibolic heat flow calorimeter's. Those were the "T", "D"[*] , "F", "G", "OHF" and "HH" cells. The general principle in these cells was that the temperature difference (ΔT) between the electrolyte and some reference varied with output power in a monotonic manner (preferably linear). When using closed cells with a recombination catalyst, a function dependent on the temperature difference between the catalyst and the same reference was added to the equation. The reference temperature was that of either air, a "blank" cell without electrolysis, or a cooling jacket on the active cell's wall. The efficiency of the heat conduction across the ΔT's could be estimated but was not used to calculate input power.

The Seebeck heat flow calorimeters were based on the measurement of some or all of the output power as a voltage proportional to the heat conducted across a set of thermoelectric elements (TE's). The cells were either heavily insulated on the cell faces not containing the elements, or elements were placed on all faces of the cell. The Heat-Helium (HH) cell was an example of the latter design, a complete envelope calorimeter. The external surfaces of the TE's were kept at a relatively constant temperature by immersing the whole cell in a water bath or attaching heat sink fins to the outer surface and cooling with forced air fans. The temperatures of both the hot and cold faces of the TE's were measured and used in the function that converts the TE's voltage to output power.

Mass Flow. In addition to the heat flow calorimeters, we used two different types of mass flow calorimeters for our longer term experiments. These experiments were designed to be completely integrating mass flow calorimeters. Ideally, all of the heat sourced in the cell is used to raise the temperature of the calorimeter fluid with no losses due to heat conduction or convection. In practice, these losses have been reduced to between 0.5% and 5% of total input power, depending on the particular calorimeter design.

By accurately measuring the inlet and outlet temperatures of the calorimetric fluid and the mass flow rate the temperature/power response curve can be calculated from first principles. The Newtonian loss factor can then be added to this function as a term proportional to ΔT (outlet-inlet).

---

[*] The "D" Series experiments were undertaken by Dr. M. Srinivasan from the Bhabha Atomic Research Center, Bombay, India, while an SRI Visiting Scientist. An account of this work can be found in Appendix A.

Labyrinth. The device we refer to as a labyrinth ("L") calorimeter has the electrochemical cell completely immersed in the flowing water inside a stainless steel vacuum flask. The water passes over all of the electrical leads as it enters the flask and travels to the bottom of the calorimeter where it passes upward over the cell and out. The temperatures are measured as the fluid enters and exits the calorimeter. All gas and liquid connections to the electrochemical cell pass through the top of the calorimeter using low heat-conduction PTFE tubing. The outer case of the cell has a resistive heater and heat transfer fins intimately contacting the cell body. As above, these heaters can be used to maintain a constant input power or to provide input power steps to be used for calibration.

Helium Tight. The Helium tight version of the labyrinth calorimeter is referred to as the "M" cell. In this design the PTFE out-going tube was replaced with a long metal tube leading out of the cell and calorimeter. To minimize heat conduction losses through this tube the top cover of the calorimeter is taller and channels the inlet flow water past this gas tube as well as the electrical lead wires. Also, in order to make the cell helium leak-tight the electrical leads were passed out of the cell through this tube to a vacuum tight electrical feed-through above the bath water level. A helium-tight manifold was attached to this system. Other than these differences the "M" cell operates identically to the "L" cell labyrinth calorimeters.

This introduction has given a general overview of the different types of calorimeters used in this project. Following we will describe each of the calorimeters and their operation in detail. Each of the cells used and their operating procedure will be detailed. Finally, the results from the cell/calorimeter assemblies and their interpretation will be presented.

F Series Experiments

Introduction. The F cell/calorimeter was designed as a thermodynamically open heat flow calorimeter which allows large temperature excursions. The experimental plan was to electrolyze the cell until the cathode was well loaded and then step the current up to yield a fast temperature rise. The inside wall of the electrode chamber was lined with a Ni cylinder 4 cm i.d. x 5 cm o.d. x 7 cm tall as an anode. An 8m long piece of 0.25mm diameter, PTFE coated Ni wire was wound in a spiral groove on the outside of the Ni cylinder as an electrolyte temperature sensor.

The side walls of the cells are fabricated from thick (~ 1 cm) PTFE as good thermal insulation. The remainder of the cells walls are fabricated from even thicker (~ 2 cm) PTFE. In this way the primary heat flow path is from the electrolyte to the bath. Since this path is a reasonably good insulator the temperature of the electrolyte rose significantly when the cell was operated at higher electrolysis currents (> 0.5A).

The F cell was operated in a bath identical to one used for the L cell/calorimeter, which was later used for the M cell/calorimeter. The data acquisition and control hardware was the same as that used for the M calorimeter. The calorimetric ΔT was calculated as the difference between the Pt wire in the Ni cylinder and the bath. Because of the insulating properties of the thick PTFE wall no external heater was employed in this design. To avoid chemical contamination problems, no internal heaters were used. Two Pt wires were mounted at the top of the electrode chamber to act as a resistive electrolyte level sensor. When the two wires read an open circuit an HPLC pump was commanded to add D_2O until the sensor read a stable resistance. A constant 0.5 mA was passed between the level sensor wires.

Two F experiments were performed. In the first experiment F1, a 3mm diameter x 3 cm long Engelhard Lot 1 Pd cathode, was used. It had a "center-tap" Pt wire spot-welded on its longitudinal center. This center-tap was used to apply axial current between the center and two ends of the cathode. Two additional identical power supplies were used for this purpose. The Ni cylinder was used as the anode. For experiment F2 a "cage" of Pt wire wrapped around quartz rods held between two PTFE plates, mounted inside the Ni cylinder was used as the anode. The Ni cylinder was coated with Pt. A newly-annealed unused Engelhard Lot 2 Pd cathode of 3 mm diameter x 3 cm long was used as the cathode. No center-tap was used in F2. The results of these experiments are given below.

F1. The purpose of the F1 experiment was to test the calorimetry in a large ΔT system, and the electrochemistry of the Pd cathode/Ni anode system. The resistance of the previously unused Engelhard lot 1 Pd cathode was 0.55 mΩ in air. Approximately 95 cm^3 of 1M LiOD with 200 ppm Al was added to the cell with 2.5V (potentiostatic) applied across the cell. After several attempts and repairs of leaks, etc., the experiment was restarted with August 6, 1993 13:48 hours as 0 elapsed time. At 75 mA cathodic the cathode loaded to $R/R° = 1.96$ and remained steady. As the current was stepped to 0.21, 0.51, 1.0, 1.5, and 2.0A the $R/R°$ never came below 1.9. The current was stepped backed down to 1A, 0.5A and 0.25A then back up to 1.5A and 2.0A. The cell was left open-circuit for ~ 1.25 hours and then 2.0 A was applied. Approximately 35 ml D_2O was added to the cell.

The bipolar axial current system was connected. The cell current was lowered to 0.5A and held there for ~ 125 hours. The cell current was stepped to 3.0A. Approximately 15 hours later 3.0A was also applied axially along the cathode with each power supply's negative terminal connected to the center of the cathode. After 32 hours I_{axial} was raised to 6.0A. An additional 20 ml D_2O was added to the cell. When the experiment was terminated the cell was less than half full of electrolyte. Most of the missing electrolyte had leaked into a connector space at the bottom of the cell.

The scatter in the calculated excess power for the cell was as high as ± 0.5W at the higher cell and axial currents. The excess power always averaged to 0W throughout the entire experiment.

Together with other experiments these results suggest that Ni anodes are not conducive to good Pd cathode loading. We also learned that better cell seals were needed before operating the next experiment.

F2. The purpose of the F2 experiment was to search for excess power in an electrochemical cell which heated rapidly during current steps. For the reasons outlined earlier, no heater was used in this cell. To avoid electrolyte contact with Ni a new Ni anode cylinder was machined and coated with Pt. This cylinder had an ~ 20 m length of 0.25 mm diameter Pt wire wound on the groove on the outside of the anode as an electrolyte temperature sensor. The calorimetric measurements were as described above. The electrolyte was identical to that used in the F1 experiment. A better seal at the connector was designed and implemented.

Fast heat steps were induced, after achieving nominal low current loading, by stepping the cell current to either 2, 3, or 4 A. Calorimetric parameters were determined during these current steps early in the experiment, with the assumption of no excess power. Figure 3-1 shows the plot of total power and excess power as the current was stepped from 0.075A to 3.075A, then to 4.075A, then to 2.075A and returned to 0.075A. The large fluctuation in excess power at ~388 and 410 hours was due to D_2O top-up. At stable electrolyte levels the scatter in excess power measurement is ~ ± 0.25W.

Figure 3-2 shows the calorimetric response of the cell when the current is alternated between 0.075A and ~3A every 12 hours. The response suggests a decreasing electrolyte level with time, even though enough D_2O was added to offset the loss due to electrolysis.

We interpret this to mean that there is significant D_2O loss due to evaporation. Due to this unmeasured electrolyte loss the calorimetry was severely compromised.

It is shown, that in future experiments D_2O must be added more frequently, the electrolyte level must be measured in some way and that, if possible, the D_2O additions should be automated. Future experiments will incorporate these recommendations.
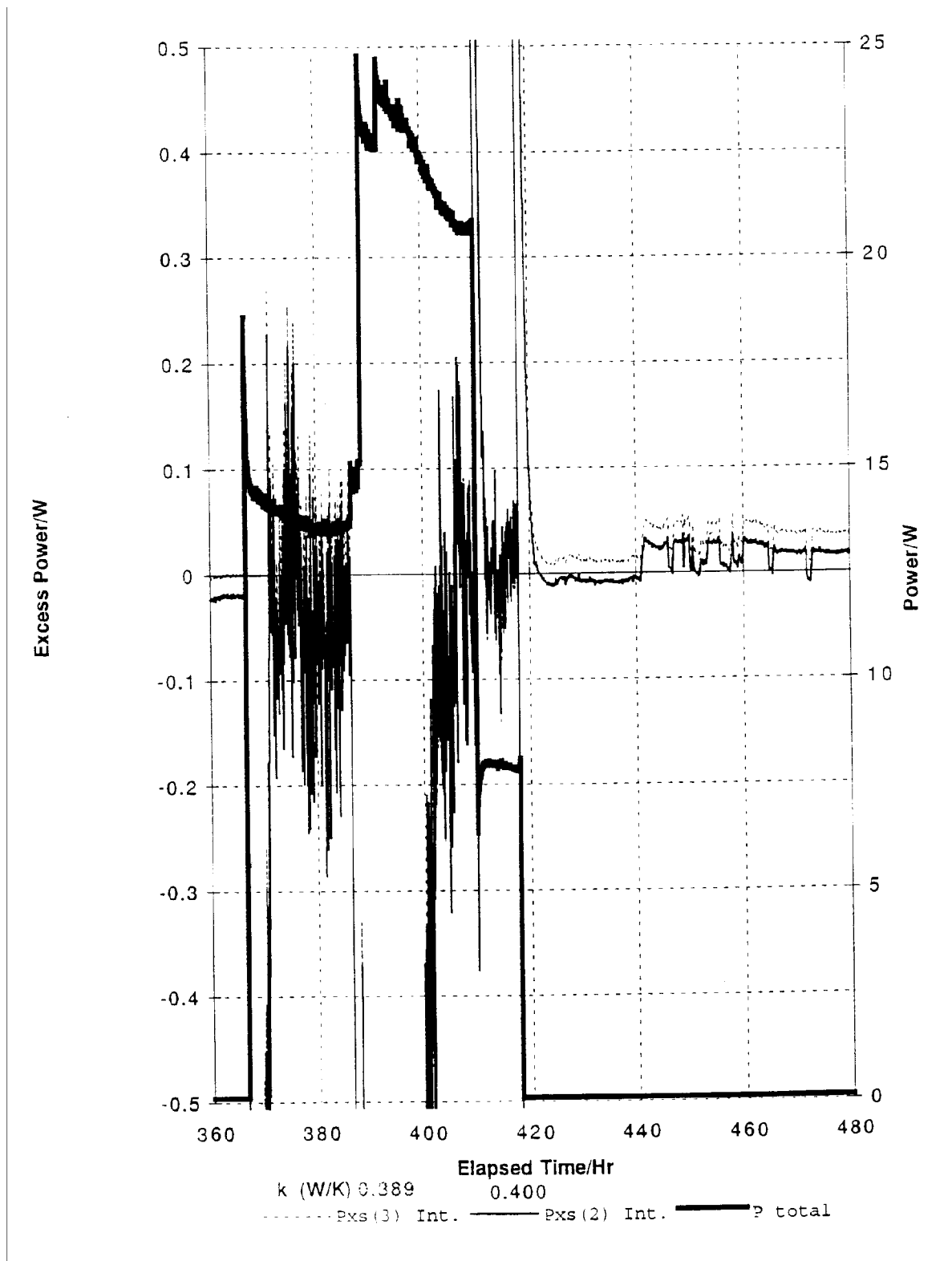
Figure 3-1
Cell F2 total power and excess power versus time during calibration steps
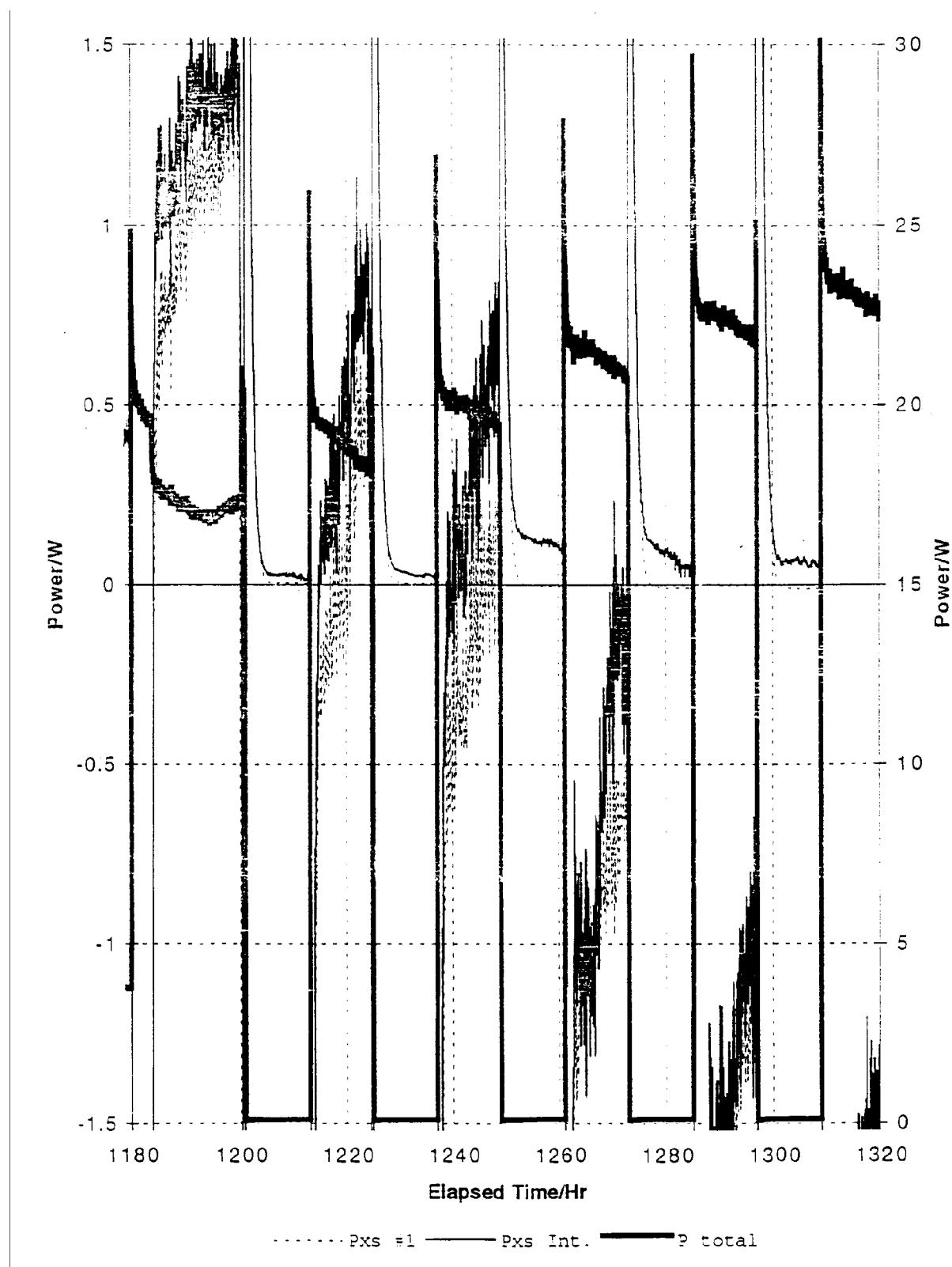
Figure 3-2
Cell F2 total power and excess power versus time during current pulses

G Series Experiments

Introduction. The G cell set of experiments were designed to allow simultaneous measurement of excess power and on-line γ-ray detection. The cell was designed to fit inside the NaI Compton-Suppressed high purity germanium (HPGE) $\hat{y}$-ray detection system (See Vol. 2 for a description). The electrode chamber has a very thin cylindrical PTFE wall intimately contacting a cooled cylindrical jacket on the outer wall of the cell (as shown in Figure 3-3). The bottom wall of the cell is also thin PTFE to minimize the absorption of any $\hat{y}$-rays sourced in the cell. This bottom is then covered with a polyethylene disc and a thick cylinder of poly-styrene foam as thermal insulation. The top of the HPGE detector is touching the bottom of the 1 cm thick polystyrene below the cell. The portion of the cell above the electrode chamber has thick insulating side walls and top plate.

The cell is designed as a heat flow calorimeter where the electrode chamber wall represents the primary heat flow path. Water is flowed through the Al jacket on the outer wall and the water's inlet and outlet temperatures measured. The electrolyte's temperature is also measured. The difference between the electrolyte temperature and the water jacket's average temperature is the heat flow calorimeter's ΔT. If the electrode chamber's walls were 100% thermally conductive and the rest of the calorimeter was 100% thermally insulating then the output power P_{out} would be a simple linear function of ΔT.

$$P_{out} = K(T_{elec.} - T_{jacket})$$

At high cooling jacket flow rate $T_{jacket} = T_{out} = T_{in}$.

Since there are other heat-loss paths, the function describing P_{out} is somewhat complicated and therefore determined empirically for each experiment. By using a compensation/calibration heater, the total input power (P_{in}) was held at the same selected values during the calibration and operation phases of the experiment. A third-order polynomial (*i.e.* $P_{out} = 0.0097.2 + 0.442 (\Delta T) +) 0.0487 (\Delta T)^2 - 0.0000553 (\Delta T)^3$ was used to describe the $P_{out}/\Delta T$ function. For the G experiments that were not fitted with a heater, the cell was calibrated using only electrochemical power during the phases when the cathode was poorly loaded with deuterium and presumably unlikely to produce excess power. The cooling jacket temperature data can also be interpreted as a crude mass-flow calorimeter by measuring the average cooling water flow rate ($\frac{\partial m}{\partial t}$) and using ΔT as the difference between the cooling water outlet and inlet temperatures. However, the imprecision in ($\frac{\partial m}{\partial t}$) and ΔT was such that this approach was only viable at higher input powers above ~ 2 watts.
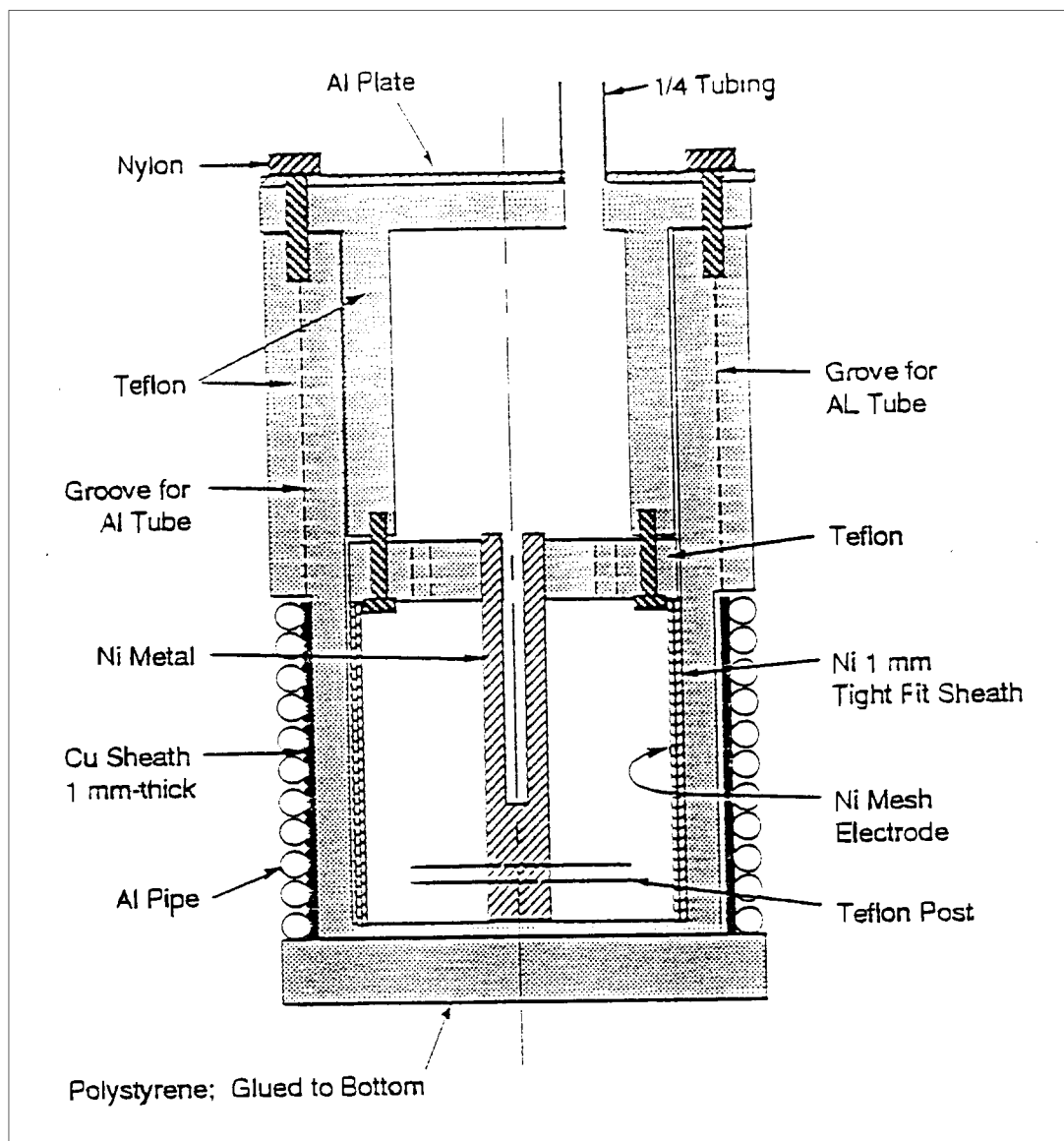
Figure 3-3
Diagram of G cell

There were the four experiments run in the G cell: G1, G2, G3 and G4. Each experiment represented a modification and improvement to the previous experiment in an attempt to yield better calorimetry and/or higher D:Pd loading.

The G1 experiment used an Aethica Metals 1mm dia., 22 cm long Pd wire cathode in the shape of a 4-point crown held between two concentric, cylindrical Ni anodes. A heater was mounted in the electrolyte and a temperature sensor in a hole drilled in the center anode. Experiment G2 was nearly identical to G1 except that the cathode was from Engelhard Pd lot 2 and the position of the heater and temperature sensor were exchanged to yield better calorimetry. Experiments G3 and G4 used our traditional Pt wire/quartz cage anode assembly. G3 used a 3mm diameter x 3 cm long Engelhard lot 2 Pd cathode while G4 had a 1mm diameter x 3 cm long Engelhard Pd cathode. We have only used one lot of 1mm Engelhard Pd.

None of the cathodes in experiments G1-G3 loaded well enough to be expected to produce excess power. Other technical problems caused us to redesign the cell to yield more reproducible calorimetry. Results of experiment G4 are described below.

G4. The G4 experiment was designed to load a 1mm diameter Pd cathode to a high D:Pd ratio and cause a high flux of D axially along the cathode. This flux is effected by passing a dc current, up to 7A, axially along the cathode. During times when axial current is passing both loading information and calorimetry were seriously inaccurate: Calorimetry was poor because the axial input power was not measured at the calorimeter boundary. Loading measurements were inaccurate because the actual temperature of the cathode could not be determined. Attempts to estimate the cathode temperature from the power input to the cathode (which was measured) yielded unreasonable results. The high DC current also interfered with the 1000 Hz AC resistance measurement.

The 1 mm diameter x 3 cm long (0.75 cm^2 area) Engelhard Pd cathode was mounted in the center of the electrode chamber. The cell used 120 mL of 1 M LiOD/D$_2$O as electrolyte. The cathode had 2 wires attached to both the top and bottom of the cathode for 4-point resistance measurement using the HP4338A resistance meter. A third lead wire was attached to the bottom of the cathode to pass electrochemical current. The cathode had a mass of 0.3616 g and a starting axial resistance of 4.653 mΩ. The cell is shown in Figure 3-3.

A new calorimetry flow system was used for this experiment. The cooled 18 mΩ cm water flowed through a small 20 x 20 x 10 cm bath with a resistive heater. The heater was controlled by an OMEGA CN2042P2 temperature controller. A PTFE insulated RTD, immersed in the bath, was used as a temperature sensor for the controller. The bath was maintained at 23° ± 0.5°C, the approximate temperature of the cubicle and lead shield. The water was pumped from the bath to the cell's cooling jacket and back to the

bath. As the experiment progressed, and especially at higher currents, the return water was warmer than the 23°C bath.

To counteract this temperature rise the warm water return was sent to the chilled water reservoir causing the chilled water to more quickly fill the mini-bath and more effectively maintain the temperature set point.

A 2-wire level sensor was used to determine when the electrolyte level had dropped by ~ 5 ml from the top plate and read open circuit. An HPLC pump was then instructed to add D_2O slowly until the level sensor read as a closed circuit. This Ti pump head HPLC pump was also used to introduce the starting electrolyte after the cell/calorimeter was installed inside the Pb shield. With the cell potential held at ~ 2.0V potentiostatic, 120 ml of 1 M $LiOD/D_2O$ was added to the cell at 20 ml/minute with N_2 flowing through the cell. The cell's power supply was then set to 0.025A galvanostatic and D_2 flowed through the cell. Zero elapsed time on this experiment was set as 8:00 a.m. on 22 December 1993. Current was first applied at 7.0 hours. For the first 25 hours of the experiment the power supply was occasionally replaced with a 1.5V battery to determine if the power supply was interfering with the γ-ray spectrometer's data collection system. No correlation was found.

After ~ 55 hours of low current the cathode's resistance ratio ($R/R°$) reached a maximum of ~ 1.96. By 100 hours the $R/R°$ had leveled at ~ 1.93. Diurnal variations in the cell temperature were ~ ± 0.5°C at this time, yielding an excess power uncertainty of ~ ± 30 mW. By 128 hours the $R/R°$ had risen to ~ 1.95 and a 20 hour ramp from 25 to 375 mA was initiated. At the end of the ramp, the $R/R°$ was ~ 1.9 but rose to 1.92 within 20 hours. At 173 hours a 20-hour ramp from 375 to 725 mA was started where the $R/R°$ reached ~ 1.89 and was steady. The steady state excess power (P_{xs}) calculation was well behaved and set to 0 W. At 271 hours a 10-hour ramp from a 725 mA to 1.05 A reduced $R/R°$ from 1.89 to 1.87 and was steady.

This 1.05 A/cm^2 was held only for ~ 13 hours before dropping the current to 25 mA at ~ 294 hours. Thirty minutes later the current was switched off and the cell removed to attach axial current leads to the outside of the cell. Data collection continued during this process. During the open circuit the $R/R°$ rose to a maximum of 1.93 and relaxed to ~ 1.89 before current was reapplied.

At 1A electrolysis current the electrolyte and cooling water temperatures reached ~ 45°C which was unacceptable. To increase the efficiency of the cooling system the warm water was sent directly to the chilled water reservoir and chilled water was used to make up the level of the mini-bath. The cell was placed back inside the γ-ray detector system. At ~ 322 hours 25 mA cathodic was applied. The cell and calorimeter took ~ 15 hours to attain an electrochemically and thermally stable environment. The $R/R°$ rose to ~ 1.98 over a 45 hour period. At 369 hours the current was stepped to 350 mA to

attempt to initiate a large flux of D into and out of the cathode. This is in contrast to the current ramps used earlier in this experiment which strived to maintain the loading at or near a steady state condition. There are reports of large D flux yielding anomalous heat and nuclear events in Pd. At 350 mA the R/R^o dropped from 1.98 to 1.95. At 392 hours the current was raised to 675 mA and the R/R^o continued to fall slowly. The excess power was 0 ± 50 mW during this time.

Unfortunately at ~ 395 hours the data collection system failed and the cell was set to open circuit. During this time the cathode deloaded significantly. The system was repaired and restarted at 482 hours and the cell was left at open circuit. The R/R^o had reached 1.58 on the left side of the maximum suggesting a D:Pd ~ 0.3. R/R^o continued to fall to 1.45 when 75 mA cathodic was applied at ~ 504 hours. The cathode loaded quickly sending R/R^o through a maximum of 1.97 and settling on 1.83. Again, to track down electronic noise sources, the power supply was turned off and a 1.5 V battery attached across the cell at ~ 512 hours. During this time the R/R^o increased to ~ 2.0 and remained relatively steady until a mild anodic strip of 10 mA was initiated at ~ 530 hours. The loading plummeted with the R/R^o reaching 1.32 before 75 mA cathodic current was applied at 534 hours. R/R^o quickly went through a maximum of 1.99 and reached ~ 1.86.

This loading level was not as high as that in the preceding step cycle suggesting that the long open-circuit established a better cathode surface for loading than did a mild 10 mA/cm² anodic current. The length and depth of the anodic deload may have contributed to the subsequently poor D loading performance. Another attempt to obtain a higher steady state loading was made by initiating two current ramps. At 554 hours a 20-hour ramp from 75 to 575 mA was started. The cathode deloaded during the ramp with R/R^o reaching ~ 1.92. At ~ 587 hours another 20 hour ramp was started from .575A to 1.075A, which did not effect the cathode loading. The continued poor loading performance gave more credence to the belief that the long anodic strip (10 mA for 4 hours) was disadvantageous to subsequent cathodic loading. During this time the excess power measured was 0 ± 100 mW. This large uncertainty in the measurement was typical of these heat flow calorimeters at higher currents.

This 1.075 A dc cell current was maintained until 889 hours elapsed time. In order to effect a high D flux on the poorly loaded cathode axial current steps were initiated with the DC current at 1.075 A. At 656 hours 1.0A was applied axially along the cathode. At ~ 678 hours the axial current was increased to 2A and then to 4A at ~ 681 hours and 7A at 769 hours. The axial current remained on until 796 hours. During the axial current experiment the scatter in the excess power measurement increased to ± 150 mW but averaged to 0 W. The cell jacket temperature remained ostensibly constant during this time. Due to instrumental interferences between the axial and cell current power supplies and difficulties in estimating the cathode temperature, the R/R^o measurement were unreliable while axial current was applied. Since the R/R^o relaxed immediately after the discontinuation of axial current to the value measured (~1.94) just before axial

current was applied, we assume that the cathode loading did not change during the axial current experiment. The axial current was again set to 7A from 848 hours to 871 hours.

At 889 hours the cell current was reduced to 25 mA cathodic and the cell stripped at 20 mA anodic for ~ 2 hours starting at 892 hours. During the strip 5 ml of 1M LiOD/D_2O saturated with Al (~ 200 ppm w/v) was added to the cell, before the current was returned to 25 mA cathodic. The current was stepped to 230 mA at ~ 941 hours, to 500 mA at ~ 961 hours and to 1.0A at ~ 964 hours. The current was returned to 25 mA cathodic at ~ 984 hours. During the low current load the R/R^o went through a maximum of ~ 2.0 and reached a minimum of ~ 1.86 before rising again to about 1.91. At 0.33A the ratio again went through a minimum of 1.86 and rose to ~ 1.9 where it remained during the 0.5 A cathodic current. At 1A cathodic current the ratio dipped to 1.88 before slowly rising to 1.92 just before the current was lowered. The excess power calculation showed 75 ± 50 mW at 0.33A and 100 ± 50 mW at 0.5 A and through the first 10 hours of 1.0 A before falling back to 0 ± 50 mW.

The cell underwent a 1.75 hour, 20 mA anodic strip at 988 hours. During the low current cycle R/R^o relaxed to 1.96, while during the strip the ratio quickly went through a maximum of 1.99 continued to deload efficiently reaching a minimum of 1.47 at 989.75 hours. During this strip, 10 ml of 1M LiOD/D_2O saturated with Al was added to the cell followed by 3ml of D_2O to wash the lines. This addition was performed in hope of forming a thick film on the cathode which would promote the attainment and maintenance of high D loading. Cathodic current of 25 mA was applied after the strip. The current was raised to 50 mA at 1034 hours and doubled every 4 hours until reaching 0.8A at 1050 hours. The current was then raised to 1.0A at 1054 hours.

During the low current level the R/R^o went through a maximum of 1.98 down to 1.93. As the current stepped every 4 hours the ratio slowly dropped to ~ 1.90.

In order to raise the temperature of the cell quickly we experimented with large axial current steps while stopping the cooling water flow. The cell current was left at 1.0A for the remainder of the experiment. When the pump flow was stopped at 1059 hours the cell temperature rose to ~ 45°C from ~ 28°C. When 7A axial current was subsequently applied for 35 minutes at ~ 1064 hours the temperature rose to 54°C, then relaxed toward 48°C. When the pump was restarted at 1070 hours the temperature returned to 28°C. No calorimetry, excess power calculations or loading determinations could be performed during the heating experiment. The cathode may have loaded after the axial current pulse but ultimately de-loaded to ~ R/R^o = 1.94. Excess power calculations resumed when the pump was restarted at 1162 hours with the no axial current.

During the high temperature excursions the level sensor was damaged and the automatic D_2O refill system failed. To compensate ~ 40 ml of D_2O was added to the cell

after 1177 hours. $R/R°$ remained above 1.95 except during the D_2O loss when the ratio dropped to < 1.9, probably on the poorly loaded side of the maximum. After the D_2O was topped off the ratio rose to ~ 1.98. The electrochemical experiment was terminated at 1186 hours. Different instruments were turned off and on for the next 36 hours in order to test for electrical noise sources, ground loops, etc.

The G4 experiment allowed us to perform good calorimetry, although less precise than in the flow calorimeters, on an electrolyzing cell in front of the γ-ray spectrometer. Except during the application of axial current or when the calorimetric flow was purposely suspended the calorimeter was precise to within ± 2% of input power. There was only one time (942-972 hours) when excess power deviated from 0W. Here the $P_{xs} \cong 75 ± 50$ mW for the thirty hours. During this experiment the Pd cathode was never loaded with D to higher than 0.87. The cathode always deloaded when the current density was greater than 100 mA/cm^2. This poor loading characteristic may be related to the excessive deloading down to D:Pd $\cong$ 0.3 during anodic strips. Figures 3-4 and 3-5 show the cell/calorimeter response from 900-1000 hours.

Shorter strips to D:Pd $\geq$ 0.6 may allow better loading to be obtained during subsequent low current regimes. The minimum D:Pd ratio, and the time at anodic currents, and the anodic potential may all contribute to the loading process. In order to continue calorimetry during times of expected high D flux we need a cell with accurate and precise measurement of the power input to the cell during the axial current experiment. Using a compensation heater should allow high electrolyte temperatures while maintaining good calorimetry.
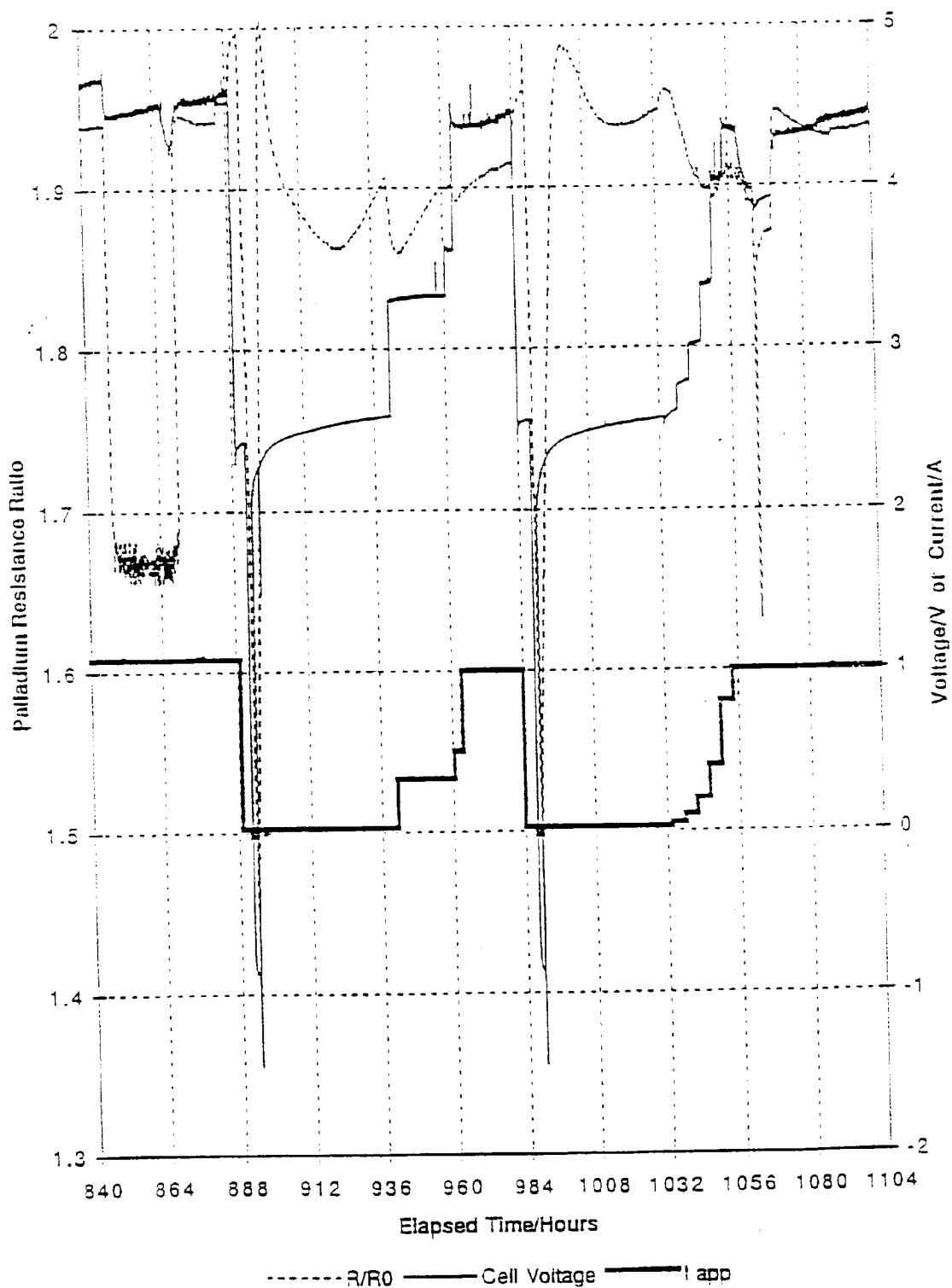
Figure 3-4
Cell G4 Electrochemical parameters versus time during current steps
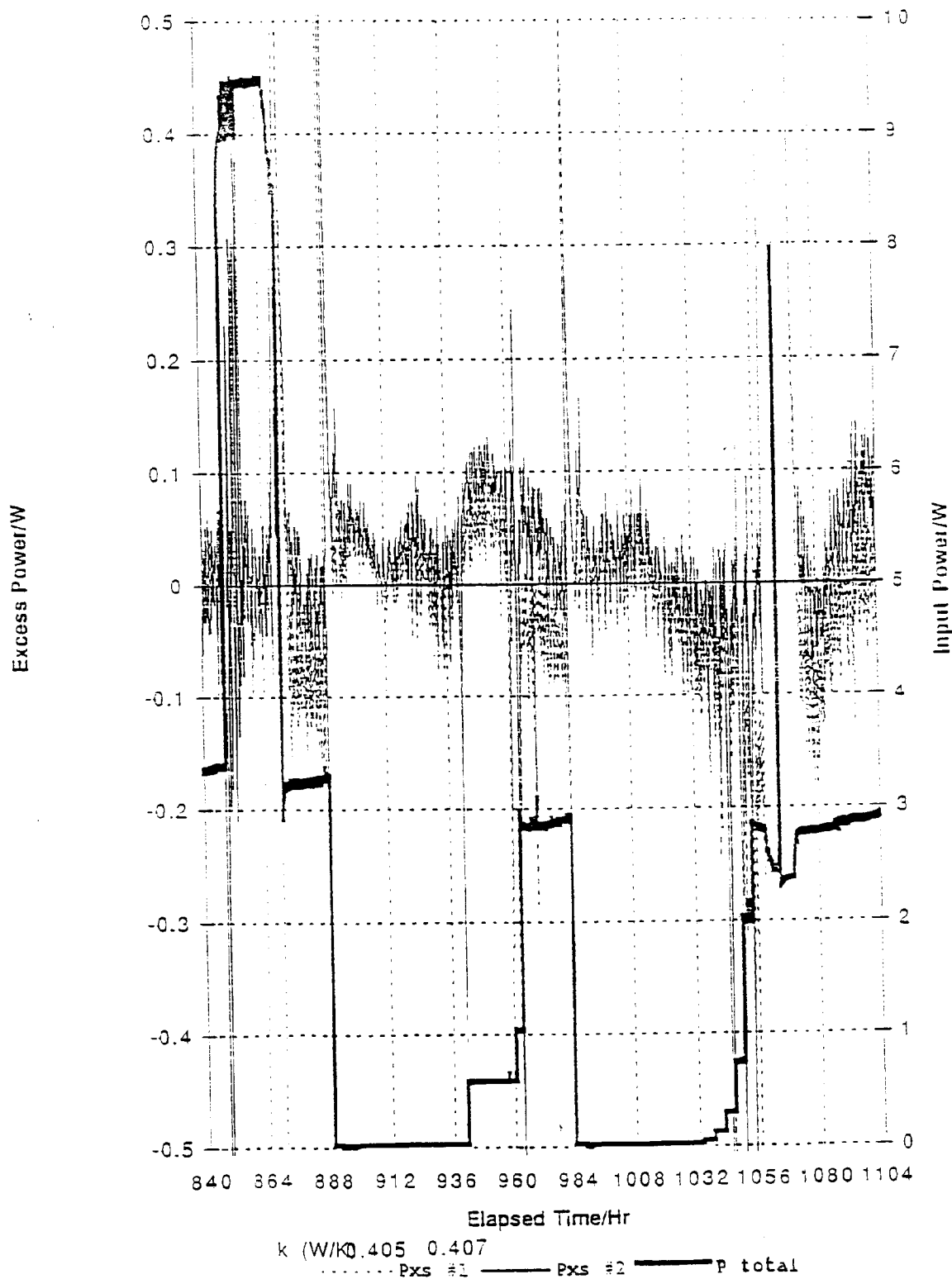
Figure 3-5
Cell G4 Total power and excess power versus time during current steps

T Series Experiments

Introduction. In preparation for the routine use of closed large-volume teflon cells in the "L" series experiments, a series of experiments were undertaken in order to establish the utility and safety of this cell design. Numerous difficulties were experienced in the prototypic experiments T1 and T2, and few meaningful calorimetric or thermometric data were collected. These experiments did, however, demonstrate the basic utility of the cell design, in particular with respect to the mode of operation of the recombination catalyst.

In experiment T3 the cathode was a Pd plate (Tanaka, 1mm thick, 1 inch square) mounted vertically in the center of a cylindrical Ni mesh anode. The electrolyte was 1 M LiOD with no additives at the outset. Three RTD temperature sensors were included; one unsheathed and mounted above the catalyst, two sheathed in Teflon and submerged in the electrolyte. The first of these (the "inner") was positioned close to and slightly above the top of the (vertically-mounted) plate. The second (the "outer") was positioned between the anode and the cell wall, at about half-height. No heater, either internal or external, was provided. The entire cell was connected to a gas-handling manifold and placed in a constant-temperature water bath. As described further below, an in-leakage of bath water occurred after 40 h of operation. The experiment was dismantled and the electrolyte replaced. Al and B electrolyte additions were made at later times.

Experiment Chronology. In order to assist with the interpretation of the accompanying result plots, Figures. 3-6 to 3-11, the following experiment chronology is provided. The data plotted are: the difference between the inner and outer temperature sensor readings (dark thin line), the input electrochemical power (medium thick line); the cell current (dark thin line); the cell voltage (medium thick line).
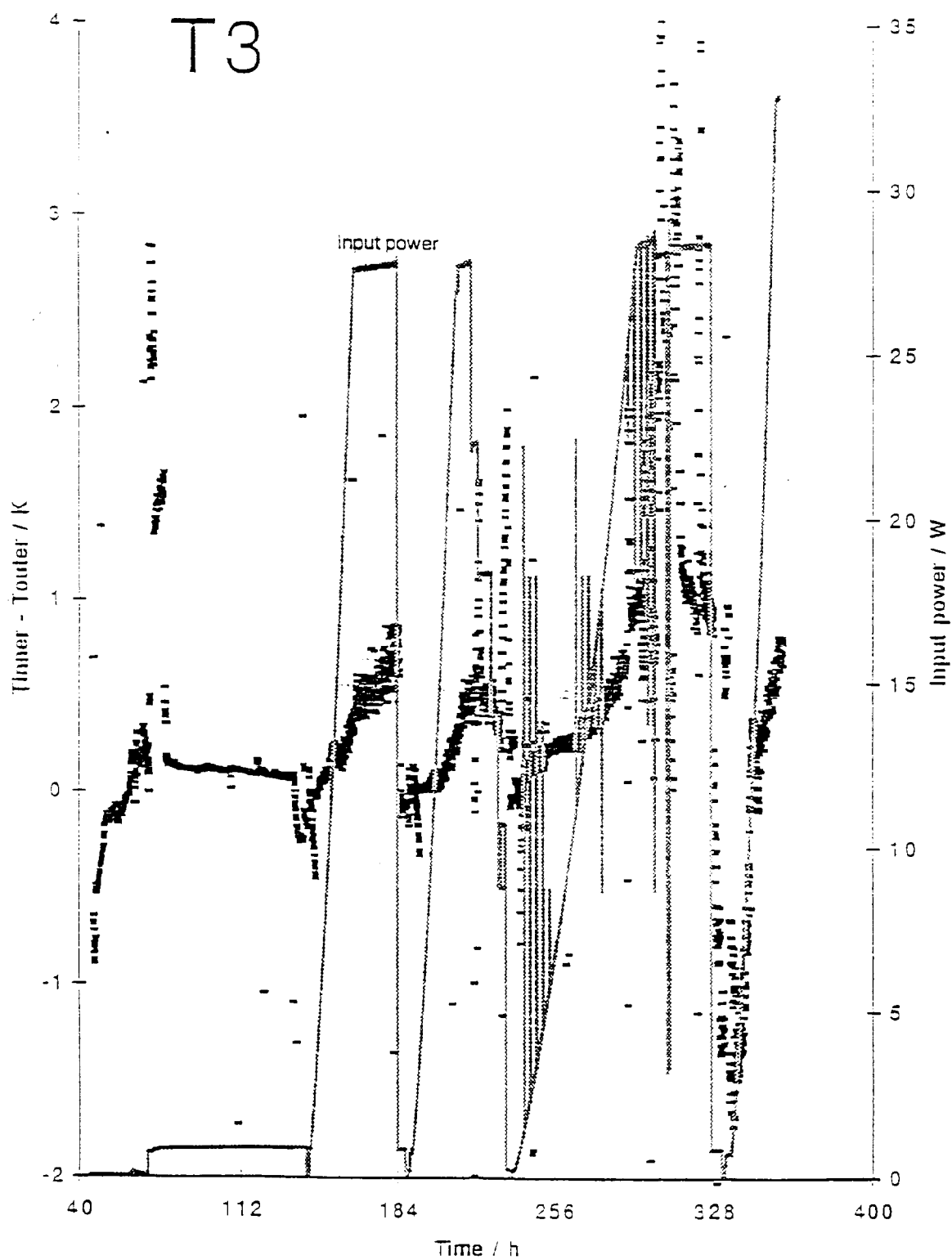
Figure 3-6
Calorimetric data for T3
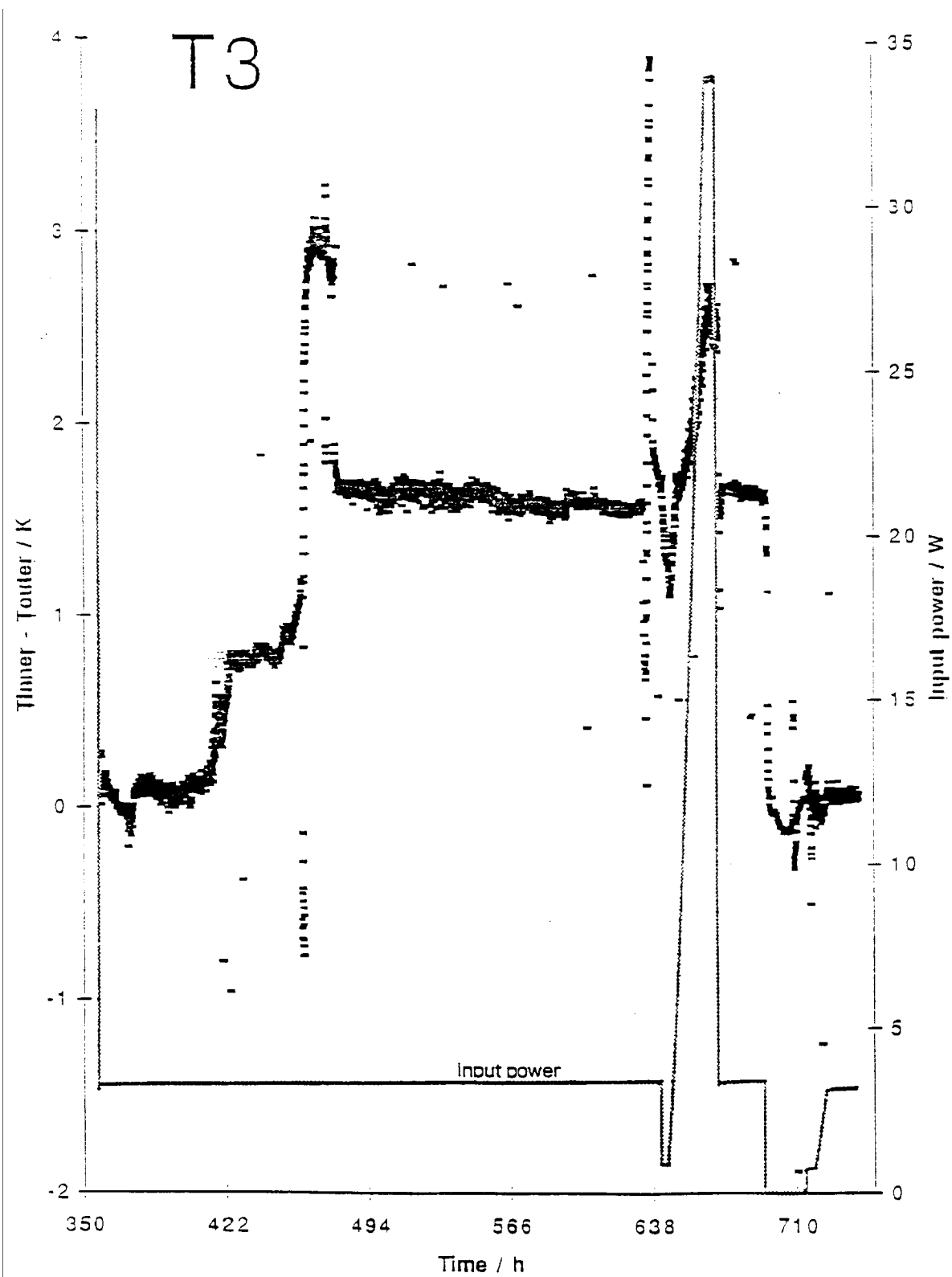
Figure 3-7
Calorimetric data for T3
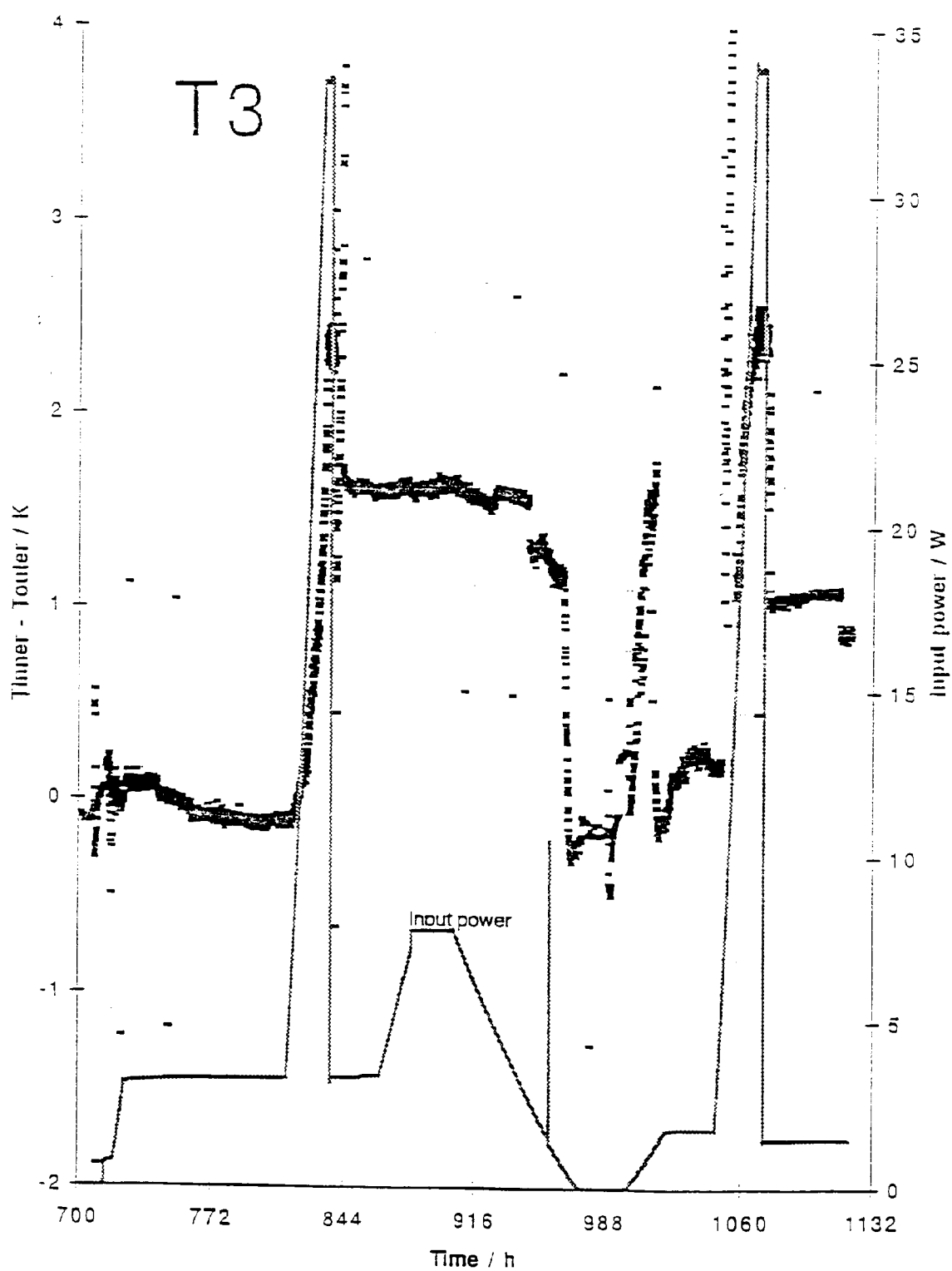
Figure 3-8
Calorimetric data for T3
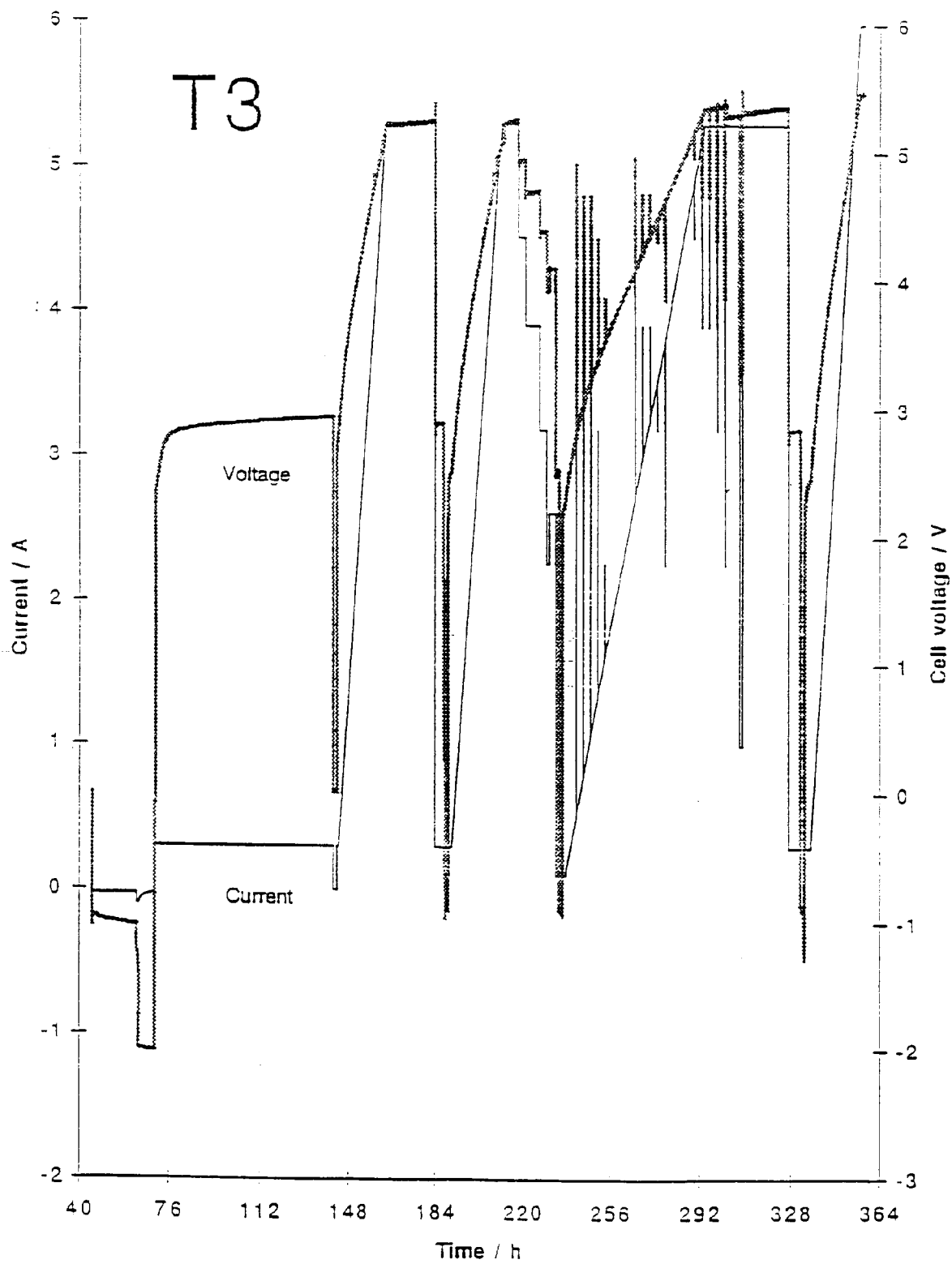
Figure 3-9
Current and voltage data for T3
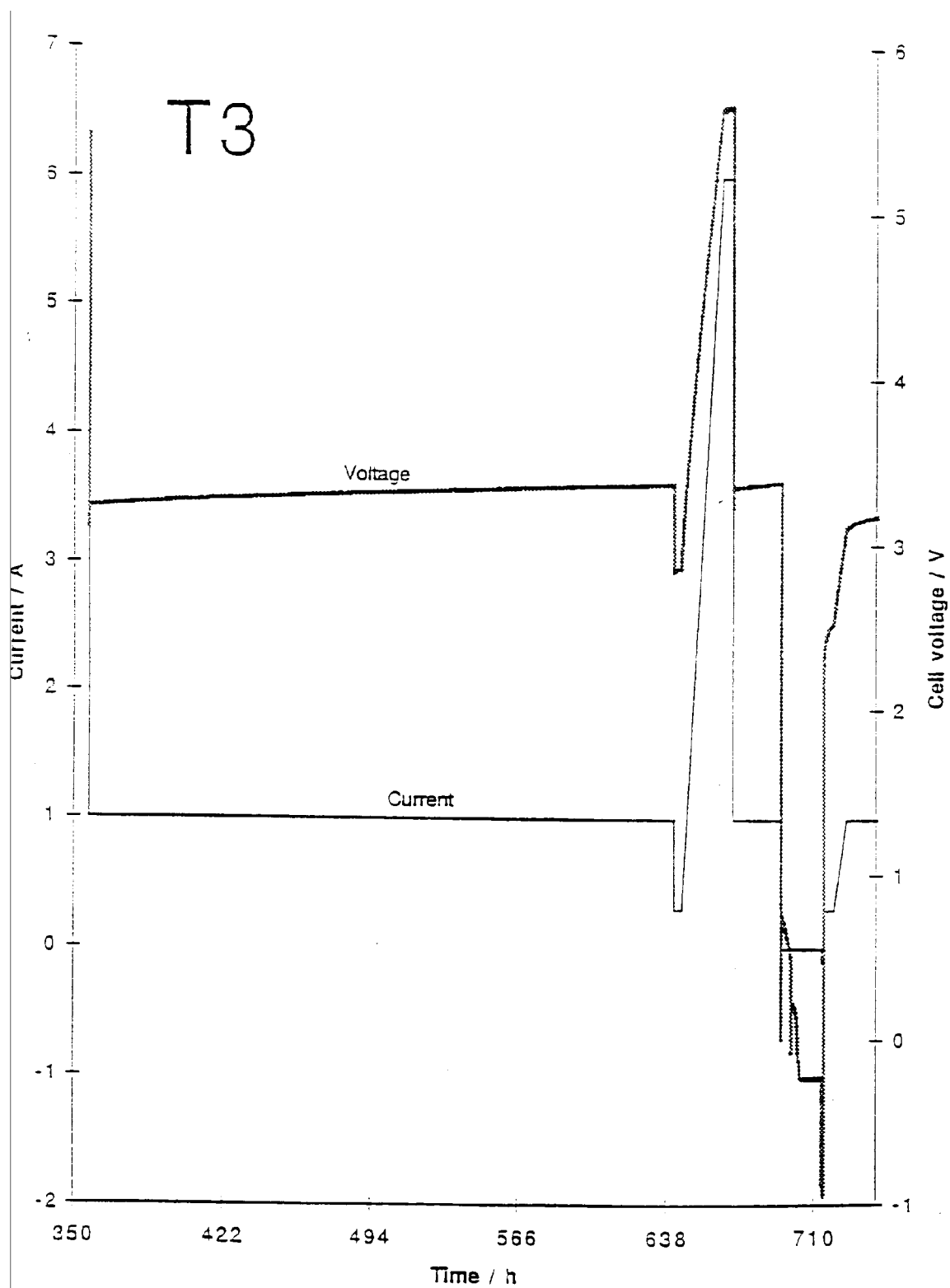
Figure 3-10
Current and voltage data for T3
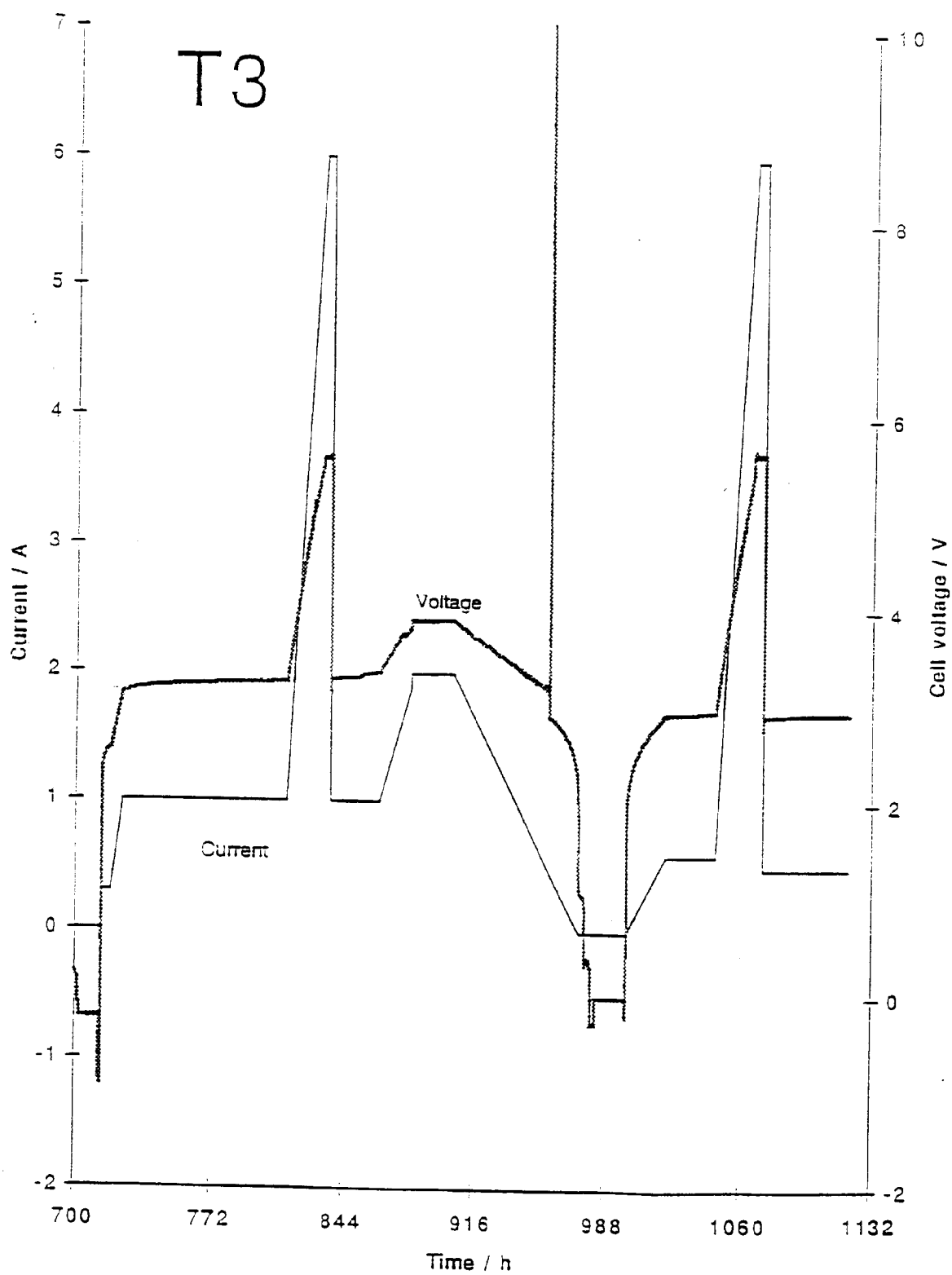
Figure 3-11
Current and voltage data for T3

Time / h	Operation	Result
40	Apparent leak from bath, experiment restarted	
188	Al added	
309	B added	
332 - 334	Apply anodic current, -0.1/-0.3 A	
334 - 336	Hold at 0.3 A	
336 - 356	Ramp to 6 A	
356 - 358	Hold at 6 A	
358	Drop current to 1 A	Temp. anomaly appears at 415 h Anomaly increases step-wise over ensuing 230 h period.
642	Drop current to 0.3 A	
645 - 665	Ramp to 6 A	
670	Drop current to 1 A	The anomaly persists throughout.
693	Drop current to 0 A (actually slightly anodic)	
714 - 715	Strip at -0.1 A	
715 - 720	Hold current at 0.3 A	
720 - 725	Ramp to 1 A	No anomaly
812 - 832	Ramp to 6 A	
832 - 837	Hold current at 6 A	
837	Drop current to 1 A	Anomaly appears at 838 h
864 - 882	Ramp to 2 A	Anomaly decreases
904 - 974	Ramp to 0 A (slightly anodic)	Anomaly increases, maximizes at 0.3 A, then decreases to zero at 0 A.
983 - 1000	Short-circuit power supply	
1000 - 1020	Ramp to 0.6 A	No anomaly
1020 - 1047	Hold at 0.6 A	No anomaly
1047 - 1067	Ramp to 6 A	
1067 - 1072	Hold current at 6 A	No anomaly
1072	Drop current to 0.5 A	Anomaly appears
1072 - 1144	Hold current at 0.5 A	Anomaly persists
1150	Experiment terminated.	

Results. In most respects, the cell behaved well and entirely as expected over its 1200 h lifetime, confirming the general utility of this cell design. A minor exception was the outer RTD which briefly recorded physically unrealistic (very high) temperatures perhaps due to water accumulation around the RTD's electrical connections in the cell head-space.

In one respect, however, the cell exhibited long-term anomalous behavior. Under reproducible conditions, after the addition of boron, the inner sensor recorded a higher temperature with respect to the outer than expected for the input power. Over a significant fraction of its lifetime, the difference between the inner temperature and the outer exhibited a reproducible dependence on the input power, as expected assuming more-or-less uniform heat loss through the cell wall surrounding the electrolyte. The temperature anomaly was manifest as a departure from this dependence, seen most clearly beginning at 415 h, where the inner-outer difference is proportionally too large. The anomaly was largest at low currents but could be removed by turning off the current.

General Observations Concerning Anomaly:

1. Initiated by ramp to high current followed by step down.

2. Turned "off" at very low or zero current; stays "off" when returned to low current.

3. Increases with decreasing current until max. at 300 mA.

4. When "on", effect is current-reproducible.

Discussion. In view of the lack of definition of heat-loss paths from the cell, it is not possible to perform quantitative calorimetry in the case of experiment T3. Therefore it is not possible to associate unambiguously the observed temperature anomalies with anything other than *local* thermal anomalies, assuming that the temperature sensors are functioning correctly. One possible cause of relative local thermal anomalies is the different electrolyte stirring patterns which will be established in the vicinity of the two sensors, and the variations of these patterns with current. The electrolyte in the vicinity of the inner sensor will be relatively well stirred by bubble evolution from the cathode; the outer sensor however, will experience relatively poor electrolyte stirring due to its placement on the outside of the anode structure.

HH Series Experiments

Experimental. An absolute (helium contamination resistant) gas handling system was developed and installed with a Seebeck calorimeter measuring the heat flowing through each of the six walls of a prismatic cell. The system was monitored using a computer data acquisition system.

In order that the system actually be free from He contamination from the air for the purpose of low level helium analysis, the system is constructed of metal. The only non-metallic parts of the system were the electrical feedthroughs which were commercial high vacuum ceramic devices, and the outlet oil bubbler which was glass; because helium diffuses through glass and ceramic materials, the feedthroughs and bubbler were immersed in the constant temperature water bath. The constant temperature water bath comprises a sealed tank continuously purged with boil-off nitrogen to provide a continuously flushed helium-free environment. The calorimeter and gas system thus comprise an all metal system designed to preclude contamination with atmospheric helium. ^{4}He is present in atmosphere-air at 5240 parts per billion by volume (ppbv).

Figure 3-12 shows the calorimeter, placed in the constant temperature bath, and connected to the gas handling manifold. The glass bubbler from the (thermodynamically) open cell can be seen immersed in the bath, adjacent to the purge tube providing a steady stream of boil-off nitrogen which served to sparge and blanket the bath.

Figure 3-13 shows the calorimeter and electrochemical cell, together with detail of a metal encapsulated resistor used for initial (pre-) calibration, and a typical palladium cathode used in the experiments performed.

The system was designed to operate at a pressure somewhat higher than atmospheric and is open in the thermodynamic sense (no recombination of D_2 and O_2). The electrolysis off-gas is used as a flushing agent so that even if helium contamination were introduced, perhaps during the addition of D_2O or gas sample flask attachment, this contamination level would be much reduced by dilution, after the interior gas volume has been flushed out several times. To avoid contamination during D_2O additions, the D_2O was sparged with liquid nitrogen boil-off gas; the liquid nitrogen boil-off gas has been found to contain no detectable helium (< 1 ppb) since boiling liquefied nitrogen is self sparging. The system was operated above atmospheric pressure, so that convective mass transport leaks will be outward, thus avoiding contamination. The gas system and calorimeter were vacuum tested prior to each experiment.
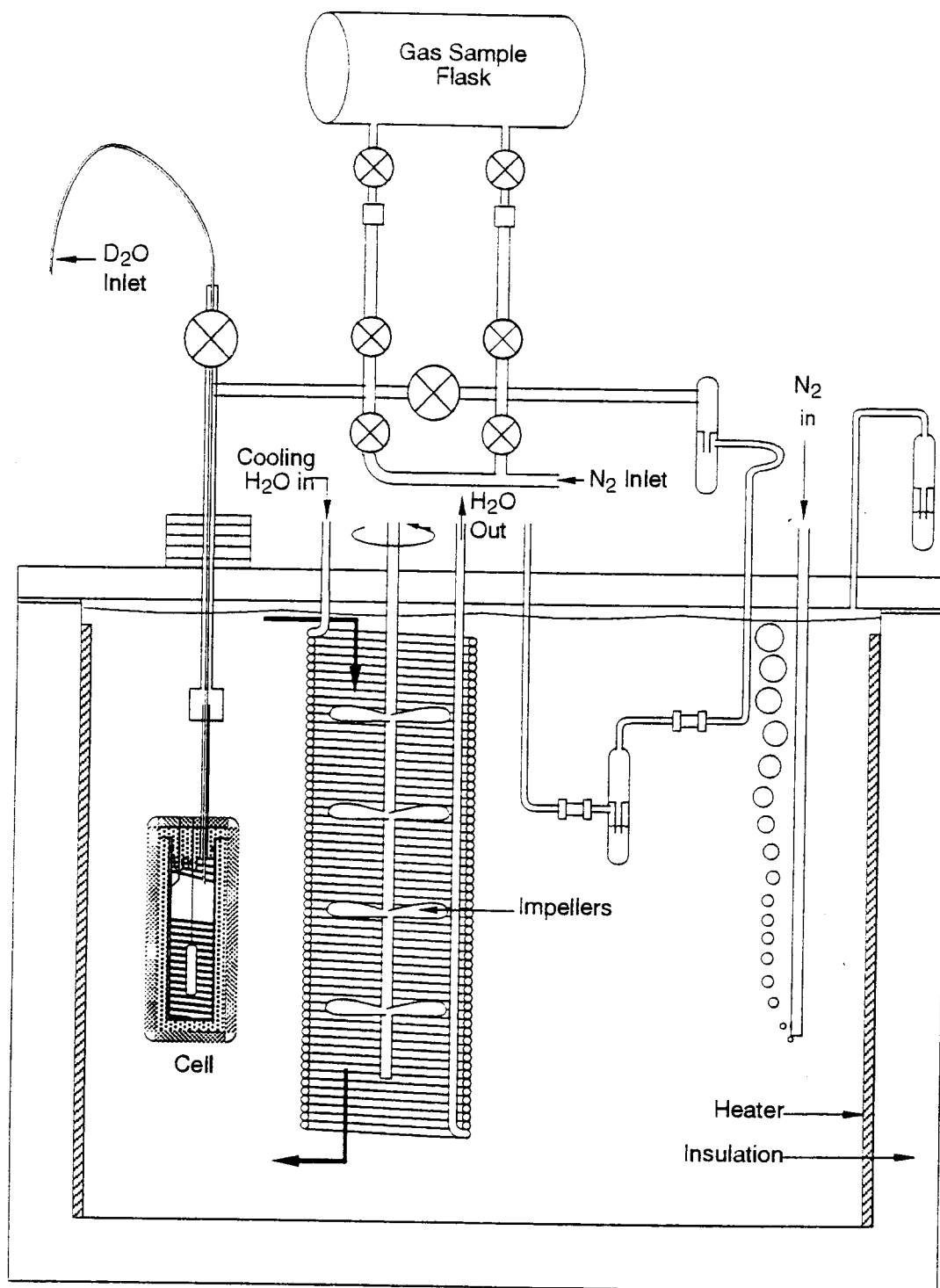
CM-4035-23

Figure 3-12
HH Calorimeter and Gas Manifold
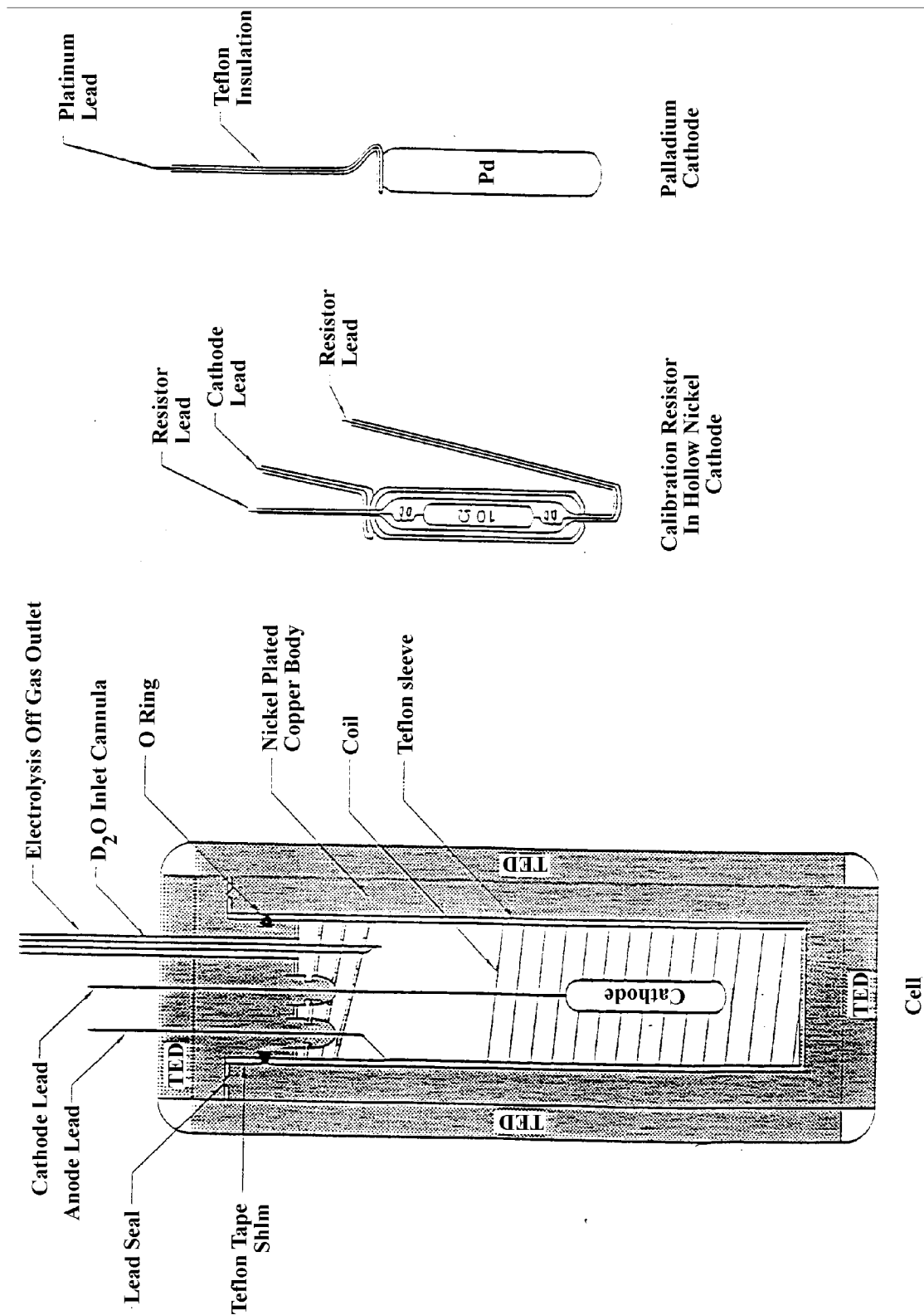
Figure 3-13
Seebeck calorimeter

Calorimeter Calibration. The first electrolysis experiment was operated for calibration purposes. It was comprised of a nickel cathode with a coaxially mounted electrical resistor mounted within the nickel cathode body. The nickel lead wires were soldered to the resistor with 96% Sn 4% Ag solder and the cathode lead itself was spot welded to the nickel casing of the resistor. The resistor was coated with fluorad conformal coating, and teflon tape wrapped along with FEP heat shrink tubing, over the leads and to mask part of the cathode surface proper. The anode was constructed from flattened 0.9 mm diameter platinum wire helically wrapped on a cylindrical cage constructed of quartz and teflon.

The anode and cathode were mounted coaxially within the teflon-sleeved nickel-plated copper can of the Seebeck calorimeter. These electrodes were wired to the nickel leads of the ceramic feedthroughs using notched nickel tubing as splints. The splint area was wrapped with teflon tape held in place with nickel wire to avoid shorting of the leads through the electrolyte solution.

In use the calorimeter was calibrated by using the heater and electrolysis both together and separately. The electrolyte was 0.1 M LiOD prepared by adding 99.99% purity Li (Aesar) to 99.9% D_2O (Aldrich). The entire Seebeck calorimeter is comprised of the electrolytic cell within six thermoelectric elements, which completely enclose the cell by contiguously forming the six surfaces of an elongated cubic cell. The sum of the voltages generated by the thermoelectric devices reflects the power passing through the TEDs. The thermoelectric coefficient (W/V) itself has a (small) temperature coefficient. Thus the copper electrolytic cell body has RTD temperature sensors mounted in it, and the bath temperature is likewise monitored, to provide data necessary for this second order correction.

An experiment was performed to demonstrate that the six TEDs effected a truly contiguous envelope of energy flow measurement, and that water currents in the water bath were not pumping heat into and out of the cell. An integrating envelope was constructed of aluminum and used to encase the Seebeck calorimeter. Good thermal contact with the bath was maintained by filling the gap between the aluminum integrating envelope and the calorimeter with granulated aluminum. No change in the integral Seebeck (TED sum) coefficient was found, indicating that the calorimeter TED envelope is truly continuous and monitors the integral of the heat flow. To stress this point; with or without the exterior integrating aluminum case the calorimetric response was the same.

After the calibration experiments, the feedthroughs and nickel wires were found to be appreciably corroded; the 0.0015" thick electroless nickel plating had been removed from the feedthroughs, and the cell electrolyte contained oxidized metal. The teflon cover slipped over the feedthroughs apparently provided inadequate protection against corrosion. The corrosion seemed to be worst at the anode and the positive lead of the

calibration resistor, and seemed to be exacerbated by a crust derived from the LiOD in the electrolyte. In spite of this corrosion, the cell was found to be vacuum tight. Further cell contamination was derived from the lead gasket that sealed the cell, when electrolyte bypassed the O-ring seal of the lid, but again the cell was gas tight.

The Second Experiment. The second experiment consisted of the same cell/calorimeter. The corroded lid was painted with flourad conformal coating and FEP heat shrink tubing. The anode and cathode leads were spot welded and coated with FEP heat shrink tubing. Two Pt leads were insulated with FEP tubing and dipped down to a level just above the cathode top, to act as an electrolyte level sensor, by monitoring electrical continuity through the electrolyte solution.

The cathode was machined from a 1/8″ diameter Engelhard Pd spool (designated E#3) and specially annealed to avoid oxidation. Its ends were ground to hemispheres and the entire surface polished with sandpaper to a very fine finish by using successively finer papers starting with 600 grit silicon carbide and ending up with 4/0 aluminum oxide specimen polishing paper to polish away the exterior damage zone, so that D loading would occur straight into the grains without an intervening damage layer of amorphous palladium. The electrolyte was 1 molar LiOD containing 200 ppm molar aluminum by dissolution of the metal.

The experiment was started with the cell empty of electrolyte (containing only boil-off N_2), and with the cathode held at -2V with respect to the anode. The electrolyte was added through the cannula, a coaxial metal tube allowing additions to the cell as electrolysis proceeded. Electrochemical current steps were employed to verify the TED calibrations obtained in the previous experiments.

At ~ 213 hours following the initial electrolyte addition (triggering initiation of current flow), the current was ramped to 0.53A (~ 320 mA cm²) in an attempt to stimulate excess power production. Figure 3-14 shows the effect of a D_2O addition (to replace material exhausted by electrolysis), and the current ramp, on the cell input power. Also shown are the consequent effects on the voltages induced across each of the six TED elements. In Figure 3-14, the TED voltages for the top and bottom elements are multiplied by a geometric factor of 3, to account for the smaller area of these surfaces. It can be seen that all six sensors respond monotonically, and rapidly, to the changes in input power.
The power changes result from three causes: electrolyte dilution due to D_2O addition (causing increased resistance in a constant current circuit); increasing cell current during the ramp; electrolyte concentration with loss of the (gaseous) electrolysis products.

Although the form of the response is the same for each of the TED sensors, the coefficients are not. On an equal area basis different coefficients apply to each of the

sides, the top, and the bottom of the calorimeter. Notably, and as expected from geometric and convective effects, thermal conduction through the cell/calorimeter bottom is substantially less than that through the other surfaces.

It is the sum of these voltages, the integrated heat flux, that is used to measure the calorimetric output heat transfer rate (or output heat power). During the course of this work a single, temperature dependent coefficient was employed as a multiplicative operator, to convert the sum of the TED voltages to output power. Two other factors are needed to estimate any "excess" power: an accurate measurement of the input power, and the effects of heat storage or release due to heat capacity (and temperature changes) of the object inside the TED boundary.

In determining the Joule heating due to the electrical input, from the measured cell current and voltage (at the calorimeter boundary), it is necessary to know the extent to which chemical energy is expelled from the cell in the form of electrolysis gases (H_2 and O_2). Throughout the work performed with the HH calorimeter we have assumed that the cell operated thermodynamically open, for which condition

$$P_{input} = I_{cell} \left(V_{cell} - V_{TN} \right)$$

where the thermoneutral voltage for D_2O, $V_{TN} = 1.54$ V.
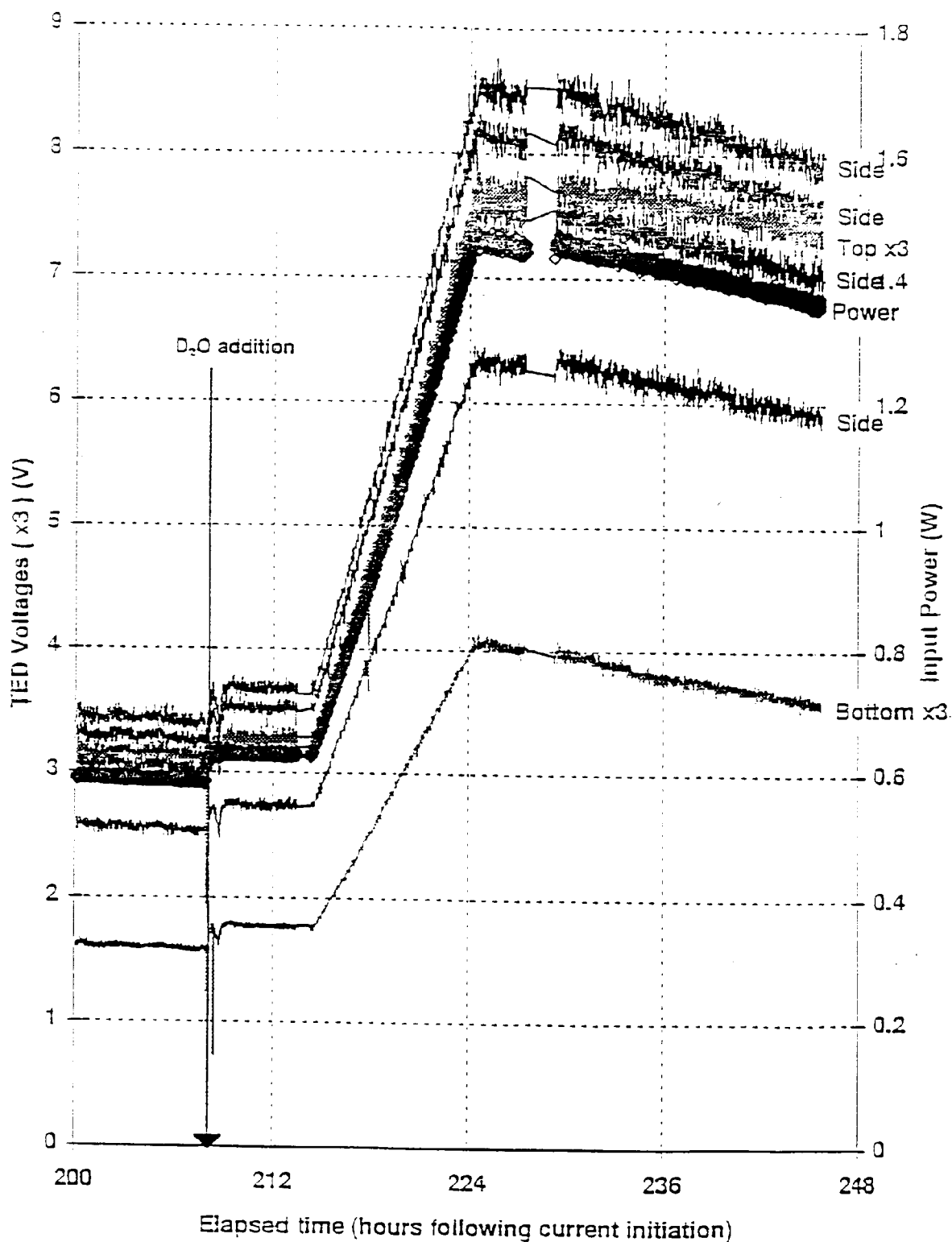
Figure 3-14
Engelhard batch 3, low O_2 anneal, slow cool

A resistive electrolyte level sensor was used in conjunction with accurate integration of the electrochemical current passed, to verify that the open calorimeter assumption was sound. In actuality, the rate of D_2O loss slightly exceeded that predicted by Faraday's Law, due presumably to transfer of D_2O vapor from the operating cell with the emerging electrolysis gases. Figure 3-15 plots the electrolyte level below full calculated from Faraday's Law, and showing a 3.4 ml addition of D_2O through the cannula.

Also shown in Figure 3-15 are the cell (TED inner wall) and bath (TED outer wall) temperatures. In part due to rather poor control in the constant temperature bath at this time, these temperatures exhibit considerable fluctuation. Immersed as it is, this fluctuating temperature difference causes heat to flow in and out of the cell, inducing transient voltages across the TED's, in an amount proportional to the heat capacity of the cell and its contents, and the time rate of change of this differential temperature. This problem was subsequently solved satisfactorily.

Figure 3-16 shows the cell electrochemical current, voltage and input power calculated using the open cell assumption. Also shown is the excess power, calculated as follows:

$$P_{xs} = P_{out} - P_{in} - P_{cp}$$

where $P_{out} = K_1 \Sigma V_{TED's}$

$$P_{in} = I_{cell} (V_{cell} - 1.54)$$

$$P_{cp} = K_2 \frac{\delta \Delta T}{\delta t}$$

and K_1 is the TED voltage coefficient
K_2 accounts for the heat capacity of the cell and its contents
ΔT is the temperature difference between cell and bath.

It can clearly be seen that operated in the mode described above, the calorimeter is a device capable of high accuracy, and very high precision. The uncertainty reflected in the data for P_{xs} shown in Figure 3-16 is less than ± 5 mW, or $< \pm 0.5\%$ of P_{in}.
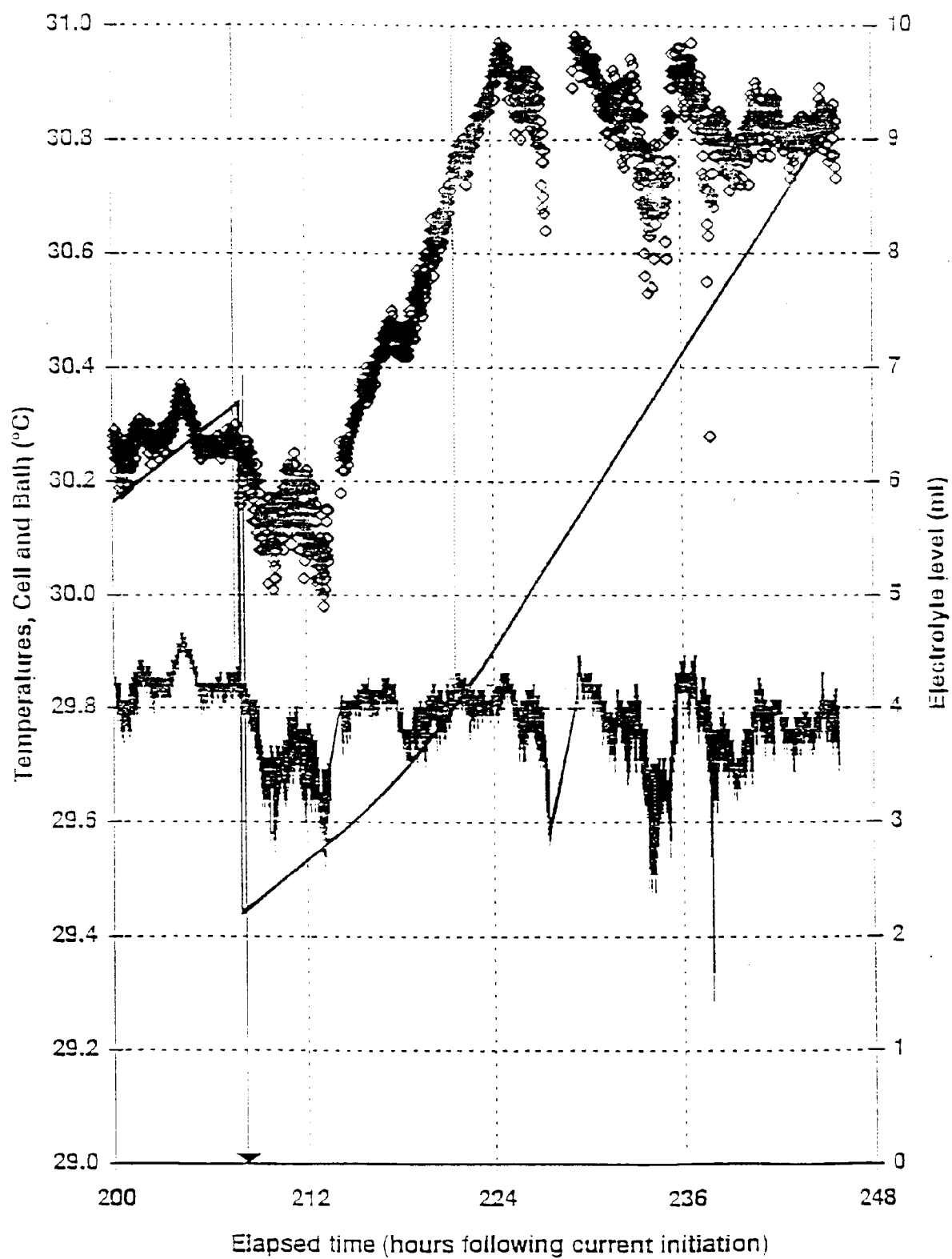
Figure 3-15
Seeback calorimeter temperature and electrolyte level
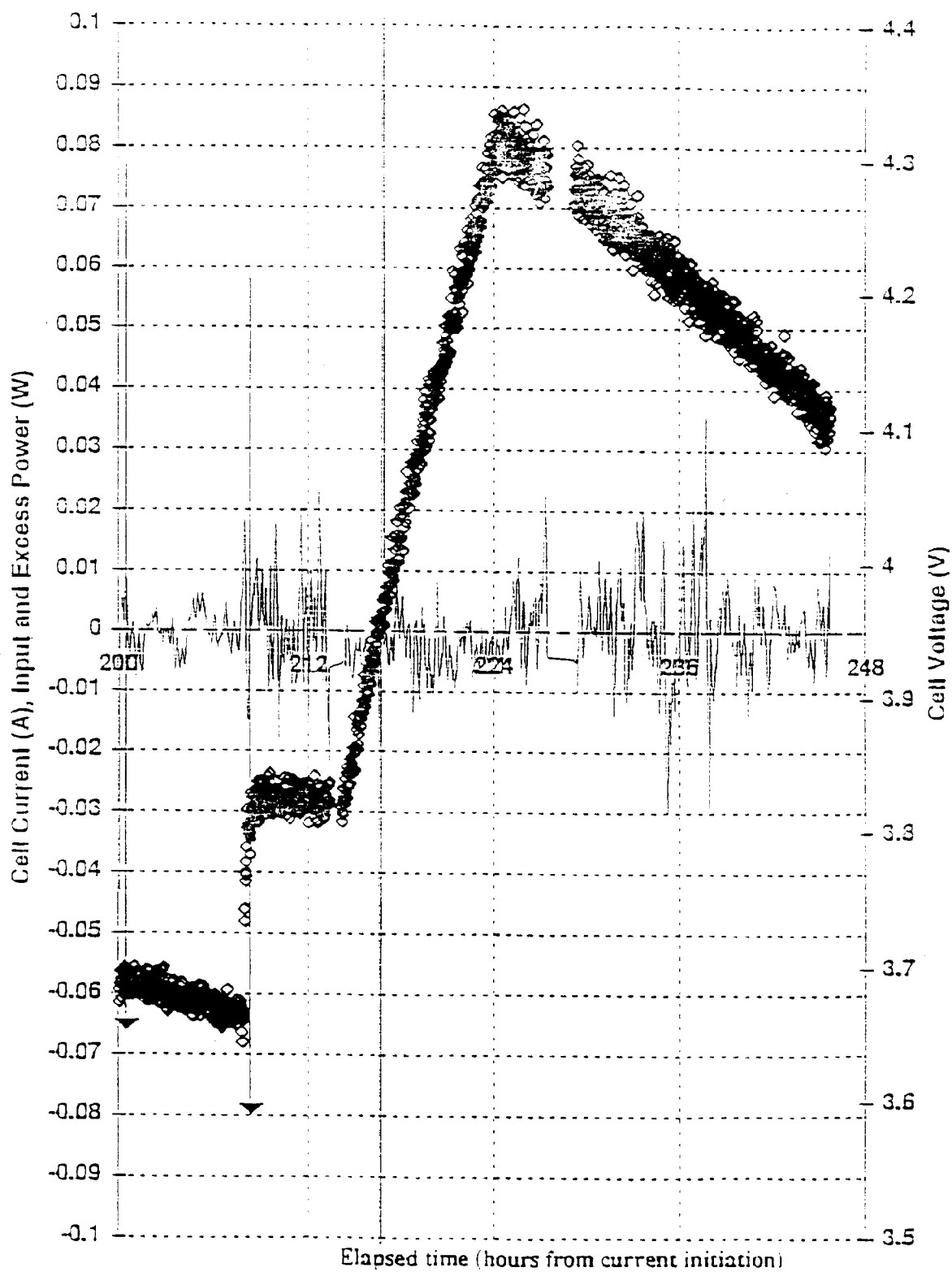
Figure 3-16
Engelhard batch 3, low O$_2$ anneal, slow cool

A synopsis of this series of helium analysis studies is as follows: Six experimental studies were performed, three of which generated excess heat. Of the three producing excess heat, helium was detected in two of them.

These studies were of two types: excess heat measurements and equipment verifications. In the latter category were the runs in the following table designed to test whether an expected null value of helium would be near the limit of detection. These gas samplings were with electrolysis using light waterelectrlyte.

Control Samples, No Excess Heat Generated, Light Water Electrolyte

Sampling Date	Helium Concentration Measured (Bureau of Mines)
8-13-93	8.2 + or - 1.4 ppb by volume He-4
8-16-93	1 + or - 1 ppb He-4 (none above background)

Subsequent leak checking of the 8-13-93 sampling flask revealed a leak in the seam of a tube attached to the flask valve apparently damaged in shipping to the Bureau of Mines Amarillo, TX laboratory. Subsequent flasks were shipped successfully without damage in foam packings.

Active Sampling of Batch 3 Engelhard Palladium, Heavy Water Electrolyte

Sampling Date	Electrolysis Current (ma)	Excess Power (mW)	Helium Found (ppbv)
9-13-93	700	47	2.4+or - 0.8
9-14-93	700	0	1 + or -1

Batch 2 Engelhard Palladium on two successive attempts generated no excess heat and were not sampled for helium. Next a palladium alloy (Pd:Ce:Sm, 92.5:5:2.5) received from Pons and Fleischmann was subjected to tests for excess power and helium-4 as follows:

Sampling Date	Electrolysis Current (ma)	Excess Power (mW)	Helium Found (ppbv)
11-25-93	350	38	1 + or -1
11-28-93	350	35	2.8 + or -1.2
12-01-93	525	55	1 + or -1
12-16-93	535	50	1 + or -1
12-17-93	525	55	3.5 + or -1.4

A few more experiments were performed in which excess power was observed but no more helium gas samplings were made because all the sampling bottles were in use.

These results while not always showing helium with the appearance of excess power, in NO CASE show helium in the ABSENCE of excess power. Thus artifacts such as from air inleakage are not observed within the limits of He-4 detection of 1 ppb by volume. The absence of helium in 3 of the 5 samplings with the palladium alloy deserve some comment.

The appearance of helium in the vapor phase of the cell implies a reaction at or extremely near the cathode surface. If not right at the surface, the absence of microcracks could be expected to trap produced helium in the metal phase. It has been observed that the alloy Pd:Ce:Sm exhibits far fewer microcracks than the nominally pure palladium of the two Englehardt batches studied here. Hence depending upon the active cathode regions juxtaposition relative to microcracks could determine capture or release of the helium produced. Other publications give greater detail for similar work performed by the author (B. Bush) and his collaborators elsewhere under different sponsorship supporting the hypothesis that the surface reaction D+D-->He-4 +23.82 Mev is the operative power and heat producer. (1,2).

1. B.F. Bush and J.J. Lagowski, "Nuclear Products Associated with the Pons and Fleischmann Effect; Helium Commensurate to Heat Generation, Calorimetry, and Radiation." Proceedings of the 6th Int'l Conf. on Cold Fusion, Toya Japan, October 13-18, 1996, Vol. 2, p.622

2. B.F. Bush, J.J. Lagowski, M.H. Miles, and G.S. Ostrum, "Helium Production During the Electrolysis of D2O in Cold Fusion Experiments", J.Electroanal. Chem. 304, (1991) 659

OHF Series Experiments

Introduction. A heat flow calorimeter was constructed (10/92) which employed Seebeck thermoelectric elements in order to characterize the calorimetric response. The calorimeter consists of two concentric cylinders, separated at their base by either four coplanar Seebeck elements (1 inch square) or a large, single disc-shaped element. The inner cylinder was Al, 1 cm thick, and served to integrate the heat flow from the cell contained within it. It was designed to accommodate a teflon cell similar in design to that employed in the "L" and "T" series experiments. No calibrating or compensation heater was provided. The cylindrical air space ("calorimeter jacket") between the metal cylinders contained metal-backed closed-cell foam for insulation, as did the region on top of the cell. Thus the primary heat loss path was downward, out of the bottom of the calorimeter. A feed-tube was provided for electrolyte/D_2O additions. For the experiments reported below, the calorimeter was contained within a bath.

Preliminary experiments, not reported here, indicated that it was not possible to perform reliable calorimetry with a closed cell due to the excessive unwanted heat loss from the top of the calorimeter at high current (hence, elevated recombiner temperatures).

Thus, in the experiments reported here, the cell was run open [hence the name open heat flow (OHF)], connected to a gas-handling manifold.

Experiment Synopses and Results

OHF1 The cell contents were:

Cathode: 3 x 35 mm Engelhard Pd rod (batch 2)

Anode: Cylindrical Ni cage

Electrolyte: 140 ml 1 M LiOD

RTDs: Two, one positioned by the cathode, the other at the
            bottom of the cell.

This experiment exhibited poor quality cathode resistance measurements, RTD shorting and severe endothermic departure from the calorimetric steady state at elevated currents. These effects were thought possibly to be due to the presence of excess liquid above the first teflon cone, causing shorting and allowing direct thermal access to the top of the cell and the metal gas vent tube. For OHF2, the metal tube was replaced with a teflon tube, and the electrolyte RTDs were brought into the cell directly (in plastic tubes) through this gas vent tube. No data are reported here for this experiment.

OHF2 The cell contents were:

Cathode: 3 x 35 mm Engelhard Pd rod (batch 2)

Anode: Cylindrical Ni cage

Electrolyte: 140 ml 1 M LiOD

RTDs: Two, one positioned by the cathode, the other at the bottom
            of the cell.

Data analysis for 216 h, is shown in Figures 3-17 and 3-18. This experiment exhibited successful operation at currents less than 3 A, corresponding to input powers less than about 10 W. Above 3 A, there was excessive electrolyte loss through the gas vent tube. Adequate cathode resistance measurements were made at low currents, although high loading was not achieved. No excess heat was observed. The need to minimize the cell current employed determined the cathode selection in OHF3.

    OHF3 The cell contents were:

      Cathode: 1 x 30 mm Pd wire (Aithica metals).

      Anode: Cylindrical Ni cage

      Electrolyte: 140 ml 1 M LiOD + 200 ppm Al at outset. One subsequent Si addition (at 220 h).

      RTDs: Two, one positioned by the cathode, the other at the bottom of the cell.

Data analysis for 265 h, is shown in Figures 3-19 and 3-20. This experiment exhibited generally successful calorimeter operation (for a maximum current of 1 A). However, unusual (and poor) loading behavior was observed. The experiment was terminated due to a Seebeck element failure due to shorting. No excess heat was observed.
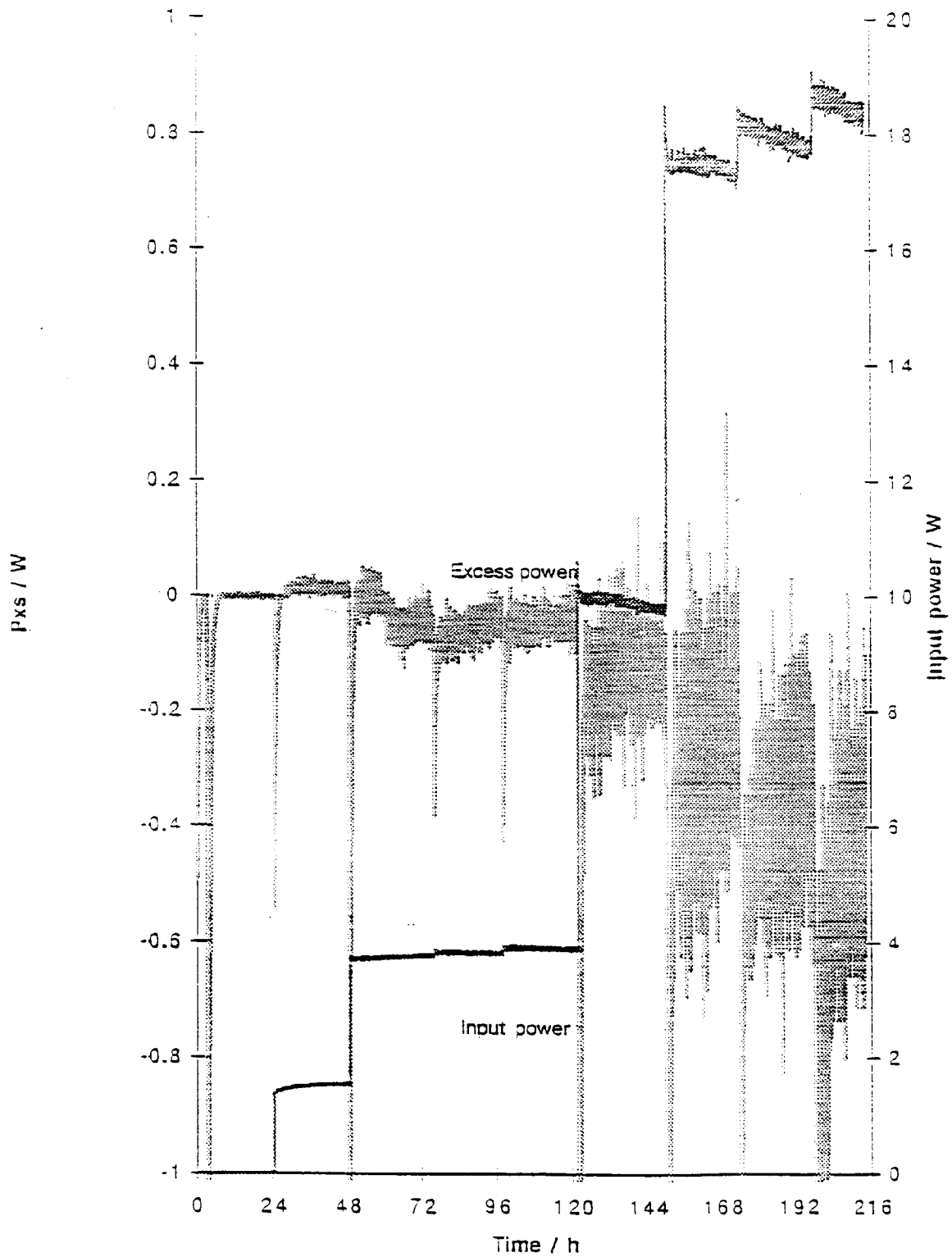
Figure 3-17
Calorimetric data for OHF2
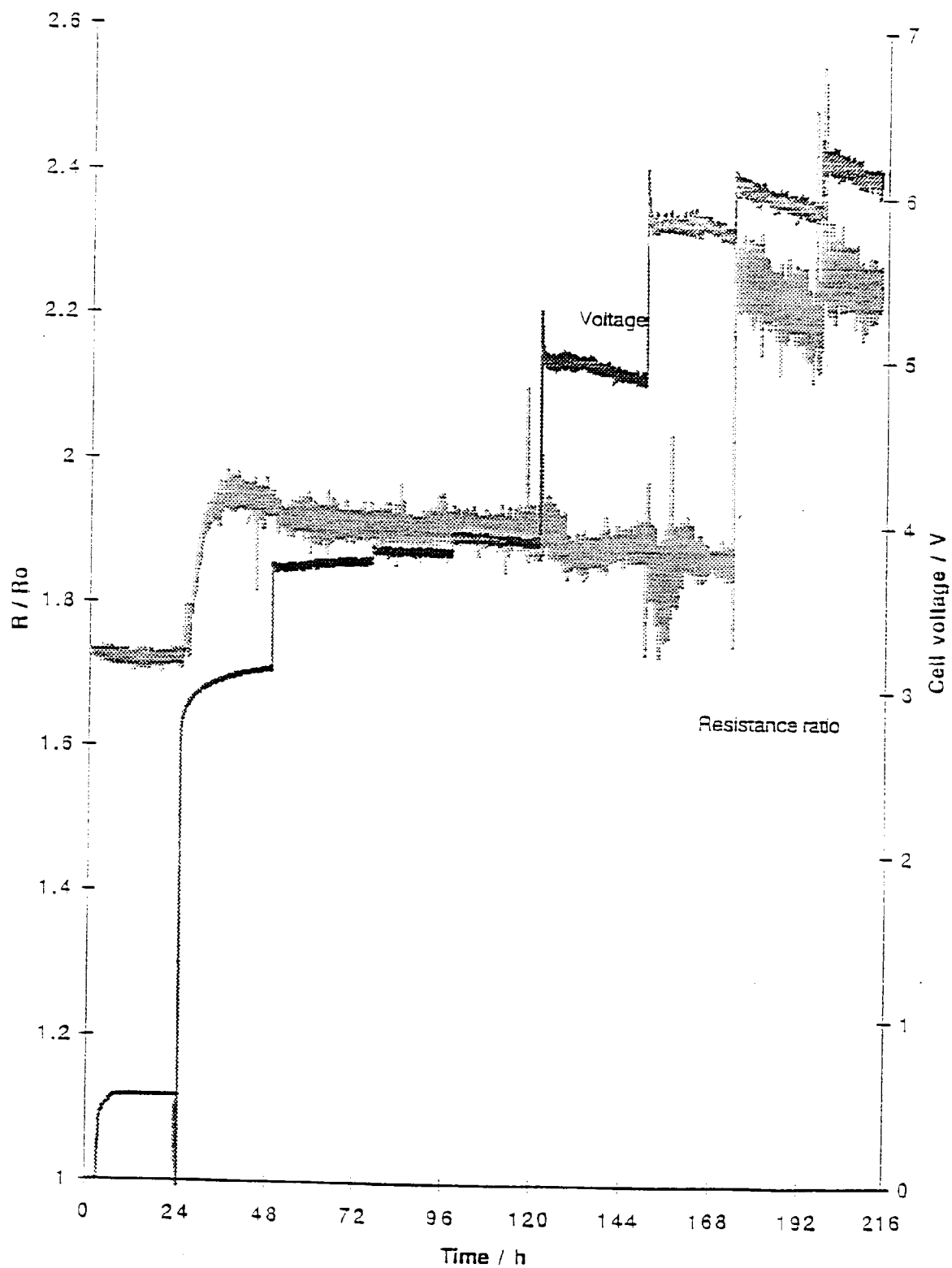
Figure 3-18
Resistance and voltage data for OHF2
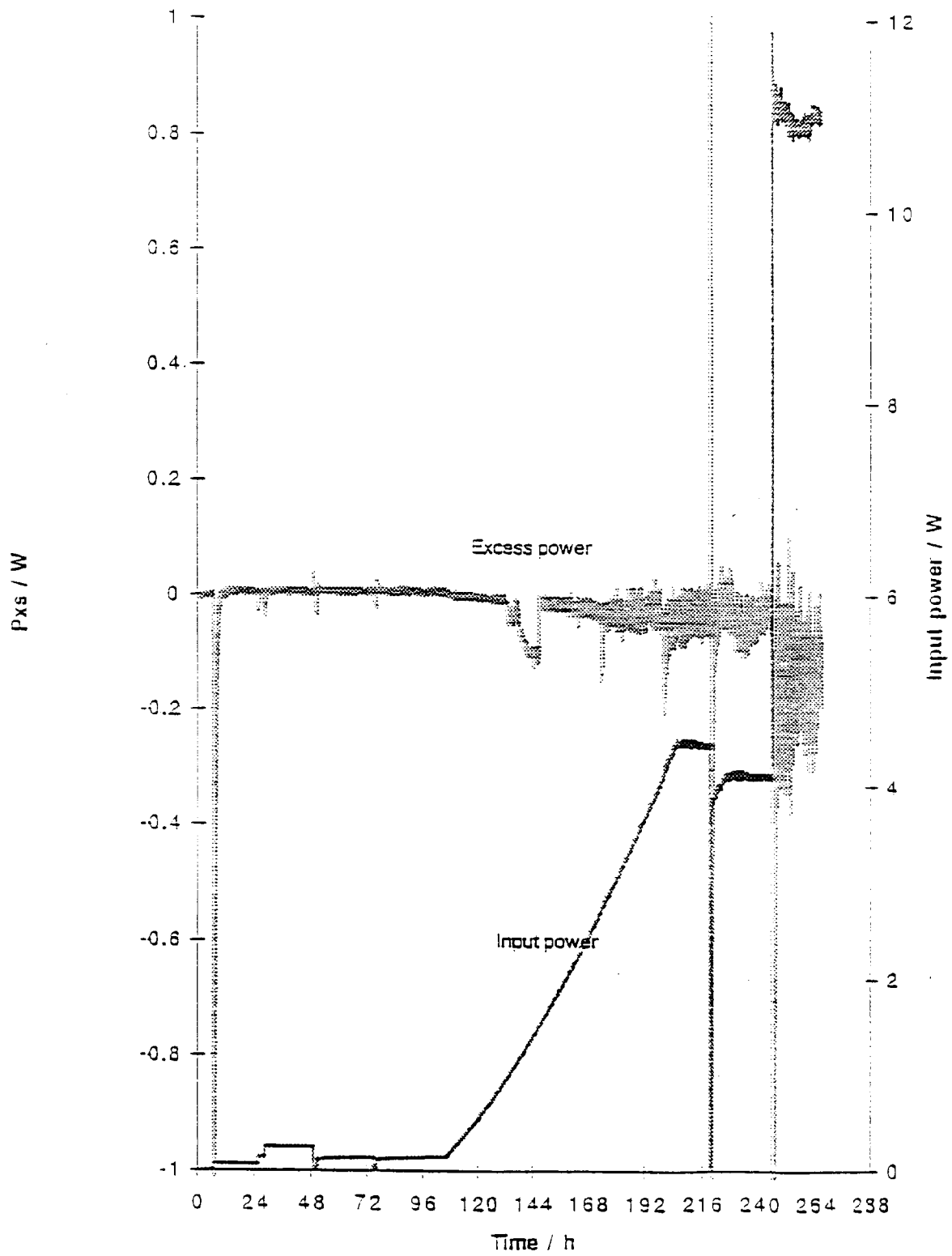
Figure 3-19
Calorimetric data for OHF3
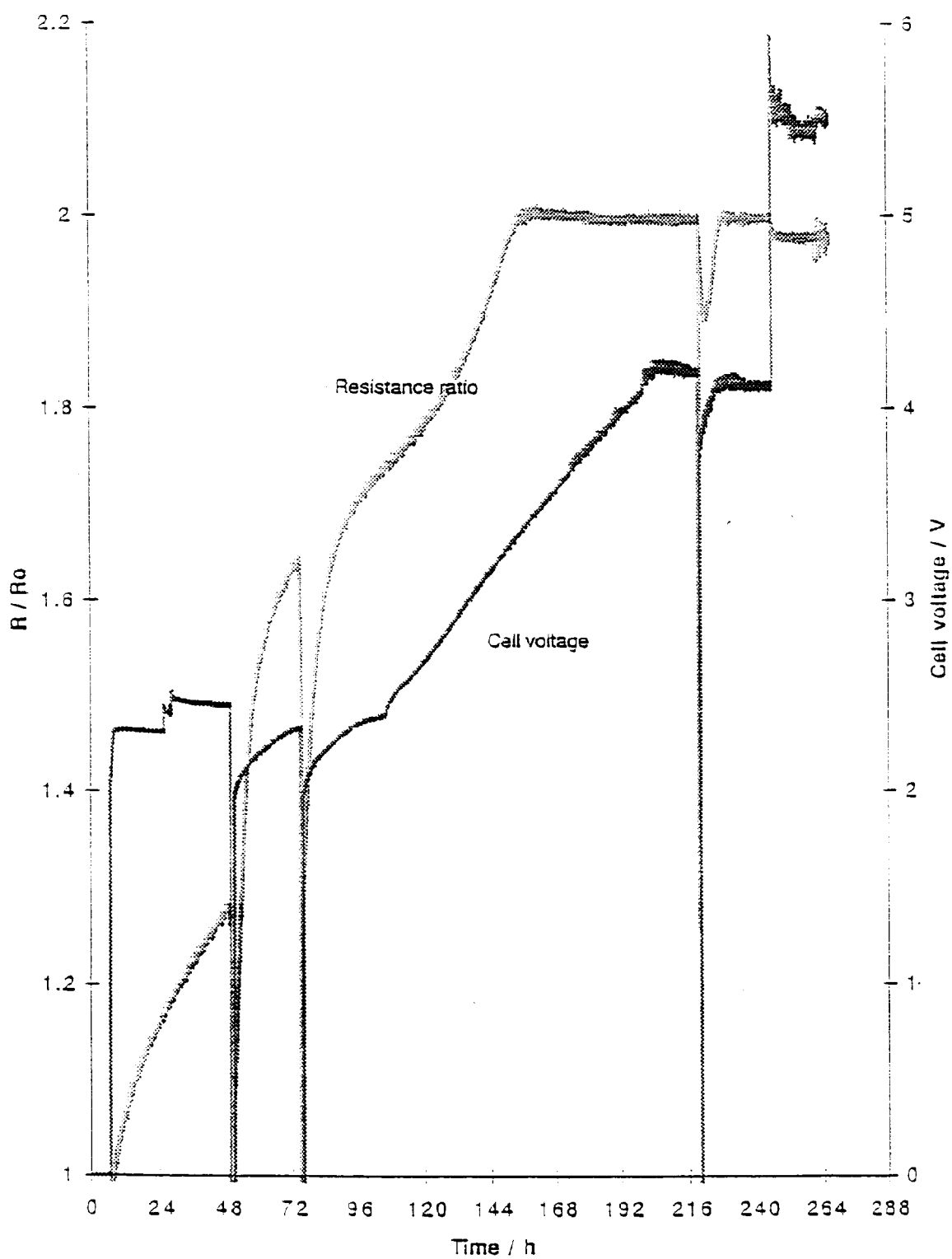
Figure 3-20
Resistance and voltage data for OHF3

Conclusions There were several limiting features inherent in this calorimeter design; therefore it has not been pursued further in this program. The need to operate at relatively low currents in order to perform acceptable calorimetry severely limited the overall usefulness, especially where relatively large surface-area cathodes were concerned. Furthermore, its rather bulky construction gave it a relatively long time constant. This became a problem at relatively high currents when frequent D_2O refills became necessary. One feature of this series of experiments (including those preliminary experiments which are not reported here), which is presumably not related to the calorimeter design, but is a feature in common with the "L" series experiments, is the poor cathode loadings which were achieved.

Mass flow

Principles. Mass flow calorimetric measurements were carried out isothermally, under constant input power conditions, whenever possible. The power input to the calorimeter by the electrochemical current was considered to be the product of that current and the voltage *at the isothermal boundary*. Under experimental conditions, this input power changed owing to voltage or resistance variations in the cell or at times when the current was ramped. This change had two undesirable consequences: First, a change in input power changed the cell temperature so that the electrochemical conditions were no longer under control, and second, a change in temperature moved the calorimeter from its steady state as the calorimeter contents took up or released heat. To minimize these effects, a compensation heater was used to correct for changes in electrochemical power so that the sum of the heater and electrochemical power inputs to the calorimeter was held constant. Computer-controlled power supplies were used for both the electrochemical power and the compensation heater element; both were operated in galvanostatic mode to avoid possible unmeasured rms heat input. The heater also was used for periodic calorimeter calibration, as described further below.

The steady-state equation for the power output from a mass flow calorimeter is

$$P_{output} = \left(C_p \frac{\delta m}{\delta t} + k^1 \right) \left(T_{out} - T_{in} \right) \qquad \text{(eq. 3-1)}$$

where C_p is the average value of the heat capacity of the calorimetric fluid in its transit through the calorimeter (4.18 J K^{-1} g^{-1} for air-saturated water), $\delta m/\delta t$ is the fluid mass flow rate, k' is an effective conductive loss constant, T_{in} is the inlet (from bath) temperature, and T_{out} is the mean temperature of the emerging fluid.

Similarly, for the power input to the calorimeter,

$$P_{input} = \left| I_c V_c \right| + \left| I_h V_h \right|$$ (eq. 3-2)

where I is the current and V is the voltage measured at the calorimeter boundary, and the subscripts c and h refer to the electrochemical cell and the compensation heater, respectively. In a closed system, the difference between the output and input powers may be described as an "excess power." In the absence of extensive, time-dependent changes in temperature, pressure, or overall composition within the system, the excess power is expected to be zero (in the absence of anomalous power-producing or consuming processes).

For the cell and heater currents,

$$I_c = \frac{V_{cr}}{R_c} \; ; \quad I_h = \frac{V_{hr}}{R_h}$$ (eq. 3-3)

where V_r is the measured voltage drop across a calibrated resistance (the subscripts c and h again refer to the electrochemical cell and compensation heater, respectively). The primary temperature measurements were made with RTDs, so that

$$T = T° + \frac{\left(R - R° \right)}{\alpha R°}$$ (eq. 3-4)

where $T°$ is the temperature at which the device resistance is $R°$, and α is the (known) temperature coefficient of resistance of platinum. Hence, we can write

$$P_{excess} = P_{output} - P_{-input}$$ (eq. 3-5)

$$= \left\{ C_p \frac{\delta m}{\delta t} + k' \right\} \left\{ \frac{R_{out}}{R_{out}} - \frac{R_{in}}{R_{in}} \right\} \frac{1}{\alpha} - \frac{V_h V_{HR}}{R_H} - \frac{V_c V_{cr}}{R_c}$$ (eq. 3-6)

The terms in this equation can be divided into three classes: (i) measured variables (δm, δt, R_{out}, R_{in}, V_h, V_{hr}, V_c, and V_{cr}); (ii) predetermined constants (C_p, α, $R_{out}°$, $R_{in}°$, R_h, and R_c); and (iii) the conductive loss constant (k').

The use of a conductive loss constant, k', requires further discussion. Conductive heat transport occurs because the electrochemical cell, its contents, and the contents of the insulating, isothermal boundary of the calorimeter vessel are at a different temperature than their surroundings. An added complexity is heat transported through the pressure pipe that emerges through the top insulating boundary. Thus, depending on the ambient and cell temperatures, heat may be conducted into or out of the calorimeter. The value of k' is negligibly influenced by the spatial distribution of these sources or the

anticipated variations in the bath and air temperatures. Thus k' was treated as a constant, its value determined during the calibration procedure, as described below. For the calorimetric fluid flow rates used (approximately 1 g s⁻¹), conductive power loss represented typically 1-2% of the total input power.

Calibration required to determine $R°$ values for the RTDs and the conductive loss constant k' was performed at the outset of the calorimetric experiment. The values of $R°$ were determined *in situ*, under flow conditions at known bath temperature and zero or low input power. The total input power was then stepped to successively higher values by using the heater (in the presence of low electrochemical power), allowing times of at least 20 calorimeter time constants (approximately 6 hours) to reach a steady state. The quantities δm, δt, R_{out}, R_{in}, V_h, V_{hr}, V_c, and V_{cr} were measured on-line and the steady-state values were used, assuming $P_{excess} = 0$, to determine k'. It should be noted that this method of calibration determines k' in terms of the other externally calibrated constants: C_p, $R_{out}^{°}$, $R_{in}^{°}$, α, R_h, R_c and the voltage calibration of the multimeter. In this way the cumulative inaccuracy of the determination of k' was greatly reduced.

To confirm that the value of k' determined during calibration was time-invariant, a second procedure was undertaken occasionally during routine operation of the calorimeter. It entailed varying the total input power (by stepping the heater power at constant electrochemical cell current) and observing the resulting excess power response (at times when the excess power was zero). For a properly calibrated calorimeter, the excess power should, of course, not change as the result of such a power step. This procedure, together with the use of redundant temperature sensors, served to check continually the results of the initial calibration procedure. It also enabled the validity of the excess power equation to be verified at very high total input powers, a procedure that was found to be more time-efficient when carried out in this manner than when undertaken at the outset of the experiment.

Typically, constant current or slowly ramped current conditions were employed. As stated above, the calorimeter was run under conditions of constant input power. Thus, during a current ramp, the heater power was reduced slowly while the electrochemical power was ramped up, thereby maintaining approximately constant total power. Under current control, the cell voltage frequently was observed to fluctuate significantly, particularly at high current densities where the presence of large deuterium (or hydrogen) and oxygen bubbles disrupted the electrolyte continuity. Because the cell current is provided from a source that is sensibly immune to noise and level fluctuations, the current operates on the cell voltage (or resistance) as a scalar. Hence, as long as the voltage noise or resistance fluctuations are random, no unmeasured rms heating can result under constant current control, provided that the average voltage is measured accurately.

Supporting Systems. The calorimeter/cell supporting systems assembly consist of hydraulics, gas manifold and data acquisition and control, Figures 3-21 and 3-22. The hydraulic systems include the water bath, the calorimetric flow system and the heat exchangers. The gas system consists of a manifold that allows the deuterium and other gases entry to and exit from the cell inside the calorimeter. Power to the electrochemical cell and the compensating heater are controlled by an Apple Macintosh computer. Temperatures in the cell, calorimeters, bath and air as well as all voltage, current, resistance, and mass measurements are controlled by and reported to the computer.

The 200-liter chilled water reservoir is kept at ~ 13°C by circulating ~ 5°C chilled water through a coiled 20m long steel tubing immersed in the reservoir. The flow is controlled (on/off) by a solenoid activated by a thermocouple in the reservoir. A Grundfos type UP15-42SF circulating pump pumps the water at ~5 gallon/hour through a Culligan model 1249 UV disinfection unit, a particle filter, a Culligan activated carbon bed, and two Culligan tri-bed ion exchange resins. A resistivity meter is used to verify that the resistivity is greater than 17 M Ω cm. The cleaned water is then pumped around the laboratory with an outlet valve in each of the five experiment cubicles. A parallel return line has an inlet valve in each of the cubicles and returns to the chilled water reservoir. Operation with high purity cooling water prevented many phenomena such as algae growth and corrosion that interfere with long time experiments (hundreds of hours).

In a particular cubicle a line from the circulating system passes through a flow meter and then is split into two lines, one entering the middle box of the bath and the other entering the inner box. The flow rate into the inner box is kept constant at approximately twice the total flow rate through all of the calorimeters operating in the bath.

The water from the inner box flows through an overflow hole into the middle box which flows out to the return line and back to the chilled water reservoir. A YSI model 72 proportional-temperature controller with a YSI 400 series thermistor and four ARI model BXD19B-126T heaters maintain the temperature of the bath to ± 3 mK.
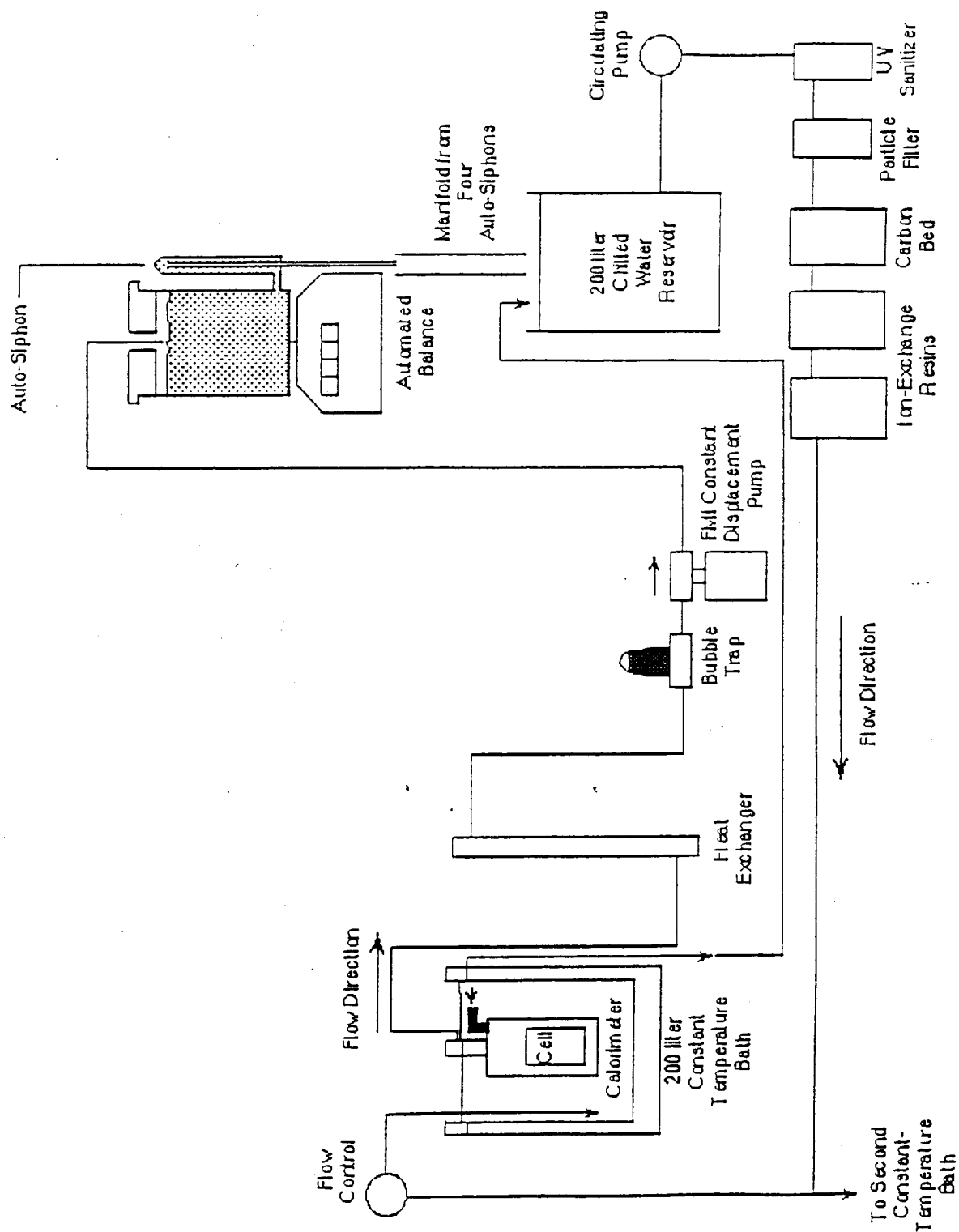
Figure 3-21
Calorimeter hydraulic system
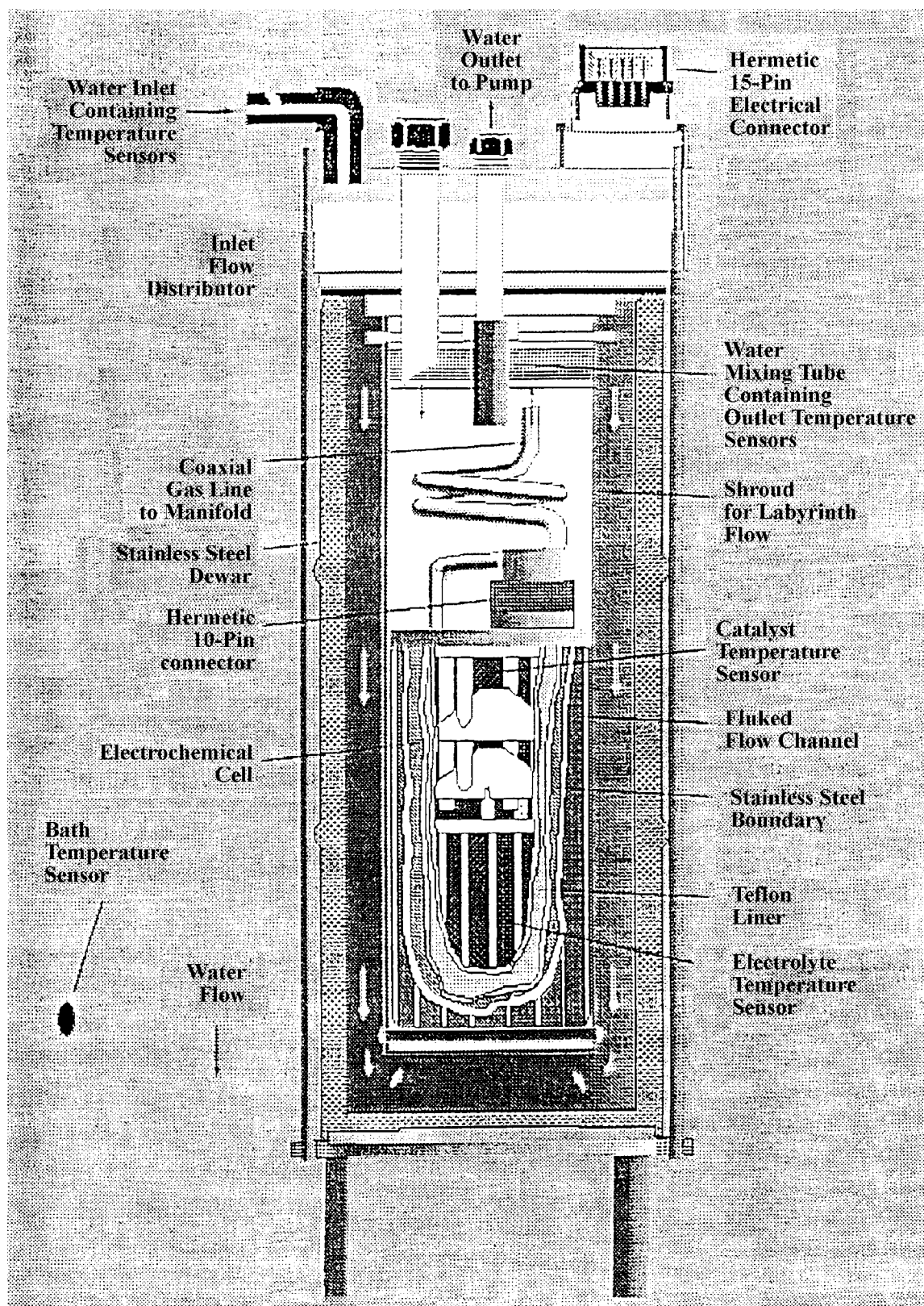
Figure 3-22
L Calorimeter

The water from the bath is drawn into the top of the calorimeter by an FMI QV-0SSY constant displacement pump. Before reaching the cell the water flows past the electrical lines outside an acrylic cylinder to the bottom of the steel dewar flask where it flows up over the cell and out of the calorimeter. Upon exiting the calorimeter the water is drawn through a standard design metal heat exchanger and an inverted bulb bubble trap into the pump. The heat exchanger is cooled by the same 5° water cooling the chilled water reservoir.

The water flows from the pump into the reservoir on the balance. When the reservoir is full the auto siphon device empties the reservoir in ~ 3 minutes. The outlet from the auto-siphons for all of the cells passes into a manifold and flows into the chilled water reservoir.

The flow through design is a safety feature used to verify that none of the gas handling lines are plugged. The D_2 (Matheson, research grade) or N_2 (prepurified 99.999%) flows through the inlet flow meter past the Omega model PX176-100S5V pressure transducer, an analog pressure gauge, and a double bubbler half filled with D_2O on its way to the cell. The narrow inlet tubing traverses the "cross" fitting atop the cell and directly into the cell's headspace. The cell's outer gas tubing, coaxial with the inlet tubing, leads to the "cross" fitting, and back through bubbler, another flow meter and out to the vent valve. The "cross" is also fitted with a spring type pressure relief valve. The two flow meters must read the same flow rate while gas is flowing into the cell to assure us that the manifold assembly is not plugged or leaking. The bubblers serve as flow indicators redundant to the flow meters as well as liquid traps to prevent liquid contamination either to or from the cell.

The Hewlett-Packard (HP) 4338A milliohmeter is a 3-1/2 digit four-terminal, single-frequency impedance meter used to measure the cathode's resistance. The instrument operates at a fixed frequency of 1000 Hz and reports the resistance (R) and reactance (X) of the cathode resistance measuring circuit. The reactance arises from the lengths of unshielded leads inside the calorimeter and cell. The instrument is instructed to generate a 10 mA AC rms 1000 Hz perturbation and measure the resulting voltage, calculating the R and X. As the resistance of the cathode is usually less than 2 mΩ, the meter operates on the 10 mΩ range with a resolution of 1 $\mu\Omega$. Each measurement reported is based on an internal average of 16 0.9 s measurements. The meter is calibrated by the manufacturer at least once a year.

The mass flow rate through the calorimeter is measured using a Setra 5000L, 5000 g. electronic balance. The mass is reported to the computer immediately when commanded with the time measured by the computers internal clock. The balance has a resolution of 0.01g and the clock's resolution is ~ 0.017 s. When the reservoir on the balance is emptying, as described earlier in this section, the average flow rate for the

time necessary to completely fill the reservoir is calculated and recorded. When the reservoir is filling, the computer calculates and records the mass flow rate for the previous data collection interval (~ 4 minutes). The balance is calibrated at least once a year.

All other measurements (voltage, resistance, current, temperature, pressure, etc.,) are measured using the Keithley model 195A digital multimeter (DMM). The DMM is connected to the various electrical inputs using the Keithley model 706 scanner using various scanner cards. The calorimetric temperatures are measured using the 4-wire scanner card and the DMM's 100 Ω Pt RTD temperature measurement mode. The meter has a fundamental resolution of 0.01°C but when averaged five times in the computer the sensitivity is ~ 0.002°C. The cell temperatures are measured using the 4-wire scanner card and the DMM's 200 Ω range with a resolution of 0.001 Ω. This is done to facilitate corrections due to extended lengths of 2-wire leads in the cell/calorimeter.

The cell voltage is measured using separate voltage leads which are connected to the current leads at the calorimeter's boundary. This allows us to measure all voltage that is impressed at the calorimeter boundary. This is measured using a 2-wire scanner card and the DMM's 20V DC range with a resolution of 10 μV. The current passing into the cell is measured across a regularly calibrated 0.1 Ω, 25W series shunt resistor (Kepco model KT-1387) using the 2-wire scanner card (Keithley model 7056) and the DMM's 2V dc range, yielding a voltage resolution of 1 μV or a current resolution of 10 μA. By always operating the cell's power supply in galvanostatic mode the current measured is identical to that passing through the calorimeter. The product of this current and the voltage measured gives the power input to the calorimeter due to the electrochemical cell.

A resistive heater, ARI Industries (Addison, IL) Model BXD 04B46-4K, ~ 85 Ω, is wound around the outside of the cell inside the heat-transfer fins. Similar to the cell's input power the heater's power is calculated from the voltage drop across the heater and leads measured at the calorimeter boundary. The current is calculated from the voltage-drop across an identical 0.1 Ω series shunt resistor. The heater's power supply is also always operated in galvanostatic mode so that the product of the voltage and current yields the power into the cell due to the heater. The sum of the heater power and the cell power is the total electrical power input to the calorimeter, and is mostly kept constant during an experiment.

The pressure is measured using an electrical strain-gage type pressure transducer Omega model #PX176-100S5V. The transducer accepts an unregulated voltage input (9-24V) and yields a voltage proportional to gage pressure. The combination of meter resolution and transducer sensitivity gives a resolution of ~ 0.001 psig. This voltage is

measured using a 2-wire scanner card and the DMM's 20V scale. A 12V dc, 0.5A power supply is used to power the transducer.

The power supplies used for the L and M calorimeters are different. The L calorimeters use a HP66000A IEEE-488 interfaced main-frame with a HP66102A 7.5A, 20V power supply module and a HP66105A 1.25A, 100V power supply module for each cell. The 7.5A power supply is for the electrochemical cell while the 1.25A supply is used for the resistive heater. The M calorimeter uses a Kepco BOP 20-20M, 4 quadrant 20V, 20A power supply with a built in IEEE-488 interface for the electrochemical cell. A Kepco ATE 100-1M 1A, 100V power supply with a Kepco SN 488-121 IEEE-488 interface supplies power to the resistive heater.

An Apple Macintosh IIsi computer controls all of the data acquisition and cell parameters. An IOtech Mac 488B serial-to-IEEE interface is connected to the computers serial port and acts as the start of the general purpose interface bus (GPIB) chain. IOtech Serial 488A devices connect the serial interfaced balances to the GPIB chain. The milliohmeter, scanner, DMM, and power supplies connect directly to the GPIB. Data is collected from each of the channels every 4 minutes and saved on the computer's hard disk. The data is transferred via Apple's Ether talk network to Apple Macintosh Quadra 950's for analysis.

L-Series Experiments

Introduction. A series of experiments were undertaken, starting in April 1993, employing the labyrinth mass flow calorimeter. Typically, two calorimeters were run together in the constant temperature bath, each with independent hydraulic and electronic systems. The calorimeter and "usual" cell design were as described below. Since a variety of cell design modifications and experimental protocols were employed in this experimental set, a brief synopsis of each experiment is given below.

Representative results are shown here for each experiment. Where possible, the data are shown with the minimum of subsequent processing.

Experimental Apparatus. The labyrinth mass flow calorimeters used to obtain the results described here are similar in operating principle to the linear mass flow calorimeters used in an earlier phase of this program. The calorimeter, Figure 3-23, consists of a metal Dewar can closed at one end. This can contains the electrochemical cell and, during use, is submerged in a constant temperature water bath. The top of the can is plugged with a polycarbonate top-piece, described in more detail later. The calorimeter contains a symmetrically disposed, inner cylindrical polycarbonate barrier (or "shroud"), about 8 cm in diameter, the bottom half of which surrounds the electrochemical cell. The shroud reduces unwanted, unmeasured conductive heat loss

from the cell by "capturing" such energy in the incoming fluid moving in the outer portion of the shroud. Bath water is pumped into the calorimeter, entering at the top and passing through the polycarbonate top-piece, is distributed evenly around the top inner can circumference, moves downward around the outside of the shroud, and then passes upward through the inner portion of the shroud. Finally, the bath water passes through a flow mixer, suspended under the polycarbonate top-piece and in which the outlet temperature sensors are located, before passing upward through the top-piece to the pumping system. The leads of the outlet RTD's are contained within thin walled PTFE tubes which pass directly downward through the inner portion of the shroud, past the electrochemical cell, and upward past the outside of the shroud. They pass intact through two separate feed-throughs mounted in the top-piece. Electrical connection to the data acquisition system is made above the water bath. This arrangement ensures that rigorous four-point temperature measurements are made by the outlet sensors.
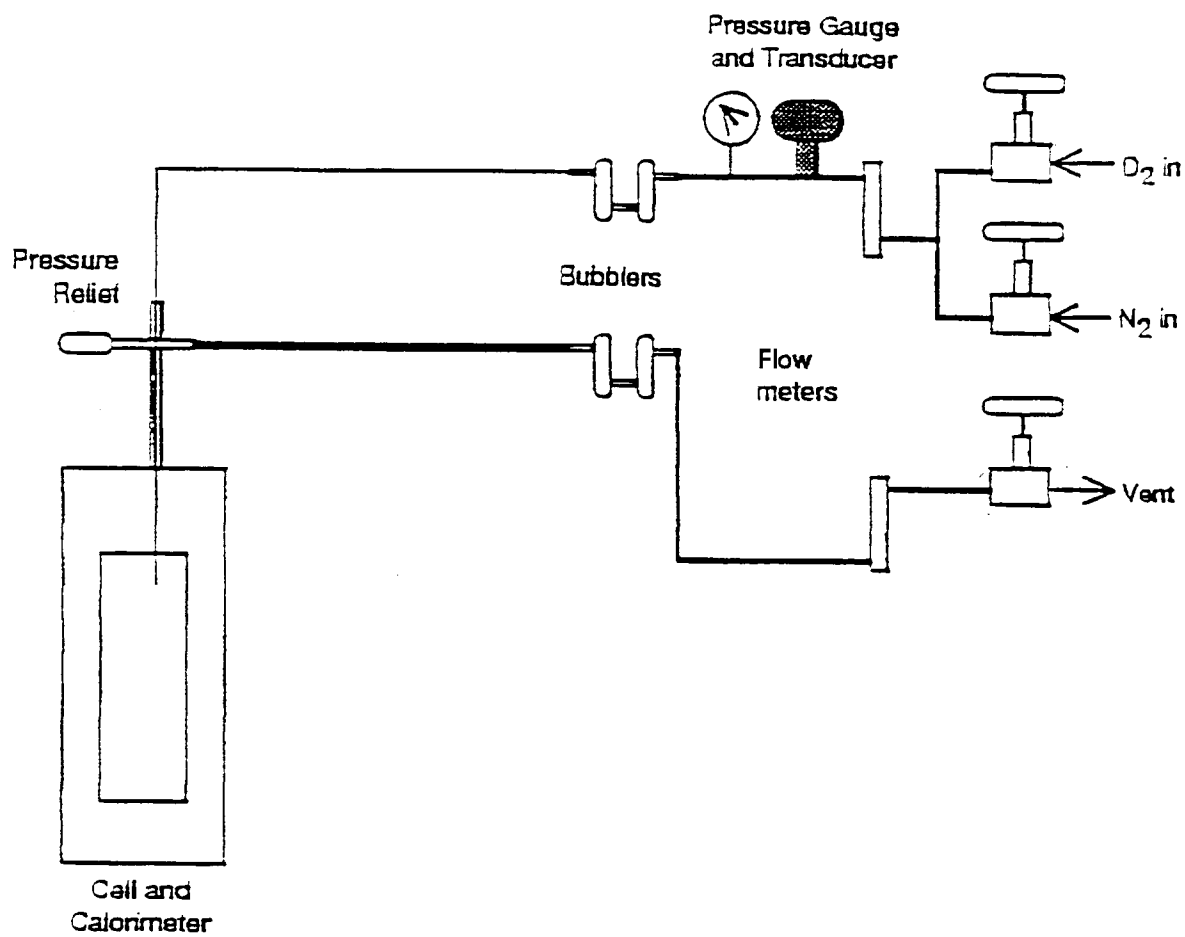
Figure 3-23
L Calorimeter gas manifold

The temperature of the inlet water is measured similarly by two independent sensors located on top of the top-piece.

The electrochemical cell is surrounded by a resistive heater contained within a brass heat-integrating jacket. Small vertical heat-exchanging fins spaced appropriately on the outside of this jacket allow bath water to move past the cell. Electrical connection is made via the outside of the shroud to an hermetic 16-pin connector mounted in the top-piece.

The electrochemical cell, is contained within a stainless steel boundary. Its inner components, predominantly teflon, are separated from the stainless steel by a teflon liner. A platinum catalyst basket is suspended about 2 cm from the top of the cell; the temperature of this region being monitored by an RTD. The lower half of the cell contains a cylindrical cage structure, consisting of teflon top- and bottom-rings separated by quartz rods. This structure, the diameter of which was varied during the experiments described here, serves to support the anode, typically Pt wire. The cathode, usually a vertical palladium rod, is mounted symmetrically within the anode cage. The lower half of the cell, which contains the electrolyte, is separated from the catalyst by two vertically-displaced teflon cones. These act to reduce contact between the catalyst and electrolyte vapor, thereby prolonging catalyst lifetime. A PTFE-sheathed RTD is situated in the electrolyte inside the anode cage.

The cell is equipped with a gas pipe which also contains a teflon catheter for electrolyte additions. The pipe and inner tube also function as two separate, parallel gas flow paths as part of the calorimeter safety-monitoring system. The gas pipe emerges through the top-piece and is connected to the gas/sample-handling manifold. Inside the calorimeter, the gas pipe is spirally wound in order to achieve better heat transfer with the calorimetric fluid. It should be noted that, for the experiments described here, the manifold, comprised largely of plastic components above the calorimeter top, was designed to be pressure tight up to approximately 2 atm., but was not designed to be specifically Helium-tight.

The top of the cell is furnished with a 10 or 16-pin hermetic connector similar to the one used on top of the calorimeter. Electrical leads pass from the cell connector to the calorimeter connector via the outside of the shroud.

The cell design described above is referred to as the "usual" cell design in the experimental accounts given in the following pages. Changes are indicated where appropriate.

Experiment Synopses and Results

L1. This experiment was designed to test the new labyrinth mass flow calorimeter design. The following cell materials were used:

      Cathode   3 mm x 3 cm Pd (Engelhard, batch 2). Pt contact and lead wires.

      Anode   Ni mesh

      Electrolyte 140 ml 1 M LiOD (Aldrich lot JZ). No element additions were made during the experiment.

      Internal sensors two electrolyte thermistors and one catalyst RTD.

When initially installed (4/20), a gas leak at cell top was observed (due to an incorrectly seated O-ring) leading to bath water entry into cell. The cell was removed and cleaned and the catalyst balls were replaced. The cell was returned to the bath on 4/23 with new electrolyte. Poor quality cathode resistance measurements were made during the experiment. There were problems with outlet sensor positioning and the thermistor response was difficult to interpret. The experiment was terminated after 1600 h due to a massive gas leak from the cell. No data from this experiment are reported here.

L2. Having observed the behavior of the prototype L1 labyrinth mass flow calorimeter, L2 was designed to determine the efficacy of the resulting design changes. The cell contents were:

      Cathode   3 mm x 3 cm Pd (Engelhard, batch 2). Pt contact and lead wires.

      Anode   Platinum coated niobium screen.

      Electrolyte   140 ml 1 M LiOD (Ontario). A Si addition was made during the experiment.

      Internal sensors two electrolyte RTDs and one catalyst RTD

After some 200 h, the experiment was removed from the bath due to poor cathode resistance measurement. The cell was later returned to the bath with the original electrolyte. In general, reasonable quality data were recorded for approximately 400 h from this time, Figure 3-24. However, cathode resistance measurements remained unsatisfactory, particularly at high current. The cathode did not load well and no excess heat was observed.
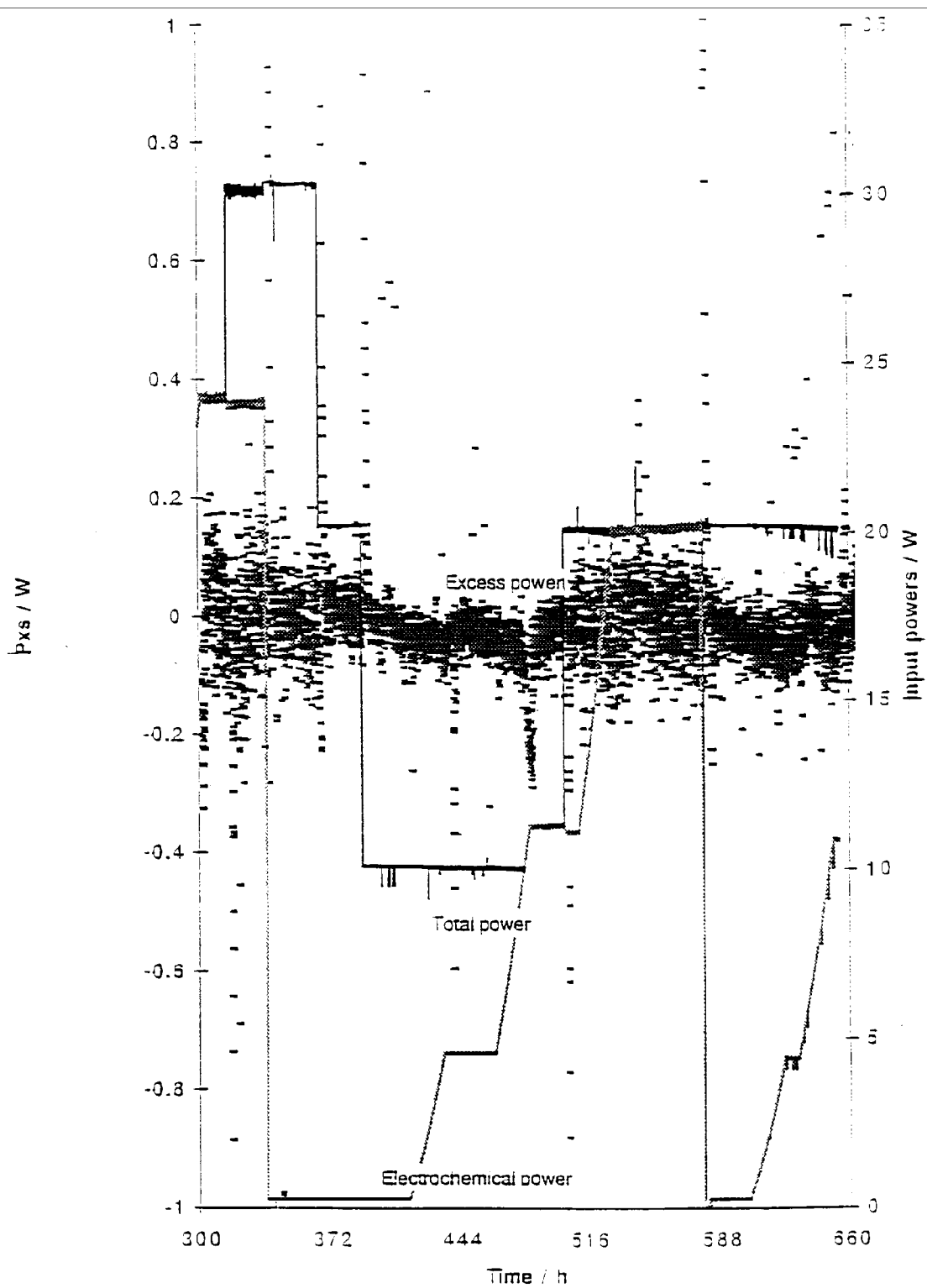
Figure 3-24
Calorimetric data for L2

L3. The cell contents were:

Cathode   3 mm x 3 cm Pd (Engelhard, batch 2). Annealed under vacuum with Ta getter. Pt contact and lead wires, 5-wire cathode contacts.

Anode   Pt wire.

Electrolyte   140 ml 1 M LiOD (Ontario Hydro). One Al addition during the experiment.

Internal sensors one electrolyte RTD and one catalyst RTD.

Calorimetrically, the experiment generally ran well. Measurements were made for approximately 2000 hours from 8/3/93. The cathode loading was, however, never particularly good. On dismantling the experiment, it was discovered that the cell voltage had been measured at the cell, instead of the calorimeter, boundary. An attempt was made retrospectively to correct for the mis-measurement of input power. Corrected calorimetric data shown in Figures 3-25 a-e were obtained by adding to the measured input power an amount proportional to I^2. The proportionality constant, the resistance of the uncompensated section of Pt lead wire, was estimated by asserting that the excess power could not sustain a negative value. While consistent with our previous experience, and with the known behavior of a Pt resistive element, we cannot be certain that the correct value was selected for the uncompensated resistance, or that this value did not change with time. As such, the values of excess power displayed in Figures 3-25 a-e must be interpreted with caution.

L4. The cell contents were:

Cathode   3 mm x 3 cm Pd (Engelhard, batch 2). The cathode was annealed in deuterium. Pt contact and lead wires, 5-wire cathode contacts.

Anode   Pt wire.

Electrolyte   140 ml 1 M LiOD (Ontario). Light water additions were made during the experiment.

Internal sensors one electrolyte RTD and one catalyst RTD

Experiment L4 was assembled and operated as a twin to experiment L3. On dismantling the cell after ~2000 hours of operation it was discovered that L4 suffered the same measurement error as L3. The cell voltage had been measured at the cell rather than at the calorimeter boundary, resulting in a significant unmeasured contribution to the input power. An attempt was made to correct the data in the same way as described above for L3. The results, shown in Figure 3-26 a-e, should be interpreted with the same caution as advised above for the results of experiment L3.
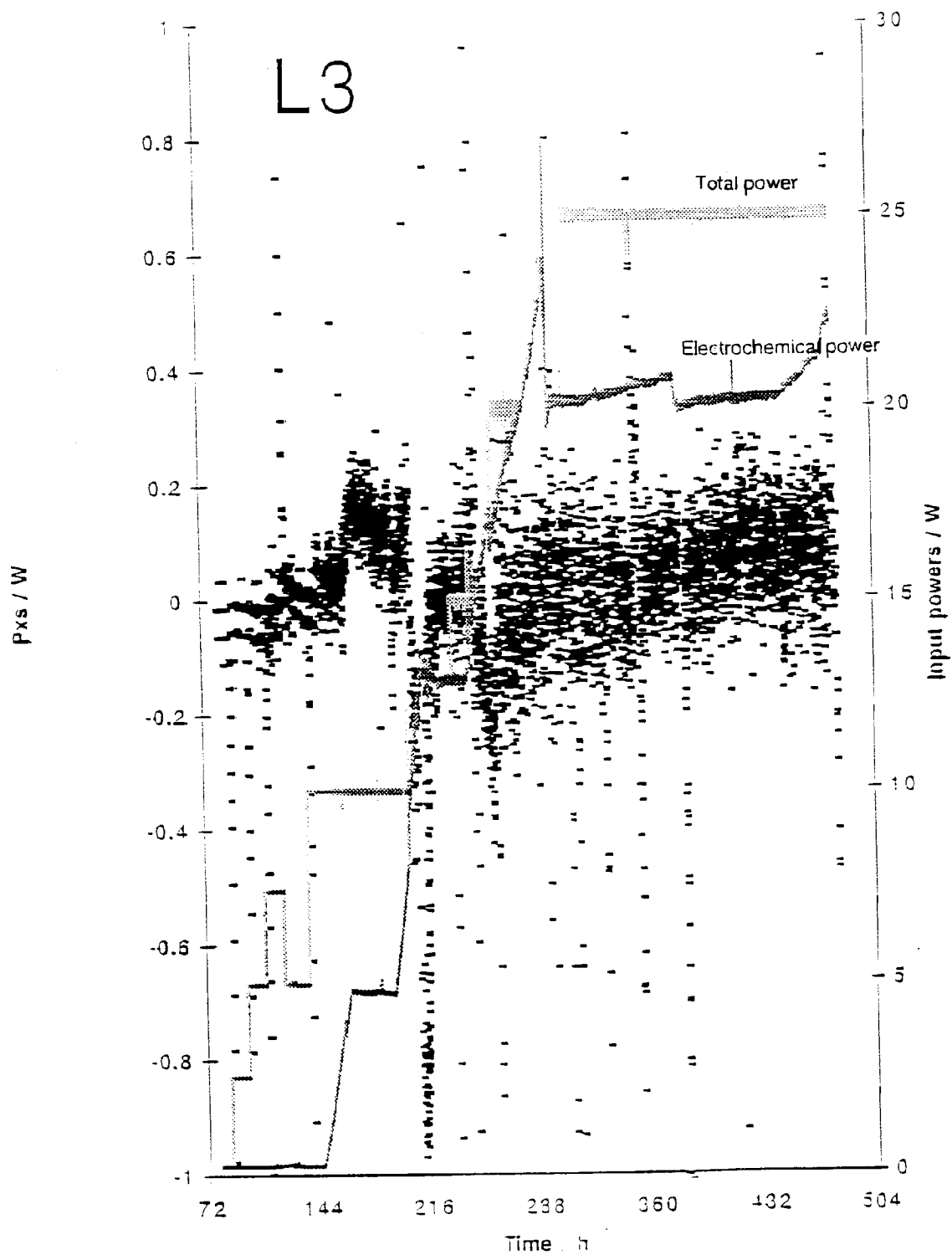
Figure 3-25a
L3 cell
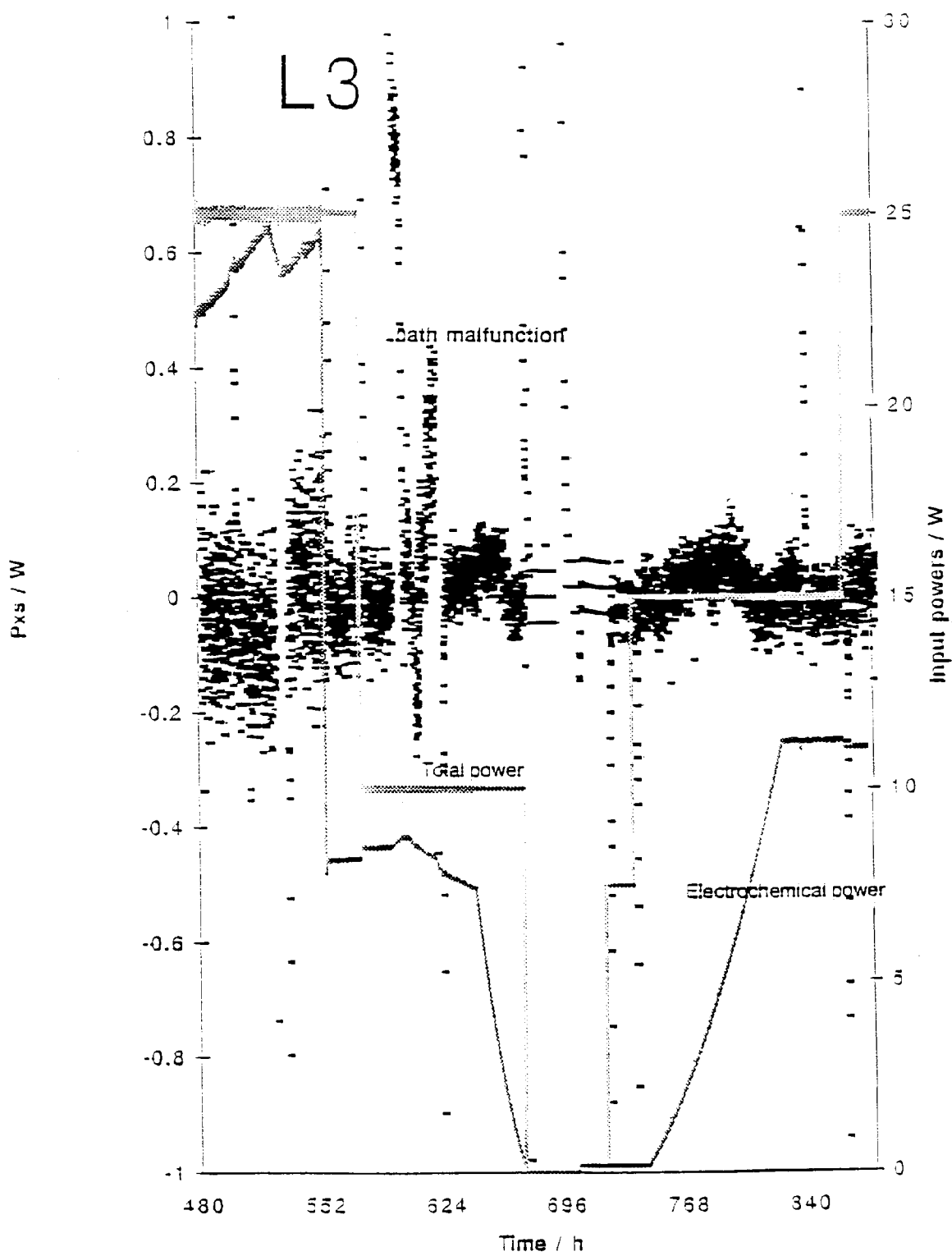
Figure 3-25b
L3 cell
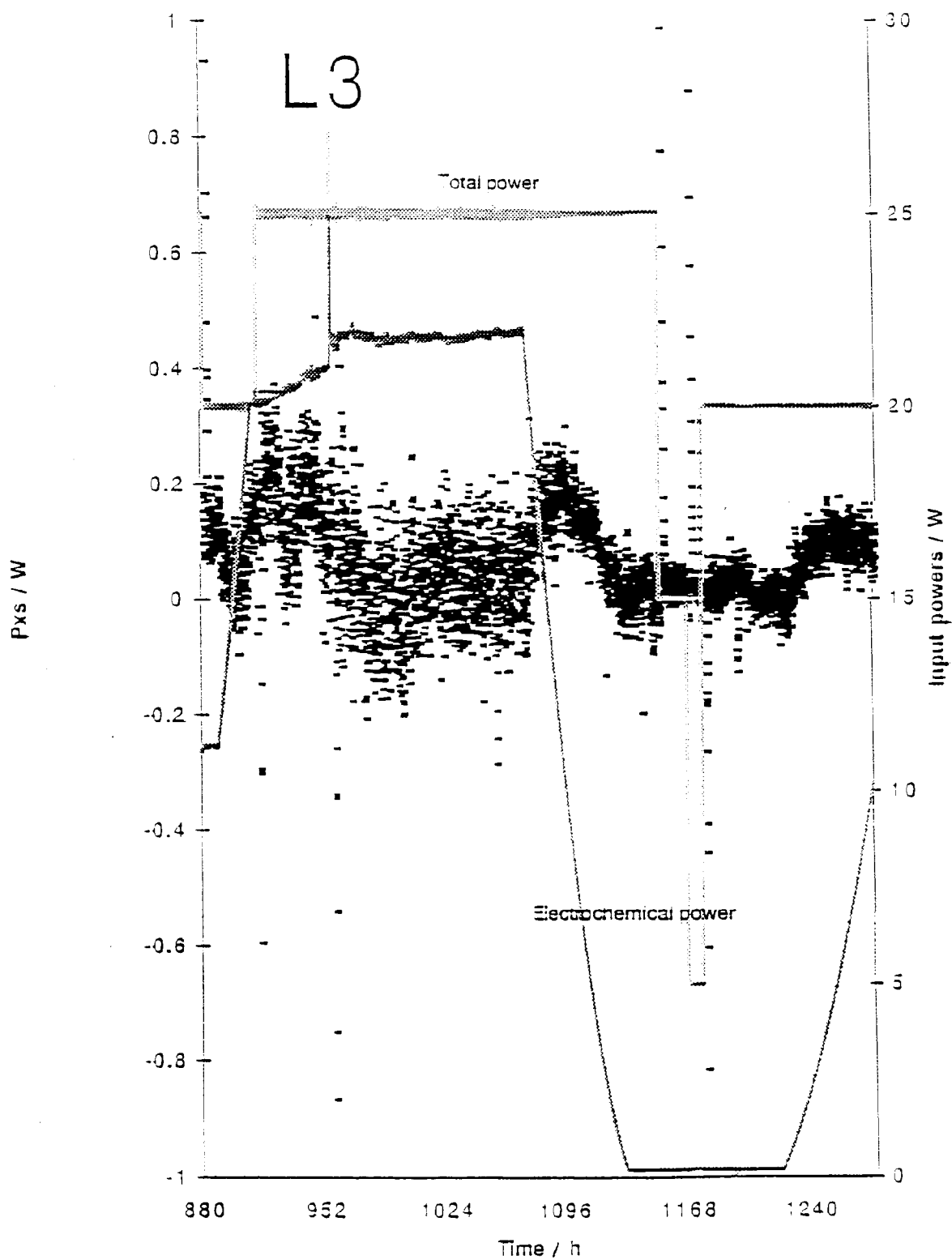
Figure 3-25c
L3 cell
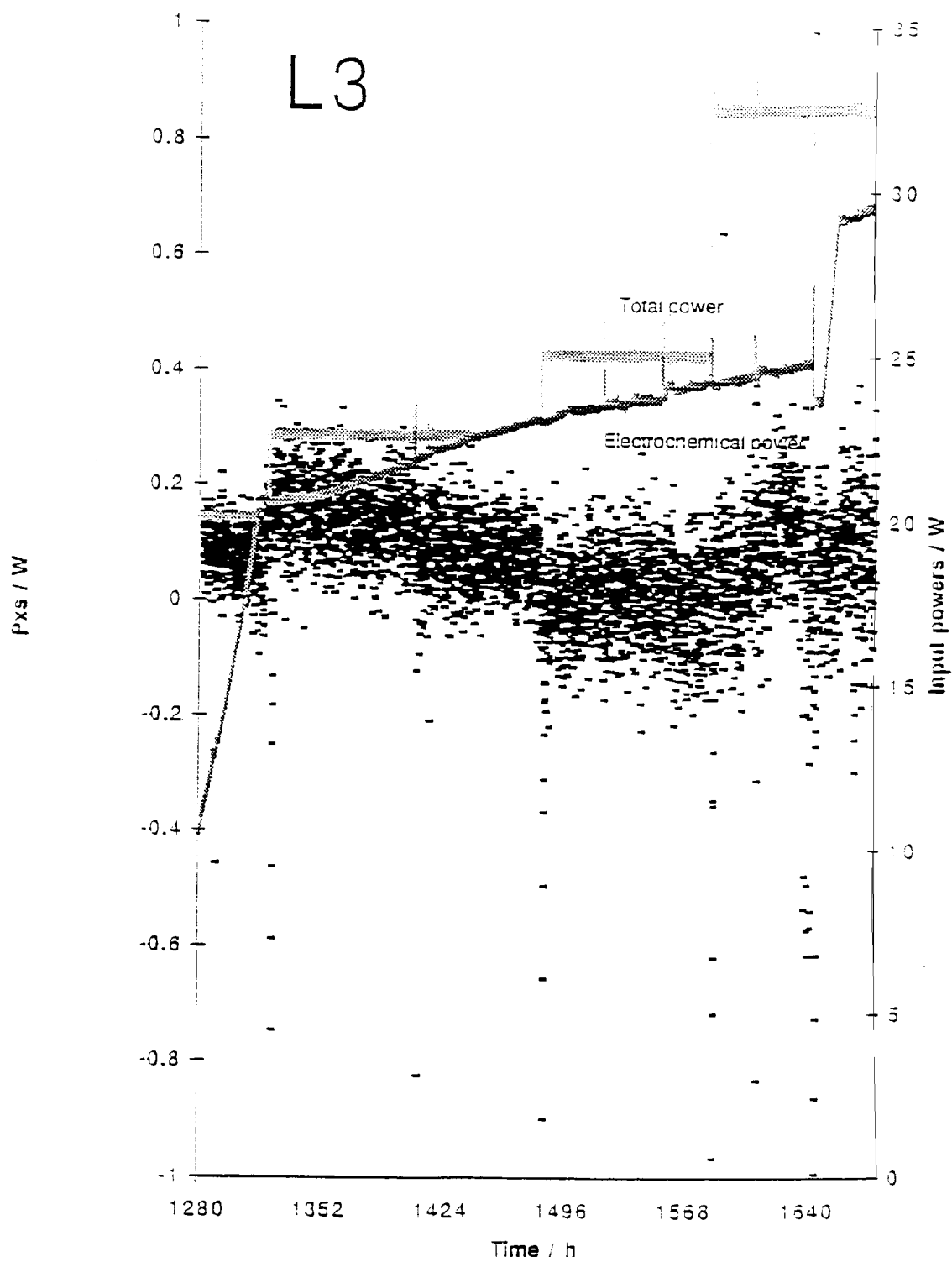
Figure 3-25d
L3 cell
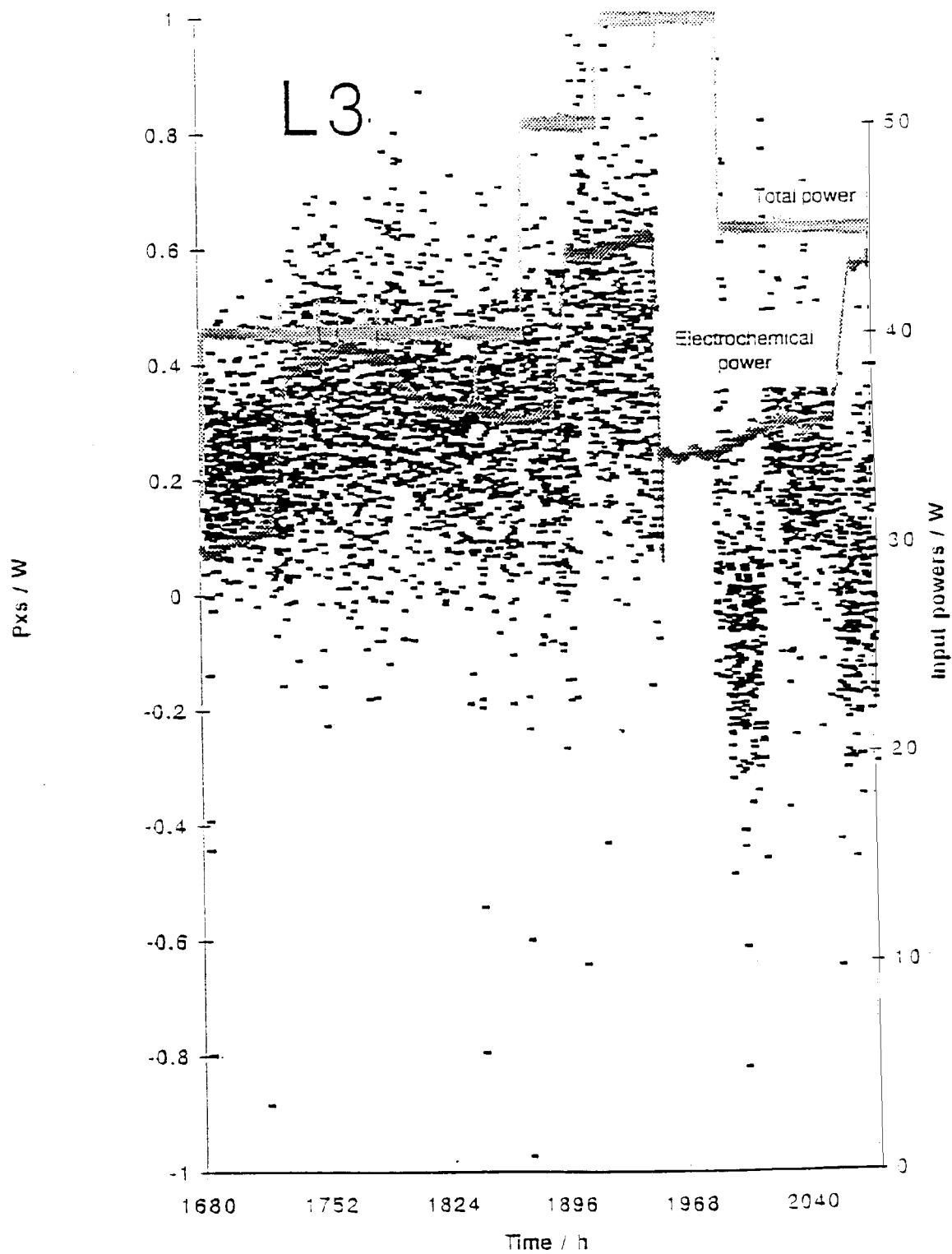
Figure 3-25e
L3 cell

L5. This experiment was designed to test the thermal behavior of a Ni cathode. The cell contents were:

Cathode	Ni Fibrex (Manufacturers designation = 80/20 ,600 g/m), 1.2 mm thick, 5 x 10 cm, rolled into cylinder. 40 mil Ni contact wires.
Anode	Pt wire.
Electrolyte	0.6 M K_2CO_3 in H_2O.

Internal sensors one electrolyte RTD and catalyst RTD; the cell was run closed.

Calorimetrically, the experiment ran well. Data were collected for 500 h beginning 12/14/93, Figures 3-27 and 3-28. The experiment was run according to an alternating cathodic/anodic current cycle protocol. No excess heat was observed, but small (< 100mW) endothermic anomalies were seen at 150 h and 380 h.

L6. This was a further experiment designed to test the thermal behavior of Ni cathodes. The cell contents were:

Cathode	1 mm Ni wire (JM 99.8%), 9 cm long total (bent into three-legged "3 cm" long cathode. 40 mil Pt contact wires.
Anode	Pt wire.
Electrolyte	1 M $LiOD/D_2O$ (Aldrich).

Internal sensors one electrolyte RTD and one catalyst RTD; cell run closed.

Calorimetrically, the experiment ran well. Data were collected for approximately 450 h beginning 12/16/93. No excess heat was observed. Results of this experiment are shown in Figures 3-29 and 3-30.
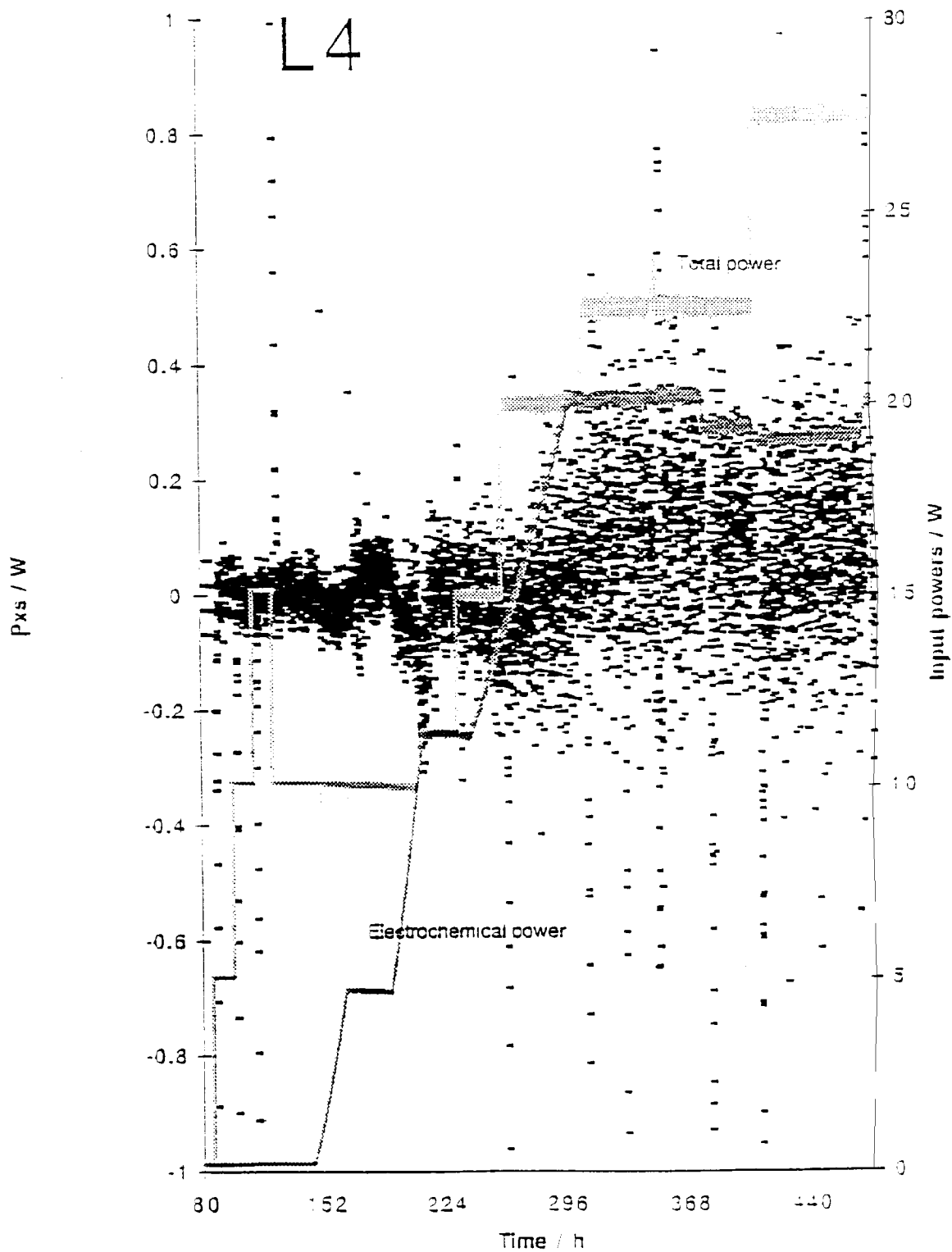
Figure 3-26a
L4 cell
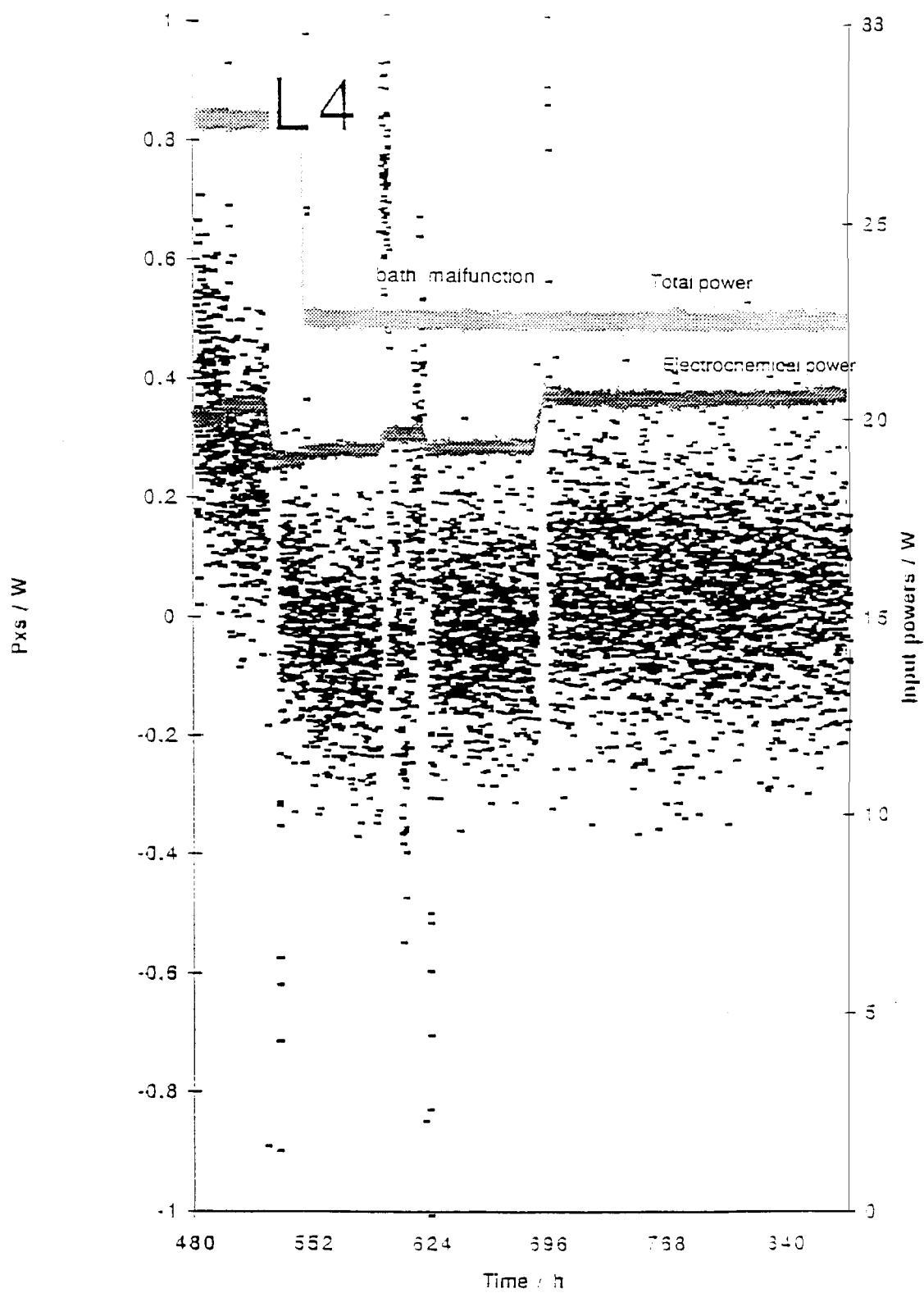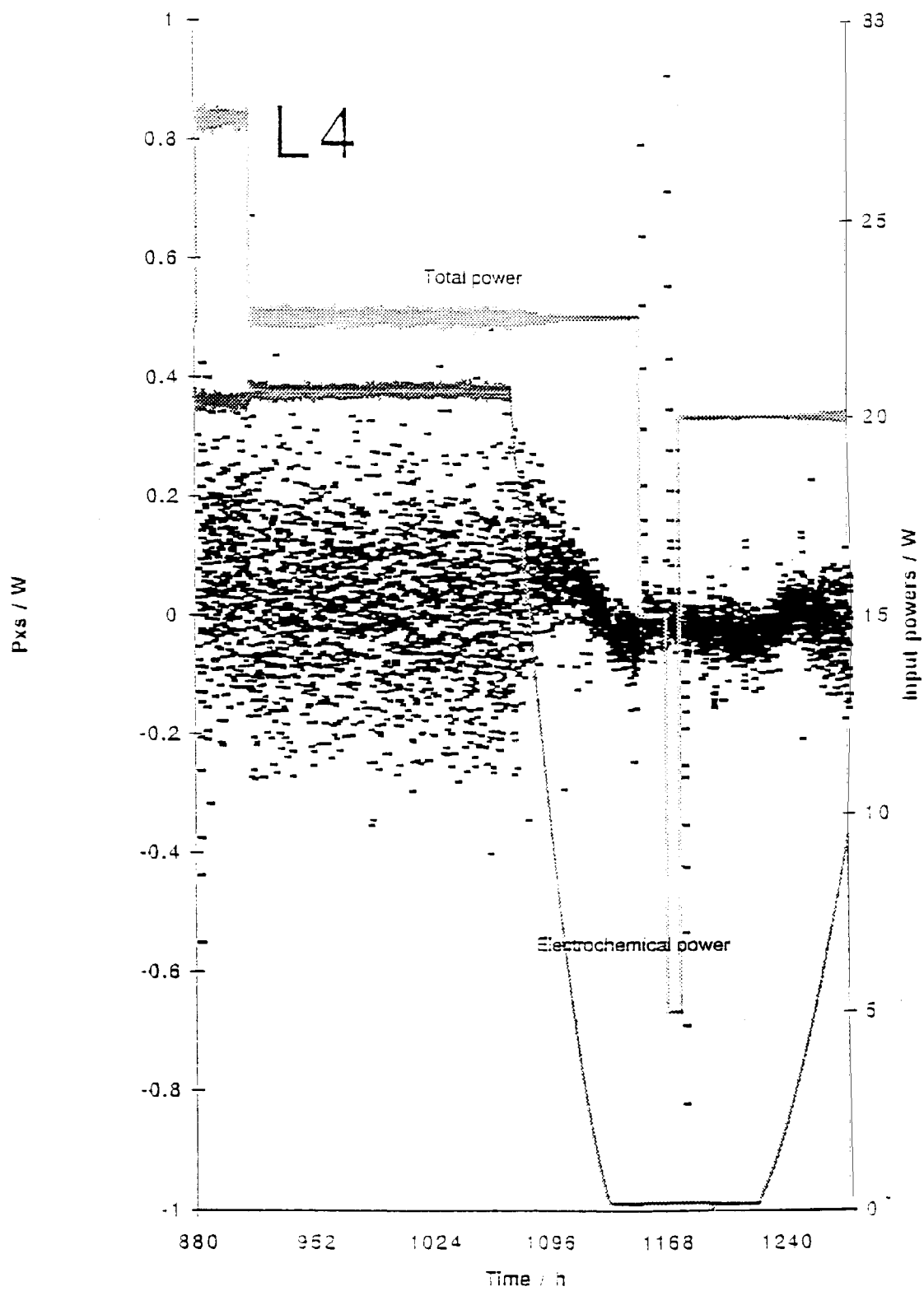
Figure 3-26b
L4 cell

Figure 3-26c
L4 cell
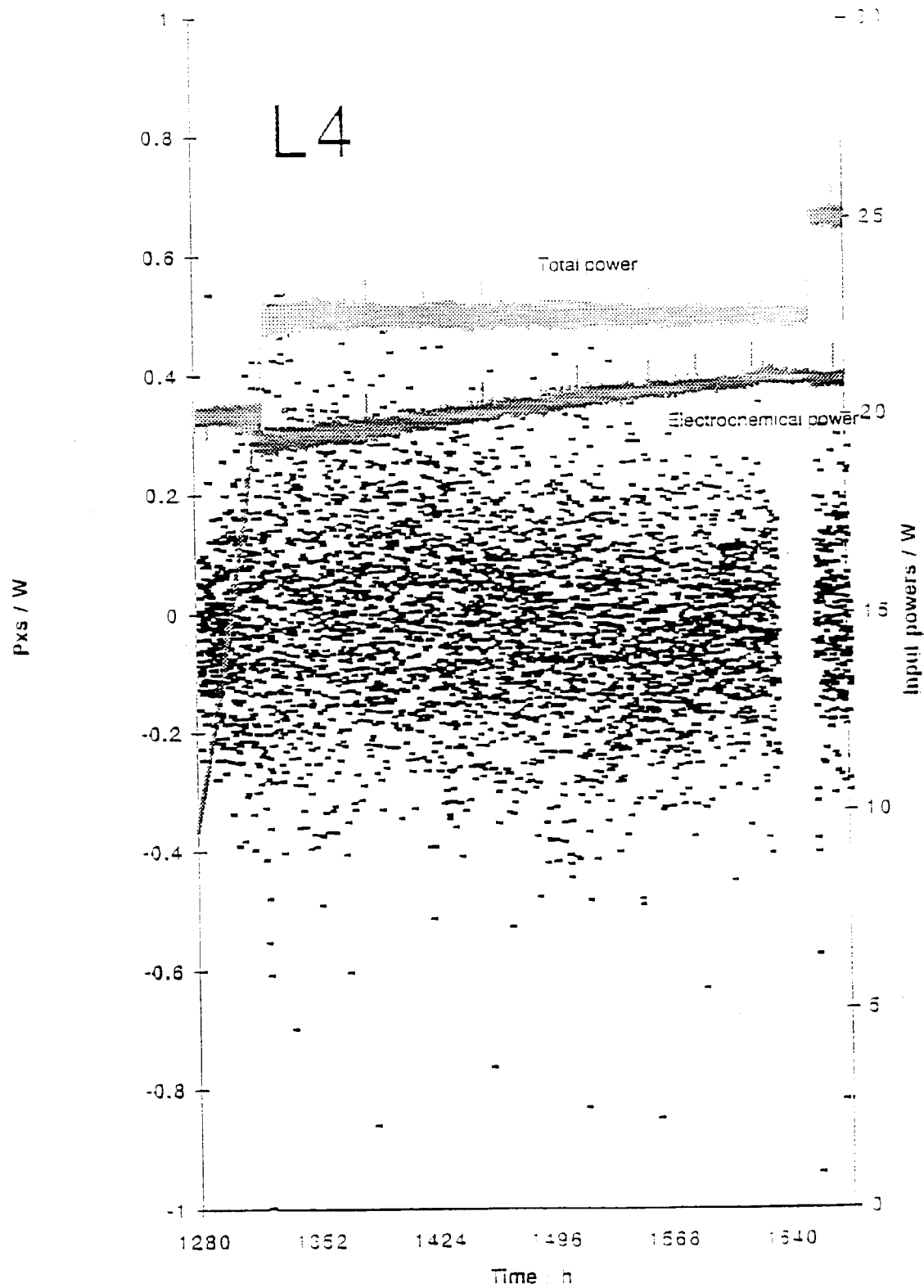
Figure 3-26d
L4 cell
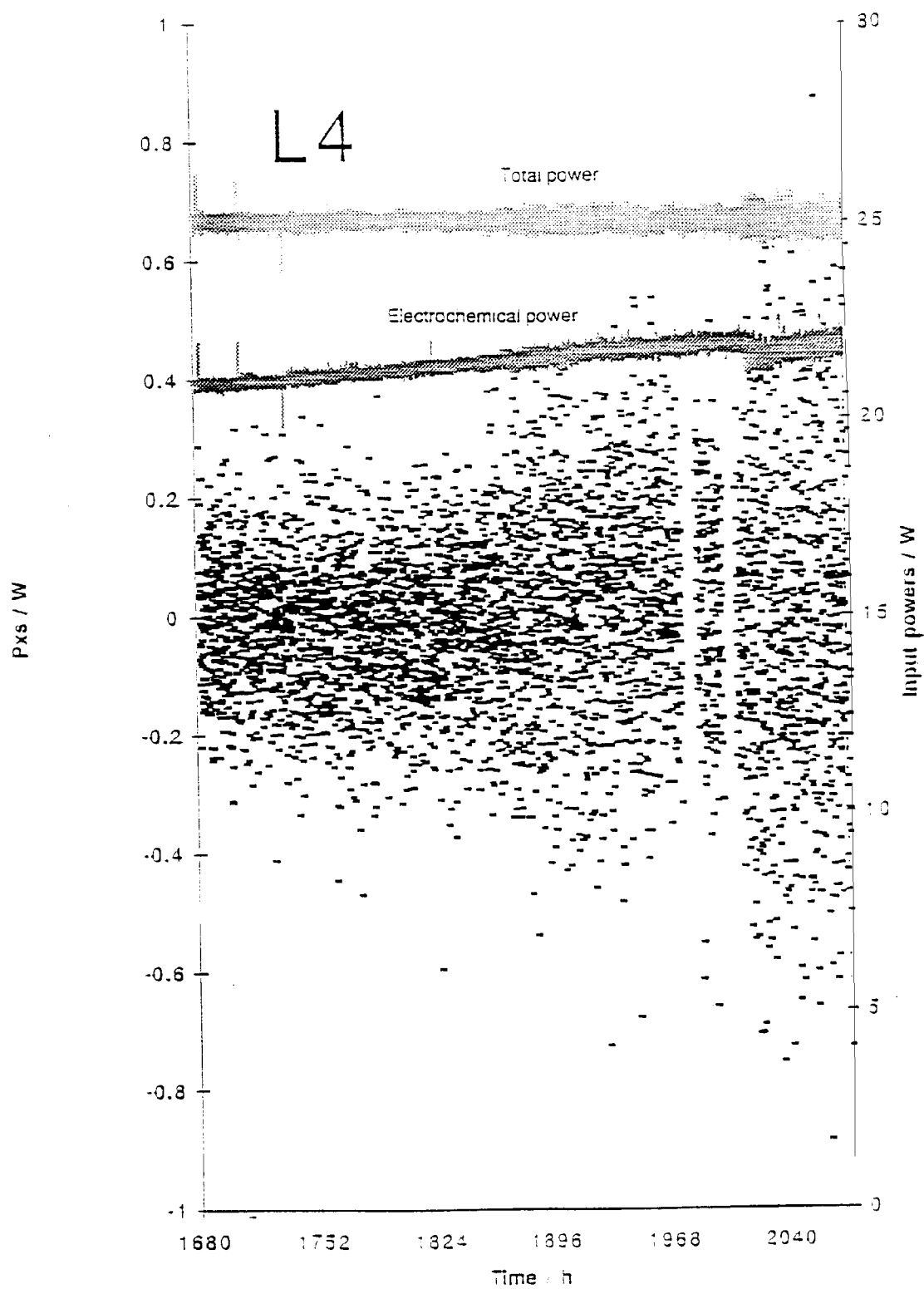
Figure 3-26e
L4 cell
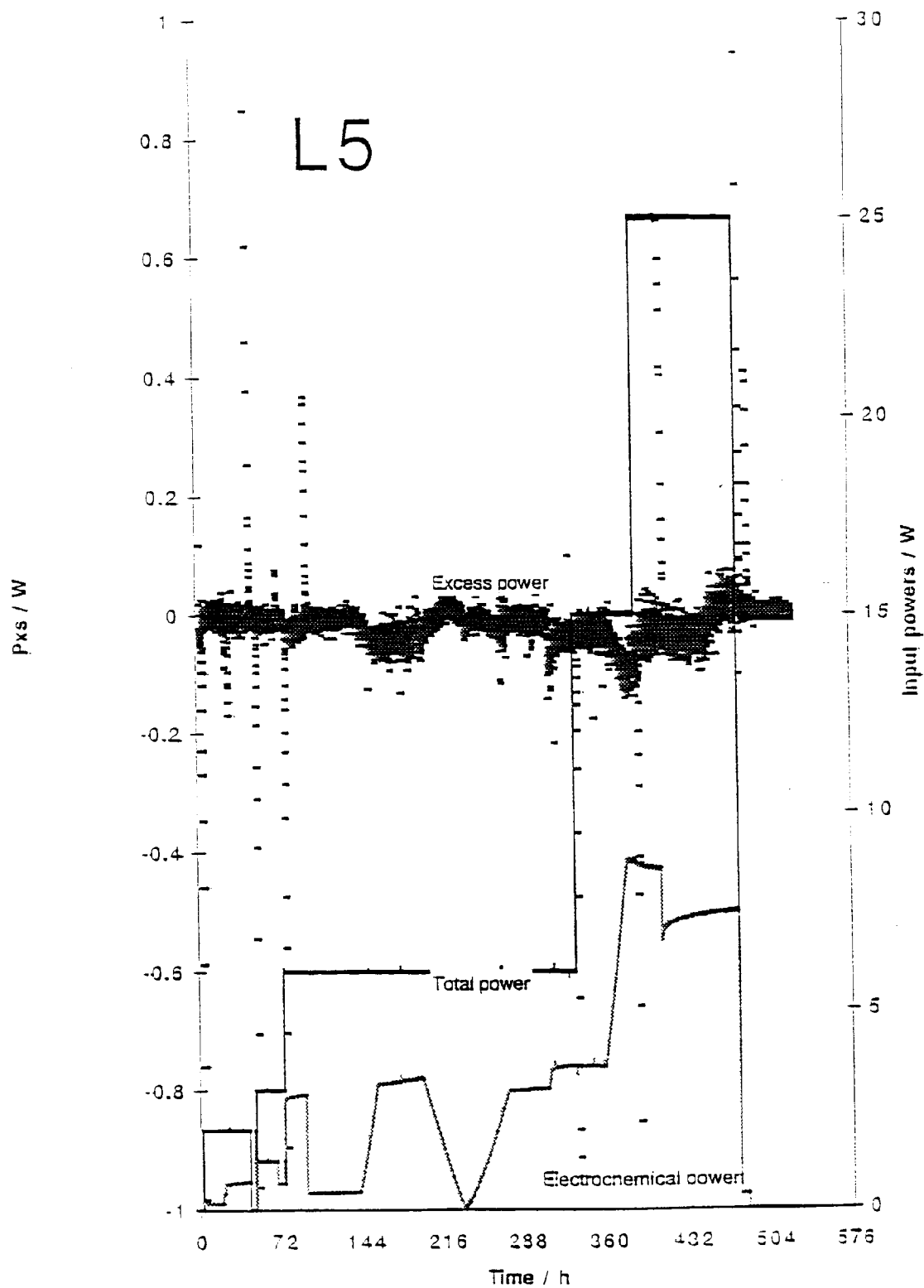
Figure 3-27
Calorimetric data for L5
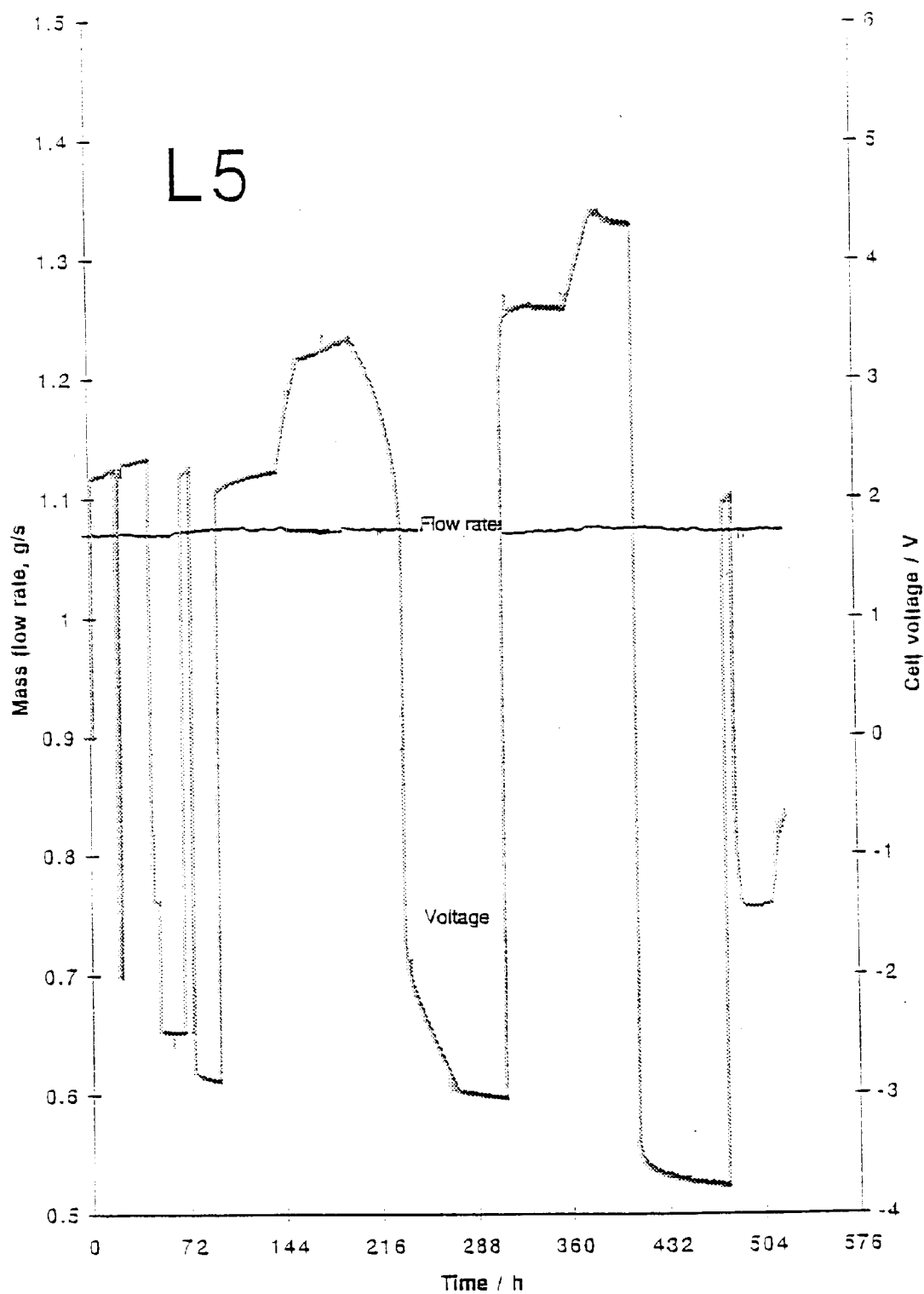
Figure 3-28
Mass flow and voltage data for L5
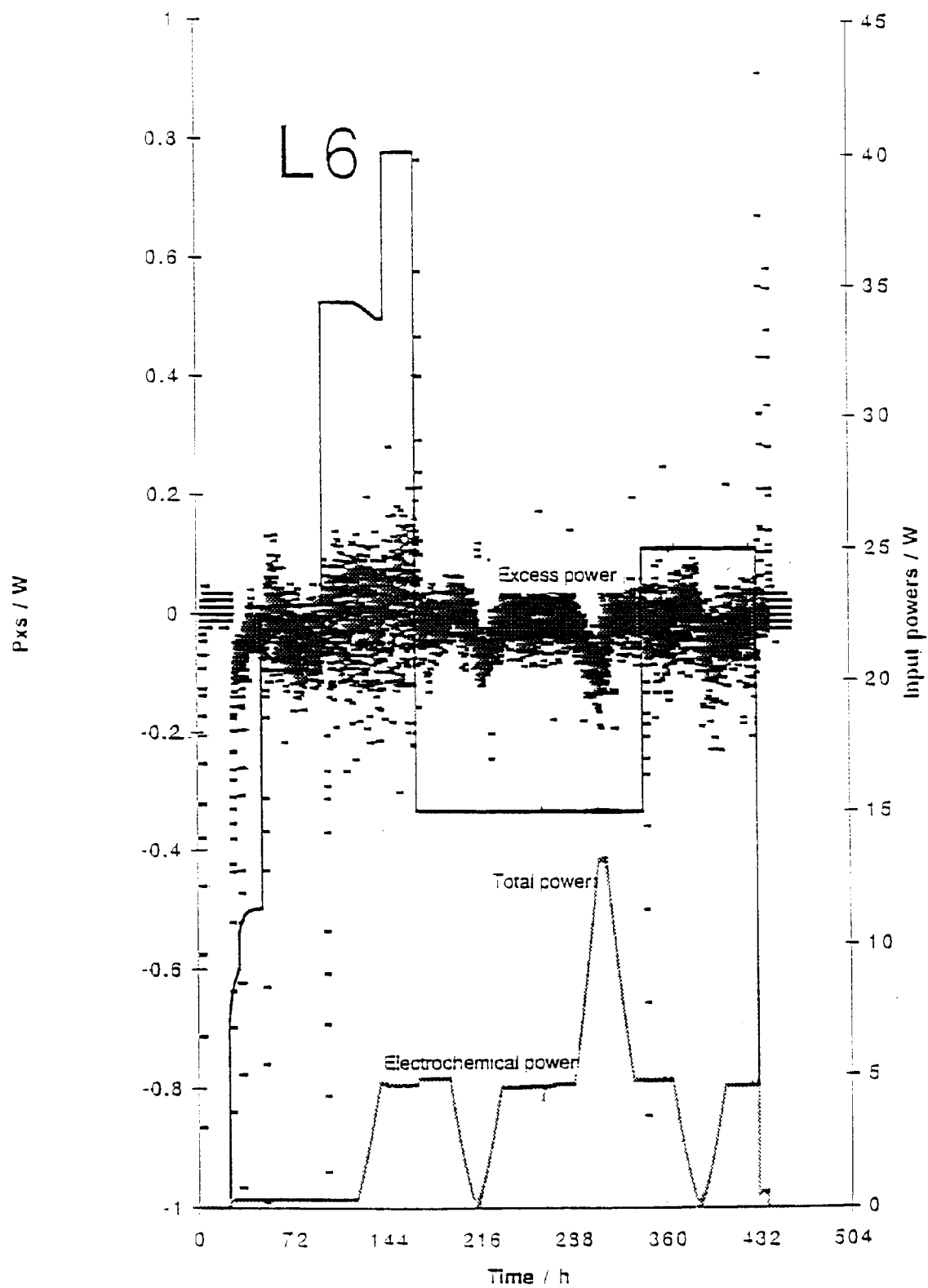
Figure 3-29
Calorimetric data for L6
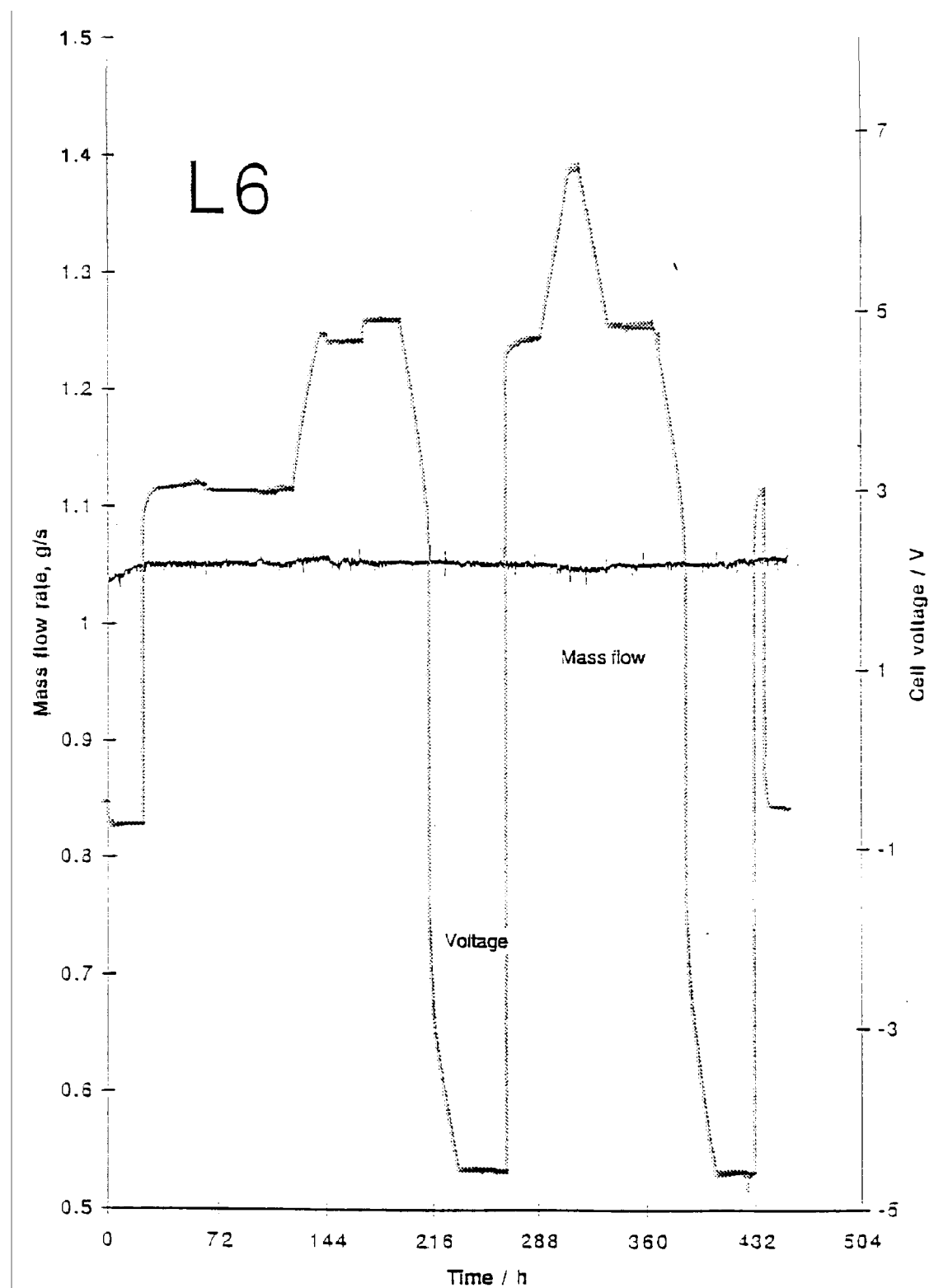
Figure 3-30
Mass flow and voltage data for L6

L7. The cell contents were:

Cathode	3 cm x 3 mm (Engelhard, batch 2), slow cool after annealing. 40 mil Pt contact wires.
Anode	Pt wire.
Electrolyte	1 M LiOD/D_2O (Aldrich) + 200 ppm Al at the outset.

Internal sensors one electrolyte RTD and one catalyst RTD; cell run closed.

Calorimetrically, the experiment ran very well. Data analysis for approximately 1000 h beginning 1/31/94. Lowest cathode $R/R°$ was approximately 1.8, corresponding to a loading of approximately 0.9. No excess heat was observed. Results of this experiment are shown in Figures 3-31 to 36.

L8. The cell contents were:

Cathode	Pd/Ce/Sm (alloy supplied by Pons and Fleischmann, IMRA, France), 1.5 cm x 4 mm rod. Heavy aqua regia etch only.
Anode	Pt wire.
Electrolyte	1 M LiOD/D_2O (Aldrich). No Al addition.

Internal sensors one electrolyte RTD and one catalyst RTD; cell run closed.

Data were collected for 1200 h beginning 1/31/94, Figures 3-37 to 3-42. No loading measurements were made. After an initial period of cathode loading, the cell electrolyte was made to boil, by increasing the heater power and lowering the mass flow rate, at 260 h. Small electrolyte temperature anomalies were observed after boiling. A small amount of apparent excess heat was observed after boiling, although data exhibited an unusually high degree of scatter at high input powers. The cell was made to boil twice more at the end of the experiment. On dismantling the experiment, it was found that plastic rods which hold the cell in place within the calorimeter had become distorted, by the very high temperatures which were sustained on the walls of the cell. The calorimeter was designed to ensure that the measured heat (output power) was insensitive to the position of the heat source within the calorimeter. As such, it is unlikely that the small displacement of the cell could result in measured apparent excess power. This possibility, while remote, cannot be ruled out as calibrations were not performed with the cell in its distorted position within the calorimeter.
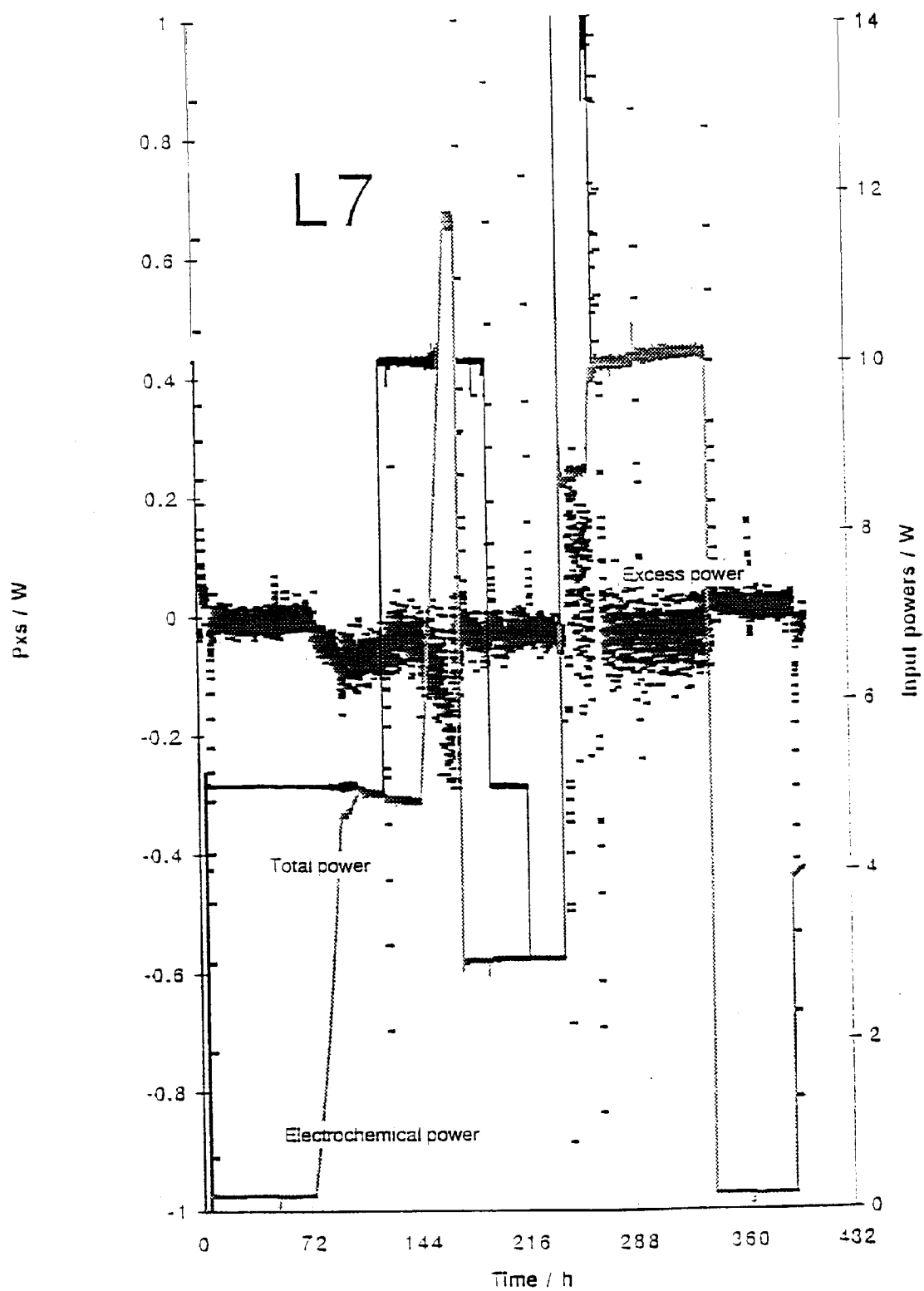
Figure 3-31
Calorimetric data for L7
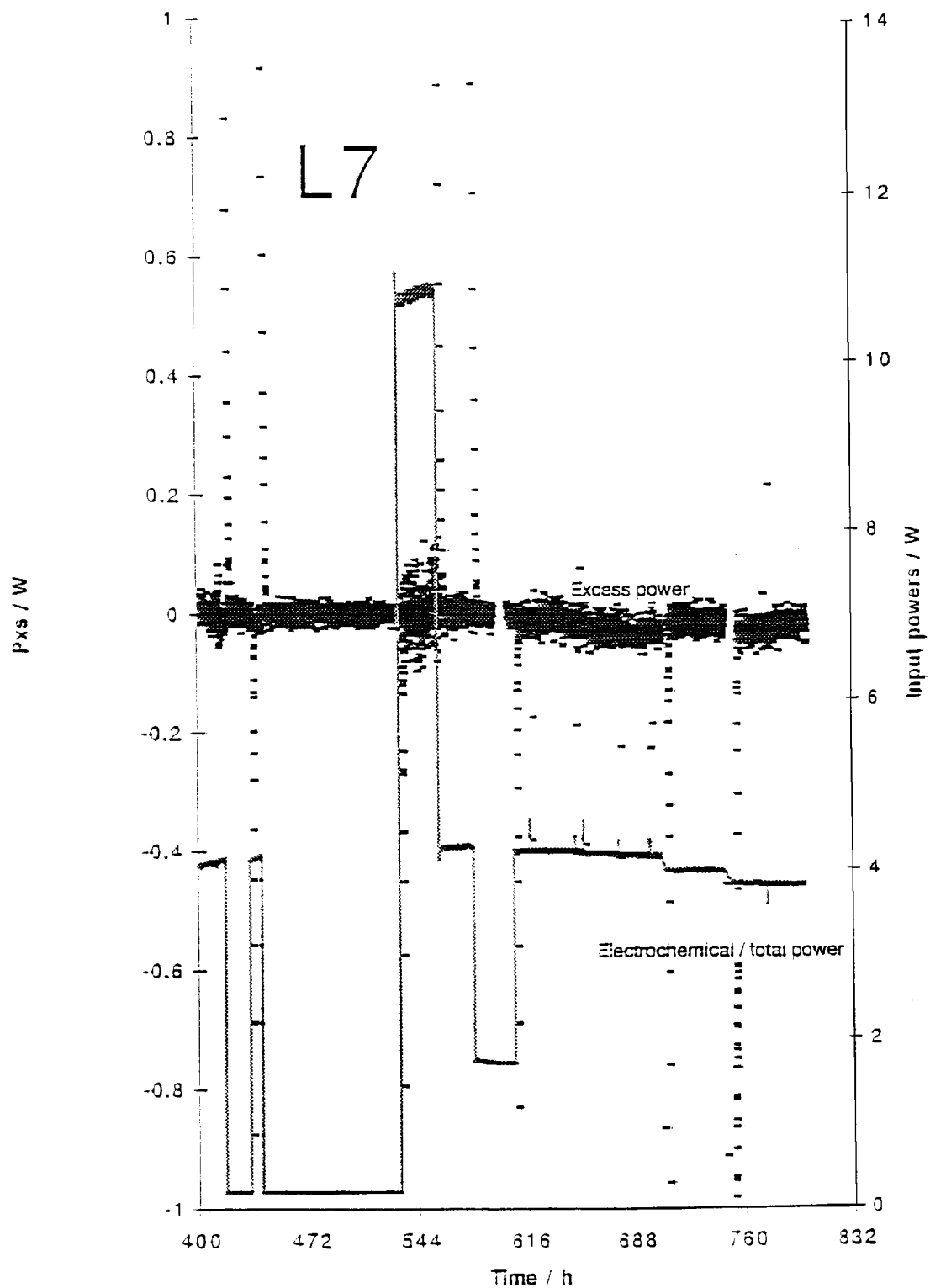
Figure 3-32
Calorimetric data for L7
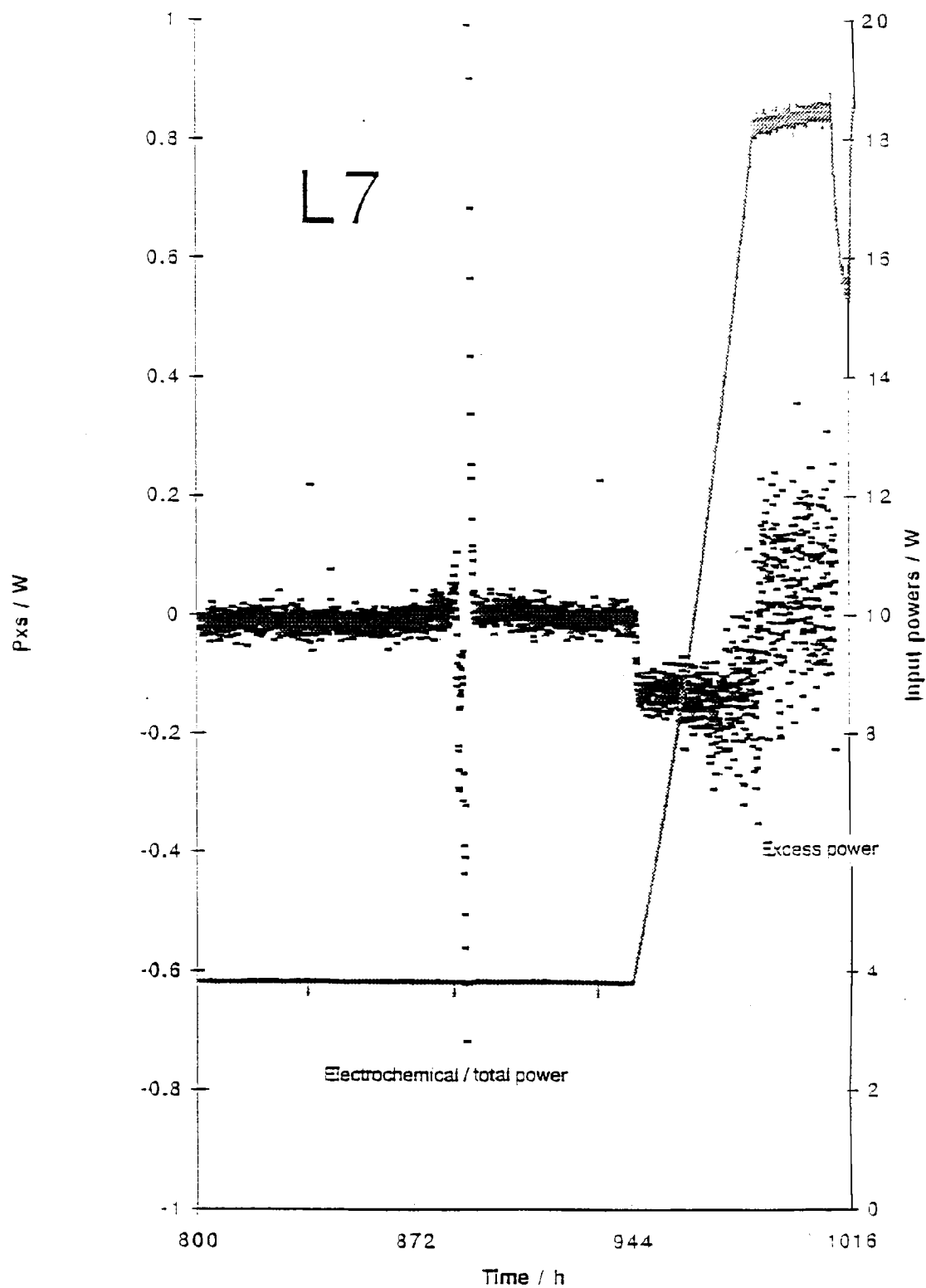
Figure 3-33
Calorimetric data for L7
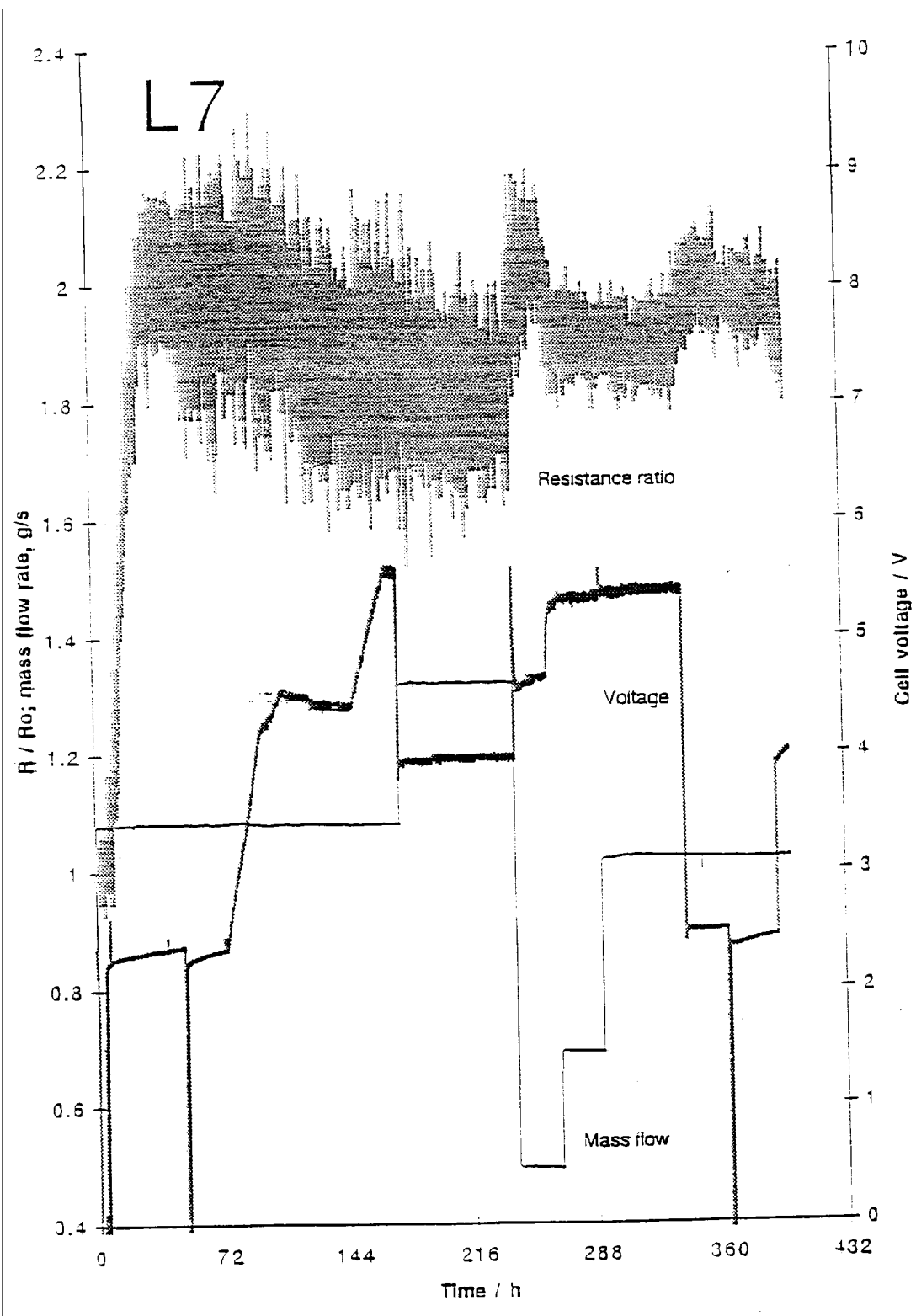
Figure 3-34
Data for L7
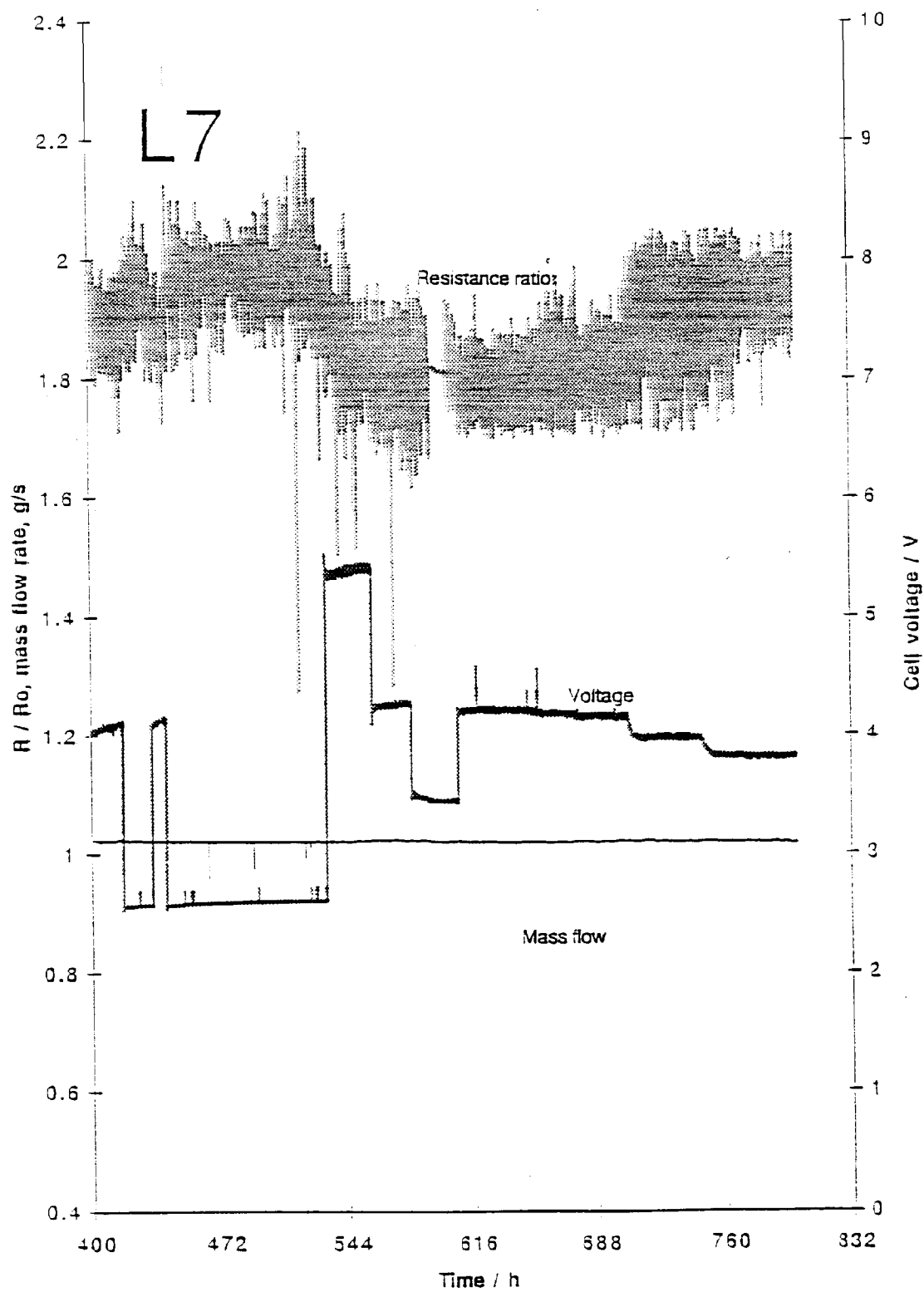
Figure 3-35
Data for L7
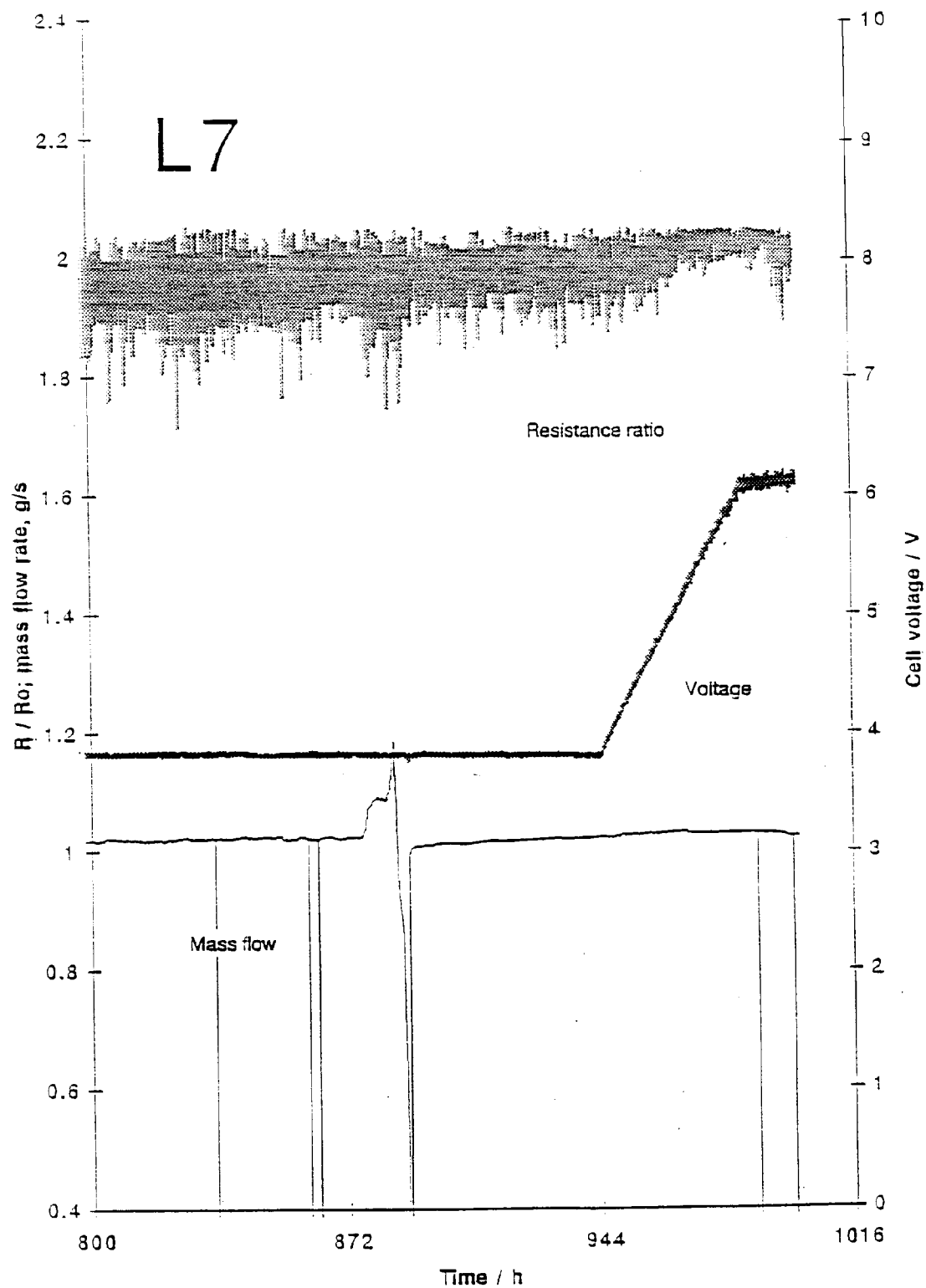
Figure 3-36
Data for L7
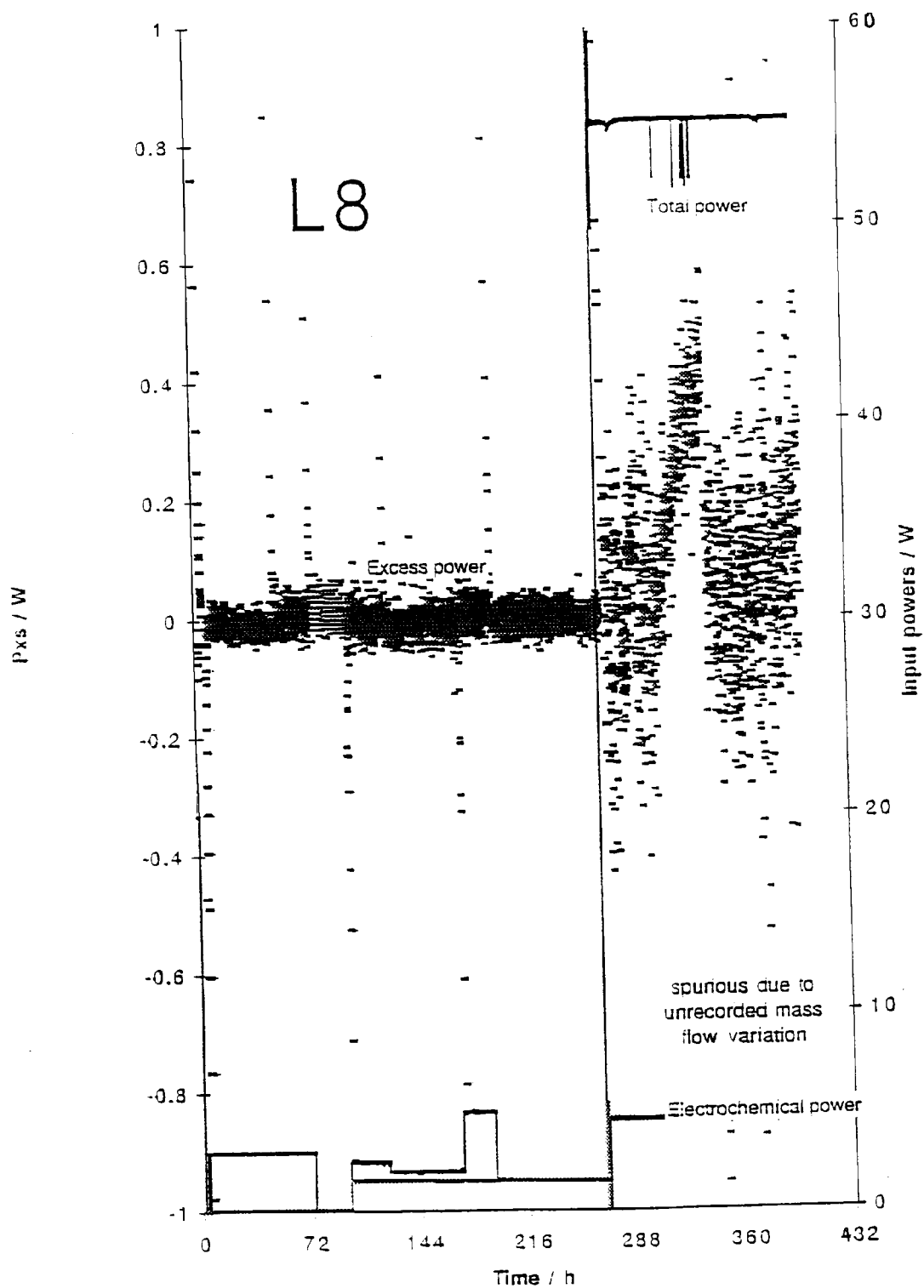
Figure 3-37
Calorimetric data for L8

Figure 3-38
Calorimetric data for L8
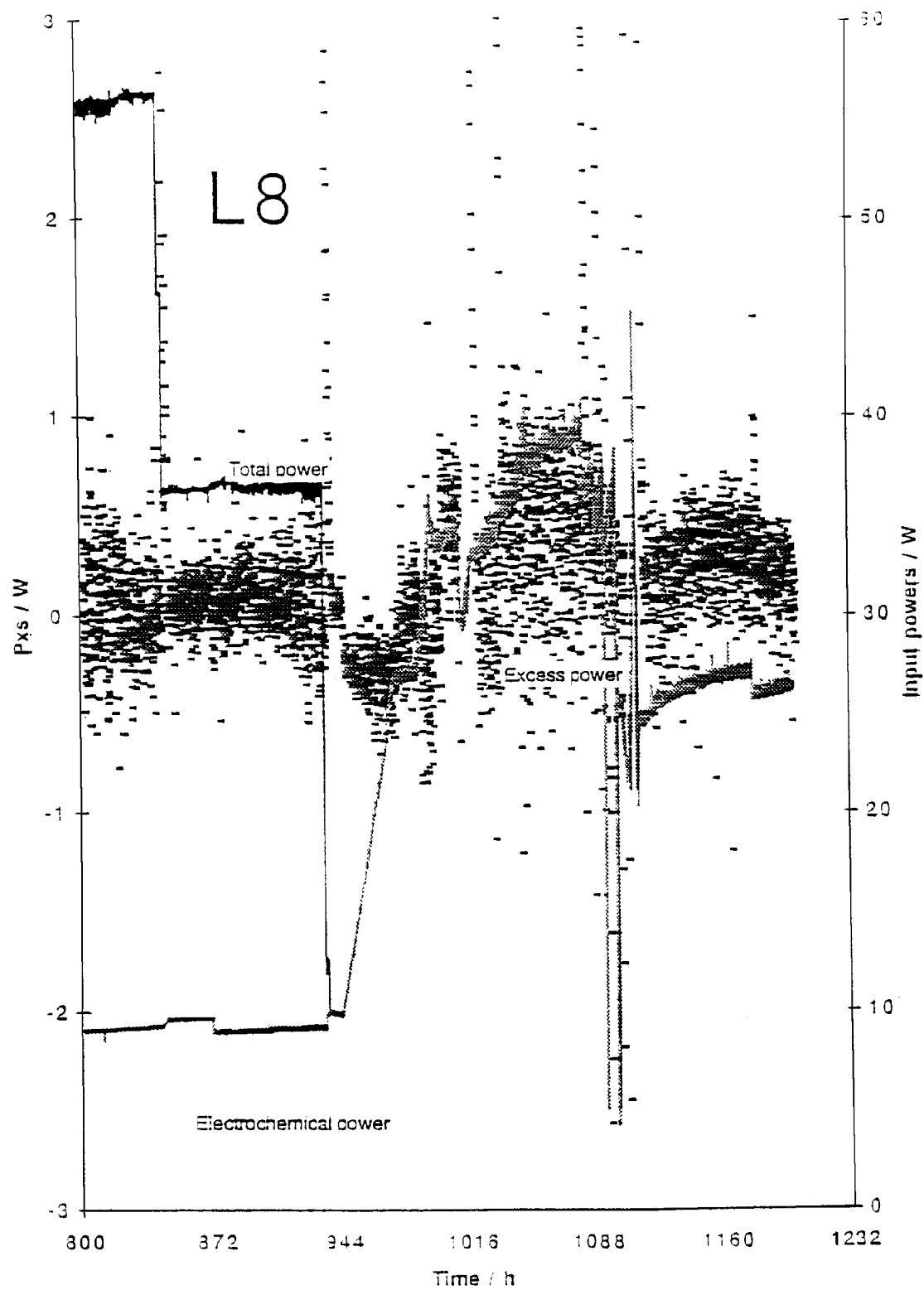
Figure 3-39
Calorimetric data for L8
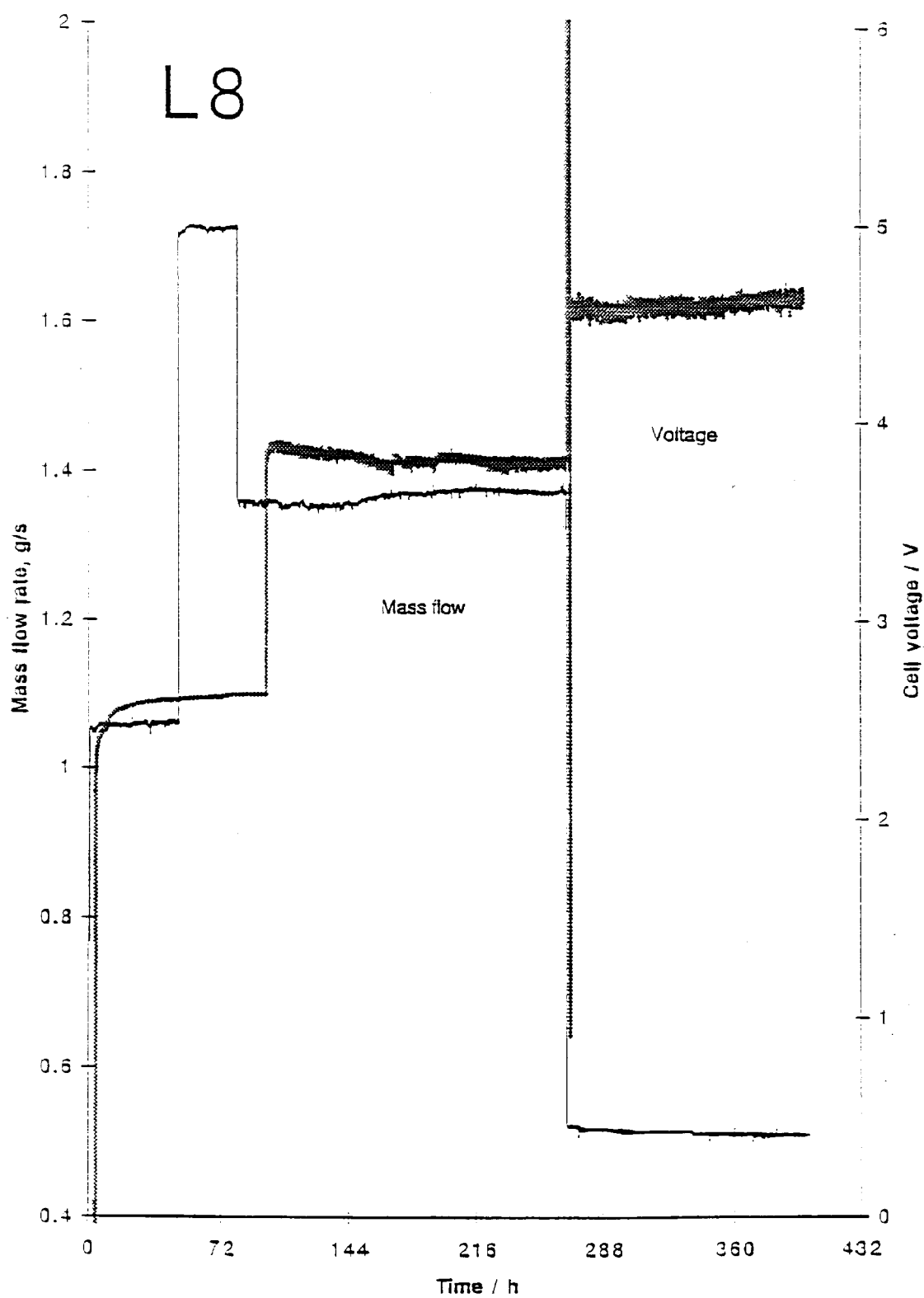
Figure 3-40
Mass flow and voltage data for L8
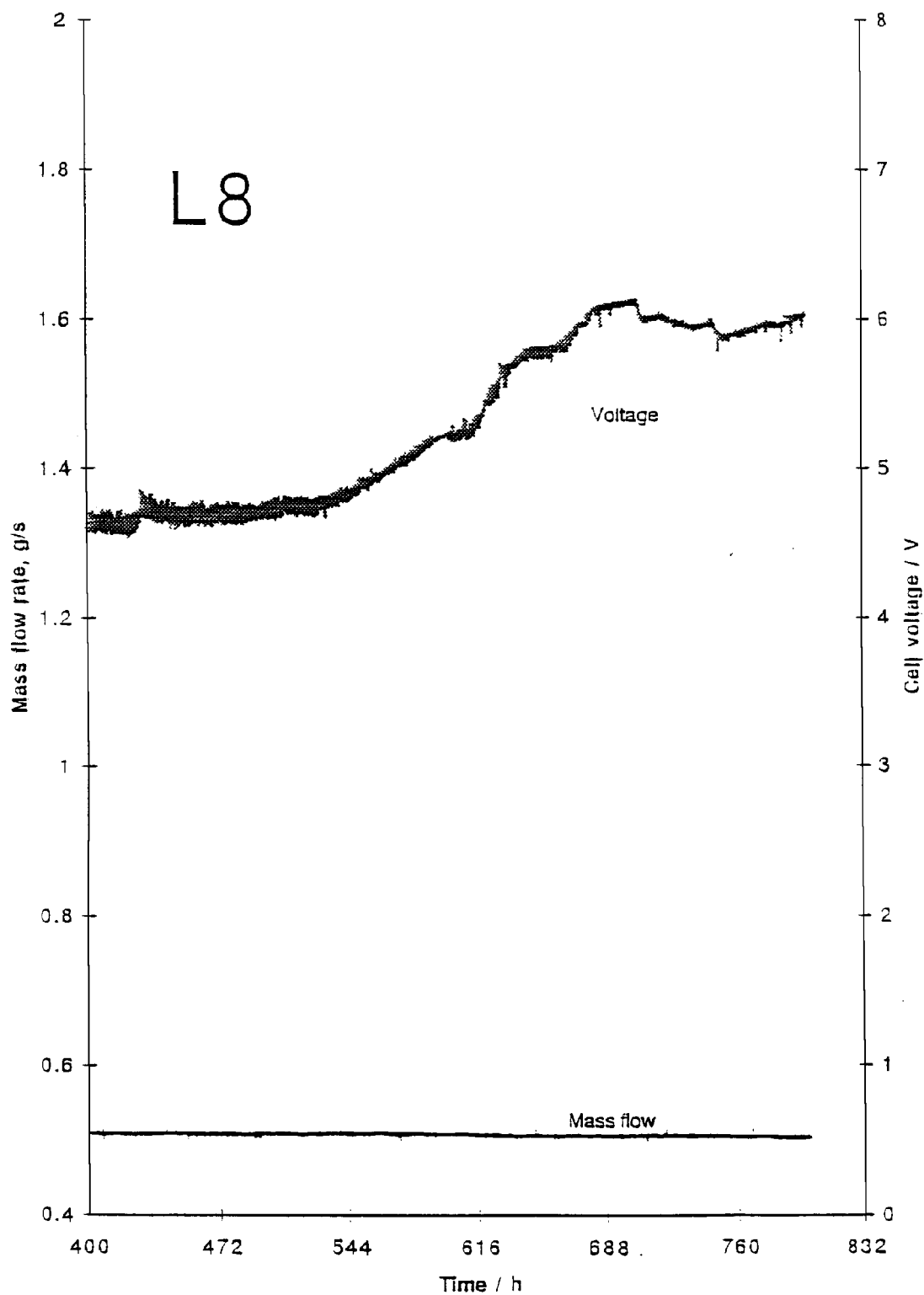
Figure 3-41
Mass flow and voltage data for L8
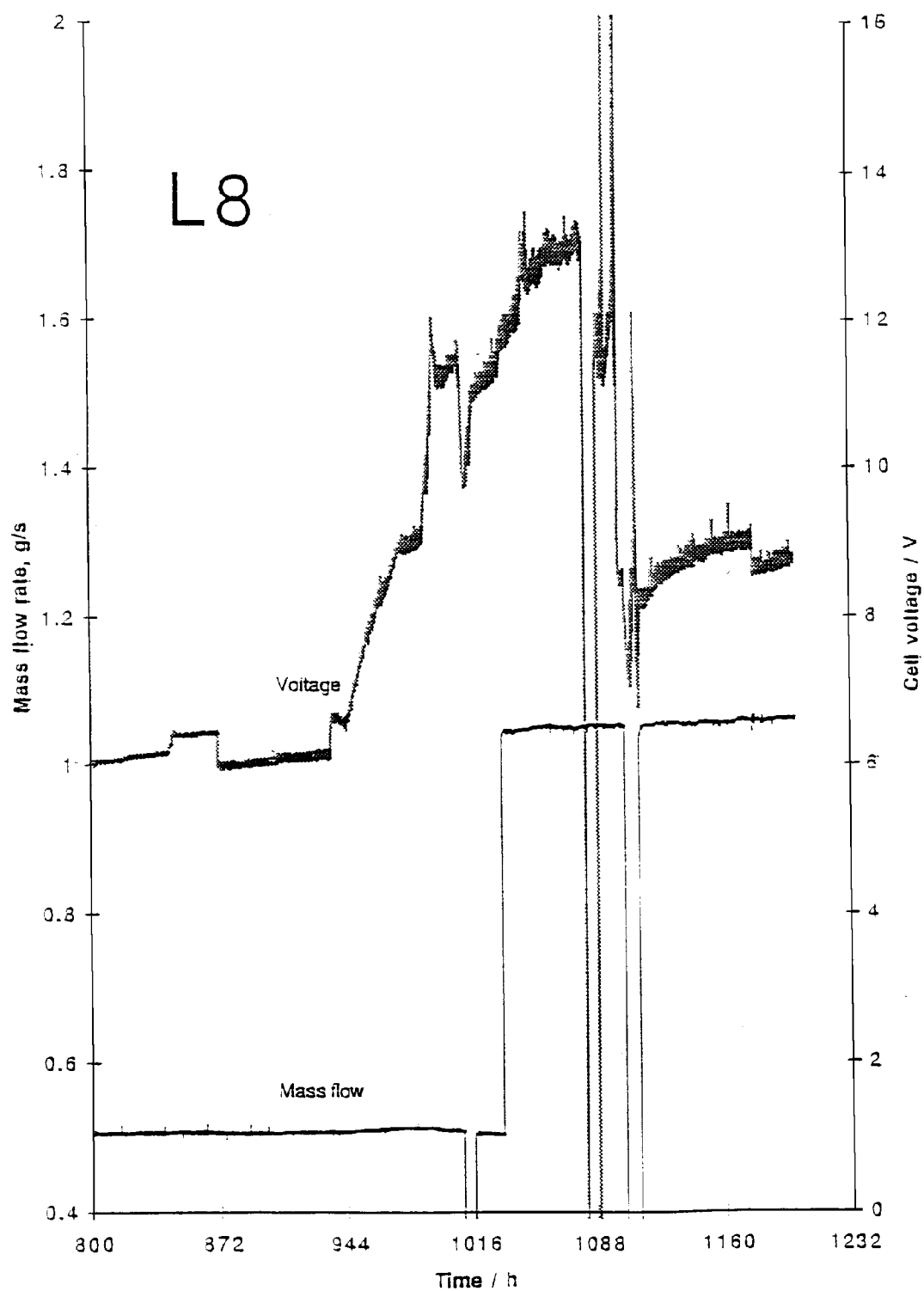
Figure 3-42
Mass flow and voltage data for L8

L9. This experiment was designed as a further attempt to investigate the properties of boiling systems. The cell contents were:

Cathode	3 cm x 3 mm (Engelhard, batch 1), originally used as a degree-of-loading cathode (P52-D26). Annealed and etched before reuse, but not remachined.
Anode	Pt wire.
Electrolyte	25 ml 1 M LiOD/D$_2$O (Aldrich). No Al.

Internal sensors one cell RTD and one catalyst RTD; cell run closed.

In this experiment, the cell design was changed somewhat in order to be able to raise the cell temperature with lower input powers. The cell contained a teflon insert in its lower half, the internal dimensions of which resembled a degree-of-loading cell. The cell temperature sensor was contained in a hole in the teflon adjacent to the electrolyte portion.

Data were collected for 580 h from 4/1/94, Figures 3-43 and 3-44. The cathode did not exhibit good loading. The calorimeter could not be calibrated satisfactorily; on disassembly, the sheathing of the outlet temperature sensors was found to be faulty-sensor heads were exposed to water. Significant silicate dissolution was observed in the cell, originating from the quartz rods.

L10. This experiment was designed to test an alternative cathode metallurgy. The normal cell design was employed. The cell contents were:

Cathode	Zone-refined Pd, 1mm x 3 cm.
Anode	Pt wire.
Electrolyte	140 ml 1 M LiOD/D$_2$O (Aldrich). No Al.

Internal sensors one electrolyte RTD and one catalyst RTD; cell run closed.

Data analysis for 140 h beginning 4/26/94, Figures 3-45 and 3-46. Excellent calorimetry was recorded. Although not extensively exercised, the cathode demonstrated very poor loading behavior and the experiment was terminated early.

Figure 3-43
Calorimetric data for L9
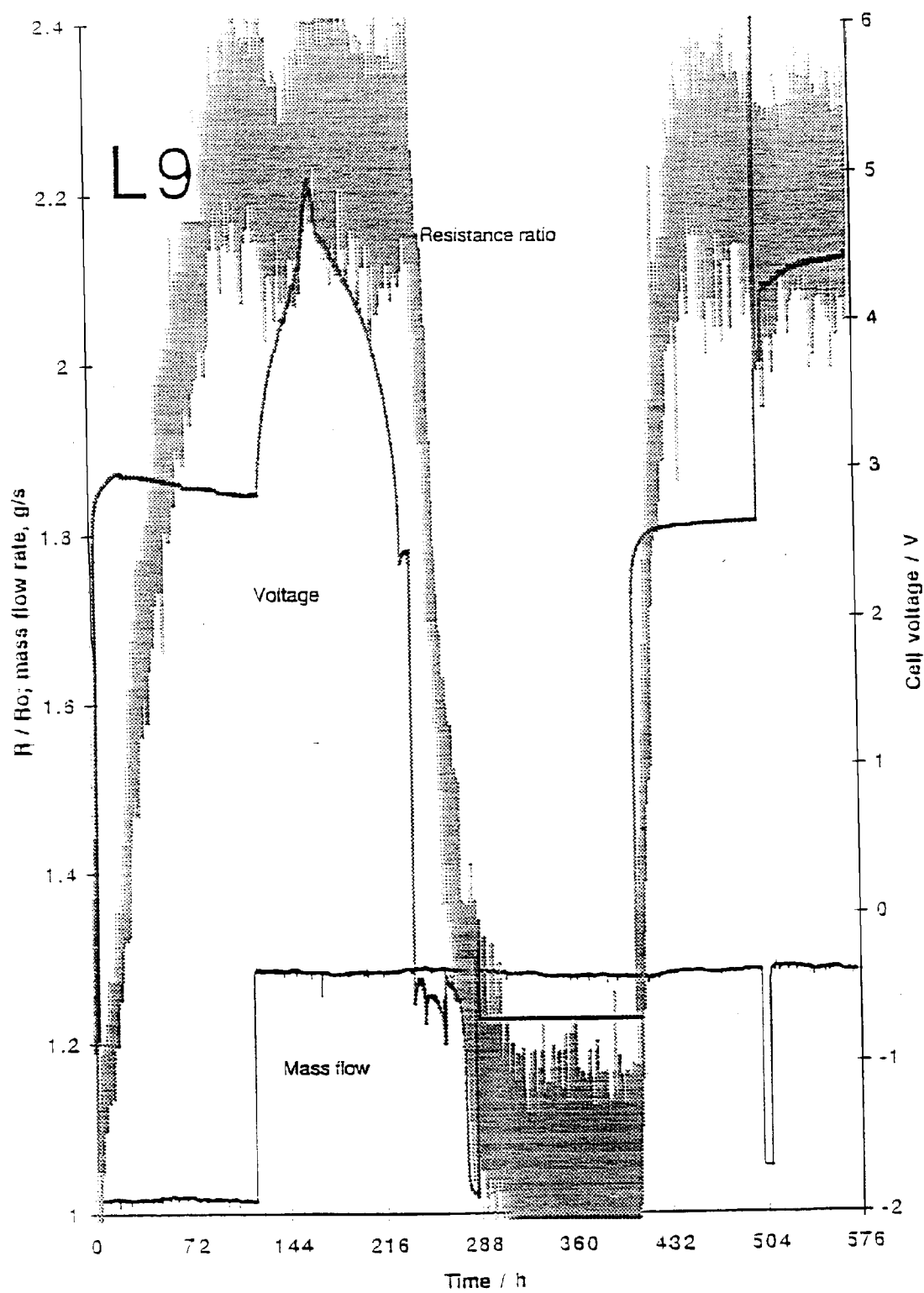
Figure 3-44
Data for L9

Figure 3-45
Calorimetric data for L10

Figure 3-46
Data for L10

L11. The cell contents were:

Cathode	Reused #1 Engelhard (originally degree-of-loading P28-D12), 2.8 mm x 3 cm. Remachined, annealed and etched.
Anode	Pt wire.
Electrolyte	25 ml 1 M LiOD/D_2O (Aldrich). No Al.

Internal sensors one electrolyte RTD and one catalyst RTD; cell run closed.

This experiment utilized the same cell body as L9. Data were analyzed for approximately 600 h beginning 5/2/94, Figures 3-47 and 3-48. Reasonable calorimetry was obtained, although the heater became excessively noisy after 100 h and was turned off (problem later traced to power supply). Cathode showed poor loading behavior (x < 0.9) and no excess heat was observed.

L12. The cell contents were:

|	
Cathode	Unused #1 Eng., 2.8 mm x 3 cm, annealed previously.
Anode	Pt wire.
Electrolyte	140 ml 1 M LiOD/D_2O (Aldrich). No Al.

Internal sensors one electrolyte RTD and one catalyst RTD; cell run closed.

Data analysis for 650 h beginning 5/10/94, Figures 3-49 and 3-50. Good calorimetry was exhibited. Cathode showed poor loading behavior and no excess heat was observed.

L13. The cell contents were:

Cathode	Re-reused Eng. #1, 3 mm x 3 cm, apparently well-loaded in degree-of-loading experiment (DoL I2) prior to transfer to L13.
Anode	Pt wire.
Electrolyte	20 ml 1 M LiOD/D_2O (Aldrich).

Internal sensors one internal RTD and one catalyst RTD; cell run open.
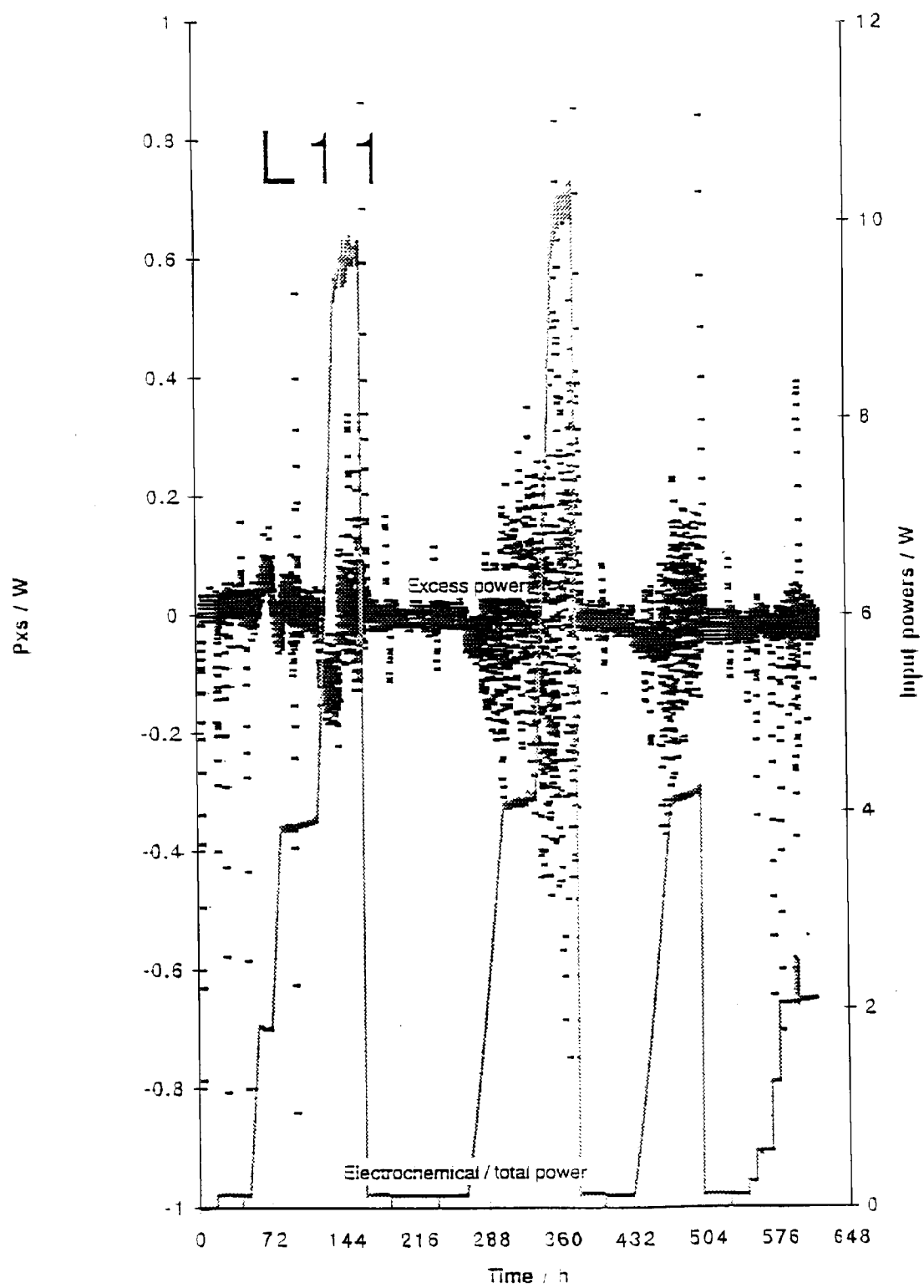
Figure 3-47
Calorimetric data for L11
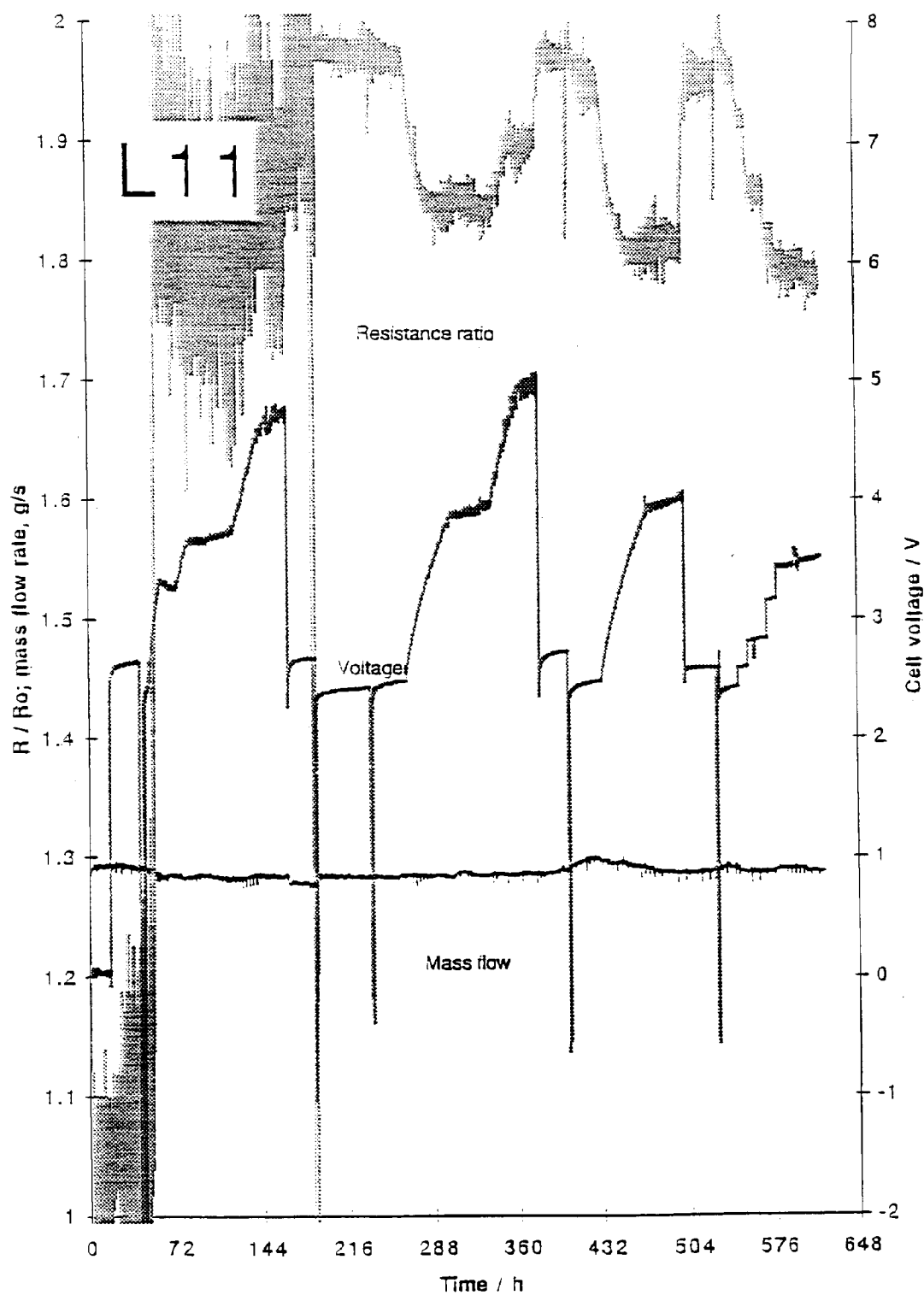
Figure 3-48
Data for L11
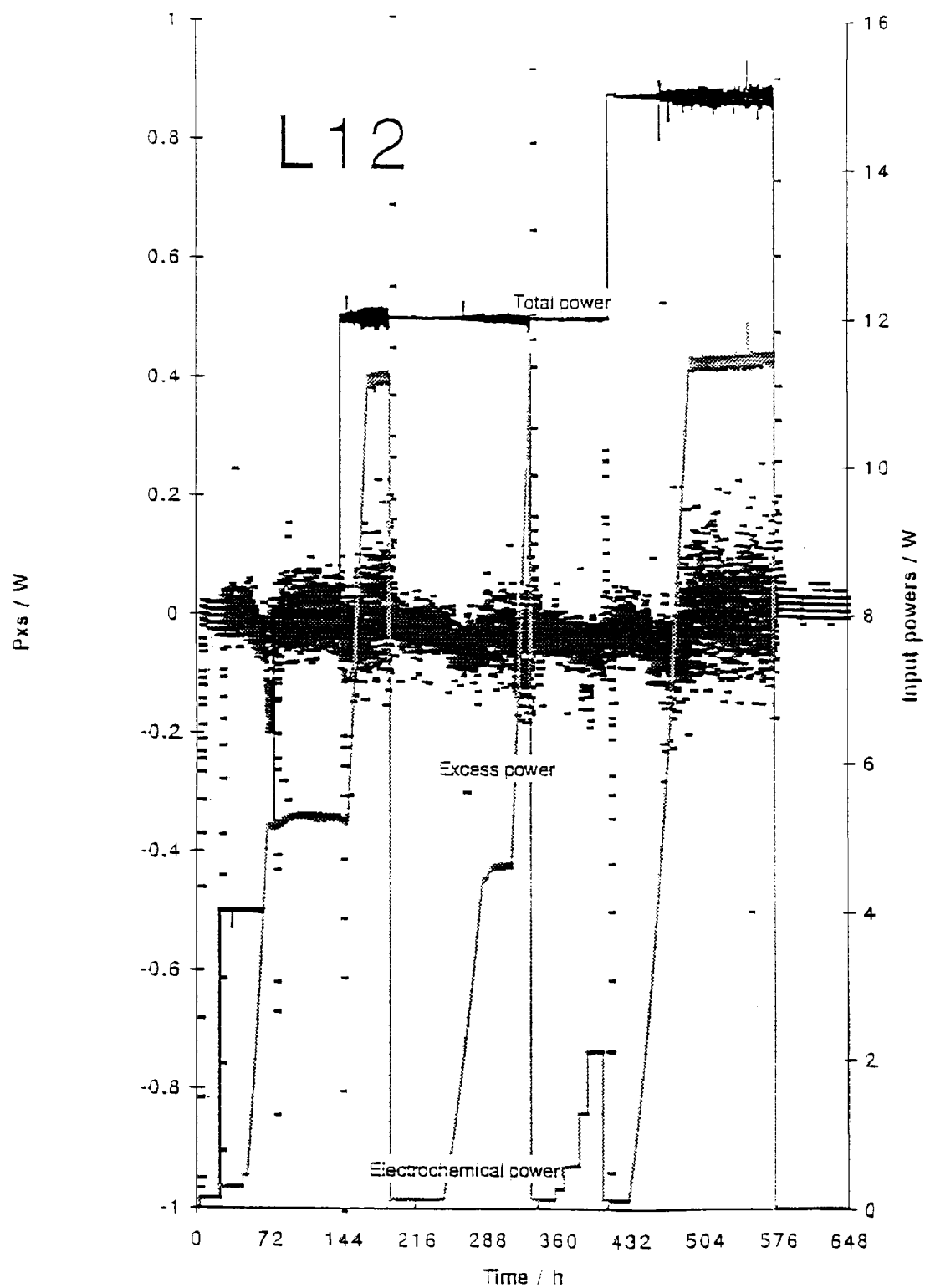
Figure 3-49
Calorimetric data for L12
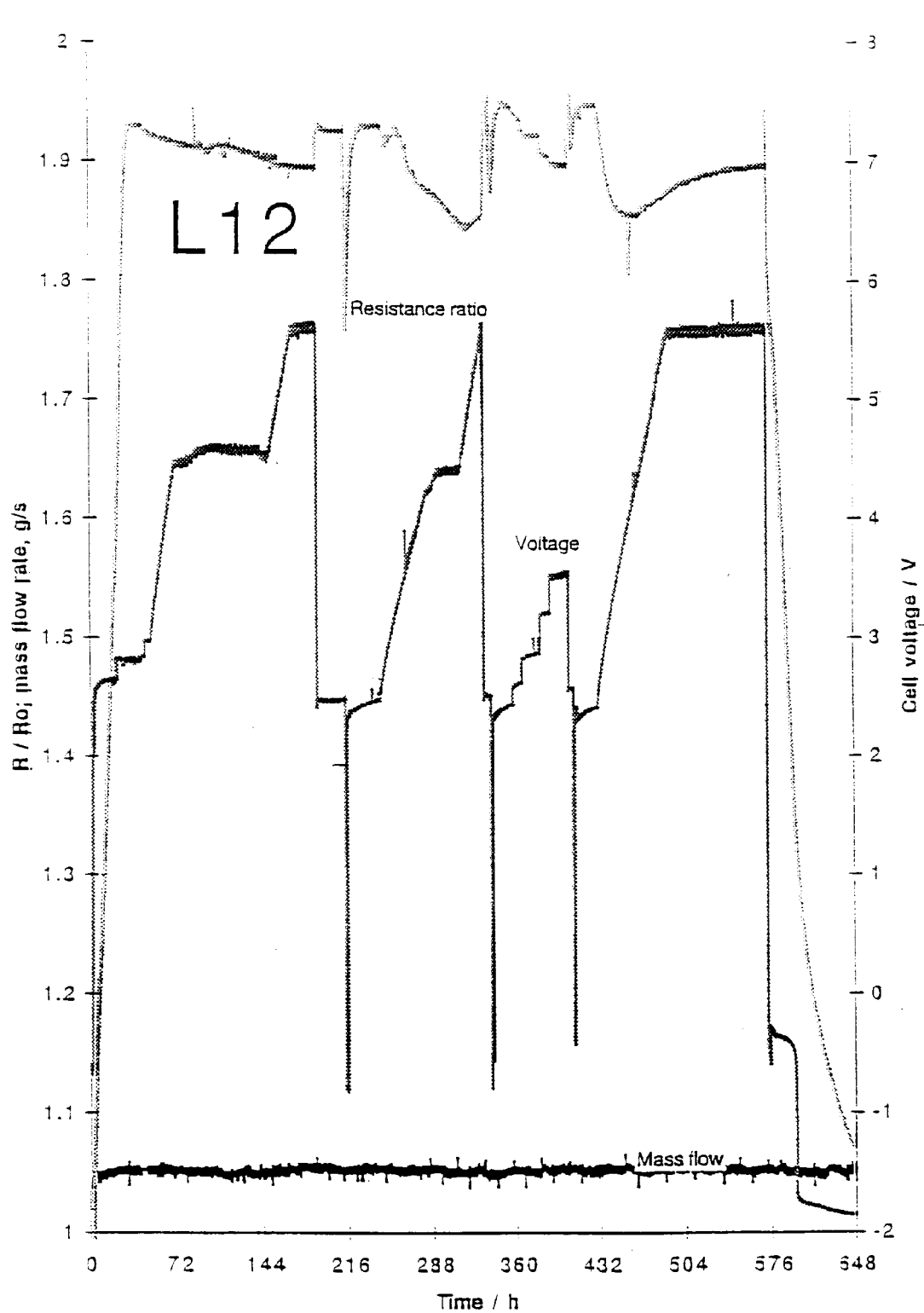
Figure 3-50
Data for L12

A new cell design was utilized in this experiment: The cones and catalyst assembly were removed from the normal cell design and an intact degree-of-loading cell containing the cathode was placed directly in cell. An RTD was placed outside the degree-of-loading cell in 125 ml D$_2$O. The cell was refilled automatically with D$_2$O using an HPLC pump placed outside the experiment cubicle. Data analysis for 720 h beginning 6/6/94, Figures 3-51 and 3-52. Good calorimetry and apparently very good loading were achieved up to about 250 h using a cell current up to 2 A. However, obvious recombination events and, eventually, a rapidly increasing voltage were observed. On inspection, the degree-of-loading refill catheter found to be outside the cell, which was half empty with top of the cathode exposed. The cell was reassembled, and data collection resumed at 375 h. Although reasonable loadings were achieved subsequently, no excess heat was observed.

L14. The cell contents were:

Cathode	Reused Engelhard batch 2, 2.8 mm x 3 cm, annealed, loaded well in degree-of-loading farm (DoL I5) prior to transfer to AS 2 prior to transfer to L14.
Anode	Pt wire.
Electrolyte	140 ml 1 M LiOD/D$_2$O (Aldrich). 200 ppm Al at outset.

Internal sensors one internal RTD + catalyst RTD; cell run closed.

A new cell design was employed for this experiment: One cone was removed from the normal cell design and a degree-of-loading type anode cage was placed in the electrolyte. A quartz liner was incorporated in the lower half of cell. Data analysis for 190 h beginning 6/9/94, Figures 3-53 and 3-54. Good calorimetry was obtained but poor loading was observed, apparently insensitive to current changes. No excess heat was observed.

L15. The cell contents were:

Cathode	Re-reused Engelhard batch 1, 3 mm x 3 cm, loaded well in degree-of-loading farm prior to transfer (DoL K5).
Anode	Pt wire.
Electrolyte	20 ml 1 M LiOD/D$_2$O (Aldrich).

Internal sensors one internal RTD; cell run open.

The cell design was as in L13. Data analysis was carried out for 400 h beginning 7/8/94, Figures 3-55 and 3-56. Severe problems with cell/calorimeter operation were encountered and only a limited portion of the data are shown here. On disassembly, one cathode resistance lead found to be disconnected; there was almost no electrolyte remaining and significant salting-out had occurred in the cell. Obviously, the cell refill protocol was inadequate. No excess heat was observed.
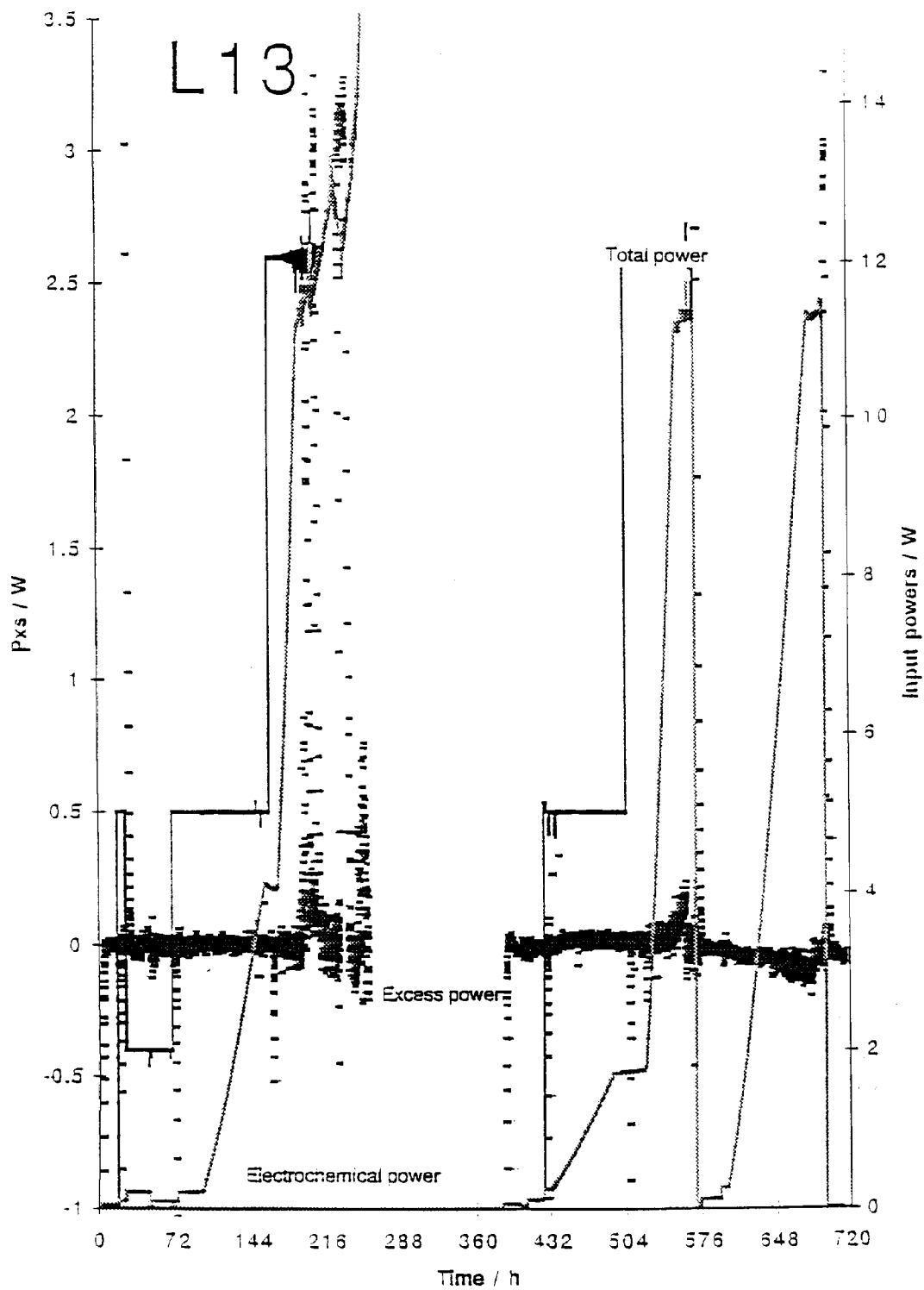
Figure 3-51
Calorimetric data for L13
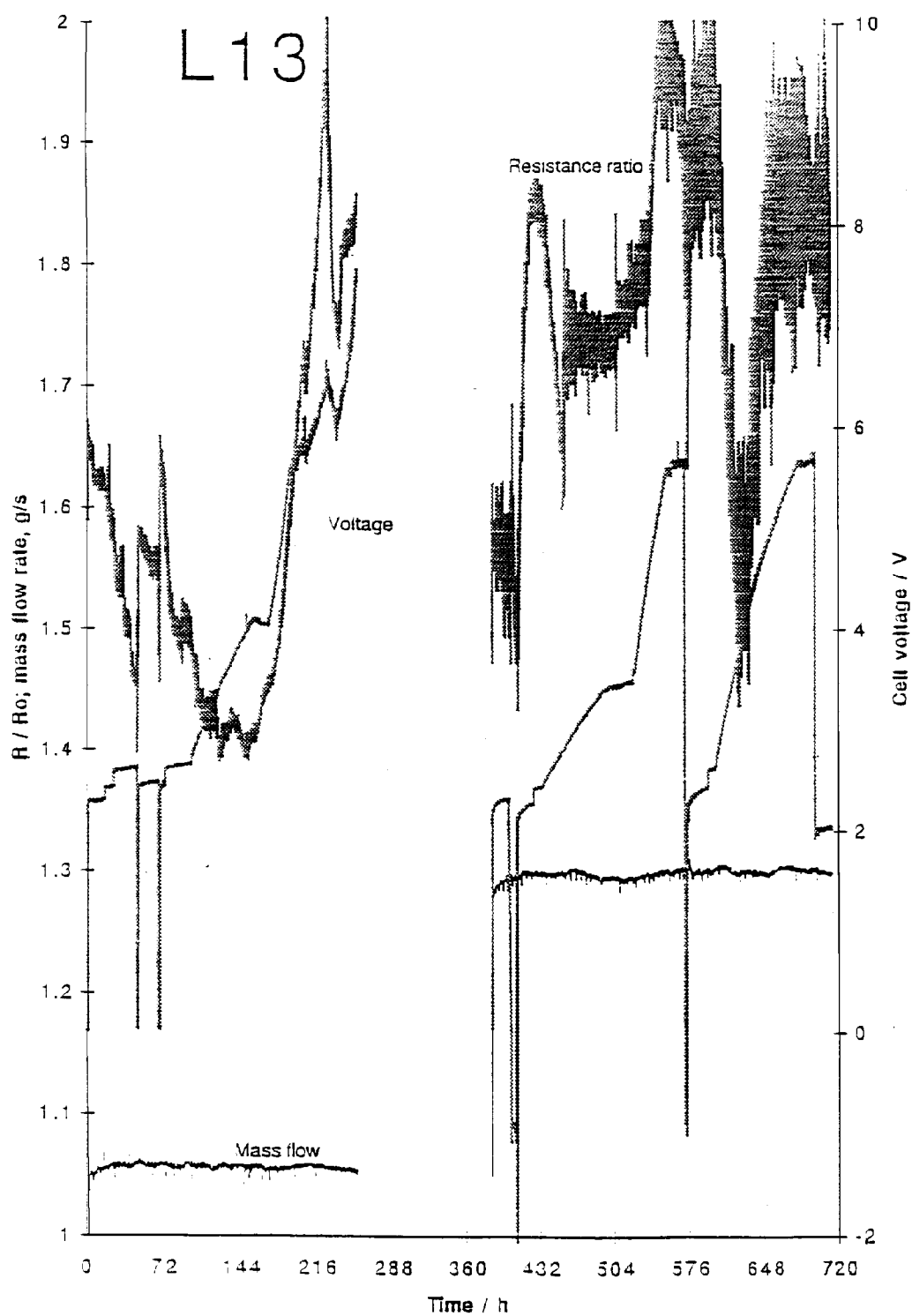
Figure 3-52
Data for L13
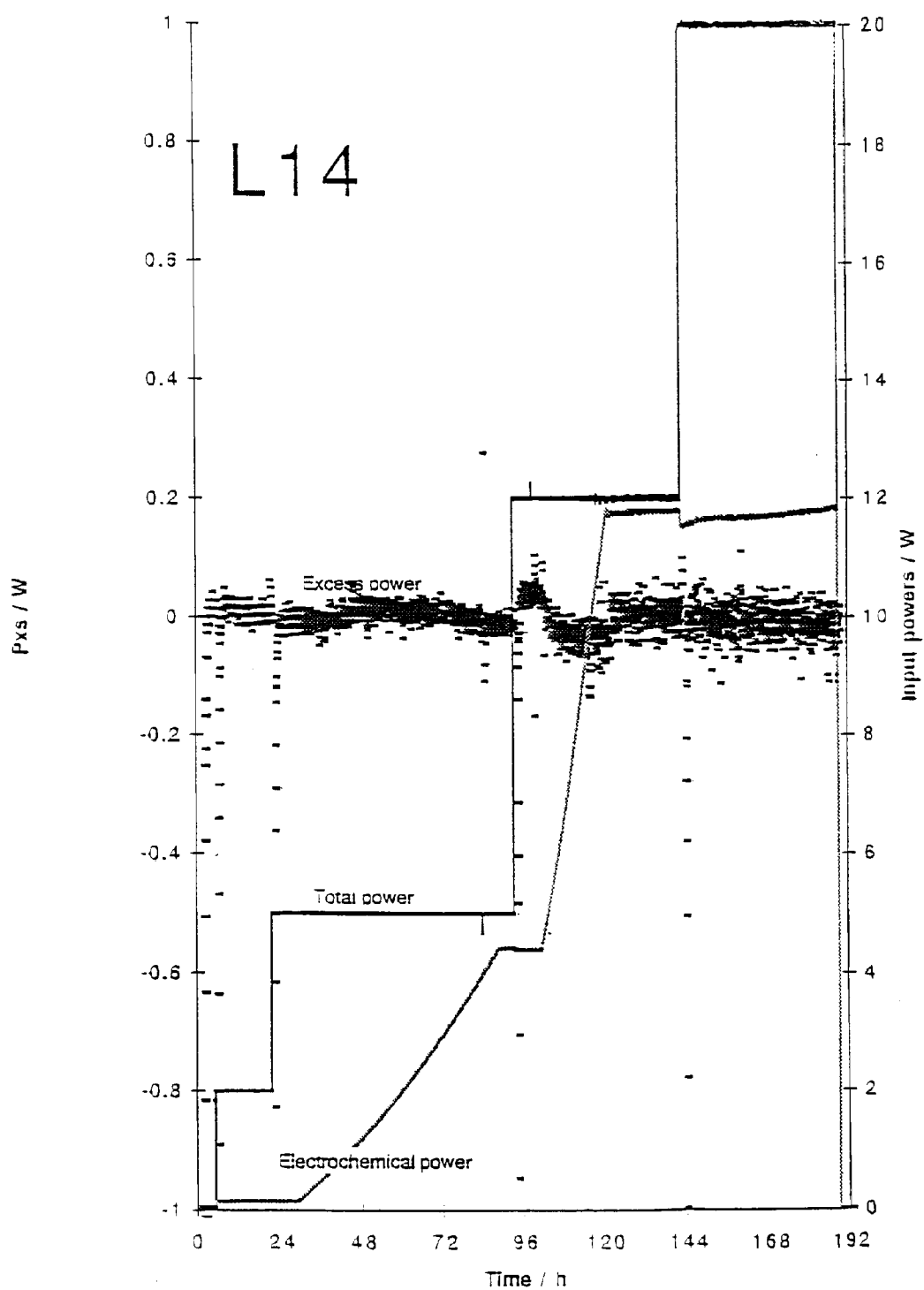
Figure 3-53
Calorimetric data for L14
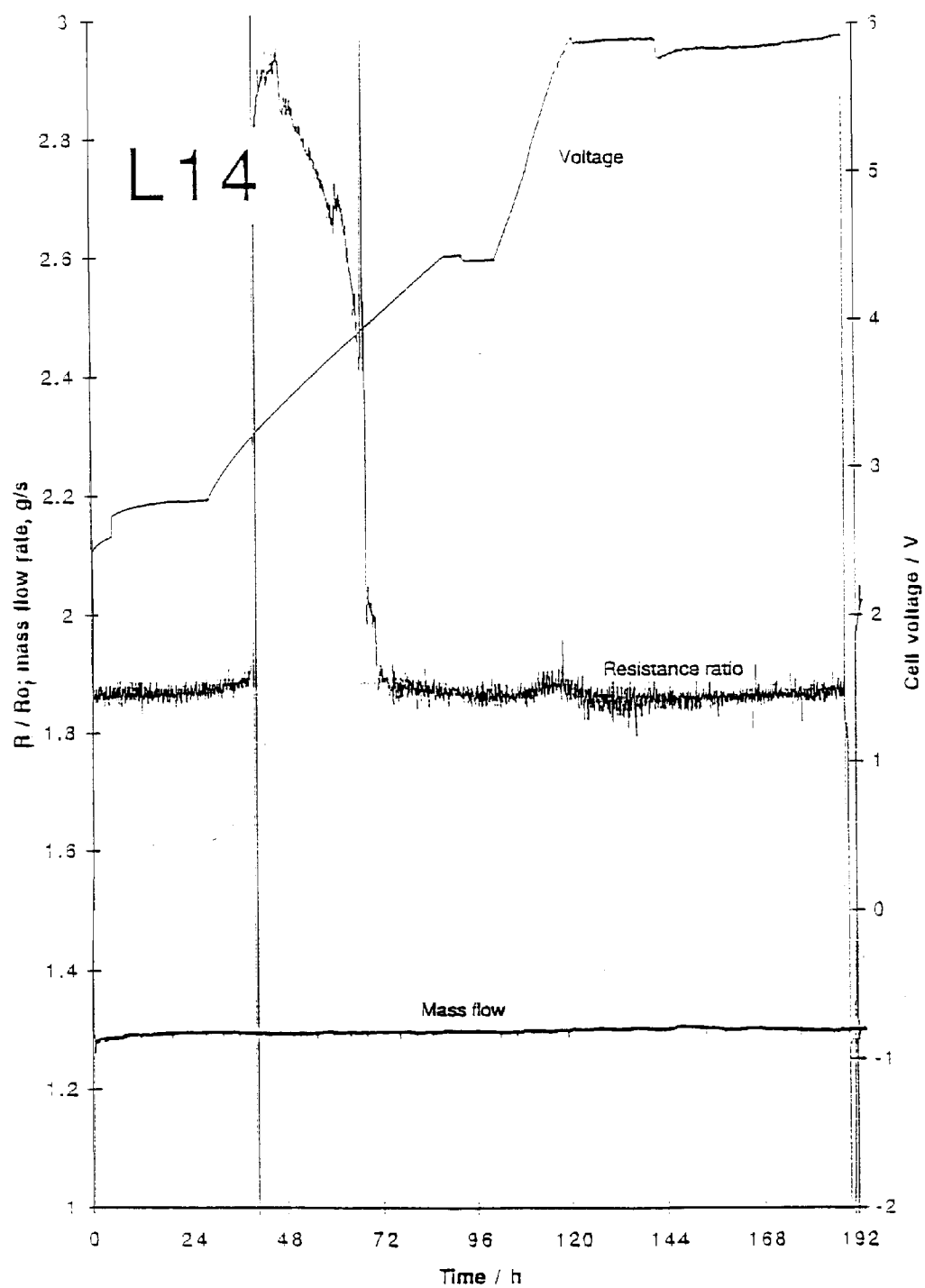
Figure 3-54
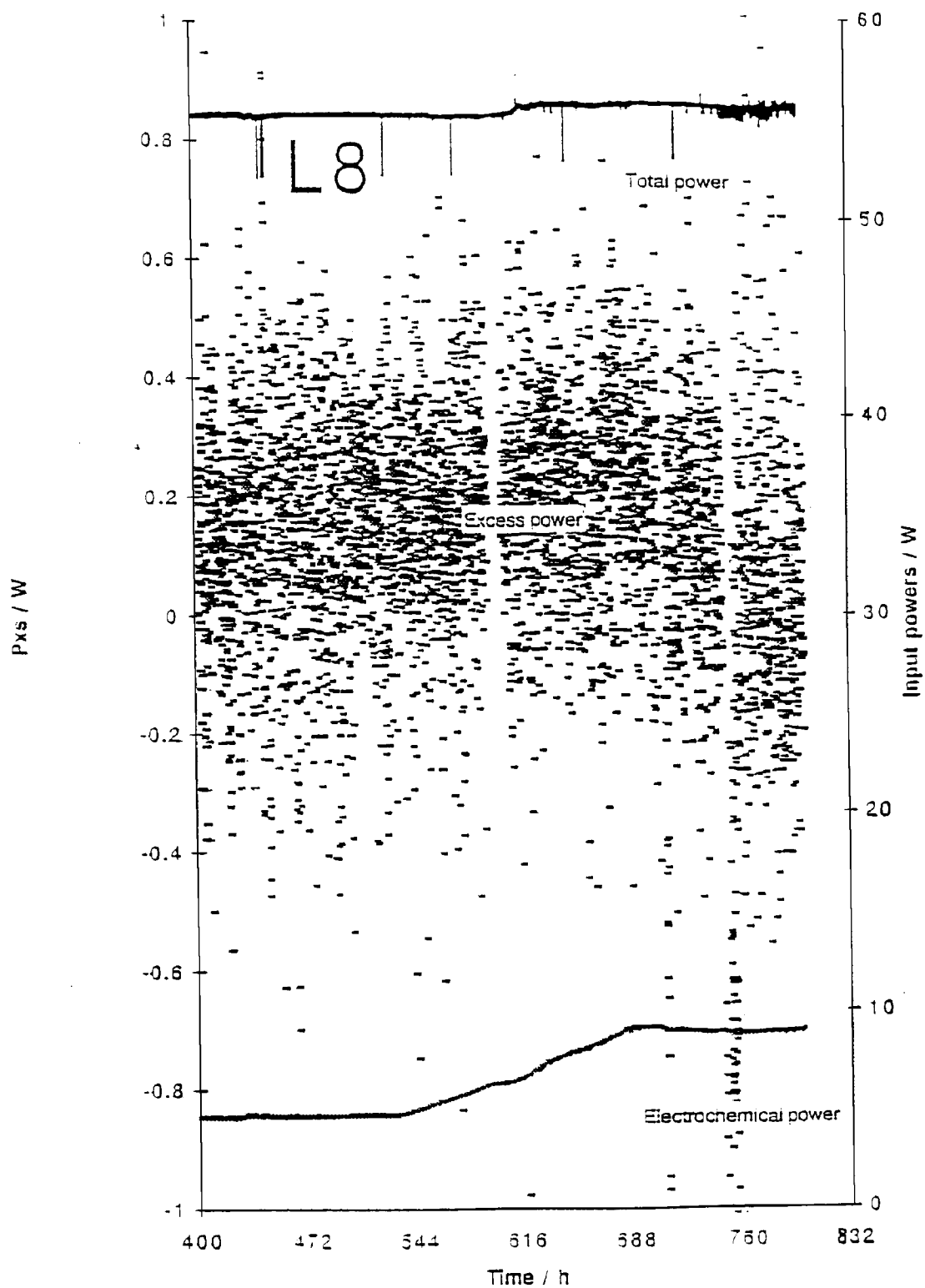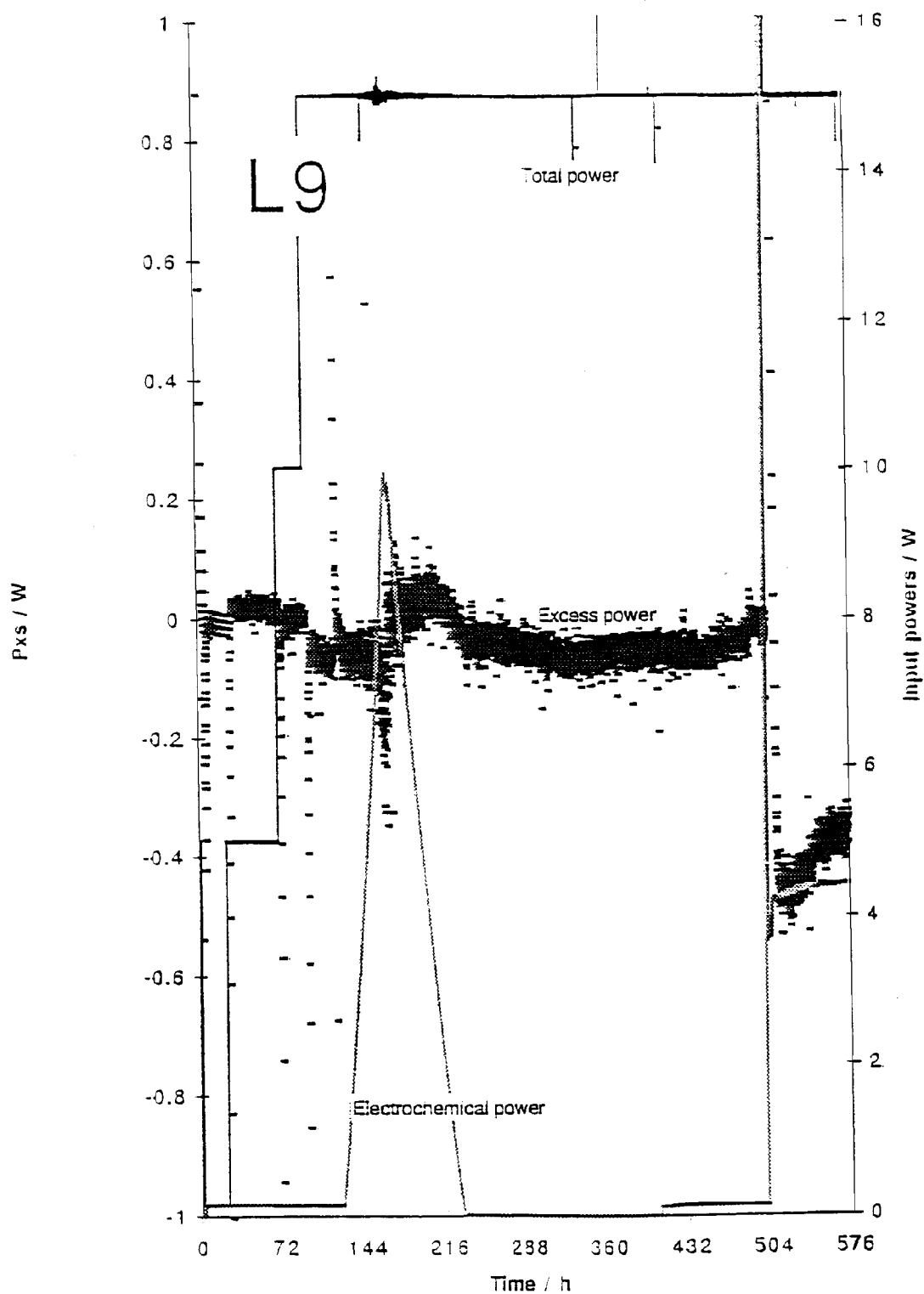**Data for L14**
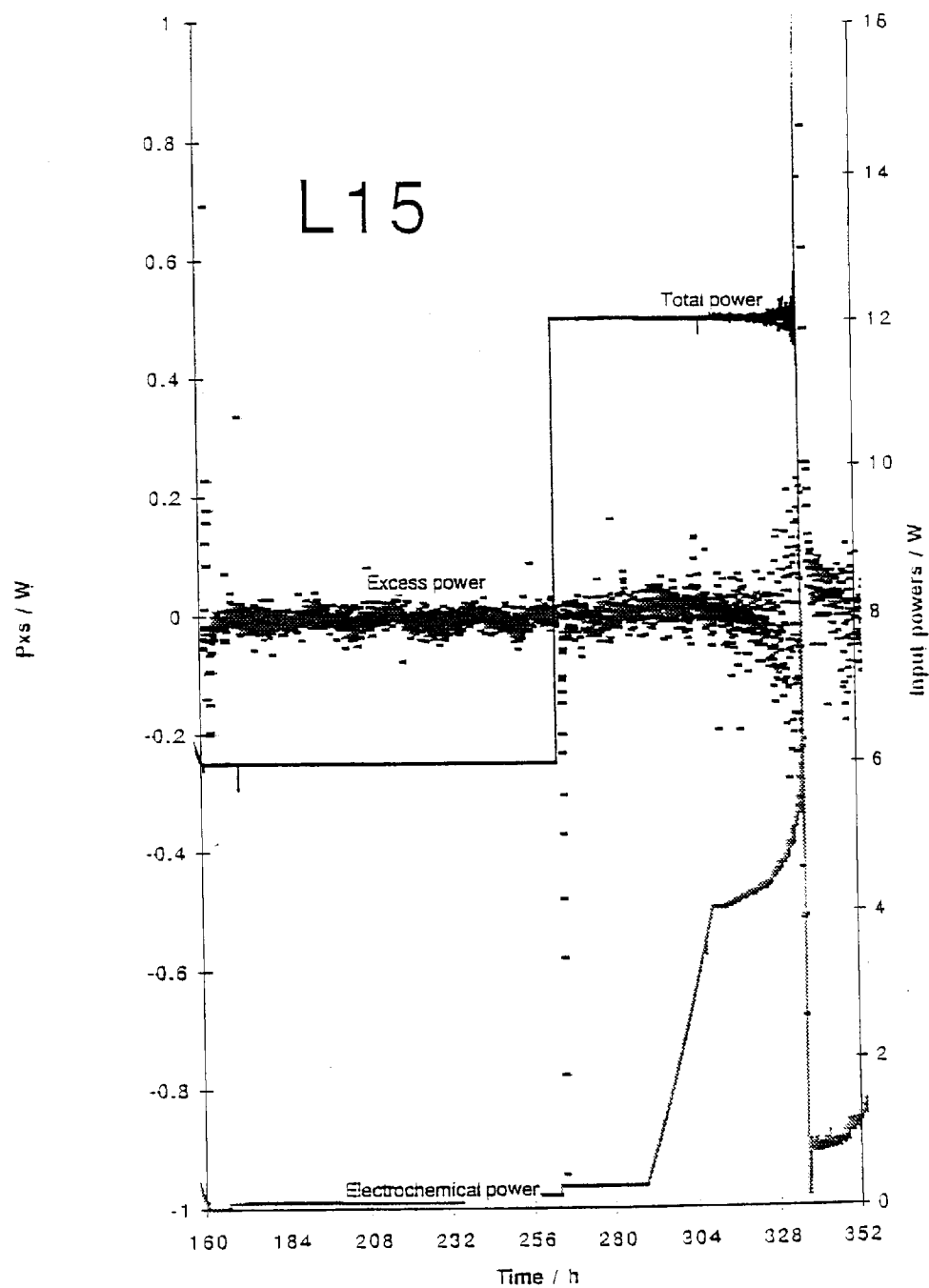
Figure 3-55
Calorimetric data for L15
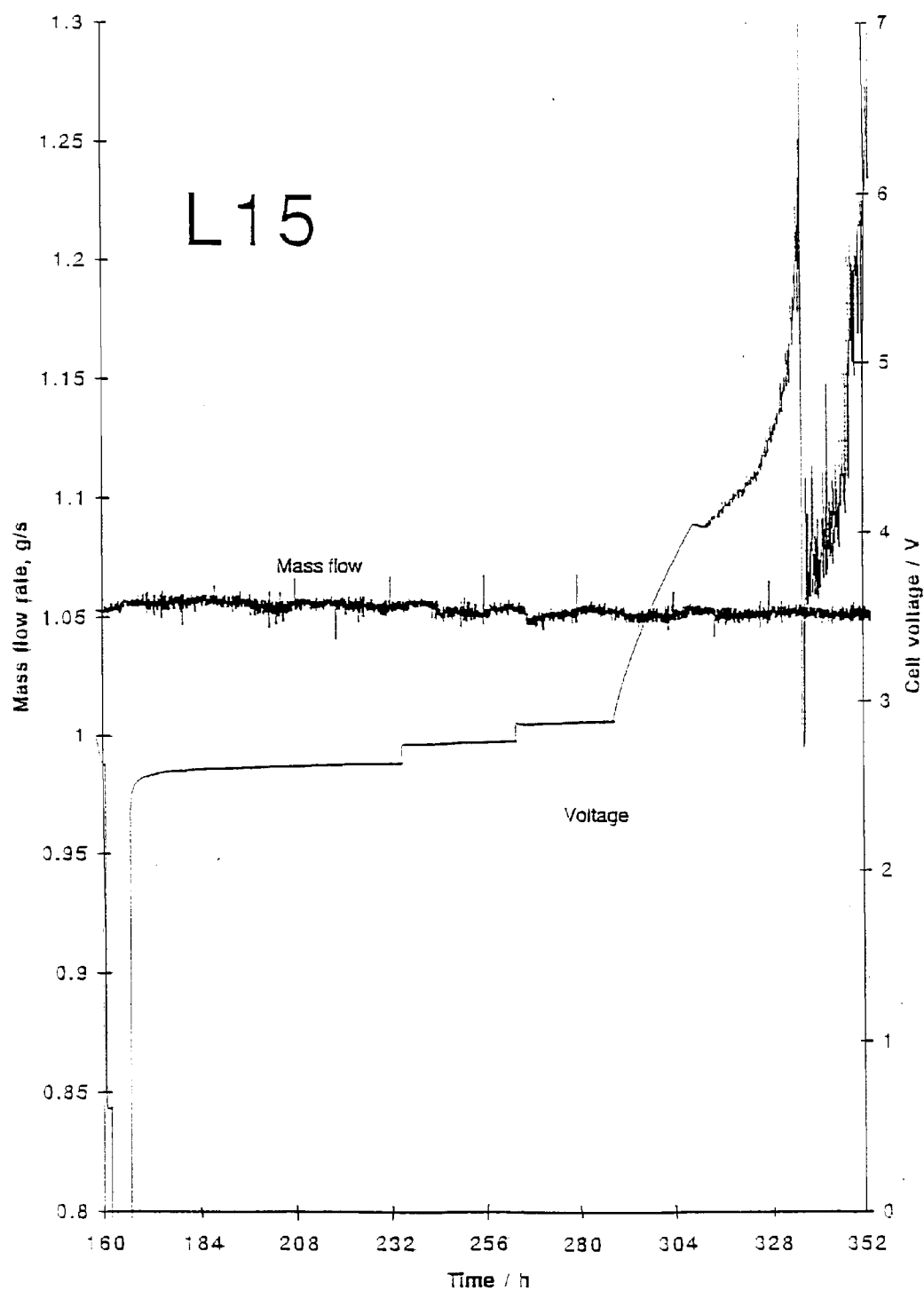
Figure 3-56
Mass flow and voltage data for L15

L16. The cell contents were:

      Cathode   Engelhard batch 4, 3 mm x 3 cm, annealed.

      Anode   Pt wire.

      Electrolyte   20 ml 1 M LiOD/D_2O (Aldrich).

      Internal sensors one internal RTD; cell run closed.

The L15 cell design was used. In this case, the system was run closed with catalyst balls placed in the top of the degree-of-loading cell. Data analysis for 100 h beginning 7/15/94, Figures 3-57 and 3-58. No excess heat was observed in this period. Problems with cell/calorimeter operation were encountered when a current ramp was attempted- no catalyst action was observed. On disassembly, almost all of the degree-of-loading cell was found to be drowned by surrounding D_2O, presumably affecting catalyst operation. No loading measurements were made.

L17. The cell contents were:

      Cathode   Engelhard batch 1, heavily machined to 2 mm x 1.2 cm, annealed.

      Anode   Pt wire.

      Electrolyte   20 ml 1 M LiOD/D_2O (Aldrich "cg") + 200 ppm Al at outset.

      Internal sensors one internal RTD; cell run closed.

The L16 cell design was employed. No loading measurements were made. Data analysis for 600 h beginning 7/29/94, Figures 3-59 and 3-60. Good calorimetry was exhibited (with some interruptions of mass flow measurement) - no excess heat was observed. Some electrolyte transport into outer D_2O reservoir was observed.
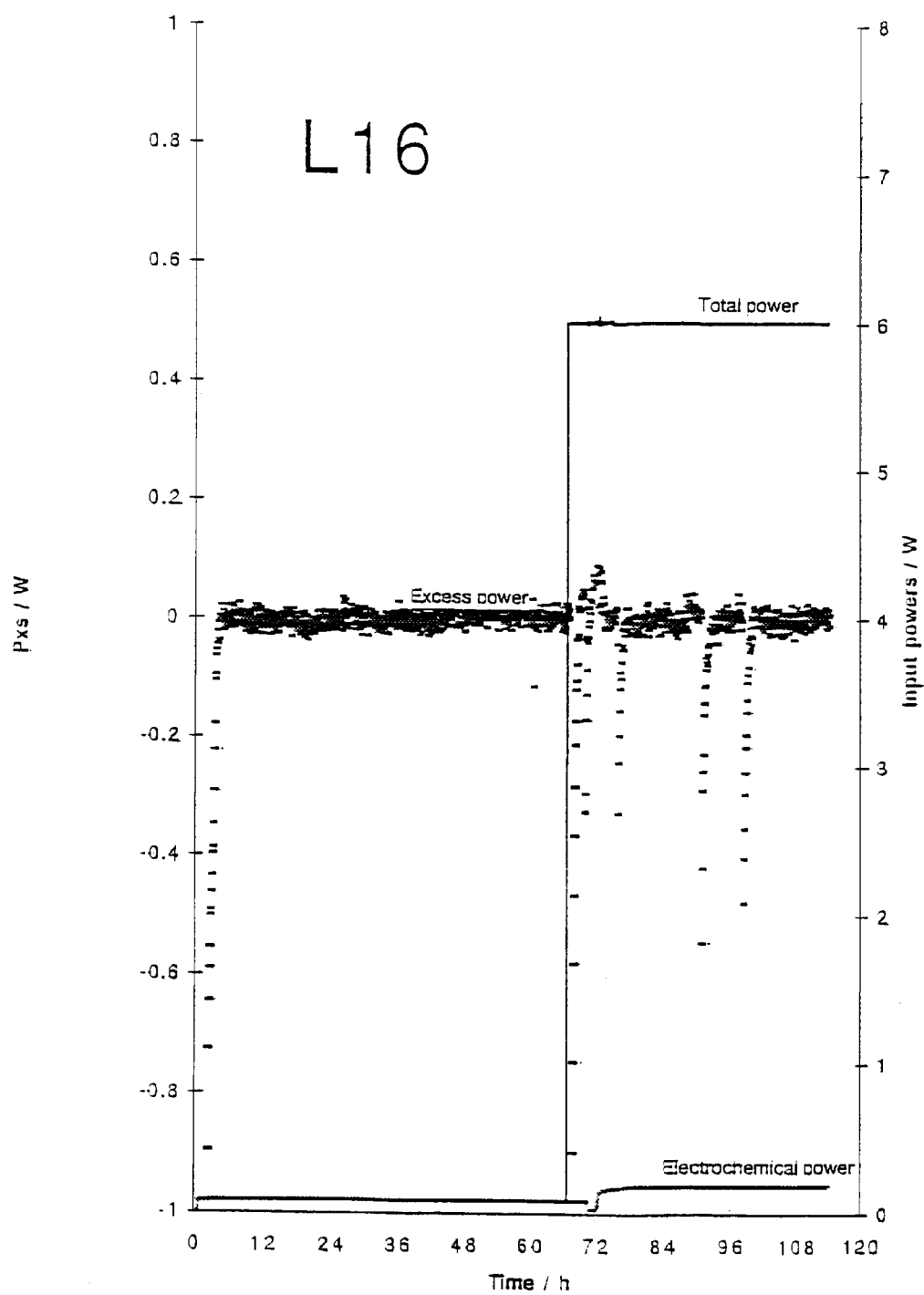
Figure 3-57
Calorimetric data for L16
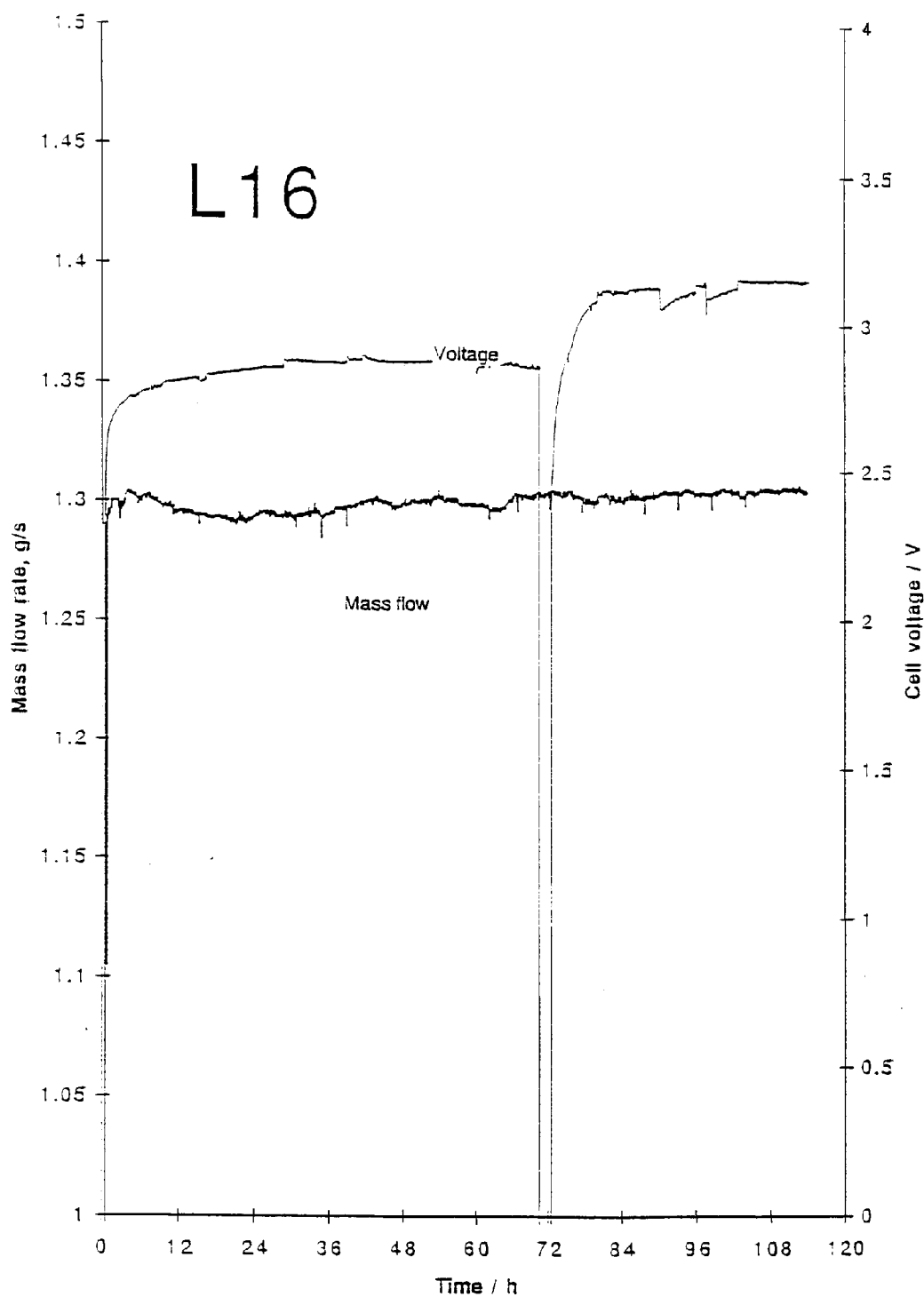
Figure 3-58
Mass flow and voltage data for L16
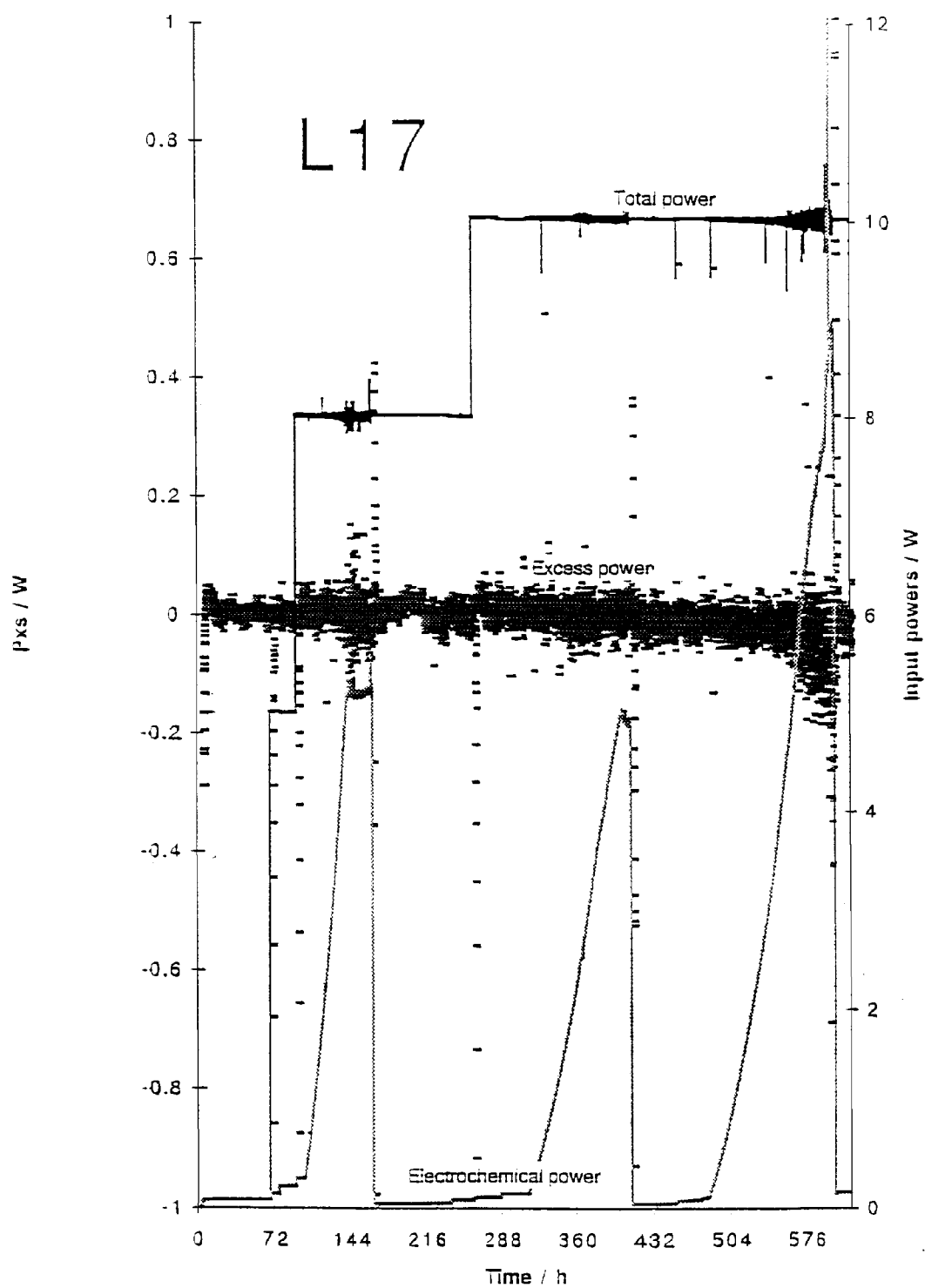
Figure 3-59
Calorimetric data for L17
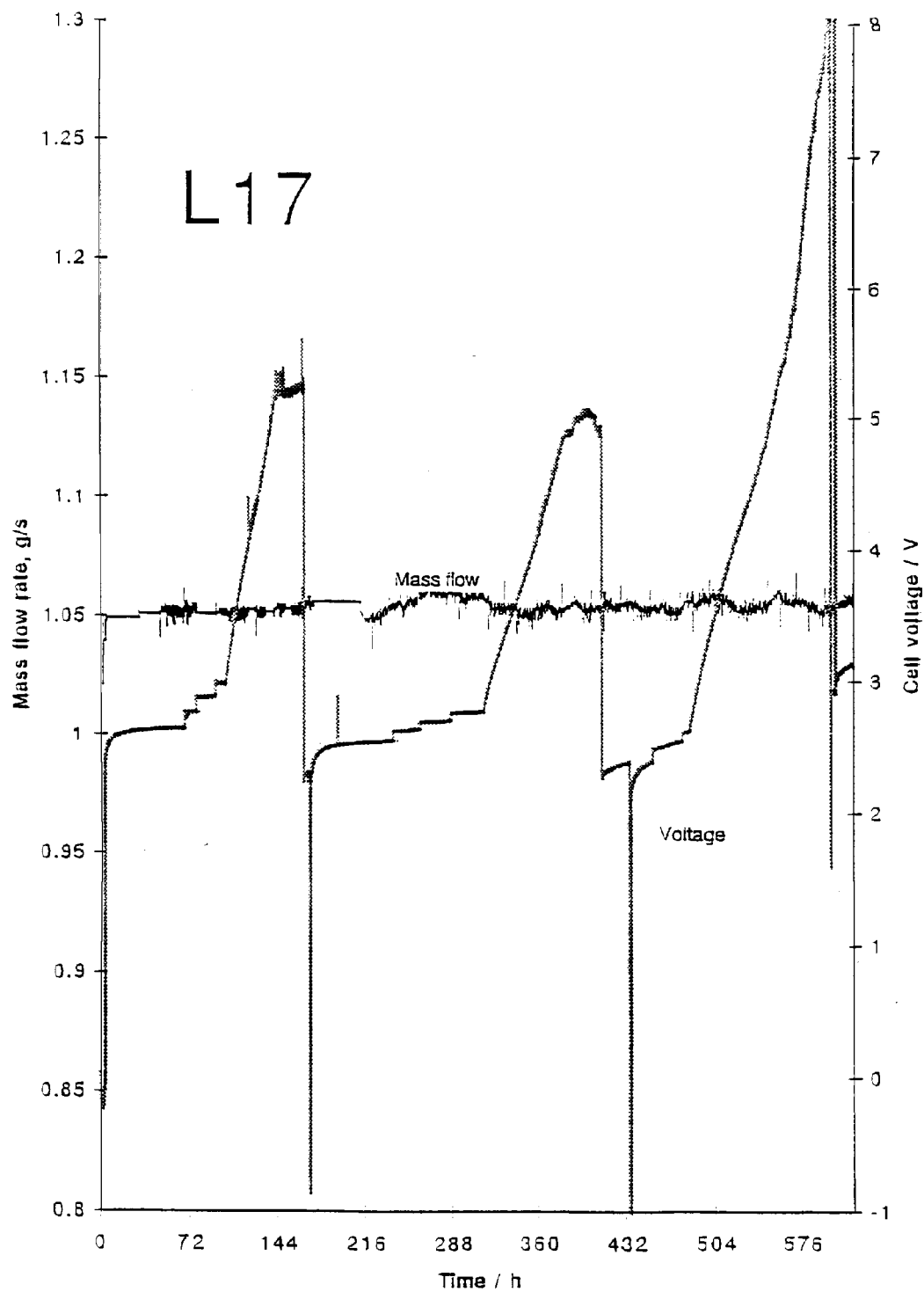
Figure 3-60
Mass flow and voltage data for L17

L18. The cell contents were:

        Cathode   Engelhard batch 1, heavily machined to 2 mm x 1.2 cm, annealed.

        Anode   Pt wire.

        Electrolyte   20 ml 1 M $LiOD/D_2O$ (Aldrich "cg") + 200 ppm Al at outset.

        Internal sensors one internal RTD and one catalyst RTD (in Degree-of-Loading cell head space); cell run closed.

The L16 cell design was employed. No loading measurements were made. Data analysis for 600 h beginning 7/29/94, Figures 3-61 and 3-62. Good calorimetry was exhibited-no excess heat was observed.

L19. The cell contents were:

        Cathode   Johnson-Matthey, 2 mm x 3 cm, annealed, polished, etched.

        Anode   Pt wire.

        Electrolyte   20 ml 1 M $LiOD/D_2O$ - pre-electrolyzed + 200 ppm Al at outset.

        Internal sensors one internal RTD; cell run closed.

The L16 cell design was used. Data analysis for 300 h beginning 8/31/94, Figures 3-63 and 3-64. Poor calorimetry was observed at high current. The calorimeter was difficult to calibrate properly, perhaps due to poor outlet sensor positioning. Very poor loading was achieved and some electrolyte loss was observed. No excess power was observed.

L20. The cell contents were:

        Cathode   Johnson-Matthey, 2 mm x 3 cm, annealed, not polished, etched.

        Anode   Pt wire.

        Electrolyte   20 ml 1 M $LiOD/D_2O$ - pre-electrolyzed + 200 ppm Al at outset.

        Internal sensors one internal RTD; cell run closed.

The L16 cell design was used. Data analysis for 270 h beginning 8/31/94, Figures 3-65 and 66. Good calorimetry was obtained until the first ramp - then catalyst action ceased leading to cell failure. Poor loading was observed and significant electrolyte loss was seen.
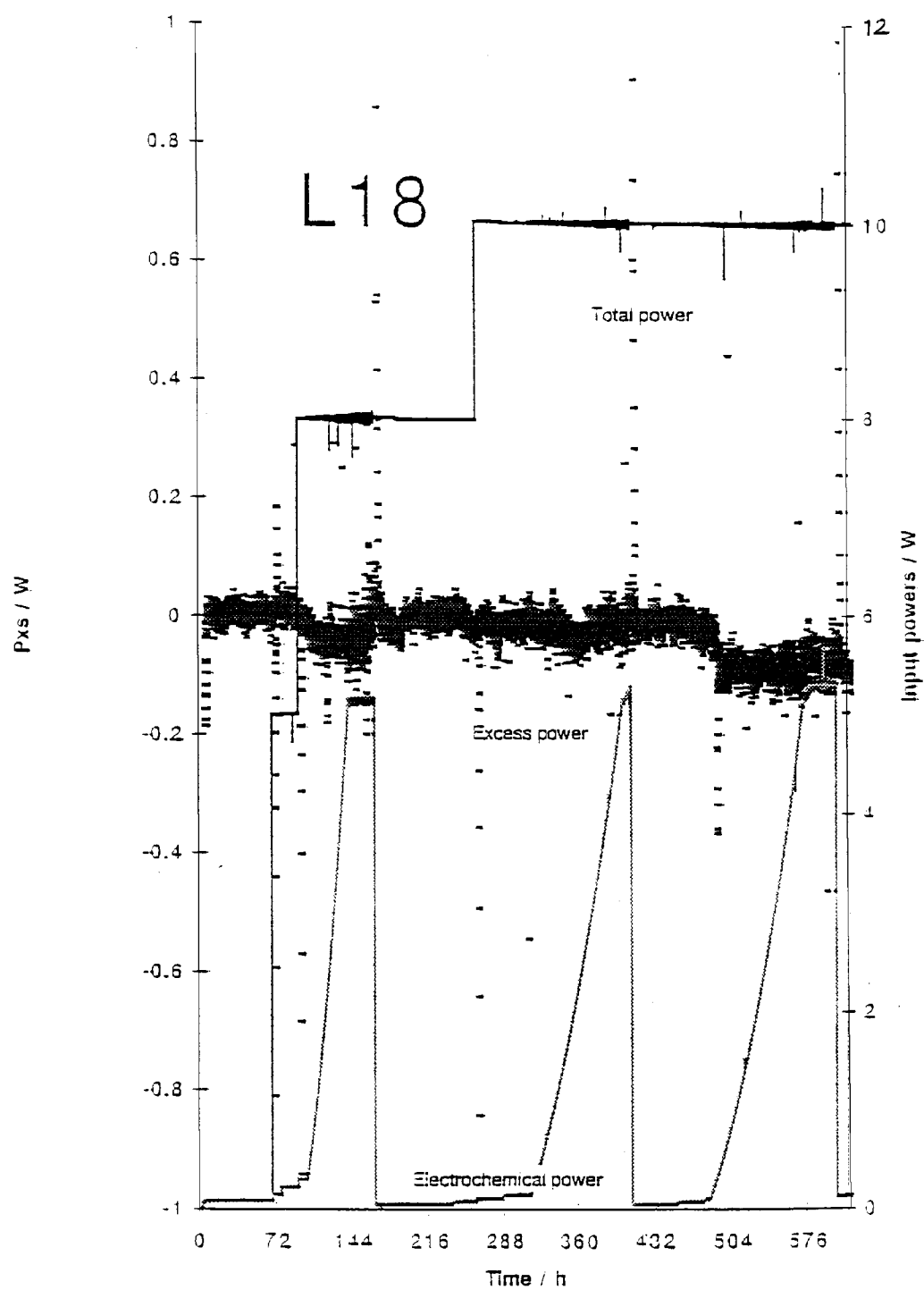
Figure 3-61
Calorimetric data for L18

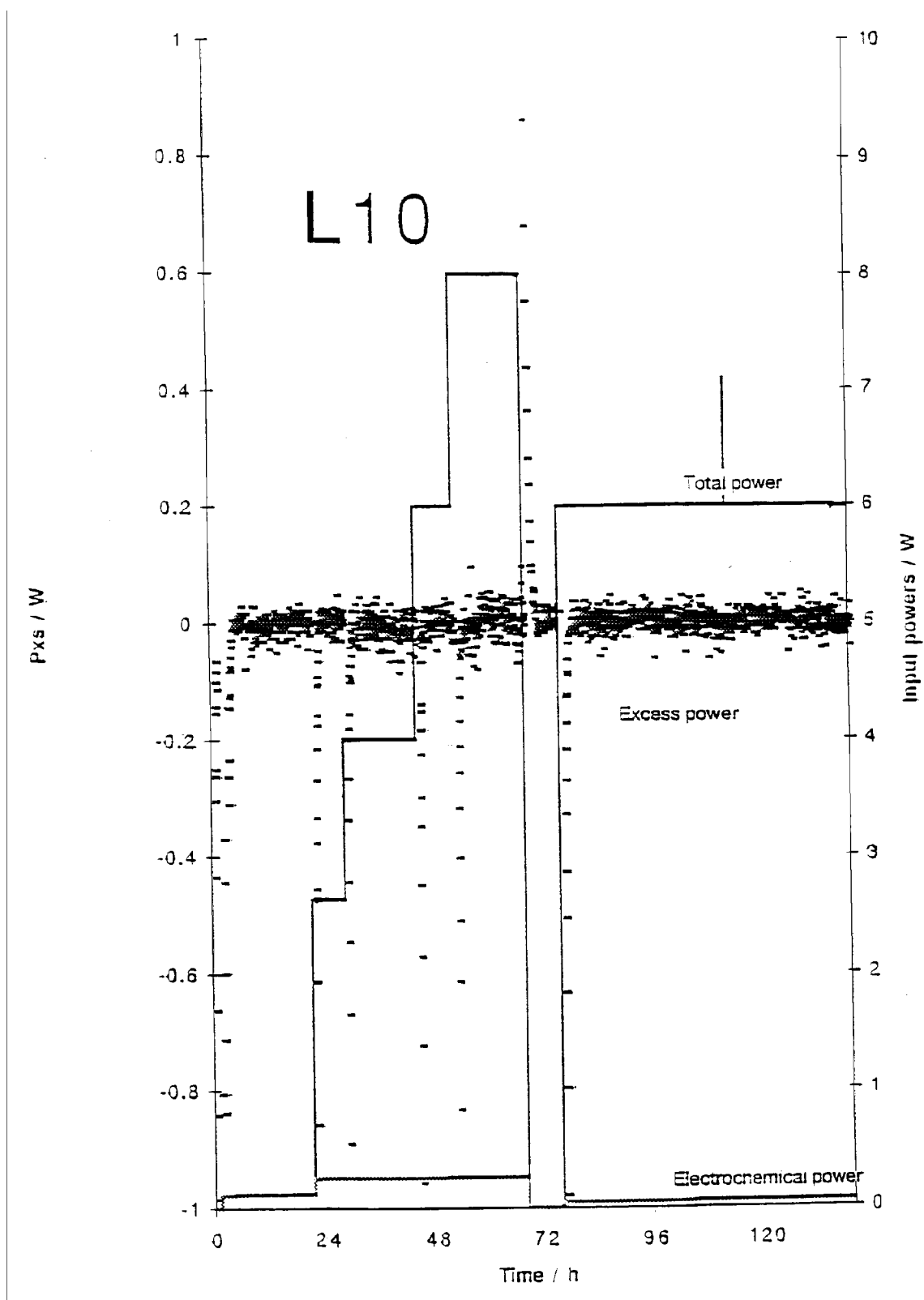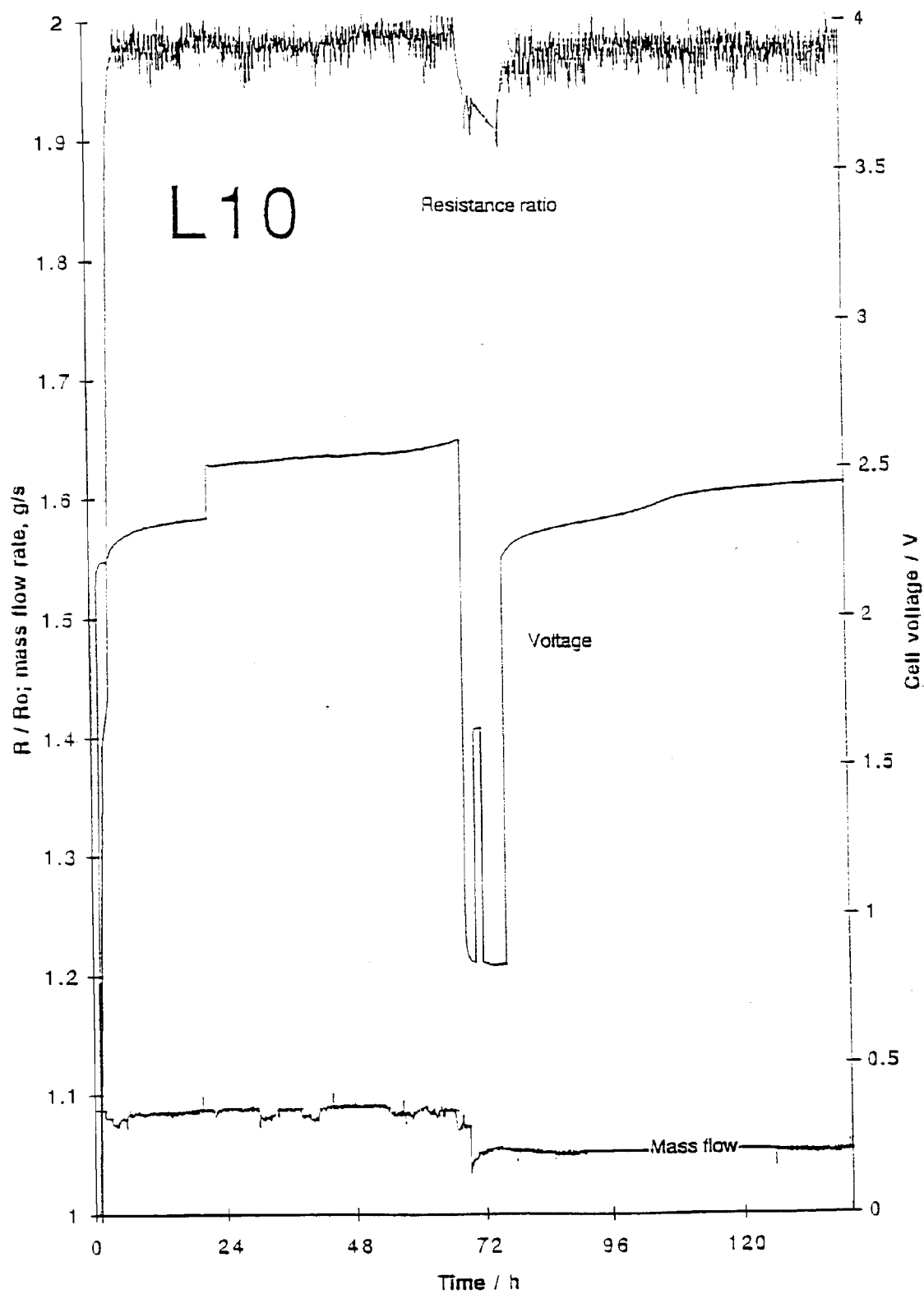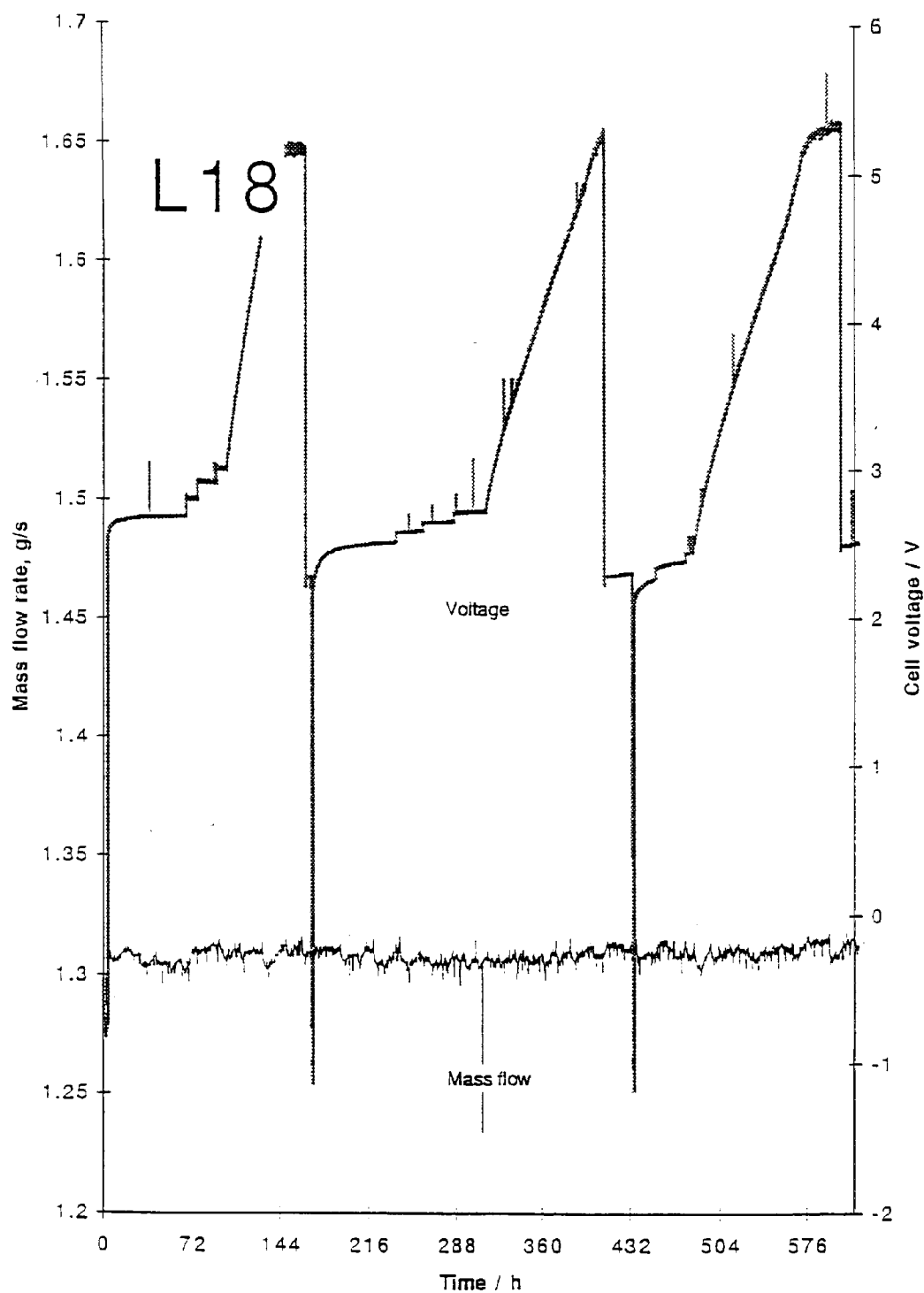**Figure 3-62**
Mass flow and voltage data for L18
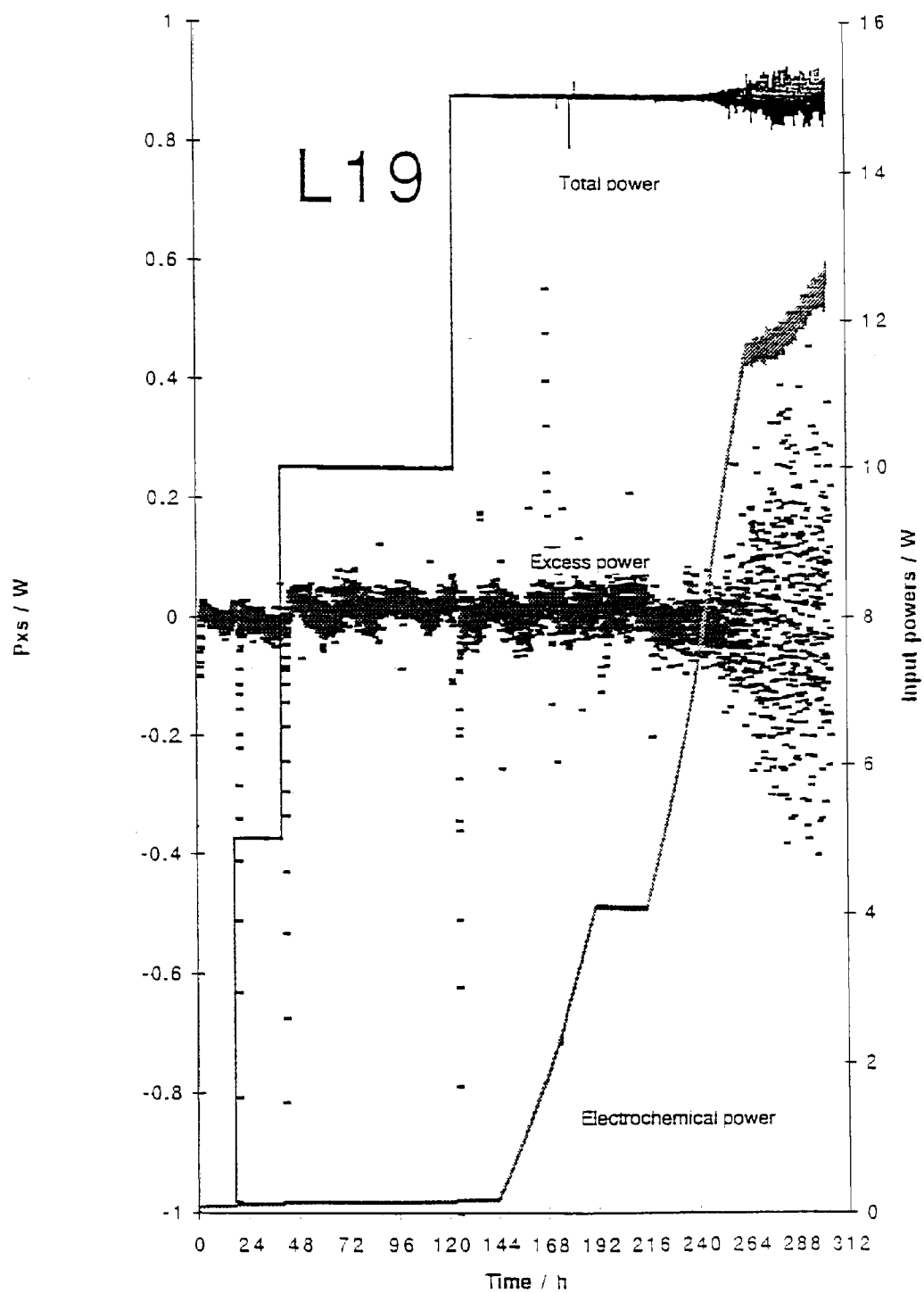
Figure 3-63
Calorimetric data for L19
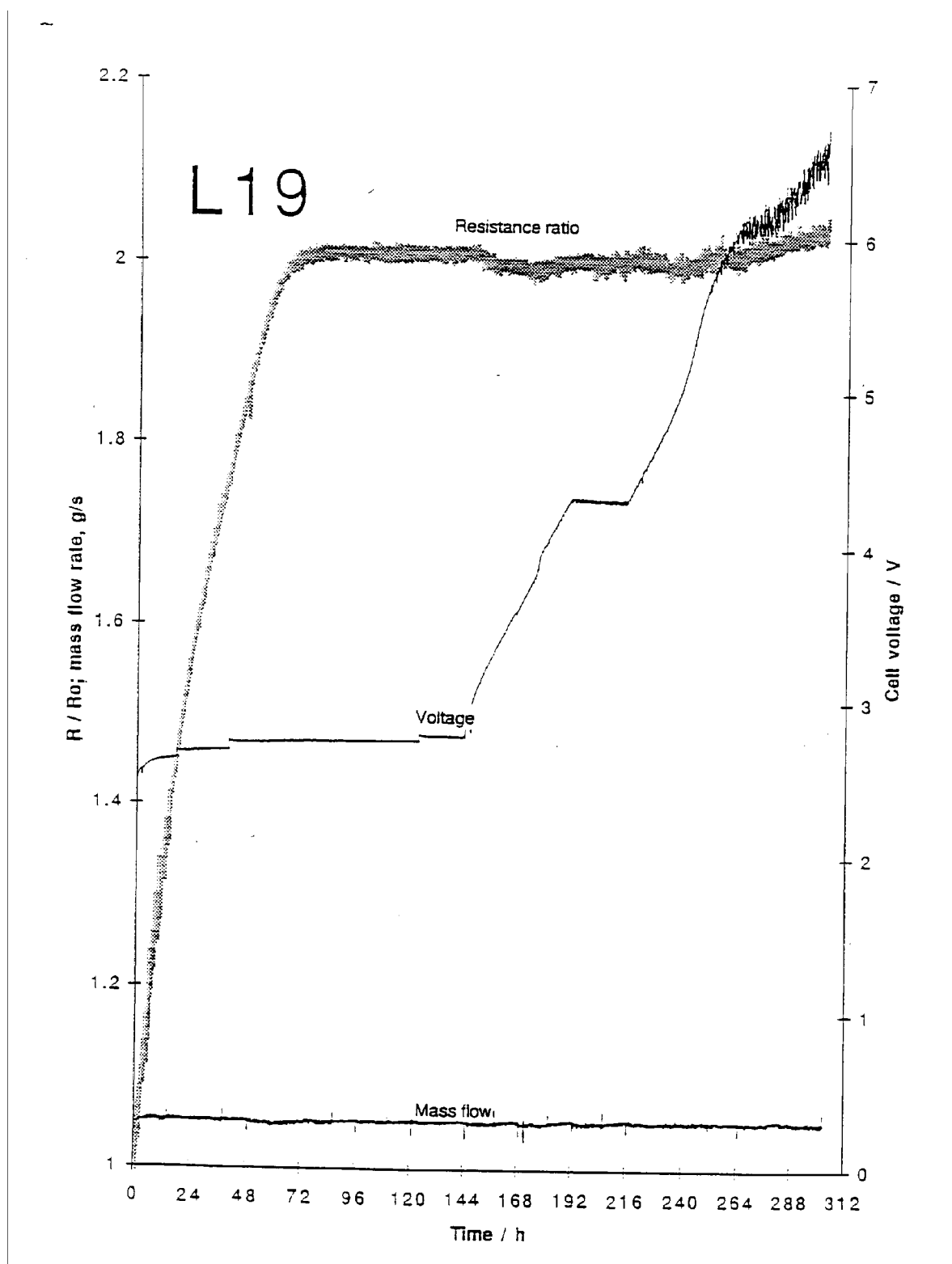
Figure 3-64
Data for L19
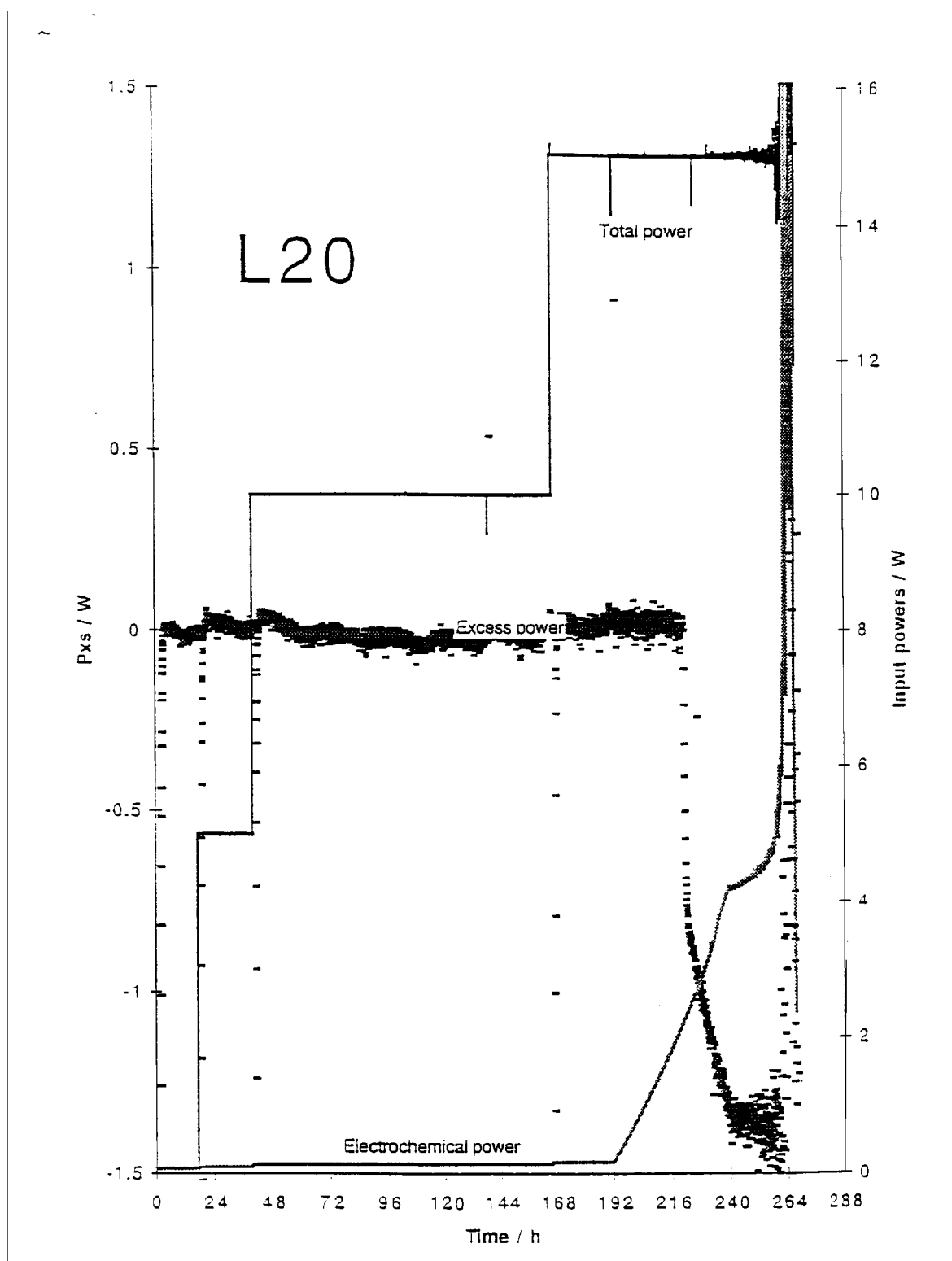
Figure 3-65
Calorimetric data for L20
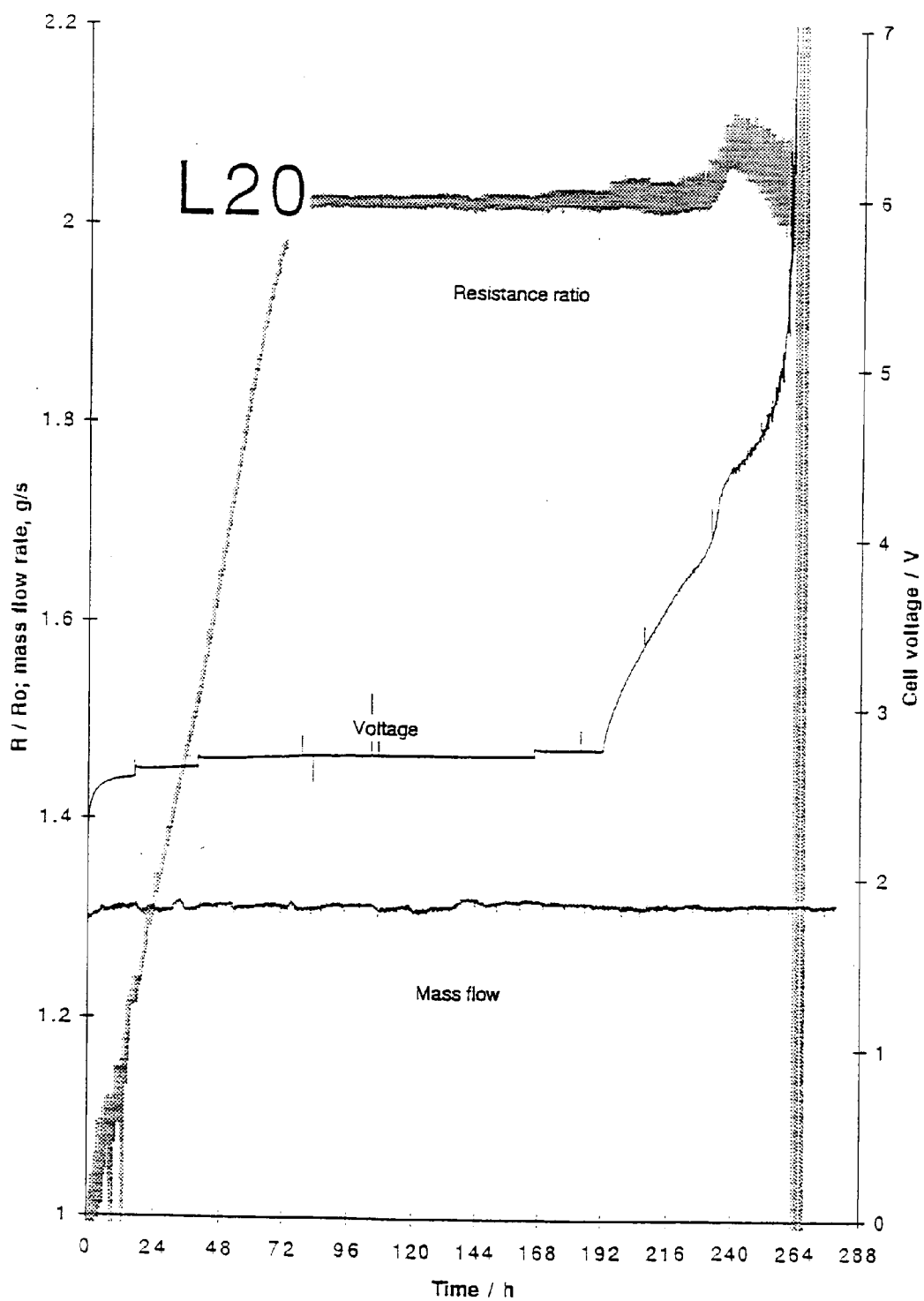
Figure 3-66
Data for L20

M-Series Experiments

System Description. The M-series calorimeters were designed as modified
L-calorimeters to incorporate two new features: a rigorous ^{4}He leak-tight enclosure and
manifold, and greater efficiency of heat recovery from water vapor within the
calorimeter boundary. These calorimeters therefore allowed a greater facility in two
classes of experiments:

a. the search for gaseous products, notably ^{3}He and ^{4}He observed by others to be
   associated quantitatively or semi-quantitatively with excess heat production

b. initiation or stimulation of excess heat or temperature effects, by rapidly stepping or
   pulsing the cell temperature, while maintaining calorimetric monitoring

The cell, water bath, hydraulic system, control and monitoring electronics were all
identical to those systems for the L-series calorimeters except that a Keithley
model 2001 7-1/2 digital multimeter was employed instead of a model Keithley
195A 6-1/2 digit DMM.

Experiment Overview. Table 3-1 provides an overview of the four experiments
performed in the M1 cell/calorimeter body.

Table 3-1
Overview of Experiments M1-M4

Expt #	Cathode (source) (dimension)	Date (start) (stop)	Duration (hours) (days)	Maximum (D/Pd)	Excess Power (mW)	(kJ)
M1	JM* (0.2x3 cm)	3/4/94 5/3/94	1340 (56)	0.927 ± 0.001	180 ± 20	50 ± 25
M2	E#1 (0.3x3 cm)	5/6/94 6/21/94	1104 (46)	0.868 ± 0.001	0 ± 50	0 ± ?
M3	E#4 (0.3x3 cm)	6/24/94 7/5/94	269 (11)	?	0 ± 50	0 ± ?
M4	JM* (0.1x10cm)	7/19/94 9/26/94	1840 (77)	0.944 ± 0.001	400 ± 25	85 ± 25

All experiments were operated thermodynamically closed after initial loading in excess D_2. In all cases the electrolyte was 1.0M LiOD prepared by dissolving 1.75 g Li metal in 250 ml D_2O. In addition, cells M1 and M4 were started with electrolyte containing 200 ppm Al obtained by dissolving 50 mg Al metal in the 250 ml prepared basic electrolyte.

For the cathode metal source, JM* designates a palladium lot specially ordered from Johnson Matthey, specified to contain a low concentration of platinum group metals (PGM's) and light elements (specifically B, C and O). The cathode source designated E indicates various lots obtained from Engelhard.

All cells contained a large area (~ 50 cm²) helical wire Pt anode formed from a 1m length of 25 mm dia. Engelhard C Pt thermocouple wire STD grade platinum. This is made from 15 turns on a 21 mm diameter quartz rod cage.

Experiment M1

Cathode:	JM* wire 0.2cm dia., 3.0 cm long, mass 1.12232 g
Anneal:	4 hours at 850°C in oxygen gettered vacuum
Contacts:	Five wire, I contacts spot-welded to ends V contacts 0.25 mm Pt wires mechanically wrapped in grooves and spot-welded
Anode:	1 m, 0.25 mm dia. Pt wire helix
Electrolyte:	140 ml, 1.0 M LiOD with 200 ppm Al by weight
Monitors:	2 TLD's in quartz tubes outside anode 2 Kodak Dental X-ray films outside PTFE liner
Cell sensors:	Gas Pressure Electrolyte temperature Recombiner gas temperature

Calibration. The cell was placed in the calorimeter, the calorimeter in the water bath, and data collection started ~ 51 hours before the application of cell current. This period was used to allow the calorimetric and cell temperature sensors to achieve thermal equilibrium with the water bath, and thus establish the R^o values of the platinum resistance temperature devices (RTD's) used for temperature sensing.

Figure 3-67 shows the initial calibration of M1. The electrolyte was added and a cathodic current of 74 mA was applied initially at 3/2/94 11:12. The cell was subjected to an inadvertent current step to 3A at 10h, resulting in ~ 27W of electrochemical power for ~ 12 hours. At 48h a sequence of five, 5W heater steps were applied, each of 12h duration. These seven power levels (two electrochemical and five largely heater) were used to establish values for the conductive loss terms (k') for each of the independent pairs of calorimetric temperature sensors, and the calorimeter time constant. At a calorimetric mass flow of 0.945 ± 0.001 g s^{-1}, the conductive loss was calculated to be k' = $1.0 \pm 0.1\%$, and the time constant $\tau = 930 \pm 30$s (15.5 minutes).

Initial load. During the inadvertent period at 3A, the cathode resistance ratio increased to a maximum, $R/R^{\circ}_{max} = 1.965$, and then decreased (on the right side of the maximum) to $R/R^{\circ} = 1.868$ corresponding to a loading D/Pd = 0.86. Between 120 and 214 h the cathode was loaded by stepping the current to successively higher values.
Table 3-2 summarizes the results of this stepped loading.

Figure 3-68 plots the steady state loading from Table 3-2 versus current density, and shows the expected roughly logarithmic dependence of loading on current density.

Ramp One. At 222h a current ramp was started from 1.2 to 2.2 A at 20 mA/hour. During this ramp the cathode achieved a maximum loading of D/Pd = 0.927, (as shown in Figure 3-69a), and a small amount of excess heat was observed. This response is shown plotted in Figure 3-69a. The maximum excess power observed during ramp 1 was 100 ± 40 mW or ~ 0.6% of the total input power. The integrated energy was 27 ± 12 kJ before the cell current was reduced. The excess power plotted in Figure 3-69b shows considerable variability, as does the loading in Figure 3-69b.
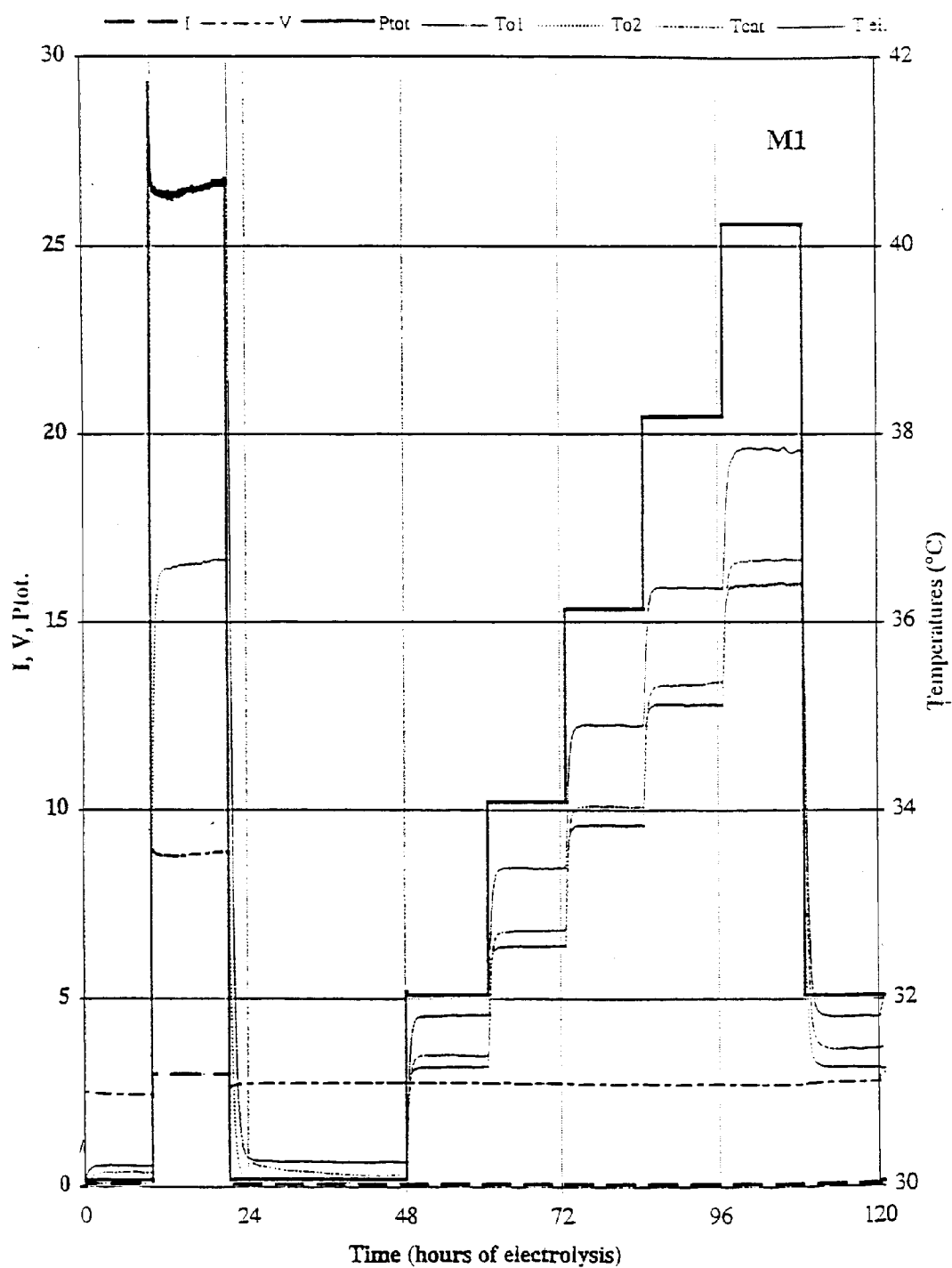
Figure 3-67
M1 Current, Voltage and total power 0-120 hours
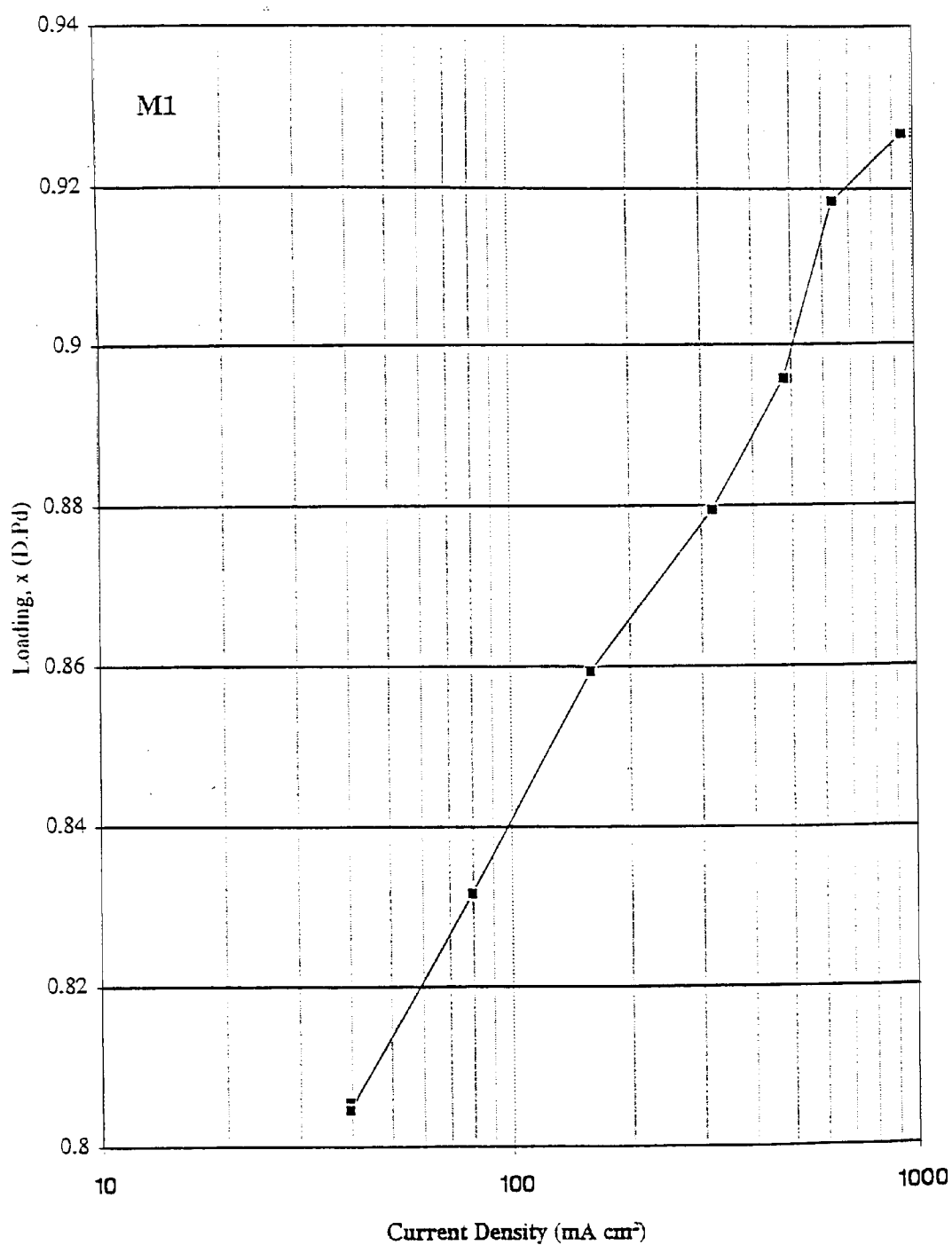
Figure 3-68
Loading of M1 cathode
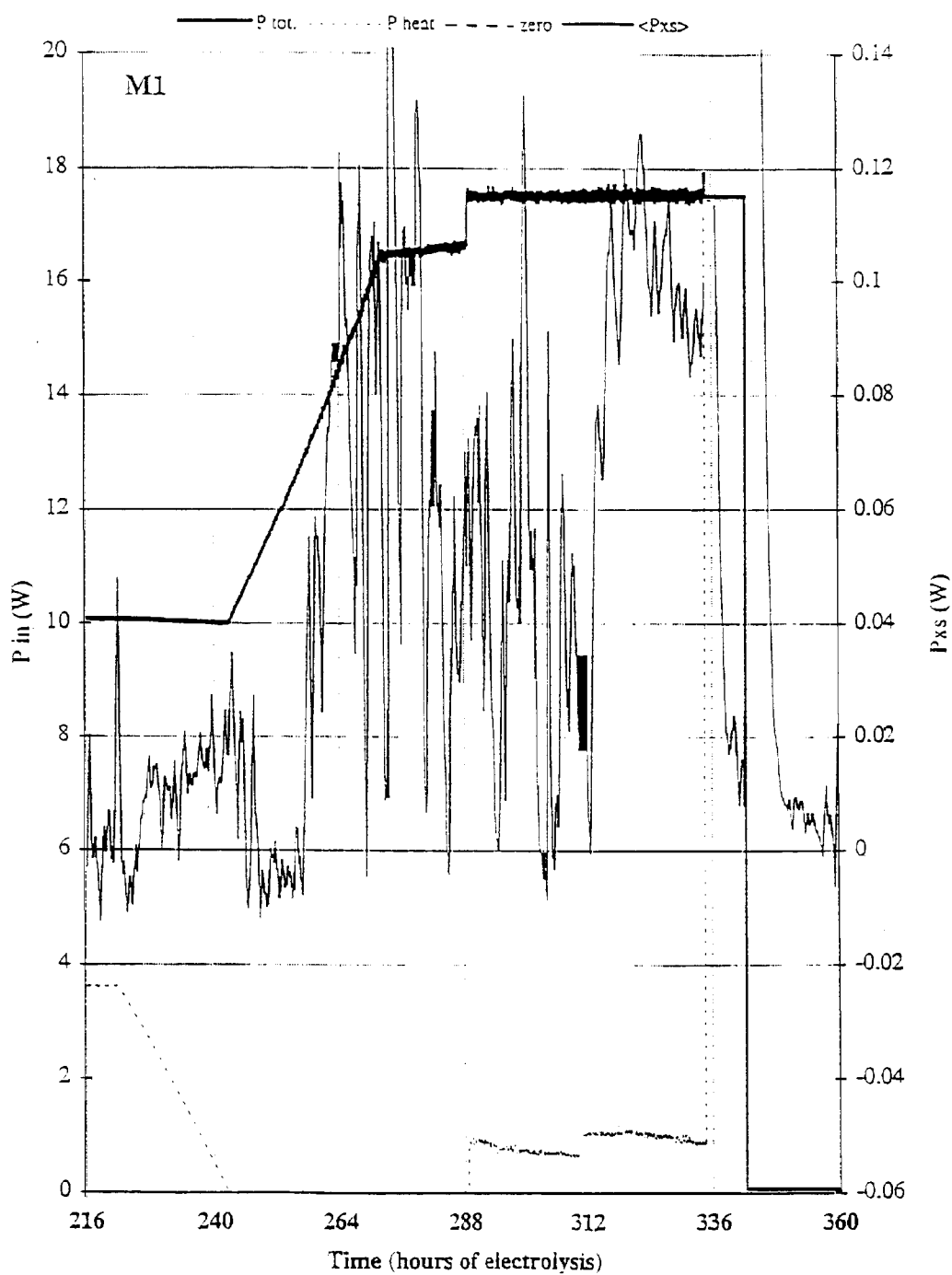
Figure 3-69a
M1 Input power 216-360 hours
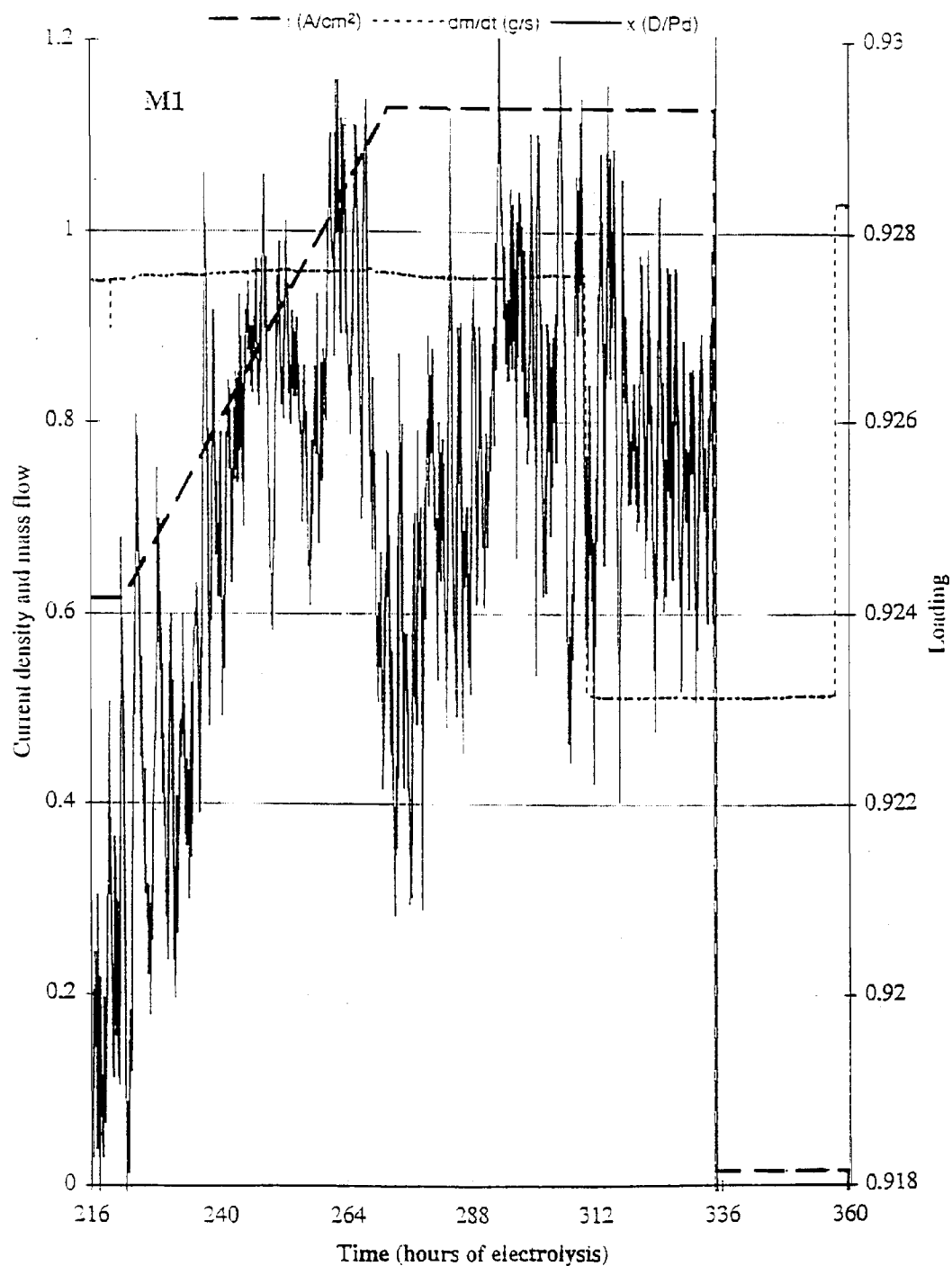
Figure 3-69b
M1 Current density 216-360 hours

Table 3-2
Initial Load of M1 Cathode

Time (h)	Current mA	Current /cm²	Tel (°C)	R/R°	D/Pd
10	74	39	30.28	1.741 ± 0.009	0.508 ± 0.005
22	3002	1593	56.93	1.867 ± 0.002	0.861 ± 0.001
48	74	39	30.27	1.946 ± 0.003	0.805 ± 0.004
120	74	39	31.81	1.948 ± 0.005	0.800 ± 0.004
132	150	79	32.05	1.911 ± 0.006	0.832 ± 0.004
144	300	159	32.56	1.869 ± 0.003	0.859 ± 0.002
160	600	318	33.84	1.835 ± 0.005	0.879 ± 0.003
192	900	477	34.86	1.804 ± 0.003	0.896 ± 0.002
222	1200	637	36.84	1.755 ± 0.006	0.918 ± 0.002
252	1786	947	41.27	1.733 ± 0.003	0.927 ± 0.001

At 288 h a 1W heater power step was applied in order to effect a calibration. The calorimeter appeared to be well calibrated, and the steady state excess power was unaffected by the heater power.

At 310 h, the calorimetric mass flow rate was reduced from 0.95 to 0.52 g s⁻¹, partly to act as a calibration. Since reducing the calorimetric mass flow results in an increased cell and cathode temperature, this also serves to test if the mechanism yielding the excess power was sensitive to temperature. While the cause is not clear, the effect of halving the calorimetric mass flow was twofold.

i. The excess power apparently increased from 40 ± 40 mW to 100 ± 40 mW. One possible explanation of this positive deviation is the subsequent current step and heater step (to zero) indicate, however, that the calorimeter was, indeed, well calibrated.

The reduction in mass flow resulted in a measured increase in the electrolyte temperature of ~ 4°C. It is possible that the small increase in excess power is due to the small increase in temperature. Alternatively, the excess power response may have been coincidental and part of the "natural" variation of the phenomenon which caused it.

ii. Following the mass flow reduction the excess power appears to be less variable with time. This effect is due simply to the increase in calorimeter time constant (and therefore, smoothing) which accompanies a decreased mass flow.

At 334 h the electrochemical current was reduced from 2.20 to 0.29 A, while maintaining the calorimeter at constant power using the compensating heater. At 343h, the heater was switched off. Large thermal transients are associated with both events; the first because of the heat capacity of the electrochemically heated cell and contents; the second due to the heat capacity of the entire calorimeter contents. Despite the clear

presence of these (expected) transients, there is an indication in Figure 3-69a that a transient release of heat occurs from the cell, following the current step at 334h, occurred with a time constant much longer (~ 4 hours) than that of the calorimeter itself (~ 15 minutes).

Ramp Two. At 360 h, the Pd electrode was stripped by making the current density -16 mA cm^{-2} (anodic) for a period of ~ 30 minutes. Following this, the current was restored to 15 mA cm^{-2} (cathodic) and then stepped progressively to ~ 493 mA cm^{-2}. At 460 h the current was returned to 15 mA cm^{-2} cathodic and held until 478 h at which point the current was ramped at 25 mA/hour to a final current density of 786 mA cm^{-2}. This sequence of steps, and its consequences, are shown in Figures 3-70a and b.

Two important results were obtained in this second loading and ramp sequence:

i.   The cathode did not load as well (as far) as it had on the first step and ramp sequence. Figure 3-68 shows the dependence of loading on current density for the first and second attempt. Both show a (roughly) logarithmic dependence, with regression fits.

     First: D/Pd = 0.088 Log (i) + 0.664 r^2 = 0.994

     Second: D/Pd = 0.051 Log (i) + 0.715 r^2 = 0.980

     This variation in slope is particularly significant. If we suppose that a critical loading of D/Pd ≈ 0.95 must be achieved before substantial excess power can be observed, then for the first loading sequence this might be achieved for i ≥ 1.7 A cm^{-2}. In the second loading sequence we would require i ≥ 40 A cm^{-2}; an essentially unobtainable value.

ii. Within the detection limits of the calorimeter, no excess power was observed. For the period 360-552 h shown in Figure 3-70, the measured excess energy

          E_{xs} = 4 ± 10 kJ
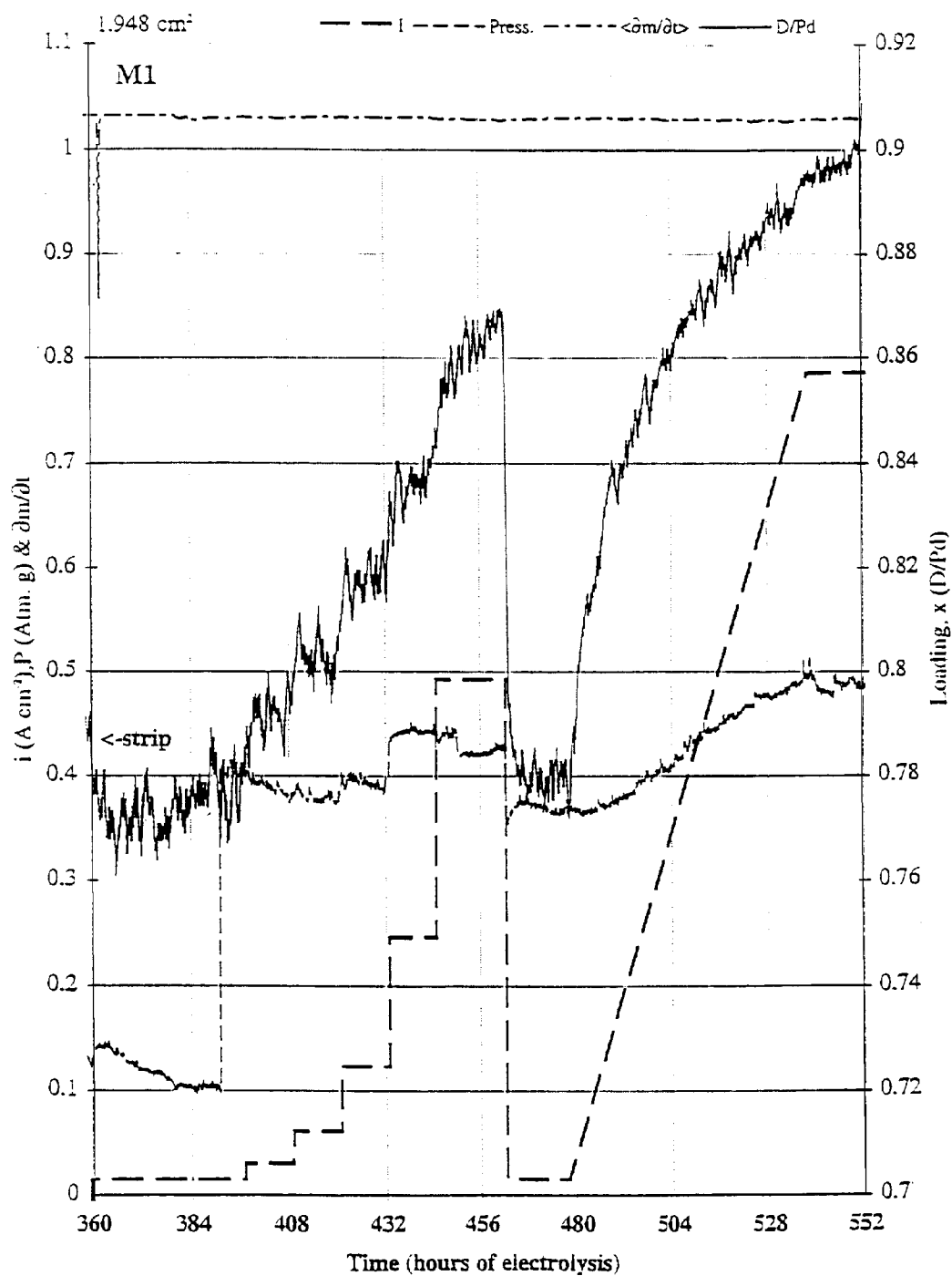
Figure 3-70a
M1 Current density and mass flow 360-552 hours
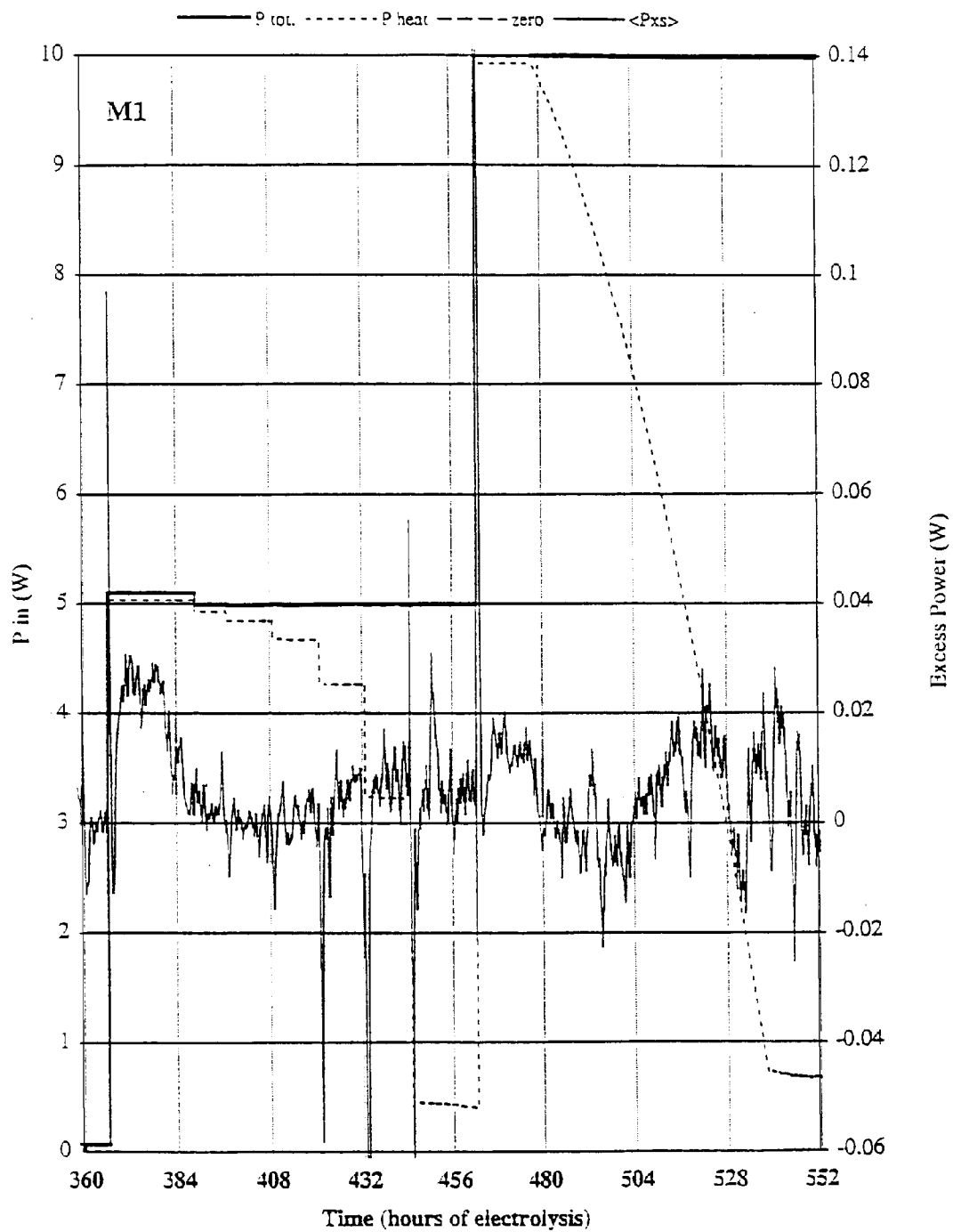
Figure 3-70b
M1 Input power 360-552 hours

The current density was held at 786 mA cm^{-2} until 648 h, at which point it was stepped to 1027 mA cm^{-2} and held until 724 h. The loading declined slightly in this period, to D/Pd $\approx$ 0.89. The excess power remained 0 ± 20 mW. The total excess energy in the period 552-742 h was

$$E_{xs} = -5 \pm 16 \text{ kJ}$$

Ramp 3. At 724 h the current density was ramped down from 1027 to 15 mA cm^{-2} at 33 mA/hour, and held for ~ 12 hours, followed by a brief anodic strip at -15 mA cm^{-2}. The current density was then held cathodically at 15 mA cm^{-2} for ~ 14 hours and ramped back to 1027 mA cm^{-2} at 50 mA/hour.

Several features of these two ramps are displayed in Figures 3-71a and b, and deserve special note:

i. With decreasing current density (Figure 3-71a) the resistance ratio increases from R/R° $\approx$ 1.80 to R/R° $\approx$ 1.98; this corresponds to a decrease in loading from D/Pd $\approx$ 0.90 to D/Pd $\approx$ 0.74. When the current density was ramped back to the same value as initially, following a strip, the resistance ratio goes over the maximum and partly down the right side to a value of R/R° $\approx$ 1.88. This corresponds to a loading of only 0.86.

ii. The voltage response to the current ramps also is not symmetric. At the same current (density) before and after the strip, the cell voltages (Figure 3-71b) differ by as much as 1 volt. Examining the period of anodic reversal, it is clear that the stripping process has resulted in a reduced cell voltage, presumably by the removal or change of a (cathode) surface film.

iii. The calorimeter remains essentially* in thermal balance during the period of these ramps (720-884 h), with

$$E_{xs} = 1 \pm 8 \text{ kJ}$$

Strip and boron addition. At 890 h the cathode was anodically stripped and the current density set to 15 mA cm^{-2} cathodic. At 964 h the current density was doubled to 30 mA cm^{-2}. At 982 h, 15 mg of H_3BO_3 was added to the cell. Figure 3-72 shows the response of the cell voltage and cathode resistance ratio. At 15 mA cm^{-2}, the voltage monotonically rises to ~ 2.2 V; the resistance ratio increases to the maximum and then slightly down the right side to a loading of D/Pd = 0.787. When the current is doubled the voltage steps and continues its slow monotonic increase, and the resistance ratio decreases to a slightly increased loading of D/Pd = 0.799.

---

*The origin of the endothermic feature at ~ 740 h is not known. The exothermic feature in the vicinity of the strip is due to the exothermic release of D_2 from the cathode. All other variations in excess power are either random fluctuations or due to departures of the calorimeter from its steady state.
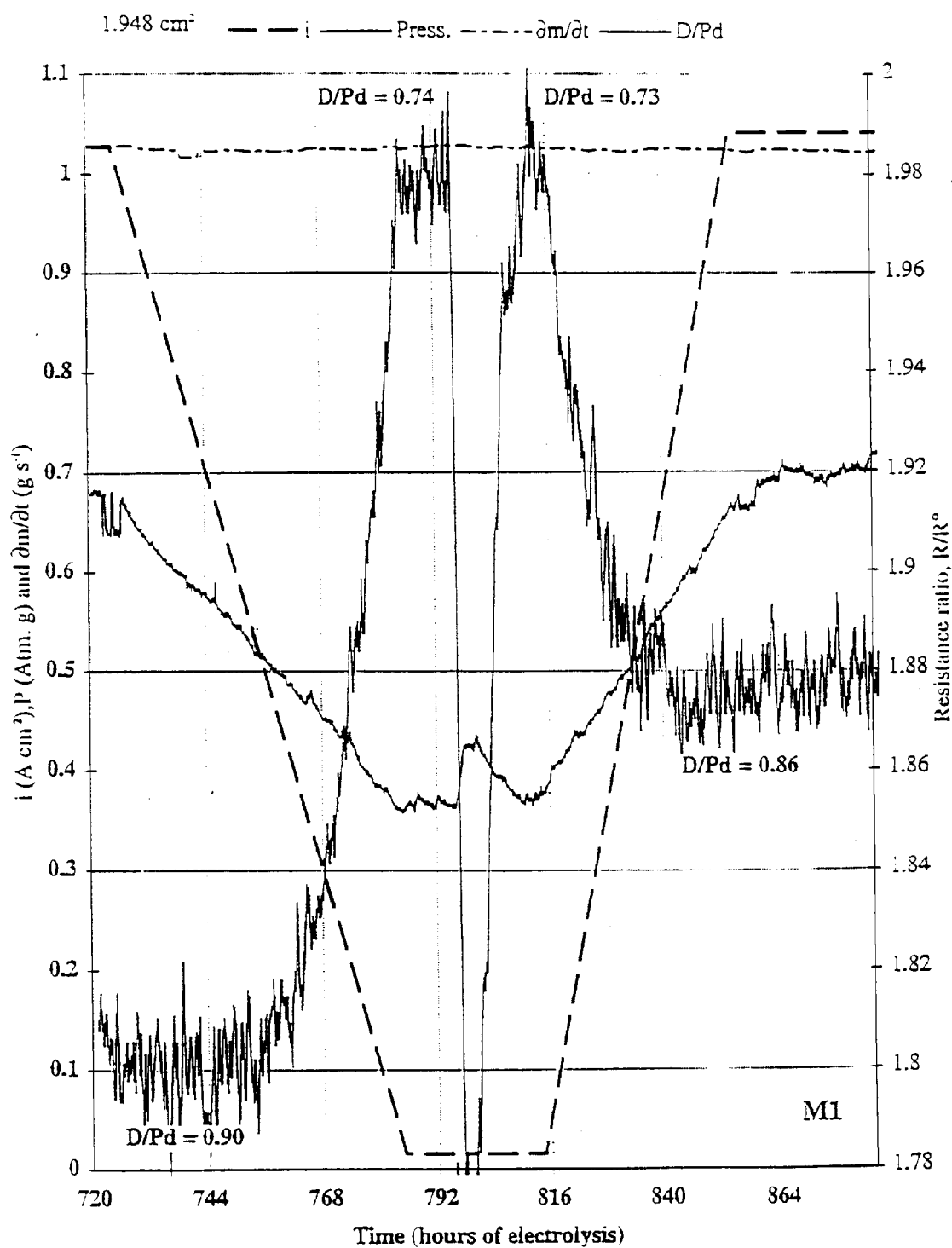
Figure 3-71a
M1 Current density and mass flow 720-864 hours
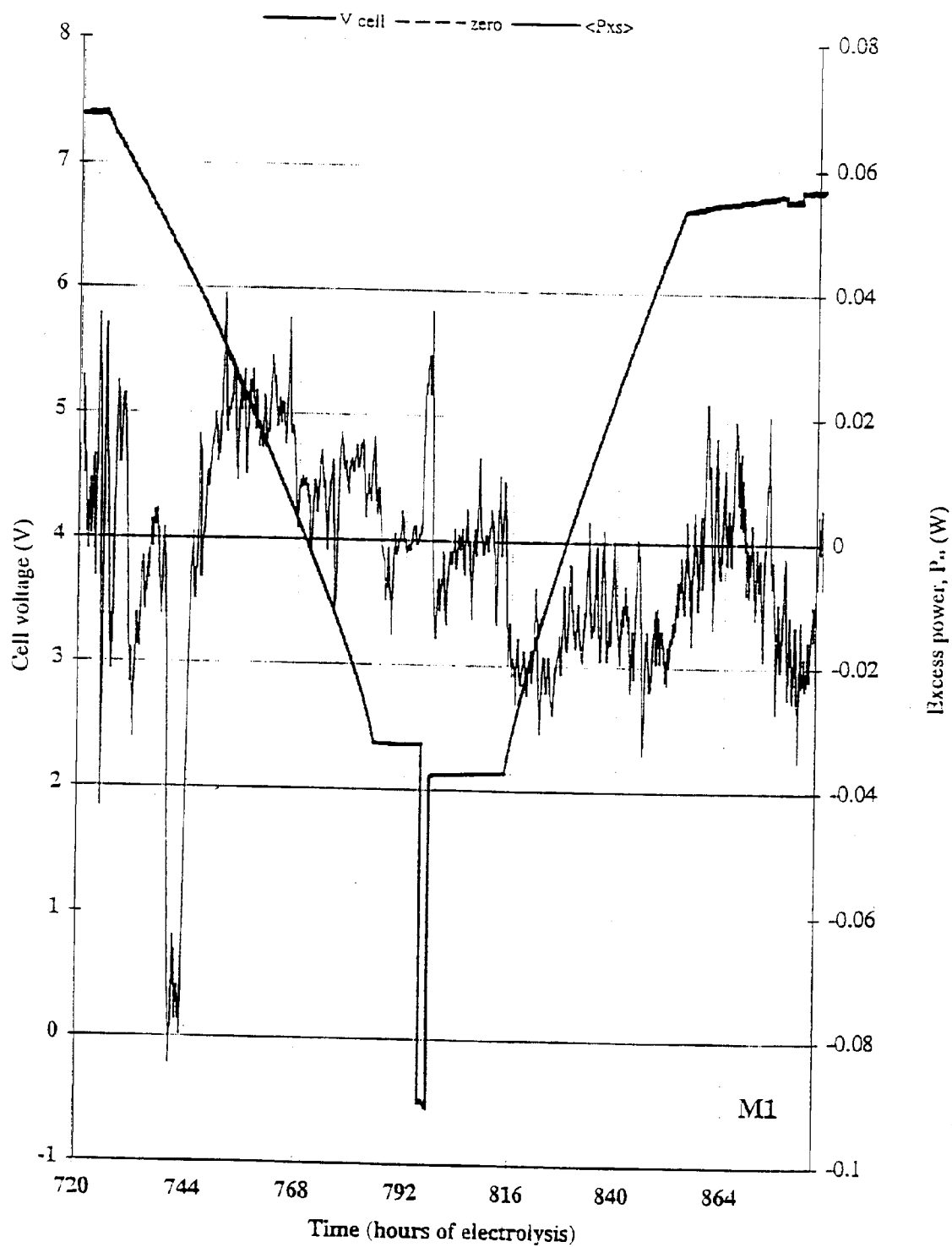
Figure 3-71b
M1 Cell voltage
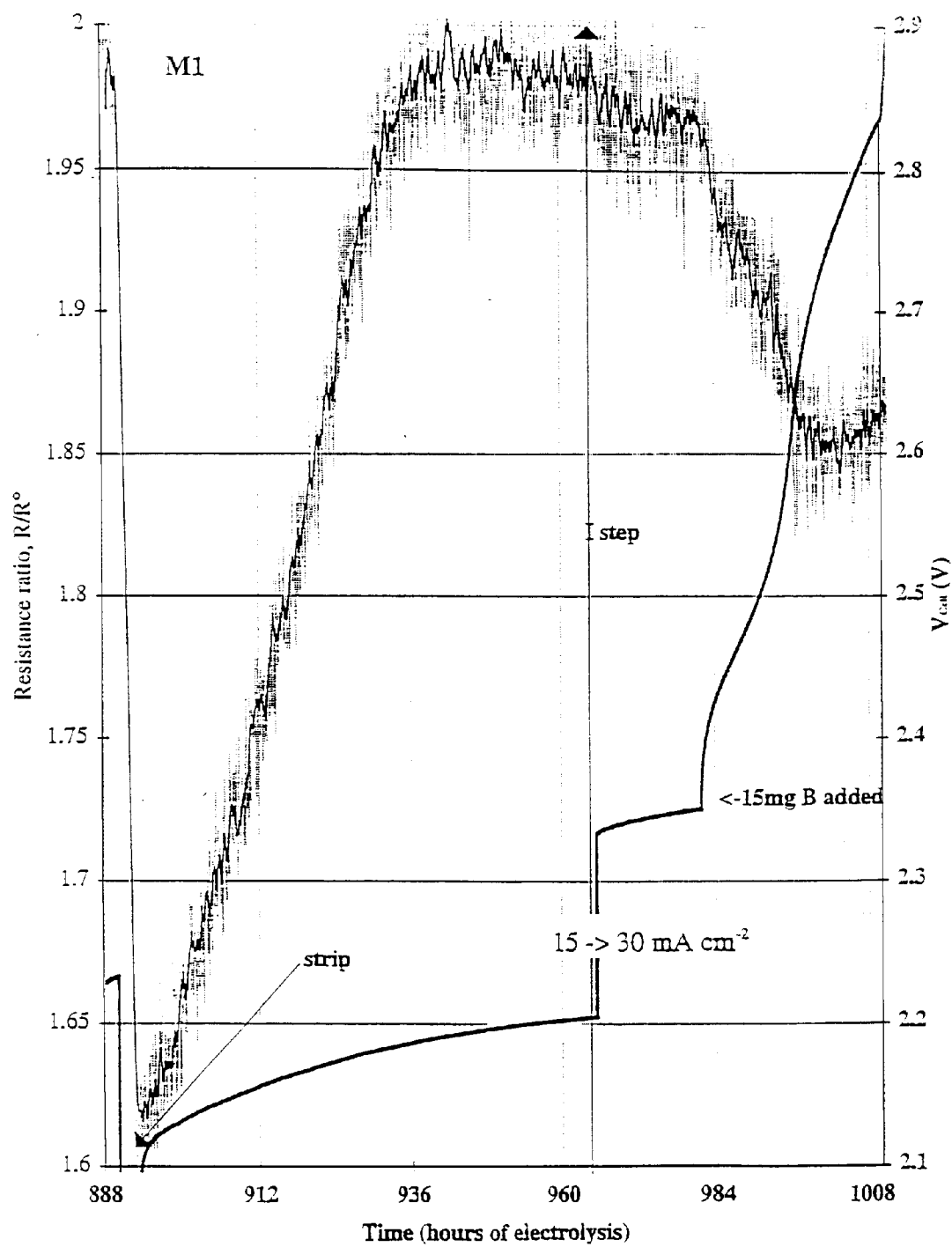
Figure 3-72
M1 Resistance ratio 888-1008 hours

When 0.015 g boric acid was added at 982 h, the cell voltage begins to increase rapidly, and the resistance drops. Two features of this response are of note:

i. The voltage rises by 433 mV. This is far larger than any likely kinetic (rate constant) effect at these low current densities. This voltage is also too large to represent the thermodynamic effect of increased loading. The effect of B on cell voltage must be due, at least in part, to the formation of a surface film.

ii. The resistance decrease, were it due entirely to the absorption of D into the Pd, would represent a new loading D/Pd = 0.877 (an increase of ~ 8%). While such absorption of D may have occurred, we must consider what effect the absorption of protons introduced with the boric acid may have on the cathode resistance.

    15 mg of H_3BO_3 contains 7.3×10^{-4} moles of H

    1.122 g Pd contains 1.05×10^{-2} moles of Pd

Had all the protons entered the Pd, they could have added to or substituted for D on 7% of the lattice sites.

Since the resistance ratio versus loading curves for D/Pd and H/Pd are different, either supplementing or substituting for D atoms in the Pd lattice will produce a measured resistance change. We can approximate the resistance of a Pd specimen containing both H and D as a linear combination of the binary functions. Thus, for $PdDH_y$

$$R/R^\circ = \frac{x}{z} * f_z (D/Pd) + \frac{y}{z} * f_z (H/Pd)$$

where f_z is the binary function for D or H calculated at the total loading z = x + y.

Using this formula we can calculate the effect of adding 7.3×10^{-4} moles of H to 1.05×10^{-2} g Pd. Note that this represents the largest possible effect, if all of the H atoms added to the electrolyte become sequestered in the cathode. Let us take two cases:

Case 1. If all the H replaces D in the lattice (that is, a 1:1 substitution of D for H), then the resistance ratio should change from the pre-addition value of $R/R^\circ = 1.97$ to *1.95*. Clearly a much larger effect than this occurred (Figure 3-72).

Case 2. If all of the H enters the Pd lattice to take up sites not occupied by D, and without expelling D, then the resistance ratio should change from $R/R^\circ = 1.97$ to *1.85*. This indeed, was observed.

Before we conclude that Case 2 correctly represents what occurred in the Pd lattice, we must consider the role of B, adsorbed and absorbed. Absorption of B does and will occur although the diffusion of B in Pd is too slow to modify our conclusions, above.

Adsorption of B may occur, changing the surface kinetics and possibly facilitating net loading of D as well as H. 15 mg of H_3BO_3 in 130 ml of LiOD represents only ~ 0.6 mol% H. It is thermodynamically unreasonable to expect all of this H to enter the lattice. Given a separation factor of ~ 8 then 30-50% of the H may enter the Pd before a new equilibrium is established with the (lowered) electrolyte H concentration.

From the above we conclude that the addition of H_3BO_3 to the electrolyte resulted:

i.   in the formation of a film of substantial resistance on the Pd cathode

ii. in increased lattice loading of D and (probably) H.

Ramp 4. At 1012 h the current was ramped at 14 mA/hour to 1027 mA cm^{-2}. At 1200 h the current was stepped from 2 to 3A to a new current density of 1.54 A cm^{-2}. The loading decreased monotonically with the current ramp (R/R° increasing); during this period of ramps and current steps there was no indication of excess power. An attempt was made at 1220 h to simulate the temperature step conditions of Fleischmann and Pons. This was accomplished by turning off the calorimetric mass flow for a period of ~ 2 hours with the total input power at ~ 27 W. The resulting temperature pulse did not obviously result in initiating excess power. It is possible that vapor transported D_2O entered the vertical section of the gas manifold, degrading the performance of the calorimeter.

Final Strip. At 1317 h the current density was reduced to 27 mA cm^2 anodic, and the cathode was extensively stripped to re-determine the value of R°.

Figure 3-73a shows the resistance and voltage response for the first 100 hours following current reversal. The horizontal axis is plotted as the logarithm of the time spent at 27 mA anodic, in order to draw attention to both short and long term features. A finer scale is shown in Figure 3-73b.

Three features of Figure 3-73a should be noted:

i.   The anodic removal of D (and H) from the Pd lattice, as measured by the resistance ratio, proceeds more slowly than is expected for a 2mm diameter cathode. This suggests either the presence of a barrier (that is stable under anodic conditions), or that the effective diffusion coefficient of D (and H) is substantially less than its initial and nominal value. Boron, adsorbed and absorbed may be responsible in each case.

ii. Upon complete removal of D (and H) from the lattice, the Pd resistance does not return to its initial value. The final value of R/R° (for stripping times ≥ 100 hours,

see Figure 3-73b) is $R/R^\circ = 0.95 \pm 0.01$, suggesting that a 5% reduction has occurred in the metal resistivity. At present we have no explanation for this effect, although we have observed it previously.

iii. The cell voltage first decreases, then goes through a maximum between 1 and 2 hours of stripping (labeled "a" in Figure 3-73b). The cell voltage then decreases monotonically, with the suggestion of two arrests labeled "b" and "c", in Figure 3-73a. The voltage then exhibits a minimum, labeled "d", before establishing a stable value for electrolysis of D_2O.

When the Pd is anodic, the large area Pt electrode (formerly the anode) acts as a cathode, reducing D_2O to evolve D_2 gas on its surface. At the current density of this experiment, the Pt electrode will be very little polarized; in the slightly elevated D_2 pressure of the cell it may be considered as a suitable reference electrode. Likewise, the IR drop in the electrolyte is likely to be constant (at constant temperature and current). We must therefore consider the source of the voltage variations discussed in (iii) above, in terms of the kinetic and thermodynamic processes of the Pd electrode as an anode.

The appearance of an inflection in the voltage-time curve (at constant current and temperature) is not easily explained. One possibility is that a resistive film, present and produced while the Pd was a cathode, is removed by dissolution, oxidation or mechanical processes associated with D_2 out-gassing. Once lost, the cell resistance is reduced, and the voltage rises (becomes less negative). In this sense, it is not the maximum "a" that is important, but the minimum that precedes it. It is very likely that the barrier film which is anodically removed is comprised of Al, Li and also, possibly, B species deposited from the electrolyte at times when the Pd was a cathode.
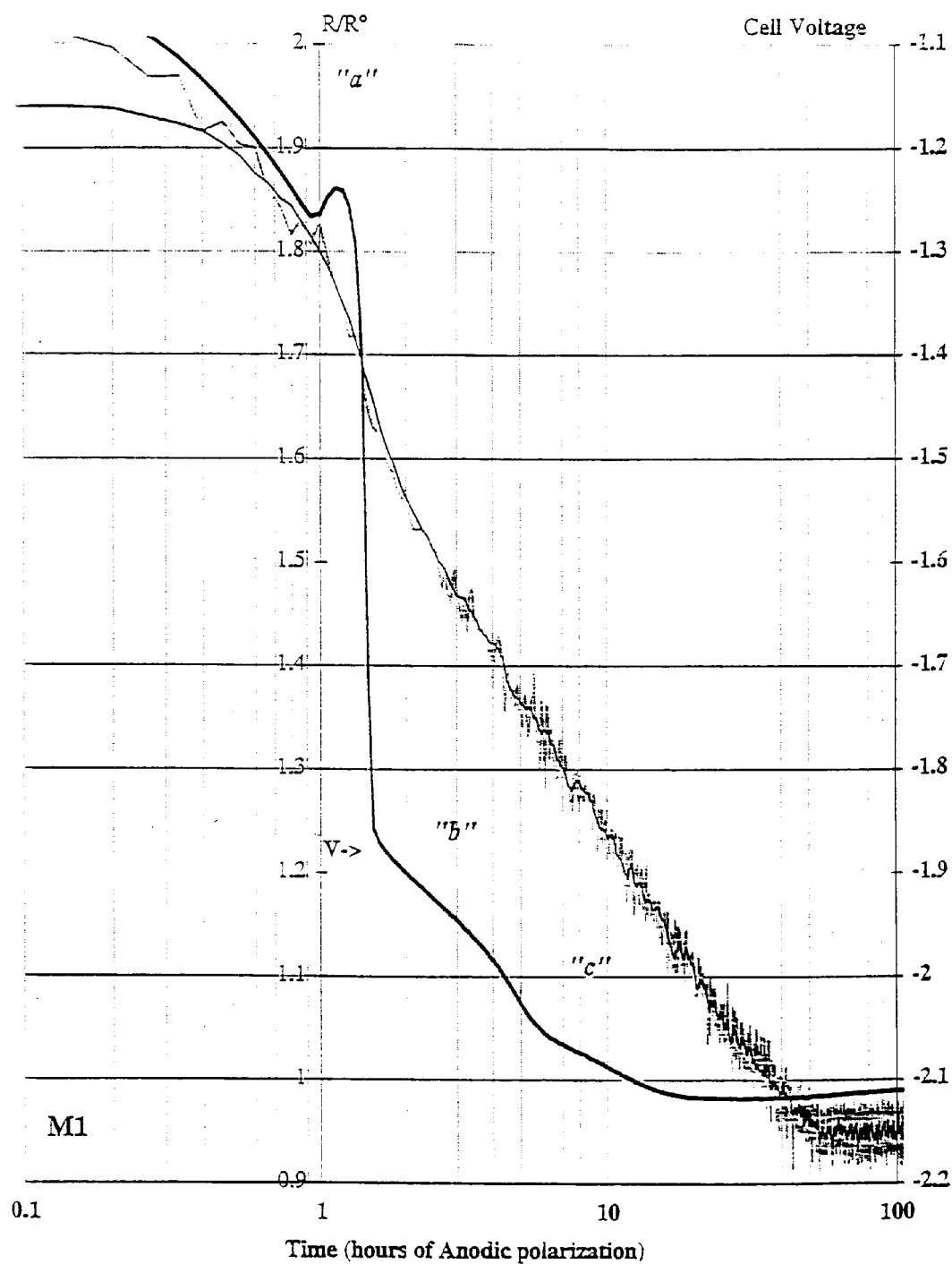
Figure 3-73a
M1 Time (hours of anodic polarization) 0.1-100 hours
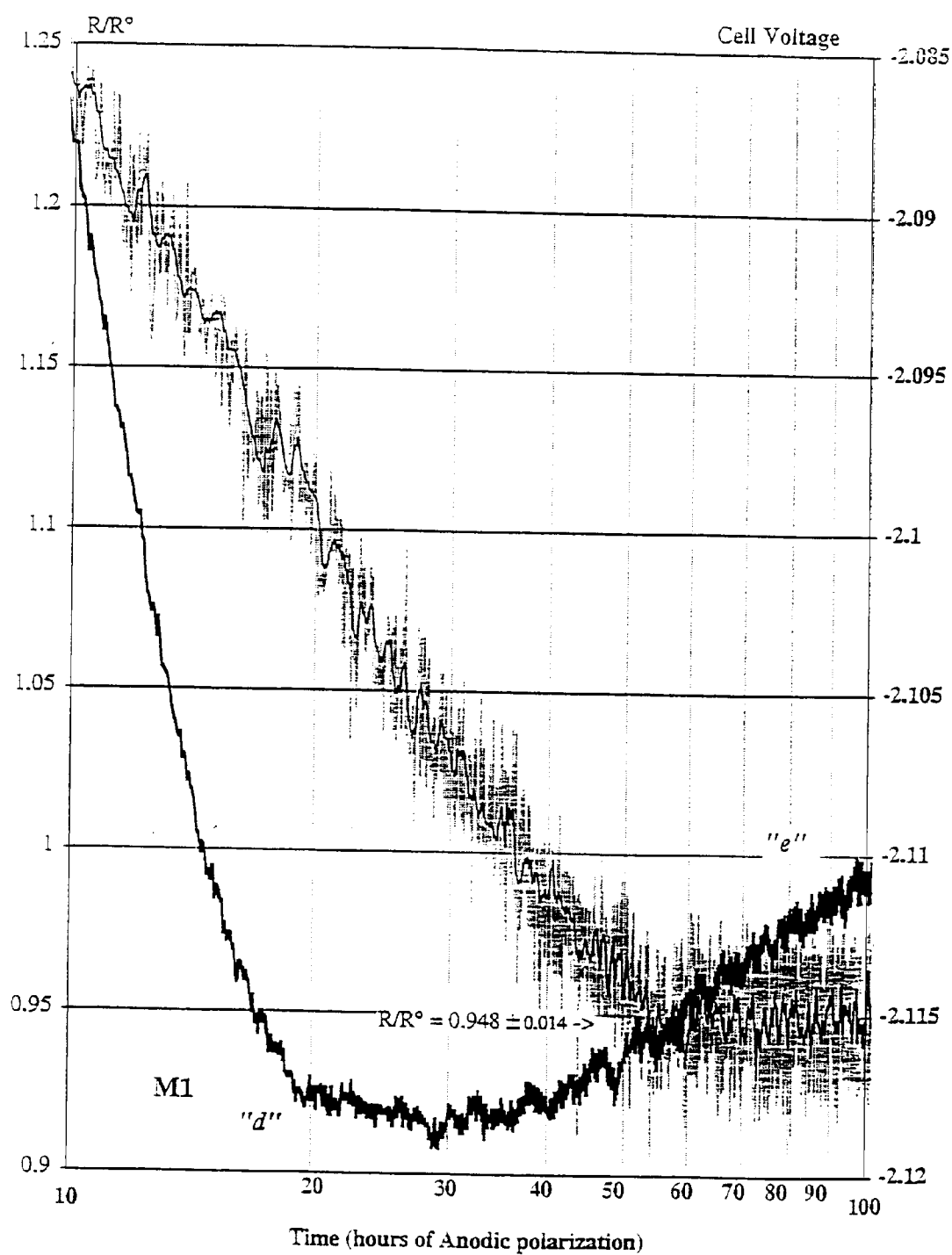
Figure 3-73b
M1 Time (hours of anodic polarization) 10-100 hours

The partial arrests, "b" and "c" in Figure 3-73a, may well be associated with the final removal first of D, then H from the Pd lattice. The minimum, "d", possibly is due to a kinetic constraint of a barrier which is ultimately removed before the Pd electrode establishes its steady state potential for oxygen evolution. Since this process takes ~ 100 hours to complete, it is likely to be due to an absorbed, not adsorbed species. The most probable candidates are B and Li, absorbed from the electrolyte at times when the Pd was a cathode.

A reduction in the final resistance is shown in Figure 3-73b. This is unlikely to be due to an artifact of the measurement system, since the same instrument was used continuously throughout the experiment. Neither is this change in resistance thought to be due to geometric effects associated with movement of the resistance voltage contacts (effective length) or change in the specimen diameter (effective area). Instead, the cause of this effect must be sought in the metal phase resistivity, itself.

Such a resistance change is not normally observed; cathodes typically return to within 1% of their initial values after loading and stripping. For a small number of cells, such a resistance reduction has been observed. In some cases, cathodes exhibit a much larger resistance drop.

For a Pd cylinder, 3.0 cm long and 0.2 cm diameter, we can calculate the expected resistance from the resistivity; at 20°C $\rho = 10.8~\mu\Omega$ cm.

	Resistance at 20°C
Expected value	$8.94 \times 10^{-4}~\Omega$
Initial value	$9.21 \times 10^{-4}~\Omega$
Final value	$8.73 \times 10^{-4}~\Omega$

Each of these numbers has a considerable uncertainty, perhaps 1%; the first because of uncertainty in dimensions, the last two because of instrumental uncertainties. The results tabulated above nevertheless are consistent with the hypothesis that the specimen resistance initially was larger than nominal (this is usually the case), and reduced to its "expected" value after extended loading and stripping. To understand how this might occur we need to consider how resistance, and thus resistance rise, occurs in a metal.

Resistance in a metallic lattice (the impediment to electron transport) occurs due to the scattering of electrons; such scattering may be introduced by mechanical or chemical imperfections in the lattice. The specimen used as a cathode in M1 was fabricated from high purity Pd 99.997%, and was subjected to our normal annealing process for 3 hours at 850°C in an oxygen gettered vacuum. It is nevertheless possible, even probable, in

light of the preceding discussion, that sufficient mechanical imperfection and/or chemical impurity remained in the cathode to measurably increase its resistivity. That charging the cathode with D, H (and B?) and then stripping caused a reduction in resistivity tends to suggest that the initial lattice imperfections were chemical, not mechanical. Charging with hydrogen is known to strain the Pd lattice and cause or exacerbate mechanical imperfections. This would tend to increase the resistivity. One might imagine that charging and discharging D, H (and B?), may act to "getter" the Pd of reactive chemical species, notably C, N and O. This may be accomplished by sequestering the resistance-inducing chemical impurities, to or from the grain boundaries. Alternatively, these species may be expelled from the lattice entirely by volatilization. Indeed, hydrogen cycling (in the gas phase, at high temperature) is used explicitly to remove light elements from Pd, prior to gas charging.

Experiment M2

Cathode:	E#1 0.28 cm dia., 3.0 cm long
Anneal:	4 hours at 850°C in oxygen gettered vacuum. [Cathode previously annealed at 3.0 cm diameter, in 1990]
Contacts:	Five wire, four notches (only outer notches used).
Anode:	1 m, 0.25 mm dia. Pt wire helix
Electrolyte:	1.0 M LiOD with no additive
Monitors:	2 Kodak Dental X-ray films outside PTFE liner
Cell sensors:	Gas Pressure Electrolyte temperature Recombiner gas temperature

Calibration. Current was applied when the electrolyte was added, ~ 4 hours after the cell and calorimeter were placed in the constant temperature bath and data collection was started.

Figures 3-74a-c show the initial load, calibration and first ramp of M2. The calibration (R^o values of RTD's and conductive loss constants) were found to be effectively unchanged from M1.

Ramp 1. Figure 3-74a plots the loading response to the initial current steps and ramps, and Figure 3-74b, the resistance ratio and cell temperature. The maximum loading of D/Pd = 0.829 ± 0.006 was obtained at 580 mA cm^{-2}.

Figure 3-74c shows the input and excess power for this period of initial loading. For times 0-264 h, the excess power and energy were,

$$P_{xs} = 0 \pm 25 \text{ mW}$$

$$E_{xs} = 4 \pm 4 \text{ kJ}$$

Strip and Al Addition. At 165 h the Pd was anodically stripped and 2 ml of 1M LiOD saturated with Al was added followed by 1 ml D_2O. The cell was flushed with He free N_2, and the manifold sealed.

Ramps 2 and 3. Figure 3-75a shows the loading, pressure and calorimetric mass flow for the second and third current ramps. A second strip was performed at 406 h, between the two current ramps. At this time, 2 ml of 1 M LiOD saturated with Si was added, followed by 1 ml D_2O; the cell was flushed with D_2 and the manifold sealed. The maximum loading achieved during the two ramps was:

Ramp 2; $\quad R/R^\circ = 0.836 \pm 0.005$
Ramp 3; $\quad R/R^\circ = 0.846 \pm 0.006$

Figure 3-75b shows the total input and excess power. For the period 256-512 hours the excess power and energy were

$$P_{xs} = 0 \pm 25 \text{ mW}$$

$$E_{xs} = 2 \pm 16 \text{ kJ}$$

Strip and B Addition. At 300 h the Pd electrode was stripped and 5 ml LiOD containing 3 mg B_2O_3 was added to the cell, followed by 1 ml D_2O. The cell was then flushed with D_2 and sealed.
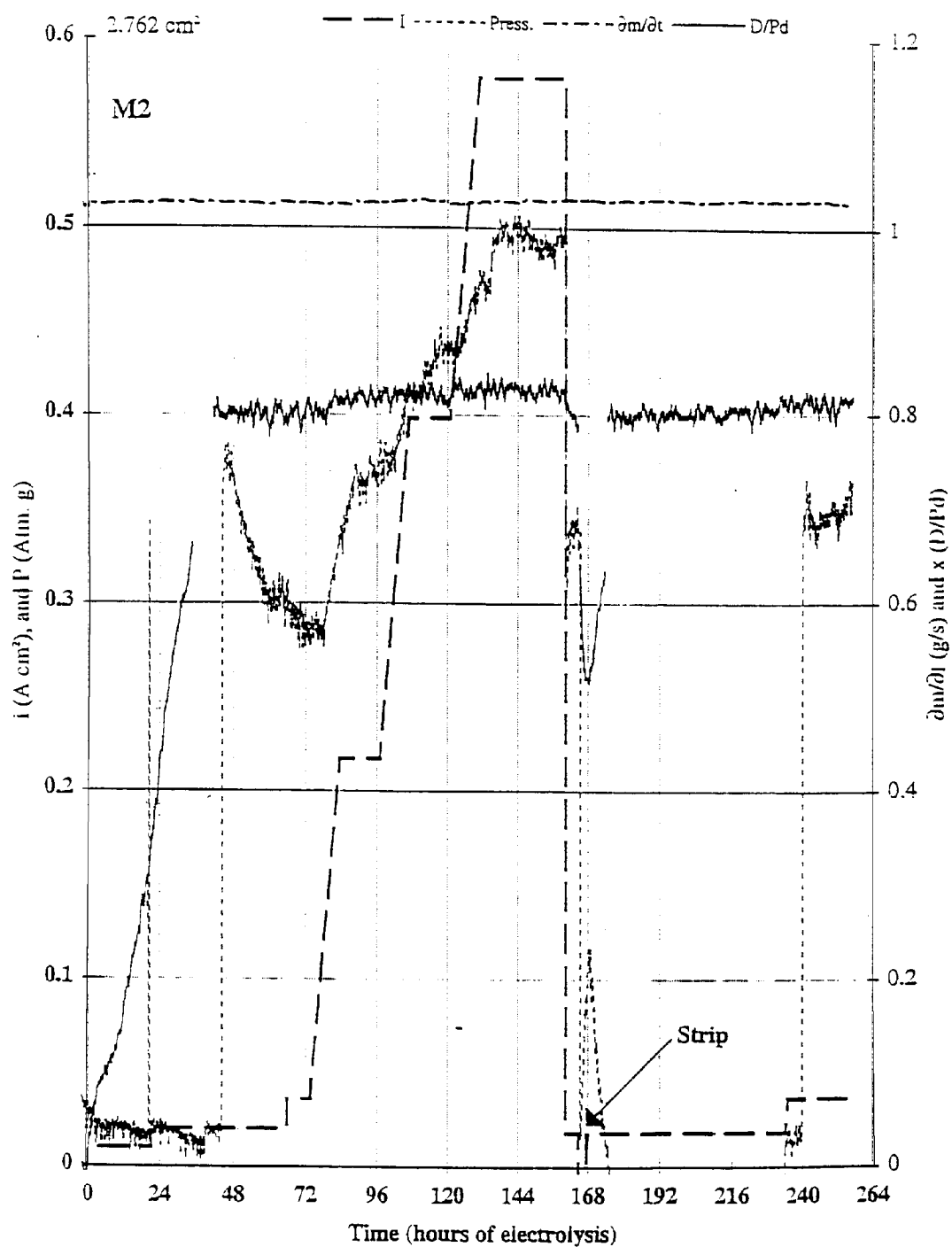
Figure 3-74a
M2 Current density and mass flow 0-264 hours
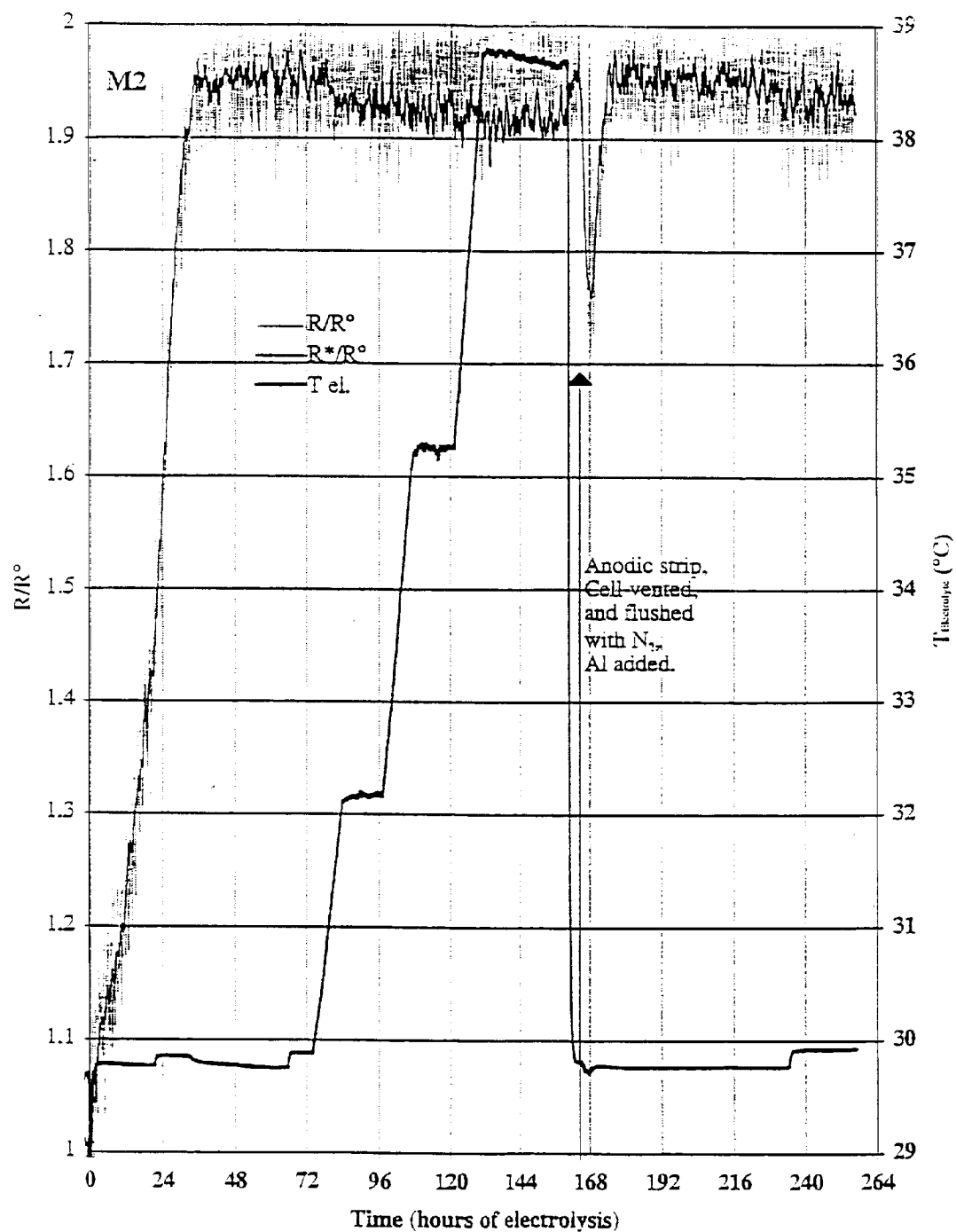
Figure 3-74b
M2 Resistance ratio 0-264 hours
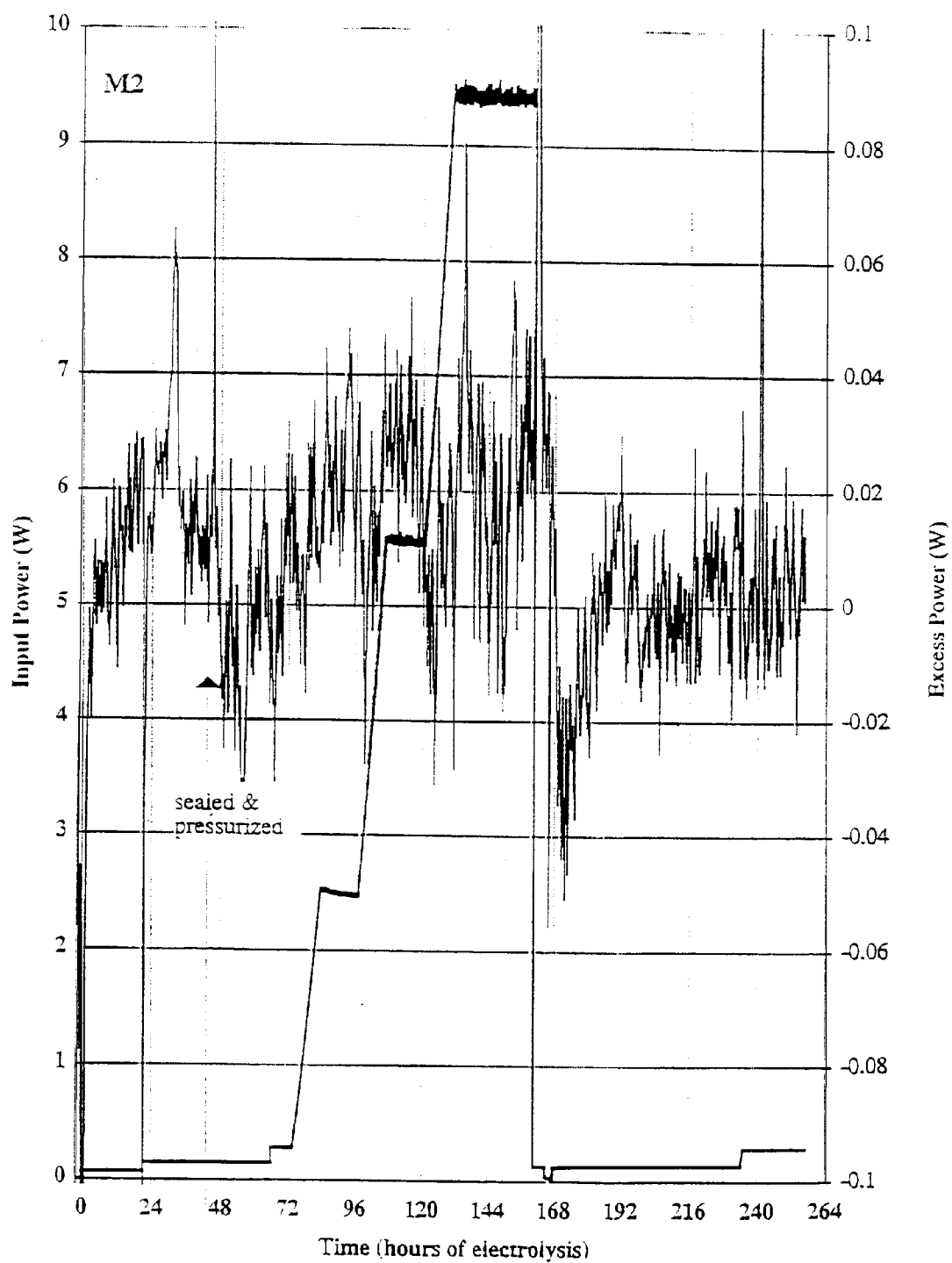
**Figure 3-74c
M2 Input power 0-264 hours**
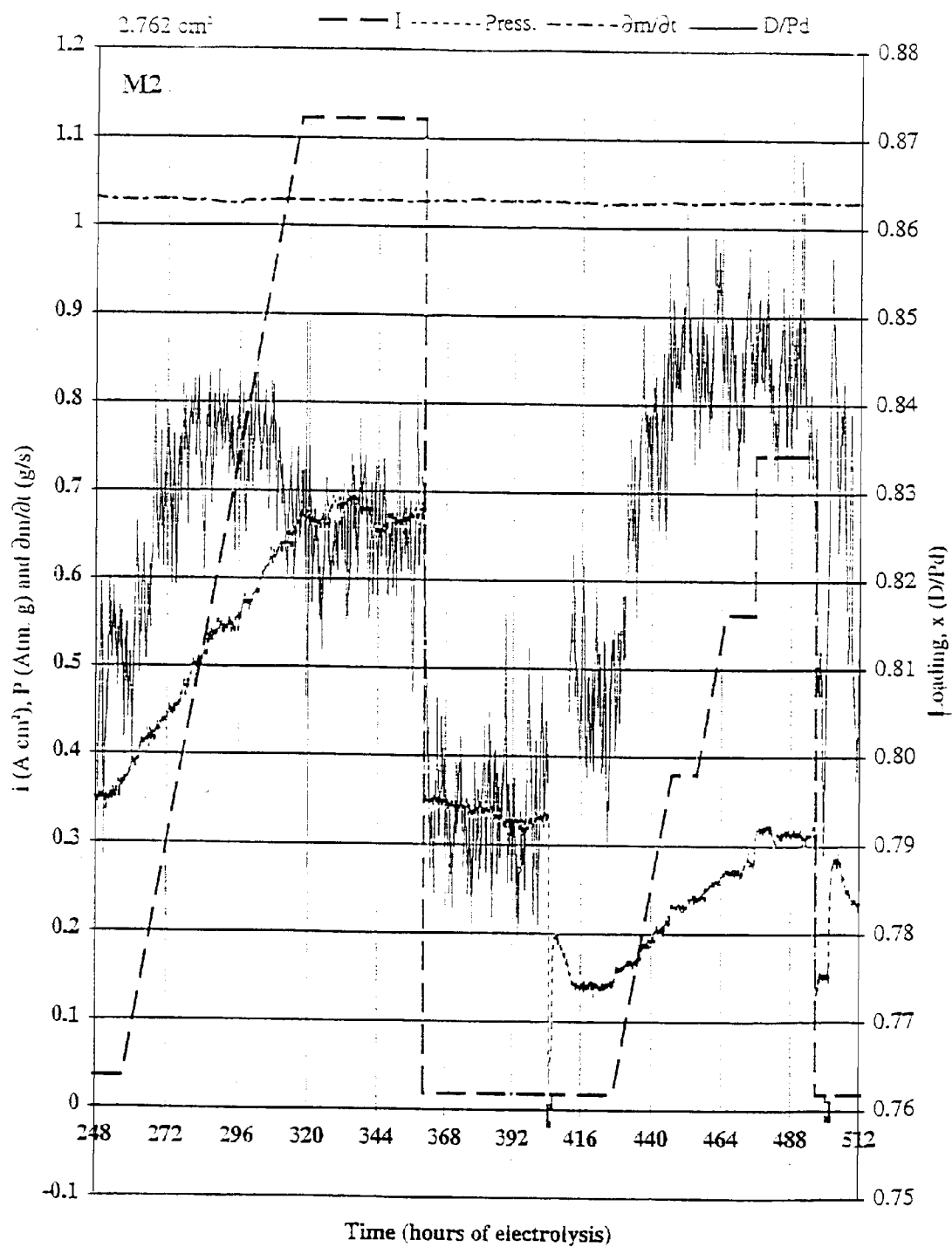
Figure 3-75a
M2 Current density and mass flow 248-512 hours
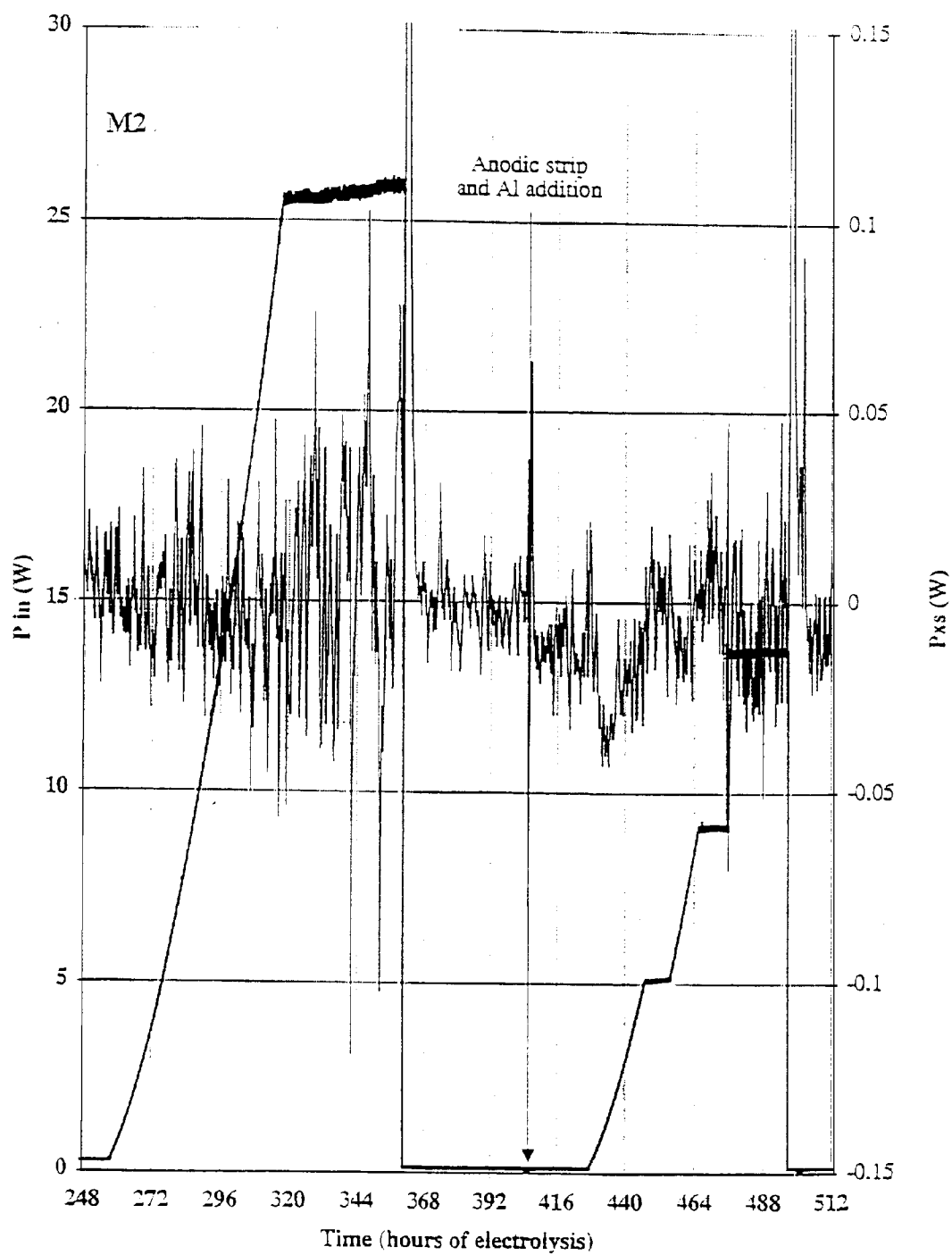
Figure 3-75b
M2 Input power 248-512 hours

Ramp 4 and Current Pulses. Figure 3-76a shows the fourth current ramp. At 623 h a 10A, 1 kHz, 10% duty cycle cathodic pulse was added to the 50 mA dc cathodic current, for a period of ~ 2 hours [Prior to this the cell voltage was inadvertently shorted (and hence = 0) for ~ 2 hours].

At 642 hr. the same pulse sequence was repeated for ~ 7 hours and the current returned to 50 mA cathodic (26 mA cm^{-2}).

At 670 h the power supply was set to deliver a 10A cathodic, 1% duty cycle, 1 kHz pulse for 2.4 s every 240 s, immediately after data collection. This pulsing was stopped at 741 h after ~ 70 hours of pulsing.

These pulse sequences neither facilitated loading, or produced any indication of excess power. Figure 3-76a shows the current and loading response of the cathode; Figure 3-76b shows the excess power response. The presence of high current pulses made the resistance measurements (loading) and the cell voltage measurements (calorimetry) inaccurate and unreliable. In Figure 3-76a, it nevertheless appears as if the continuous, 1 kHz, 10% duty cycle, 10A cathodic pulses (labeled "p1" and "p2"), caused net de-loading.

Ramp 5, intermittent pulses and RF. To avoid the measurement difficulty and inaccuracy introduced when sensitive voltage and resistance measurements are made in the presence of large amplitude cell current pulses, an intermittent mode of pulsing was developed. The power supply was set to deliver a current pulse of variable amplitude, frequency and duty cycle, for a controlled period immediately after data collection.

Table 3-3 details the application of such pulses, and their characteristics. At 912 h, current ramp 5 was started (0.05 - 2.05 A in 10 hours), in the presence of an *anodic* pulse sequence.

Pulsing was stopped at 979 h, and later replaced with an attempted radio frequency ac current stimulation at various frequencies specified in Table 3-3. To accomplish this, the output of an HP 8601 RF signal generator with an ENI 603L RF power Amplifier was connected in parallel with the dc power supply used for the cell current. This was done both with, and without transformer coupling. Because of impedance matching difficulties and radiative losses, it was estimated that very little RF power ($\leq$ 30 mW) entered the calorimeter at any of the frequencies employed.
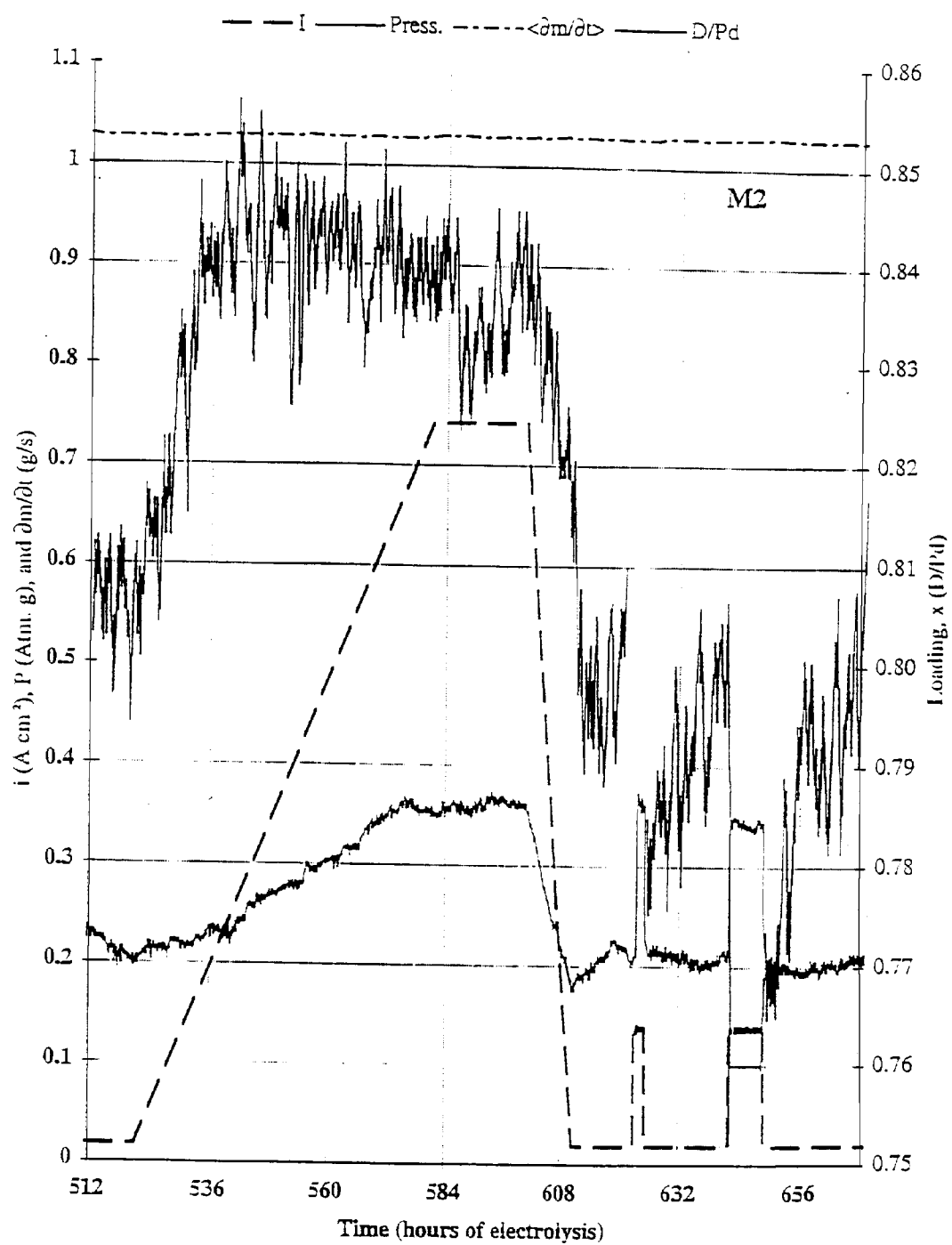
Figure 3-76a
M2 Current density and mass flow 512-668 hours
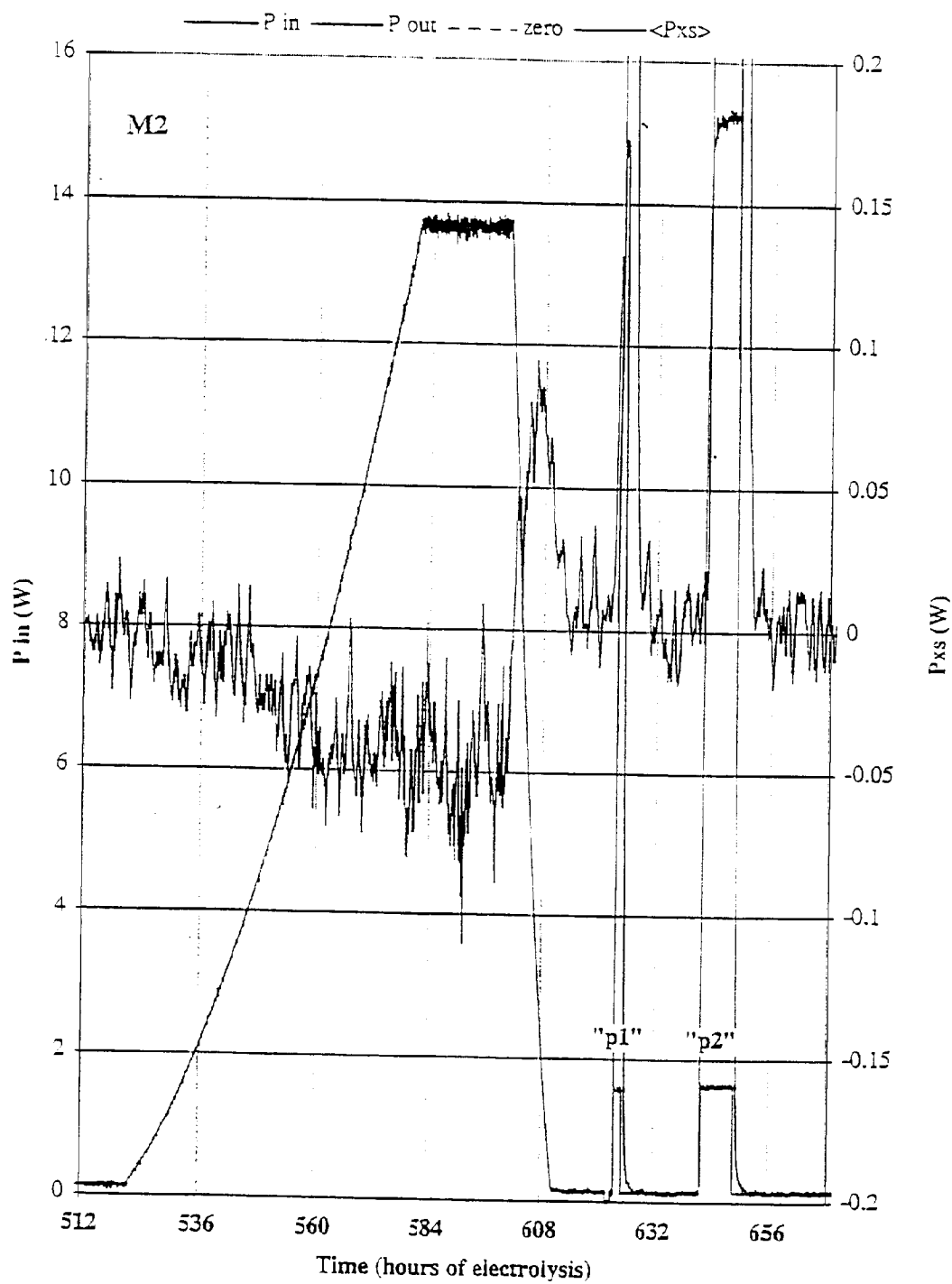
Figure 3-76b
M2 Input power 512-668 hours

Table 3-3
M2 Pulse Sequences

Date/Time		Hours	Action	Low I* (A)	High I* (A)	Freq.(Hz)	Duty Cycle	Duration	
5/6/94 16:44			Pulses:						
6/1/94	15:42	623.0	On	0.05	10	1000	10%	240	240 s
6/1/94	17:38	624.9	Off	0.05	0				
6/2/94	10:44	642.0	On	0.05	10	1000	10%	240	240 s
6/2/94	17:50	649.1	Off	0.05	0				
6/3/94	15:08	670.4	On	0.05	10	1000	1%	2.4	240 s
6/6/94	13:30	740.8	Off	0.05	0				
6/7/94	9:16	760.5	On	0.05	10	1000	10%	2.4	240 s
6/8/94	17:47	793.0	Increase	0.05	10	1000	10%	24	240 s
6/9/94	10:42	810.0	Reverse	0.05	-10	1000	10%	24	240 s
			Ramp:						
6/13/94	17:08	912.4	Start	0.05	-10	1000	10%	24	240 s
6/14/94	3:12	922.5	Stop	2.05	-10	1000	10%	24	240 s
6/14/94	11:52	931.1	Reduce	2.05	-10	1000	10%	2.4	240 s
6/15/94	0:00	943.3	Reverse	2.05	10	1000	100%	2.4	240 s
6/16/94	11:52	979.1	Stop						
			RF			(mega Hz)			
6/16/94	15:26	982.7	On	2.05	0.01	81.950	100%	240	240 s
6/16/94	15:45	983.0	*f*	2.05	0.01	81.930	100%	240	240 s
6/17/94	8:48	1000.1	*f*	2.05	0.01	81.915	100%	240	240 s
6/18/94	12:20	1027.6	*f*	2.05	0.01	90.000	100%	240	240 s
6/19/94	12:04	1051.3	*f*	2.05	0.01	95.000	100%	240	240 s
6/19/94	12:16	1051.5	*f*	2.05	0.01	88.000	100%	240	240 s
6/20/94	9:12	1072.5	*f*	2.05	0.01	85.000	100%	240	240 s
6/20/94	17:44	1081.0	Off						
6/21/94	9:01	1096.3	DC Off	0					
6/21/94	10:30	1097.8	Gas Samples Collected						
			Experiment ended						
6/21/94	11:40	1098.9							

*Cathodic positive

Figures 3-77a and 3-78a present the dc current profile and loading response for the period 668 h to the end of the experiment. It is clear that the application of current pulsing and RF stimulation provides little benefit to the cathode loading.

Figures 3-77b and 3-78b show the measured input and output power, and the excess power for the period 668 h to the experiment end. The excess power response to current pulsing is less easily interpreted than the loading response because of the unmeasured input power components during the application of pulses, which are deliberately out of phase with the measurement cycle, and the RF input of unknown power. Nevertheless, the calorimetric response does not suggest that excess power initiated or was stimulated by any of the current pulses attempted.
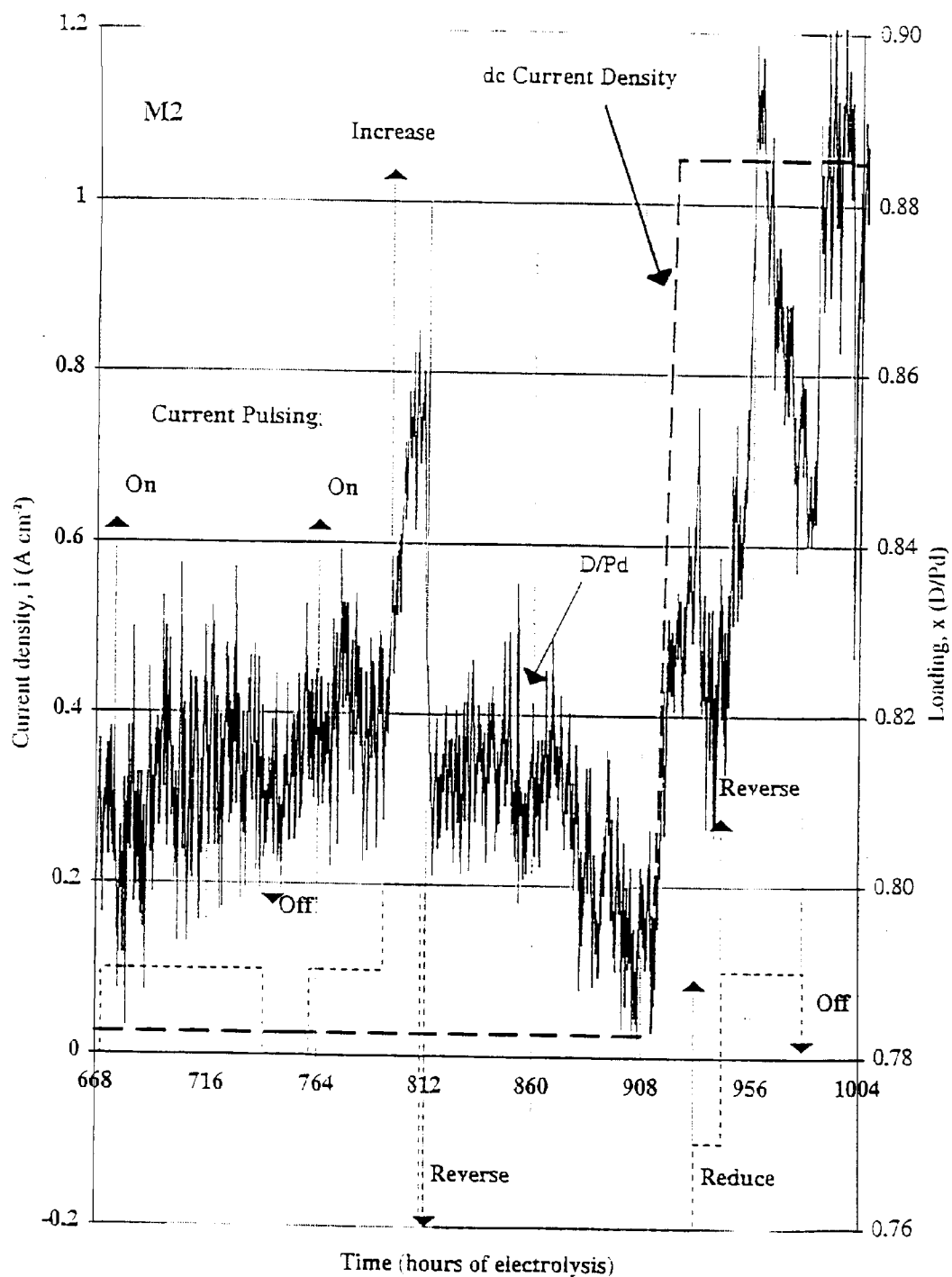
Figure 3-77a
M2 Current density and Mass flow 668-1004 hours
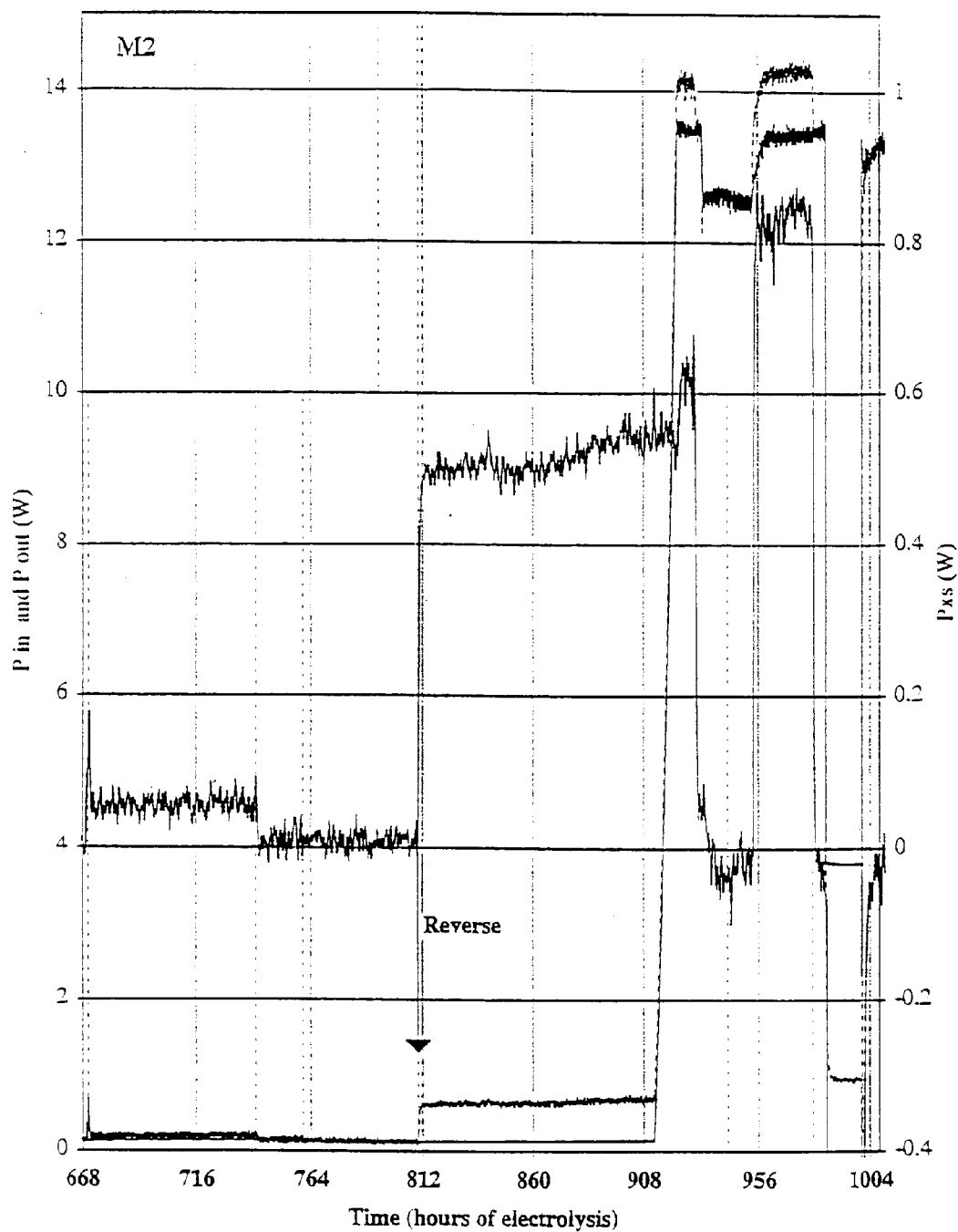
Figure 3-77b
M2 Input and output power 668-1004 hours
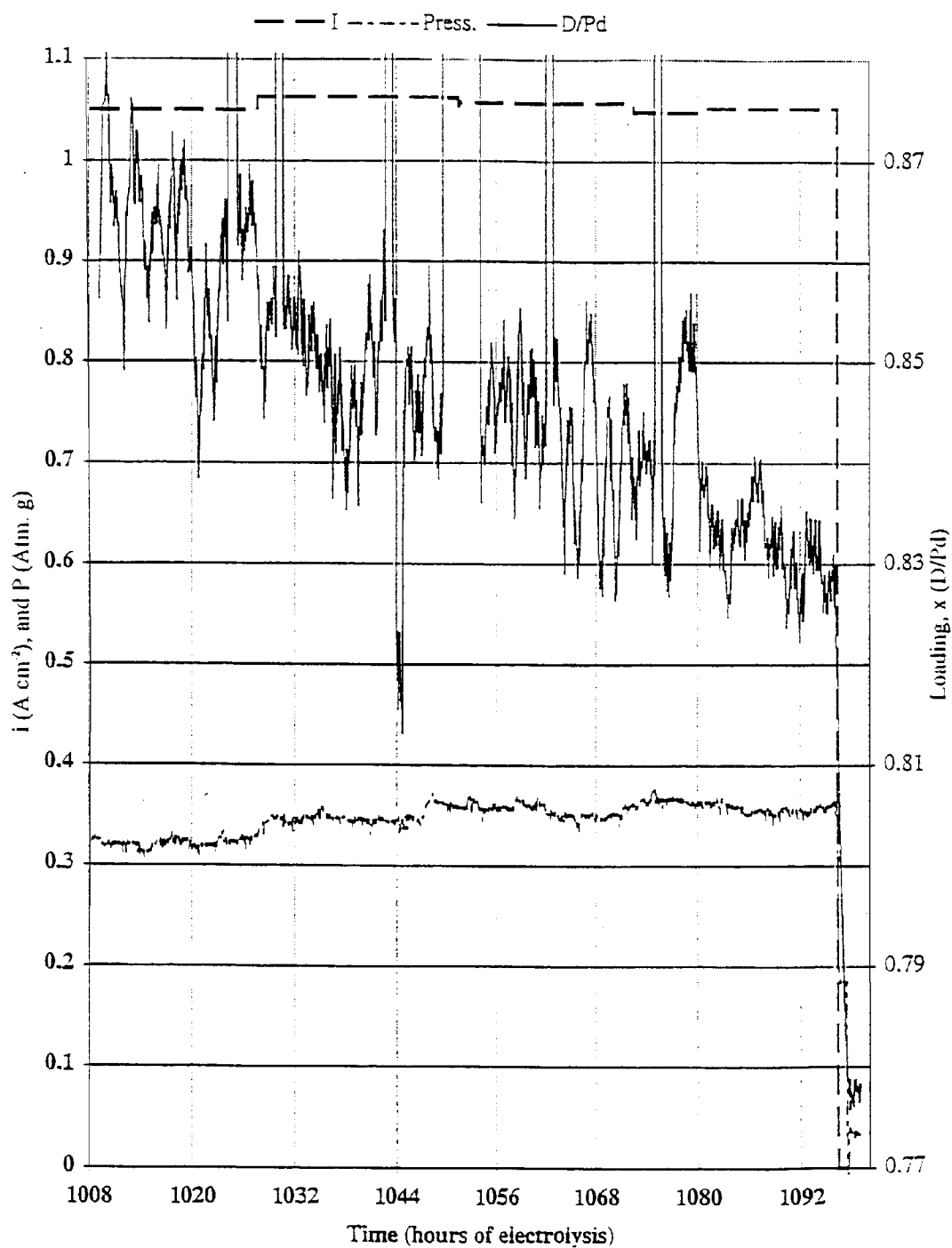
Figure 3-78a
M2 Current density and mass flow 1008-1092 hours
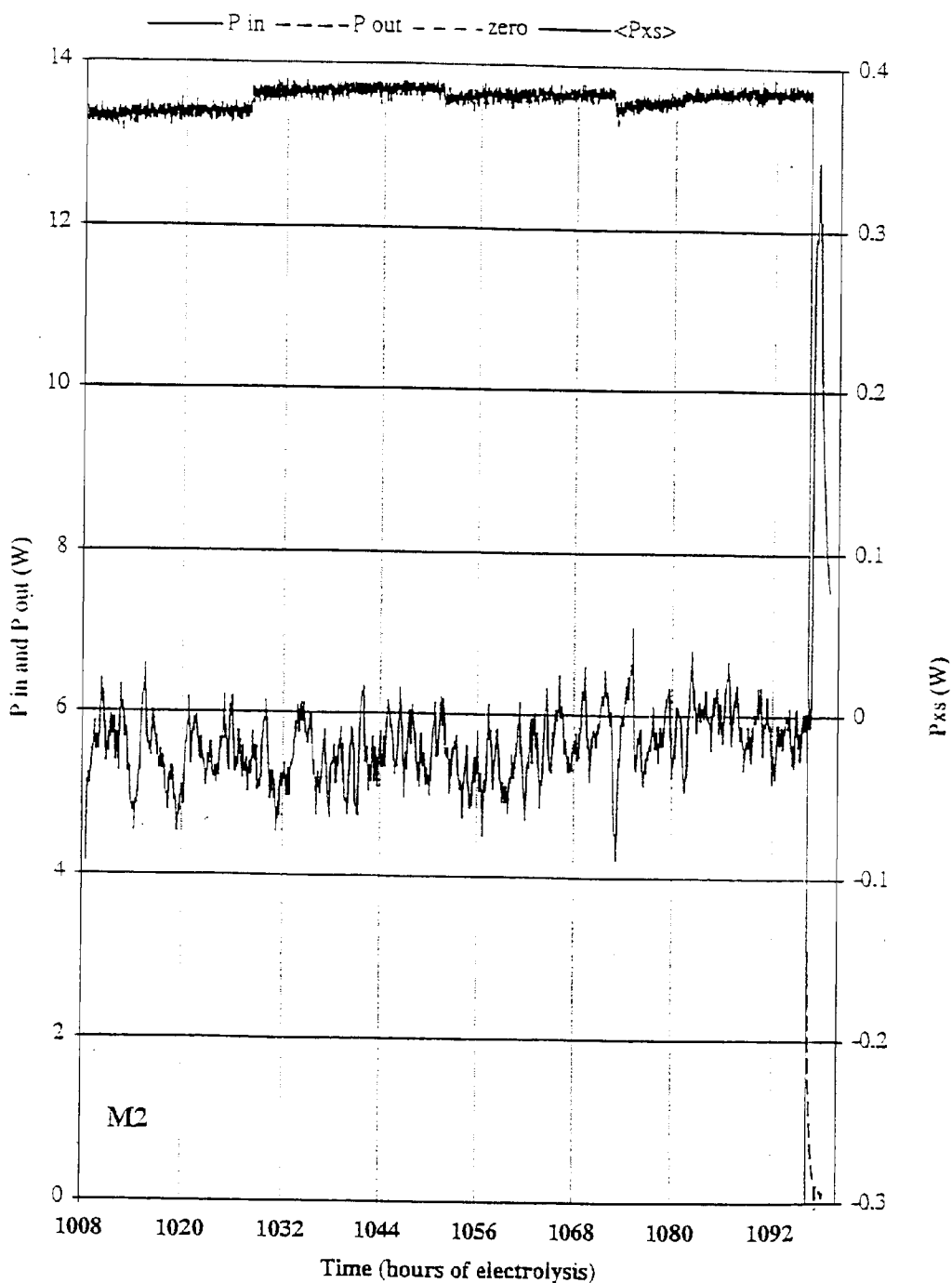
Figure 3-78b
M2 Input and output power 1008-1092 hours

Experiment M3

Cathode:	E#4 0.30 cm dia., 3.0 cm long, 2.44709 g
Anneal:	4 hours at 850°C in oxygen gettered vacuum
Contacts:	Five wire, two notches
Anode:	1 m, 0.25 mm dia. Pt wire helix
Electrolyte:	140 ml, 1.0 M LiOD with 200 ppm SiO_2
Monitors:	2 TLD's in quartz tubes outside anode 2 Kodak Dental X-ray films outside PTFE liner
Cell sensors:	Gas Pressure Electrolyte temperature Recombiner gas temperature

Calibration and initial load. The cell and calorimeter were placed in the water bath ~ 17 hours before electrolyte addition and the application of cathodic current. Electrolyte was added using a PTFE catheter while the cell voltage was maintained at 0.8V cathodic. The calibration of the RTD's (R^o values) were found to be effectively unchanged from M2 (and M1).

Following electrolyte addition, the power supply was set to control the current at 50 mA (17 mA cm^{-2}). The initial loading was performed under flowing D_2 gas (~ 15 cm^3 min^{-1} at ~ 0.45 atm. gauge).

Current steps and ramp. Figure 3-79a shows the current density, cell pressure and resistance ratio response from time - 24 h (with respect to current initiation) to 250 h. Three features of the resistance ratio appear to be anomalous:

i. R/R^o appears to be rising at times before the application of cathodic current, when the cell was empty of liquid, and the cathode was exposed only to (flowing) N_2 gas.

ii. R/R^o rises rapidly to "impossibly" large values (> 2), and continues to rise with time and applied current.

iii. R/R^o exhibits an abrupt step decrease, when the cell pressure was increased at ~ 123 h.
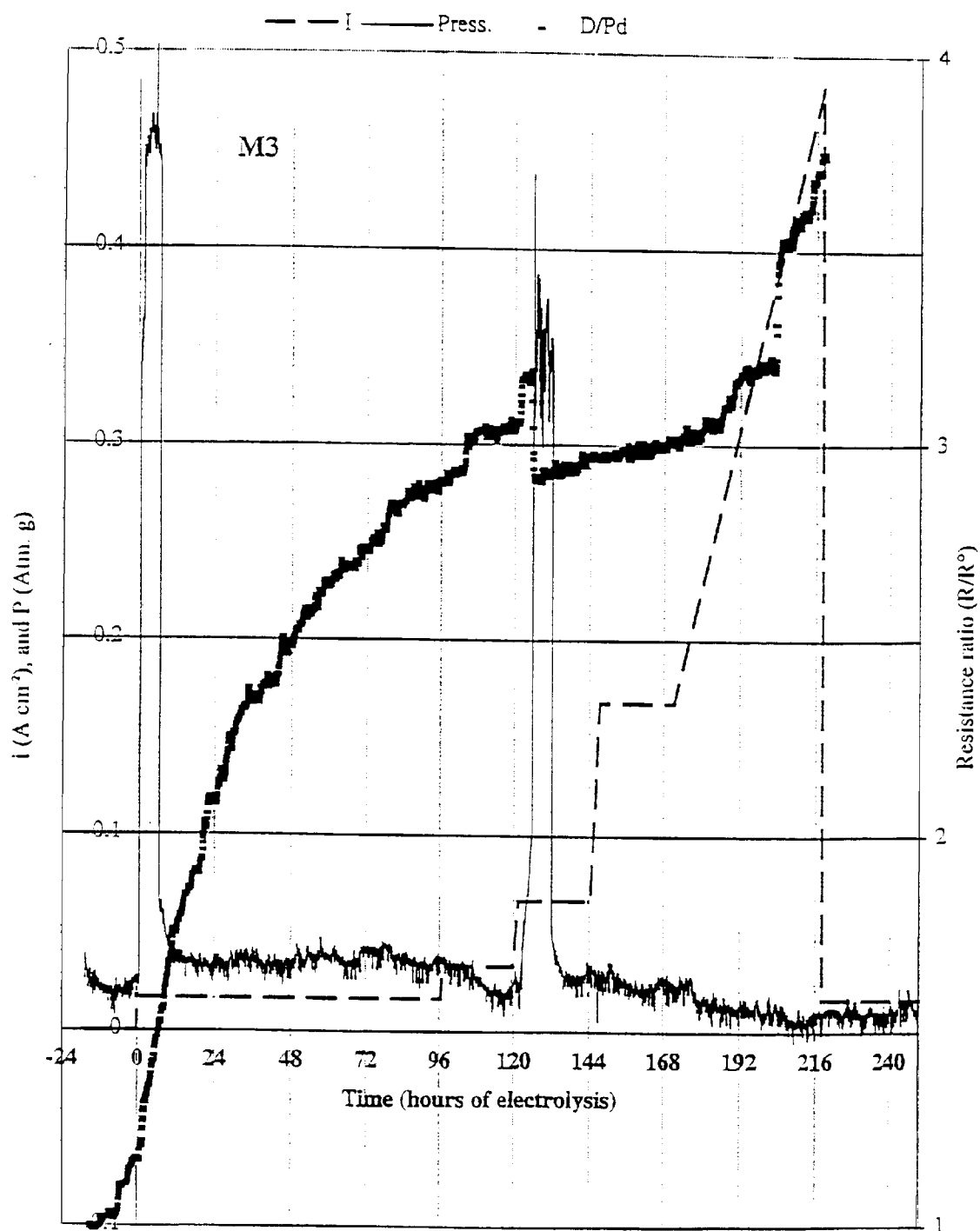
Figure 3-79a
M3 Current density and mass flow -24-240 hours

Figure 3-79b shows the input, output and excess power measured in response to the current stimulus shown in Figure 3-79a. Three features are of note:

iv. Using the same values of conductive loss terms determined for M2, the average excess power (at least for the first 144 h) is very close to zero, suggesting that the calorimeter is well calibrated.

v. Although the average value is very close to zero, P_{xs} exhibits a periodic variation for the first ~ 100 hours of operation.

vi. The calorimeter shows a small endothermic departure from thermal balance with the current ramp. This is expected as the calorimeter is moved from its steady state.

vii. Towards the end of the ramp, the calorimeter exhibits a large, and unexpected endothermic excursion.

The cause of excess power variability (point v, above) was determined to be poor, or intermittent, operation of the recombination catalyst. Figure 3-79c shows the cell current and gas pressure, and the temperature sensed at a point immediately above the platinum basket containing platinum on alumina recombination catalyst. The temperature can be seen to fluctuate at constant cell current, indicating unstable operation. This temperature oscillation is correlated (or anti-correlated) with changes in cell pressure, and excess power. It is clear that the recombination catalyst has not achieved steady state operation. The pressure builds up as electrolysis gases are unrecombined, resulting in a temporary endotherm. At some critical pressure or condition, the catalyst "lights up", recombining gases, reducing the pressure and producing a temporary exotherm. This mode of operation is not calorimetrically desirable, or safe.

Conclusion. Because of the implausible resistance measurements, unstable recombiner function and poor calorimetry, experiment M3 was terminated after 262 hours of operation. On inspection, it was evident that a faulty electrical contact within the cell was the cause of the anomalous resistance measurements (points i-iii, above). No obvious reason was found for the imperfect operation of the recombiner, although this, combined with cell venting, may have produced the endotherm at the end of the current ramp (point vii).
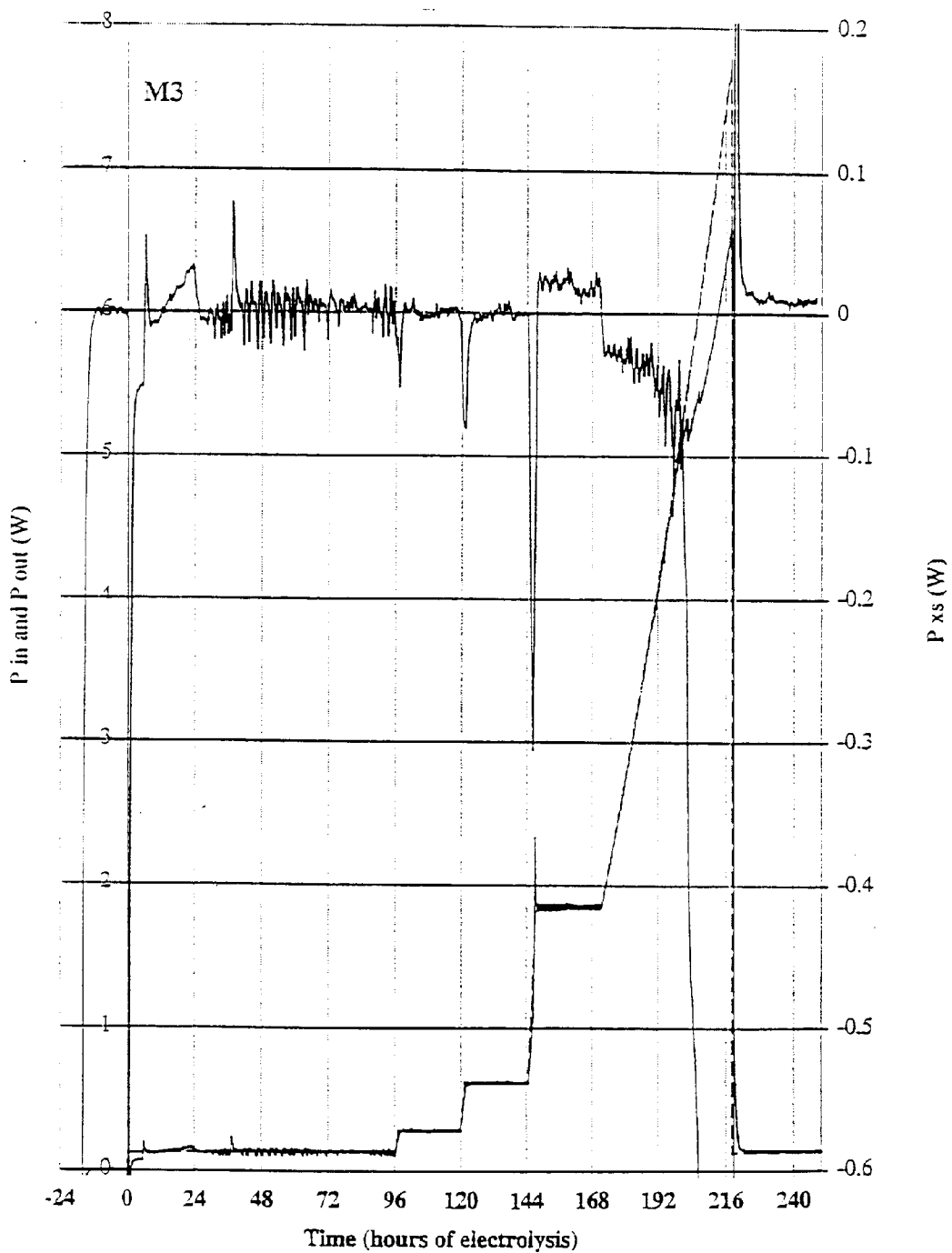
Figure 3-79b
M3 Input and output power -24-240 hours
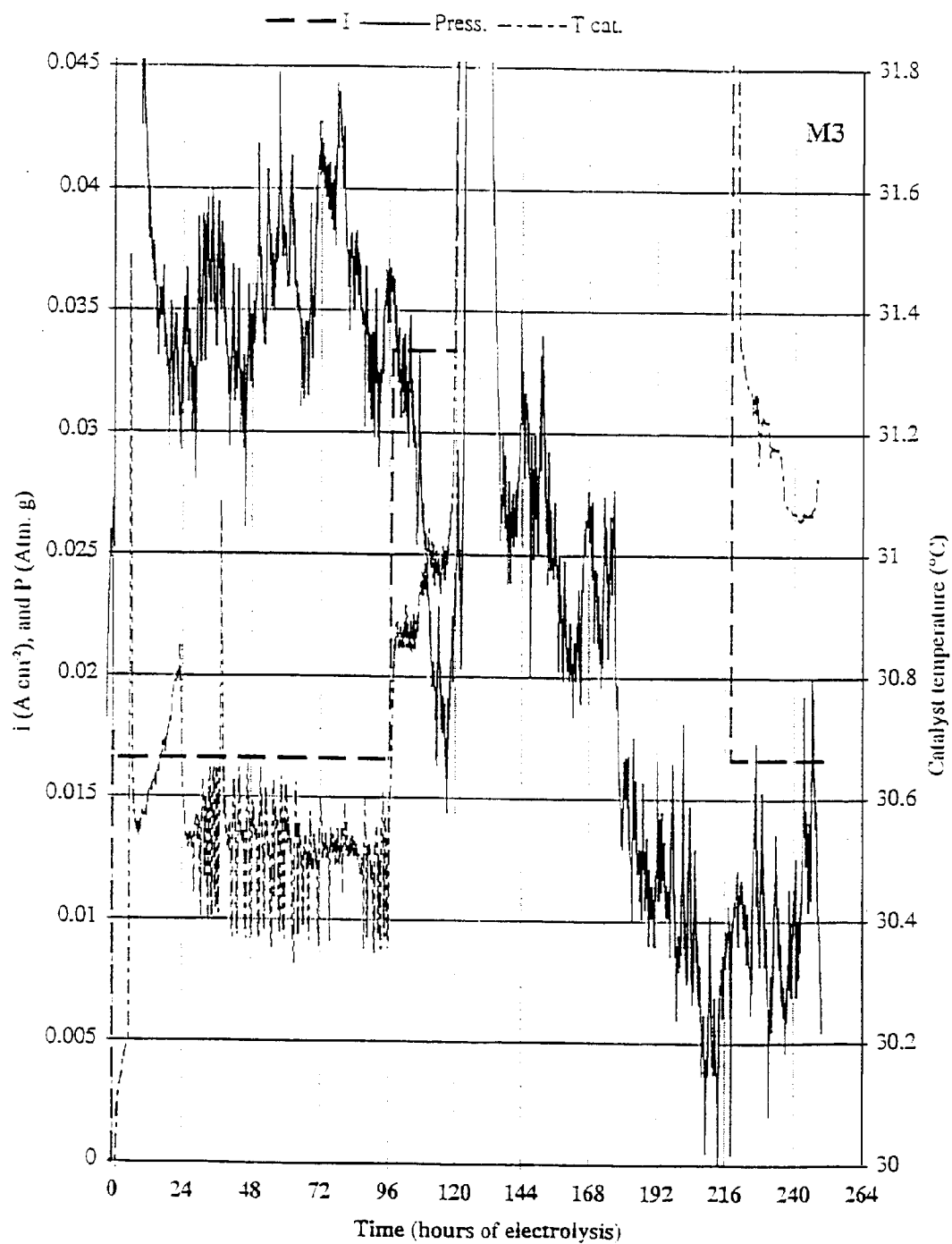
Figure 3-79c
M3 Current density and pressure 0-264 hours

Experiment M4

Cathode:	JM* (low PGM), 0.1 cm dia., x 10 cm long formed into the shape of a "lasso" (see Figure 3-80).
Anneal:	Oxygen gettered vacuum
Contacts:	Five wire, I contacts across ends, V contacts wrapped and spot welded
Electrolyte:	1.0 M LiOD with 200 ppm Al
Monitors:	2 X-ray films outside PTFE liner
Cell sensors:	Pressure Electrolyte temperature Recombiner gas temperature

Calibration and initial load. The empty cell and calorimeter were placed in the water bath ~ 1 hour before electrolyte addition and the application of cell current. Electrolyte was added through a PTFE catheter, with the electrochemical power supply set to control potentiostatically at 2.0V cathodic. When the electrolyte addition was complete it was determined that one of the electrochemical current wires was broken. The cell was removed from the calorimeter and bath, and the fault corrected. The cell was returned to the calorimeter, and the power set to control galvanostatically at 59 mA (19 mA cm^{-2}), approximately 3 hours later. This time of current initiation is the reference point for experiment duration.

Initial loading of the cathode was performed with flowing D_2 gas (~ 0 psig, ~ 10 cm^3 min^{-1} flow). At ~ 22 h, the cell was pressurized to ~ 5 psig (~ 0.3 atm. gauge) and the cell and manifold sealed.

First ramp. Figure 3-81a shows the initial current ramps for M4 to a final current density of 956 mA cm^{-2}. The loading monotonically increased with current density to a final value of D/Pd = 0.857 at 264 h. The pressure shown in Figure 3-81a first decreases (after the cell is sealed at ~ 22 h) with loading of the cathode, then increases with cell temperature as the input power is increased.

I V

V

I

Pt Contact
Wires

Pd Wire
(1 mm diode)

Pt Anode

NM-340581-4
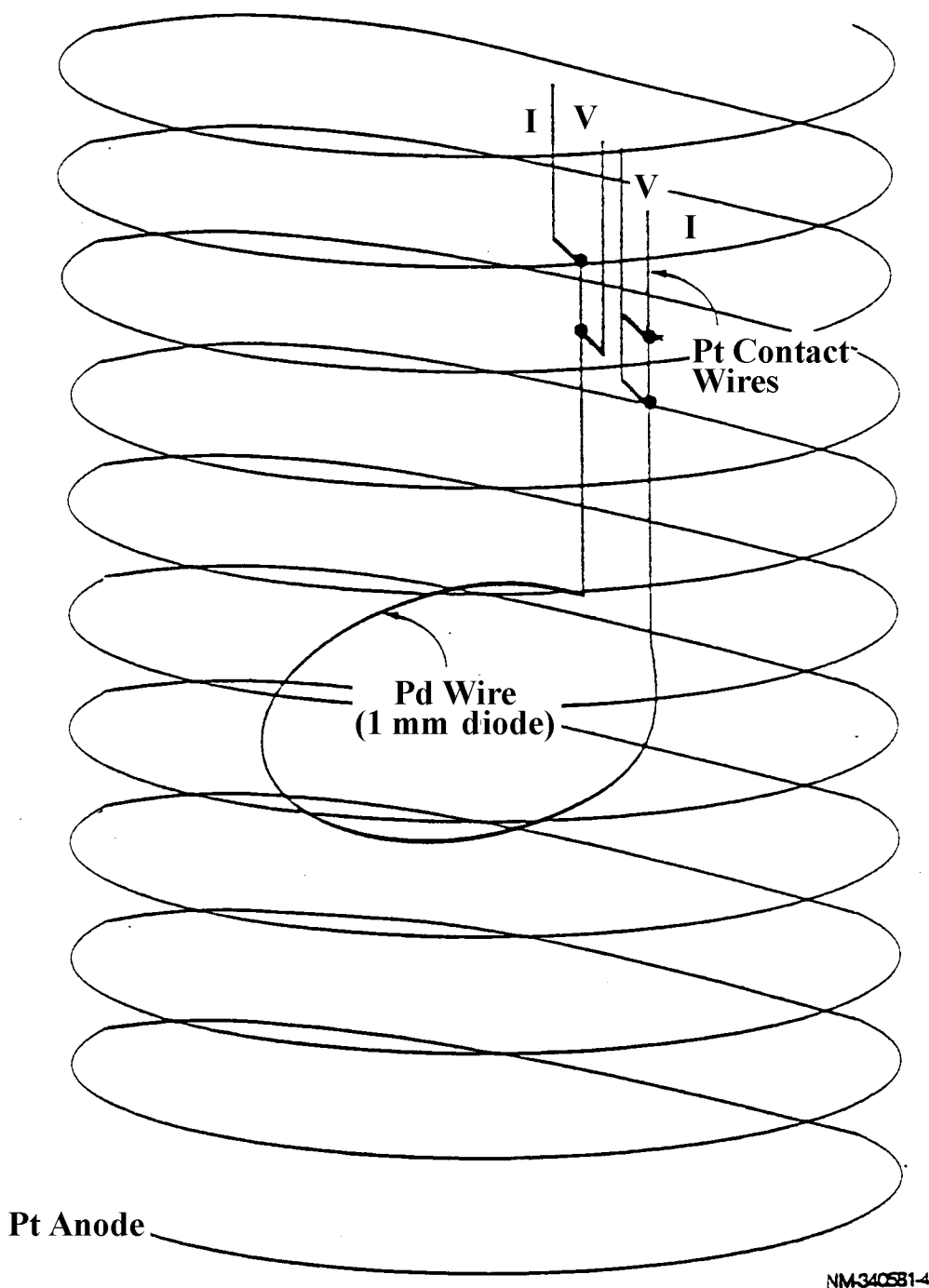
Figure 3-80
M3 Loading
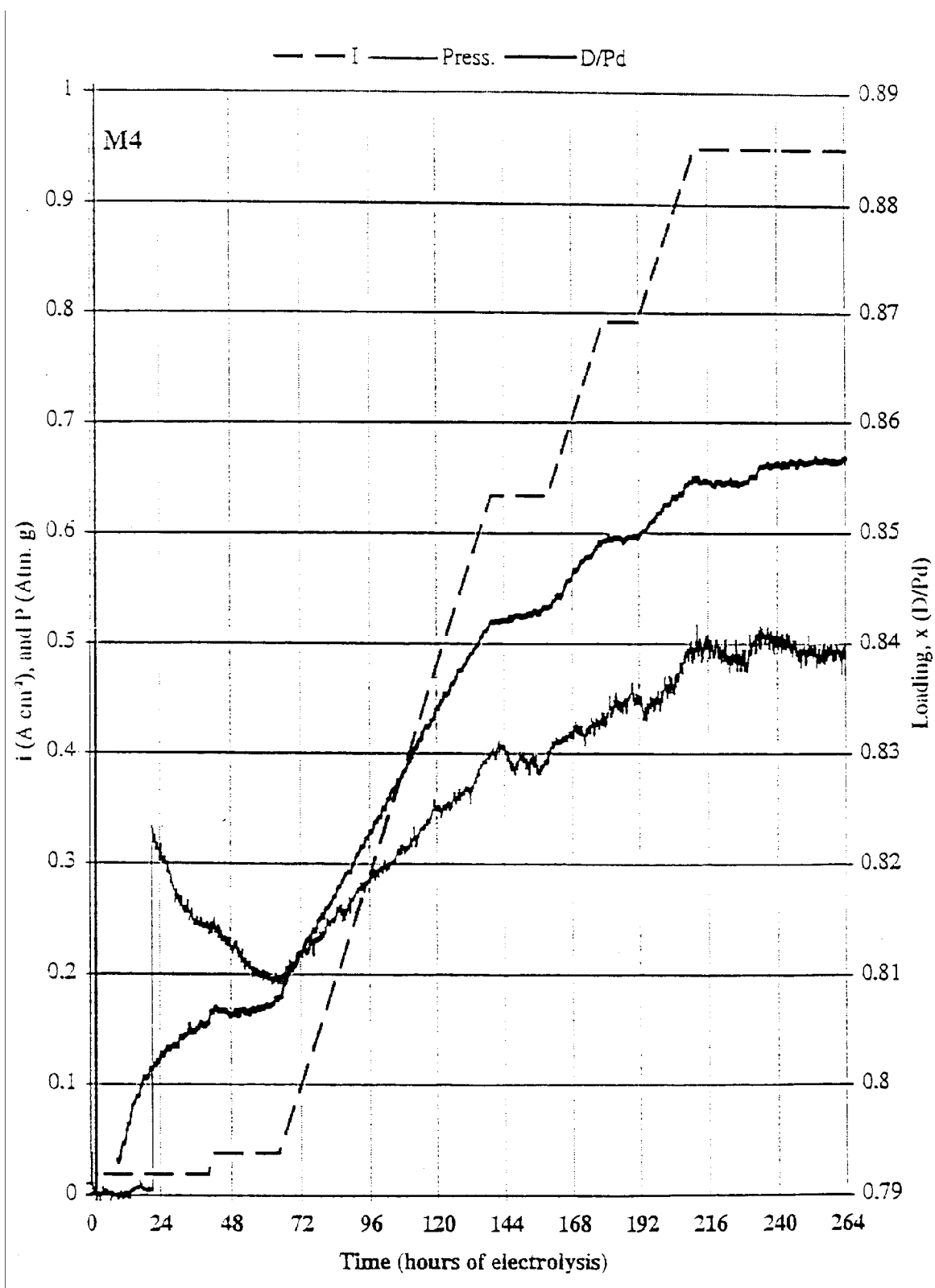
Figure 3-81a
M4 Current density and pressure 0-264 hours

Figure 3-81b shows the input, output and excess power observed during this period. The input and output power, referenced to the left axis, monotonically increase with current density and time. The excess power, referenced to the right hand axis, is shown both as raw data (light) and with application of a non-steady state correction. A small exotherm is observed during the rapid loading phase at $t \leq 20$ h. Apart from this, the calorimeter appears to be in thermal balance, and thus well calibrated. At the highest levels of loading, there is an indication of very small levels of excess power, with $P_{xs} \leq 70 \pm 25$ mW.

For the period shown in Figure 3-81, $0 \leq t \leq 264$ h,

$$E_{xs} = 12 \pm 18 \text{ kJ}$$

$$P_{xs} = 12 \pm 21 \text{ mW}$$

The response of the cathode loading to current density for this cell was slightly unusual. Figures 3-81c and d show loading plotted against current density as both linear and logarithmic plots. It can be seen that, for $i \leq 0.5$ A cm^{-2}, the loading increases linearly with current density;

$$D/Pd = 0.805 + 0.061 \text{ I} \qquad\qquad r^2 = 0.997$$

For $i \geq 0.5$ A cm^{-2}, the loading increases logarithmically with current density, as is more normally observed (see discussion of M1, Figure 3-68).

$$D/Pd = 0.857 + 0.074 \text{ Log [i]} \qquad\qquad r^2 = 0.991$$

Strips, Cu addition, second ramp. At ~ 308 h the cell current density was reduced from 956 to 16 mA cm^{-2}, and shortly thereafter reversed in polarity to strip the Pd surface. During the period of the anodic strip, the cell manifold was opened and 2 ml of 1 M LiOD containing 200 ppm (wt) Cu was added to the cell with D_2 gas flowing. The copper-containing LiOD was followed with 1.5 ml D_2O. The pressure was then set to ~ 5 psig, the cell and manifold sealed, and the current reversed to 16 mA cm^{-2} cathodic.

The cell was held at 16 and then 32 mA cm^{-2}, and then given a brief current ramp to 670 mA cm^{-2}. At ~ 400 h the current was reduced to 16 mA cm^{-2}, and the strip and Cu addition procedure described above was repeated.
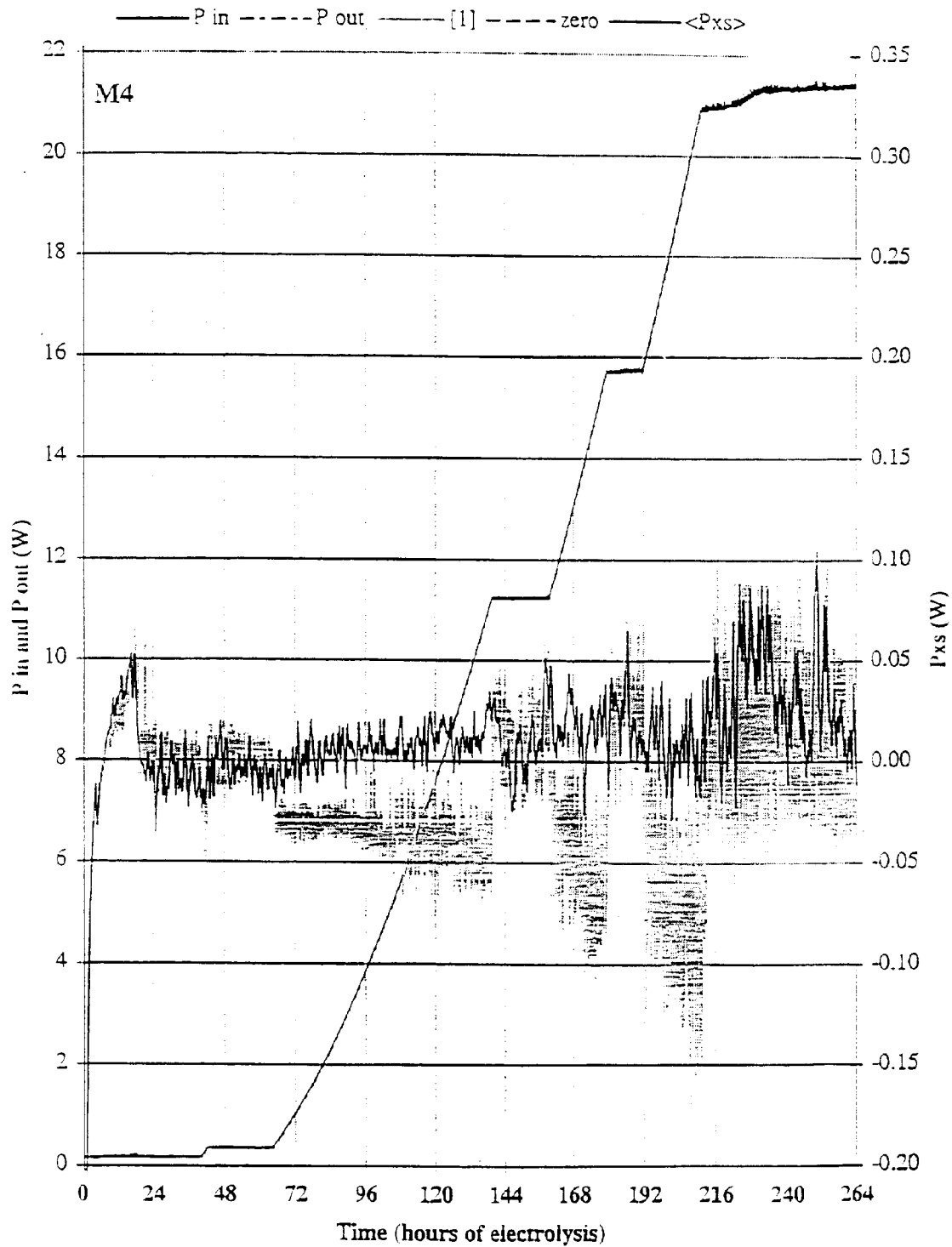
Figure 3-81b
M4 Input and output power 0-264 hours
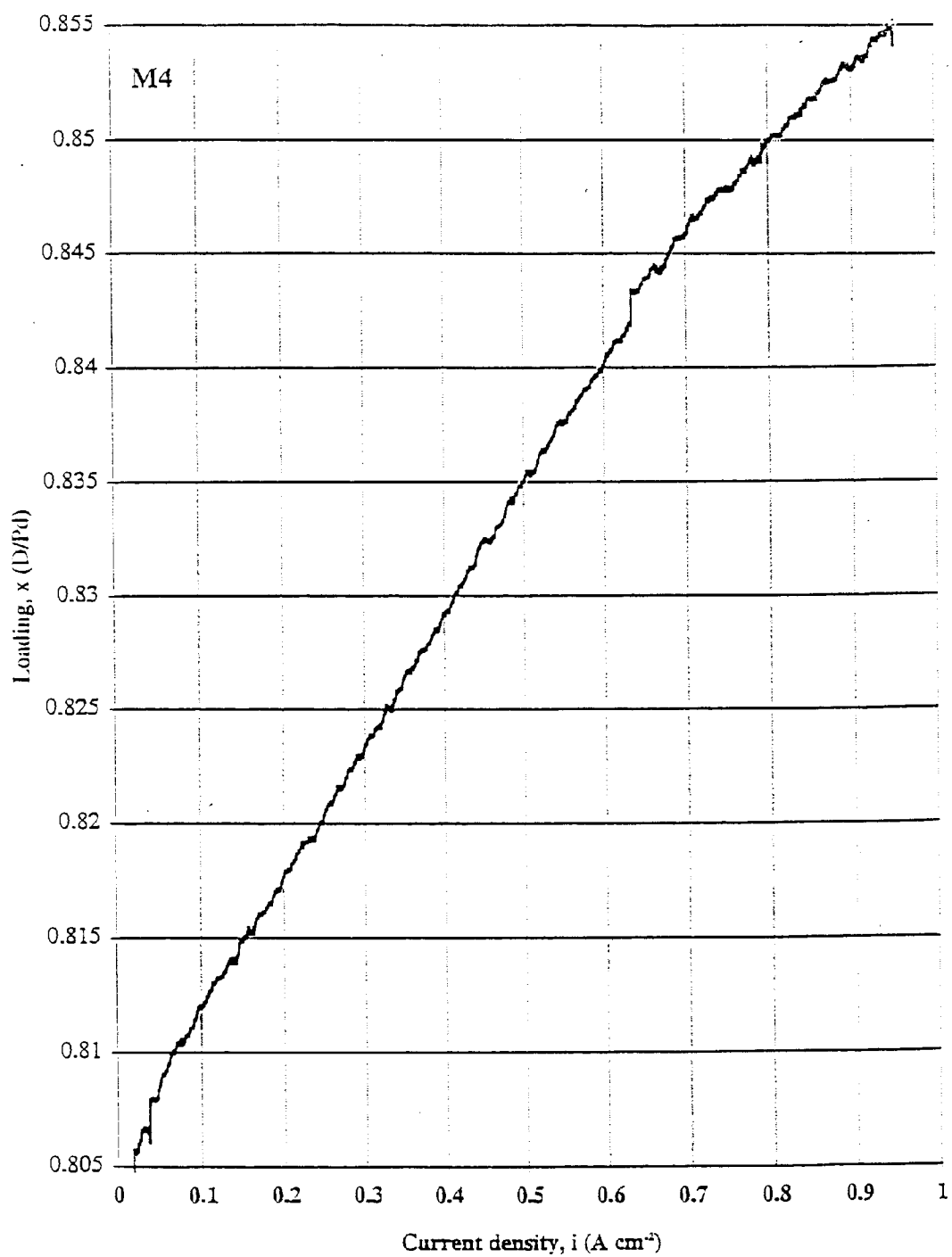
Figure 3-81c
M4 Loading
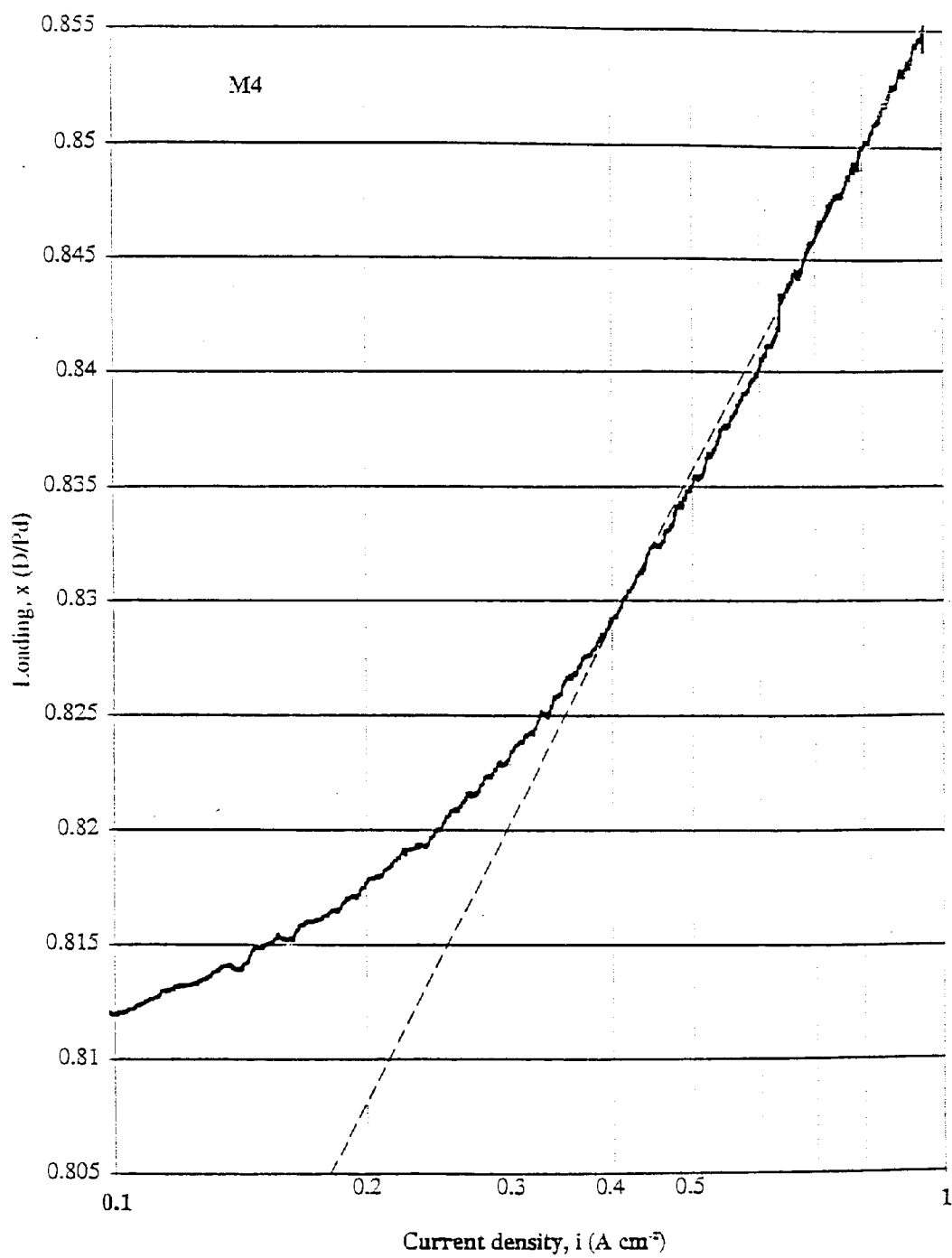
Figure 3-81d
M4 Loading

Figure 3-82a shows the current profile, steps, strips and Cu additions. Following the first strip and Cu addition, the Pd cathode achieved a slightly improved loading (over the first attempt) of D/Pd = 0.862 at 32 mA cm^{-2}. During the current ramp the loading improved to D/Pd = 0.867 at i $\approx$ 150 mA cm^{-2}, but declined as the ramp continued.

Following the second strip and Cu addition, the Pd cathode demonstrated a further improvement in loading, and obtained a loading D/Pd = 0.854 at 16 mA cm^{-2}, and D/Pd = 0.864 at 32 mA cm^{-2}.

In very close association with the current step from 16 to 32 mA cm^{-2} at 472 h, a possibly important change was observed in the properties of the measured resistance ratio (and, consequently, in the inferred loading); the measured resistance exhibited spontaneous fluctuations. No change was made (knowingly) to the electrical circuit at this time, other than repeating a previously made current step. We will discuss this observation further in the analysis of ramp 3.

Figure 3-82b shows the input, output and excess powers for the period 264-504 hours. Until the time of the current reduction at 306h,

P_{xs} = 53 $\pm$ 25 mW

During the subsequent current step, ramp and hold periods,

P_{xs} = 0 $\pm$ 13 mW

The second ramp therefore shows the calorimeter to be extremely well calibrated and operating with very good accuracy and precision. The excess power observed at 956 mA cm^{-2} which persists from 220 to 306, must therefore be treated as a real, although small effect. During this period (220-306 h),

E_{xs} = 17 $\pm$ 8 kJ

This is only a 0.24% response, which is the limit of calorimeter accuracy.
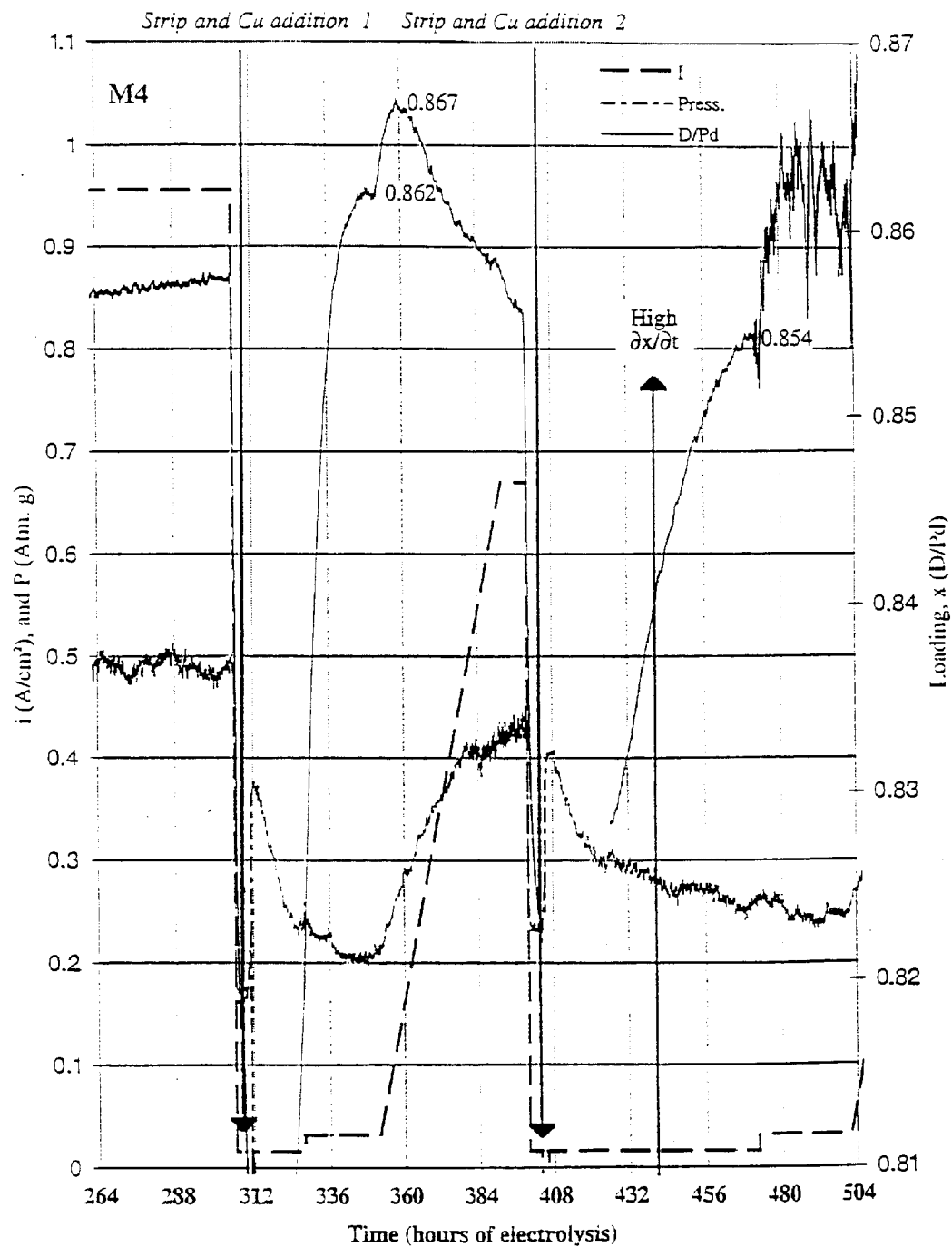
Figure 3-82a
M4 Current density and pressure 264-504 hours
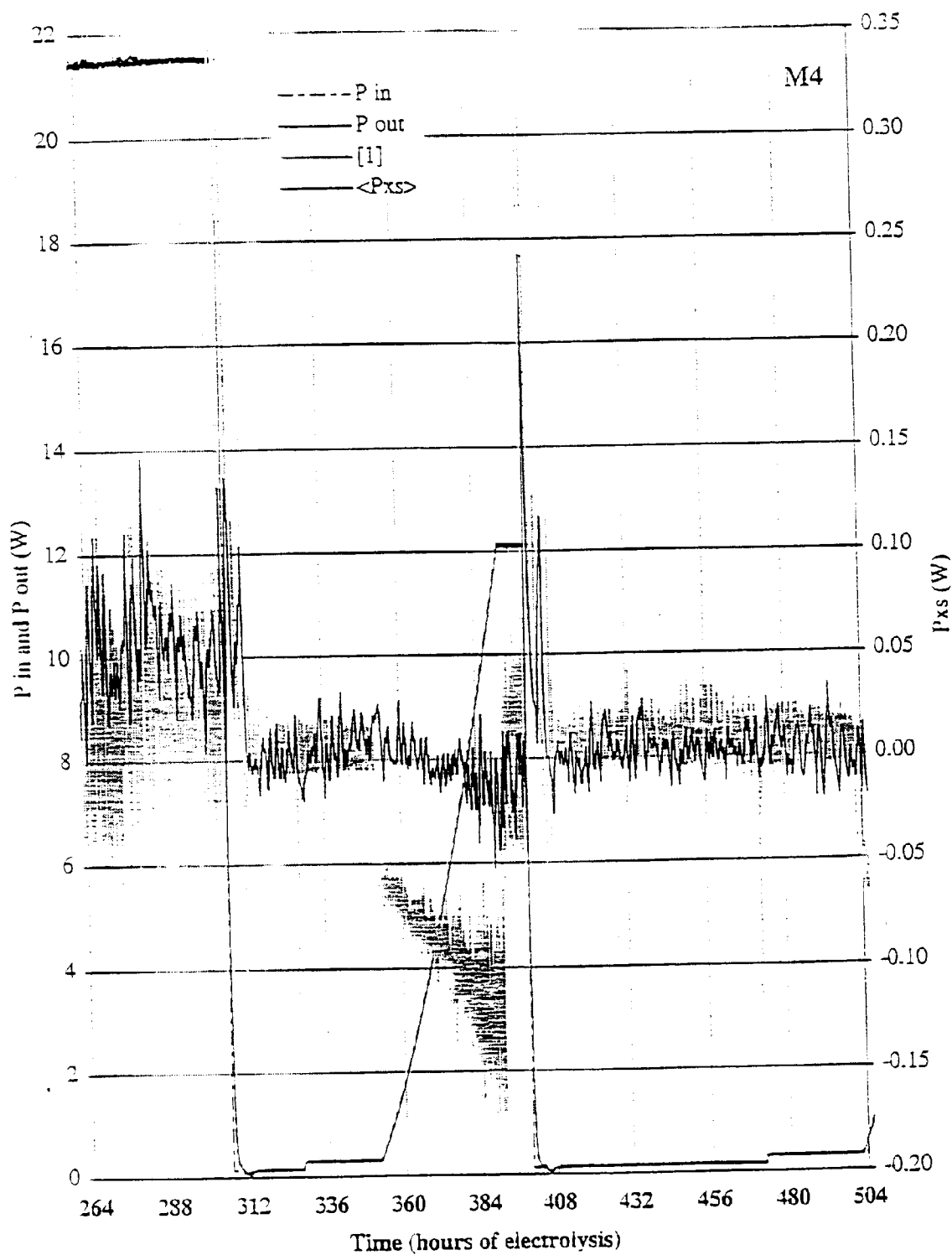
Figure 3-82b
M4 Input and output power 264-504 hours

It should be noted that no measurable excess power was observed during the second ramp to 670 mA cm^{-2}, even though the loading achieved was higher than that obtained on the previous ramp at 956 mA cm^{-2}.

Ramp 3. At ~ 504 h a current ramp was started at 32 mA cm^{-2}. Figure 3-83a shows the current density, cell pressure and loading response of the Pd cathode. Also shown numerically at the top of the graph is the calorimetric mass flow rate, which was varied to permit additional calibration with the calorimeter operating at high input and output power. This graph displays the following features:

i.   The overall envelope of loading responds to the current steps and ramp, but declines with time.

ii. A maximum loading of 0.88 ± 0.01 was achieved at a current density of ~ 376 mA cm^{-2}.

iii. The amplitude of the loading variations, $|\delta x / \delta t|$, varies with time and applied current density. The amplitude increases markedly at 472 h in association with the current step to 32 mA cm^{-2} as noted above. The amplitude $|\delta x / \delta t|$ then generally increases with time but is relatively small during the 24 hour period from ~ 594 to 618 h. The amplitude $|\delta x / \delta t|$ then markedly decreases in close association with the gas sampling at 667 h, and the consequent reduction in cell pressure.

Figure 3-83b shows the input, output and excess power for the period of the third ramp. This plot shows several interesting features.

iv. Excess power appears in two "bursts", each of ~ 2.5 days duration, separated by ~ 1 day.

v.   In the first instance, excess power appears to initiate with the current ramp at a current density i ≈ 425 mA cm^{-2}.

vi. The excess power reaches a local maximum of ~ 340 mW, shortly following the end of the current ramp at 562 h.

vii. At constant current, the excess power is highly variable, displaying a minimum of 0 ± 50 mW, and a maximum of 400 ± 25 mW.

viii. In some instances, changes in excess power appear to be anti-correlated with changes in input power; that is, when the excess power steps down, the input power steps up, and vice versa. [While these changes appear in Figure 3-83b as abrupt steps, they are in fact not. The data reflect a period of 11 days].

ix. Deliberate mass flow variations at the times noted in Figure 3-83a, result in no apparent change in the excess power, in the presence or absence of excess power. The calorimeter thus appears well calibrated, and the effect insensitive to mass flow rate.
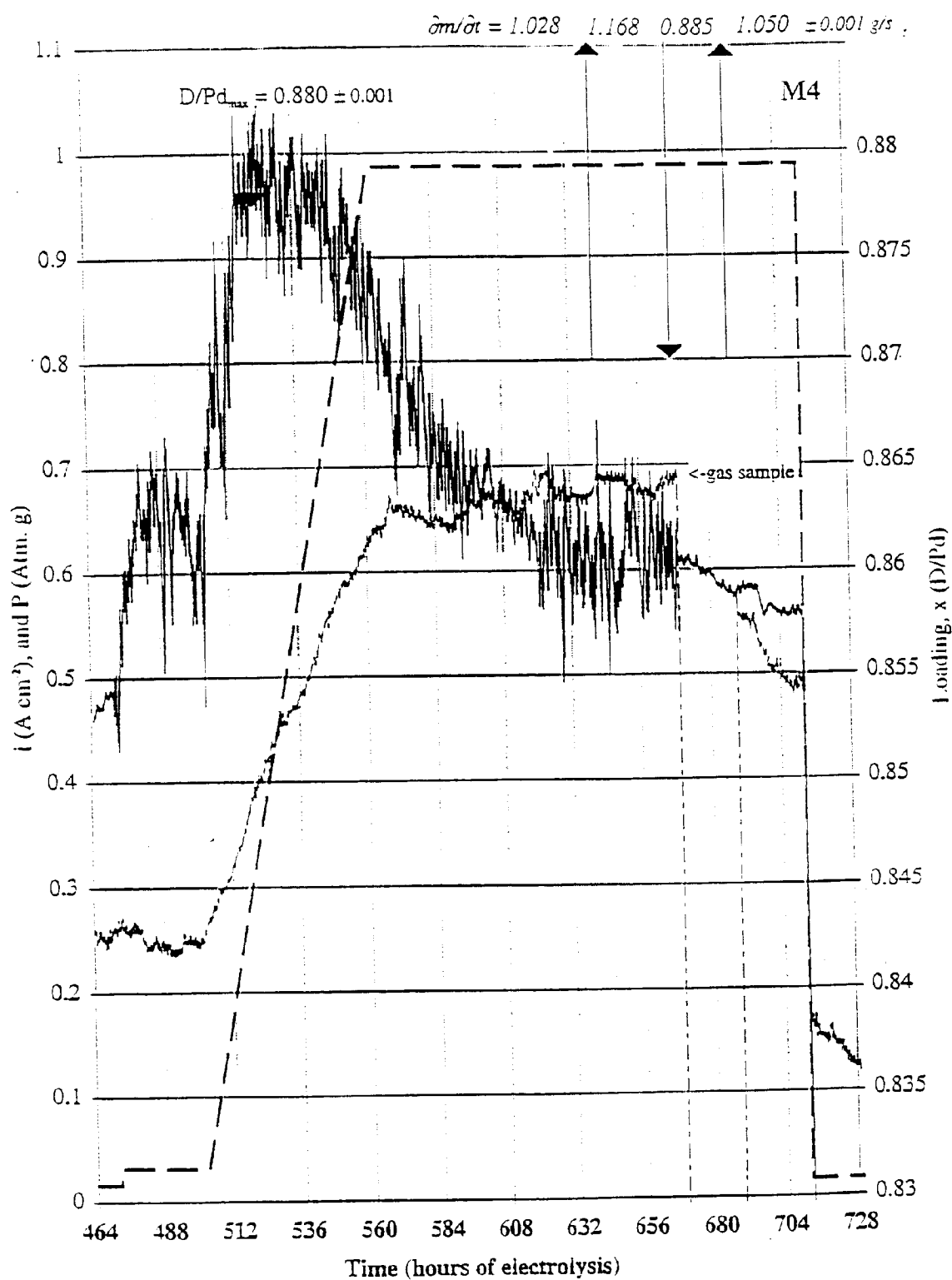
Figure 3-83a
M4 Current density and pressure 464-728 hours
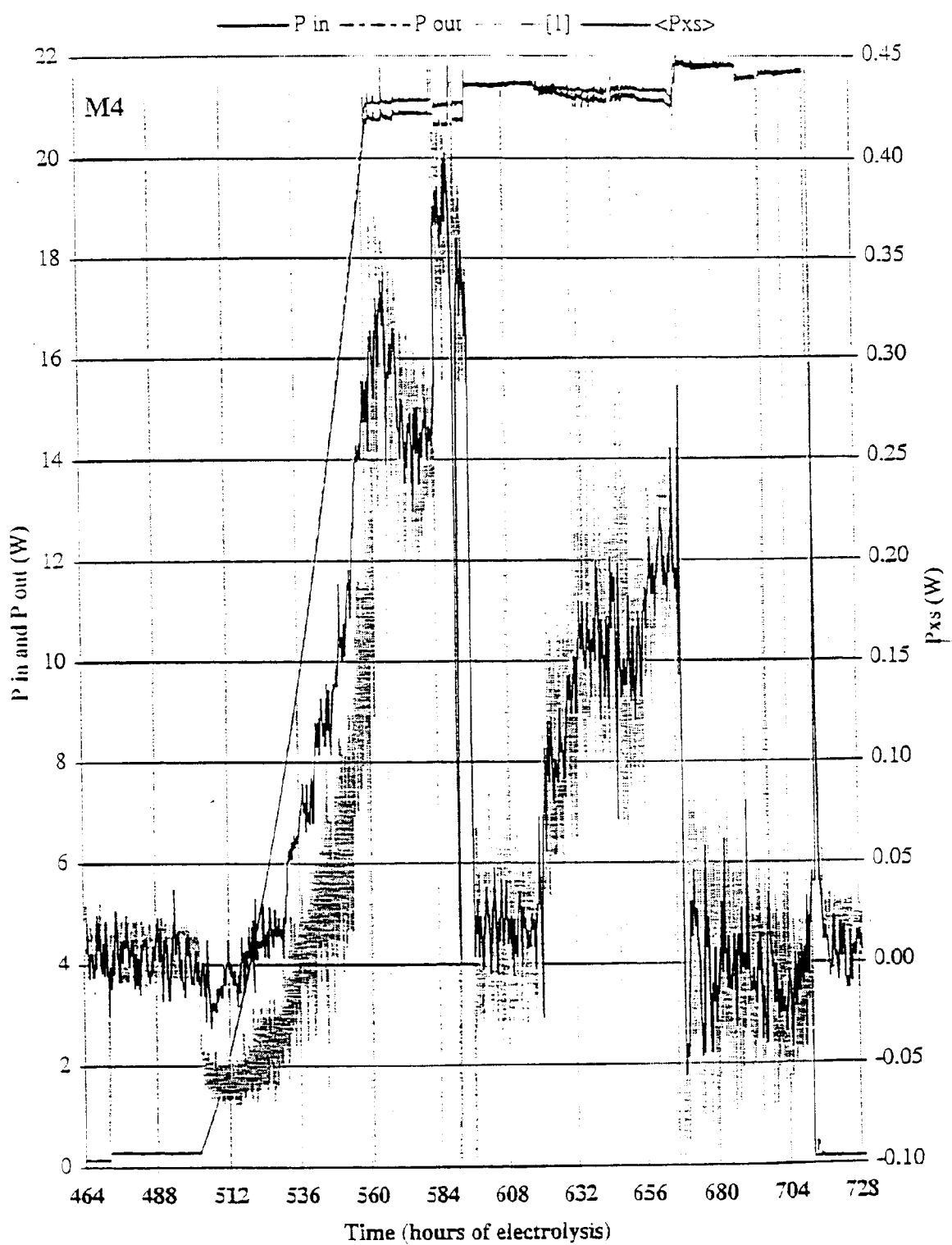
Figure 3-83b
M4 Input and output power 464-728 hours

At constant current, the variability in input power noted in viii above, is reflected in the cell voltage. Figure 3-83c presents the cell voltage and the excess energy (the integral of excess power from t^o = 464 h). The total excess energy observed during ramp 3 was 82.45 ± 27 kJ, or 9.27 MJ/Mole of Pd.

The implications of these data are discussed more fully in the Conclusions to this section. In subsequent experiments with the M4 cell attention was paid to an apparent correlation between excess power and the variation in loading $|\delta x/\delta t|$. Experiments were designed to enhance this variable loading, in an attempt to stimulate excess power production.

Third Cu addition and Ramp 4. At 740 h, the cell was stripped and a third Cu addition made. At 758 h a series of three, six hour heater power steps were made at 5.5, 11 and 22 W, to verify calorimeter calibration, with the cell current at 16 mA cm^{-2}. The current was then stepped to 32 mA cm^{-2} for a period of 12 hours, and the fourth current ramp commenced.

Figure 3-84a shows the current density, cell pressure and cathode loading response. The loading achieved a maximum of 0.898 ± 0.001, shortly into the current ramp, at a current density of ~ 150 mA cm^{-2}. It is clear from Figure 3-84a that the loading variability manifest during ramp 3 (at i ≥ 32 mA cm^{-2}), is not present during ramp 4.

At 1000 h, with the cell current at 3.1 A (956 mA cm^{-2}), an attempt was made to induce a fluctuation in loading with the hope of stimulating excess power production. A current bias of increasing amplitude and alternating sign was applied to the electrochemical current, immediately following the collection of data for each measurement (period 240 s). The increase in amplitude was stopped at a perturbation current of 3.1 ± 1 A; this condition was maintained for ~ 24 hours.

At 1054 h a new pulsing regime was started during which the power supply was controlled to set the cell current to zero for 477 ms every 240 s, immediately following data collection. It is clear from Figure 3-84a that current perturbation of this form did not result in a measurable increase in $|\delta x/\delta t|$; the loading monotonically (and smoothly) declines with time, before, during and following the period of current oscillation. [The measured pressure, temperatures and output power do reflect the current oscillations].
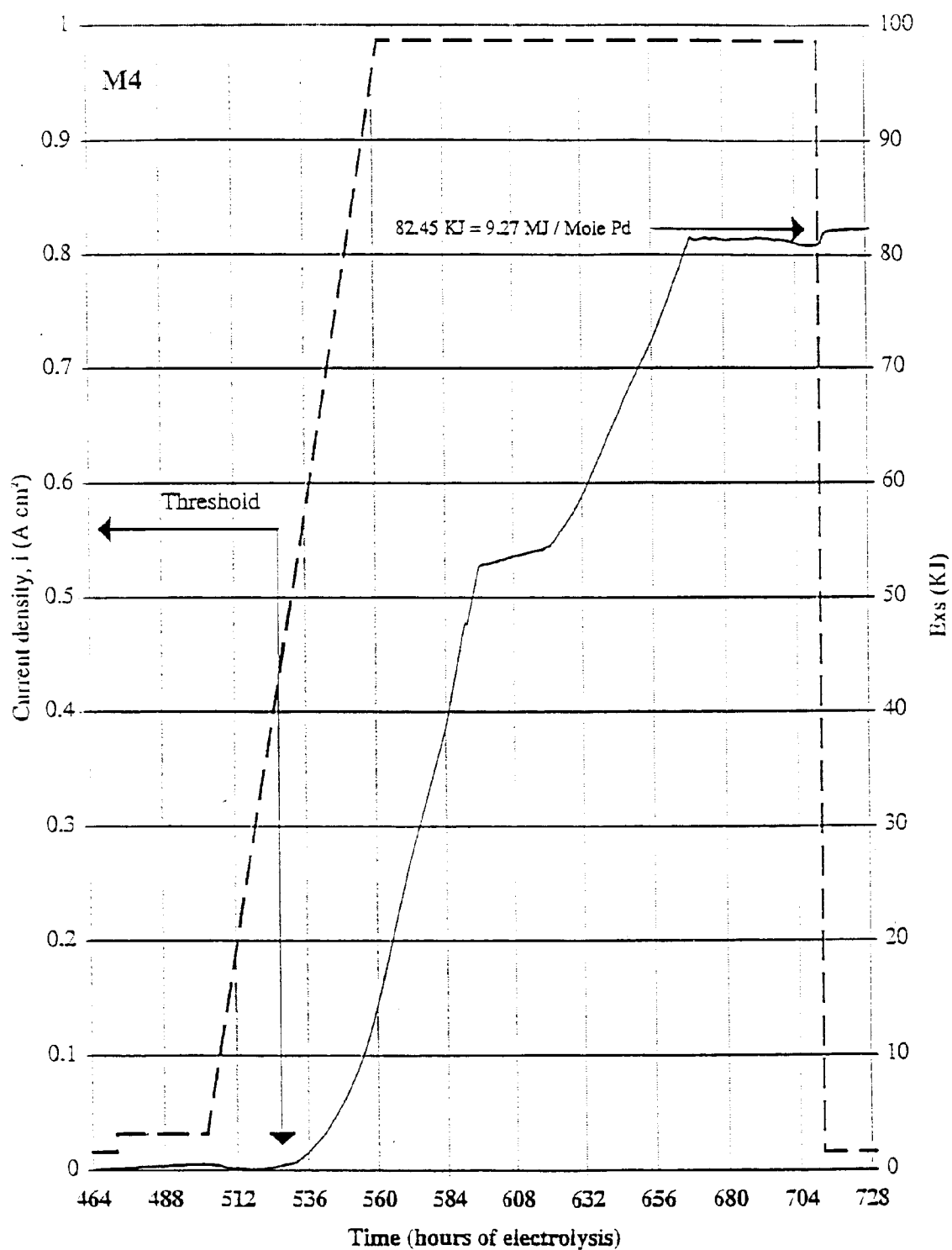
Figure 3-83c
M4 Current density 464-728 hours

$\partial m/\partial t = 1.050 \pm 0.001 \ g/s$

M4

i

D/Pd$_{max}$
= 0.898
$\pm$ 0.001

D/Pd

P

gas sample

i (A cm^{-2}), and P (Atm. g)

Loading, x (D/Pd)

728   776   824   872   920   968   1016   1064   1112

Time (hours of electrolysis)
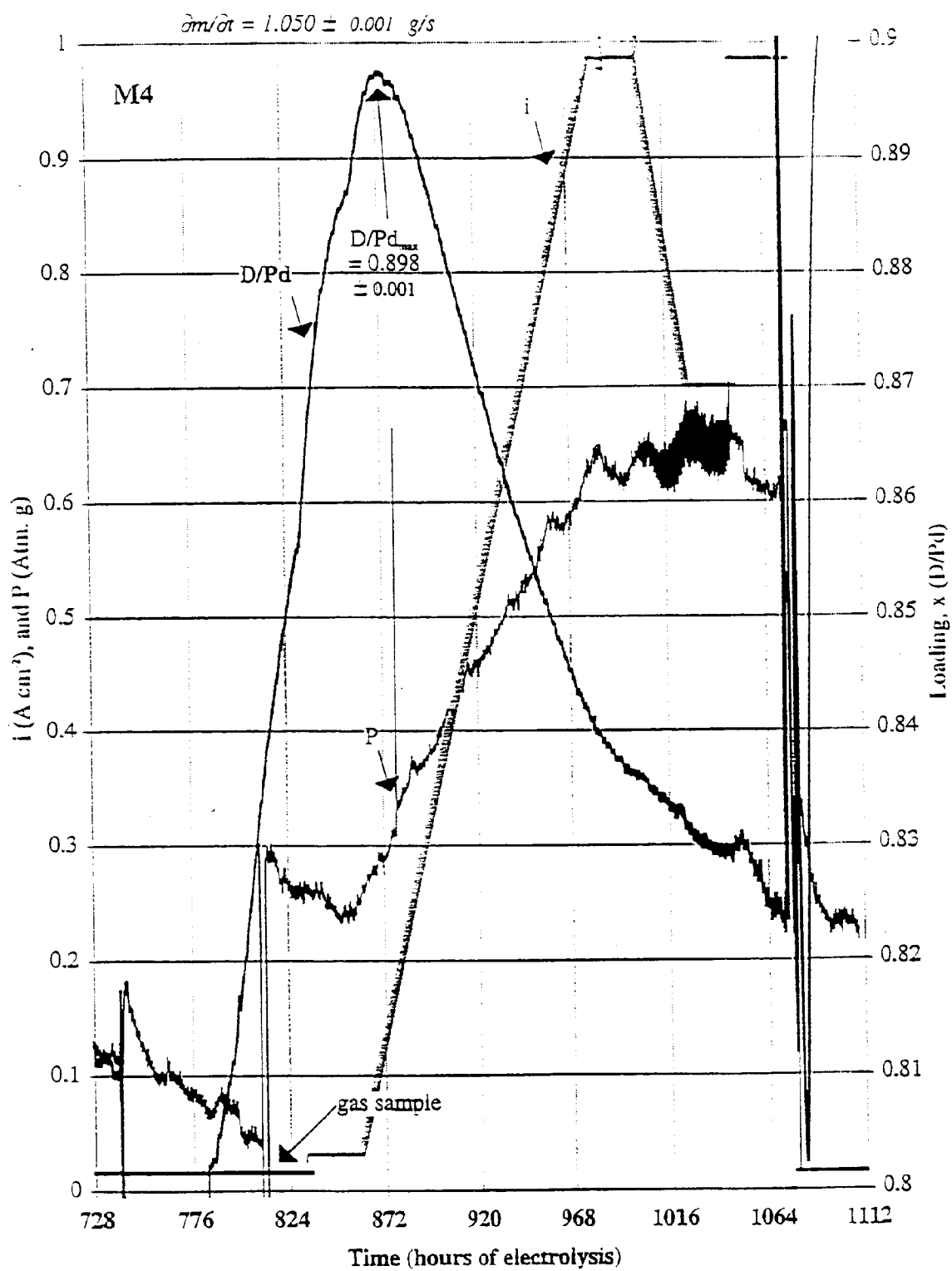
Figure 3-84a
M4 Current density and pressure 728-1112 hours

Figure 3-84b shows the input, output and excess power for ramp 4. The raw data are not shown for P_{xs} because, without non-steady state correction, these are unintelligible. However, the fact that we are able, using the non-steady state correction, to maintain a calorimetric measurement accurate to 50 mW, in the presence of an input power source oscillating by 18W (from ~ 13 to ~ 31 W), is a substantial tribute to the design, execution, performance and accuracy of this calorimeter.

Despite the higher maximum loading, and identical current densities, the cell M4 exhibited no detectable excess power during ramp 4 either in the presence or absence of induced current oscillations. For the period 728-1076 h (when the current was reduced back to 16 mA cm^{-2})

$$P_{xs} = 0 \pm 40 \text{ mW}$$

$$E_{xs} = 4 \pm 26 \text{ kJ}$$

Al addition and Ramp 5. At 1077 h the cell was stripped and 2 cm^3 of 1 M LiOD with 200 ppm Al was added to the cell, followed by 1 cm^3 D_2O, with flowing D_2. At 1078 h the cell was pressurized to ~ 5 psig, the D_2 flow stopped and manifold sealed, and the current was returned to 16 mA cm^{-2}.

At 1154 h the manifold was opened and D_2 gas flow started at ~ 10 cm^3/hour. At 1174 h, a gas sample was taken while D_2 was still flowing. The cell was sealed and pressurized to ~ 5 psig and a current ramp started from 0.1 A to 3.1 A at 25 mA/hour.

At 1336 h a further attempt was made to induce loading variation by switching the current on alternate measurement cycles between 3.1 A cathodic and 0.001 A anodic. Figure 3-85a shows the current, cell pressure and cathode loading response for the current ramps, steps and pulse sequence described above. During the initial ramp the loading reached a maximum of D/Pd = 0.918 ± 0.001 at a current density of ~ 175 mA cm^{-2}. The cathode de-loads monotonically with current density and time. With the introduction of the first cathodic/anodic pulsing at 1334 h, the cathode briefly loads and then de-loads, roughly to its initial value. There is, however, a small indication that this pulse sequence somewhat reversed the trend of slow de-loading; it also introduced a variability in loading, as desired, but the response was small.

$$\partial m/\partial t = 1.050 \pm 0.001 \ g/s$$

M4
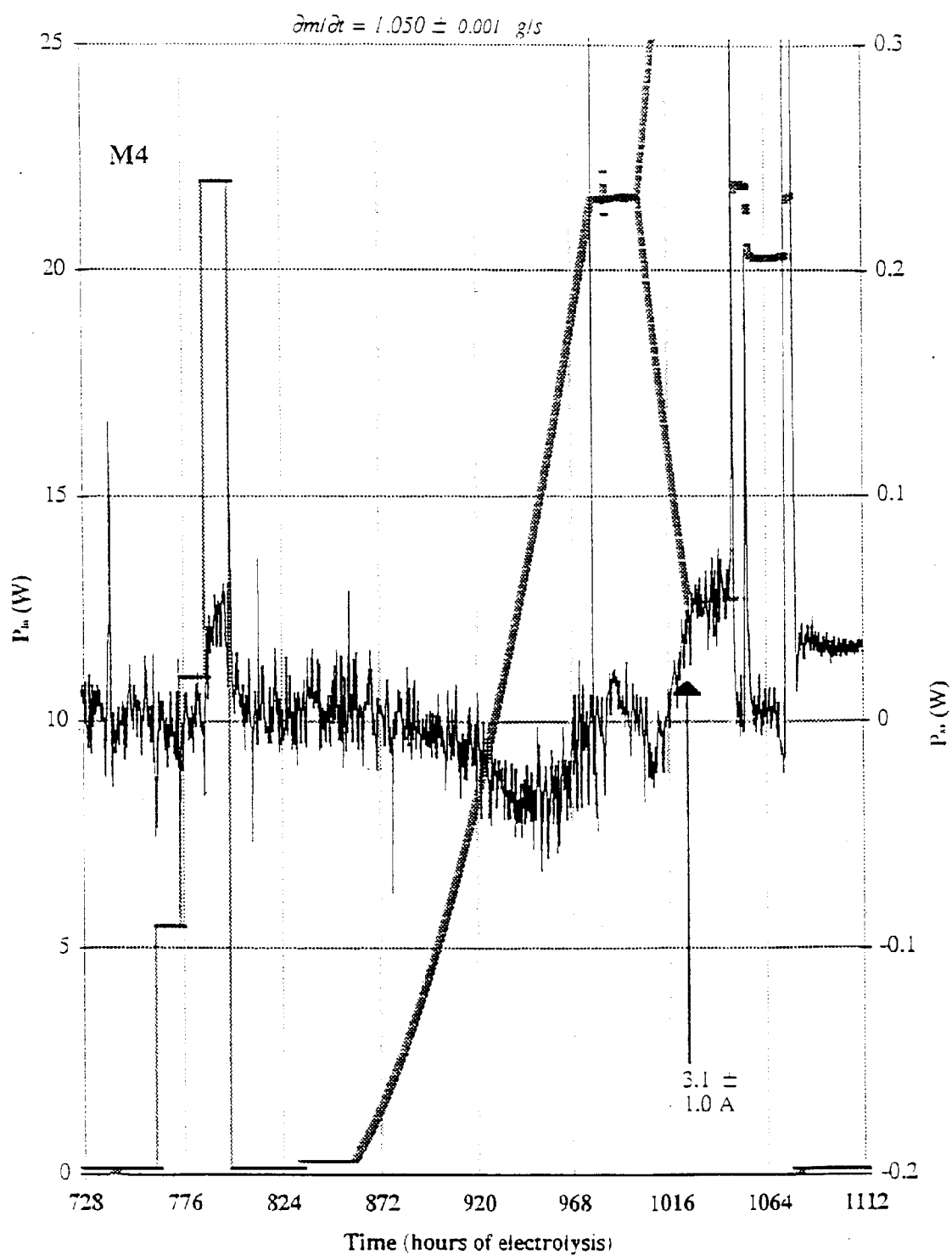
Figure 3-84b
M4 Input power 728-1112 hours
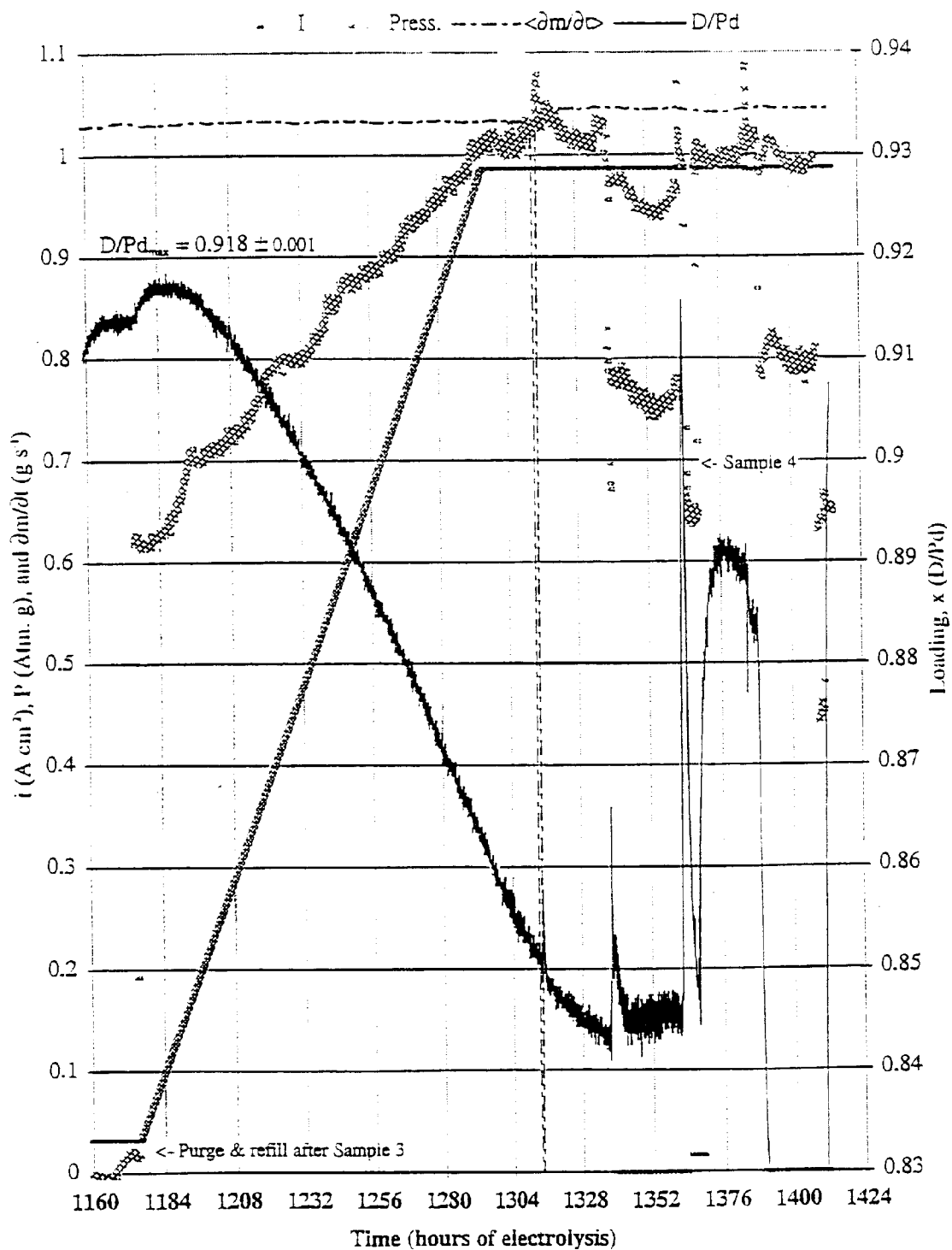
Figure 3-85a
M4 Current density, pressure and mass flow 1160-1424 hours

On terminating the current pulses and re-establishing a constant cathodic current of 3.1 A (956 mA cm^{-2}), the cathode loaded rapidly, and then de-loaded when the current was dropped to 50 mA cathodic (16 mA cm^{-2}). The implications of this observation, and the success of attempts to reproduce the effect which gave rise to rapid loading are discussed subsequently in the section in **M-Series Conclusions.**

Figure 3-85b plots the input, output and excess power for the period of ramp 5. The raw data are calculated as the average of adjacent pairs of data points to somewhat remove the effect of the imposed power oscillation. As for ramp 4, the excess power initially shows a small endothermic response that is not fully corrected for by the non-steady state correction. During periods of current oscillation the calorimeter appears to be slightly endothermic; this effect is due to asymmetric voltage transients associated with switching to and from high current. It is clear, however, from Figure 3-85b that the cell M4 exhibited no detectable positive excess power during ramp 5 (as for ramp 4), either in the presence or absence of induced current oscillations. For the period 1076-1408 hours.

$$P_{xs} = -25 \pm 25 \text{ mW}$$

$$E_{xs} = -4 \pm 24 \text{ kJ}$$

Attempts at pulsed loading. A series of experiments was performed to determine the conditions under which loading enhancement might be achieved by a variety of anodic strips, current interrupts, and anodic/cathodic pulse sequences. Table 3-4 summarizes the procedures employed, and the results achieved. Figure 3-86a plots the current density, cell pressure and cathode loading obtained during the period covered by Table 3-4. Figure 3-86b plots the input, output and excess power for the same period.

It is clear from Table 3-4 that a benefit is obtained in achieving enhanced loading after the following procedures:

i.   Maintaining the cell at open circuit for a period of time (operation 17 in Table 3-4).

ii. Anodic/cathodic pulsing, with the anodic limit ~ 1 mA cm^{-2} (operations 1, 3, 5, 7, 9, 21 and 24 in Table 3-4).

iii. Brief anodic strips at ~ 1 mA cm^{-2} (increasing benefit with increasing hold time; operations 11, 13, 15).
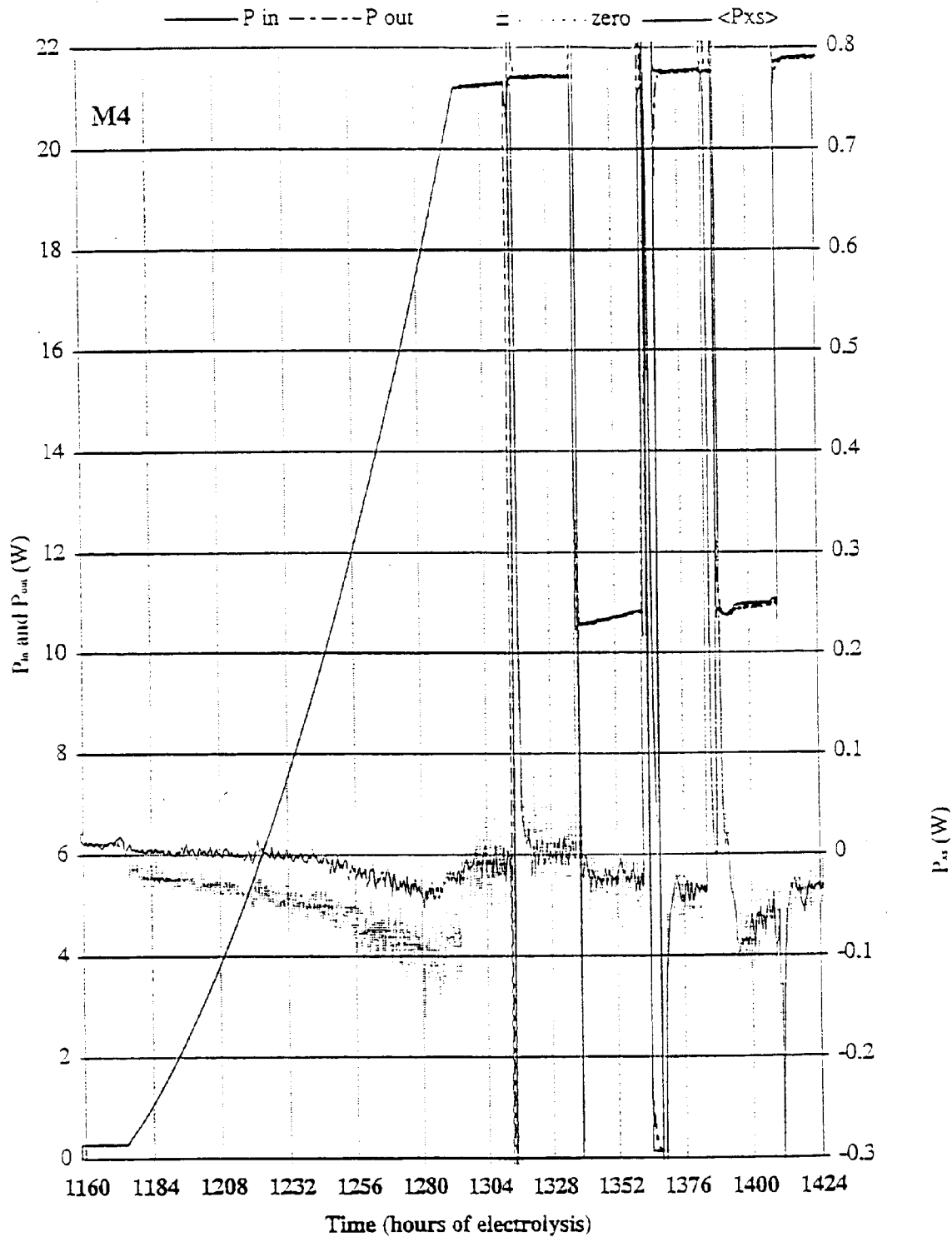
Figure 3-85b
M4 Input and output power 1160-1424 hours
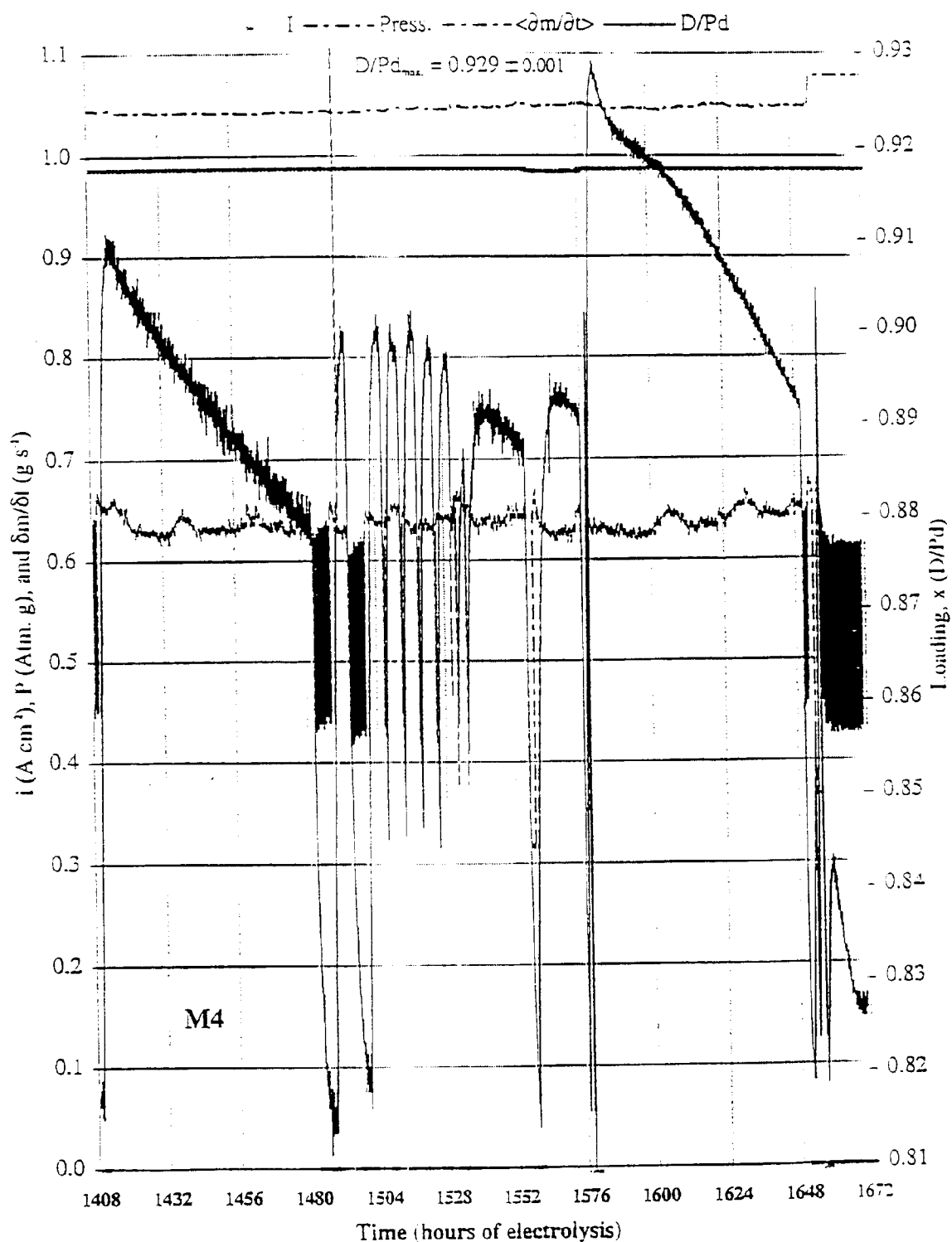
Figure 3-86a
M4 Current density, pressure and mass flow 1408-1672 hours
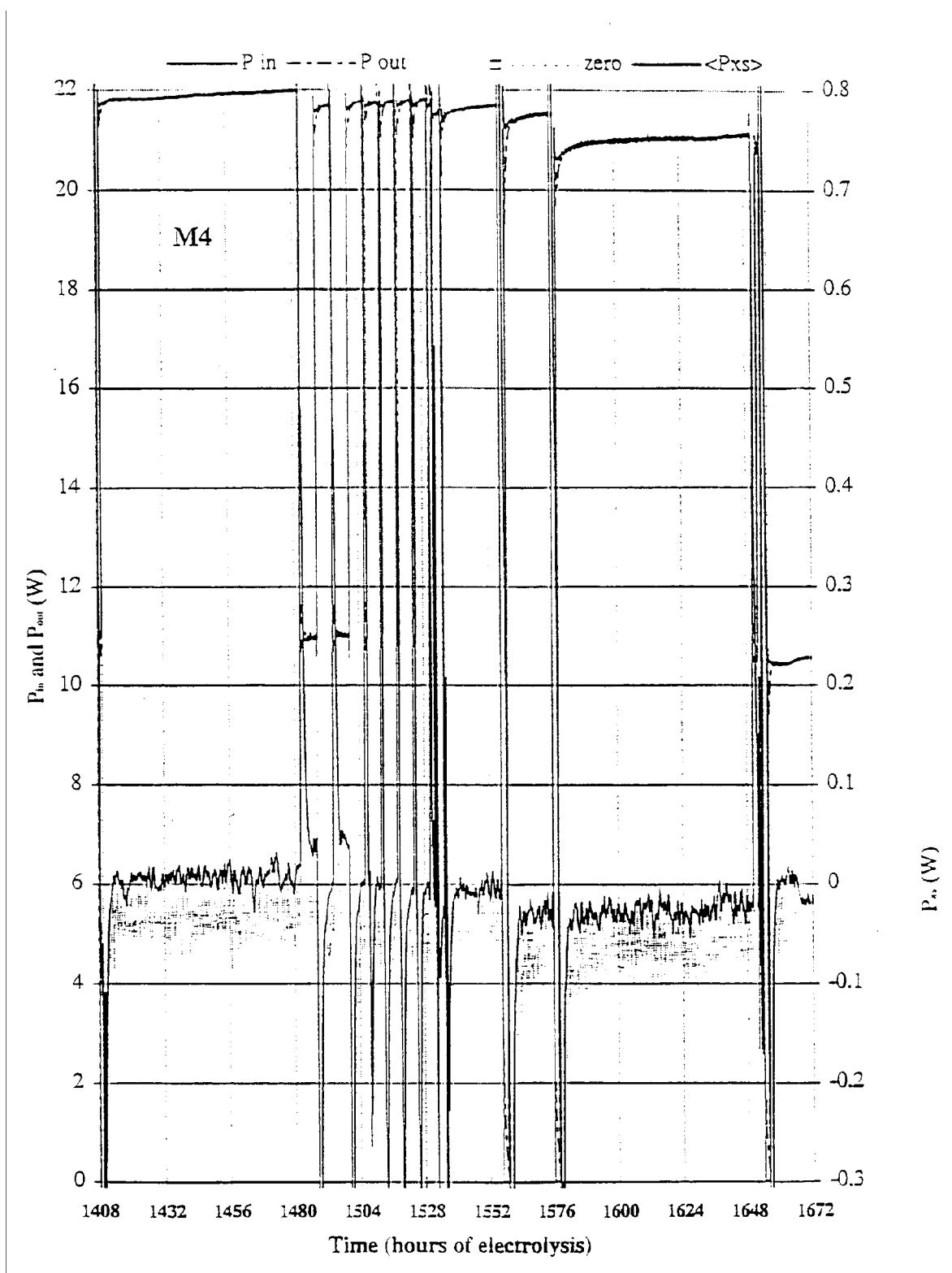
Figure 3-86b
M4 Input and output power 1408-1672 hours

Table 3-4
Summary of Pulse Procedures

	Time		Duration (h) Expt.	Duration (h) Process	i low (mA/cm^{-2})	i high (mA/cm^2)	D/Pd	Max	Min
1	9/16/94	10:24	1408.6	1.3	-0.001	0.987 pulse	0.818		0.817
2	9/16/94	11:44	1410.0	72.3	0.987	0.987 dc	0.818	0.909	
3	9/19/94	12:04	1482.3	6.1	-0.001	0.987 pulse	0.879		0.816
4	9/19/94	18:12	1488.4	5.9	0.987	0.987 dc	0.817	0.900	
5	9/20/94	0:04	1494.3	6.1	-0.001	0.987 pulse	0.900		0.819
6	9/20/94	6:12	1500.4	5.9	0.987	0.987 dc	0.822	0.901	
7	9/20/94	12:04	1506.3	1.1	-0.001	0.987 pulse	0.900		0.846
8	9/20/94	13:12	1507.4	4.9	0.987	0.987 dc	0.845	0.900	
9	9/20/94	18:04	1512.3	1.1	-0.001	0.987 pulse	0.895		0.848
10	9/20/94	19:08	1513.4	16.9	0.987	0.987 dc	0.848	0.902	
11	9/21/94	12:00	1530.2	0.1	-0.001	4 min. anodic	0.896		
12	9/21/94	12:04	1530.3	1.8	0.987		0.892	0.882	
13	9/21/94	13:54	1532.1	0.2	-0.001	10 min. anodic	0.880		
14	9/21/94	14:04	1532.3	3.2	0.987		0.870	0.887	
15	9/21/94	17:17	1535.5	0.3	-0.001	16 minutes anodic	0.885		
16	9/21/94	17:33	1535.8	20.9	0.987		0.865	0.894	
17	9/22/94	14:24	1556.6	2.5	0.000	Open Circuit	0.888		0.814
18	9/22/94	16:52	1559.1	16.9	0.985	Close Circuit	0.818	0.894	
19	9/23/94	9:444	1576.0	2.1	-0.016	Anodic Strip	0.890		0.560
20	9/23/94	11:52	1578.1	72.2	0.987	Cathodic	0.576	0.929	
21	9/26/94	12:04	1650.3	2.0	-0.001	0.987 pulse	0.891		0.819
22	9/26/94	14:04	1652.3	0.0	0.987	0.987 dc	0.819	0.857	
23	9/26/94	15:48	1652.3	3.7	-0.013	Strip at -0.8V	0.819		0.545
24	9/26/94	17:44	1656.0	21.2	-0.001	0.987 pulse	0.551	0.843	
25	9/27/94	14:56	1677.2	23.9	-0.988	0.987 oscillation	0.599		
26	9/28/94	14:48	1701.0		0.987	0.987 dc	0.817		

iv. A more extended anodic strip under galvanostatic conditions at ~ 16 mA cm^{-2} (operation 19)

v. A constant voltage anodic strip, up at ~ -0.8V (operation 23).

The benefits achieved by these processes, thought to clean or refurbish the Pd surface, appear to increase with increasingly aggressive procedures. That is, the larger the anodic current (or voltage) and the longer the procedure, the greater the benefit observed in subsequent re-load steps. None of the procedures attempted, however, yielded the benefits observed following the initial pulsing sequence from 1336-1362 h. This first instance of pulsing, also, was the only one which did not result in net cathode de-loading.

One procedure which did not yield a beneficial effect on loading was the ~ ± 1A cm^{-2} oscillation (25 in Table 3-4). This oscillation did appear to have profound effects on the cathode which are discussed more fully below.

Because of the large number of power steps in the period covered by Table 3-4, an accurate determination of the total excess energy cannot be made. Figure 3-86b shows the input, output and excess power calculated for this period; the raw data for P_{xs} are offset slightly for clarity. From observation of Figure 3-86b it is clear that no appreciable amount of excess power was observed, even at times when the loading was as high as D/Pd ≈ 0.929. For the period 1408-1672 h we estimate

$$E_{xs} = 0 \pm 35 \text{ kJ}$$

At 1701 h the pulsing was stopped and the power supply was set to deliver a 3.1 A continuous cathodic current. At 1718 h the current was reversed in polarity for nearly 30 h in order to strip all D from the Pd and re-determine a value for R$^{\circ}$. At 1744 h the cathode was re-loaded, and attained a (modest) loading of 0.83 at 3.1 A (956 mA cm^{-2}).

Figure 3-87a shows the current density, cell pressure, calorimetric mass flow and resistance ratio until the termination of M4. At 1672 h, under the influence of alternating current pulses ~ 1 A cm^{-2} cathodic and ~ 1 mA cm^{-2} anodic, the resistance ratio was stable at ~ 1.93 on the right side of the maximum; a loading of D/Pd ≈ 0.83. When the pulsing begins, at the point indicated by the first arrow in Figure 3-87a, several interesting features are observed in the measured resistance.
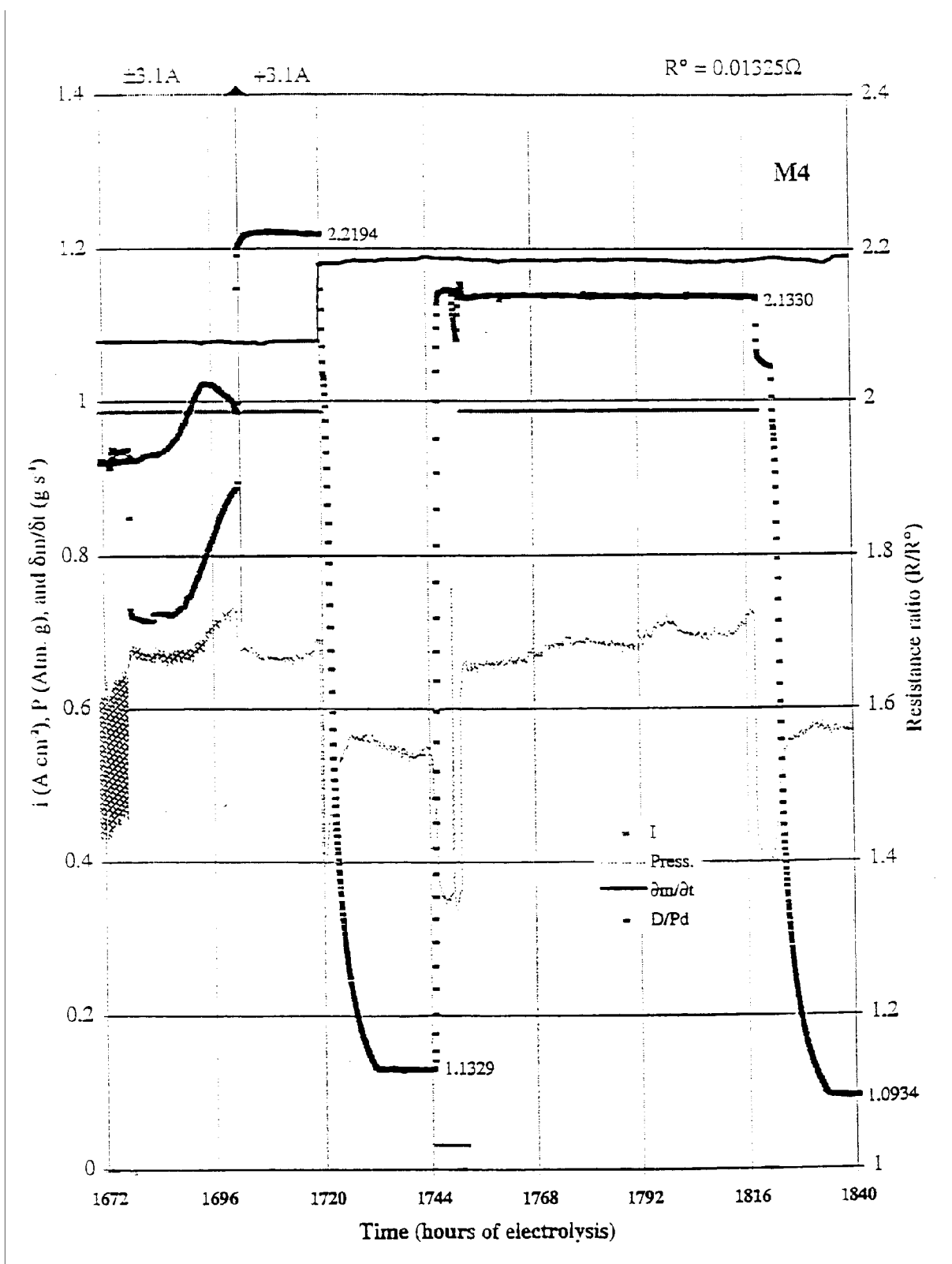
Figure 3-87a
M4 Current density, pressure and mass flow 1672-1840 hours

i. Unlike the preceding pulse regime, under the influence of ± 1 A cm⁻² current oscillation, the cathode displays marked loading and de-loading on alternate cycles, as shown by the divergence of the R/R^o trace in Figure 3-87a.

ii. The resistance of the branch measured at the end of the cathodic half cycle (the upper branch between the arrows in Figure 3-87a) increases from the initial value, passes through a maximum and begins to decrease.

iii. The resistance of the branch measured at the end of the anodic half cycle (the lower branch between the arrows in Figure 3-87a) increases in value, essentially monotonically, by ~ 13%.

iv. When the current was restored to ~ 1 A cm⁻² cathodic, the resistance ratio rises to a roughly constant value of $R/R^o \approx 2.22$. When stripped completely, at 1744 h, the measured resistance ratio $R/R^o \approx 1.133$.

v. When this cycle was repeated, the resistance ratio rises on loading to $R/R^o \approx 2.13$, and when fully stripped falls to $R/R^o \approx 1.09$.

Provided that the Pd electrode does not undergo mechanical change, and is influenced only by the absorption and desorption of D, we expect the resistance ratio to be bounded such that $1 \leq R/R^o \leq 2$. Clearly, something unusual must have happened to the Pd electrode.

Figure 3-87b shows the input, output and excess power from 1072 - 1840 h. During the period of ± 1 A cm⁻² current oscillation, the calorimeter appears to be operating endothermically by about 0.5 W. In fact, this is due to the asymmetric transient voltage responses to the up-going and down-going current steps. These transients were integrated completely by digitizing the transient waveform to calculate the net power for each cycle. The open squares plotted in Figure 3-87b show the results of this calculation for a selected set of data. Clearly, these data coincide with the alorimetrically determined endotherm. We can conclude, therefore, that, during the period of current oscillation and up until the experiment end at 1840 h, $P_{xs} = 0 \pm 50$ mW and $E_{xs} = 0 \pm 17$ kJ.

Table 3-5 summarizes the measured resistances during this period. In the column labeled "$R^{o\prime}$", we calculate the presumed value based on the measured R/R^o, with the following assumptions:

a. All temperature corrections have been correctly handled.

b. The value of R^o before the current oscillations is the same as that measured at the start of the experiment.

c. The maximum described by the cathodic branch during the period of oscillation, is a de-loading maximum (point ii, above).

d. The rise in R/R° described by the anodic branch during the period of oscillation (point iii, above) is due to an increase in R°, and not due to increased loading.

e. The Pd cathode at 1720 and 1818 h is loaded approximately to the resistance maximum, for which $R/R^\circ \approx 1.95$ (the largest value observed for this cathode).

f. The Pd cathode at 1744 and 1840 h is fully stripped ($R/R^\circ = 1.00$)

The final column in Table 3-5 shows the rise in this estimated resistance as a percentage of the initial value. This percentage is plotted in Figure 3-87c; these data points are shown as squares, connected by straight lines. Also plotted in Figure 3-87c is the resistance rise during the period of oscillation, calculated on the basis of assumption (d), alone.
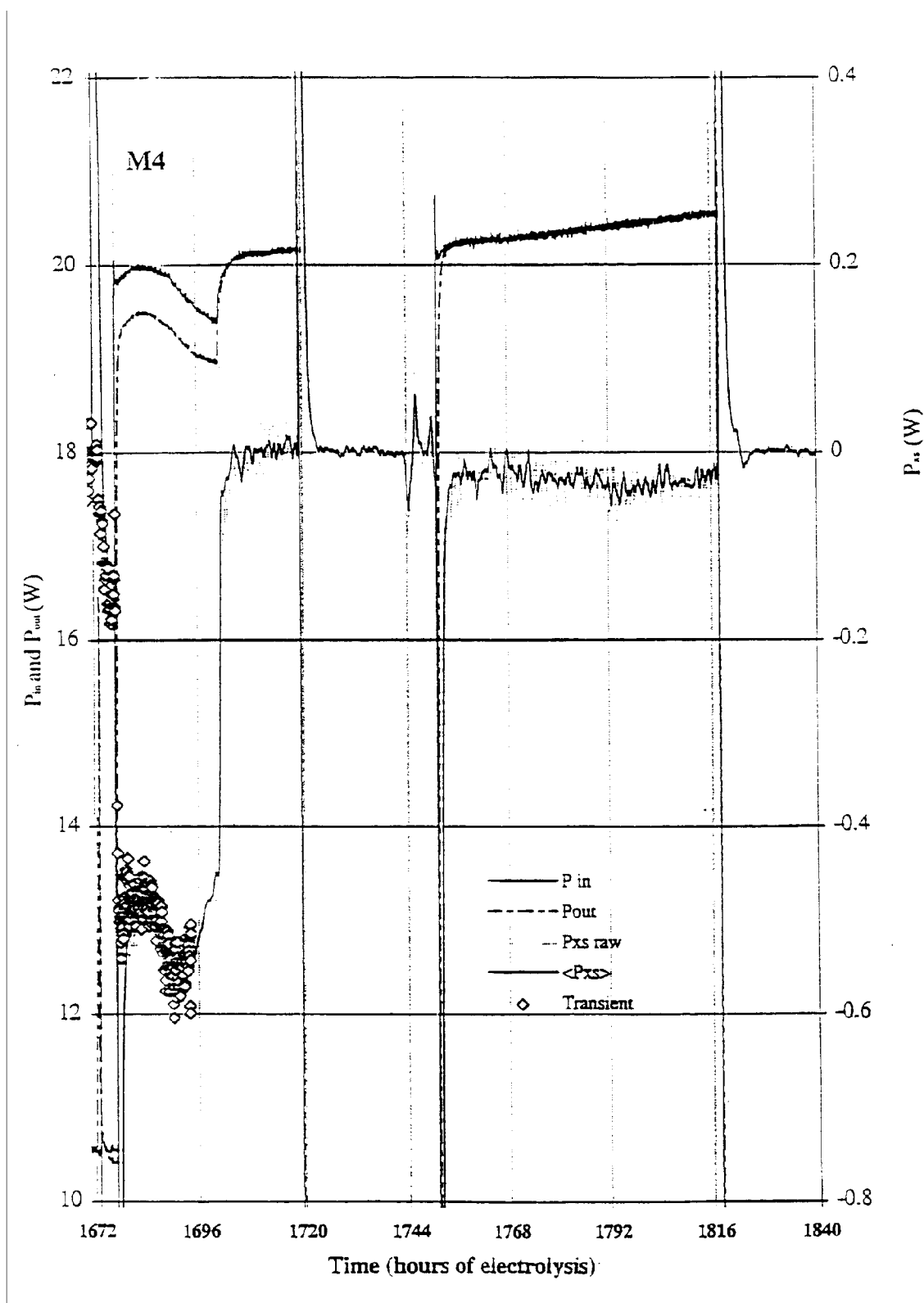
Figure 3-87b
M4 Input and output 1672-1840 hours
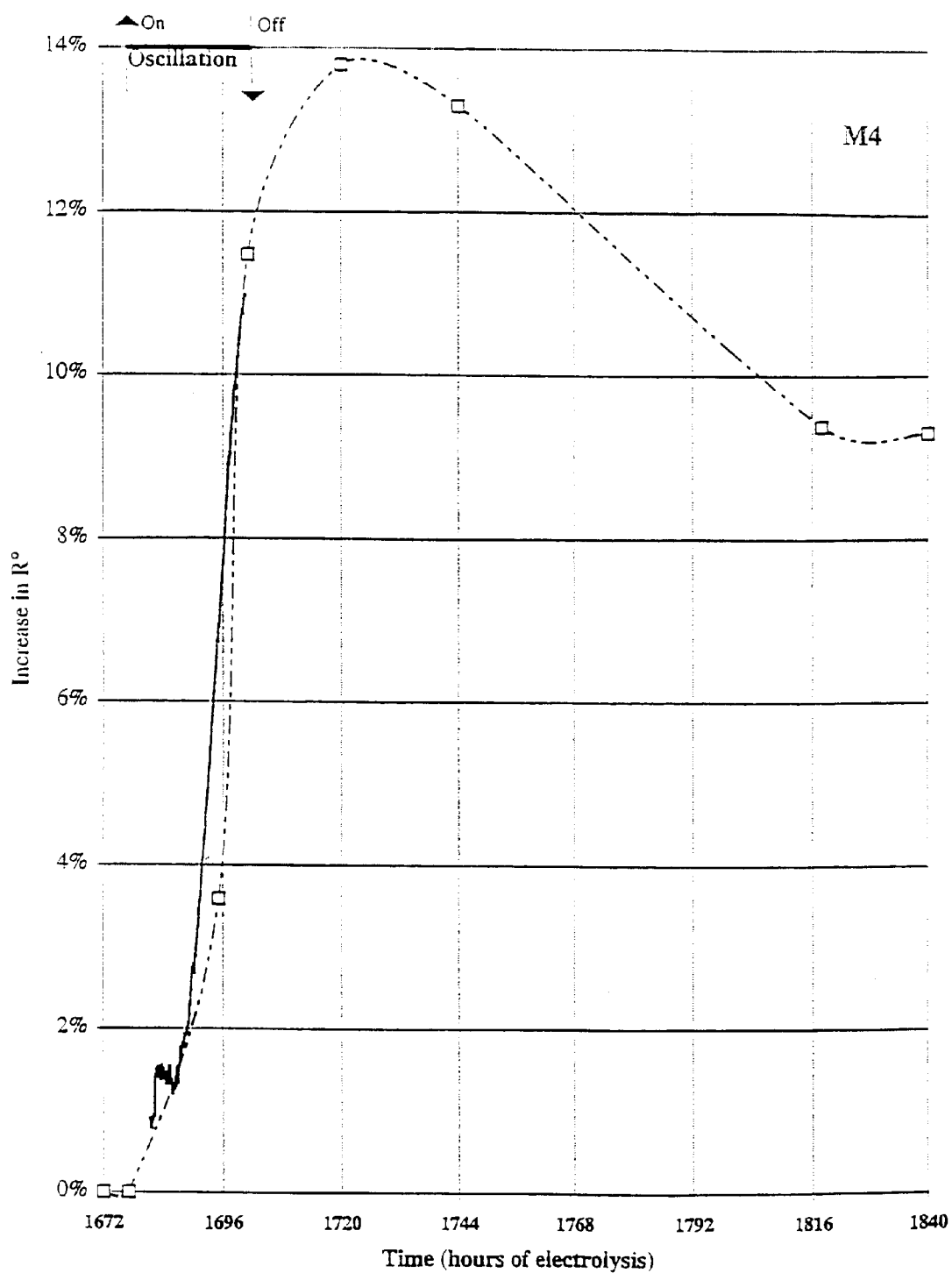
Figure 3-87c
M4 Increase in Resistance ratio 1672-1840 hours

Table 3-5
Components of Measured Resistance

Duration (h)	Condition Branch		R/R° Cathodic	R/R° Anodic	"R°" (½)	
1672	Pulse		1.92	1.92	0.0133	0%
1677	Oscillation:	start	1.91	1.70		0%
1695		R max	2.02	1.85	0.0137	4%
1701		end	1.99	1.90		11%
1720	dc 3.1A cathodic load		2.22		0.0151	14%
1744	dc 0.05A anodic strip		1.13		0.0150	13%
1818	dc 3.1A cathodic load		2.13		0.0145	9%
1840	dc 0.05A anodic strip		1.09		0.0145	9%

The changes in resistance calculated in Table 3-5 and plotted in Figure 3-87c are consistent with the following picture. The period of ± 1 A cm^{-2} current oscillation causes a change in the resistance of the Pd electrode, which is manifest in both its loaded and unloaded state. The resistance increase may continue for a short period after the oscillation is stopped but, this resistance rise is partially, but not completely removed at longer times and/or with subsequent load/unload cycles.

M-Series Discussion and Conclusions

Introduction. The purpose of the series of experiments described in this section was to determine the conditions under which the phenomenon which gives rise to calorimetrically determined excess power can be initiated and sustained. Having achieved this goal a secondary goal was to demonstrate whether or not the excess heat produced, correlated with the production of species from nuclear reactions; the primary nuclear product sought was helium, but integrating monitors were included in the M-cells for neutrons and x-rays.

In the light of these goals, the M-series experiments must be regarded as being only partially successful. The excess power observed was infrequent, and of small magnitude. The experiments, and their results summarized here, nevertheless contain a wealth of information. In this section we attempt to discuss these results, and draw conclusions from them, within the frame-work of the following four questions.

i. What can we learn from the excess power observed; can we refine the conditions necessary for its production?

ii. What can we learn from the extended periods where excess power was not observed; given the previous experience generated on this project and in the rest of the world, ought we to have observed this phenomenon more frequently or at greater amplitude under the circumstances of these experiments?

iii. What other information has been learned, in these experiments, about the D/Pd system; in what way is this information valuable?

iv. Using the information obtained, how can we achieve our goal of demonstrating conclusively whether or not nuclear processes contribute to the phenomenon of excess heat production?

Loading. The D/Pd loading has been shown to be closely correlated with excess power production. Identifying the conditions under which high loadings can be achieved, and maintained has been an important, even crucial, part of our experimental program (see Section 2, Degree of Loading). Our knowledge is, as yet, incomplete; the results of the M-series experiments provides some illumination.

It is clear from past and present studies of the D/Pd system that one of the factors which controls the ability of palladium to take up and retain deuterium (and hydrogen) is contained within the metal itself. A metallurgical or mechanical property, which may vary from manufacturer-to-manufacturer, lot-to-lot, or section-to-section within a single rod, may control the rate and extent of deuterium absorption. Cathodes selected for M-cell calorimetry were from lots supplied by two manufactures, Johnson Matthey and

Engelhard, found previously to load satisfactorily. All cathodes were subjected to a single annealing process previously found to be beneficial. A considerable variation in loading was nevertheless observed; in no case was a maximum loading obtained $D/Pd \geq 0.95$, a value previously observed to be necessary for reproducible excess heat production.

The M-series experiments were performed as a series of current ramps, normally followed with anodic strips, often accompanied by chemical species additions. [Other features of these experiments are discussed below under the heading *Pulses*]. Table 3-6 summarizes the loading response to successive ramps in experiment M1, M2 and M4.

In general, we observe two characteristics of loading which somewhat conflict during current ramps: an increased loading (D/Pd) with increased current density (i) - this relationship is often logarithmic; a tendency towards decreased loading with time when a cathode is held at high current densities (≥ 100 mA cm^{-2}).

Reviewing the data in Table 3-6 we see three different types of response for the three cathodes:

i.   The 2mm JM* cathode used in M1, initially loaded quite well ($D/Pd \approx 0.927$) in the presence of 200 ppm Al. This high loading was obtained at very high current densities (or, perhaps more importantly, high loading was sustained at high current densities). With successive ramps, following strips with no chemical species additions, the maximum loading obtained during a ramp declined progressively. This decrease is due to the change in slope of the Log [i] versus D/Pd relationship (see Figure 3-68). Until the addition of H_3BO_3 at 890 h, the M1 cathode showed very little tendency for decreased loading with time (or i during a ramp). A small (but significant) improvement in *net* loading was seen at low current densities on adding H_3BO_3; this improvement does not sustain to high current densities and completely changes the functional relationship between i and D/Pd.

ii.   The 2.8 mm E#1 cathode used in M2 initially displayed poor loading in an electrolyte containing no deliberate additive. With anodic strips accompanied by the addition first of Al, then of Si, the maximum loading obtained during a ramp increased progressively (but not sufficiently). This cathode showed little tendency for decreased loading with time (or i during a ramp).

Table 3-6
Loading Response to Current Ramps in Experiment M1, M2 and M4

Expt. #	Ramp #	Rate (mA/hour)	Maximum (D/Pd)	at i (mA cm^{-2})	at t - t^{o} (h)	Additive[†]
JM* 2mm x 3 cm					0	
M1	1	20	0.927	900	250	Al[1]
M1	2	25	0.900	800[2]	552	None
M1	3	50	0.867	800	844	None
M1	4	50[5]	0.877[6]	30[4]	1000	B[3]
E#1 2.8mm x 3cm						None
M2	1	50	0.829	580[2]	144	None
M2	2	50	0.840	490	280	Al
M2	3	50	0.854	525	460	Si
M2	4	50	8.846	280	542	B[7]
JM* 1 mm x 10 cm						
M4	1	25	0.857	956[2]	264	Al[1]
M4	2	25	0.867	150[5]	360	Cu
M4	3	25	0.880	376	524	Cu
M4	4	25	0.898	150[5]	872	Cu
M4	5	25	0.918	175[5]	1184	Al
M4	Step to	956	0.929[8]		1580	None

[1] 200 ppm Al in starting electrolyte, [2] Highest current density obtained on this ramp

[3]. 15 mg H_3BO_3, containing 7.3 x 10^{-4} moles of H [4] Maximum loading obtained at start of ramp

[5]. Loading declined markedly with increasing current density, [6] D/Pd not well known due to influence of H and B

[7]. 3 mg B_2O_3, [8]. Loading declined markedly with time

† Unless otherwise noted, chemical species additions were made by adding the element dissolved in 1.0 M LiOD

iii. The 1mm JM* cathode used in M4 initially displayed modest loading in an electrolyte containing 200 ppm Al. [Note that this is the same material as used in M1 varying only in dimension, and nominally the same electrolyte]. On the first ramp, in the presence of Al only, the relationship between i and D/Pd was monotonic (and logarithmic at i > 500 mA cm^{-2}). Thus the cathode obtained its highest loading at the highest current density, and, for ramp 1, showed little tendency for decreased loading with time.

With three successive ramps following Cu additions and one further ramp following Al addition, the maximum loading obtained increased progressively. A final current step following a strip with no chemical species addition shows yet higher maximum loading. In every case, however, following the first addition of Cu, the cathode shows a strong tendency to de-load with time so that the maximum loading occurs at low current density.

Figure 3-88a plots the Loading versus Log [current density], for the first current ramp of M4 (M4.1), and the first four current ramps of M2 (M2.1-M2.4). For the M2 cell ramps we observe a roughly log-linear relationship, and a family of parallel lines of the form

$$x = x^o + \alpha \, Log[i]$$

where x = D/Pd, and the slope, $\alpha \approx 0.0033$ with i in mA cm^{-2}. This family of lines is bounded approximately by the dashed lines showing upper and lower limits in Figure 3-88b. The increase in loading on successive ramps of the M2 cathode, apparently has occurred by increasing the initial value, x^o, and not by changing the slope (these x^o values are printed in Figure 3-88c). On the fourth ramp, the value of x^o actually decreases slightly; a higher loading was achieved only because a higher current density was attained.

The curve for M4 is slightly different than those for M2. The initial value (x^o) is somewhat higher, but the initial slope is lower than the value of 0.033 which characterizes the M2-cathode. At larger current densities (500 mA cm^{-2}) a log-linear relationship is observed for M4, with a similar slope to M2.

Figure 3-88b shows the limiting lines from Figure 3-88a, together with data taken from the first three ramps of the M1 cathode. These data also show a linear relationship between loading and Log [current density], and describe a family of lines with common slope, 0.085, but different from the value which characterizes the M2 and M4 cathodes (0.033). This increased slope obviously provides the facility to obtain satisfactorily high loading at accessible current densities. A significant (and disappointing) feature of the family of linear curves for the M1 ramps, however, is the steady decrease in the intercept value with ramp number (*i.e.* time).

3-192
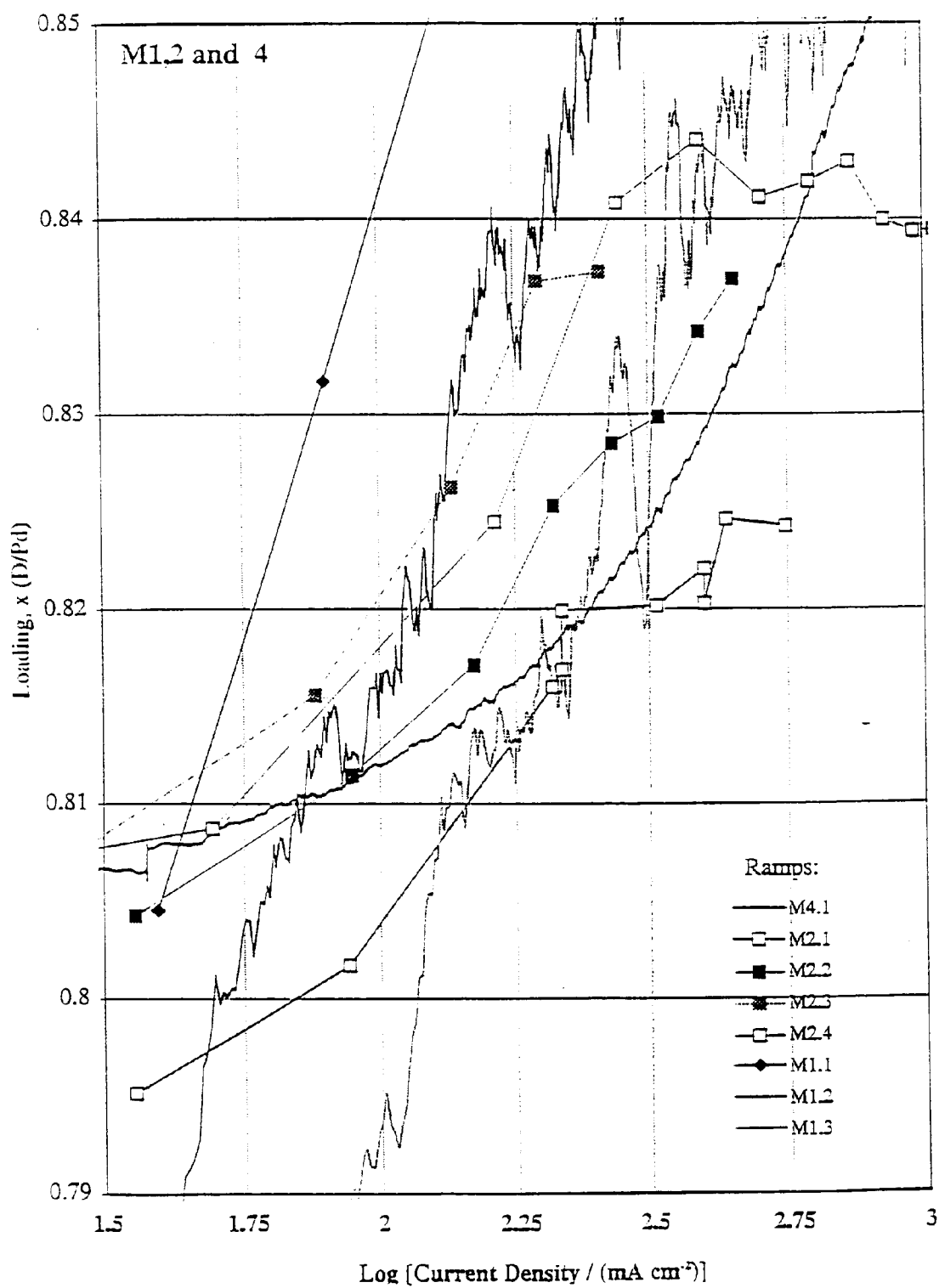
Figure 3-88a
M4 Loading

Figure 3-88b
M4 Loading

M1 ramps

Ramp	Slope	Intercept (at 1mA cm^{-2})
1	0.085	0.670
2	0.085	0.645
3	0.085	0.620
4	0.033	0.735
5	0.033	0.760
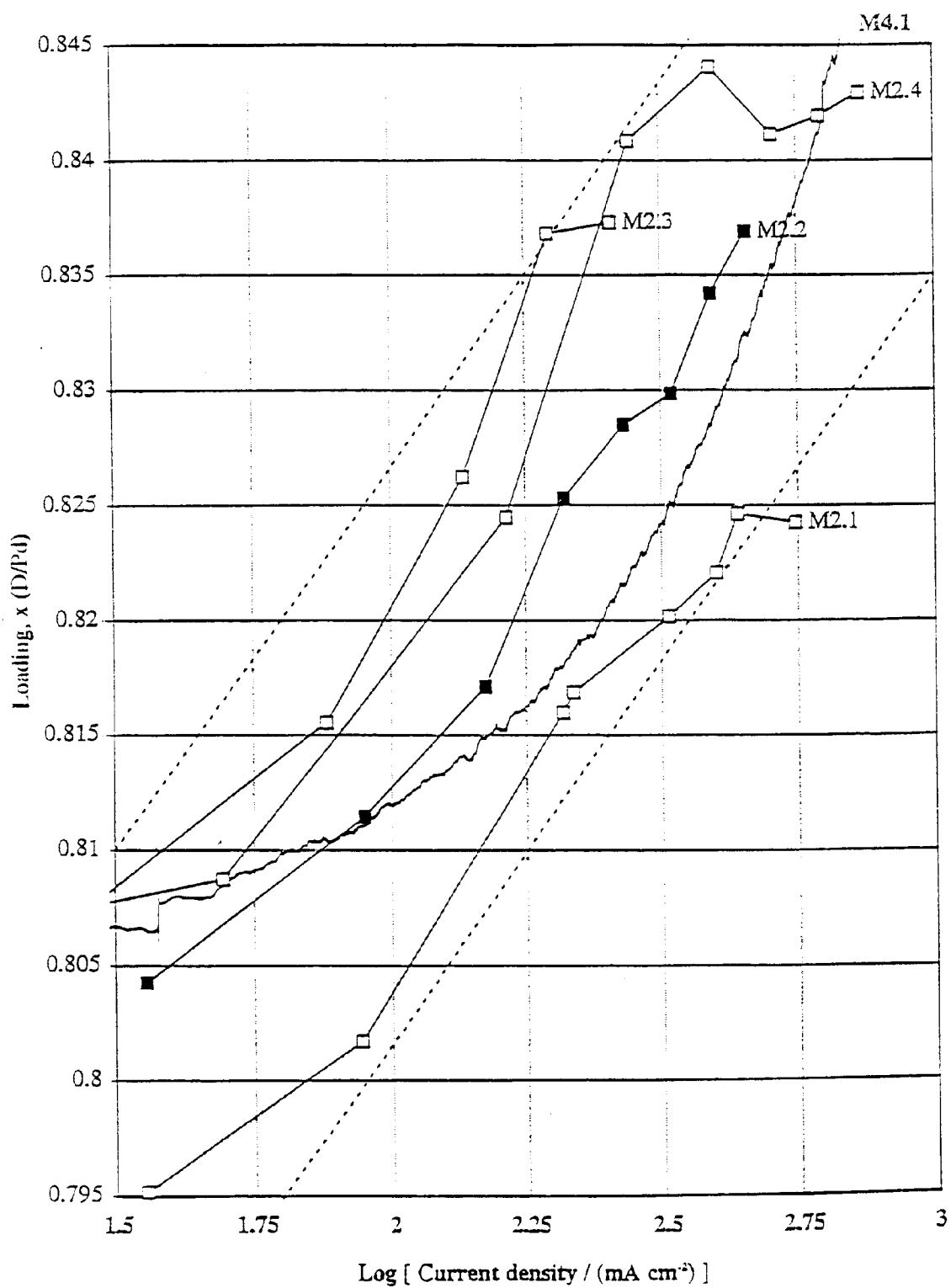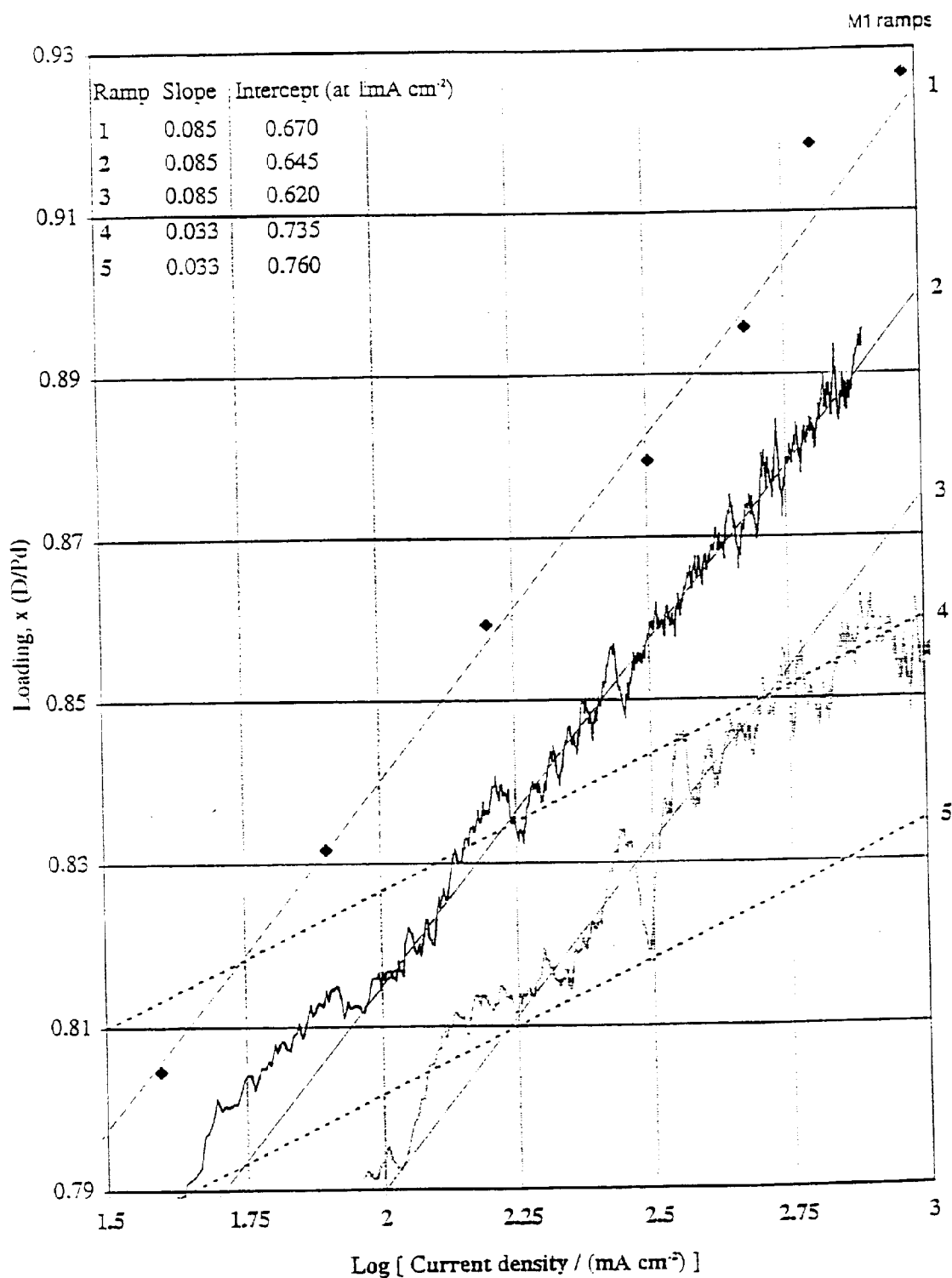
**Figure 3-88c
M4 Loading**

It is perhaps significant that the M1 cathode was started with electrolyte containing Al, but that further chemical species additions were not made in the strips between ramps 1 and 2, and 2 and 3 (see Table 3-6). A completely different mode of response is observed for the M2 cathode (although also log-linear). The M2 cathode was started with electrolyte containing no (deliberate) additive other than Li. The four ramps, interspersed with strips accompanied by chemical species additions: Al, Si then B, show a (generally) increasing loading. Satisfactory (high) loading was not obtained for M2, apparently, because of the very low slope of the loading versus log[i] relationship.

On the basis of this set of experiments we may (tentatively) conclude the following:

i. The D/Pd loading of a cathode during current steps or ramps is controlled by two processes:

   a. one which yields a linear increase in average loading with logarithmic increase in current density (over a range of current densities)

   b. a second effect which causes a monotonic decrease in loading with time, particularly at high current densities.

ii. The slope of the process defined in (ia), is not influenced by time, ramp and strip cycles, or the addition of Al and Si. This slope therefore appears to be a property intrinsic to a cathode or to an experiment.

iii. The intercept of the process defined in (ia) can be improved (made larger) by the addition of Al or Si during strip cycles between ramps, at least of cathodes started in electrolytes not containing these species.

iv. For cathode M1, started in electrolyte containing Al, the intercept of the process defined in (ia) is reduced in strip cycles without Al or Si addition.

v. The addition of B and Cu may increase loading transiently, may change the slope of the process defined in (ia), but appears to precipitate or exacerbate the de-loading process defined in (ib), above.

Resistance. Upon complete removal of D from the Pd lattice by anodic stripping at the end of the experiments, cathodes M1 and M4 (both JM* palladium) showed unusual responses. In Figure 3-73b, the final value of R is seen to be only 95% of its initial value ($R/R^o = 0.95$). In Figure 3-87a, and Table 3-5, the resistance on anodically stripping the cathode M4 is seen to be first 13% higher and then 9% higher than the initial value ($R/R^o = 1.13$ and 1.09).

The causes of these two effects are quite different. The resistance drop in M1 probably is attributable to a change in the intrinsic resistivity of the palladium. One method by which this may be accomplished is if the absorption then desorption of hydrogen helps to remove or redistribute chemical impurities from the bulk or grain boundaries of the polycrystalline palladium wire. Such impurities act as electron scattering sites and increase the metal resistivity. In the hypothesis proposed here, the initial Pd resistance is larger than the intrinsic value, due to the presence of chemical impurities. The act of hydrogen loading and de-loading either removes these impurities from the lattice, or moves them to sites where they have a lesser impact on the specimen resistance. As a consequence, the resistivity falls to, or towards, its intrinsic value.

The increased resistance of M4 is not thought to be due to a change (increase) in the metal phase resistivity. Instead we look for a geometric cause (a change in the ratio length/area). In concert with the calculated rise in M4 resistance (shown in Figure 3-87c), the cell voltage at constant current dropped. Since the electrolyte resistivity and anode kinetic characteristics are unlikely to change, the change in cell voltage most probably reflects a change in the effective cathode area (surface roughness).

As indicated in Figures 3-87a-c the predominant change in increasing resistance and decreasing cell voltage occurred during the period of $\pm 3.1A$ (± 1 A cm^{-2}) current oscillation. (This response is not indicative of a change in the cathode wire cross-section, but an increase in the cathode area). When removed from the cell at the end of the experiment the M4 cathode was observed to have experienced a severe modification of the Pd surface. Instead of a smooth shiny surface as at the beginning of the experiment, or a mildly tarnished surface as is commonly observed at the end of a long experiment, the surface of the M4 cathode was covered with faceted, metallic protrusions. These protrusions had approximately the form of flat cylinders which were apparently randomly but roughly uniformly spaced, covering the entire cathode surface. These cylindrical protrusions were found by subsequent analysis to be composed of palladium; or conductive palladium oxide.

It seems clear that, primarily during the period of $\pm 3.1A$ current oscillation, a surface rearrangement or decoration has occurred, which causes Pd to move from some sites, and deposit preferentially on others. It is likely that this process has occurred by an electrochemical dissolution/precipitation mechanism.

This surface rearrangement gives rise to the observed effects of increased resistance and surface roughness. We have modeled the expected effects of such surface rearrangement, using the following assumptions:

a. Metal is not lost (or gained) but is simply moved from trenches to protrusions.

b. The protrusions are cylinders, uniformly spaced.

c. The conductivity of the cylinders is the same as that of the substrate Pd wire, but,

d. The axial current used to probe the specimen resistance has access only to a portion of the cylindrical protrusion, defined by the Resistance Factor.

The results in Figure 3-89a and b were calculated for a range of conditions covering those observed on the M4 cathode. Figure 3-89a shows the calculated resistance ratio as a function of diameter of protrusion for a number of values of reciprocal spacing (protrusions/cm). For this calculation, the resistance factor is taken to be 50%. Superimposed on this graph are the resistance ratios measured at the end of the first and second strips.

From visual inspection of M4, the reciprocal spacing appears to be ~ 5 (5 rotrusions/cm or, an average spacing of 0.2 cm between centers). We can calculate the dimensions of the (presumed cylindrical) protrusions necessary to achieve the two measured values of resistance ratio:

Dimensions of Protrusion

Strip	R/R°	r	Spacing (cm)	Diameter (cm)	Height Surface Roughness (cm)	
First	1.133	50%	0.2	0.046	0.036	1.20
Second	1.090	50%	0.2	0.041	0.032	1.16

It appears, therefore, that the act of anodic/cathodic cycling at 1A cm^{-2} has caused the redistribution of surface atoms, moving Pd from some areas, and depositing it on others.
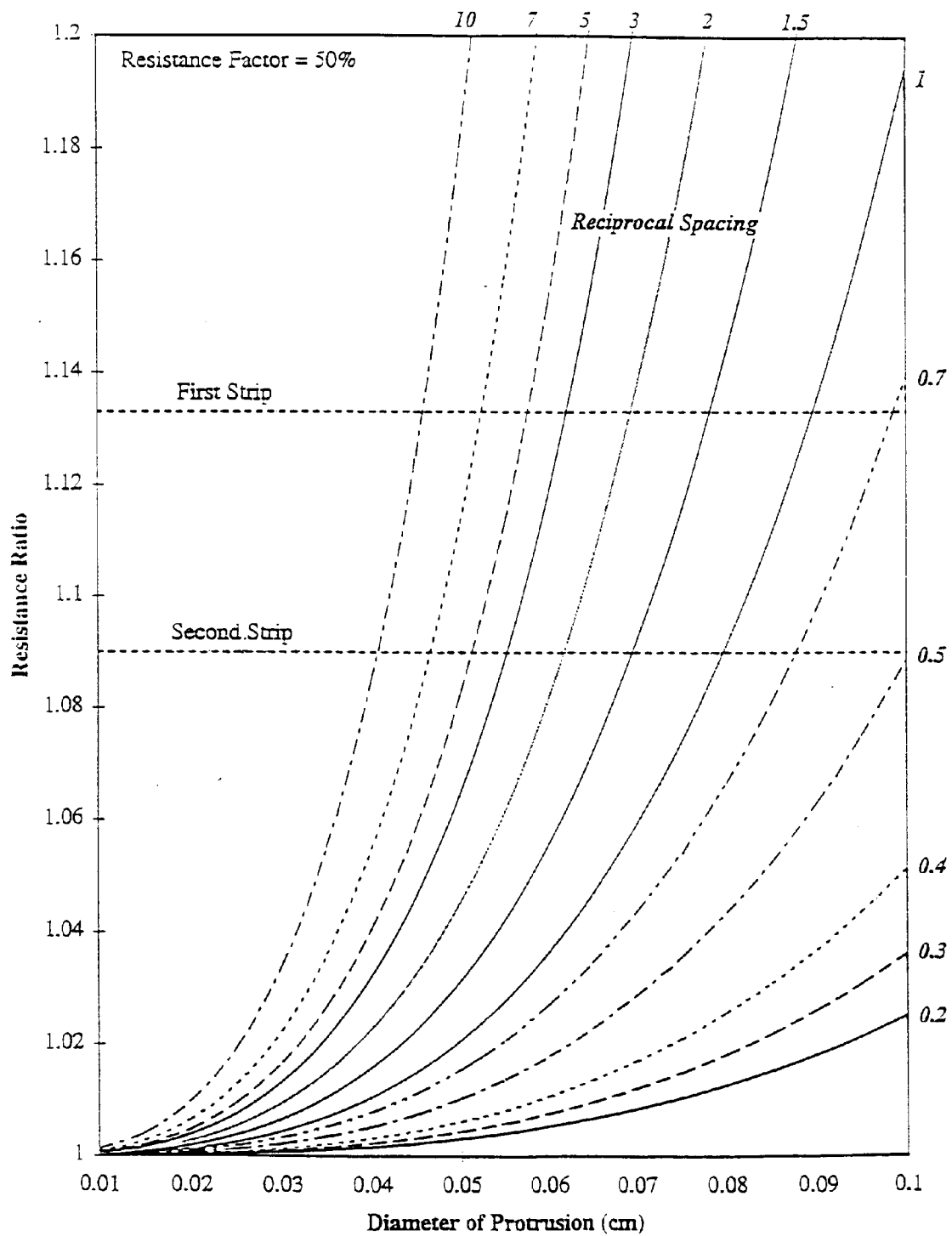
Figure 3-89a
M4 Resistance ratio
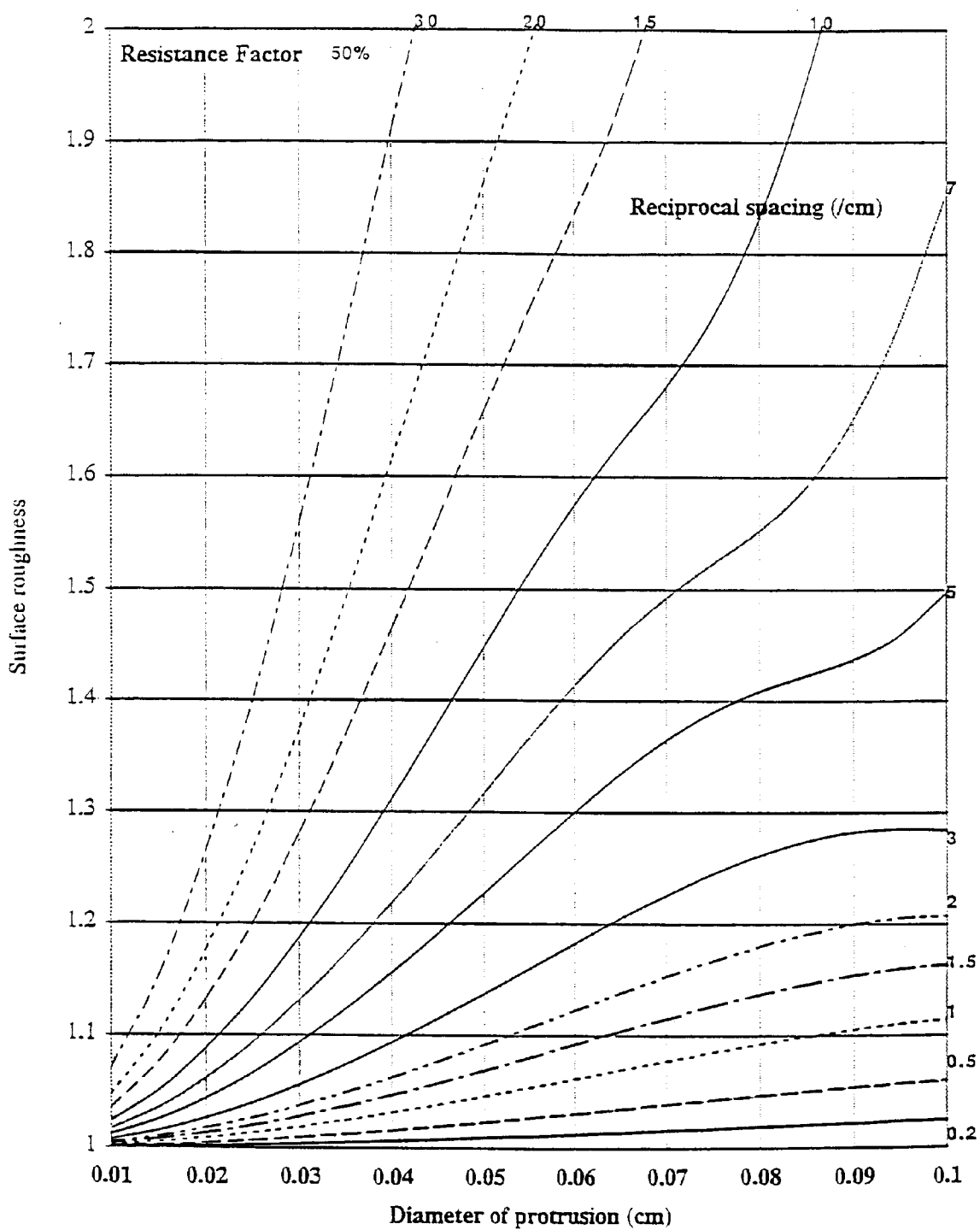
Figure 3-89b
M4 Surface roughness

After hours of cycling, the surface protrusions are electrically equivalent to cylinders, 0.046 cm in diameter, 0.036 cm high and at average spacing ~ 0.2 cm. A small amount of redistribution occurs after the high current anodic/cathodic cycling is stopped. Later it appears as if the protrusions have somewhat reduced in size (or, at least, effect on R/R^o).

This dramatic redistribution of surface does not appear to be beneficial in facilitating deuterium uptake.

Excess Power. In a total of 14 current ramps in experiment M1-M4, excess power was observed on only 3 occasions: the first ramp of M1, and the first and third ramps of M4. In two instances, the amount of excess power observed was very small, not much larger than the determined accuracy of the calorimeter (~ 0.2-0.4%). Only in the case of M4 ramp 3 was excess power and energy observed with sufficient resolution to perform further analysis and draw conclusions about the causes and conditions.

Figure 3-83a shows the input, output and excess power for the period of the third ramp of experiment M4. This plot shows two "bursts" of excess power, each separated by a period of small (or no) excess power, each lasting about one day. In the first instance, excess power appears to initiate, with the current ramp, at a current density threshold of approximately 425 mA cm^{-2}. At constant current the excess power is highly variable. Two features of the excess power, and its variability, deserve special attention:

i. In some instances there appears to be a correlation between excess power and input power, at constant input current.

ii. There appears to be a correlation between excess power (shown in Figure 3-83b), and an apparently spontaneous variation observed in the measured cathode resistance (interpreted in Figure 3-83a as a variation in loading).

Both of these apparent correlation's warrant further scrutiny.
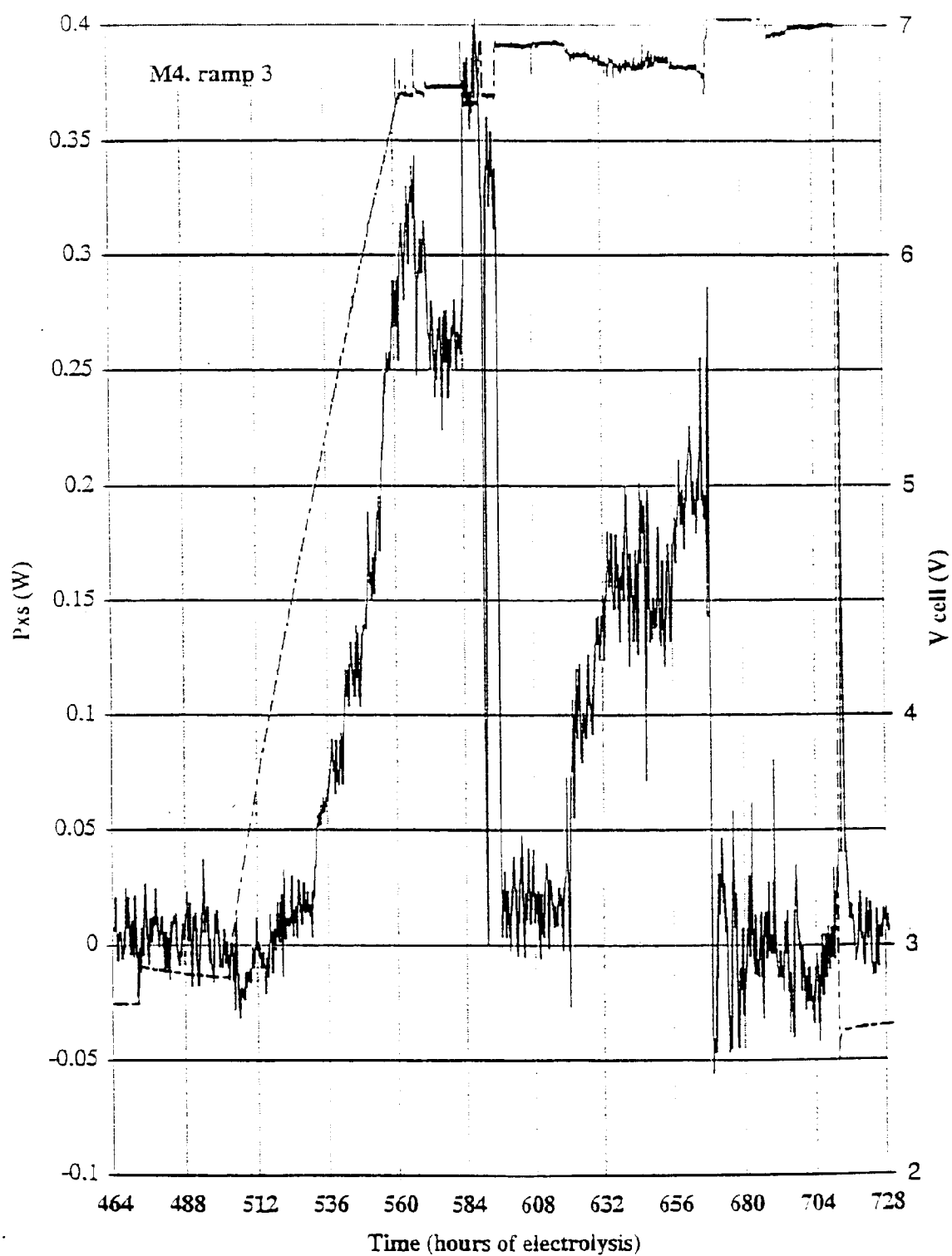
Figure 3-90a
M4 Excess power 464-728 hours
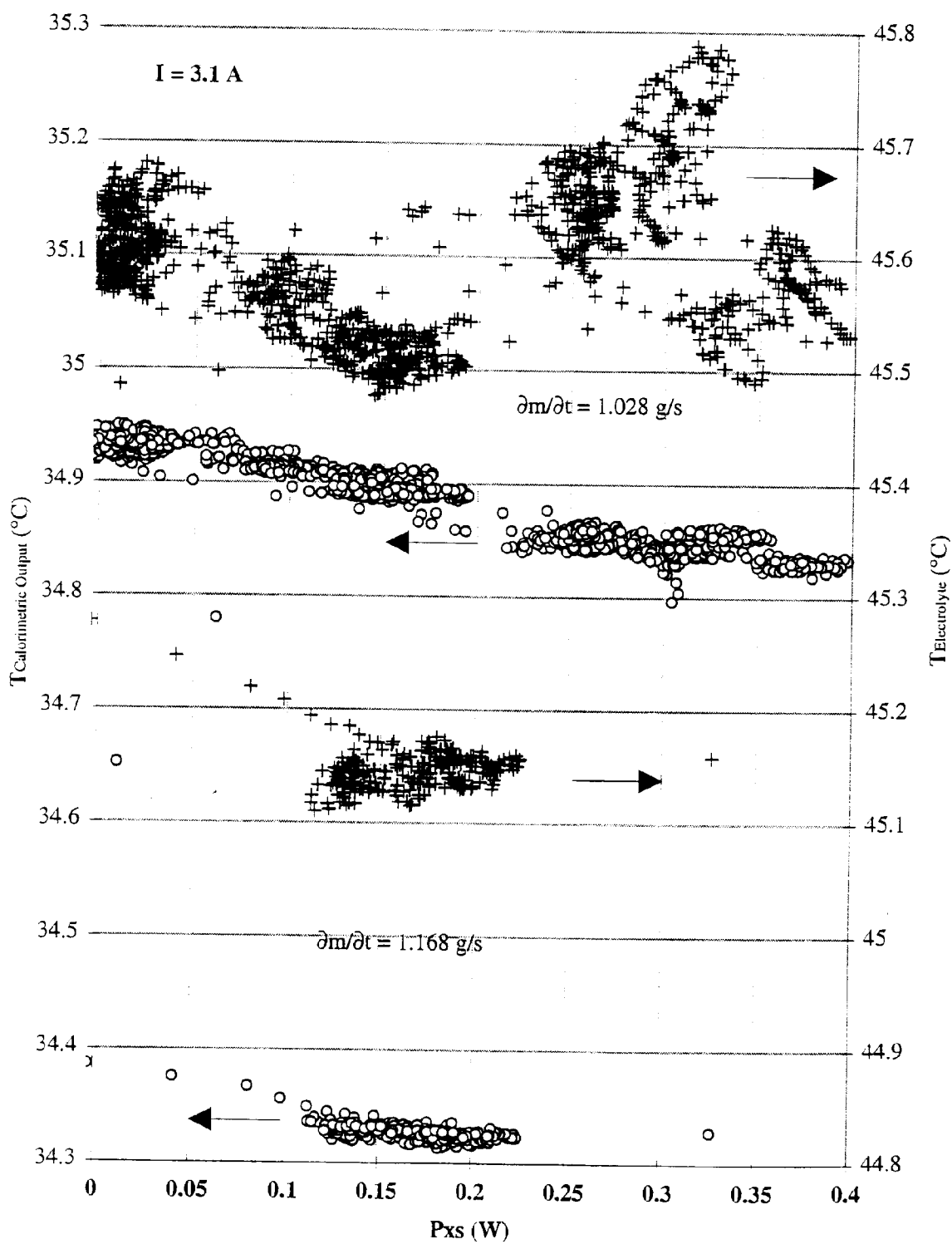
Figure 3-90b
M4 Excess power

The correlation between excess and input power in Figure 3-83b reflects, more fundamentally, an apparent correlation between excess power and cell voltage. Figure 3-90a shows the excess power and cell voltage plotted for the period of ramp 3. It is clear that when the voltage increases (apparently spontaneously) on some, but not all occasions, the excess power decreases, and *vice versa*. The obvious concern prompted by such a correlation, is the possibility that the excess power is electrical in origin, and is associated not with processes occurring in the cell but with the mis-measurement of input power. We must examine the possibility that the voltage is not being measured accurately, that is, does not change in the manner shown in Figure 3-90a, and the excess power merely reflects the changes in this mismeasurement. Several points can be made from inspection of the data:

i. Voltage measurements are made three times during the measurement cycle, using two different methods, and a meter with calibrated accuracy at least two orders of magnitude better than that needed to resolve the apparent voltage swings. This meter is also used to make other voltage measurements (including a redundant measurement of the cell current). There is very little reason therefore, to suppose that the voltage measurement itself is in error.

ii. The voltage swings in some instances are correlated with the excess power, but not intimately. Figure 3-90a shows different regions of interest labeled "a-d". While for regions "a" and "b", there appears to be a close correlation between P_{xs} and V_{cell}, for the spontaneous step in V_{cell} at the point labeled "c", there is no change in P_{xs}. Furthermore, the large voltage step caused by current reduction at "d" induces no change in P_{xs}, showing the calorimeter to be well calibrated.

iii. A close inspection of the data reveals that the changes in cell voltage occur within the four minute measurement cycle, but that the changes in P_{xs} occur more slowly and with a small time lag. The fact that the voltage change is rapid, itself gives us no clue as to cause since electrical, electrochemical or even thermal effects may easily result in a 250 mV change at 3.1A input current in a 240s interval. The calorimeter response, however, appears to be appropriate to the cell voltage changes (as if these were real), but a secondary effect occurs which yields more or less power than expected from Joule heating.

iv. The central question is whether the measured excess power, is the result of variable under-measurement of an effectively constant input power, or due to a fluctuating power source within the electrochemical cell, that has some causal association with cell voltage. Information is available from the electrolyte temperature sensor. Figure 3-90b plots the temperature measured at one of the calorimetric outlet sensors, and the electrolyte temperature, versus excess power for the period in Figure 3-90a with constant cell current (3.100 ± 0.001A). The outlet temperatures are

plotted as open circles referenced to the left axis; the cell electrolyte temperatures are plotted as "+" referenced to the right axis. Both scales are the same, but are displaced vertically for clarity; the cell electrolyte is warmer than the bathing calorimeter fluid, since the heat sources (electrochemical and recombination) are contained within the cell.

At constant input (but variable excess) power, and constant inlet temperature and mass flow rate we expect a linear correspondence between P_{xs} and T_{out}, with positive slope

$$\frac{\delta P_{xs}}{\delta T_{out}} \bigg|_{T_{in}} = \frac{\delta m}{\delta t} C_p + k$$

In fact, the data in Figure 3-90b show a (roughly) linear correlation with negative slope *because of* the inverse correlation between P_{xs} and V_{cell}. The data in Figure 3-90b reflect two different mass flow rates: the upper points were obtained and $\delta m/\delta t = 1.028 \pm 0.001$ g s^{-1}; the lower points (reflecting more efficient cooling) were obtained at $\delta m/\delta t = 1.168 \pm 0.001$ g s^{-1}.

The slope (or, more correctly, slopes at different $\delta m/\delta t$) of T_{out} versus P_{xs} nevertheless define(s) the expected slope of $T_{electrolyte}$ versus P_{xs}. If "real" excess power is sourced within the electrolyte then the electrolyte should be disproportionately hotter than the bathing calorimetric fluid, reflected by T_{out}. If, on the other hand, there is no excess power, just a mismeasurement on the input voltage, then the electrolyte temperature should parallel exactly, the outlet temperature, T_{out}. Thus, if genuine (and no artifactual) excess power is sourced within the cell electrolyte then the temperature by which the electrolyte exceeds the calorimetric fluid ($T_{xs} = T_{electrolyte} - T_{out}$) should increase with increasing P_{xs}.

Figure 3-90b shows that T_{xs} indeed does increase with P_{xs}. The data are too scattered to define a good functional relationship but it is clear that at both mass flow rates the electrolyte temperature somewhat increases with P_{xs}, while T_{out} falls for the reason stated above.

Thus it is clear that the electrolyte temperature sensor responds as if the excess power was a genuine heat source (and not an artifact), and that the source of the heat was within the electrolyte or closely coupled to the electrolyte. A simple analysis of the expected distribution of temperature within the cell and calorimeter (not presented here) is consistent with the source of heat, of variable power equal to P_{xs}, being at the cathode.

Fitting Function. It seems likely, therefore, that the excess power observed in experiment M4 reflects the presence of a heat source at, or in, the Pd cathode. It is useful, therefore,

to examine the time series data for the various parameters measured, in light of the questions enumerated in the introduction to this section. Specifically, what can we learn from the excess power observed; can we refine our knowledge of the conditions necessary for its production? In the following section(s) we will assess the information obtained in experiment M4 to help elucidate the question central to our research: do nuclear processes contribute to the phenomenon of excess power production?

In previous studies in this laboratory and others, excess power has been observed to correlate with current density and with loading. It is clear that these two variables are not orthogonal in that loading is achieved by the application of electrochemical current. Furthermore, in experiments in which the cell electrolyte is not well coupled to an isothermal reservoir, or deliberately maintained at constant temperature by using an auxiliary heater (or cooler), the electrolyte and especially the cathode temperature will rise with current, and cathode temperature is coupled to loading through the Pd/D phase diagram.

In our laboratory, in experiments performed under approximately isothermal conditions, we have observed the following functional relationships between excess power (P_{xs}), loading ($x = D/Pd$) and current density(i), for times following a critical initiation period.

$$P_{xs} \; \alpha \; (x - x^o)^a$$

$$P_{xs} \; \alpha \; (i - i^o)^b$$

where a=2, b=1, and x^o and i^o are threshold values which may vary (particularly i^o) from experiment-to-experiment and from ramp-to-ramp. The threshold value of x^o is approximately 0.8-0.85.

In other laboratories, notably in the experiments of Fleischmann and Pons, experiments are performed under more nearly adiabatic conditions. Thus the cathode temperature rises markedly with both current density and excess power. For these experiments the same functional relationships are observed as described above, but the coefficients, a and b, may not be the same. The coefficient, a, is not known for Fleischmann and Pons' experiments. This is for two reasons. In their experiments, the loading is not measured directly, or has not been reported; the existence of a threshold value, x^o, is known or can be inferred from their data, but the loading criterion is normally expressed by them in terms of an achieved cathode overvoltage. *More subtly, it is possible, even probable, that the critical variable is not the loading concentration, x, but the deuterium chemical potential or activity.* The equation of state that relates these two thermodynamic properties is known for D, and is a strong function of temperature in the range 30-100°C.

Thus in other than isothermal conditions, the functional relationship between P_{xs} and x may be very difficult to determine.

The value of the coefficient, b, has been determined in Fleischmann and Pons' and other similar experiments to be between 2 and 3. This contrasts with the value of ~ 1 found in our experiments under approximately isothermal conditions. It is likely, however, that the difference in the values determined for b is attributable to the (complex) effects of current density on cathode temperature, and cathode temperature on loading and on deuterium activity, and on the phenomenon itself. We believe, therefore, that a value of $b \approx 1$ expresses a more fundamental relationship at isothermal condition.

In developing a function to fit the observation of excess power, we must proceed empirically. Whatever the phenomenon we are studying, its cause is not yet known, and no theory exists to guide us. Probably the most comprehensive and rigorous mathematical development of a theory capable of explaining our observations is that of Hagelstein[1]. We may use this, as a model, to shed some light, if only by suggesting variables against which we may test our observations.

In the theory of Hagelstein, excess power is produced by coherent, solid state, nuclear processes, triggered and coupled by lattice phonon excitation. The detailed mechanism has been expounded in numerous publications, but is not important for the purpose of this discussion.[2] What is important is that the lattice phonons needed to produce excess power derive from the exothermic desorption of D. This imposes two constraints on excess power production. Deuterium loads endothermically into palladium only at loading levels above a threshold value of approximately 0.8-0.85. On the basis of this theory one might, therefore, expect the rate of phonon generation (and therefore excess power?) to be a function of two variables:

$$f(x-x^o)$$
$$f(J_D)$$

where $x-x^o$ measures the extent by which the adsorption of a deuteron is endothermic, and J_D is the flux of (desorbing) deuterons across the surface.

---

[1] P. Hagelstein "Update on Neutron Transfer Reactions", in *Proceedings of the Fifth International Conference on Cold Fusion* (ICCF5), Monte Carlo (April 1995).

[2] P. Hagelstein "Anomalous Energy Transfer between Nuclei and the Lattice", in *Proceedings of the Sixth International Conference on Cold Fusion* (ICCF6), Hokkaido, Japan (October 1996).

The functionality predicted for phonon generation is very similar to that observed for excess power. Let us make a very simple approximation, that excess power production can be expressed as a linear combination of (at least) three variables. We can define a test function:

$$P_{x_s} = K \, (x\text{-}x^0)^a \, (i\text{-}i^0)^b \, J_D$$

The constant K may include other dependencies, such as temperature, sample volume or area, or alloy type. From our data, we expect a $\approx$ 2 and b $\approx$ 1. The flux needs to be defined, carefully, in terms of variables we can measure. A unidirectional flux of deuterons into or out of the palladium cannot be sustained. A steady state will be established when the lattice contains no deuterons (x=0), or when the activity of deuterons inside the lattice equals that the adsorbed deuterons established on the surface by the prevailing conditions of current density, temperature, and the presence of other chemical species *etc.* One might imagine a condition where a net adsorption of deuterons occurs at one site, these deuterons then diffuse to a region of lower D activity and desorb at a second site. In this way, a net flux of deuterons may be sustained, in the steady state, at least in one region of the cathode. Since the flux is limited by the rate of diffusion between the adsorption and desorption sites, unless these sites are closely proximate, the flux would be small.

A far more practical way of creating a net flux under close to steady state conditions, is to cause a small fluctuation in the adsorbed deuteron activity. If one imagines a sinusoidal perturbation of the surface activity, a flux of deuterons will cross the interface due to the oscillating surface activity. In the steady state, a damped, semi-infinite, oscillating activity profile will penetrate into the metal. The time averaged flux will be zero, but a flux of deuterons of appreciable amplitude and alternating sign will cross the interface on each half cycle. The amplitude of this flux for a given average loading, x

$$\left| J_D \right|_x \, \alpha \, \left| a \right| \, D \sin (\omega t)$$

where |a| is the amplitude of oscillation of the sinusoidal surface activity, D is the diffusion coefficient of deuterons in palladium at the average loading, x, and ω is the oscillation frequency.

In our experiments we cannot measure such a flux, directly. We can impose a periodic perturbation on the system in the hope of perturbing the surface activity. We can measure the average loading periodically, and interpret the net change in moles per unit time as a net flux. Thus, the rate of change of the loading $\delta x/\delta t$ is a measure of the flux. It is clear from the preceding equation, however, that for a periodically varying loading, the sample period (frequency) will also affect the apparent flux.

Understanding that considerable approximation is involved, let us define a simplified test function for P_{xs}, and test this against the time series data. Figure 3-91 shows the excess power measured during M4, ramp 3, compared to the test function

$$P_{xs.test} = K (x - x^o)^2 (i - i^o)^1 \, \delta x/\delta t.$$

The coefficients a and b have been set to 2 and 1, respectively, to be consistent with our previous results obtained under near isothermal conditions. The proportionality constant K was determined to be 2.33×10^5 cm^2 s A^{-1} in order to set the two functions to equal energy. The threshold values, x^o and i^o were determined by maximizing the correlation between the two functions P_{xs} and $P_{xs.test}$.

The Correlation function is defined as:

$$\rho_{xy} = \frac{1}{n} \ (x_i - \mu_x) (y_i - \mu_y)/ \sigma_x \sigma_y$$

$$\sigma_x^2 = \frac{1}{n} \ (x_i - \mu_x^2)$$

$$\sigma_y^2 = \frac{1}{n} \ (y_i - \mu_y^2)$$

where μ and σ are the mean value and standard deviation of the data sets x and y. This function measures the extent to which two ranges of data move together, independent of the unit of measure. For the two data sets shown in Figure 3-91, the correlation coefficient

$$\rho = 0.853$$
with $\quad x^o = 0.83 \ (D/Pd)$
and $\quad I^o = 0.45 \ (A \ cm^{-2})$
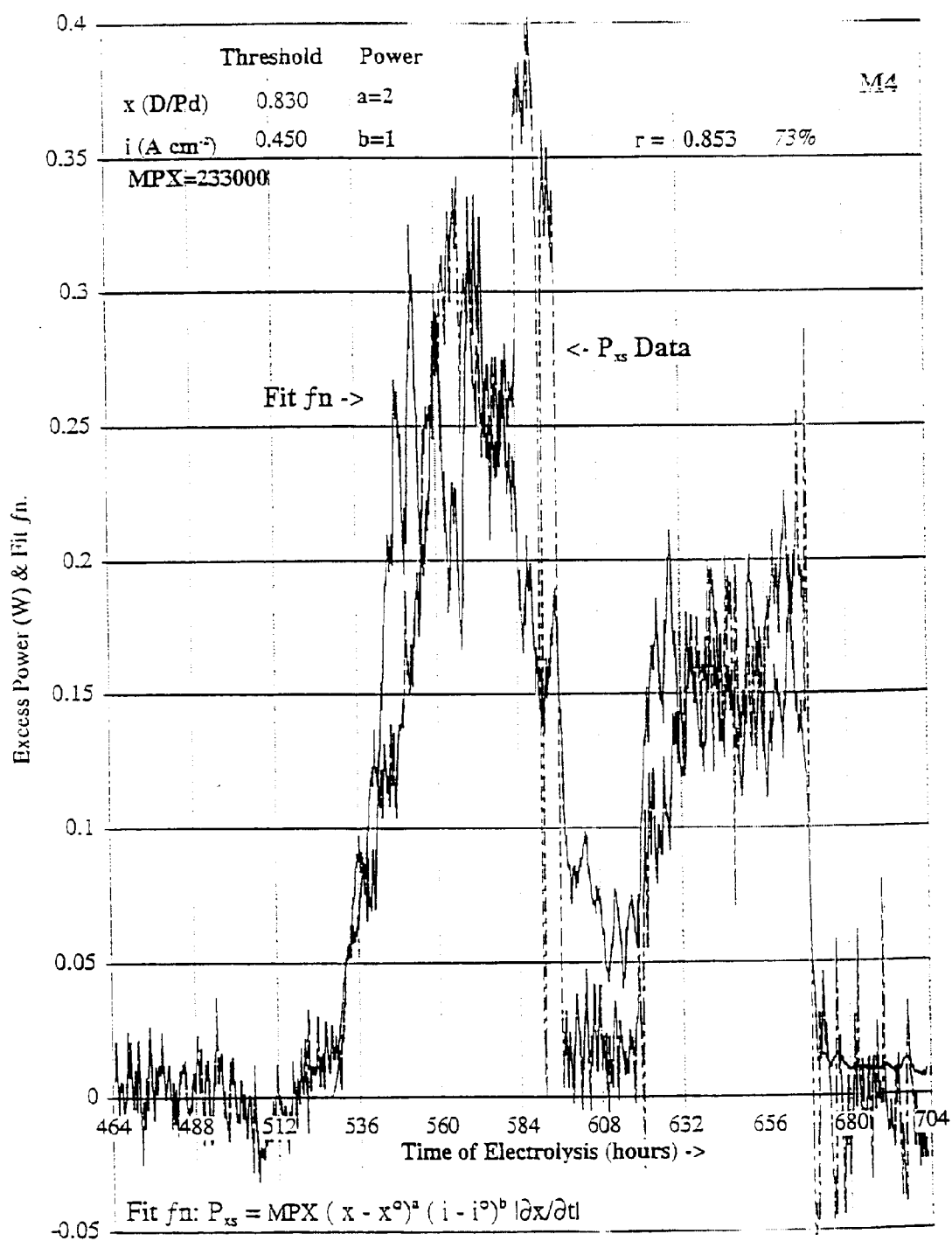
Figure 3-91
M4 Excess power 464-1704 hours

A value of 0.853 indicates that ~ 73% of the excess power is related linearly to our test function. Other variables may be involved (the test function is not complete) or the coefficients may not be precisely right (the test function is not completely correct); this is nevertheless a remarkable degree of correlation when the approximations and simplifications involved in generating the test function are considered.

A factor not taken into account in the simple Correlation function is the possibility of temporal displacement between the two data sets. If one imagines that the test function is a generating function and the measured excess power is the response (that our test function is *causal*) then one might expect P_{xs} to be delayed with respect to $P_{xs.test}$, and to have large amplitude (high frequency) features somewhat smoothed. Close inspection of Figure 3-91 reveals that this may indeed be the case. Treating the two data sets we should, perhaps more appropriately, calculate the Cross-Correlation function

$$R_{xy} = \frac{1}{T} \int_o^T x(t)y \, (t + \tau) \, dt$$

where T is the time interval over which the correlation is sought and τ is a time displacement or delay. By Fourier transform of the Cross-and Auto-Correlation functions we can calculate frequency domain power spectra of the two time domain data series, and ultimately the Coherence function. This latter would allow us to determine whether there is only one input and to what extent the "response function", P_{xs}, is linearly related to the "input" test function, $P_{xs.test}$. This analysis has not yet been performed.

One reason not to embark on a more rigorous time-domain correlation approach, is the difficulty in handling the variable $\delta x/\delta t$ in our test function. Because of the need to move a calorimetric fluid of appreciable heat capacity at finite velocity to the outlet temperature sensors, the calorimetric output represents necessarily a damped and phase shifted response to a (thermal) perturbation at the cathode or in the electrochemical cell. The calorimetric response to an impulse function in fact closely approximates that of an exponential low-pass filter of time constant, τ, determined by

$$\tau = \left(\frac{M + WE}{\delta m/\delta t} \right)$$

where M is the mass of the moving water in the calorimeter, WE (the Water Equivalent) is the mass of water having a heat capacity equivalent to that of all of the cell parts and contents, and $\delta m/\delta t$ is the calorimetric flow rate of water.

For M4, M + WE $\approx$ 900g, so that, at 1.028 g s^{-1} τ = 876 s ($\approx$ 15 minutes). In assessing the Correlation function, ρ_{xy}, it is important that the input and output (test and response) functions vary on the same time scale; that is, that both are subjected to the same averaging or smoothing.

If we examine our test function, again;

$$P_{xs.test} = K (x - x^o)^a (i - i^o)^b \, \delta x / \delta t$$

the explicit variables are x, i, and $\delta x / \delta t$. In our experiments we arrange for i to be constant or to slowly and monotonically change with time. For the purposes of this analysis, however, we may treat i as static. In the preceding and subsequent analyses, the variables x and $\delta x / \delta t$ have been treated as follows:

The time series data presented in this report are averaged values collected within a fixed sampling period; for experiment M4 this period was 4 minutes (240 s). The sampling period limits the highest frequency response ($\approx 1 / 240$ s, ≈ 4 m Hz), but is still faster than that permitted by the calorimetric "output" filter. The most appropriate way to establish P_{xs} and $P_{xs.test}$ (specifically x and $\delta x / \delta t$) on the same time scales may be to apply a symmetric exponential filter to x. This is computationally complex, and, given the approximations already employed, probably unwarranted. It is a mathematically trivial exercise to show that the weighting of a symmetric exponential filter is the same as a seven point average for Δt = 240 s and τ = 875 s:

$$\int_{-\infty}^{\infty} \exp\left[-t / \tau\right] \delta t \ = \ 2\tau \ = \ 1751 \text{ s}$$
$$7 \ \Delta t \ = \ 7 * 240 \ = \ 1680 \text{ s}$$

Simply for mathematical convenience, therefore, the values of x (strictly, $\bar{x}$) used in correlation calculation and to generate our test functions, were calculated as 7-point moving averages of the "raw" values of x (determined from R/R^o). The values of $\delta x / \delta t$ were taken as

$$\delta x = \bar{x}_i - \bar{x}_{i+1} + \bar{x}_i - \bar{x}_{i-1}$$

$$\delta t = \Delta t$$

[In fact, since Δt is constant, the period of the variation was taken up in the proportionality constant, K].

Having defined our terms and procedures, we can go back and examine how well our test function applies to the excess power observed in experiment M4, and other similar experiments, and what this teaches us about the phenomenon under study.

The first point of interest is that the coefficients a=2 and b=1 do not provide the best fit between $P_{xs.test}$ and P_{xs} for experiment M4, ramp 3.

Figure 3-92 plots the Correlation Coefficient, ρ_{xy}, versus the threshold value for loading, x^o, for various values of the threshold current density, with

$$x = P_{xs} \text{ (M4, ramp 3)}$$

$$y = K \, (\overline{x} \quad - x^o)^2 \, (i - i^o)^2 \, \delta x / \delta t$$

where $(\overline{x}$ and $\delta x / \delta t$ were calculated as described above). Notice that the coefficients a and b are both set to 2, rather than a=2 and b=1 as used to calculate the data plotted in Figure 3-91.

In Figure 3-92 we see a family of curves calculated for different values of i^o, and displaying a maximum Correlation fit at different values of x^o. From the envelope of this family of curves we see that the "best" best fit, with a Correlation coefficient of $\rho \approx 0.873$, occurs for a value of $x^o \approx 0.833$, and i^o between 400 and 425 mA cm^{-2}. On the basis of this maximization we are able to assign $x^o \approx 0.833 \pm 0.001$ and $i^o = 415 \pm 20$ mA cm^{-2} as the "most probable" values for a=2 and b=2.

We can compare the best Correlation fits obtained in the two cases examined so far (Figures 3-91 and 3-92) to see how sensitive the fitting procedure is to the values of coefficient b.

Figure	a	x^o (D/Pd)	b	i^o (mA cm^{-2})	ρ	ρ^2
3-91	2	0.833	1	425	0.853	73%
3-92	2	0.830	2	415	0.873	76%
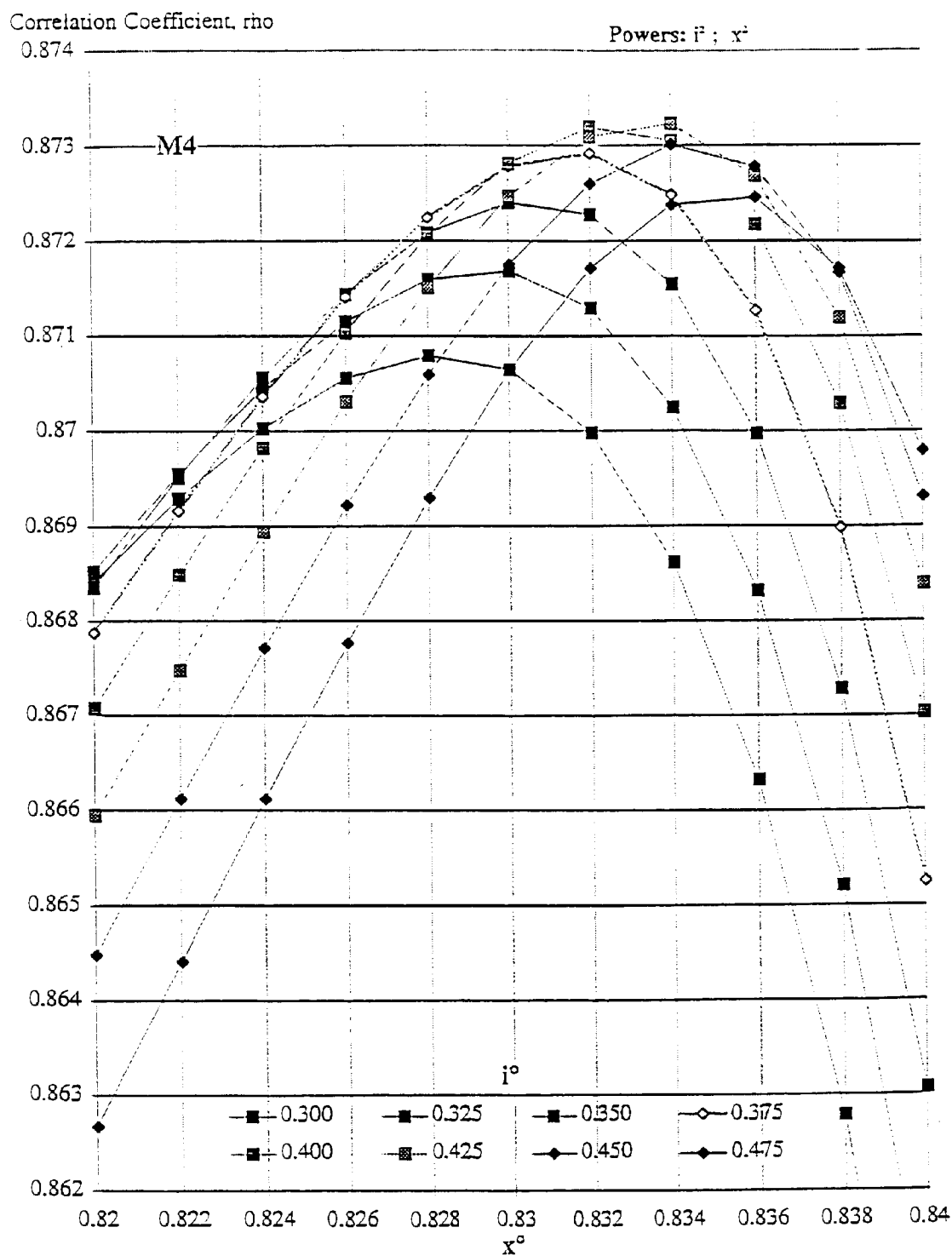
Figure 3-92
M4 Correlation Coefficient, ρ_{xy}, versus the threshold value for loading, x

Clearly there is some sensitivity to b, and b=2 must be taken as the more probable value (if, indeed, the exponent is integral). It is perhaps worth remembering here that a value of b between 2 and 3 can be estimated from the calorimetric results of Fleischmann and Pons.

In the last column, ρ^2 reflects the component of P_{xs} that relates *linearly* to changes in the test function, $P_{xs.test}$. It is quite remarkable that more than three quarters of the variability in P_{xs} can be accounted for by a function as simple as that employed in this analysis.

Figure 3-93 shows P_{xs} and $P_{xs.test}$ (with the coefficients determined from Figure 3-92) plotted against each other as a scatter graph. The value of K is taken to be 5×10^5, and a straight line is plotted at 45° to indicate a 100% linear correlation. While the covariance is generally good, there is a significant cluster of data at $P_{xs.test} = 0.1 \pm 0.05W$, where the test function underestimates P_{xs}. Nevertheless, it is clear that there are large regions of correspondence at zero, intermediate and "large" excess powers.

Important questions are raised by the apparent success of our test function:

i.   how generally applicable is this function?

ii. is the function predictive or responsive to other (hidden) stimuli?

iii. can the function be used to explain the appearance of excess power in some experiments, but not in others?

iv. by controlling the variables in this function can we induce excess power more controllably?

v.   what can this function teach us about the phenomenon under test?

On the question of general applicability we are limited in our choice of comparative experiments. It would be desirable to select reference experiments having the same cathode geometry and dimension as the M4 cathode. Very few of our experiments have been performed with 1mm wires, and none, previously, with the "lasso" geometry employed in M4. In practice we are more constrained in our choice by the need for high data quality in cathode resistance measurements, so that random measurement errors are not introduced into the values of $\delta x/\delta t$. Simply because the signal-to-noise ratio for 1mm wires is better than the 3 or 4 mm cross-section wires more typically (and successfully) employed, we are reduced in our selection of comparative experiments to one only; C1.

$$\text{Fit } fn: P_{xs} = MPX \ (\ x - x^o)^a (\ i - i^o)^b |\partial x/\partial t|$$
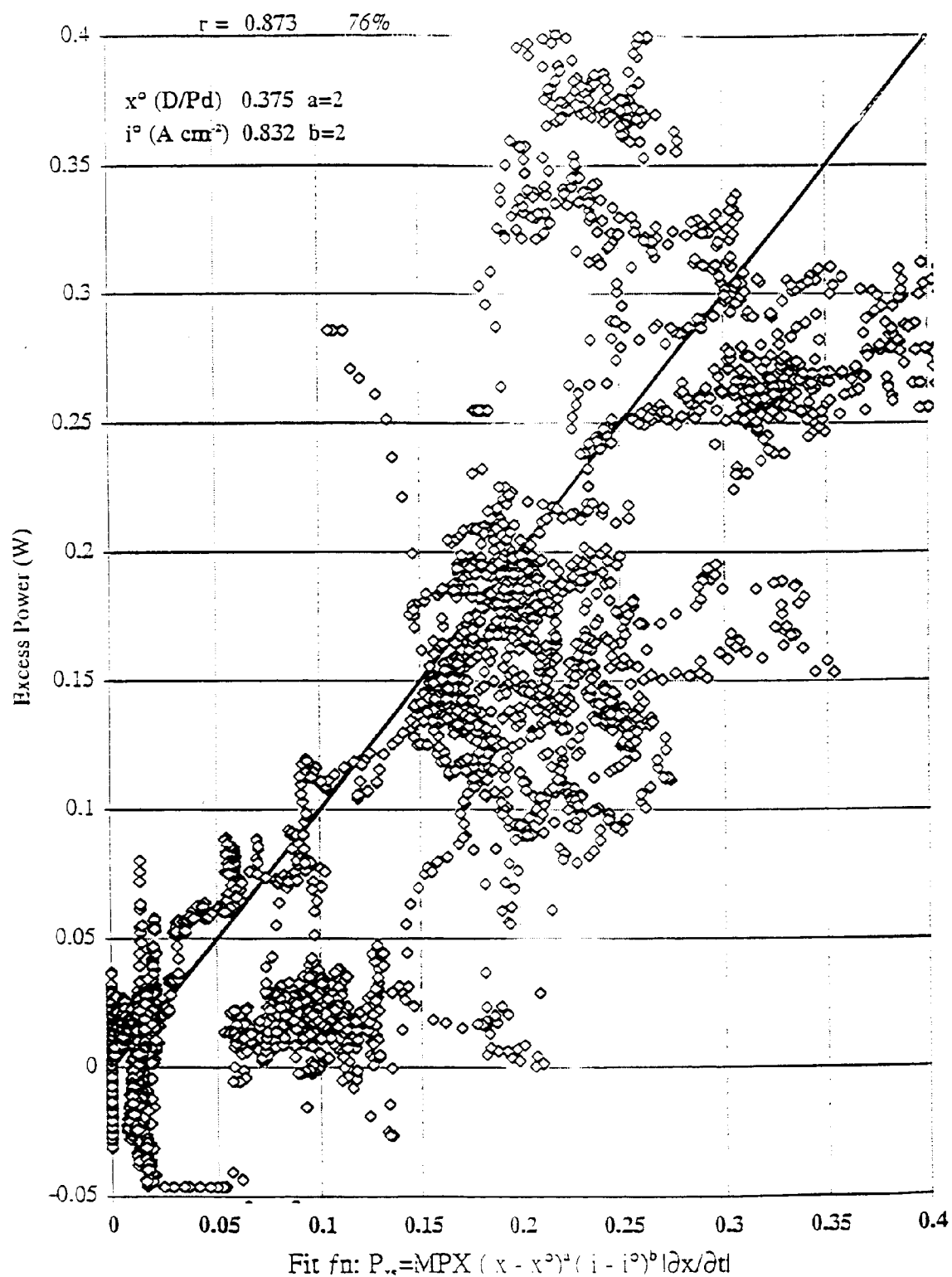
Figure 3-93
M4 Excess power from figure 3-92, scatter graph

Experiment C1 has been described fully in previous reports and publications[3].
The cell and calorimeter were very similar to those employed in M4, the cell being slightly larger (200 cm^3 rather than 140 cm^3 electrolyte), and the mass flow calorimeter was of flow-through rather than labyrinth flow design. The electrolyte in C1 was 1M LiOD + 200 ppm Al.

Two concentric-cylinder palladium sheets were employed as anodes in C1, rather than the helical platinum anode used in M4. The cathode in C1 was a vacuum annealed, 1 mm, Johnson Matthey palladium wire, approximately 45 cm long, with 36 cm submerged in the electrolyte. The cathode was secured by four PTFE pegs from below and mounted between the concentric anode in the shape of a crown.

Excess power was observed during the first (and only) ramp of C1. The same procedure was employed for C1, Ramp 1 to define the coefficients of the test function, as was described above for M4, ramp 3. For the case of C1, ramp 1, a better fit was found to the measured P_{xs} values with b=1, Figure 3-94 shows the time series data for P_{xs} and $P_{xs.test}$ calculated using the best fit parameters. Because of the great similarity between these two data series, they are offset by 1W in Figure 3-94, with $P_{xs.test}$ (the lower set) referred to the left axis, and P_{xs} referred to the right.

It was immediately clear that there is a striking similarity between P_{xs} and our test function, not only in general form, but in detail. The measured excess power looks like a damped, delayed response to the test function. This is reflected in the calculated Correlation Coefficient between the two sets of 0.94; more than 88% of P_{xs} is related linearly to our test function.

The data in Figure 3-94 can be compared directly with those in Figure 3-91. Both were calculated with coefficients a=2 and b=1, but the best fit threshold values differ significantly

---

[3] M. McKubre, et al in "Excess Power Observations in Electrochemical Studies of the D/Ps System; The Influence of Loading", in *Frontiers of Cold Fusion* , Universal Academy Press, Tokyo, 1993.
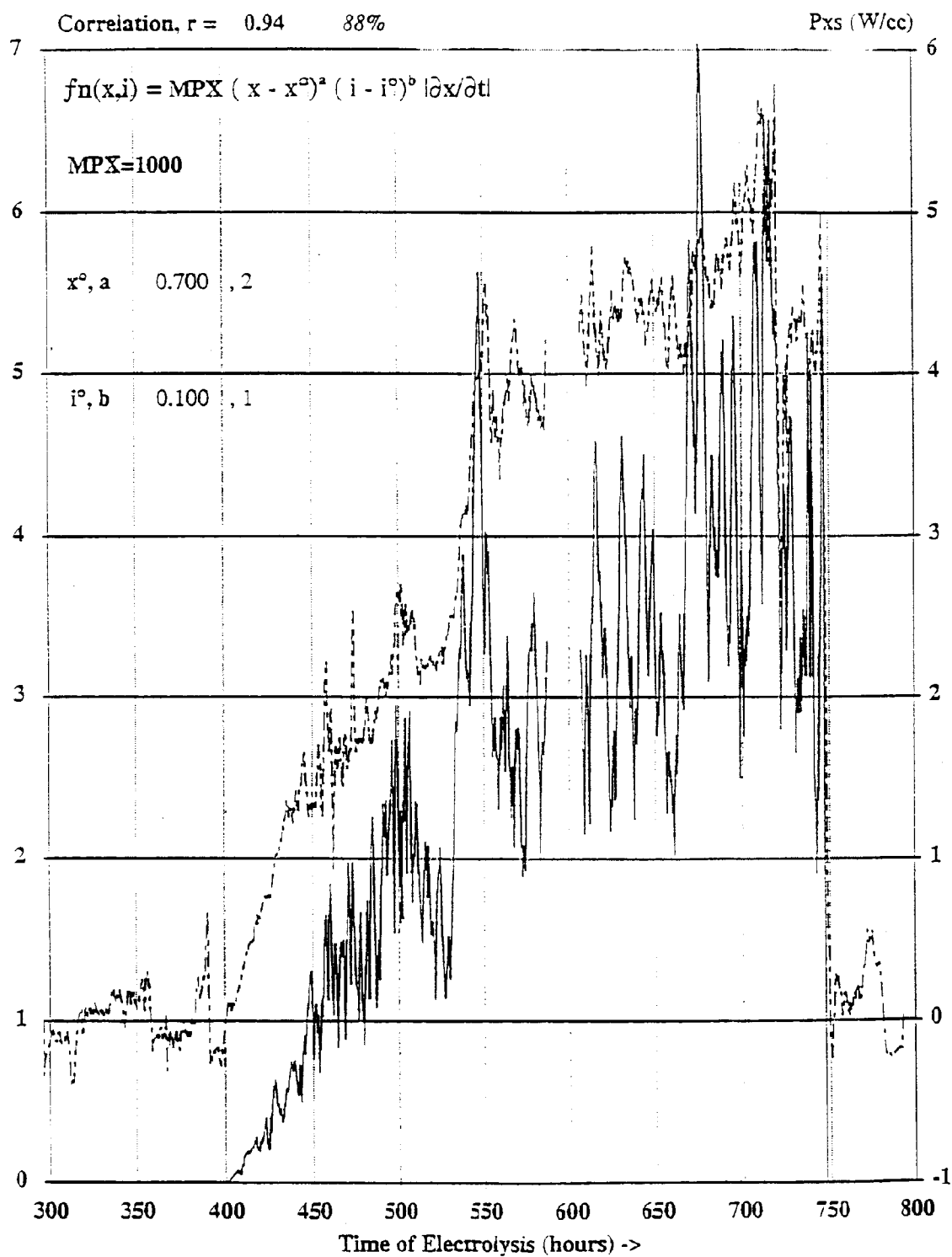
Figure 3-94
M4 time series data for P$_{xs}$ and P$_{xs.test}$

Coefficients for $P_{xs.test}$

Expt.	a	x^o (D/Pd)	b	i^o (mA cm^{-2})	K (V*)	ρ	ρ^2
M4	2	0.833	1	425	2.3×10^5	0.873	73%
C1	2	0.700	1	100	10^3	0.940	88%

*With b=1, K has units of Volts
*With b=2, K has units of Ohms

It is useful to compare these "results", with the maximum input functions and results for the two experiments.

Maximum Values for P_{XS}

Expt.	i (mA cm^{-2})	x (D/Pd)	P_{xs} (W)
M4	972	0.88	0.4
C1	758	0.98	5.0

Maximum Values of Excess Parameters

Expt.	$(i - i^o)$	$(x - x^o)^2$	P_{xs}/Volume (W cm^{-3})
M4	546	2.2×10^{-3}	5.1
C1	658	7.8×10^{-2}	17.7
C1/M4	1.2	35.5	3.6

In terms of the "excess" parameters there is not a great deal of difference in $(i-i^o)$ between experiments M4 and C1. Although the threshold value for M4 is much higher, the current density attained in experiment M4, ramp 3 also was higher, and the exponent of 1 makes this not a very strong variable. A significant difference does exist in the "excess loading" variable $(x-x^o)^2$. In this case, due both to a higher attained loading and *equally important* a much lower threshold loading value, the excess loading variable for C1 exceeded that of M4 by a factor of 35.

This latter observation is exceedingly important. Assuming that we can, as seems reasonable, use our test function as a predictor or, at least diagnostic for P_{xs}, then we need to pay close attention to the variables which give rise to large increases in the magnitude of the test function. A factor of 35 difference in our experiments is the difference between indiscernible levels of excess power ($\sim$ 50 mW) and a very large and

interesting effect (1.75 W). Between M4 and C1 this increase was achieved by two means: increasing $x_{max,}$ and decreasing x^o. The former is very difficult to achieve, reproducibly. It is not at all clear why the threshold value of x^o for C1 was low, or how it was lowered. Obviously it is important that we achieve such an understanding.

The product of 1.2 and 35.5 is 43. As indicated in the final row of the Table in the previous page, however, the volume (or area) weighted maximum excess power for C1 exceeded that of M4 by only 3.6. This difference is contributed, at least in part, by the much larger value of the rate of change of loading, $\delta x/\delta t$, observed in M4. If we attribute all of the difference in the specific excess power generation rate between C1 and M4 that is not due to the quantitative difference in the excess parameters $(i - i^o)$ and $(x - x^o)^2$, then the value of $\delta x/\delta t$ for M4 was 12 times larger than for C1.

A factor of 12 is the difference between one experiment and another. This also would be important as the difference between experiments in which scientifically interesting levels of excess power were observed and those which are rejected as yielding null or ambiguous results. Had this factor of 12 difference in $\delta x/\delta t$ between M4, ramp 3 and C1, ramp 1 not occurred (or in M4 it had been a factor of 12 less), then the excess power observed would have been at the threshold of calorimetric detection.

It is important to recognize that in neither case, M4 or C1, was an attempt made to maximize $\delta x/\delta t$. Quite the contrary. Both experiments were operated at constant (or slowly changing) currents, temperatures, and gas pressures; the three variables most likely to influence loading. What fluctuation in loading did occur, and in both cases it was significant and varied, occurred apparently spontaneously; we observed the effect, we did not control it.

As for the threshold values, particularly x^o, it is important that we understand what causes fluctuating loading, how we can control it and increase it to produce excess power more efficiently.

Attempts made to stimulate $\delta x/\delta t$ by stepping and pulsing the current at low and high (RF) frequencies were not successful. Even the very large current perturbations and oscillations, the values of $\delta x/\delta t$ induced were small compared to those which occurred apparently spontaneously during M4, ramp 3. Furthermore, large current perturbations (at least those examined so far), appear to reduce the average loading, so that neither a loading flux or excess power was observed.

Nuclear Products. A significant amount of excess energy was produced in experiment M4, more than can be accounted for by known chemical and mechanical processes. It is therefore appropriate to search for products of potential nuclear reactions which may give rise to excess power and energy.

The mass flow calorimeters, because of their size, complexity and the need for environmental isolation, are not provided with on-line nuclear detection capability. Instead, three integrating monitors were provided for experiment M4. These monitors had the capability of detecting integrated:

> X-rays
> neutrons
> helium.

The capability to detect x-rays, integrated over the experiment duration, was provided by placing Kodak dental x-ray films, size 00, outside of the 1 mm PTFE liner around the electrolyte chamber. At the termination of the experiment, after 1840 hours (> 2.5 months) of operation, it was found that water damage had rendered the radiation film badges unreadable. We are therefore not able to draw conclusions regarding the production of X-rays or other penetrating radiation, and its association to excess heat production.

The capability to detect integrated neutron flux, as well as x- and gamma rays, was provided by placing commercial (Radiation Detection Company, Sunnyvale, CA) LiF Thermoluminescent Dosimeters (TLD's) inside quartz tubes in the electrolyte. Four TLD's were placed inside two quartz tubes. Two other TLD's were kept as blanks in a lead storage container during the experiment. These blanks were developed along with the TLD's from the cell. The results from the cells M1, M3 as well as the blank samples were all less than 30 mRem as shown in Appendix 2. The configurations for cells M2 and M4 were such that no TLD's could be placed in the cell. It is obvious from these results that no neutron flux was detected by this method. In fact, the output measured in these cells was always somewhat less than that measured in the blanks because the duration of time spent underwater reduced the exposure to ambient neutrons to below that seen by the blanks in a 2" thick lead cabinet.

In an attempt to measure rates of helium production, the gaseous contents of cell M4 were sampled four times during the experiment, and subjected to analysis for ^{4}He. These analyses were performed by the U.S. Bureau of Mines at Amarillo, Texas. The sample times and results are presented in Table 3-7.

Table 3-7
Summary of Helium Analysis

Sample	Duration	Date	Time	ppm
1	669.4h	8/16/94	15:07	1.556
2	810.2h	8/22/94	11:55	1.661
3	1172.7h	9/06/94	14:30	0.340

| 4 | 1407.7h | 9/16/94 | 09:30 | 2.077 |

Excess power was first observed in M4 during the third current ramp at ~ 530 hours (8/10/94 19:44). At this time the current density i = 475 mA cm^{-2} and the loading D/Pd = 0.88. Excess power continued with some variability, reaching a maximum of 375 mW (~ 2% of P_{in}), and terminated abruptly at ~ 668h. At this time the current density i = 987 mA cm-2 and the loading D/Pd = 0.86. The energy integrated from the excess power in this period was 82.45 kJ or 9.27 MJ/mole of Pd.

A sample of gas was taken almost immediately following termination of P_{xs} (Sample 1, at 669 h) and found to contain 1.556 ± 0.007 ppm of ^{4}He. A second sample was taken 5.9 days later (Sample 2, at 810.2 h) and found to contain 1.661 ± 0.009 ppm of ^{4}He.

Sample 1. If ^{4}He is produced in the manner suggested by Miles and Bush via the reaction

$$D + D \rightarrow {}^4He + 22.4 \text{ MeV}$$

then from 82.45 kJ we expect

$$\Delta ppm = \frac{\delta \text{ atoms x } 10^6 \text{ x } 22400 \text{ cm}^3/\text{mole (at STP)}}{N \text{ x } V}$$

where   N = Avagrodo's constant = 6.022 x 10^{23} atoms/mol

V = Volume of cell plus manifold ≈ 250 cm^3

$$\Delta \text{ atoms} = \frac{82.45 \text{ x } 10^3 \text{ J}}{\left(22.4 \text{ x } 10^6 \text{ eV/atom}\right)\left(1.6 \text{ x } 10^{-19} \text{ J/eV}\right)}$$

$$= 2.30 \text{ x } 10^{16}$$

thus

$$\Delta ppm = 3.42 \text{ ppm}$$

Given an (assumed) starting concentration of [^{4}He] = 0.34 ppm (the value in the starting D$_2$ gas - see subsequent discussion of samples 3 and 4), then the "expected" concentration of ^{4}He is

$$ppm_{expected} = 3.42 + 0.34 = 3.76 \ ppm$$

In sample 1, only 41% of this amount was found.

Sample 2. The gas sampled at 669h (Sample 1) had 1.556 ppm ^{4}He. The volume of this sample, reduced the system pressure by 0.73 Atm., from 0.69 to - 0.04 Atm. gauge. Using gas from the D_2 source, the system pressure was increased by 0.59 Atm, to 0.55 Atm. gauge.

Given a system volume of 250 cm^3, and a helium content of 0.34 ppm in the make-up D_2 gas (subsequently verified), we can calculate the expected value of ^{4}He in Sample 2.

$$ppm_{expected} = \frac{0.96 \ Atm. \ x \ 1.556 + 0.59 \ Atm. \ x \ 0.34}{1.55 \ Atm.}$$

$$= 1.13 \ ppm$$

Sample 2 contained 1.66 ppm; 0.53 ppm more than "expected".

Discussion of Samples 1 and 2. Sample 1 was lower in ^{4}He, than predicted by the Miles Bush mechanism, and sample 2 was high. Two opposed hypotheses are offered:

1. Helium is not sourced with P_{xs} by the mechanism of reaction [1], and the ^{4}He measured originates by air in-leakage or by poor sampling procedures.

2. Reaction [1] is relevant, the integral power excess is measured accurately, but the release of ^{4}He to the gas phase is subject to an appreciable delay.

These hypotheses are discussed below with reference to the analyses of Samples 3 and 4.

Sample 3. Sample 3 was measured after extensively flushing the (operating) calorimeter with D_2 gas. This sample reflects any residual ^{4}He in the cell, the ^{4}He level in the D_2 purge gas, and any in-leakage of ambient air due to poor sampling technique. The value of 0.34 ± 0.01 ppm is consistent with samples previously taken by B. Bush of other D_2 gas cylinders, suggesting:

a. The gas in the cell was adequately purged

b. The sampling effectively excludes room air.

Sample 4. Sample 4 was measured 9.79 days (8.46 x 10^5 s) after Sample 3. During this time the cathode was ramped from 0.1 to 3.1A at 25 mA/hour, held at 3.1A for ~ 2 days,

and subjected to current oscillations 3.1/-0.001A with a 4 minute period twice for a total of ~ 2 days. The cell was also subjected to a "mini-boiloff", with the mass flow stopped for 76 minutes; during this time the cell electrolyte temperature rose to 57°C (from 45°C)

In the period between samples there were 5 instances of rapid loading or de-loading (large $\delta x/\delta t$) and the cathode attained a maximum loading of D/Pd = 0.918.

Excess power was not noted during the period between samples. Under steady state conditions, P_{xs} = 0 + 20/-50 mW. Several features of the calorimetric balance should, however, be noted as unusual.

i. Because of the temperature step and current steps, the calorimeter was at significant remove from its steady state for long periods of time (10-20% of the between sample period).

ii. The thermal baseline was not well established. Prior to the ramp, the calorimeter was 10-20 mW above thermal balance, while at the end of the ramp the calorimeter was 40-50 mW below thermal balance even with the non-steady state correction applied.

iii. During the two periods of current oscillations the calorimeter was apparently endothermic, by as much as 100 mW.

Hypothesis 1 The helium sourced between purging at Sample 3 and Sample 4 can be calculated as:

$$\Delta \text{ atoms } = \frac{\Delta ppm}{10^6} \frac{350cc}{22400} \; 6.022 \times 10^{23}$$

$$= 1.17 \times 10^{16}$$

$$\Delta \text{ time } = 9.79 \text{ days} = 8.46 \times 10^5 \text{ s}$$

$$\text{Source } = 1.38 \times 10^{10} \text{ atoms/s}$$

We can imagine that the source of this helium is one of the following:

i. Diffusional in-leakage of ^{4}He contained in room air.

ii. Convective in-leakage of ^{4}He contained in room air, either progressively, or at the time of sampling.

iii. Unobserved production via D + D → ^{4}He (or some other reaction)

iv. Slow release of ^{4}He previously produced or occluded.

i. *Diffusion*

Diffusional flux, $F = \dfrac{D\,\Delta C\,A}{l}$ moles s^{-1}

where   D   =   diffusion coefficient

ΔC   =   concentration gradient

A   =   available area for in-diffusion

l   =   effective thickness of diffusing area

We can define a parameter

$$X = \frac{DA}{l} = \frac{F}{\Delta C}\quad cm^3\ s^{-1}$$

Assuming constant and uniform in-diffusion,

$$\overline{\Delta C} = C_{air} - \frac{C_{initial} + C_{final}}{2}$$

$$= C_{air} - \frac{C_{initial} + C_{final}}{2}$$

$$C_{air} = 5.7\ ppm$$

$$C_{initial} = 0.34\ ppm$$

$$C_{final} = 2.077\ ppm$$

⇒ $\overline{\Delta C} = 4.49\ ppm$

$$= 4.49\ ppm$$

$$F = \frac{(\Delta ppm)\ 250\ cm^3}{\Delta t}$$

$$= \frac{(2.077 - 0.34)\ 250}{8.46 \times 10^5}$$

$$= 5.13 \times 10^{-4}$$

$$X = F/\overline{\Delta C} = 1.14 \times 10^{-4}\ cm^3\ s^{-1}$$

This diffusional rate is large. It represents $\sim 0.4\ cm^3/day$ which seems too much. If we ascribe all of this diffusion to the ceramic member holding the electrical feed-throughs ($A \approx 10\ cm^2$, $l \approx 0.2\ cm$), then $D_{ceramic} = 2 \times 10^{-6}\ cm^2\ s^{-1}$; this is much too large a number.

ii. Convection

The pressure in the system varied from 0.6 to 1.05 atmospheres *above* ambient in the period between Samples 3 and 4. When corrected for temperature, the pressure was not noted to change at all. There is therefore no reason to suspect convective leakage of gas out of the system, and much less reason to suspect convective in-leakage.

Had in-leakage occurred, we can calculate how much room air (at 5.7 ppm ^4He) would be needed to increase the concentration in 250cc from 0.34 to 2.077 ppm.

$$V_{leak} = \frac{2.077 - 0.34}{5.7}\ 250$$

$$= 76\ cm^3$$

This value seems implausibly large.

iii. Production

If ^4He were produced by a reaction such as

$$D + D \rightarrow {}^4He + 22.4\ MeV$$

we must ask the question whether or not we should have expected to observe calorimetrically the associated power or energy.

From the previous calculation, we need to account for 1.17×10^{16} atoms sourced in 8.46×10^5 s (1.38×10^{10} atoms s^{-1}).

For reaction [1]

$$\text{\AE}_{xs} = (1.38 \times 10^{10})\ (22.4 \times 10^6)\ (1.6 \times 10^{-19})$$

$$= 4.95 \times 10^{-2} \text{ W}$$

$$E_{xs} = (1.17 \times 10^{16}) (22.4 \times 10^{6}) (1.6 \times 10^{19})$$

$$= 4.18 \times 10^{4} \text{ J}$$

Given the state of the calorimeter and the number of transient events occurring it is possible (but not likely) that there is a baseline error of 50 mW; this reflects < 0.4% of the average input power, which is the nominal accuracy of the calorimetry. It is also possible (but not likely) that 40 kJ of excess heat could have been sourced during one or more of the calorimetric transients, and not seen.

We therefore cannot rule out the possibility that ^{4}He was sourced, with excess heat, in the method reported by Miles and Bush.

iv. Hideout

Excess power was observed in this calorimeter, and ^{4}He measured, some 20 days prior to sample 3. Immediately prior to sample 3 the cell was flushed with D_2 at ~ 10 cm^3/min. for ~ 18 hours; in this time the gas in the cell and manifold was presumed to be equilibrated with that in the D_2 bottle.for ~ 18 hours; in this time the gas in the cell and manifold was presumed to be equilibrated with that in the D_2 bottle.

Since the gas flow enters and leaves at the top of the cell, this equilibration is less likely to have taken place with the ^{4}He contained in the cell electrolyte (130 cm^3), the cathode (0.08 cm^3) or the PTFE parts of the cell (~ 100 cm^3). We do not know what the partition coefficient for ^{4}He is between D_2 gas, LiOD, PTFE and Pd metal. Nor do we know the effective diffusion coefficient of ^{4}He in PTFE or the rate at which ^{4}He sourced within Pd might be expected to leave. Given a Henry's law coefficient of 5-8 ppm for ^{4}He in D_2O and PTFE, however, there is certainly sufficient storage capacity to source the observed helium even with some removal during purging with D_2 gas. We do need to consider to what extent the cell parts, including the electrolyte, were saturated with helium (equilibrated with 5.7 ppm in the air) at the outset of the experiment.

Hypothesis 2. In attempting to evaluate a ^{4}He mass balance on the basis of hypothesis 2 (nuclear source), two critical pieces of information are missing: the helium content of the cell immediately before the initiation of excess heat production at 530h, and before purging at 1154h. We can make progress by assuming that, as intended (a, b) or claimed (c):

a. the system is helium leak tight

b. the initial helium content is that of the D_2 gas cylinder (= Sample 3)

c. helium is produced by reaction [1]

Sources of ^4He		Atoms
Initial inventory from D_2		3.9×10^{15}
Excess power 530-658 h		2.30×10^{16}
D_2 top-up 690 h		1.4×10^{15}
D_2 top-up 815 h		1.0×10^{15}
D_2 fill 1173 h		3.7×10^{15}
	Sum	*3.30×10^{16}*

Sinks of ^4He		Atoms
Sample 1 at 669 h		7.6×10^{15}
Sample 2 at 810 h		2.2×10^{15}
Purged volume before Sample 3		Unknown
System volume at Sample 4		1.40×10^{16}
	Sum	*2.38×10^{16}*

Clearly, if volume purged before Sample 3 contained $\geq 9.2 \times 10^{15}$ atoms (≥ 1.14 ppm), then a mass balance can be achieved. The inequality is employed because we cannot be certain that all ^4He had been released into the gas at the time of Sample 4. This estimated concentration is entirely plausible, but not provable.

In this model, ^4He is created before Sample 1 (presumably in the cathode, by reaction [1]). This helium is not, however, immediately available in the gas phase where it is accessible for sampling. Instead, the helium is slowly released over a period of a month or more.

Diffusion within the metal itself, might explain this time-constant. Alternatively, hold-up in the electrolyte or PTFE parts could supply the mechanism of delay. It is possibly of significance that the large ^4He concentration in Sample 4, followed the extended period of temperature pulsing and a temperature step in this sample period.

Conclusions

1. We cannot rule out the possibility that ^4He was sourced during the period between samples 3 and 4, or that the measured helium represents a hold-over from helium previously dissolved in D_2O or PTFE.

2. In the event of delayed release, a satisfactory mass balance can be obtained for ^4He on the assumption that

    a. the system is helium leak tight, and

b. the helium is sourced by reaction [1].

3. Convective in-leakage during cell operation or sampling seems a very unlikely source of the measured ^{4}He, and diffusional in-leakage, while possible, would be very hard to account for quantitatively.

4. The possibility of ^{4}He hide-out and slow emergence into the gas phase must be tested by experiment. This applies to both the ^{4}He thought to be produced by reaction [1] and to an initial inventory of ^{4}He in the LiOD and PTFE, due to equilibration with the ambient.

5. Definitive statements will be difficult to make about ^{4}He production in this or future experiments unless or until it is measured at several times the ambient background level.

4

CONCLUSIONS

Summary of Work Performed

At the outset of this program, the following overall project objectives, broadly speaking, were established: (1) To further quantify, and increase the rate of, excess heat production. (2) To identify the nuclear product(s) of the "cold fusion" phenomenon. (3) To investigate the correlation between excess heat and nuclear product formation.

In pursuit of these goals, the following experiment groups were undertaken.

(i) Mass flow calorimetry/nuclear product detection. Approximately 20 L-series, and 4 M-series, experiments were undertaken in high precision mass flow calorimeters. These experiments were designed primarily to investigate the excess heat producing capabilities of differing batches of palladium under differing pre-treatment and electrochemical conditions. Typically, experiments were run in isothermal mode at modest temperatures; however, a few were performed at elevated temperatures. The M-series experiments were provided with a He-tight gas-handling manifold in order to test for the production of He. All cathodes were analyzed with a Ge-detector and autoradiographically at the end of an experiment. Similarly, the tritium content of all used electrolytes was established. A majority of the cells tested were provided with shielded dental X-ray film for the in situ detection of energetic radiation.

(ii) Heat flow calorimetry/nuclear product detection. Several heat flow calorimeter designs were used in the investigation of excess heat production. Some 30 experiments were carried out within this group. The variables studied, from a calorimetric point of view, were similar to those studied in mass flow calorimetry.

(iii) Degree-of-loading experiments. Degree-of-Loading experiments were performed in order to investigate primarily the batch-to-batch variation in palladium loading behavior. Attractive cathodes were occasionally transferred to other experiments as they became available. Used cathodes were analyzed for gamma-emission.

Results Obtained

The following key results were obtained:

(i) In two experiments, M1 and M4, excess power production was observed at levels significantly above the sensitivity of the M calorimeter. Although the power levels attained were smaller than those measured previously in this program, their observation serves to confirm the key result of our earlier studies, *i.e.*, that the D/Pd system will act as a source of excess energy.

(ii) In the HH series of experiments, levels of excess power and He production were observed which, although relatively small, were deemed to be significant relative to their respective detection sensitivities. Taking these results at face value, the excess heat and He formation are apparently connected, via a multiplier of several tens of MeV/He.

(iii) Results obtained from both calorimetric and degree-of-loading studies served to emphasize the irreproducibility of palladium loading behavior. In addition, a possible systematic difference between loading results obtained from small, silica degree-of-loading cells and large, teflon lined calorimetric cells was identified. In general, it was found that loadings obtained in calorimetric experiments were lower than those obtained in degree-of-loading experiments. In addition, and perhaps most importantly, the loadings obtained in the calorimetric experiments reported here were significantly lower than those obtained (in a different cell design) in an earlier phase of this work (EPRI TR-104195) during which larger, and more frequent, excess heat production was observed.

(iv) In studies of the Ni/light water system, an experimental artifact was identified which, when operative, will serve to complicate significantly the interpretation of results obtained from this system. Based on this observation, it was decided not to pursue vigorously this line of research.

(v) Studies of excess heat production at high temperatures will, in general, require purpose-built calorimetric systems. The systems employed in this study were not entirely satisfactory when adapted to this task.

(vi) No tritium generation was observed.

(vii) While not definitive because of high background levels, the data obtained in experiment M4 are consistent with a quantitative, but temporally displaced correlation between excess heat and helium-4 production.

Concluding Remarks

At the outset of this work, it was assumed that the encouraging excess heat/loading results obtained in a previous phase of this study (EPRI TR-104195) would underpin the attainment of the broad objectives listed previously. The more-or-less repeatable attainment of significant levels of excess heat production was clearly identified as an obvious pre-requisite for continued, efficient study of all aspects of the "cold fusion" phenomenon. An experimental plan was constructed accordingly and the results of the execution of this (necessarily fluid) plan are described here.

With hindsight, we may now conclude that the presumption of repeatable excess heat production was premature, and that this has limited the progress achieved in this study. In particular, it has not been possible to address directly the issue of heat-commensurable nuclear product generation. Although this question remains unanswered, we may nevertheless state with some confidence that tritium is not a routinely produced product of the electrochemical loading of deuterium into palladium.

Using the observation of excess heat production in M1 and M4, together with the sum total of results published in this field in the period 1992-1995, we have no reason to abandon the view that the palladium loading plays a key role in the production of excess heat. Further, the excess heat results obtained in this program have reinforced the view that the electrochemical current, as well as some dynamic feature of the loading behavior, are also important. Results obtained elsewhere have indicated that the exact nature of the thermal boundary conditions imposed on the cathode are of critical importance for significant rates of excess heat production; in particular, that approximately isothermal conditions may not be the most advantageous.

Future work in this area, the experimental plan of which is primarily designed to identify and study the nuclear product(s) associated with the excess heat produced in an electrochemical system, must initially reinvestigate thoroughly those areas of electrochemistry and materials science associated with cathode loading, and the other parameters which are believed to be relevant to excess heat production. Success in this area is a necessary precondition for an efficient search for any associated nuclear products.

During the time period covered by this report, some alternative methods of producing excess heat have been described. These include raising the temperature of the cell electrolyte to the boiling point by a large current step following a low current "soak" phase, radio-frequency stimulation and acoustic stimulation. These approaches may prove useful in attempts to produce excess heat reproducibly enough in order to mount a systematic search for potential nuclear products.

A

D SERIES EXPERIMENTS

Objective of the Experiments Mills and Kneizys first reported observing excess heat during the electrolysis of light water solutions of alkali carbonates using nickel as cathode and Pt wire as anode. Several other groups have since reported having confirmed these intriguing observations. Most of these cells, including that of Mills and Kneizys[1], were of the open type. However, Bush and Eagleton[2] of CalPoly, Pomona, CA, who have carried out closed cell calorimetric studies on such systems, have also reported measuring excess heat. Thermacore Inc. have reported successfully scaling up the experiments to tens of watts levels. They used a pulsed power source, as recommended by Mills and Kneizys.

As for the origin of excess power in such systems, the originator of the concept, namely Randell Mills, claims it arises from the formation of "compact hydrogen atoms", rather than any nuclear reactions. On the other hand Robert Bush has hypothesized that the excess heat is due to the exothermic capture of protons (from the hydrogen of H_2O) by the alkali atom nuclei, catalyzed by the nickel cathode during electrolysis. He has since published experimental data which he claims supports his nuclear transmutation hypothesis. He has reported detection of an increase in calcium concentration in the K_2CO_3 solution after electrolysis and likewise an increase in level of strontium isotopes following electrolysis of Rb_2CO_3 solution. "Evidence" for potassium to calcium transmutation has also been reported by R. Natoya of the Catalysis Research Center, Hokkaido, Japan. Besides, both the BARC group at Bombay India and Natoya have reported observing a significant increase in tritium activity of the electrolyte following electrolysis for several days.

In the context of all these intriguing reports it was decided to carry out calorimetric studies on similar $Ni-H_2O$ light water cells during the six month sabbatical of Dr. Mahadeva Srinivasan (of BARC, Bombay) at SRI International taking advantage of his prior experience with similar systems at Bombay as well as the availability of considerable expertise and equipment at ERC for carrying out such studies.

In the first phase of the program, Srinivasan was given a free hand to reproduce the BARC "excess heat" results at SRI by setting up similar open cells and adopting a similar calorimetric technique as that employed in the BARC work. It took about three to four weeks for the initial planning of the experiments, fabrication of the cells and

commencement of calorimetric studies. The first open cell Ni-H$_2$O experiments commenced on 1 November 1993. In the second phase some of the calorimeters available at ERC, of both open and closed type, were deployed to independently study the "temperature anomalies" which appeared to be present in the phase I experiments.

Brief Description of the Open cells and Experimental Methodology Employed in the Phase I Experiments. The cells were fabricated out of a pair of concentric glass cylinders with dished bottoms which were fused along their top rims leaving a sealed air gap between them. This double-walled air-insulated clear-glass dewar was mounted inside a protective (6mm thick) perspex enclosure with a flat bottom. A couple of low density expanded Styrofoam spacer rings glued to the inner surface of the perspex enclosure served to locate the dewar centrally inside it. A similar foam pad at the bottom served as a shock resistant seating for the dished bottom of the glass dewar. The cell was provided with a T-shaped push fit teflon top plug (~ 50 mm thick) with six through holes for inserting RTDs and taking out electrode lead wires. A tube connected to an inert gas supply line was inserted into one of these holes to facilitate flushing of the gas volume above the electrolyte, prior to handling the cell for carrying out any checks/changes. The capacity of the inner cell vessel (~ 50 mm ID, 180 mm free height below top plug) was ~ 300 ml.

The electrode holder was also made of teflon. Upper and lower teflon spacer discs helped to locate the electrode assembly centrally inside the cell. A number of holes were drilled in these discs to facilitate connective circulation of electrolytic solution as well as for electrolytic gases to escape freely.

The nickel cathode was cut out of mesh stock or foil stock and was mounted centrally in the teflon holder to provide either cylindrical or planar geometry for the electrode assembly. 0.5mm dia. Pt anode wire was wound symmetrically around the nickel cathode. A Ni lead wire was spot welded to the upper part of the nickel cathode. Thin teflon sleeving was inserted over the anode and cathode lead wires so as to ensure that no part of the electrode connections in the air space above the electrolytic solution was left bare to avoid sparking or recombination effects. The electrode assemblies were subject to ultrasonic cleaning for about 30 minutes prior to loading into the cells.

The electrolyte was a light water solution of either 0.6 M K$_2$CO$_3$ or 0.1 M Li$_2$CO$_3$. Typically about 200 ml of electrolytic solution was charged into the cell. The level of the solution was adjusted to be at least a cm above the top of the electrode assembly.

Two RTD's were employed in each cell for temperature measurements. They were carried inside separate bottom-sealed teflon tubing to prevent the sensors from coming into direct contact with the electrolyte. One of the RTD's was located in the central part of the cell between the anode and cathode, while the other monitored the upper outer part of the electrolyte. The RTD's could sense temperature changes correct to 0.01°C.

No separate stirrer was employed for mixing the solution. The vigorous bubbling caused by the escaping electrolytic gases was reasonably efficient in this context, as evidenced by the fact that the difference in temperatures read by the two RTD's was typically < 0.8°C only.

A one meter long thin (~ 1mm dia.) heating element encased inside heat shrunk Teflon tubing, wound in the form of a coil around the electrode assembly served to calibrate the system for calorimetric purposes. An identical cell without electrochemical current flow, filled up to a similar level as the operating cell with either distilled water or electrolyte, served as a reference or dummy cell. It also had two RTD's mounted at two different elevations in the solution. The temperature difference δT at steady state between the average temperature readings of the operating cell RTD's (T_c) and dummy cell RTD's (T_{ref}) was taken as a measure of the total heat deposition rate (or power dissipation) in the operating cell.

Standard data acquisition system and software employed at the Energy Research Center for monitoring the various other calorimeters was employed for these experiments also. Besides the temperature sensor output, the cell voltage (V) and current (I) was also monitored continuously every two minutes. Being open cells, the power input to the cell, was computed as (V-1.482) * I, and was also recorded continuously.

The electrolyte level was periodically made-up by the addition of H_2O (typically every morning) to ensure that it does not fall too much below the pre-marked level. The see through nature of the cell was extremely helpful in this respect. The ability to observe the bubble formation and rise pattern during electrolysis was also very instructive.

There were two test cells for calorimetric studies and one common dummy cell. The cells were housed in the central cubicle of the middle compartment of the ERC safety enclosure. A temperature sensor suspended in this cubicle monitored ambient temperature variations. Prior to opening the door of the cubicle for checking electrode/RTD connections or for adding make-up water etc. the cell was turned off and inert gas (argon) flushed through the upper air-filled volume of the cells, as a routine safety precaution.

General Remarks on Thermal Characteristics and Performance of Cells.
Calorimetry involved determining the steady state δT between the temperature (T_c) of the operating cell and the temperature (T_{ref}) of the dummy cell for various input Joule heat powers. The time constant of the cell being in the region of about an hour, it normally required a few hours to reach temperature equilibrium after any change in cell current. However, we soon realized that we could attain equilibrium conditions in less than an hour (when going from a lower to a higher electrolytic power) by using the Joule heater to quickly raise the cell temperature to the expected level and then switching it off. The cell was then allowed to relax to its steady state condition in a

period of 15-20 minutes. The plot of δT versus Joule Power input to the cell was linear or almost linear in the range of interest which was up to ~ 2.5W in most cases; at times powers up to ~ 4W was studied. The calibration constant (slope of the calibration curve) varied from cell to cell in the range of 8 ~ 11°C/W. Since the δT at steady state could be determined to an accuracy better than 0.1°C, the typical error margin on the data points works out to only about 10 mW (derived from the calibration constant).

The main contribution to the error margin in δT arises from (a) differences in temperature gradients between heater calibration runs (where there is no bubbling to stir the electrolyte) and electrolysis runs where there is vigorous bubbling. But, surprisingly, in spite of this obvious source of error/uncertainty, in several experiments where no "excess heat" was measured, the electrolysis points and heater calibration points fell on a single smooth curve, (b) the second source of error is from the fact that when the data is recorded assuming it is in steady state, the system may in fact not be in equilibrium - the cell temperature may be very slowly rising or falling. To avoid this, for a given required accuracy, the required "waiting time" to confirm equilibrium condition needs to be allowed. For overnight runs this source of error is not present, (c) another source of error could be of electrochemical origin. The power may never attain a steady state if the overvoltage continuously changes due to ingress of hydrogen into the cathode surface. However, in the case of nickel, the overvoltage appeared to attain a steady value after a change in current, by the time the cell temperature attains a steady value, (d) Yet another possible source of error is the change in calibration constant following changes in electrolyte level in the cell vessel due to evaporation/Faraday loss. In this context a peculiar problem observed in the present series of experiments was an apparent slow increase in electrolyte level due to formation and growth of large bubbles on the surfaces of the teflon holder in which the electrodes were mounted. The cold region below the bottom spacer disc (dished and portion of cell bottom) as well as surface of heater coil was particularly prone to accumulating gas bubbles. The electrolyte level swelled by as much as a centimeter at times on account of this phenomenon. However, the effect of this on calibration constant (changes in heat loss characteristics) was not significant. To minimize errors due to this effect, the cells were periodically gently tapped to dislodge the large bubbles that were trapped.

The electrolytic runs were usually carried out in a galvanostatic mode. After every four or five electrolysis runs a few heater calibration runs were performed. In several cases, calorimetry was also done with reversed polarity operation   with the nickel driven anodically. We were rather surprised to observe that in many cells, the data points (δT for a given input power) in case of reverse electrolysis fell below the calibration curve. This behavior is discussed further later.

For cells which appeared to be showing temperature anomalies, between 20 to 45 stable points at different power levels (either during electrolysis or with heater or both together) were recorded. However in the case of cells wherein electrolysis and heater

points fell on the same curve the experiments were terminated after only 10 or 12 data points.

Summary of Results of Phase I Ni-H₂O Electrolysis Experiments. The first phase of the experiments lasted for about three months (November 1, 1993-January 31, 1994). During this period 23 cells were studied. Except for three cells which used 0.1 M Li_2CO_3, all other cells employed 0.6 M K_2CO_3 solution as electrolyte. In most cases either Johnson Matthey Ni foil or Fibrex nickel mat (similar to that used by Robert Bush at Pomona) was used. Other types of Ni material tested as cathodes were a type of Ni netting, an expanded low density nickel marketed as "Foam-metal" and a nanocrystalline Ni sheet specially procured from Queens University in Canada. One cell even used soft solder wire (Sn-Ag alloy) wound as a coil at the cathode. Table A-1 summarizes the results. Of the 22 cells in which calorimetry was carried out, 10 cells appeared to indicate some apparent "excess power" with respect to (V-1.482) * I.

Table A-1
Summary of first month results: Ni-H$_2$O open cell calorimeter 4 November to 3 December 1993

No	Cell#	Dates (Nov-Dec'93)	Dur. of Exp./d	Cathode Description	Electrolyte	# of Stable Points	Calibration Constant C/W	Apparent Excess Power	Tritium if measured (CPM/ml electrolyte)
1	HTA-01	4-9 Nov.	5	Ni Netting	0.6 M K$_2$CO$_3$	12	9.5°	n.o.*	
2	HTA-02	9-10 Nov.	2	Fibrex Mesh	0.6 M K$_2$CO$_3$	6	9.5°	n.o.*	
3	HTA-22	10-11 Nov.	2	JM Ni Foil	0.6 M K$_2$CO$_3$	6		n.o.*	
4	HTC-22	12-18 Nov.	6	JM Ni Foil (after anodic run)	0.6 M K$_2$CO$_3$	34	~ 10°- 11°	100 mW	n.o. (18.9 ± 1.9)
5	HGY-21	4-16 Nov.	4	JM Ni Foil	0.6 M K$_2$CO$_3$	45	8.3°	150 mW (0.15)	n.o. (18.9 ± 1.9)
6	HTA-21	16-29 Nov.	13	JM Ni Foil (after RE)	0.6 M K$_2$CO$_3$	8	9.5°	250 mW	
7	HGY-02	19-30 Nov.	11	Fibrex mesh (after RE)	0.6 M K$_2$CO$_3$	41	10.2°	200 mW	n.o. (16.6 ± 1.6)
8	HTA-31	29 Nov. 1 Dec.	2	Notoya Ni	0.6 M K$_2$CO$_3$	11	8.7°	n.o.*	n.o. (16.6 ± 1.6)

*n.o. = Not observed

Table A-1 (continued)
Summary of second month results: Ni-H$_2$O open cell calorimeter 4 December to 4 January 1994

No	Cell#	Dates (Nov-Dec'93)	Dur. of Oper.	Cathode Description	Electrolyte	# of Stable Points	Calibration Constant C/W	Apparent Excess Power	Remarks Figure #	Page # in Log Book
9	HTA-31L	2-16 Dec.	12d	Natoya Ni	Li$_2$CO$_3$	27	8.7	n.o.*	Fig. 9	pp. 59-63 (II)
10	HBO-21	10-15 Dec.	6d	JM Ni Foil	K$_2$CO$_3$	n.o.	—	n.o.*		pp. 23-24 (II)
11	HGY-44	14-17 Dec.	4d	Soft solder wire (Sn-Ag alloy)	K$_2$CO$_3$	9	12.8	30 mW	Fig. 11	pp. 24-28 (II)
12	HTA-56L	16-17 Dec.	2d	Foametal Ni	Li$_2$CO$_3$	9	9.3	² 50 mW	Fig. 12	pp. 64-68 (II)
13	HTA-56	17 Dec.-5 Jan.	19d	Foametal Ni	K$_2$CO$_3$	33	9.3	5200 mW	Fig. 13	pp. 68-75 (II)
14	HGY-67	17-20 Dec.	4d	Nano Ni	K$_2$CO$_3$	5	12.8	n.o.	Fig. 14	pp. 29-30 (II)
15	HGY-02R	20-21 Dec.	2d	Fibrex Ni (old used M4)	K$_2$CO$_3$	7	9.6	30 mW	Fig. 15 Cu on anode	pp. 30-33 (II)
16	HTC-21	22 Dec. 5 Jan.	15d	JM Ni Foil (old used cathodes)	K$_2$CO$_3$	10	10.3	n.o.	Fig. 16	pp. 34-37 (II)
17	HTC-04	6-14 Jan.	8d	Fibrex Ni Sandwich assy.	K$_2$CO$_3$ + copper shots	28	10.5	100 mW	1 mm Cu shot	pp. 37-45 (II)
18	HTC-04L	17-18 Jan.	2d		Li$_2$CO$_3$	4	10.5	n.o.*		pp. 45&89 (II)

A-7

Table A-1 (concluded)
Summary of second month results: Ni-H₂O open cell calorimeter 4 December to 4 January 1994

No	Cell#	Dates (Nov-Dec'93)	Dur. of Oper.	Cathode Description	Electrolyte	# of Stable Points	Calibration Constant C/W	Apparent Excess Power	Remarks Figure #	Page # in Log Book
19	HTA-23	7-13 Jan.	7d	J4 M Ni Fed (New)	K_2CO_3 + Cu	16	9.2	n.o.*		pp. 75-82 (II)
20	HTA-67	13-14 Jan.	2d	Nano Nickel (used)	K_2CO_3 + Cu	6	8.7	n.o.*		pp. 83-85 (II)
21	HTC-04	18-21 Jan.	4d	Fibrex	K_2CO_3	12	9.34			pp. 2-7 (III)
22	HTA-05	18 Jan.-17 Feb.	8d	Fibrex	K_2CO_3	39	—	n.o.*		pp. 51-57 (III)
23	HGY-58	21-31 Jan.	11d	Foametal	K_2CO_3		10			pp. 9 - (III)
24	HTA-06	22-25 Feb.	4d	Fibrex	K_2CO_3	7	9		Two balance	
25	HTA-05R	25 Feb.-1 Mar.	5d	Fibrex	K_2CO_3	8	9.6		Not on balance	
26	HGY-59	26 Feb.-1 Mar.	4d	Foametal	K_2CO_3	8	9.4		Two balance	
27	HTA-06R	2-16 Mar.	15d	Fibrex	K_2CO_3		8.6		Two balance	

*n.o. = Not observed

The "excess power" margin varied from 30 mW to a maximum of 200 mW. In the cells indicating apparent excess power, the electrolysis data points fell on a line almost parallel to the calibration line, very similar to the observations reported by the BARC group. Unfortunately, however, the excess heat margin was such that it always fell short of 1.48 x I. In other words, the δT values indicated power dissipation in the cell more than (V-1.482) * I, but less than V*I.

There was one other puzzling feature of the results which was somewhat disturbing. In several cells the data points corresponding to reverse electrolysis fell below the calibration line. This was also observed in one closed cell operated with a Fibrex Ni cathode and an electrolyte of 0.6 M K_2CO_3 solution in light water. (This experiment is described separately).

While we were trying to understand the different temperature anomalies observed in the Phase I Ni-H$_2$O experiments, we learned that Shkedi *et. al* of Bose Corporation had found evidence for in cell recombination effects (Faraday efficiency less than 100%) in their Ni-H$_2$O studies using semi-open cells wherein the electrolytic gases were recombined in a neighboring test tube containing a Pt catalyst. By weighing the mass of water reformed periodically and correlating it with coulombs passed, they concluded that recombination was occurring giving rise to an apparent "excess heat" margin in their "open" cells. If such effects were indeed present in Ni-H$_2$O cells, then the temperature anomalies or "apparent excess heat" observed in the Phase I experiments at ERC could also perhaps be explained by recombination effects.

The Phase II experiments were therefore designed to measure the Faraday efficiency while simultaneously performing calorimetry.

Phase II Ni-H$_2$O Experiments: Simultaneous Measurement of Power Dissipation in Cell and Faraday Efficiency

Introduction. Two different types of experiments were carried out for this. In the first a semi-open cell was set up, similar to the Bose Corporation experiment discussed earlier, with the difference that the recombiner flask along with the bubbler was mounted on a second electronic balance while the cell wherein calorimetric measurements were done was placed on the first electronic balance. In the second type of experiment an open heat flow calorimeter was used wherein the majority of the heat loss occurred through its bottom. The magnitude of heat flow was determined by means of a thermoelectric panel measuring the voltage developed across the thickness of the panel. The gas production rate from the cell was deduced by measuring the rate of displacement of a soap film in a graduated burette. These two experiments which started operating on 22 February 1994 are described in the following page.

Principle of the Two-Balance Experiment. The basic objective of the experiment is to measure simultaneously the mass of water lost from a cell due to electrolysis (Faraday efficiency) as well as mass of water reformed in a neighboring flask containing a large area Pt catalyst, into which the electrolytic gases are directed through flexible tubing. These two masses are to be measured while open cell calorimetry is performed. The output of the recombiner flask is connected to ambient atmosphere via a water bubbler. The electrolysis cell and recombiner flask (along with attached bubbler) are placed separately on two independent electronic balances reading to an accuracy of 0.01g. After inserting the usual temperature sensors and electrode connection leads via the top plug of the electrolytic cell, all gas leakage paths are sealed. The water bubbler serves additionally as an on-line manometer monitoring system pressure thereby confirming gas tightness.

There are four possible outcomes of such an experiment: (a) Mass of water lost from cell equals mass of water reformed in recombiner and both correspond to the Faraday value. Simultaneously if calorimetry confirms absence of "excess heat", then all is well and there is no anomaly to be explained. (b) However, in the above case when Faraday efficiency is 100%, if there is also some "excess heat" observed, then one may postulate the presence of some new phenomenon, as that suggested by Robert Bush. (c) Alternately, if mass of water lost equals mass of water reformed but both fall short of the Faraday value, then clearly it must be due to recombination effects. If further, calorimetry indicates some amount of "excess heat" generation, then it may be compared quantitatively with the heat due to recombination. (For the present we rule out the possibility that in the case wherein Faraday efficiency is less than 100%, there could be a situation wherein no "excess power" is observed with respect to [V-1.482]*I). (d) In the event however that mass of water lost from cell corresponds to the Faraday value but that of water reformed is less, then Mills theory of formation of dihydrino molecules gains support. This is what in fact Mills claims for his cells. (Before concluding that there is indeed an imbalance between masses of water lost and gained, it has to be ensured that the Pt catalyst is functioning properly and that there is negligible gas leakage).

Two-Balance Experiments: Preliminary Results. During the three week period 22nd February to 16th March 1994 three cells were run in the two balance mode: They were HTA-06 (22nd-25 Feb.), HGY-59 (26th Feb.-1 Mar.) and HTA-06R (2nd-16th Mar.). The open cell and the bubbler-recombiner were each placed on two separate SETRA electronic balances whose outputs were connected to the data acquisition system. Unfortunately, it was found subsequently, that these balances have a built-in auto zeroing feature as per which the balances are reset to 0.00 if the change during a scanning interval is less than a minimum value. As such if the initial readings are set to 0.00, or it so happens that it reaches a reading of 0.00 during the course of an experiment, weight changes during a two minute interval being very small, the balance

would get stuck at 0.00, showing no weight change during electrolysis. During the period 22nd Feb. to 16th Mar. this happened several times.

However, there were several data sets where neither of the balances misbehaved in this fashion, and these data could be interpreted. In most instances it was noticed that mass of water lost was higher by up to 20% as compared with mass of water reformed. The difference was larger at higher cell currents (higher temperatures), and therefore is attributable to evaporative loss. This was also evident from the fact that water was found to be condensing inside the tygon tubing connecting the cell to bubbler-recombiner.

For 100% Faraday efficiency we expect -0.335 grams of water loss (or reformed) per Ampere-hour of electrolysis. (This corresponds to .0011 grams per minute at a current of 200 mA) For good accuracy however, it is advisable to note differences that clearly emerged from these results is that invariably, during anodic operation of the nickel electrode, the Faraday efficiency is more than 100% while for cathodic runs it was less than (or sometimes equal to) 100%. The absolute Faraday efficiency during anodic operation was as high as 115-120% while for cathodic operation it dipped as low as 80% at times.

However, from the first three weeks of experimentation with the two-balance method it is difficult to draw any firm conclusions. Unfortunately, none of the three cells tested showed "excess heat" in an unambiguous manner so as to correlate "excess heat" with Faraday efficiency. It is easy to jump to the conclusion that Faraday efficiencies of 80% seen during some cathodic runs must be the cause of the apparent excess heat, suggesting recombination as the explanation. But how can one explain Faraday efficiencies of 120% during anodic runs accompanied by "negative excess heat"? One can at best conclude that there is a "temperature anomaly" and a "Faraday efficiency anomaly" and that the direction of the two are such as to suggest a correlation between the two. But rather than re-combination effects it may perhaps be some other electrochemical phenomenon, such as for example a shift in the thermoneutral potential of 1.482 due to the presence of carbonate in the electrolyte.

Open Cell Calorimetry Using a Heat Flow Calorimeter With Simultaneous Measurement of Gas Production Rate.

Cell # OHF-4 with a nickel fibrex - Pt wire coil electrode assembly dipped in a 0.6M K_2CO_3 solution in H_2O was used for this purpose. The heat flow calorimeter used a thermoelectric panel affixed to the bottom of the cell for measurement of total heat dissipation in the cell. Adequate insulation provided on the sides and top of the cell ensured that the major component of the heat loss occurred via the cell bottom. The entire calorimeter was immersed in a constant temperature water bath. No separate joule heater was provided for calibration of the calorimeter. Instead it was calibrated during electrolysis with the nickel electrode driven anodically when the cell was freshly installed. (Earlier experience at the Energy Research Center

had confirmed that anodic calibration is a valid procedure provided the electrodes are freshly installed, and not used for any electrolysis runs earlier).

Within a few days of commencement of the OHF-4 experiments, it became clear that there was a distinct difference in the slopes of the plots Thermoelectric device output voltage (V_{Ted}) against cell thermal power between the anodic and cathodic runs. Thus if the anodic operation is taken as a reference, the cathodic runs show clearly a steady 20% "apparent excess power". This finding corroborates similar observations made both during the Phase I experiments as well as the two-balance experiments of Phase II.

In order to measure the gas production rate the electrolytic gases issuing from the top of the cell were directed into the bottom region of a vertically mounted graduated burette. By means of a rubber bulb pumping arrangement containing soap solution and feeding into the bottom part of the same burette, it was possible to inject a soap film in the path of the escaping electrolytic gases. From a measurement of the time elapsed for the film to sweep 10 ml volume of the burette, during its upward traverse the production rate of electrolytic gases could be determined. For example, if the Faraday efficiency is assumed to be 100%, it should take 52.69 seconds to generate 10 ml of H_2 and O_2 gases during electrolysis at a cell current of 1 ampere. The gas production rate of cell OHF-4 was measured using this technique at intervals of about 20 minutes. Typically 5 or 6 time elapse measurements were recorded and averaged. The gas measurement system became operational on 8 March 1994.

A noteworthy feature of the gas production rate measurements on cell OHF-4 was that the time to generate 10 ml of gases was invariably smaller during anodic operation of the nickel fibrex electrode. The Faraday efficiency corresponded to 115%, both during 1.0 amp and 1.5 amp operation. In contrast during cathodic runs, the Faraday efficiency was always <100%. It fluctuated widely between 60% and 95% during cathodic runs at 1.0 and 1.5 amps. These observations thus generally corroborate the two-balance experiment results.

The gas production rate method of Faraday efficiency measurement has one advantage over the cell weight loss method in that it can detect short term variations, almost from minute to minute, whereas the balance method integrates over time intervals of tens of minutes.

A startling observation made on cell OHF-4 during cathodic operation of the fibrex nickel electrode was that the gas production rate becomes zero at times, meaning that there appeared to be no gas evolution at all for durations as long as 10 or 15 minutes. Subsequently the gas evolution resumed once again attaining 70% to 80% of the Faraday value. This observation indicates that 100% recombination of the gases occurs at times within the cell. Examination of the cell power output as recorded by the thermoelectric panel voltage confirmed a higher power dissipation in the cell during

such episodes. Thus it appears that in-cell recombination seems to occur only when the nickel is driven cathodically and not anodically. Here again it needs to be emphasized, that recombination postulate cannot explain 120% Faraday efficiency during anodic operation.

It is cautioned that the above observations/conclusions are of a preliminary/tentative nature and need to be confirmed after conducting further experiments of a similar nature.

1. R. L. Mills, S. P. Kneizys; "Excess Heat Production by the Electrolysis of an Aqueous Potassium Carbonate Electrolyte and the Implications for Cold Fusion" Fusion Technol. 20 (1991) 65.

2. R. T. Bush, R. D. Eagleton; "Cold Nuclear Fusion: A Hypothetical Model to Probe an Elusive Phenomenon" J. Fusion Energy 9 (1991) 397.

B

THERMOLUMINESCENT DOSIMETER RESULTS

Thermoluminescent Dosimeters (TLD), consisting of LiF crystals sealed in polyethylene tubes inside quartz tubes, were placed in five different experiments. Background data were collected on equivalent TLD's shielded by 5 cm thick lead walls in an adjacent laboratory. Background samples were also collected on TLD's stored at Radiation Detection Company, Sunnyvale, CA, where all TLD's were developed and analyzed. Results of all samples collected and their appropriate background and calibration results are shown.

Table B-1
TLD Exposure Results

Experiment	Sample	Background (Menlo Park)	Exposure (mrem) Background (Sunnyvale)	1000 mrem Calibration
L9	<30	<30	—	—
M1	<30	<30	—	—
M3	19±2	20±1	24±1	1000±15
H1	16±2	21±1	25±1	1000±10
L11	17±1	21±1	25±1	1000±10

It is obvious from these results that no exposure above background was measured by the TLD's in any of the five electrochemical cells. In fact, within experimental error, exposure was always less in the cells than in the background samples. This could be due to the neutron scattering of the 200 liter water baths in which the experiments were performed.

Export Control Restrictions

About EPRI

EPRI creates science and technology solutions for the global energy and energy services industry. U.S. electric utilities established the Electric Power Research Institute in 1973 as a nonprofit research consortium for the benefit of utility members, their customers, and society. Now known simply as EPRI, the company provides a wide range of innovative products and services to more than 1000 energy-related organizations in 40 countries. EPRI's multidisciplinary team of scientists and engineers draws on a worldwide network of technical and business expertise to help solve today's toughest energy and environmental problems.

EPRI. Electrify the World

Program:

Nuclear Power

TR-107843-V1